PROPERTIES, PROCESSING AND APPLICATIONS OF

Glass and Rare Earth-Doped Glasses for Optical Fibres

Edited by

DAN HEWAK

Optoelectronics Research Centre
University of Southampton, UK

IEE

INSPEC
THE INSTITUTION OF ELECTRICAL ENGINEERS

Published by: INSPEC, The Institution of Electrical Engineers,
London, United Kingdom

© 1998: The Institution of Electrical Engineers

This publication is copyright under the Berne Convention and the Universal Copyright Convention. All rights reserved. Apart from any fair dealing for the purposes of research or private study, or criticism or review, as permitted under the Copyright, Designs and Patents Act, 1988, this publication may be reproduced, stored or transmitted, in any forms or by any means, only with the prior permission in writing of the publishers, or in the case of reprographic reproduction in accordance with the terms of licences issued by the Copyright Licensing Agency. Inquiries concerning reproduction outside those terms should be sent to the publishers at the undermentioned address:

The Institution of Electrical Engineers,
Michael Faraday House,
Six Hills Way, Stevenage,
Herts. SG1 2AY, United Kingdom

While the author and the publishers believe that the information and guidance given in this work is correct, all parties must rely upon their own skill and judgment when making use of it. Neither the author nor the publishers assume any liability to anyone for any loss or damage caused by any error or omission in the work, whether such error or omission is the result of negligence or any other cause. Any and all such liability is disclaimed.

The moral right of the author to be identified as author of this work has been asserted by him/her in accordance with the Copyright, Designs and Patents Act 1988.

British Library Cataloguing in Publication Data

A CIP catalogue record for this book
is available from the British Library

ISBN 0 85296 952 X

Printed in England by Short Run Press Ltd., Exeter

Introduction: a history of glass for optical fibres

by W. Alexander Gambling, FRS
City University of Hong Kong, August 1998

Silica is an extraordinary material. It is strong, stable, abundant, easily processed, can be manufactured in extremely pure form and, above all, is remarkably transparent to light of visible, and particularly near infrared, wavelengths. Even more crucial for its application in optical fibre communications is the fact that its material dispersion parameter becomes negative at wavelengths greater than 1.3 μm and, in fibre form, can be compensated by simple, appropriate fibre design. Silica fibres can also be fabricated with a high degree of precision. As a result of these properties, silica fibres, lightly doped with suitable modifying oxides which induce small changes in refractive index, have transformed telecommunications. It is now possible to transmit information by modulated laser light over single-mode, silica-based optical fibres for millions of kilometres, at enormous information capacity, with almost zero distortion [1] and at greatly reduced cost compared with earlier methods. Not surprisingly optical fibres and laser light have swiftly replaced copper wire and electric current in telephone networks and long-distance transmission for all but short distances.

Silica is a glass of simple chemical structure containing only the two elements silicon and oxygen. It has a softening temperature at which it can be stretched, i.e. drawn, into fibre of about 2000°C. Other glasses of more complex composition, the so-called 'soft' glasses, have drawing temperatures in the region of 1000°C but are far less transparent to light. Soft-glass fibres have been known for many years: for example a patent was issued in France in 1836 [2] to cover 'weaving glass ... either pure or mixed with silk, wool, cotton or linen'. In 1840 when the body of Napoleon was transported to Les Invalides in Paris the funeral draperies were 'woven of silk and glass fibre dyed in the mass and giving the appearance of gold brocade'. Silica fibre was later fashioned in a spectacular way by Sir Charles Boys [3] who wanted a very fine, but strong, suspension in a sensitive instrument for the measurement of gravity. Silica was superior to metal because it was perfectly free from hysteresis and, after twisting, always returned to its original position. Sir Charles heated a rod of silica quartz in a crossbow (to a temperature of about 2000°C) which was then fired across the width of two laboratories. In this way exceptionally fine silica fibres were produced in varying diameters down to less than 100,000th of an inch (i.e. 0.2 μm). He also experimented with the rapid drawing of a heated quartz rod into fibre with the aid of a rocket, but concluded that the method 'does not seem altogether convenient'.

A more controlled method of drawing glass rods into fibre emerged much later and was based on soft glasses. Because of the lower fictive temperature the heating could be carried out in a cylindrically-wound, resistance-wire furnace open at both ends and mounted vertically. The temperature was measured by a thermocouple and set to within a degree or so by controlling the heater current. The glass rod was inserted gradually into the top of the furnace and the temperature in the hot zone adjusted so that the viscosity of the glass became low enough for fibre to be drawn off at the bottom.

A glass fibre is able to guide light if its refractive index is greater than that of the surrounding medium, air in this case. Several hundred such fibres could be bound together in the form of a bundle, the ends of which were then cut and polished, and used to transmit light. If the

individual fibres were sufficiently thin, ~100 μm, the fibre bundle formed a flexible light 'guide', sometimes erroneously called a light 'pipe'.

Unfortunately these fibre bundles had three severe limitations. Firstly, in addition to the launching loss at the input end, the transmission loss was such that the useful length was only a metre or two. Secondly, flexing of the bundle caused adjacent fibres to abrade each other causing breakages and the number of useful fibres decreased with use, thus increasing the loss still further. Thirdly, the individual fibres were not completely surrounded by air but made line contact with six neighbouring fibres. For incoherent bundles which were intended only to transmit a patch of light for which the spatial distribution was not important the latter fault was not serious. However for coherent bundles intended to convey images, for example in medical endoscopes, light leakage between fibres caused a progressive decrease in resolution along the length.

In 1951 H.H. Hopkins and N.S. Kapany in England [4] and A.C.S. van Heel in the Netherlands began to experiment with a coating on the guiding glass fibre, the former with a glass cladding and the latter with a plastic one. If the cladding had a lower refractive index than the core, total internal reflection would now occur at the core/cladding interface and no light would leak into adjacent fibres. The spatial resolution would not deteriorate along the length of the fibre bundle and providing the cladding thickness was small, in practice a few micrometres, there was no great reduction in launching efficiency at the input end of the bundle. Such a fibre structure, with a glass cladding, is now almost universally used in fibre bundles and in single fibres for information transmission. Kapany, a research student of Hopkins, subsequently published an excellent and comprehensive book describing the state of knowledge at the time [5].

As far as optical fibre communication is concerned the first crucial step came in 1966 with the estimation by C.K. Kao and G.A. Hockham [6] that the optical transmission loss in bulk glass might, if the impurities could be reduced sufficiently, be as low as 20 dB/km at a wavelength of about 0.6 μm. This was thought to be the level required for practical application. The best known value for bulk silica was then just over 100 dB/km and for soft glasses about 200 dB/km. However, the techniques available for drawing bulk glass into cladded glass fibre were primitive. Firstly, two low-loss glasses were required, one for the core and the other for the cladding, and they had to be compatible, which means primarily that they must have similar drawing temperatures, whilst the refractive index and thermal expansion coefficient of the core glass must be larger than those of the cladding glass. The cladded fibres available at the time had losses of many thousands of dB/km due to imperfections at the core/cladding interface. A problem with silica was that no other compatible glass was known because of its high drawing temperature, low expansion coefficient and low refractive index.

From 1966 to 1970 improvements in fibre-drawing techniques, particularly at Southampton, reduced considerably the optical loss of fibres drawn from commercially-available soft glasses. Nevertheless the results achieved, approaching 100 dB/km, were still well above the target figure of 20 dB/km and attempts to improve the bulk properties of the glasses concerned had not progressed far. Then in 1970 came the startling announcement from Corning Glass Works [7] that a silica-based single-mode fibre with a loss of 20 dB/km had been fabricated. Few details were given but it subsequently emerged that titania had been deposited on the inside surface of a silica tube which was then drawn into a fibre. During drawing the titania diffused into the internal silica surface which formed the core of the emerging fibre. The titania-doped

core was of higher refractive index than the surrounding pure silica cladding, thus producing the required optical guidance.

This 'existence theorem' excited considerable interest and the number of laboratories actively researching optical fibres for communications rapidly increased from the three in England (STC led by Charles Kao, British Telecom led by Frank Roberts and Southampton University led by Alec Gambling) to many, worldwide. New dopants were introduced for raising and lowering the refractive index of silica for alternative core and cladding compositions (germanium, phosphorus, boron, fluorine, aluminium, etc.) and new fabrication techniques were devised, the most important commercially today being OVD (Corning), MCVD (Southampton University [8] and Bell Laboratories [9]), VAD (NTT Laboratories [10]) and PCVD (Philips [11]). In a few years the attenuation was reduced to less than 1 dB/km and later (1986) reached nearly the theoretical minimum of 0.3 dB/km at a wavelength of 1.3 μm, and a remarkable 0.15 dB/km at 1.55 μm, in a fibre with a pure silica core and a cladding of fluorine-doped silica [12]. These results have never been improved upon in any material despite considerable effort being expended on fluoride, chalcogenide and other glass systems.

In 1975 it was shown [13] that the material dispersion

$$\frac{\lambda}{c}\frac{d^2n}{d\lambda^2}$$

in silica falls to zero at a wavelength, λ, of 1.3 μm so that the signal capacity of multimode fibres operated with light-emitting diode sources is greatly increased at this wavelength. It was further [14] shown that at longer wavelengths the material dispersion becomes negative and, in single-mode fibres operated with laser sources, can be counteracted by appropriate fibre design. The latter result, together with the low and minimum loss at 1.55 μm, meant that enormous bandwidths were possible at this wavelength, together with spacings between the electrical repeaters in an optical fibre transmission line of 100 km or so. This compares with the last electrical fibre to be installed across the Atlantic Ocean which had repeater spacings of 10 km and a modest capacity of only 4,000 circuits (about 20 MHz). The first TransAtlantic optical fibre cable, laid in 1986, had twice the capacity and the number of submerged repeaters was reduced from 1,200 to only 200. The cost per circuit was reduced by a factor of two.

The 1970s were also the era of a breakthrough in a totally unrelated family of glasses. Marcel Poulain, working as a student on research dealing with the synthesis of crystals based on zirconium fluoride, surprised his co-workers when, rather than the desired single crystal, a large glassy sample was produced [15]. Further work by the team at the University of Rennes led to the establishment of a family of heavy metal fluoride glasses. Like silica, fluoride glass also has a wavelength of minimum loss, but at wavelengths between two and three micrometres depending on the specific composition. A consequence of the longer wavelength is a reduced intrinsic loss, theoretically near 0.01 dB/km, an order of magnitude lower than in silica. The promise of even longer repeaterless spans of fibre, drawn from fluoride glass, prompted a flurry of research around the world [16].

However the development of optical amplifiers suitable for use with silica fibres and the inability to realise in practice the low predicted losses saw an equally rapid decline of interest in the application of fluoride fibres to optical transmission. Nevertheless fluoride fibres have taken on a new life of their own. When doped with appropriate lasing ions they form the basis

for new, more efficient fibre lasers and amplifiers because of the lower radiative decay rates in this heavy metal glass structure.

In addition to the advances being made in silica technology and its applications the associated techniques of coating, cabling, jointing and so on were steadily improving. It was also necessary to develop new laser diodes for operation at the preferred wavelength of 1.55 μm; considerable, and successful, efforts were made by device manufacturers to fulfil this need. The next major advance in silica technology, which was to have a rapid and major commercial impact, was the announcement from Southampton University that a standard single-mode fibre doped additionally with erbium ions could amplify at the optimum wavelength of 1.55 μm [17]. The erbium-doped fibre amplifier turned out to have remarkable properties. Not only did it operate, by a great coincidence, at precisely the wavelength where the fibre loss was a minimum and at which material and mode dispersions can effectively be cancelled, but a gain of over 50 dB was possible with a bandwidth of 4,600 GHz, together with a noise figure very close to the quantum limit of 3 dB. So importance was this development that only three years after the initial announcement the first commercial product appeared and, in a further three years, amplifiers began to be installed in operating systems. As a result of the erbium fibre amplifier, electronic repeaters are no longer required. The fibre system thus becomes transparent so that changes to the signalling protocol and format are easily made whilst the bandwidth, formerly limited by the repeaters, can be as large as that of the amplifier. The cost per circuit has fallen from US$30,000 in the first underwater cable to US$500, whilst the capacity has increased from 8,000 to 600,000 circuits. The number of underwater cables worldwide is now increasing rapidly.

Even before silica fibres revolutionised optical communication, a large family of infrared red glasses, formed from metals such as arsenic, germanium and antimony and combined with one or more of the chalcogenides (sulphur, selenium and tellurium), were being actively developed in fibre form. Early applications in the 1960s were in infrared transmission and thermal imaging at wavelengths where other glasses such as silica were completely absorbing. Today, chalcogenide fibres have a wide range of applications, from new passive infrared waveguides for wavelengths beyond ten micrometres, to high-power laser delivery systems, thermal imaging, aerospace and sensing applications, as well as active applications such as high-speed photonic switching compatible with silica optical fibres [18].

Until recently optical fibres simply carried information from point to point; any signal processing, other than amplification, had to be carried out by extracting the signal from the fibre and processing it electronically. Increasingly, both passive and active fibre components are becoming available and what I have described elsewhere as a technology of integrated fibre circuits is emerging. By far the most important of these components is the fibre grating [19]. It is now possible to 'write' directly into the core of a silica-based fibre a wide variety of gratings which can be suitably designed to carry out a multitude of functions, such as narrow and broad-band filters, dispersion compensation, wavelength selection, fibre lasers, fibre taps, gain equalisation in fibre amplifiers and a host of others. The application of silica to optical fibre communications has produced a succession of revolutionary, rather than evolutionary, developments and the advent of fibre gratings is yet another which is likely to have just as great an impact as the erbium-doped silica fibre amplifier.

Nearly half a century ago the element silicon began the electronic and information technology revolution which it continues to supply and control. A quarter of a century ago the simplest of

glasses, silica, initiated the optical communication revolution which is in full swing. Will this sequence continue, and if so where will it lead us? At this point I take a hint from Groucho Marx who is reputed to have said, 'Never make predictions - especially about the future'.

REFERENCES

[1] M. Nakazawa, K. Suzuki, E. Yamada, H. Kubota, Y. Kimura, M. Takaya [*Electron. Lett. (UK)* vol.29 (1993) p.729-30]

[2] G. Gintrand [*Vetrolux Fiberworld* vol.14 (1982) p.2]

[3] C.V. Boys [*Philos. Mag. (UK)* vol.23 (1887) p.489]

[4] H.H. Hopkins, N.S. Kapany [*Nature (UK)* vol.173 (1954) p.39]

[5] N.S. Kapany [*Fiber Optics: Principles and Applications* (Academic Press, 1967)]

[6] C.K. Kao, G.A. Hockham [*Proc. Inst. Electr. Eng. (UK)* vol.113 (1966) p.1151-8]

[7] F.P. Kapron, D.B. Keck, R.D. Maurer [*Appl. Phys. Lett. (USA)* vol.17 (1970) p.423]

[8] D.N. Payne, W.A. Gambling [*Electron. Lett. (UK)* vol.10 (1974) p.289-90]

[9] W.G. French, J.B. O'Connor, G.W. Tasker [*Bell Syst. Tech. J. (USA)* vol.52 (1974) p.951]

[10] T. Izawa, S. Kobayashi, S. Sudo, F. Hanawa [*Proc. Int. Conf. on Integrated Optics and Optical Communications* Japan, July 1977 (Institute of Electronics and Communication Engineers of Japan, 1977) vol.C1-1 p.375-8]

[11] D. Küppers, H. Lydtin, F. Meijer [*Proc. Int. Conf. on Integrated Optics and Optical Communications* Japan, July 1977 (Institute of Electronics and Communication Engineers of Japan, 1977) vol.C1-1 p.319-22]

[12] H. Yokota et al [*Proc. Int. Conf. on Optical Fibre Communications* USA, February 1986 (Optical Society of America, 1986) vol.P.D.3-1 p.11-8]

[13] W.A. Gambling, H. Matsumura, C.M. Ragdale [*Electron. Lett. (UK)* vol.14 (1978) p.618-20]

[14] W.A. Gambling [*Proc. European Conf. on Optical Communications* Genoa, Italy, 12-15 Sept. 1978, Invited Plenary Paper]

[15] M. Poulain, M. Poulain, J. Lucas [*Mater. Res. Bull. (USA)* vol.10 (1975) p.273]

[16] P.W. France (Ed.) [*Fluoride Glass Optical Fibres* (Blackie, London, 1989)]

[17] R.J. Mears, L. Reekie, I.M. Jauncey, D.N. Payne [*Proc. Int. Conf. on Integrated Optics and Optical Communications/Optical Fibre Communications* Reno, Nevada, USA, January 1987 (Optical Society of America, 1987) paper W12]

[18] D.W. Hewak, D.N. Payne [*Proc. Int. Conf. on Integrated Optics and Optical Communications/ European Conference on Optical Communications* Edinburgh, UK, 22-25 Sept. 1997]

[19] K.O. Hill, G. Meltz [*J. Lightwave Technol. (USA)* vol.15 (1997) p.1263-76]

Contributing Authors

J.L. Adam
C1.1, C1.2
Universite de Rennes, Laboratoire des Verres et Ceramiques
Campus de Beaulieu, 35042 Rennes Cedex, France

I.D. Aggarwal
D4.3, D4.4
Naval Research Laboratory
4555 Overlook Ave S.W., Washington DC 20375-5338, USA

G.P. Agrawal
A1.4
Institute of Optics, University of Rochester
PO Box 270186, Rochester, NY 14627, USA

H. Aoki
B3.1
Hoya Corporation, R&D Center
3-3-1 Musashino, Akishima-shi, Tokyo 196-8510, Japan

M. Asobe
D5.3
NTT Optical Network System Laboratories
1-1 Hikarinooka, Yokosuka-shi, Kanagawa-ken 239, Japan

M.O. Berendt
A3.1
Technical University of Denmark, Dept. Electromagnetic Systems
Building 348, DK-2800, Lyngby, Denmark

A. Bjarklev
A3.1
Technical University of Denmark, Dept. Electromagnetic Systems
Building 348, DK-2800, Lyngby, Denmark

D.J. Brady
D1.1, D1.2, D2.1, D2.2
University of Southampton, Optoelectronics Research Centre
Highfield, Southampton, SO17 1BJ, UK

M. Braglia
C2.2
CSELT, Optical Syst. & Technology - Optical Fibre Devices
Via Reiss Romoli 274, 10148 Torino, Italy

W.S. Brocklesby
D3.1
University of Southampton, Optoelectronics Research Centre
Highfield, Southampton, SO17 1BJ, UK

J. Broeng
A3.1
Technical University of Denmark, Dept. Electromagnetic Systems
Building 348, DK-2800, Lyngby, Denmark

A. Bruce
A4.3
Lucent Technologies, Bell Laboratories, Rm 1D-431
600 Mountain Avenue, Murray Hill, NJ 07974, USA

R. Caspary
C3.3
TU Braunschweig, Institut fur Hochfrequenztechnik
Postfach 3329, D-38023 Braunschweig, Germany

T. Catunda
C1.4
Instituto de Fisica de Sao Carlos
Cx.P.369, 13560-970 Sao Carlos, SP, Brazil

M.F. Churbanov
D4.2
Inst. Chemistry of High Purity Substances, Russian Acad. Sciences
49 Tropinin St., GSP-75, 603600 Nizhny, Novgorod, Russia

M.J.F. Digonnet
B5.1
Stanford University, Edward L. Ginzton Laboratory
Stanford, California 94305, USA

L. Dong
A4.2
Corning Inc.
Sullivan Park, Corning, New York 14381, USA

K. Dridi
A3.1
Technical University of Denmark, Dept. Electromagnetic Systems
Building 348, DK-2800, Lyngby, Denmark

L. Duffrene
A2.2
Saint-Gobain Recherche
39 Quai Lucien Lefranc, BP 135, 93303 Aubervilliers Cedex, France

M.G. Dyndgaard
A3.1
Technical University of Denmark, Dept. Electromagnetic Systems
Building 348, DK-2800, Lyngby, Denmark

A.J. Faber
D4.1
TNO-TPD, Den Dolech 2, Building SL
PO Box 595, 5600 AN Eindhoven, The Netherlands

K. Fujiura
C4.4
NTT Optoelectronics Labs, Nippon Telegraph and Telephone Corp.
Tokai, Ibaraki 319-11, Japan

G. Ghosh
A1.3
Electrotechnical Laboratory, Femtosecond Technol. Res. Assoc.
1-1-4 Umezono, Tsukuba, Ibaraki 305, Japan

J. Heo
D3.3
Pohang University of Sci. & Technol., Dept. Materials Sci. & Eng.
San 31, Hyoja-dong, Nam-ku, Pohang, Kyungbuk 790-784, Korea

D.W. Hewak
various
University of Southampton, Optoelectronics Research Centre
Highfield, Southampton, SO17 1BJ, UK

E. Ishikawa
B3.1
Hoya Corporation, R&D Center
3-3-1 Musashino, Akishima-shi, Tokyo 196-8510, Japan

A. Jha
C2.1, C2.3, C2.4
University of Leeds, Dept. Materials
Clarendon Road, Leeds, LS2 9JT, UK

T. Kanamori
C5.1
NTT Optoelectronics Labs, Nippon Telegraph and Telephone Corp.
Tokai, Ibaraki 319-11, Japan

I. Kang
A3.1
Technical University of Denmark, Dept. Electromagnetic Systems
Building 348, DK-2800, Lyngby, Denmark

J. Kieffer
A2.2
University of Illinois, Dept. Materials Sci. & Eng.
1304 West Green Street, Urbana, IL 661801, USA

R.I. Laming
A5.1
University of Southampton, Optoelectronics Research Centre
Highfield, Southampton, SO17 1BJ, UK

W. Luethy
C5.2
University of Bern, Institute of Applied Physics
Sidlerstrasse 5, CH-3012 Bern, Switzerland

M.J. Matthewson
A4.4
Rutgers University, Ceramic & Materials Engineering
607 Taylor Road, Piscataway, NJ 08854-8065, USA

J. Minelly
A3.2
Corning Inc., Sullivan Park
Corning, New York 14381, USA

W. Miniscalco
C3.5
GTE Laboratories Inc.
40 Sylvan Road,Waltham, MA 02254, USA

N. Neuroth
B1.1
Schott Glaswerke
Postfach 2480, Hattenbergstrasse 10, D-55014 Mainz, Germany

J.L. Philipsen
A3.1
University of Southampton, Optoelectronics Research Centre
Highfield, Southampton, SO17 1BJ, UK

M. Poulain
C1.3, C4.1
Universite de Rennes 1 - Brittany, Laboratoire des Materiaux
Photoniques, Campus de Beaulieu, F-35042 Rennes, France

L. Reekie
A5.2
University of Southampton, Optoelectronics Research Centre
Highfield, Southampton, SO17 1BJ, UK

M. Saad
C4.2, C4.3
National Optics Institute
369 rue Franquet, Ste Foy, Quebec, G1P 4N8, Canada

S. Sakaguchi
A1.1, A1.2, B1.2, B4.2, B4.3
NTT Optoelectronics Labs, Nippon Telegraph and Telephone Corp.
Tokai, Ibaraki 319-11, Japan

T. Sakamoto
C3.4
NTT Optical Network Systems Laboratories
Y-805A, 1-1 Hikarinooka Yokosuka 239, Japan

B. Samson
D3.4
Corning Inc.
Sullivan Park, Corning, New York 14381, USA

J.S. Sanghera
D4.3
Naval Research Laboratory
4555 Overlook Ave. S.W., Washington DC 20375-5338, USA

T. Schweizer
D5.2
University of Southampton, Optoelectronics Research Centre
Highfield, Southampton, SO17 1BJ, UK

W. Seeber
B4.1
Friedrich-Schiller-University of Jena, Otto-Schott-Inst. Glass Chem.
Fraunhofferstrasse 6, D-07743 Jena, Germany

A. Soufiane
C4.2, C4.3
National Optics Institute
369 rue Franquet, Ste Foy, Quebec, G1P 4N8, Canada

H. Takebe
B1.3, D1.3
Kyushu University, Dept. Materials Science & Technology
Kasuga, Fukuoka 816, Japan

K. Tajima
A2.1
NTT Optoelectronics Labs, Nippon Telegraph and Telephone Corp.
Tokai, Ibaraki 319-11, Japan

S. Tanabe
B3.2, C3.2
Kyoto University, Faculty of Integrated Studies
Sakyo-ku, Kyoto 606-8501, Japan

H. Tawarayama
D5.1
Hoya Corporation, R&D Center
3-3-1 Musashino, Akishima-shi, Tokyo 196, Japan

S. Todoroki
A1.1, A1.2, B1.2, B4.2, B4.3
National Institute for Research, IMSTA
Nimiki 1-1, Tsukuba, Ibaraki 305-0044, Japan

M. Tomozawa
A2.3
Rensselaer Polytechnic Institute, Materials Sci. & Eng. Dept.
110 8th Street, Troy, New York 12180-3590, USA

P.W. Turner
A4.2
Corning Inc.
Sullivan Park, Corning, New York 14381, USA

U.B. Unrau
C3.3
TU Braunschweig, Institut fur Hochfrequenztechnik
Postfach 3329, D-38023 Braunschweig, Germany

J. Wang
D2.2
University of Southampton, Optoelectronics Research Centre
Highfield, Southampton, SO17 1BJ, UK

H.P. Weber
C5.2
University of Bern, Institute of Applied Physics
Sidlerstrasse 5, CH-3012 Bern, Switzerland

F. Wise
A3.1
Technical University of Denmark, Dept. Electromagnetic Systems
Building 348, DK-2800, Lyngby, Denmark

H. Yanagitav
B3.1
Hoya Corporation, R&D Center
3-3-1 Musashino, Akishima-shi, Tokyo 196-8510, Japan

K. Yoshida
A4.1
Furukawa Electric Co. Ltd., Yokohama R&D Laboratories
2-4-3 Okano, Nishi-ku, Yokohama 220-0073, Japan

M. Zervas
A5.1
University of Southampton, Optoelectronics Research Centre
Southampton, SO17 1BJ, UK

Abbreviations

AOM	acousto-optic amplitude modulator
APM	additive-pulse mode-locking
ASE	amplified spontaneous emission
BGO	Boling-Glass-Owyoung (formula)
CCD	charge-coupled device
CCR	critical cooling rate
CIP	cold isostatic pressing
CVD	chemical vapour deposition
CW	continuous wave
DCF	dispersion-compensating fibre
DFB	distributed feedback
DSC	differential scanning calorimetry
DSF	dispersion shifted fibre
DTA	differential thermal analysis
EDF	erbium-doped fibre
EDFA	erbium-doped fibre amplifier
EPR	electron paramagnetic resonance
ESA	excited-state absorption
EXAFS	extended X-ray absorption fine structure
FM	fibre modulator
FM	frequency modulated
FOM	figure of merit
FTIR	Fourier transform infrared
FWM	four-wave mixing
GLS	gallium lanthanum sulphide
GSA	ground state absorption
GVD	group velocity dispersion
HMF	heavy metal fluoride
HMFG	heavy metal fluoride glasses
IR	infrared
IS	isomer shift
JMA	Johnson-Mehl-Avrami (equation)
J-O	Judd-Ofelt (calculations)
K-K	Kramers-Kronig
MCVD	modified chemical vapour deposition
MFD	mode field diameter
MI	modulation instability
MIR	mid infrared
MOPA	master oscillator power amplifier

MSP	mechanically shaped preform
NA	numerical aperture
NALM	non-linear amplifying loop mirror
NBOHC	non-bridging oxygen hole centre
NF	noise figure
NIR	near infrared
NOLM	non-linear optical loop mirror
NPM	non-linear polarisation modulation
NR	non-radiative
NWM	network modifier
ODC	oxygen deficient centre
OLA	optical limiting amplifier
OVD	outside vapour deposition
P	preform method
PCVD	plasma chemical vapour deposition
PDFA	praseodymium-doped fibre amplifier
PL	population lens
POR	peroxy radicals
RAP	reactive atmosphere
RE	rare earth
RF	radio frequency
RH	relative humidity
SEM	scanning electron microscopy
SPM	self-phase modulation
T	transmission
TEM	transmission electron microscopy
THG	third harmonic generation
TL	thermal lens
TPA	two photon absorption
t-t-t	time-temperature-transformation
UV	ultraviolet
VAD	vapour-phase axial deposition
VAD	vertical axis deposition
WAT	weak absorption tail
WC	double-crucible method
WDM	wavelength-division- multiplexed/multiplexing
XPM	cross-phase modulation
ZMDW	zero material dispersion wavelength

Contents

Introduction: a History of Glass for Optical Fibres ix

Contributing Authors xiv

Abbreviations xviii

Part A. Silica

A1. Optical Properties 1
A1.1 Transmission of Silica Glass 3
A1.2 Intrinsic Scattering Losses of Silica Glass 8
A1.3 Refractive Index and Dispersion of Silica Glass 12
A1.4 Non-Linear Refractive Index of Silica Fibres 17
A2. Thermal and Mechanical Properties 23
A2.1 Viscosity of Silica Glass 25
A2.2 Elastic Moduli of Silica Glass 29
A2.3 Stability of Silica Glass 35
A3. Rare-Earth Spectroscopy 41
A3.1 Spectroscopy of Erbium-Doped Silica 43
A3.2 Spectroscopy of Neodymium-Doped Silica 48
A4. Optical Fibre Manufacture 53
A4.1 Preparation and Preform Fabrication of Silica Optical Fibres 55
A4.2 Drawing of Silica Optical Fibres 62
A4.3 Loss of Silica Optical Fibres 65
A4.4 Reliability of Silica Optical Fibres 69
A5. Applications 73
A5.1 Fibre Amplifiers Based on Rare Earth-Doped Silica 75
A5.2 Fibre Gratings in Silica Optical Fibre 80

Part B. Oxide Glass

B1. Optical Properties 85
B1.1 Transmission of Oxide Glass 87
B1.2 Intrinsic Scattering Losses of Oxide Glass 92
B1.3 Refractive Index and Dispersion of Oxide Glass 95
B1.4 Non-Linear Refractive Index of Oxide Glass 99

This page has been reformatted by Knovel to provide easier navigation.

B2. Thermal and Mechanical Properties 105
B2.1 Mechanical Properties of Oxide Glass 107
B2.2 Viscosity of Oxide Glass 110
B2.3 Stability of Oxide Glass 114
B3. Rare-Earth Spectroscopy 117
B3.1 Spectroscopy of Neodymium-Doped Oxide Glass 119
B3.2 Spectroscopy of Erbium-Doped Oxide Glass 126
B4. Optical Fibre Manufacture 131
B4.1 Preparation and Melting of Oxide Glass 133
B4.2 Drawing of Oxide Glass Optical Fibres 138
B4.3 Loss of Oxide Glass Optical Fibres 142
B5. Selected Applications 147
B5.1 Fibre Lasers Based on Rare Earth-Doped Oxide Glass 149
B5.2 Optical Fibre Amplifier Based on Rare Earth-Doped Oxide Glass 156

Part C. Halide Glass

C1. Optical Properties 159
C1.1 Transmission of Halide Glass 161
C1.2 Intrinsic Scattering Losses of Halide Glass 170
C1.3 Refractive Index and Dispersion of Halide Glass 176
C1.4 Non-Linear Refractive Index of Halide Glass 180
C2. Thermal and Mechanical Properties 187
C2.1 Characteristic Temperatures of Halide Glass 189
C2.2 Viscosity of Halide Glass 194
C2.3 Elastic Moduli of Halide Glass 202
C2.4 Stability of Halide Glass 206
C3. Rare-Earth Spectroscopy 211
C3.1 Spectroscopy of Praseodymium-Doped Fluoride Glass 213
C3.2 Spectroscopy of Erbium-Doped Halide Glass 218
C3.3 Spectroscopy of Holmium-Doped Halide Glass 224
C3.4 Spectroscopy of Thulium-Doped Halide Glass 236
C3.5 Spectroscopy of Neodymium-Doped Halide Glass 241
C4. Optical Fibre Manufacture 247
C4.1 Preparation and Melting of Halide Glass 249
C4.2 Drawing of Halide Glass Optical Fibres 253
C4.3 Loss of Halide Glass Optical Fibres 260
C4.4 Reliability of Halide Glass Optical Fibres 265
C5. Selected Applications 269
C5.1 Optical Amplifiers Based on Rare Earth-Doped Halide Glass 271
C5.2 Fibre Lasers Based on Rare Earth-Doped Halide Glass 275

This page has been reformatted by Knovel to provide easier navigation.

Part D. Chalcogenide Glass

D1. Optical Properties 281
D1.1 Transmission of Chalcogenide Glass 283
D1.2 Intrinsic Scattering in Chalcogenide Glass 289
D1.3 Refractive Index and Dispersion of Chalcogenide Glass 294
D1.4 Non-Linear Refractive Index of Chalcogenide Glass 298
D2. Thermal and Mechanical Properties 303
D2.1 Characteristic Temperatures of Chalcogenide Glass 305
D2.2 Viscosity of Chalcogenide Glass 309
D3. Rare-Earth Spectroscopy 313
D3.1 Spectroscopy of Praseodymium-Doped Chalcogenide Glass 315
D3.2 Spectroscopy of Neodymium-Doped Chalcogenide Glass 320
D3.3 Spectroscopy of Thulium/Holmium-Doped Chalcogenide Glass 326
D3.4 Spectroscopy of Dysprosium-Doped Chalcogenide Glass 330
D4. Optical Fibre Manufacture 335
D4.1 Preparation and Melting of Chalcogenide Glass 337
D4.2 Purification of Chalcogenide Glass 340
D4.3 Drawing of Chalcogenide Glass Optical Fibres 344
D4.4 Loss of Chalcogenide Glass Optical Fibres 348
D5. Selected Applications 353
D5.1 Fibre Amplifiers Based on Rare Earth-Doped Chalcogenide Glass 355
D5.2 Fibre Lasers Based on Rare Earth-Doped Chalcogenide Glass 358
D5.3 Optical Switches Based on Chalcogenide Glass 362

Index **367**

This page has been reformatted by Knovel to provide easier navigation.

PART A: SILICA

CHAPTER A1

OPTICAL PROPERTIES

A1.1 Transmission of silica glass
A1.2 Intrinsic scattering losses of silica glass
A1.3 Refractive index and dispersion of silica glass
A1.4 Non-linear refractive index of silica fibres

A1.1 Transmission of silica glass

S. Sakaguchi and S. Todoroki

June 1997

A INTRODUCTION

Silica glass is the only material whose ultimate optical loss is realised in optical fibre fabricated using an elaborate technique based on a vapour-phase reaction [1]. The optical absorption of silica glass has been extensively investigated over a wide range of wavelengths [2]. Although transition metal and OH impurity absorption bands have been virtually eliminated from the fibres, bands related to gaseous species and defects are apparent in recent applications such as fibre Bragg grating devices and UV lithography [3,4]. On the other hand, the Kramers-Kronig (K-K) analysis, which is used to examine the absorption properties through a complex index N (where $N = n - ik$, n is the refractive index and k is the extinction coefficient), has been shown to be useful for investigating glass structure [5]. K-K analysis is also used for describing the IR absorption tail determining theoretical loss in fibres [6]. This Datareview provides a brief overview of optical absorption of silica glass.

B FUNDAMENTAL (UV/IR) ABSORPTION

The fundamental optical absorption bands in silica glass appear in a UV region of 0.1 μm (10 eV) due to electronic transitions and in an IR region of 10 μm (0.1 eV) due to molecular vibrations in $[SiO_4]$ tetrahedral molecules [7]. The absorption diminishes in the region between these UV and IR regions. Additional bands appear in this transparent region. Absorption due to defect centres and the Urbach tail [8] appears in the UV-visible region, while impurity absorption due to transition metal and OH ions appears in a region from UV to IR.

The UV absorption peaks are located at 10.2, 11.7, 14.3 and 17.2 eV and are understood as electronic transitions from various valence bands to conduction bands of O_{2p} electrons. The 10.2 eV peak is the strongest and has an absorption coefficient α with a magnitude of the order of 10^6 cm^{-1} based on K-K analysis, in which α is given by $\alpha = 4\pi k/\lambda$ (where λ is the wavelength) [9].

The IR absorption peaks appear at 9.1, 12.5 and 21 μm and are assigned to molecular vibrations as asymmetric bond stretching vibration (ν_3), symmetric bond stretching vibration ($\nu_1 = 2\nu_4$) and bond bending vibration (ν_4), respectively [10]. The 9.1 μm (1100 cm^{-1}) peak is the main one and its α value has a magnitude of the order of 10^4 cm^{-1} [11]. Overtone and combination modes appear in the shorter wavelength region, as summarised in TABLE 1. They form an IR absorption tail together with the fundamental modes. This tail is measured for silica specimens with various lengths in the 3 - 6 μm region [12].

TABLE 1 Peak positions and intensities of IR absorption bands in silica glass [11].

Wavelength (μm)	Intensity (dB/km)	Identification
21.3	5×10^9	ν_4
12.5	2×10^9	ν_1
9.1	1×10^{10}	ν_3
6.2	8×10^7	$2\nu_1$, $\nu_3 + \nu_4$
5.3	1×10^8	$\nu_1 + \nu_3$, $\nu_2 + \nu_3 + \nu_4$, $2\nu_1 + \nu_2$
5.1	6×10^7	$3\nu_2 + \nu_3$, $\nu_1 + \nu_2 + 2\nu_4$
4.5	4×10^6	$2\nu_3$, $\nu_1 + \nu_2 + \nu_3$
4.2	1×10^6	$3\nu_1$, $\nu_1 + \nu_3 + \nu_4$
3.8	6×10^5	$2\nu_3 + \nu_4$, $2\nu_1 + 2\nu_4$
3.2	6×10^4	$4\nu_1$, $2\nu_3 + 2\nu_4$, $2\nu_1 + \nu_3 + \nu_4$
3.0	5×10^4	$3\nu_3$, $\nu_1 + \nu_2 + 2\nu_3$

FIGURE 1 shows the absorption properties of silica glass [2] and a pure silica fibre [1,13]. Model absorption curves derived by K-K analysis are also shown, assuming that the curves are given by an empirical form [6]. These curves can be calculated to reproduce the measured refractive index, using the K-K relation [6], as

$$n(\nu_i) = 1 + \frac{1}{\pi}\int_0^\infty \frac{\nu k(\nu)}{\nu^2 - \nu_i^2} d\nu = 1 + \frac{1}{2\pi^2}\int_0^\infty \frac{\alpha(\nu)}{\nu^2 - \nu_i^2} d\nu \quad (1)$$

$$k(\nu_i) = \frac{2\nu_i}{\pi}\int_0^\infty \frac{n(\nu)}{\nu_i^2 - \nu^2} d\nu \quad (2)$$

where ν is the wavenumber $1/\lambda$, giving $\alpha = 4\pi\nu k$. This method is useful for determining the IR absorption tail, because it avoids the effects of OH impurities.

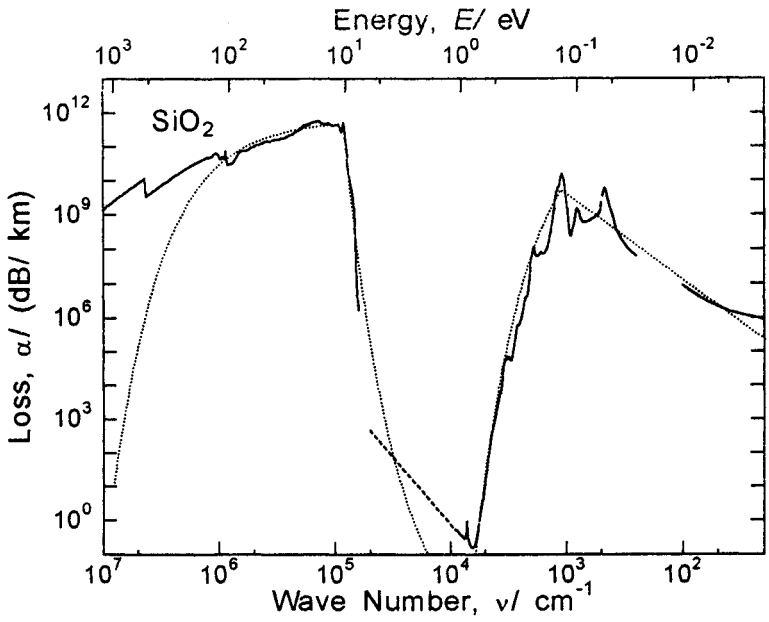


FIGURE 1 Absorption spectra of silica glass. Dotted curves: model absorption spectra calculated to reproduce the measured refractive index curve [6]; solid curves: measured absorption spectra [2]; broken line: Rayleigh scattering and loss spectrum of a low loss pure silica core single-mode fibre [1].

C ABSORPTION DUE TO DEFECT CENTRES

Silica glass contains disordered bonding structures such as oxygen deficient centres (ODC) and peroxy linkages. They can be turned into electronic defects by irradiation by high energy photons and particles such as γ rays and neutrons [14]. Typical defects are Si-E′ centres (electron trapped Si), non-bridging oxygen hole centres (NBOHC, hole trapped non-bridging O) and peroxy radicals (POR) [15]. Absorption bands which appear at 7.6, 5.8, 5.0 and 4.8 eV are correlated to the defects [16], as summarised in TABLE 2.

TABLE 2 Correlation between absorption bands and defects in silica glass [16,4].

Absorption band (eV)	Defect	Remark
7.6	ODC	≡Si-Si≡[1]
5.8	E′ centre	≡Si•[2]
5.0	Unrelaxed ODC	≡Si...Si≡
	E′ centre	≡Si•
	Silicon lone pair centre	≡Si:
4.8	NBOHC	≡Si-O•
	POR	≡Si-O-O•
	Ozone molecule	O_3
3.8	Peroxy linkage	≡Si-O-O-Si≡
2.0	NBOHC	≡Si-O•
	POR	≡Si-O-O•
	Ozone molecule	O_3

[1] ≡ represents bonding to 3 oxygen atoms; [2] • denotes unpaired electron.

Defects are formed in silica fibres during drawing, in which disordered structures initiated at high temperatures above 2000°C are quenched in the fibres at extreme rates of above 10^3 °C/s [17]. A drawing induced band appears at 2.0 eV (0.62 μm) in high purity silica fibres. Although this band is correlated to NBOHC [18], it has also been suggested that it is related to ODC or O_3 [4,19].

Defects initiated by irradiation with excimer lasers such as KrF (248 nm) and ArF (193 nm) lasers induce bands in the UV region. The photo-induced bands have a substantial effect on silica glass used as lens and photomask for UV lithography. The laser irradiation increases the E′ and NBOHC concentrations and such increases are correlated to bands of 7.6 and 5.8 eV [4]. The induced band tends to be small in silica glass with high OH content [20].

Fibre Bragg grating devices are attracting increasing attention because they offer a variety of light manipulating functions based on Bragg reflection [3]. The Bragg grating is written in Ge:SiO_2 fibres by modulated laser irradiation. This irradiation causes a refractive index increase and the modulated index profile forms the grating. The index increase is understood to result from the increased absorption due to the increase in defects such as Ge-E′ through the K-K relation, the formation of electric dipoles at defects through the Pockels effect, and the increased density of glass through the Lorentz-Lorentz law [21-23]. Photo-induced Ge-E′, which exhibits an absorption band at 5 eV similar to that of Si-E′, dominates the index increase. The index increase in Ge:SiO_2 fibres is enhanced to 10^{-3} by H_2 loading, compared with 10^{-4} for unloaded fibres [24].

D ABSORPTION DUE TO IMPURITIES

Common impurities in silica glass are transition metal ions such as Fe, Co, V, Cu and Cr and OH groups. Absorption bands due to these ions appear over a wide range from UV to near IR because of the complex transition process of 3d electrons, and the bands depend on their valence states in glass [25]. Although the amount of each transition metal impurity must be reduced to a few ppb, these impurities are completely removed from the fibres based on the difference between the vapour pressures of $SiCl_4$ and impurity chlorides.

OH groups in silica glass induce fundamental absorption at 2.7 μm. The OH groups exist in silica as isolated (free) and hydrogen bonded states. The isolated OH induces a sharp peak at 3672 cm^{-1} and the hydrogen bonded OH induces a broad peak at 3608 cm^{-1}. Absorption due to water molecules appears at 1611 cm^{-1} [26,27]. The typical OH induced losses in the fibres appear at 1.38, 1.24 and 0.95 μm due to the overtone and combination modes of isolated Si-OH. The 1.38 μm loss is the most intense and its absorbance corresponds to 60 dB/(km ppm) as summarised in TABLE 3 [28]. OH groups in the fibres are removed by dehydration in a Cl_2 atmosphere.

TABLE 3 Peak positions and intensities of OH absorption bands in silica glass [28].

Wavelength (μm)	Intensity (dB/km ppm)	Identification
2.72	10000	ν_3
2.21	201	$\nu_3 + \nu_1$
1.38	62.7	$2\nu_3$
1.25	2.7	$2\nu_3 + \nu_1$
1.14	0.07	$2\nu_3 + 2\nu_1$
0.94	1.6	$3\nu_3$
0.88	0.08	$3\nu_3 + \nu_1$
0.72	0.08	$4\nu_3$

E ABSORPTION DUE TO DISSOLVED GASEOUS SPECIES

Absorption due to gaseous species such as O_2 and Cl_2 has been apparent in recent high purity silica glass. The dissolved O_2 exhibits absorption in the UV region above 7.5 eV [4]. O_2 is turned into O_3 by ArF laser irradiation and the initiation of O_3 is correlated to the 4.8 and 2.0 eV bands. Absorption due to Cl_2 appears at 3.8 eV [4].

Dissolved H_2 molecules have special importance in relation to the optical absorption of the fibre. H_2 loading is a key technique for fabricating fibre Bragg grating devices as noted above. The dissolved H_2 caused serious problems in terms of the long-term reliability of fibre cables installed for commercial use more than a decade ago [29]. The H_2 induced loss in Ge:SiO_2 fibre appears over a wide region of 1 - 2 μm [30]. When the dissolved H_2 molecules react with the glass network over a long period of time or by heating, they form Ge-OH and Si-OH, resulting in OH loss increase. Ge- and Si- E′ centres are suggested as the reaction sites. When SiH is present, it induces absorption at 1.53 μm in the fibre [31].

F CONCLUSION

The application of silica glass in the optoelectronics field in recent decades has demanded a further understanding of its absorption properties. K-K analysis is useful for understanding not only glass structure but also the IR absorption tail which is needed for attempts to realise further reduction in

optical loss in the fibres. Absorption bands induced by defect centres and dissolved gaseous species are utilised in forming fibre Bragg grating devices and in managing photo-induced bands in UV lithography. Further investigation into fabrication methods must be undertaken to expedite silica glass application.

REFERENCES

[1] H. Kanamori et al [*J. Lightwave Technol. (USA)* vol.LT-4 (1986) p.1144-9]

[2] H.R. Philipp [*Handbook of Optical Constants* Ed. E.D. Palik (Academic Press, Orlando, 1985) p.749-63]

[3] I. Bennion, J.A.R. Williams, L. Zhang, K. Sugden, N.J. Doran [*Opt. Quantum Electron. (UK)* vol.28 (1996) p.93-135]

[4] K. Awazu, H. Kawazoe [*J. Non-Cryst. Solids (Netherlands)* vol.179 (1994) p.214-25]

[5] A.M. Efimov [*Optical Constants of Inorganic Glasses* (CRC Press, New York, 1995)]

[6] S. Todoroki, S. Sakaguchi [*J. Non-Cryst. Solids (Netherlands)* to be published]

[7] G.H. Sigel Jr. [in *Optical Absorption of Glasses, Treatise on Materials Science and Technology* vol.12, Eds. M. Tomozawa, R.H. Doremus (Academic Press, New York, 1977) p.5-89]

[8] F. Urbach [*Phys. Rev. (USA)* vol.92 (1953) p.1324]

[9] D.L. Griscom [*J. Non-Cryst. Solids (Netherlands)* vol.24 (1977) p.155-234]

[10] W. Wadia, L.S. Balloomal [*Phys. Chem. Glasses (UK)* vol.9 (1968) p.115-24]

[11] H.R. Philipp [*J. Appl. Phys. (USA)* vol.50 (1979) p.1053-7]

[12] T. Izawa, N. Shibata, A. Takeda [*Appl. Phys. Lett. (USA)* vol.31 (1977) p.35-7]

[13] S. Sakaguchi, S. Todoroki, T. Murata [*J. Non-Cryst. Solids (Netherlands)* vol.220 (1997) p.178-86]

[14] E.J. Friebele, D.L. Griscom [in *Radiation Effects in Glass, Treatise on Materials Science and Technology* vol.17, Eds. M. Tomozawa, R.H. Doremus (Academic Press, New York, 1979) p.257-351]

[15] R.A. Weeks [*J. Non-Cryst. Solids (Netherlands)* vol.179 (1994) p.1-9]

[16] D.L. Griscom [*J. Ceram. Soc. Jpn. (Japan)* vol.99 (1991) p.923-42]

[17] H. Hanafusa, Y. Hibino, F. Yamamoto [*Phys. Rev. B (USA)* vol.35 (1987) p.7646-51]

[18] L. Skuja [*J. Non-Cryst. Solids (Netherlands)* vol.179 (1994) p.51-69]

[19] G.R. Atkins et al [*J. Lightwave Technol. (USA)* vol.11 (1993) p.1793-801]

[20] D.R. Sempolinski, T.P. Seward, C. Smith, N. Borrelli, C. Rosplock [*J. Non-Cryst. Solids (Netherlands)* vol.203 (1996) p.69-77]

[21] L. Dong, J.L. Archambault, L. Reekie, P.St.J. Russell, D.N. Payne [*Appl. Opt. (USA)* vol.34 (1995) p.3436-40]

[22] J.P. Bernardin, N.M. Lawandy [*Opt. Commun. (Netherlands)* vol.79 (1990) p.194-9]

[23] B. Poumellec, P. Niay, M. Douay, J.F. Bayon [*J. Phys. D (UK)* vol.29 (1996) p.1842-56]

[24] P.J. Lemaire, R.M. Atkins, V. Mizrahi, W.A. Reed [*Electron. Lett. (UK)* vol.29 (1993) p.1191-3]

[25] P.C. Schultz [*J. Am. Ceram. Soc. (USA)* vol.57 (1974) p.309-13]

[26] M.L. Hair [*J. Non-Cryst. Solids (Netherlands)* vol.19 (1975) p.299-309]

[27] K.M. Davis, M. Tomozawa [*J. Non-Cryst. Solids (Netherlands)* vol.201 (1996) p.177-98]

[28] O. Humbach, H. Fabian, U. Grzesik, U. Haken, W. Heitmann [*J. Non-Cryst. Solids (Netherlands)* vol.203 (1996) p.19-26]

[29] N. Uchida, N. Uesugi [*J. Lightwave Technol. (USA)* vol.LT-4 (1986) p.1132-8]

[30] K. Noguchi, Y. Murakami, N. Uesugi, K. Ishihara [*Electron. Lett. (UK)* vol.44 (1983) p.491-3]

[31] S. Sakaguchi, H. Itoh, F. Hanawa, T. Kimura [*Appl. Phys. Lett. (USA)* vol.47 (1985) p.344-6]

A1.2 Intrinsic scattering losses of silica glass

S. Sakaguchi and S. Todoroki

June 1997

A INTRODUCTION

Intrinsic scattering loss, which determines transmission loss of optical fibres along with the infrared absorption tail, is composed of Rayleigh, Raman and Brillouin components, and the Rayleigh scattering is dominant. The slope of the transmission loss versus λ^{-4} plot, where λ is the wavelength, is accepted as the Rayleigh scattering loss α_R of the fibres [1]. Although the α_R value depends on the fabrication process, an α_R value of around 0.76 (dB/km) μm^4 is obtained with good reproducibility for pure silica core fibres [2,3]. By contrast, various magnitudes of scattering intensity have been measured for bulk silica glass [4,5]. Recent investigations confirm that the Rayleigh scattering intensity varies in proportion to the fictive temperature (T_f) of the glass specimen [6-8]. This Datareview offers a brief overview of scattering loss in silica glass and fibres.

B MEASUREMENT

The intrinsic scattering loss in glass materials, composed of Rayleigh, Raman and Brillouin components, exhibits a λ^{-4} dependence and the Rayleigh scattering contributes more than 85% [9]. Rayleigh scattering is induced by local structural fluctuations such as density and concentration fluctuations. The scattering due to density fluctuations occurs in a single component glass such as silica. Raman and Brillouin scattering losses are induced by the interaction between the incident light and optical and acoustic phonons, respectively.

The scattering intensity in bulk silica glass is measured from two standpoints: scattering by small particles [4,10,11] and scattering by thermodynamic fluctuations [5,11,12].

Scattering by small particles is formulated as the Rayleigh-Gans theory for small particles (relative to wavelength) and the Mie theory for large particles [10,11]. The Rayleigh scattering intensity is evaluated using the Rayleigh ratio R, and the scattering loss is given as $\alpha = 7.3\ R_{90}$ dB/km, where R_{90} is the scattered light intensity at a right angle in a unit of $\times 10^{-6}$ cm^{-1} [4]. The scattered light in this measurement generally includes Raman and Brillouin components.

When scattering is considered in terms of the local fluctuation of the electric susceptibility, the Rayleigh ratio is evaluated using the temperature correlation of thermodynamic parameters such as density, entropy and pressure [11,12]. Since these parameters have a time-dependent nature, the scattered light has spectral components of Brillouin doublets. The scattering is described with the Landau-Placzek ratio, R_{LP} ($\equiv I_C/2I_B$, where I_C is the central Rayleigh intensity and I_B is the Brillouin intensity). The Rayleigh scattering loss can be derived from the Rayleigh-Brillouin spectrum through R_{LP} and the Brillouin scattering loss [5].

Raman scattering is usually used, along with infrared absorption, for examining glass structure. Although the Raman scattering loss has been evaluated theoretically [9], there seems to be no effective experimental method for determining the absolute intensity.

The intrinsic scattering loss in optical fibres appears as the slope of the loss versus λ^{-4} plot. This λ^{-4}-dependent loss is generally accepted as the Rayleigh scattering loss for optical fibres [1], although it also includes the Raman and Brillouin scattering losses. α_R derived by this plot has practical meaning as an inherent measure for determining the loss property of the fibres. Additional scattering loss may arise depending on the fabrication conditions. Such loss is generally λ-independent and is induced by an imperfection at the core/cladding interface, microbending or residual stress [1].

When the input power to silica fibres becomes large, stimulated Raman and Brillouin scattering phenomena are induced due to the non-linear effect. The former phenomenon is used for Raman amplification in the 1.3 μm band, while the latter limits the input power to the fibres (see [13]).

In addition, the Rayleigh scattering intensity of fibre preform glasses can be changed by heat treatment. The scattering intensity of reheated preform glass increases to 5 - 10% higher than that of annealed preform glass [16].

A theoretical evaluation of the scattering loss in alkali-doped silica glasses suggests that the intensity can be reduced for elements such as Na, K and Rb when the concentration is very small, that is less than 2 mol % [17]. The scattering loss for these alkali-doped silica glasses can be reduced to up to 20% lower than that of pure silica. In addition, when F is co-doped with alkali, the alkali concentration extends further [18]. Similarly, it has been shown that the scattering of Na-implanted silica decreases even though the concentration is 10 ppm [19].

C BULK SILICA GLASS

Various magnitudes of Rayleigh scattering loss were reported for pure silica glasses in the early 1970s and they range from 0.3 to 0.8 (dB/km) μm^4 [4,5]. This variation seems to be a result of the uncontrolled quality of the silica specimen itself. An investigation has shown that the scattering intensity obtained from recent silica glass varies depending on the fabrication method and that such dependence can be related to the glass transition temperature of the specimen [7].

This temperature dependence of Rayleigh scattering in silica glass has been examined in relation to T_f. The result, based on R_{LP} measurements, reveals a linear relationship between α_R and T_f, by which α_R increases from 0.5 to 0.9 (dB/km) μm^4 for a T_f range of 830 to 1230°C [6]. This linear relation is confirmed by a measurement of the scattered light intensity for silica samples whose T_f is changed by heat treatment, in which the relative intensity increases proportionally with increasing T_f [8]. Since the glass structure is solidified at T_f, equilibrium structural fluctuation at temperatures just above T_f is frozen. Structural fluctuations such as density fluctuations depend on T_f. Although the refractive index and the isothermal compressibility, which affect the Rayleigh scattering, also change with T_f, their effects are small [6,8]. Thus, the Rayleigh scattering primarily exhibits a proportional dependence on T_f. Therefore, the variation in scattering intensity can be understood as the effect of T_f which is a resultant temperature of thermal history. Scattering loss values obtained from silica glass and silica fibres are summarised in TABLE 1.

On the other hand, T_f values of around 1600°C are obtained from pure silica core single-mode and multi-mode fibres [21]. If the linear T_f - α_R relation is valid for this temperature range, this suggests that a further reduction may be expected in the transmission loss in silica fibres by reducing the T_f of the fibres.

TABLE 1 Scattering loss in silica glass and silica fibres.

Sample	Scattering loss (dB/km) μm^4 or relative value	Measurement*	Ref
Silica fibres			
pure silica	0.76	s	[2,3]
doped silica P:SiO_2	0.66	s	[3]
Ge, F:SiO_2	1.5 ~ 4.0	s	[15]
Silica glass			
pure silica	0.3 ~ 0.8	ls, lp	[4,5]
heat treatment	0.5 ~ 0.9	lp	[6]
heat treatment	20% low	ls	[7,8,20]
alkali-doped (<2 mol%)	20% low	th	[17,18]
Na-implanted (10 ppmw)	13% low	ls	[19]

* s: the slope of the loss versus λ^{-4} plot; ls: total scattered light measurement; lp: R_{LP} measurement; th: theoretical estimation.

D CONCLUSION

A Rayleigh scattering coefficient of around 0.76 (dB/km) μm^4 is typical of current pure silica glass. For doped silica fibres other than P:SiO_2 fibre, α_R tends to increase with dopant concentration and becomes more sensitive to the drawing conditions. A recent investigation of the Rayleigh scattering loss in silica glass confirms that the scattering loss increases in proportion to T_f. This result suggests that a further reduction can be expected in the scattering loss of pure silica core fibres if T_f is reduced.

REFERENCES

[1] K. Inada [*Opt. Commun. (Netherlands)* vol.19 (1976) p.437-9]

[2] H. Kanamori et al [*J. Lightwave Technol. (USA)* vol.LT-4 (1986) p.1144-9]

[3] K. Tajima, M. Tateda, M. Ohashi [*Tech. Digest Opt. Fiber Commun.* vol.4, San Jose, California, 20-24 Feb. 1994 (Opt. Soc. America, Washington DC, USA, 1994) p.2-3]

[4] H.N. Daglish [*Glass Technol. (UK)* vol.11 (1970) p.30-5]

[5] J. Schroeder, R. Mohr, C.J. Montrose, P.B. Macedo [*J. Non-Cryst. Solids (Netherlands)* vol.13 (1973/74) p.313-20]

[6] I.V. Pevnitskii, V.Kh. Khalilov [*Sov. J. Glass Phys. Chem. (USA)* vol.15 (1989) p.246-50]

[7] S. Sakaguchi, S. Todoroki, S. Shibata [*J. Am. Ceram. Soc. (USA)* vol.79 (1996) p.2821-4]

[8] S. Todoroki, S. Sakaguchi [*J. Ceram. Soc. Jpn. (Japan)* vol.105 (1997) p.377-80]

[9] M.E. Lines [*J. Appl. Phys. (USA)* vol.55 (1984) p.4058-63]

[10] H.C. van de Hulst [*Light Scattering by Small Particles* (Dover, New York, 1981)]

[11] B. Chu [*Laser Light Scattering, 2nd edition* (Academic Press, New York, 1991)]

[12] J. Schroeder [in *Light Scattering of Glass, Treatise on Materials Science and Technology* vol.12, Eds. M. Tomozawa, R.H. Doremus (Academic Press, New York, 1977) p.158-222]

[13] G.P. Agrawal [*Nonlinear Fiber Optics, 2nd edition* (Academic Press, New York, 1995)]

[14] K. Tsujikawa, M. Ohashi, K. Shiraki, M. Tateda [*Electron. Lett. (UK)* vol.30 (1994) p.351-2]

[15] A.A. Abramov et al [*Tech. Digest Opt. Fiber Commun.* vol.4, San Jose, California, 20-24 Feb. 1994 (Opt. Soc. America, Washington DC, USA, 1994) p.1-2]

[16] K. Tsujikawa, M. Ohashi, K. Shiraki, M. Tateda [*Electron. Lett. (UK)* vol.31 (1995) p.1940-1]

[17] M.E. Lines [*J. Non-Cryst. Solids (Netherlands)* vol.171 (1994) p.209-18]

[18] M.E. Lines [*J. Non-Cryst. Solids (Netherlands)* vol.171 (1994) p.219-27]

[19] K. Saito, A.J. Ikushima, T. Ito, A. Itoh [*J. Appl. Phys. (USA)* vol.81 (1997) p.7129-34]
[20] S. Sakaguchi, S. Todoroki, T. Murata [*J. Non-Cryst. Solids (Netherlands)* to be published]
[21] S. Sakaguchi, S. Todoroki [*Tech. Digest, Int. Workshop Structure and Functional Optical Properties of Silica and Silica-Related Glasses* Shizuoka, Japan, 10-11 July 1997 (*Jpn. J. Appl. Phys. Suppl. (Japan)* suppl.37-1)]

A1.3 Refractive index and dispersion of silica glass

G. Ghosh

June 1997

A INTRODUCTION

The refractive index and its variation with wavelength, called dispersion, are the fundamental parameters of the optical materials including silica. Silica glasses have been used to make fibres for the optical communication network and optical imaging for the last three decades. The refractive indices of silica are measured at specific wavelengths lying within the transmission region, with sufficient accuracy. It is worthwhile to relate these measured refractive indices with a suitable empirical or mathematical expression having physical meaning and being more accurate than experiment. The evaluated optical constants of silica can be used to compute dispersion throughout the transmission region. A brief review of various relations between refractive indices and wavelengths is presented in Section B. The measured up-to-date data for refractive indices have been analysed in a physically meaningful model using the Sellmeier equation as described in Section C. The dispersion characteristic is computed from the UV to the near IR and is described in Section D. Section E presents the concluding remarks.

B SELLMEIER EQUATIONS

To relate the measured refractive indices with wavelength for fused silica, Malitson [1] used a three-pole Sellmeier equation. The same type of Sellmeier equation was also used by Matsuoka et al [2] for the wavelength dispersion of silica glass in the UV and visible region. Tatian [3] also used the same form of Sellmeier equation for several optical materials. Kitamura et al [4] represented the refractive indices of densified silica glass in a modified form of three-pole Sellmeier equation. Recently, the three-pole Sellmeier equations have been used in many optical glasses [5-7] including silica glass. The three-pole Sellmeier equation is of the following form:

$$n^2 = 1 + A\lambda^2/(\lambda^2 - B) + C\lambda^2/(\lambda^2 - D) + E\lambda^2/(\lambda^2 - F) \quad (1)$$

In this three-pole Sellmeier equation, two poles are lying in the VUV/UV region, whereas the remaining pole is lying in the IR region of the optical materials. However, in practice, it is very difficult to know precisely all the absorption peaks. Therefore, it is scientifically useful and physically acceptable to use an average electronic absorption bandgap and also an average lattice absorption bandgap. The two-pole Sellmeier equation [8] can be written as:

$$n^2 = A + B\lambda^2/(\lambda^2 - C) + D\lambda^2/(\lambda^2 - E) \quad (2)$$

where λ is the wavelength in μm. The first and second terms represent, respectively, the contributions to refractive indices due to higher-energy and lower-energy bandgaps of electronic absorption, and the last term accounts for the decrease in refractive indices due to lattice absorption. The optical constants A, B, C, D, E and F are called Sellmeier coefficients of the optical materials.

C DERIVATION OF THE SELLMEIER COEFFICIENTS

The refractive indices of silica have been measured in the UV, visible and near IR regions. The measurement accuracy is within five to six decimal places. At present, there are two-pole and three-pole Sellmeier equations for silica. However, the fitting accuracy should be the dominant consideration in choosing a dispersion formula having fewer optical parameters. Recently [9] I have analysed the refractive indices of the various optical materials including silica glass in the above two-pole Sellmeier equation (EQN (2)). This is the most accurate of the dispersion equations, and can fit index data to an accuracy consistent with the measurements and the accuracy needed for most optoelectronic applications.

The Sellmeier coefficients are evaluated by the least squares analysis. The normal approach is to first find the initial values of the parameters and then to add corrections by an iterative process so as to minimise the deviation between the measured and the computed values. The Sellmeier coefficients A, B, C and D are evaluated by taking beforehand a reasonably estimated value for E, the lattice absorption frequency. The choice of the value for E is not critical since the materials stop transmitting long before the lattice absorption frequency is reached. It is possible to estimate the average electronic absorption bandgap from the evaluated Sellmeier coefficient C by the following equation:

$$E_{ag} = 1.2398/\sqrt{C} \tag{3}$$

The room temperature values of refractive indices for silica are used to compute the Sellmeier coefficients A, B, C, D and E from different sources. These coefficients are shown in TABLE 1 along with the data sources. Some of these Sellmeier coefficients are already cited in [9].

It is worthwhile to compare the estimated values of the average electronic absorption bandgaps (11.8 ~ 11.9 eV) with the experimental values of 11.6 eV [2,11] and 11.8 eV [12]. Therefore, the present two-pole model Sellmeier equation not only expresses the refractive indices with sufficient accuracy but also provides us with the estimated value of the average electronic absorption bandgap. The refractive indices vary with change of ambient temperature. These variations in silica and other optical materials have been analysed satisfactorily for the first time in a physical model [9].

D DISPERSION OF REFRACTIVE INDICES

The group velocity dispersion (GVD) is an important parameter of the silica glass. It plays a vital role in optical fibre communication systems. Since the refractive indices are fitted using a physically meaningful Sellmeier equation, it is possible to satisfactorily calculate the GVD, $M(\lambda)$, from the Sellmeier equation using the following relation:

$$M(\lambda) = -\lambda/c\,[d^2n(\lambda)/d\lambda^2] \tag{4}$$

$$M(\lambda) = 1/(cn)[-4/\lambda^5\{BC^2/(1 - C/\lambda^2)^3 + DE^2/(1 - E/\lambda^2)^3\} + \lambda(dn/d\lambda)^2 + 3n(dn/d\lambda)] \tag{5}$$

where

$$dn/d\lambda = -1/(n\lambda^3)[BC/(1 - C/\lambda^2)^2 + DE/(1 - E/\lambda^2)^2] \tag{6}$$

and c is the speed of light.

TABLE 1 Sellmeier coefficients for silica at room temperature.

Temp (°C)	Sellmeier coefficients					Expt. accuracy (10^{-5})	Fit rms error (10^{-5})	Absorption bandgap E_{ag} (eV)	Ref for n
	A	B	C ($\times 10^{-2}$)	D	E				
20.0	1.30912262	0.79514557	1.09439467	0.92107106	100	± (0.5 - 2.0)	1.66	11.9	[1]
20.5	1.31138256	0.79429689	1.09514652	0.99952574	100	± 0.3	0.39	11.9	[2]
25.0	1.29553631	0.80985310	1.07945942	0.91714598	100	± 1.0	0.59	11.9	[4]
20.0	1.32581994	0.77858053	1.11311064	0.92659879	100	-	4.55	11.8	[6]
26.0	1.31563132	0.78910058	1.10325933	0.91298262	100	± (9.6 - 21)	9.35	11.8	[10]

The chromatic dispersion characteristics are computed throughout the transmission region of silica and are shown in FIGURE 1 from the optical constants cited in TABLE 1. The behaviour is not linear. The values of M(λ) are shown in TABLE 2 at the three optical windows, i.e. at 0.85, 1.33 and 1.55 μm.

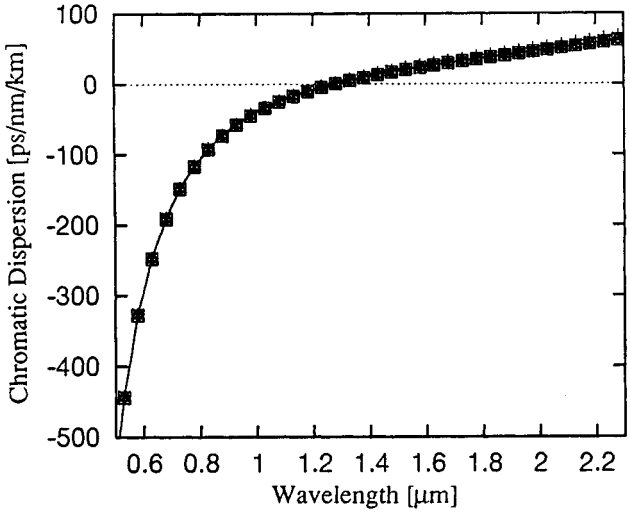


FIGURE 1 Dispersion behaviour of silica at room temperature from 0.5 to 2.3 μm.

TABLE 2 Chromatic dispersion and zero-dispersion wavelength of silica at room temperature.

Sellmeier	Abbé number	Chromatic dispersion (ps/nm/km) at			Zero-dispersion wavelength (μm)
		0.85 (μm)	1.33 (μm)	1.55 (μm)	
[1]	67.9813	-83.4100	5.6530	22.0900	1.2700
[2]	67.5492	-81.7321	8.3875	25.4154	1.2455
[4]	67.8694	-83.8650	5.4032	21.8461	1.2725
[6]	68.1185	-82.9667	5.9416	22.3860	1.2670
[10]	68.0049	-83.6540	5.3557	21.7358	1.2728
Average [except 2]	67.9935	-83.4739	5.5884	22.0145	1.2706

The zero-dispersion wavelengths are also evaluated and the average value is 1.2706 μm. Here, the material dispersion dominates over the waveguide dispersion of optical fibres made of silica glass. The values of refractive index are available only from 0.238 μm to 0.546 μm [2] in fused silica. Therefore, the extrapolated refractive indices gave a value of the zero-dispersion wavelength accurate to only one decimal point. The variation of the zero-dispersion wavelength with temperature is 0.025 nm/°C in silica. Interested readers may consult [9] for the temperature-dependent characteristics of refractive indices and dispersion of silica and other important optical materials.

E CONCLUSION

The up-to-date values of the refractive indices of silica have been fitted satisfactorily using a two-pole physically meaningful model of the Sellmeier equation. The estimated average electronic absorption bandgap has agreed well with the experimental value. The behaviour of chromatic dispersion has been analysed and it is confirmed here that the material dispersion of silica glass dominates over the waveguide dispersion of the optical fibre.

ACKNOWLEDGEMENT

A part of this work was supported by NEDO under the management of FESTA.

REFERENCES

[1] I.H. Malitson [*J. Opt. Soc. Am. (USA)* vol.55 (1965) p.1205-9]
[2] J. Matsuoka, N. Kitamura, S. Fujinaga, T. Kitaoka, H. Yamashita [*J. Non-Cryst. Solids (Netherlands)* vol.135 (1991) p.86-9]
[3] B. Tatian [*Appl. Opt. (USA)* vol.23 (1984) p.4477-85]
[4] N. Kitamura, Y. Toguchi, S. Funo, H. Yamashita, M. Kinoshita [*J. Non-Cryst. Solids (Netherlands)* vol.159 (1993) p.241-5]
[5] [*Schott Optical Glass Catalogue* (Schott Glass Technologies Inc., Duryea, PA, USA, 1992)]
[6] [*CVI Laser Corporation Catalogue* (CVI Laser Corp., Albuquerque, NM, USA, 1994-95) p.2.6-7]
[7] [*Ohara Optical Glass Catalogue* (OHARA Inc., Kanagawa, Japan, 1995)]
[8] G. Ghosh, M. Endo, T. Iwasaki [*J. Lightwave Technol. (USA)* vol.LT-12 (1994) p.1338-42]
[9] G. Ghosh [*Handbook of Thermo-Optic Coefficients of Optical Materials with Applications* (Academic Press, in press)]
[10] J.H. Wray, J.T. New [*J. Opt. Soc. Am. (USA)* vol.59 (1969) p.774-6]
[11] S. Hirota, T. Izumitani, R. Onaka [*J. Non-Cryst. Solids (Netherlands)* vol.72 (1985) p.39-50]
[12] K. Platzoder, W. Steinmann [*J. Opt. Soc. Am. (USA)* vol.58 (1968) p.588-9]

A1.4 Non-linear refractive index of silica fibres

G.P. Agrawal

April 1998

A INTRODUCTION

The use of silica fibres for transmitting information optically has become widespread in recent years. Since 1980, more than 50 million kilometres of fibre have been installed worldwide, and this number is growing each year. With the advent of optical amplifiers in 1990, the non-linear effects occurring inside silica fibres [1] have become extremely relevant since such effects can accumulate over thousands of kilometres [2]. This realisation has led to renewed efforts for measuring accurately the non-linear refractive index for different types of optical fibre [3-17]. This Datareview summarises the measured results with emphasis on the experimental techniques used.

An optical fibre consists of a thin central core (diameter ~10 μm) surrounded by a cladding layer whose refractive index is made slightly lower than that of the core. The refractive-index difference (<1%) between the core and the cladding is realised by the selective use of dopants during the fabrication process. Dopants such as GeO_2 and P_2O_5 increase the refractive index of pure silica (SiO_2) and are suitable for the core, while materials such as boron and fluorine are used for the cladding because they decrease the refractive index of silica. The core diameter determines the number of modes supported by the fibre at a given wavelength. Single-mode fibres are designed to support a single mode and have a microscopic core with a diameter <10 μm. Single-mode fibres are used almost exclusively for fibre-optic communications systems [2].

B NON-LINEAR REFRACTIVE INDEX

The dominant non-linear effects in optical fibres are governed by the third-order susceptibility $\chi^{(3)}$, a tensor quantity of rank four that is responsible for phenomena such as non-linear refraction, third-harmonic generation and four-wave mixing. Here we focus on non-linear refraction resulting from the intensity dependence of the refractive index that can be written as

$$n(\omega,I) = n_0(\omega) + n_2(\omega)I \qquad (1)$$

where $n_0(\omega)$ is the linear part of the refractive index at the frequency ω and I is the optical intensity. The parameter n_2 is called the non-linear refractive index and is related to one or more components of $\chi^{(3)}$. For a continuous-wave (CW) beam, linearly polarised along the x axis, n_2 can be written as [1]

$$n_2(\omega) = \frac{3}{8n_0}\chi^{(3)}_{xxxx}(\omega) \qquad (2)$$

Several different mechanisms contribute to n_2, the dominant one being the electronic contribution resulting from the anharmonic motion of atomic electrons under the influence of an applied optical field. Since electrons respond on a femtosecond time scale, the frequency dependence of electronic n_2 is relatively weak, changes occurring only over a wavelength scale of 100 nm or more. For example, the measurements of n_2 for bulk silica, made at the wavelength of 1.06 μm, yield a value $n_2 = 2.7 \times 10^{-20}$

m^2/W [18]. This value increases by 10 - 15% at wavelengths near 0.5 μm and decreases by about 5% for wavelengths near 1.5 μm.

When measuring n_2 for silica fibres, one must consider several important issues. First, as mentioned earlier, the core of silica fibres is doped with other materials such as GeO_2 and Al_2O_3. These dopants affect the measured value of n_2. Second, standard optical fibres do not maintain polarisation of light during its propagation. Since light polarisation changes randomly in such fibres, one measures an average value of n_2 that is reduced by a factor of 8/9 compared to the value expected for bulk samples that maintain the linear polarisation of the incident light [13,19].

The measured value of n_2 is also affected by the experimental technique used to measure it. The reason is that two other mechanisms, related to molecular motion (the Raman effect) and excitation of acoustic waves (electrostriction), also contribute to n_2. However, their relative contributions depend on whether the pulse width is longer or shorter than the response time associated with the corresponding non-linear process. The electrostrictive contribution vanishes for pulses shorter than 100 ps but attains its maximum value (about 16% of total n_2) for pulses longer than 10 ns [13]. In contrast, the Raman contribution does not vanish until pulses become shorter than 50 fs and is about 18% for pulses longer than 10 ps [20]. One should be careful when comparing measurements made by using different pulse widths. The largest value of n_2 is expected to occur for pulses longer than 10 ns (or for CW beams).

TABLE 1 Summary of n_2 measurements.

Technique	λ (μm)	Fibre type	n_2 (m^2/W)	Comments
SPM	1.319	silica core	2.36×10^{-20}	110 ps pulses, Nd:YAG laser, [7]
	1.319	DSF	2.62×10^{-20}	110 ps pulses, Nd:YAG laser, [7]
	1.548	DSF	2.31×10^{-20}	34 ps pulses, DFB laser, [8]
	1.550	DSF	2.50×10^{-20}	5 ps pulses, colour-centre laser, [12]
	1.550	standard	2.20×10^{-20}	CW DFB lasers ($\Delta\lambda \sim 0.4$ nm), [14]
	1.550	DSF	2.32×10^{-20}	CW DFB lasers ($\Delta\lambda \sim 0.4$ nm), [14]
	1.550	DCF	2.57×10^{-20}	CW DFB lasers ($\Delta\lambda \sim 0.4$ nm), [14]
XPM	1.550	silica core	2.48×10^{-20}	slow pump modulation, [9]
	1.550	standard	2.63×10^{-20}	slow pump modulation, [9]
	1.550	DSF	2.98×10^{-20}	slow pump modulation, [9]
	1.550	DCF	3.95×10^{-20}	slow pump modulation, [9]
	1.548	standard	2.73×10^{-20}	pump modulation at 10 MHz, [17]
	1.548	standard	2.23×10^{-20}	pump modulation at 2.3 GHz, [17]
FWM	1.555	DSF	2.25×10^{-20}	CW DFB lasers ($\Delta\lambda = 0.8$ nm), [6]
	1.553	DSF	2.64×10^{-20}	modulation instability, [11]

Several different non-linear effects have been used to measure n_2 for silica fibres; the list includes self-phase modulation (SPM), cross-phase modulation (XPM), four-wave mixing (FWM) and modulation instability (MI). In the following sections, several experimental techniques are discussed together with the measured n_2 values. TABLE 1 summarises the results obtained in recent experiments. The uncertainty is estimated to be about 5% for the n_2 values in TABLE 1.

C SELF-PHASE MODULATION

The SPM technique makes use of broadening of the pulse spectrum occurring because of the non-linear phase shift [1]

$$\phi_{NL} = \frac{2\pi n_2 L_{eff}}{\lambda A_{eff}} P \qquad (3)$$

acquired by the pulse during its propagation inside the fibre. Here $L_{eff} = [1 - \exp(-\alpha L)]/\alpha$ is the effective length for a fibre of length L, α accounts for the fibre loss, A_{eff} is the effective fibre-core area, and P is the optical power. The non-linear phase shift is time dependent for a pulse, resulting in a frequency chirp across the pulse. As a result, the pulse spectrum develops a multi-peak structure, and the number of peaks can be used to estimate n_2 [1]. This technique was first used in 1978 [3] and has been used extensively in recent years. The uncertainty in n_2 depends on how accurately one can estimate A_{eff} from the mode-field diameter and how well one can characterise input pulses.

In one set of measurements [7], mode-locked pulses of 110 ps duration, obtained from an Nd:YAG laser operating at 1.319 μm, were used. Uncertainty in the measurements was estimated to be about 5%. For a silica-core fibre (no dopants inside the core), the measured value of n_2 was 2.36×10^{-20} m^2/W. Before comparing it to the accepted value of 2.7×10^{-20} m^2/W for bulk silica [18], we must correct it by a factor of 9/8 to account for the random polarisation state inside optical fibre. The resulting value of 2.66×10^{-20} m^2/W is in excellent agreement with the measured bulk value of n_2 in silica glasses. The measured values of n_2 for several dispersion-shifted fibres (DSFs) were larger (average value 2.62×10^{-20} m^2/W) by 11% because of the dopant contribution.

The SPM technique has been used to measure n_2 in the wavelength region near 1.55 μm [8] that is used for optical communication systems because of relatively low losses of silica fibres occurring in that spectral region. A gain-switched, distributed feedback (DFB), semiconductor laser [21] provided 34 ps optical pulses whose spectral broadening inside silica fibres was used to measure n_2. Measurements were made over eight DSFs, resulting in an average value of 2.31×10^{-20} m^2/W with an uncertainty of about 5%. Although a smaller value is expected at longer wavelengths, the 12% difference between the measured n_2 values at 1.319 and 1.548 μm is much larger than that expected (<2%) on theoretical grounds [7].

In another SPM-based approach, the non-linear phase shift was measured in the time domain by using an all-fibre Sagnac interferometer [12]. Mode-locked pulses of about 5 ps width, obtained from a colour-centre laser operating near 1.55 μm, developed a multi-peak structure because of the SPM-induced phase shift given by EQN (3). The non-linear phase shift was estimated from autocorrelation traces and used to measure n_2. For several DSFs, the average value of n_2 was about 2.5×10^{-20} m^2/W with an uncertainty of 5%.

Perhaps the simplest SPM-based technique is the one used in [14]. It makes use of two CW DFB semiconductor lasers whose wavelength difference (0.3 - 0.5 nm) is stabilised by controlling the laser temperature. The optical signal entering the fibre oscillates sinusoidally at the beat frequency (~50 GHz). The optical spectrum at the fibre output exhibits peaks at multiples of this beat frequency because of the SPM-induced phase modulation (FM sidebands). The ratio of the peak heights depends only on the non-linear phase shift ϕ_{NL} of EQN (3), where P is now the average signal power and can be used to deduce n_2. For standard telecommunication fibres, the measured value was 2.2×10^{-20} m^2/W. The technique was used to measure n_2 for many DSFs and dispersion-compensating fibres (DCFs) having different amounts of dopant. The average values of n_2 for these two types of fibre are listed in TABLE 1.

C CROSS-PHASE MODULATION

In the XPM technique, two optical beams (called pump and probe) are launched simultaneously inside the test fibre. The total non-linear phase shift acquired by the probe beam is given by [1]

$$\phi_{NL} = \frac{2\pi n_2 L_{eff}}{\lambda A_{eff}} \left(P_{probe} + 2bP_{pump} \right) \qquad (4)$$

where the second term is due to XPM. The probe is typically weak enough that the SPM term can be neglected. The parameter b depends on the relative polarisation states of the pump and probe and takes its maximum value of 1 when the two beams remain linearly polarised along the same direction. If the fibre does not maintain polarisation, b = 2/3 when the polarisation state varies randomly [9].

Although the XPM technique was used in 1987 to measure n_2 for silica and fluorozirconate fibres [5], it was only in 1995 that systematic measurements of n_2 for many different kinds of fibre were reported [9]. In these measurements, both pump and probe signals were obtained from CW sources. When the pump light was modulated at a frequency of ~5 MHz, the probe signal developed FM sidebands because of the XPM-induced phase modulation. To ensure that the relative polarisation state of the pump and probe varied randomly, the pump light was depolarised before entering the fibre. The average values of n_2 for several kinds of fibre are listed in TABLE 1. Note that the measured n_2 values in this experiment are consistently larger than those obtained using the SPM-based techniques. The most likely explanation for this discrepancy is related to the electrostrictive contribution to n_2 that occurs for pulses longer than 1 ns (or modulation frequencies below 1 GHz). The 7.36 MHz modulation frequency for the pump beam is small enough that the measured values of n_2 include the full electrostrictive contribution. Thus, the values reported in [9] should be larger by about 16%. Indeed, this appears to be the case within the experimental uncertainty. The XPM technique has also been used to study the frequency dependence of the electrostrictive contribution by changing the pump-modulation frequency from 10 MHz to above 1 GHz [16,17].

E FOUR-WAVE MIXING

The FWM phenomenon [1] manifests itself through the appearance of spectral sidebands at the frequencies $2\omega_1 - \omega_2$ and $2\omega_2 - \omega_1$ when two pump beams at the frequencies ω_1 and ω_2 are launched simultaneously into the test fibre. The power contained in these two sidebands depends, among other things, on n_2, and its measurement can be used to deduce n_2. In a 1993 experiment [6], the CW output of two DFB lasers, operating near 1.55 μm with a wavelength separation of 0.8 nm, was amplified by using a fibre amplifier and then injected into a 12.5 km length of DSF. The powers in the FWM sidebands were fitted numerically and used to estimate a value of $n_2 = 2.25 \times 10^{-20}$ m^2/W for the test fibre. This value agrees with other measurements if we assume that electrostriction did not contribute to n_2, a reasonable assumption if we note that the laser line width was broadened to ~600 MHz through current modulation to avoid the onset of stimulated Brillouin scattering inside the test fibre.

The MI can be treated as a special case of FWM, the difference being that only a single pump beam is needed at the fibre input. Two spectral sidebands centred at the frequencies $\omega_0 \pm \Omega$ appear at the fibre output, where ω_0 is the pump frequency. The frequency shift Ω as well as the sideband amplitudes depend, among other things, on n_2 [1] and can be used to deduce n_2. In a 1995 experiment [11], a DFB laser operating at 1.553 μm was modulated externally to produce 25 ns pulses at a repetition rate of 4 MHz. Such pulses were amplified by using two cascaded fibre amplifiers and then launched into a 10.1 km section of DSF. The amplitude of MI sidebands was used to deduce a value of $n_2 = 2.64 \times 10^{-20}$ m^2/W for the test fibre. This value includes the electrostrictive contribution because of relatively long pump pulses used in the experiment. Indeed, if the 16% electrostrictive contribution is removed from the measured value, we recover $n_2 = 2.22 \times 10^{-20}$ m^2/W, a value close to other measurements in which the electrostrictive contribution was absent.

F CONCLUSION

The non-linear refractive index of silica fibres has been measured by using several different non-linear techniques. These measurements can differ by 15 - 20% depending on the concentration of dopants inside the fibre core and on the width of optical pulses (or modulation frequency) used during the experiment. The full electrostrictive contribution (about 15% of the total) is measured only for pulse widths larger than 10 ns (or modulation frequencies below 100 MHz). For standard silica glass fibres, $n_2 = 2.63 \times 10^{-20}$ m^2/W (within an experimental uncertainty of about 5%) but reduces to $n_2 = 2.21 \times 10^{-20}$ m^2/W if the 16% electrostrictive contribution is excluded during the measurement. For a DSF, these values increase by a few percent depending on the level of dopants.

REFERENCES

[1] G.P. Agrawal [*Nonlinear Fiber Optics* 2nd ed. (Academic Press, San Diego, 1995)]

[2] G.P. Agrawal [*Fiber-Optic Communication Systems* 2nd ed. (Wiley, New York, 1997)]

[3] R.H. Stolen, C. Lin [*Phys. Rev. A (USA)* vol.14 (1978) p.1448]

[4] W.L. Smith [in *CRC Handbook of Laser Science and Technology* vol.3, Ed. M.J. Weber (CRC, 1986) p.259-81]

[5] M. Monerie, Y. Durteste [*Electron. Lett. (UK)* vol.23 (1987) p.961]

[6] L. Prigent, J.P. Hamaide [*IEEE Photonics Technol. Lett. (USA)* vol.5 (1993) p.1092]

[7] K.S. Kim, R.H. Stolen, W.A. Reed, K.W. Quoi [*Opt. Lett. (USA)* vol.19 (1994) p.257]

[8] Y. Namihira, A. Miyata, N. Tanahashi [*Electron. Lett. (UK)* vol.30 (1994) p.1171]

[9] T. Kato, Y. Suetsugu, M. Takagi, E. Sasaoka, M. Nishimura [*Opt. Lett. (USA)* vol.20 (1995) p.988]

[10] T. Kato, Y. Suetsugu, M. Nishimura [*Opt. Lett. (USA)* vol.20 (1995) p.2279]

[11] M. Artiglia, E. Ciaramella, B. Sordo [*Electron. Lett. (UK)* vol.31 (1995) p.1012]

[12] M. Artiglia, R. Caponi, F. Cisternino, C. Naddeo, D. Roccato [*Opt. Fiber Technol. (USA)* vol.2 (1996) p.75]

[13] E.L. Buckland, R.W. Boyd [*Opt. Lett. (USA)* vol.21 (1996) p.1117]

[14] A. Boskovic, S.V. Chernikov, J.R. Taylor, L. Gruner-Nielsen, O.A. Levring [*Opt. Lett. (USA)* vol.21 (1996) p.1966]

[15] K. Li, Z. Xiong, G.D. Peng, P.L. Chu [*Opt. Commun. (Netherlands)* vol.136 (1997) p.223]

[16] E.L. Buckland, R.W. Boyd [*Opt. Lett. (USA)* vol.22 (1997) p.676]

[17] A. Fellegara, A. Melloni, M. Martinelli [*Opt. Lett. (USA)* vol.22 (1997) p.1615]

[18] D. Milam, M.J. Weber [*J. Appl. Phys. (USA)* vol.47 (1976) p.2497]

[19] P.K.A. Wai, C.R. Menyuk, H.H. Chen [*Opt. Lett. (USA)* vol.16 (1991) p.1735]

[20] R.H. Stolen, J.P. Gordon, W.J. Tomlinson, H.A. Haus [*J. Opt. Soc. Am. B (USA)* vol.6 (1989) p.1159]

[21] G.P. Agrawal, N.K. Dutta [*Semiconductor Lasers* 2nd ed. (Van Nostrand Reinhold, New York, 1993)]

PART A: SILICA

CHAPTER A2

THERMAL AND MECHANICAL PROPERTIES

A2.1 Viscosity of silica glass
A2.2 Elastic moduli of silica glass
A2.3 Stability of silica glass

A2.1 Viscosity of silica glass

K. Tajima

April 1998

A INTRODUCTION

The viscosity of silica glass is determined by the type and amount of dopant used in the glass. Fused silica glasses contain high levels of contamination which includes transition metal ions, OH ions and alkali metals. Such contamination is negligible in synthesised glasses. Almost all the glasses used for optical fibre are made with synthesised glasses by vaporisation processes.

Germanium or fluorine is frequently used to construct a waveguide in optical fibre. The addition of these dopants to silica glasses will reduce the viscosity of the glasses. In this Datareview, we focus on the viscosity characteristics of synthesised glasses with dopants of germanium and fluorine.

B VISCOSITY MEASUREMENT

A large quantity of viscosity data has been published, but there have been few reports on the high purity glass used for optical fibres. Silica glass for optical fibres is made by an oxidation or oxyhydration process using $SiCl_4$ as a starting material. We prepared glasses using the VAD technique [1]. We used germanium and fluorine as dopants and all our measurements were made on dehydrated glasses.

We measured viscosity using the elongation technique [2,3]. With this technique, first we prepared a glass rod. This glass rod was placed in a furnace and elongated at a high temperature of more than 1000°C. We measured the tension and temperature during the elongation process and then, once it was over, we measured the outer diameter of the elongated glass rod. We determined the viscosity from these data.

C VISCOSITY OF SILICA GLASSES

C1 Pure Silica Glasses

The measurement results are shown in FIGURE 1. We used a high quality sample with an OH and transition metal ion content of less than 1 ppbw.

In the temperature range 1600 to 2000°C, the viscosity is expressed as

$$\eta = 1.05 \times 10^{-10} \exp(E_0/RT) \qquad (1)$$

where $E_0 = 620.9$ kJ/mol is the activation energy and $R = 8.3145$ J/K/mol is the gas constant. Some viscosity data for other silica glasses are shown in FIGURE 1. These glasses are made with different processes and they contain different dopants. The activation energy of our result is a little higher than values reported by Hofmaier [4] and Bowen [5] and is close to that reported by Weiss [6]. The difference in viscosity energy is due to the dopant content of these glasses. We attribute the viscosity difference to the OH ions and/or aluminium.

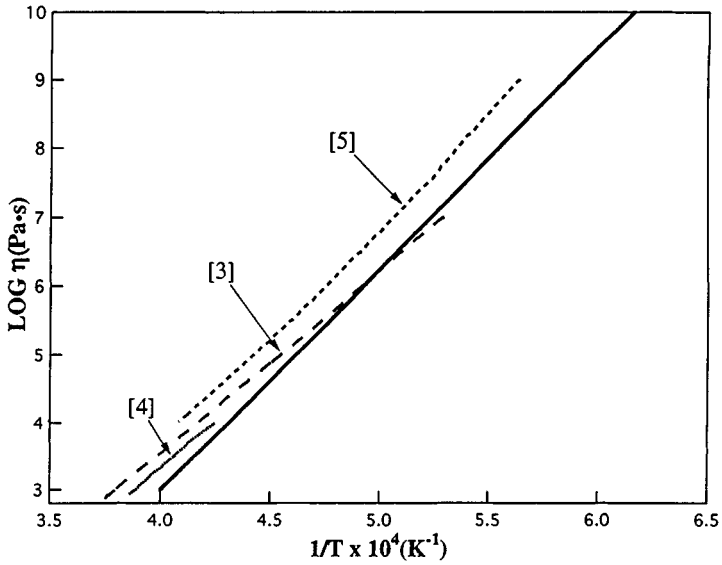


FIGURE 1 Temperature dependence of viscosity for silica glasses (identified by reference number). Solid line indicates silica glasses made by VAD technique.

C2 Germanium-Doped Silica Glasses

We fabricated germanium-doped silica glasses with OH ion content less than 1 ppbw. In general, the addition of germanium reduces the viscosity [7]. We used the relative index difference Δ to represent the dopant content. Δ is expressed as

$$\Delta = (n_1^2 - n_0^2)/2\, n_1^2 \tag{2}$$

where n_1 is a refractive index of germanium-doped silica and n_0 is that of pure silica glass.

The relationship between germanium content ρ mol % and Δ is approximated as follows:

$$\rho = 10\, \Delta \tag{3}$$

FIGURE 2 shows the temperature dependence of viscosity for germanium-doped silica glass with Δ equal to 0.48%. The viscosity of pure silica glass is also shown for comparison. The activation energy of the germanium-doped silica glass was the same as that of pure silica glass.

The dopant dependence of viscosity for germanium-doped silica glass is shown in FIGURE 3. The logarithm of viscosity is proportional to Δ up to a value of 1%. The relation between viscosity and Δ is

$$\eta = \eta_0\, 10^{-0.5\Delta} \tag{4}$$

where η_0 is the viscosity of pure silica glass.

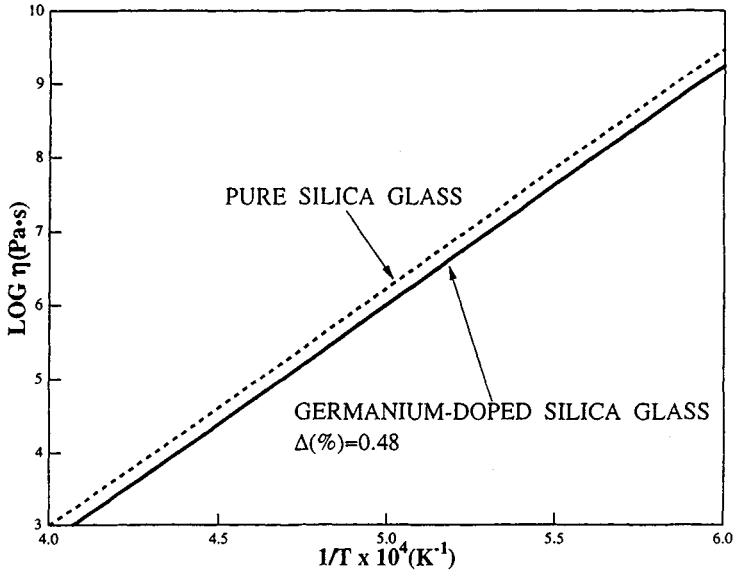


FIGURE 2 Temperature dependence of viscosity for germanium-doped silica glass.

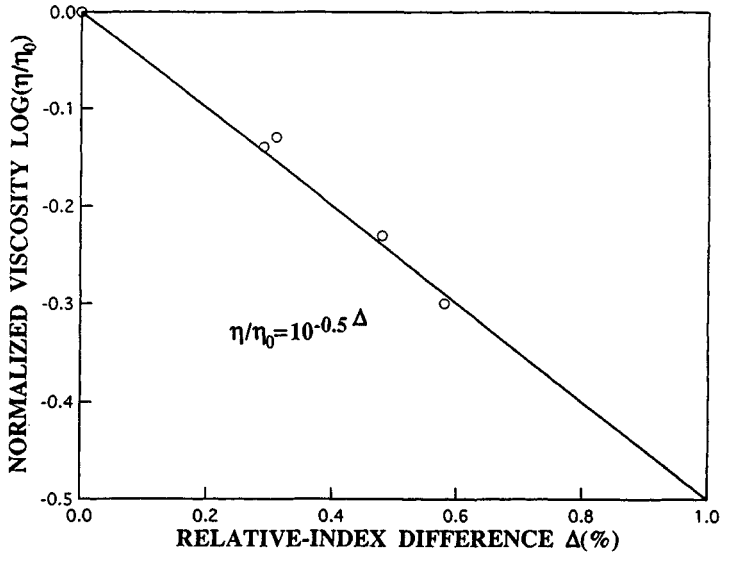


FIGURE 3 Relation between relative index difference and viscosity for germanium-doped silica glass.

C3 Fluorine-Doped Silica Glasses

The temperature dependence of viscosity for fluorine-doped silica glass [8] is shown in FIGURE 4.

The Δ value of the fluorine-doped silica glass was -0.32%. FIGURE 4 also shows the temperature dependence of viscosity of pure silica glass. The viscosity is expressed as

$$\eta = 5.76 \times 10^{-9} \exp(E_1/RT) \qquad (5)$$

where E_1 = 536.1 kJ/mol is the activation energy of the fluorine-doped glass. This value is smaller than that of pure silica glass. The viscosity difference between pure silica and fluorine-doped silica glass increases as the temperature decreases.

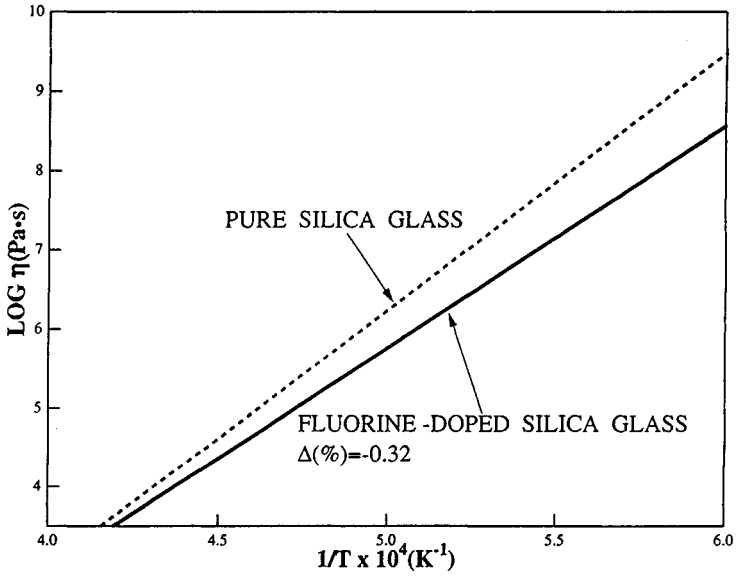


FIGURE 4 Temperature dependence of viscosity for fluorine-doped silica glass.

D CONCLUSION

We investigated the temperature dependence of viscosity for pure silica glass, germanium-doped silica glass and fluorine-doped silica glass. The addition of these dopants reduces the viscosity. The activation energy of germanium-doped silica glass is the same as that of pure silica glass. The activation energy of fluorine-doped silica glass is smaller than that of pure silica glass.

REFERENCES

[1] T. Izawa, S. Sudo, F. Hanawa [*Trans. Inst. Electron. Commun. Eng. Jpn. E, Engl. (Japan)* vol.62 (1979) p.779]
[2] U.C. Paek, R.B. Runk [*J. Appl. Phys. (USA)* vol.49 (1978) p.4417]
[3] U.C. Paek, C.M. Schroeder, C.R. Kurkjian [*Glass Technol. (UK)* vol.29 (1988) p.263]
[4] G. Hofmaier, G. Urbain [*Science of Ceramics* vol.4, Ed. G.H. Stewart (The British Ceramic Society, 1968) p.25]
[5] D.W. Bowen, R.W. Taylor [*Am. Ceram. Soc. Bull. (USA)* vol.57 (1978) p.818]
[6] W. Weiss [*J. Am. Ceram. Soc. (USA)* vol.67 (1984) p.213]
[7] K. Tajima, M. Tateda, M. Ohashi [*J. Lightwave Technol. (USA)* vol.12 (1994) p.411]
[8] M. Ohashi, M. Tateda, K. Tajima, K. Shiraki [*Electron. Lett. (UK)* vol.28 (1992) p.1008]

A2.2 Elastic moduli of silica glass

L. Duffrène and J. Kieffer

April 1998

A INTRODUCTION

Silica glass finds wide application in optical fibres because of its very low acoustic loss and high degree of elastic isotropy. For that reason, elastic moduli of silica glass have been investigated as a function of various factors, such as temperature, pressure, annealing and relaxation effects and OH ion concentration [1]. Typical values of standard temperature and pressure elastic constants for silica glass obtained from fused quartz have been determined by Spinner [2] using the dynamic resonance method: Young's modulus E = 73 GPa, shear modulus G = 31.4 GPa, bulk modulus K = 36.1 GPa and the Poisson ratio $\nu = 0.162$. The anomalous behaviour of the elastic properties of silica glass is well-known, as is that of many other properties such as the thermal expansion coefficient, the low temperature specific heat, the refractive index and the acoustic loss peak [3,4]. Various explanations have been given to describe the physical origin of these anomalous behaviours.

B EXPERIMENTAL OBSERVATIONS

The temperature dependence of the elastic moduli of silica glass is anomalous in the sense that the moduli increase with increasing temperature above 60 K [5-7]. As illustrated in FIGURES 1 and 2, the compressibility, which is the inverse of the bulk modulus, continuously decreases between 60 and 1200 K. Correspondingly, the Young's modulus and the shear modulus increase with temperature [7]. The Young's modulus versus temperature curve of Marx and Sivertsen [8] is essentially linear from 25 to 1000°C. The Brillouin scattering technique has also revealed the anomalous temperature dependence behaviour of the elastic moduli of silica glass [9-11].

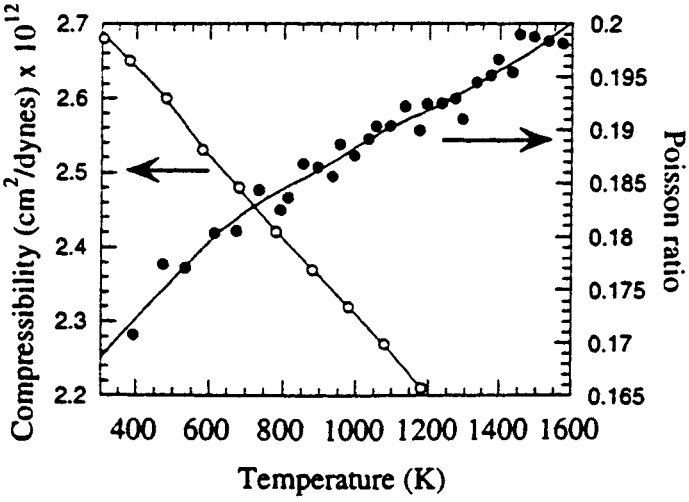


FIGURE 1 Temperature dependence of the Poisson ratio [11] and the compressibility [6,7] of silica glass at zero pressure (above 300 K).

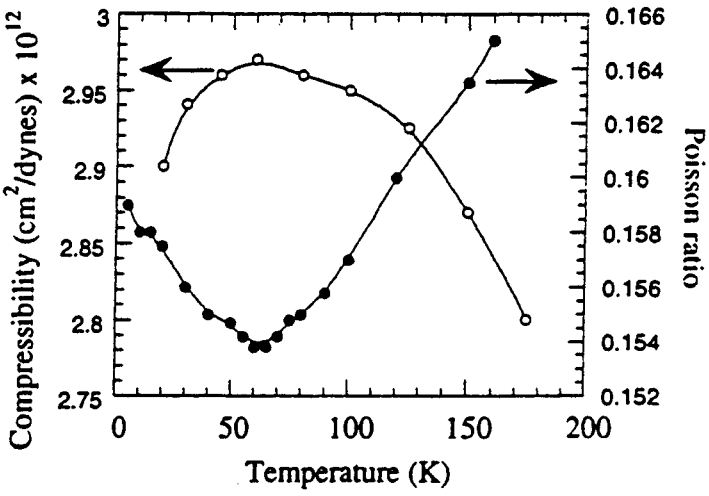


FIGURE 2 Temperature dependence of the Poisson ratio [7] and the compressibility [5] of silica glass at zero pressure (below 300 K).

In silica glass, the Poisson ratio is unusually low which means that the contraction perpendicular to the applied stress is low in comparison to the expansion in that direction. In the same way as for the elastic moduli, the temperature dependence of this ratio also shows a change at 60 K (FIGURES 1 and 2).

It is a well-known fact that the compressibility of silica glass increases with pressure, at least in the lower pressure range (FIGURE 3) [12-17]. This anomalous behaviour, which is not found in quartz, indicates that silica glass becomes 'softer' as the volume decreases. Correspondingly, the Young's modulus and the shear modulus decrease with increasing pressure [18,19]. As shown in FIGURE 3, the anomalous elastic behaviour of silica glass persists until the pressure of about 3 GPa is reached. Above this pressure, the silica glass behaves like a normal solid. Simple relationships have been determined by Anderson and Dienes [3] using ultrasonic measurements of McSkimin [6] in order to calculate the elastic moduli of silica glass in a temperature range of -77 to 75°C and in a pressure range of 0 to 3 GPa.

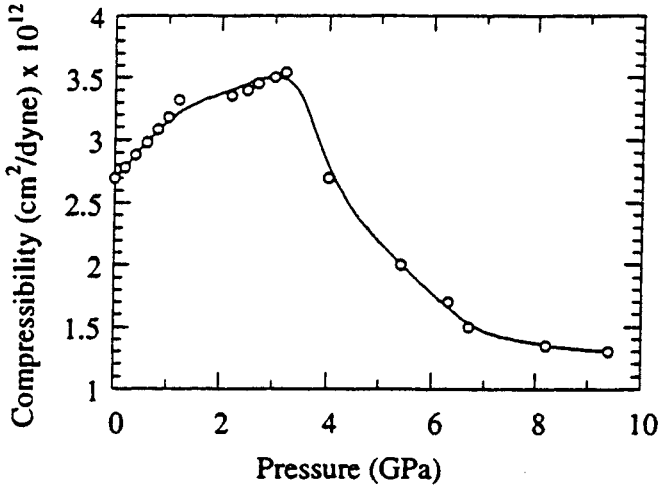


FIGURE 3 Pressure dependence of the compressibility of silica glass at room temperature [12-14].

Large longitudinal elastic strain imposed on silica glass fibres also shows anomalous behaviour [20] through the positive coefficient in the following expressions:

$$E = 7.33\ (1 + 5.75\ \varepsilon) \times 10^3\ \text{kg/mm}^2$$

$$G = 3.21\ (1 + 3.06\ \varepsilon) \times 10^3\ kg/mm^2$$

The Poisson ratio of a silica glass fibre, calculated from the above expressions, increases strongly with increasing longitudinal strain as shown in FIGURE 4 [20]. When under zero strain, silica glass is isotropic, but when under a fairly large tensile stress, the material has one preferred direction, namely that of the applied stress. Its elastic properties in all other directions perpendicular to the applied stress are the same, i.e. it is transversely isotropic and has five elastic constants.

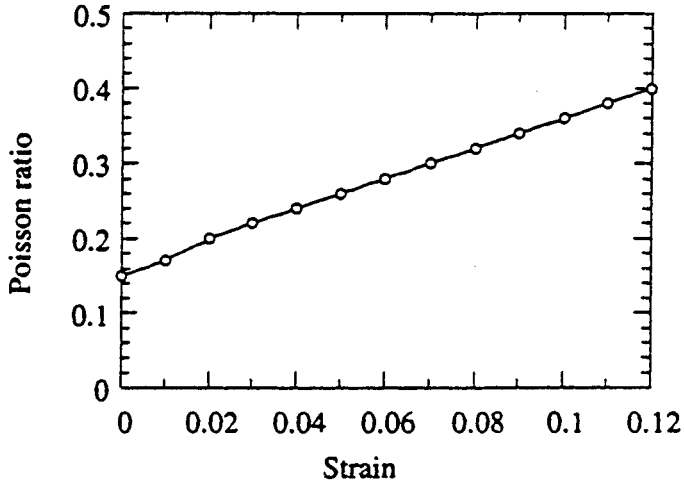


FIGURE 4 Poisson ratio versus strain
for silica glass at room temperature [20].

From the results of Fraser [1], it is evident that thermal history and OH content influence the acoustic properties, i.e. the elastic moduli, of silica glass. Of these, thermal history is the dominant factor with changes of 13 - 16 ppm in the shear velocity for a 1 deg change in fictive temperature (FIGURE 5). The temperature variation of the elastic properties has also been found by Fraser to depend on thermal history. Silica glass destined for critical ultrasonic applications obviously must have a carefully controlled thermal history. Large scale variations of OH content were found to influence the magnitude of the shear modulus (FIGURE 6). However, small velocity fluctuations, which have been measured in a large piece of silica glass and which may degrade the performance of optical silica glass fibres, have not been related to the OH content nor to the fictive temperature variations [1]. Similarly, attempts to relate shear-velocity fluctuations to differences in Na content were inconclusive. Other possible sources of the shear velocity spread such as state of oxidation, granularity and inhomogeneities due to fluctuations during the fusion process have been considered. Of these, inhomogeneities introduced at the time of fusion appear to be the source of velocity spread.

The Brillouin scattering data of Grimsditch [17] have revealed a behaviour suggesting polymorphism, i.e. the existence of more than one non-crystalline polymorph, of silica glass when compressed to high pressure. Upon releasing the constraint, the sound velocity in silica glass did not return to its original value. Grimsditch concluded that silica glass had undergone irreversible structural changes under compression. Such behaviour of the elastic properties under strong compression has been related to the anomalous properties of silica glass [11].

In FIGURES 5 and 6, I.R. Vitreosil is a silica glass made from natural quartz by electrically fusing the starting material under vacuum or inert atmosphere; Spectrosil and Corning 7940 materials are synthetic silica glasses produced by feeding $SiCl_4$ into an oxygen-hydrogen flame; the OH content of the latter varies from 900 to 1400 ppm.

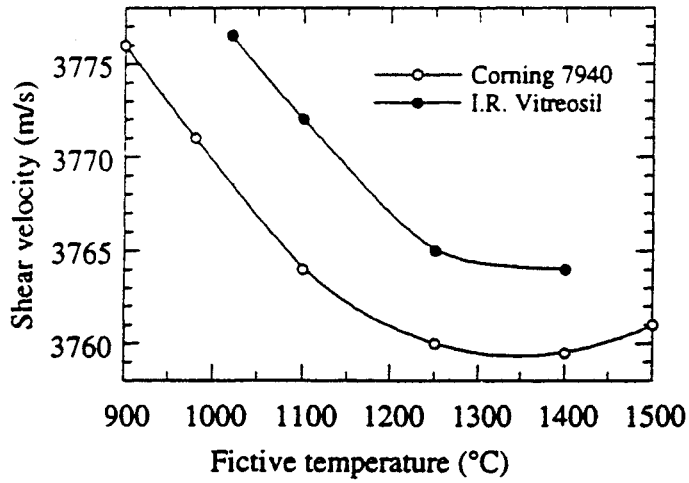


FIGURE 5 The dependence of shear velocity on fictive temperature [1].

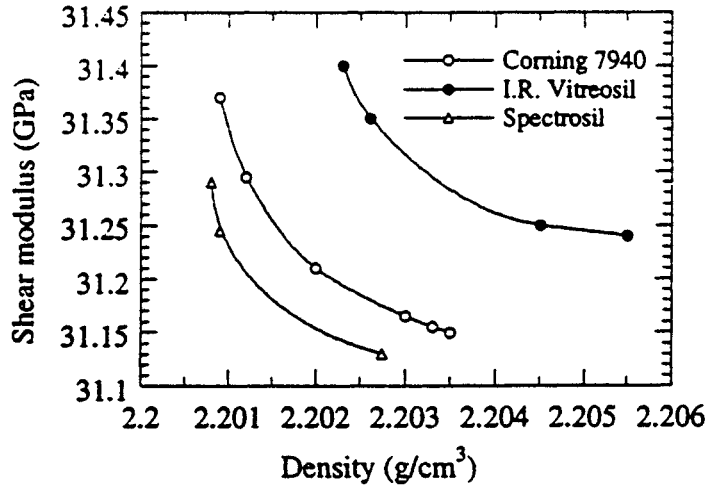


FIGURE 6 The variation of shear modulus with density for a number of silica glasses [1].

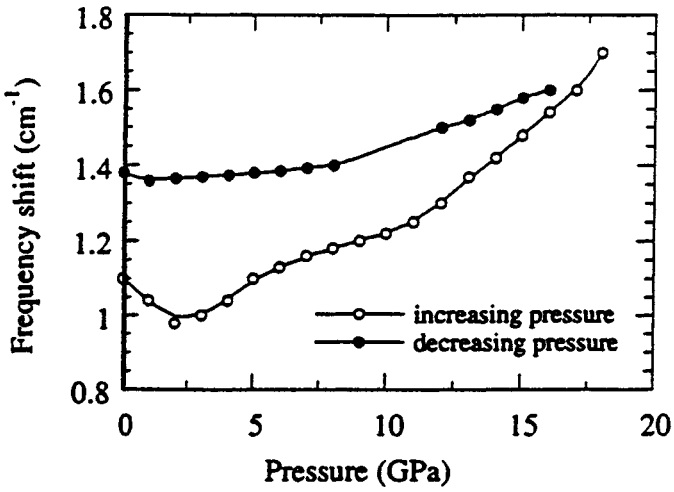


FIGURE 7 Brillouin frequency shift of silica glass as a function of pressure [17].

C PHYSICAL EXPLANATIONS

Since silica is the most important glass-forming material, its anomalous behaviour, in particular the elastic properties, have received considerable attention. The first theories only explained one or two of the anomalies, and are only qualitative [21-23]. Some of them indicate that the anomalous modulus-temperature dependence behaviour is phenomenologically related to the small coefficient of thermal expansion of silica. In the course of time, several new models have been proposed to explain these phenomena. All these models are based on the assumption of two energetically distinct states. Gaskell [24] attributed the negative thermal expansion coefficient to the partially covalent bonding in silica glass. Babcock et al [25] assumed that the structure of silica glass consists of two, or more, distinctly different arrangements which coexist in a homogeneous equilibrium in proportions that vary with temperature and pressure. By examining the superposition of simple central force inter-atomic potentials, Strakna [22] has postulated two equivalent positions for the oxygen atoms, which arise in between two silicon atoms upon increasing the distance between them. Vukcevich [26] has taken up the concept of two positions for the oxygen atoms, by taking into account the covalence of the Si-O bonds. The two oxygen positions are associated with distinct intertetrahedral angles, 138° and 145°, analogous to those in the α and β modifications of quartz. The increase in compressibility of silica glass with pressure arises from a negative volume change associated with the transition between the two bond angles. At pressures above 3 GPa, this reaction is nearly saturated and the compressibility behaves like that of a normal solid.

Vukcevich's concept is interesting in that it introduces analogies to phase transitions in crystalline counterparts of silica, although the mechanisms that he assumed can be refuted based on inelastic neutron scattering [27,28] and computer simulations [29,30]. Anderson and Dienes [3] have also pointed out that, since a crystalline phase of silica, i.e. the β-cristobalite polymorph, has a negative expansivity, it appears that the negative expansivity of silica glass reflects remnants of crystallinity [1]. Recent molecular dynamic simulations [11] have shown that silica glass can undergo local volume changes without the disruption of chemical bonds. The underlying mechanism, which is key to the phase transition between α- and β-cristobalite, is also assumed to be responsible for the positive temperature dependence of the elastic moduli below T_g [30]. This transition involves a cooperative rotation of Si-O-Si bonds about the Si-Si axis by 90°. For temperatures close to that of the transition, β-cristobalite, the high temperature phase of cristobalite, has a smaller density, but a larger elastic modulus. Hence, when arriving at the stability limit of α-cristobalite, as a result of thermal expansion or tensile deformation, the transformation produces a phase which adjusts to the imposed volume change and at the same time is more rigid. The increased elastic modulus is due to a more symmetric orientation of network bridges. In silica glass, individual bridges exhibit similar abrupt rotations. But not all Si-O-Si bonds in the glassy structure rotate simultaneously, as in the crystal. In the glass, the rotations remain localised and occur gradually over a range of densities. Each rotation is a reaction to a local stress field, which, when compressive, leads to the collapse of a network ring to better accommodate the densification. The collapsed ring is, in its geometry, closer to those in α-cristobalite and hence softens the structure. Upon expansion the reverse process takes place. Due to the disorder, there are fluctuations in the local stress fields, so that individual network bridges are affected at different degrees of expansion. Consequently, the elastic modulus increases gradually as a function of temperature in silica glass.

D CONCLUSION

Silica glass is known for a relatively large magnitude and a high degree of isotropy in its elastic moduli. However, these moduli can be affected by temperature, pressure, annealing conditions, relaxation effects and OH ion concentration [1]. When compared to those of crystalline solids, the elastic properties of silica glass appear to be anomalous. In some temperature regimes it has a negative thermal expansion

coefficient, and the elastic moduli decrease upon compression and increase with temperature [3]. Several models have been proposed to explain these phenomena, most of them based on the assumption of different structural or energetic states available to the system. A detailed description of such structural states, and the mechanism of transition between them, has recently been derived using molecular dynamic simulations [11].

REFERENCES

[1] D.B. Fraser [*J. Appl. Phys. (USA)* vol.39 (1968) p.5868]
[2] S. Spinner [*J. Am. Ceram. Soc. (USA)* vol.39 (1956) p.113]
[3] O.L. Anderson, G.J. Dienes [in *Non-Crystalline Solids* Ed. V.D. Fréchette (Wiley, New York, 1960) p.449]
[4] R. Brückner [*J. Non-Cryst. Solids (Netherlands)* vol.5 (1970) p.123]
[5] S. Spinner, G.W. Cleek [*J. Appl. Phys. (USA)* vol.31 (1960) p.1407]
[6] J.M. McSkimin [*J. Appl. Phys. (USA)* vol.24 (1953) p.988]
[7] M.E. Fine, H. VanDuyne, N.T. Kenney [*J. Appl. Phys. (USA)* vol.24 (1954) p.402]
[8] J.W. Marx, J.M. Sivertsen [*J. Appl. Phys. (USA)* vol.24 (1953) p.81]
[9] J. Pelous, R. Vacher [*Solid State Commun. (USA)* vol.18 (1976) p.657]
[10] R. Vacher, J. Pelous, F. Flicque, A. Zarembowitch [*J. Non-Cryst. Solids (Netherlands)* vol.45 (1981) p.397]
[11] R.E. Youngman, J. Kieffer, J.D. Bass, L. Duffrène [*J. Non-Cryst. Solids (Netherlands)* vol.222 (1997) p.190]
[12] P.W. Bridgman [*Proc. Am. Acad. (USA)* vol.57 (1925) p.360]
[13] P.W. Bridgman [*Proc. Am. Acad. (USA)* vol.76 (1945) p.9]
[14] P.W. Bridgman [*Am. Acad. Arts Sci. (USA)* vol.76 (1948) p.55]
[15] F. Birch, R.B. Dow [*Bull. Geol. Soc. Am. (USA)* vol.47 (1936) p.1235]
[16] J. Reitzel, I. Simon, J. Walker [*Rev. Sci. Instrum. (USA)* vol.28 (1957) p.828]
[17] M. Grimsditch [*Phys. Rev. B (USA)* vol.34 (1986) p.4372]
[18] E.H. Borgadus [*J. Appl. Phys. (USA)* vol.36 (1965) p.2504]
[19] L. Peselnick, R. Meister, W.H. Wilson [*J. Phys. Chem. Solids (UK)* vol.28 (1967) p.635]
[20] F.P. Mallinder, B.A. Proctor [*Phys. Chem. Glasses (UK)* vol.5 (1964) p.91]
[21] O.L. Anderson, H.E. Bömmel [*J. Am. Ceram. Soc. (USA)* vol.38 (1955) p.125]
[22] R.E. Strakna [*Phys. Rev. (USA)* vol.123 (1961) p.2020]
[23] S.H. Mahle, R.D. McCammon [*Phys. Chem. Glasses (UK)* vol.10 (1969) p.222]
[24] P.H. Gaskell [*Trans. Faraday Soc. (UK)* vol.62 (1966) p.1354]
[25] C.L. Babcock, S.W. Barder, K. Fanjans [*Ind. Eng. Chem. (USA)* vol.46 (1954) p.161]
[26] M.R. Vukcevich [*J. Non-Cryst. Solids (Netherlands)* vol.11 (1972) p.25]
[27] H. Boysen, B. Dorner, F. Frey, H. Grimm [*J. Phys. C (UK)* vol.13 (1980) p.6127]
[28] G. Dolino, B. Berge, M. Vallade, F. Moussa [*J. Phys. (France)* vol.2 (1992) p.1461]
[29] F.S. Tautz, V. Heine, M.T. Dove, X. Chen [*Phys. Chem. Miner. (Germany)* vol.18 (1991) p.326]
[30] L. Duffrène, J. Kieffer [*J. Phys. Chem. Solids (UK)* in press]

A2.3 Stability of silica glass

M. Tomozawa

August 1997

A INTRODUCTION

In this Datareview, the stability of silica glass against mechanical stress, i.e. fracture strength, at or near room temperature will be discussed since this type of stability is important in the applications of optical fibres. Silica glass can transform into crystalline silica at high temperature and the stability of silica glass in thermal and mechanical properties can also include stability against crystallisation. However, this type of phase stability of silica glass will not be discussed since it becomes important only at high temperatures. The theoretical (or intrinsic) strength of silica glass is extremely high but the real strength is, often, much lower for two reasons. One cause of weakening is the existence of flaws on the glass surface and the other is the presence of moisture. A surface flaw amplifies the applied stress [1] at the flaw tip and makes the real strength expressed in terms of the nominal stress appear much lower than the intrinsic strength being evaluated at the flaw tip. It is possible to manufacture silica glass without surface flaws; well made silica glass optical fibre is believed to be flaw-free [2]. However, even flaw-free silica glasses do not exhibit the theoretical (or intrinsic) strength. This is because of the strength reduction effect of ubiquitous water vapour. Water or water vapour causes the weakening of silica glass, the effect of which increases with the time of loading. This strength degradation with static loading time is called static fatigue. The same strength degradation can be detected by measuring the strength under steadily increasing load at various rates; the strength is lower when a glass is loaded more slowly since the glass has a longer time to degrade. This type of fatigue under varied loading rates is called dynamic fatigue. Static fatigue measurement, in general, is more time-consuming than dynamic fatigue measurement but simulates the real usage of the optical fibre better.

B STATIC FATIGUE DATA

There have been numerous experimental data on the static fatigue of silica glasses. One of the early and thorough measurements was performed by Proctor et al [3] and their results are reproduced in FIGURE 1. It is clear from the figure that the strength decreases with time of loading in the presence of water vapour. The strength reduction is small in vacuum and is absent at liquid nitrogen temperature. The strength on a logarithmic scale plotted against logarithmic time to failure often gives a straight line and the static fatigue data can be represented by the following equation:

$$\log \sigma_f = A - (1/n)\log t_f \qquad (1)$$

where σ_f is the fracture strength, t_f is time to failure and A and n are constants. The fatigue parameter, n, represents the severity of the mechanical fatigue, the glass with a smaller n value exhibiting the greater tendency to strength degradation. The typical value of n for bulk silica glasses is 20 to 40. The existence of the fatigue limit or the lowest strength below which a glass never fails is expected but has not been demonstrated for silica glass. In fact, the static fatigue data of silica optical fibres [4-7] exhibit an alarming trend of seemingly faster rate of fatigue for longer loading time on a logarithmic time scale. An example is shown in FIGURE 2 [7]. The anomalously small n value of silica optical fibre for longer loading time was observed even after the plastic coating of the optical fibre was removed [5,7] suggesting that the origin is in the optical fibre itself.

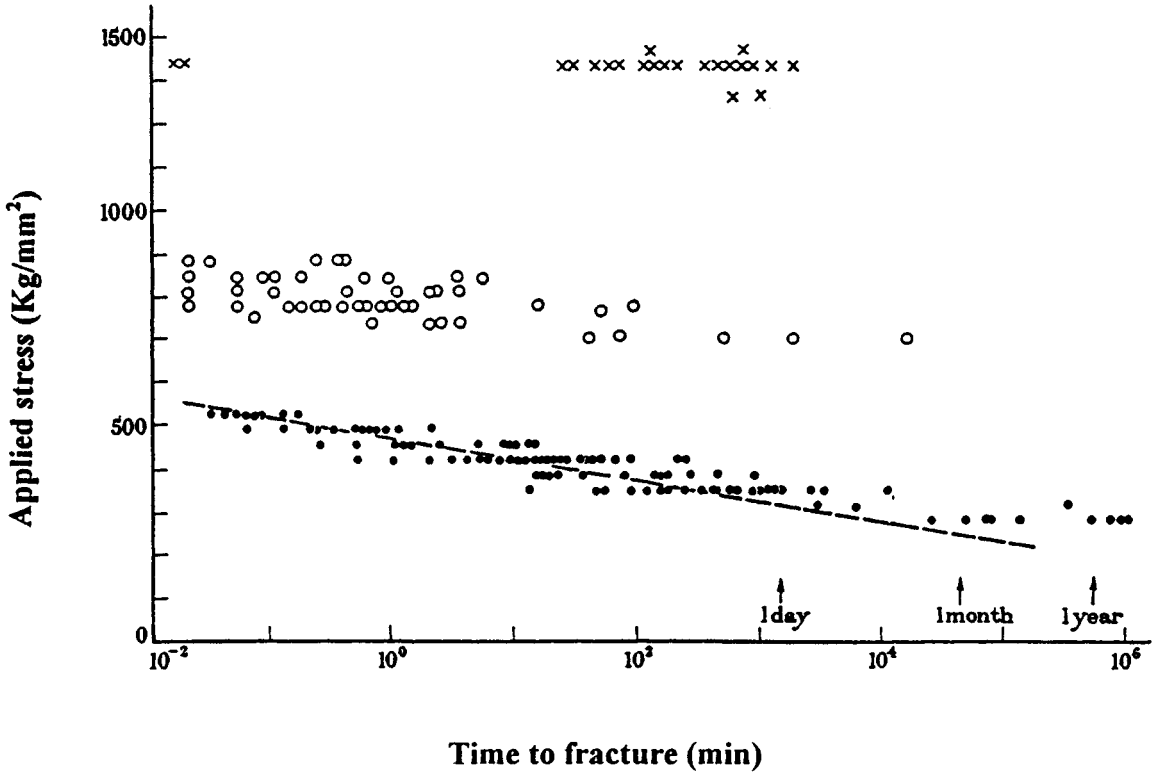


FIGURE 1 Static fatigue of silica fibres at room temperature in air and in vacuum, and at liquid nitrogen temperature in vacuum. Filled circle: in air at room temperature; open circle: in vacuum at room temperature; cross: in vacuum at -196°C; the line is an approximation (after Proctor et al [3]).

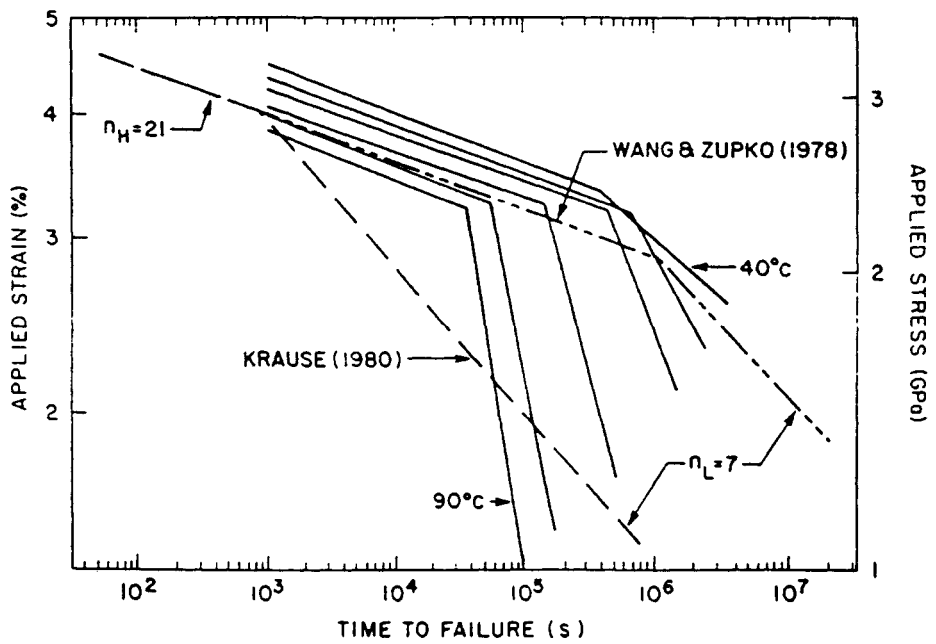


FIGURE 2 Static fatigue of silica optical fibres obtained by Wang and Zupko [4], Krause [5] and Chandan and Kalish (solid lines) [6] compiled by Matthewson and Kurkjian [7].

Reprinted with permission of The American Ceramic Society.
© 1988 by The American Ceramic Society. All rights reserved.

C FATIGUE MECHANISMS

The conventional explanation of static fatigue was slow crack growth, i.e. a surface flaw of silica glass extends slowly under a tensile stress and reaches the critical length at which the glass fails. In such a case, using crack velocity data, one can predict the fatigue lifetime of silica glasses. There have been numerous measurements of growth rate of macroscopic cracks on the surfaces of silica glasses [8-10]. One such example is shown in FIGURE 3 as a function of stress intensity [9]. The crack growth rate has been represented by several different equations, the two most popular equations being

$$v = A_1(K/K_c)^n \tag{2}$$

$$v = A_2 \exp[n'(K/K_c)] \tag{3}$$

where v is the crack velocity, K is the stress intensity factor, K_c is the critical stress intensity factor, and A_1, A_2, n′ are constants. EQN (3) has the better physical basis but EQN (2) is easier to handle mathematically. Crack velocity measurement in a wide range of stress intensity is necessary to distinguish these two equations. Using EQN (2) and assuming that slow crack growth is responsible for the static fatigue, it is possible to derive EQN (1). It has been found that the n value obtained from the static fatigue measurement and that obtained by the slow crack growth measurement agree reasonably well when the specimens have freshly formed surface flaws. The slow crack growth in the presence of water or water vapour is sometimes called stress corrosion cracking [11,12]. Various explanations have been offered as to how slow crack growth takes place in the presence of water or water vapour. One explanation is the weakening of the Si-O bond by water adsorption [9] and the other is water entry into silica glass at the crack tip accelerated by the applied tensile stress and the consequent weakening of the glass [13]. The static fatigue data at longer loading time correspond to the slower crack growth rate. In order to clarify the issue of the fatigue limit, some researchers have attempted to measure the rate of extremely slow crack growth in silica glass [10]. The slowest crack velocity measured so far does not indicate the presence of a fatigue limit.

Reprinted with permission of The American Ceramic Society.
© 1983 by The American Ceramic Society. All rights reserved.

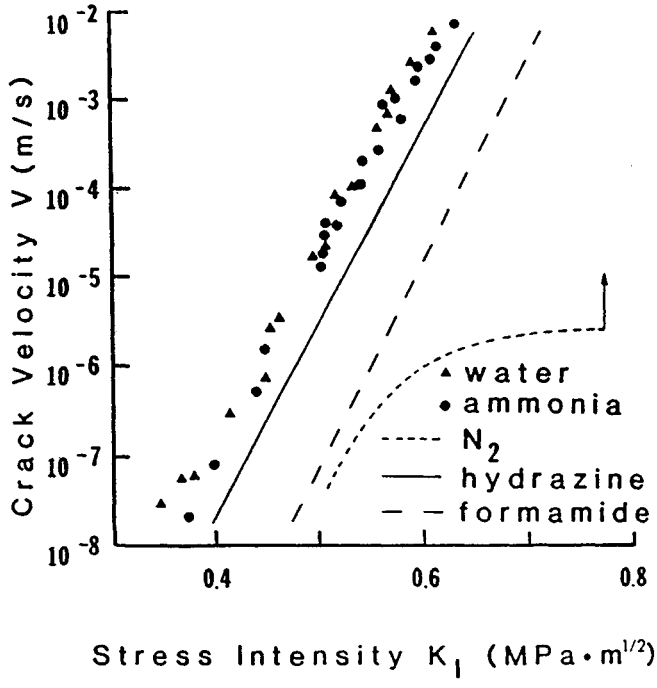


FIGURE 3 Crack velocity (V) versus stress intensity factor (K_I) for silica glass at room temperature in various environments. After Michalske and Freiman [9].

When the glass does not have any surface flaw or when the surface flaw has a blunt tip, the above explanation based upon slow crack growth is not strictly applicable since the generation of a crack with a sharp tip can take a longer time than the subsequent crack propagation. Thus, the fatigue behaviour of these glasses is expected to be different. In fact, the fatigue parameter, n, of these glasses is different from that obtained by slow crack growth. In particular the strange static fatigue behaviour of the optical fibre shown in FIGURE 2 cannot be explained by the slow crack growth data. Kurkjian et al suggested that etch pit formation on the silica glass fibre surface may be the mechanism of the strength degradation

[14]. However, there is no direct experimental evidence that the etching of silica glass is promoted by tensile stress.

The strength degradation model based upon water entry into the glass promoted by the tensile stress may explain the strength degradation of these glass samples, also. Water entry can accelerate the structural relaxation of glasses and make the glass weaker. As-produced silica glass optical fibre has a high fictive temperature on its surface as shown in FIGURE 4 [15]. The decrease of this high surface fictive temperature by relaxation was accelerated by water vapour in the atmosphere and applied tensile stress as shown in FIGURE 5 [16]. Since silica glasses with lower fictive temperature are weaker [17], the lowering of the fictive temperature can cause strength degradation.

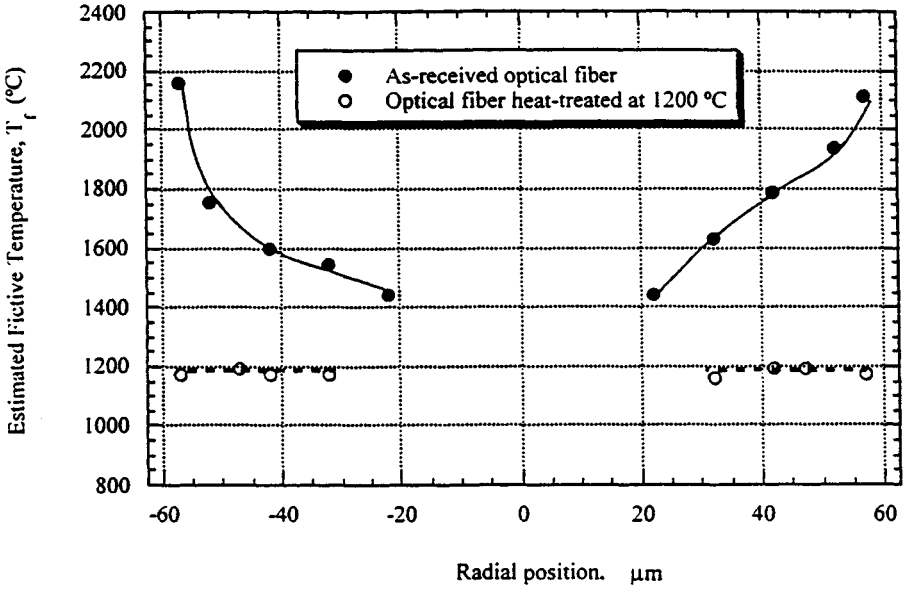


FIGURE 4 Fictive temperature distribution on a cross-section of a silica glass optical fibre. After Peng et al [15].

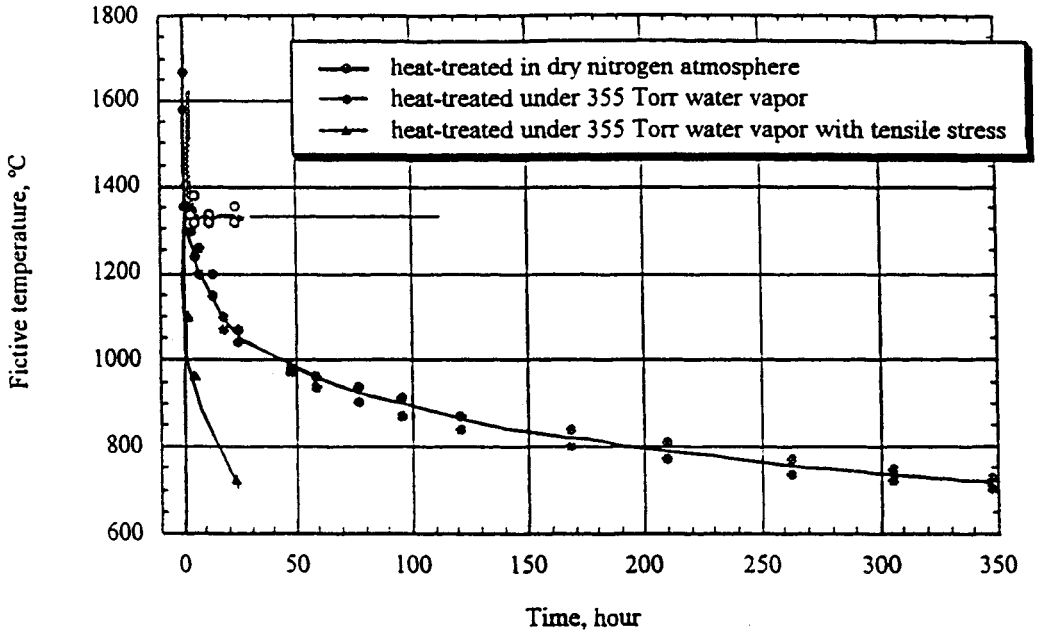


FIGURE 5 Time variation of the surface fictive temperature of a silica glass optical fibre at 650°C. Tensile stress was 0.52 GPa at time zero. After Peng et al [16].

D CONCLUSION

Current knowledge of static fatigue of silica glass, in particular of silica glass optical fibre, has been described. Silica glass optical fibres appear to exhibit different mechanical strength degradation from bulk silica glasses. It is possible that the strength degradation of silica glass in the presence of water involves water entry into the glass accelerated by tensile stress, which consequently weakens the glass.

REFERENCES

[1] C.E. Inglis [*Trans. Instn. Nav. Archit. (UK)* vol.55 (1913) p.219-30]

[2] C.R. Kurkjian, U.C. Paek [*Appl. Phys. Lett. (USA)* vol.42 (1983) p.251-3]

[3] B.A. Proctor, F. Whitney, J.W. Johnson [*Proc. R. Soc. Lond. A (UK)* vol.297 (1967) p.534-57]

[4] T.T. Wang, H.M. Zupko [*J. Mater. Sci. (UK)* vol.13 (1978) p.2241-8]

[5] J.T. Krause [*J. Non-Cryst. Solids (Netherlands)* vol.38/39 (1980) p.497-502]

[6] H.C. Chandan, D. Kalish [*J. Am. Ceram. Soc. (USA)* vol.63 (1982) p.171-3]

[7] M.J. Matthewson, C.R. Kurkjian [*J. Am. Ceram. Soc. (USA)* vol.71 (1988) p.177-83]

[8] S.M. Wiederhorn, L.H. Bolz [*J. Am. Ceram. Soc. (USA)* vol.53 (1970) p.543-8]

[9] T.A. Michalske, S.W. Freiman [*J. Am. Ceram. Soc. (USA)* vol.66 (1983) p.284-8]

[10] J.D. Helfinstine, S.T. Gulati, D.G. Pickels [*The Physics of Non-Crystalline Solids* Eds. L.D. Pye, W.C. LaCourse, H.J. Stevens (Taylor & Francis, London, UK, 1992) p.654-8]

[11] R.J. Charles, W.B. Hillig [*Symposium on Mechanical Strength of Glass and Ways of Improving It* (Union Scientifique Continentale du Verre, Charleroi, Belgium, 1962) p.511-27]

[12] W.B. Hillig, R.J. Charles [*High Strength Materials* Ed. V.F. Zackey (Wiley, New York, 1965) p.682-705]

[13] M. Tomozawa [*Phys. Chem. Glasses (UK)* to be published (1998)]

[14] C.R. Kurkjian, J.T. Krause, U.C. Paek [*J. Phys. (France)* vol.C9 (1982) p.585-90]

[15] Y.-L. Peng, A. Agarwal, M. Tomozawa [*J. Non-Cryst. Solids (Netherlands)* vol.217 (1997) p.272-7]

[16] Y.-L. Peng, M. Tomozawa, T.A. Blanchet [*J. Non-Cryst. Solids (Netherlands)* vol.222 (1997) p.376-82]

[17] H. Li, A. Agarwal, M. Tomozawa [*J. Am. Ceram. Soc. (USA)* vol.78 (1995) p.1393-6]

PART A: SILICA

CHAPTER A3

RARE-EARTH SPECTROSCOPY

A3.1 Spectroscopy of erbium-doped silica
A3.2 Spectroscopy of neodymium-doped silica

A3.1 Spectroscopy of erbium-doped silica

A. Bjarklev, M.G. Dyndgaard, M.O. Berendt, J. Broeng, K. Dridi and J.L. Philipsen

April 1998

A INTRODUCTION

Erbium is added to silica in order to obtain amplification of optical signals in the 1530 - 1570 nm transmission window that is of special interest for use in optical communications. Amplification has been demonstrated at room temperature using low-power pump light at wavelengths around $\lambda = 665$ nm, $\lambda = 807$ nm, $\lambda = 980$ nm and $\lambda = 1480$ nm [1]. It is thus possible to pump the erbium-doped-fibre amplifiers (EDFAs) using visible or infrared laser diodes. For these reasons, combined with very high gain and low noise performance, the EDFAs have become key elements in the progress of optical communication towards the present wavelength-division-multiplexed (WDM) systems. This development, however, raises a new challenge to the erbium-doped optical amplifiers, since it is no longer sufficient to provide a satisfactory gain and noise coefficient at a single wavelength, but has become necessary to consider a whole wavelength interval, in which near-constant amplification properties are required. Yet another aspect has become central in the development of spectral properties of the EDFAs, and that is the need for relatively short physical lengths of the amplifying waveguides. These requirements appear as we today aim at applications of erbium-doped-silica waveguides in, for example, distributed-feedback (DFB) fibre lasers, or in zero-loss integrated-optical components. In these applications, the pump-power must be absorbed over a short path length, and this makes a relatively high Er^{3+} concentration necessary. However, pure-silica glass has a very rigid structure, and this decreases the solubility of the Er^{3+} ions, leading to a clustering of the ions. Although this clustering may be reduced for example by adding co-dopants such as Al_2O_3 to the silica [2], it is still a significant concern, and a major part of the research into spectroscopic properties of erbium-doped waveguides has, consequently, been directed towards the solution of this problem. For these reasons, we have in the following text chosen to focus on the spectroscopic aspects of erbium-clustering effects.

B TRANSITIONS IN Er^{3+}

One of the most commonly used pumping schemes, 980 nm pumping, is illustrated in FIGURE 1. The pump laser will excite the erbium ions to the $^4I_{11/2}$ manifold, from which they relax to the metastable $^4I_{13/2}$ level by fast phonon transitions. From this level the erbium ions may then relax to the $^4I_{15/2}$ state by emitting light in a band around 1530 nm. We thus have a three-level system, where the population builds up in the metastable $^4I_{13/2}$ manifold, serving as the upper laser level. However, interaction between closely situated erbium ions introduces another relaxation mechanism known as energy-transfer upconversion. The $^4I_{9/2}$ level in erbium has an energy nearly twice as high as that of the $^4I_{13/2}$ level. This means that one ion excited to $^4I_{13/2}$ (the donor) may transfer all of its excitation energy to another ion in $^4I_{13/2}$ (the acceptor), so that the donor is transferred to the $^4I_{15/2}$ ground level, while the acceptor is upconverted to the $^4I_{9/2}$ manifold. From this level, the acceptor will relax to $^4I_{13/2}$ by very fast phonon transitions, and thus the net result of the process is the loss of one ion in the upper laser level $^4I_{13/2}$. Inside clusters, the energy-transfer upconversion takes place very rapidly (on a sub-μs scale, lifetimes as low as 50 ns have been measured [3]) due to the short inter-ionic distances, but also the non-clustered erbium ions take part in energy-transfer upconversion, although at a slower rate (ms timescale). Another energy transfer process is migration of the excitation energy from a donor in the metastable $^4I_{13/2}$ level to an acceptor in the ground level $^4I_{15/2}$ (the two ions switch energy states). This process has only indirect

influence on the excited population via its influence on upconversion [4]. Finally, energy transfer to impurities, such as OH-groups, may occur, also leading to a depopulation of the $^4I_{13/2}$ level.

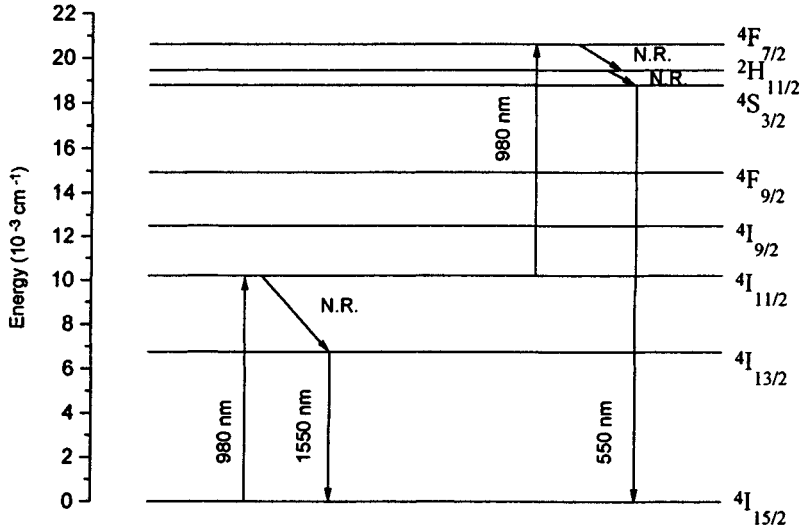


FIGURE 1 Energy level diagram for Er^{3+}. To the left are shown the transitions that lead to amplification when pumped at 980 nm. To the right ESA and corresponding green fluorescence is shown. N.R. indicates a non-radiative (phonon) transition.

C ABSORPTION

One way of obtaining information on the clustering of erbium in silica glass is to study the absorption of light sent through a fibre. It has been shown by Delevaque et al [5] that in erbium-doped fibres, even at high powers, there is a residual absorption that cannot be saturated. This phenomenon has been attributed to energy-transfer upconversion between clustered erbium ions. Due to rapid upconversion, only one erbium ion can be inverted per cluster. Thus, a total fraction of

$$k = \sum_m r_m \frac{m-1}{m}$$

(where r_m is the fraction of erbium ions sitting in clusters with m erbium ions) of the erbium ions in the glass are unbleachable at realistic (CW) pump powers. Davis et al [6] have made transmission studies of rare-earth-doped fibres, where the transmission of a 980 nm pump beam was measured. They showed that in the presence of clusters, the transmission versus power curves of the fibres exhibit a plateau. This plateau corresponds to a bleaching of a fraction 1 - k of the absorption compared to the absorption at low power.

The fraction k of erbium ions that are unbleachable is an important figure for an erbium-doped material, since the maximum obtainable gain (in dB) will be reduced by a factor

$$1 - k[1 + \sigma_a(\lambda_s)/\sigma_e(\lambda_s)]$$

(where $\sigma_a(\lambda_s)$ and $\sigma_e(\lambda_s)$ are the absorption and emission cross sections at the signal wavelength) compared to the situation without clustering.

D FLUORESCENCE

The dominant fluorescence transition for erbium is the $^4I_{13/2} \rightarrow {}^4I_{15/2}$ transition. At high 980 nm pump power, however, a population will grow in the $^4I_{11/2}$ level. Apart from leading to increased 980 nm fluorescence from the $^4I_{11/2} \rightarrow {}^4I_{15/2}$ transition, this will also increase the possibility of absorbing another pump photon. The $^4F_{7/2}$ manifold has an energy corresponding to two 980 nm photons, and may, therefore, be reached via excited-state absorption (ESA): see FIGURE 1. From the $^4F_{7/2}$ level, the erbium ions will relax to the $^2H_{11/2}$ or $^4S_{3/2}$ level by fast phonon transitions, and then to either the $^4I_{9/2}$, $^4I_{11/2}$, $^4I_{13/2}$ or $^4I_{15/2}$ levels by emitting light around 1720 nm, 1220 nm, 850 nm or 550 nm, respectively [2]. However, due to the high phonon energy in silica, this fluorescence is weak compared to the case of certain other erbium-doped materials [7].

The combination of high pump power and clustering of the erbium ions increases the $^4I_{11/2}$ population due to energy transfer upconversion and thus makes 980 nm ESA more likely to happen, which can be observed as an increased green fluorescence (550 nm). By comparing the green fluorescence with the 1530 nm infrared fluorescence, one may thus obtain information on the clustering in the glass. Quimby et al [8] have studied this problem, and found that when Er^{3+}-doped glass is pumped at 980 nm, the resulting upconverted green fluorescence shows both a saturable component and a non-saturable component analogous to that observed for the absorption. In [8] a method for determining the degree of clustering from measurements of the 1530 nm and the green fluorescence versus pump power is presented. FIGURE 2 shows the fraction of erbium ions that are unbleachable (predominantly due to clustering) as measured by this method for a series of erbium-doped silica fibres [9].

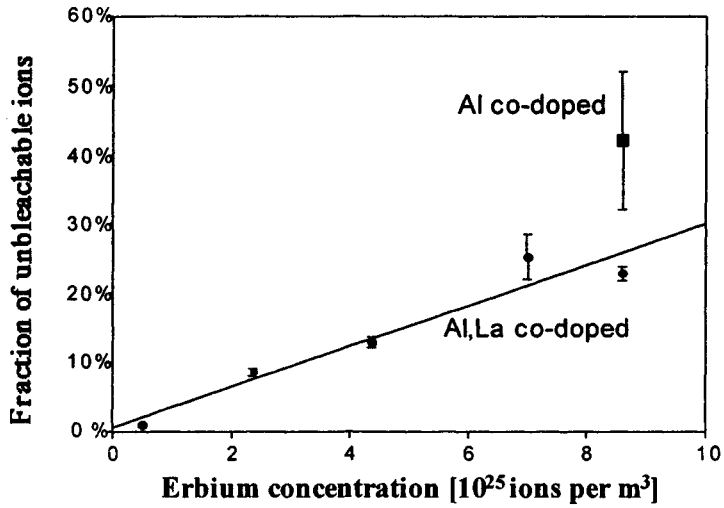


FIGURE 2 Fraction of erbium ions that are unbleachable [9].

E FLUORESCENCE LIFETIME

The fluorescence lifetime of the erbium ions is an important parameter. The inherent, long lifetime of around 10 ms (the exact value depends on the co-dopants) for the erbium ions in the metastable $^4I_{13/2}$ level makes it possible to obtain a high population inversion between this level and the $^4I_{15/2}$ level with moderate pump power. This leads to a high gain and low noise figure for the fibre/waveguide amplifier. However, at high erbium concentrations, the effective lifetime is reduced due to energy transfer upconversion. Ainslie et al [10] have shown that, in the case of clustering of the erbium ions, the fluorescence will have a fast decay component superimposed on a slowly decaying component. Furthermore, the decay rate becomes a very strong function of the pump power. Also, the fast

component may be attributed to the upconversion mechanism by comparing the fluorescence intensity decay curves for decay of the $^4I_{13/2}$ and $^4I_{9/2}$ levels [10].

F ABSORPTION AND EMISSION CROSS-SECTIONS

The absorption and emission cross-sections $\sigma_a(\lambda_s)$ and $\sigma_e(\lambda_s)$ at the signal wavelength λ_s are very important parameters for the characterisation of the active properties of erbium-doped fibres. $\sigma_a(\lambda_s)$ may be measured by standard absorption measurement techniques, but $\sigma_e(\lambda_s)$ cannot easily be determined directly. However, McCumber's theory determines a relation between the emission and absorption cross-sections, and has proven highly accurate (error < 3% [11]). Zech [12] has proposed a simple measurement technique for measuring the quotient of cross-sections $\sigma_e(\lambda_s)/\sigma_a(\lambda_s)$, where the spontaneous emission perpendicular to a fibre pumped at 980 nm is used to determine the quotient. For an erbium-doped Al-Ge-silica fibre, the quotient was thus determined to be $\sigma_e(\lambda_s)/\sigma_a(\lambda_s) = 0.91$ at $\lambda_s = 1530$ nm. Barnes et al [13] have determined the quotient for a similar fibre pumped at $\lambda_p = 978$ nm by measuring the ratio of gain to loss of a length of doped fibre as a function of pump power. The quotient is very close to the value obtained by Zech ($\sigma_e(\lambda_s)/\sigma_a(\lambda_s) = 0.94$). Cross-section ratios on other types of fibres have also been published by Barnes et al; for Ge-silica $\sigma_e(\lambda_s)/\sigma_a(\lambda_s) = 0.84$, and for Al-silica $\sigma_e(\lambda_s)/\sigma_a(\lambda_s) = 0.82$. These ratios were determined in the same way as for the Al-Ge-silica fibre. From these values it was possible to calculate the emission and absorption cross-sections at 1530 nm which are shown in TABLE 1.

TABLE 1 Absorption and emission cross-sections for different types of erbium doped silica fibres.

Fibre type	σ_e ($\times 10^{-25}$ m)	σ_a ($\times 10^{-25}$ m)
GeO_2-SiO_2	6.7 ± 0.3	7.9 ± 0.2
Al_2O_3-SiO_2	4.4 ± 0.6	5.1 ± 0.6
GeO_2-Al_2O_3-SiO_2	4.4 ± 1.0	4.7 ± 0.8

Recently Samson et al [14] showed that the presence of erbium clusters affects the absorption spectra of erbium-doped germano-silica fibres. The presence of clusters can be observed as a broadening of the spectrum on the short-wavelength side of the spectrum. On the other hand, it has been observed that very high erbium doping may lead to phase separation in the glass, with formation of large, crystalline clusters [15]. In this case, absorption and emission spectra with sharp peaks superimposed would be expected, in analogy with observations for neodymium doped glasses [16].

G CONCLUSION

Spectroscopic techniques have provided us with very useful information on the characteristics of erbium-doped silica, and in particular on the clustering of erbium in silica. From absorption and fluorescence measurements, information on the size of clusters and the degree of clustering can be inferred. This has great importance for the fabrication of efficient optical fibres, DFB fibre lasers and integrated optical components.

REFERENCES

[1] A. Bjarklev [*Optical Fiber Amplifiers: Design and System Applications* (Artech House, Boston-London, 1993)]

[2] E. Desurvire [*Erbium-Doped Fiber Amplifiers* (John Wiley & Sons, Inc., 1994)]

[3] P. Myslinski, J. Fraser, J. Chrostowski [*Proceedings of the Topical Meeting on Optical Amplifiers and Their Applications (OAA) 1995* paper ThE3-1, p.100-3, June 1995 (Opt. Soc. America, Washington DC, USA, 1995)]

[4] J.L. Philipsen, A. Bjarklev [*IEEE J. Quantum Electron. (USA)* vol.33 no.5 (1997) p.845-54]

[5] E. Delevaque, T. Georges, M. Monerie, P. Lamouler, J.-F. Bayon [*IEEE Photonics Technol. Lett. (USA)* vol.5 no.1 (1993) p.73-5]

[6] M.K. Davis, M.J.F. Digonnet, R.H. Pantell [*J. Lightwave Technol. (USA)* vol.13 no.2 (1995) p.120-6]

[7] M. Beukema et al [*Proceedings of the European Conference on Integrated Optics (ECIO) 1997* paper EThH25, p.392-5, April 1997 (Opt. Soc. America, Washington DC, USA, 1997)]

[8] R.S. Quimby, W.J. Miniscalco, B. Thompson [*J. Appl. Phys. (USA)* vol.76 (1994) p.4472-8]

[9] J.L. Philipsen, J. Broeng, A. Bjarklev, J.E. Pedersen, B. Pàlsdòttir [*OSA Trends in Optics and Photonics (TOPS)* vol.5 p.142-7 (Opt. Soc. America, Washington DC, USA, 1996)]

[10] B.J. Ainslie et al [*IEE Proc. J (UK)* vol.137 no.4 (1990) p.205-8]

[11] W.J. Miniscalco, R.S. Quimby [*Opt. Lett. (USA)* vol.16 no.4 (1991) p.258-60]

[12] H. Zech [*IEEE Photonics Technol. Lett. (USA)* vol.7 no.9 (1995) p.986-8]

[13] W.L. Barnes, R.I. Laming, E.J. Tarbox, P.R. Morkel [*IEEE J. Quantum Electron. (USA)* vol.27 no.4 (1991) p.1004-10]

[14] B.N. Samson, W.H. Loh, J.P. de Sandro [*Opt. Lett. (USA)* vol.22 no.23 (1997) p.1763-5]

[15] L.-L. Lee, D.-S. Tsai [*J. Mater. Sci. Lett. (UK)* vol.13 (1994) p.615-7]

[16] B.J. Ainslie, S.P. Craig, S.T. Davey, D.J. Barber, J.R. Taylor, A.S.L. Gomes [*J. Mater. Sci. Lett. (UK)* vol.6 (1987) p.1361-3]

A3.2 Spectroscopy of neodymium-doped silica

J.D. Minelly

February 1998

A INTRODUCTION

Nd^{3+} ion lasers in glass and crystal form have been the workhorses of the laser industry for three decades. Silica exhibits excellent optical and mechanical properties thereby providing an excellent host for Nd^{3+} glass lasers and amplifiers. In a silica fibre environment the spectroscopic properties of Nd^{3+} doped silica enable the construction of highly efficient devices with low pump power requirements. In this Datareview the properties of Nd^{3+} doped silica are summarised with emphasis given to the impact of the spectroscopy on the realisation of practical devices.

B ABSORPTION AND FLUORESCENCE

Representative absorption and fluorescence spectra [1], taken from a germano-silicate Nd^{3+} doped silica fibre, are shown in FIGURE 1. They show strong absorption peaks centred at 590 nm, 750 nm, 805 nm and 890 nm, and fluorescence peaks around 950 nm, 1090 nm and 1320 nm. The three longest absorption wavelengths coincide with the operating wavelengths of semiconductor lasers. Therefore convenient low cost pump sources are available. The most commonly employed is the 805 nm wavelength due to the lower cost and production yield of AlGaAs lasers at that wavelength. While efficient lasing operation has been demonstrated at 940 nm [2,3] on the $^4F_{3/2}$-$^4I_{9/2}$ transition, and at 1088 nm on the $^4F_{3/2}$-$^4I_{11/2}$ transition [4,5], operation at the technologically important 1300 nm wavelength is frustrated by the presence of an excited state absorption band centred near the fluorescent peak from the $^4F_{3/2}$ metastable level to the $^2G_{9/2}$ and $^2G_{7/2}$ levels [6]. These levels correspond to ground

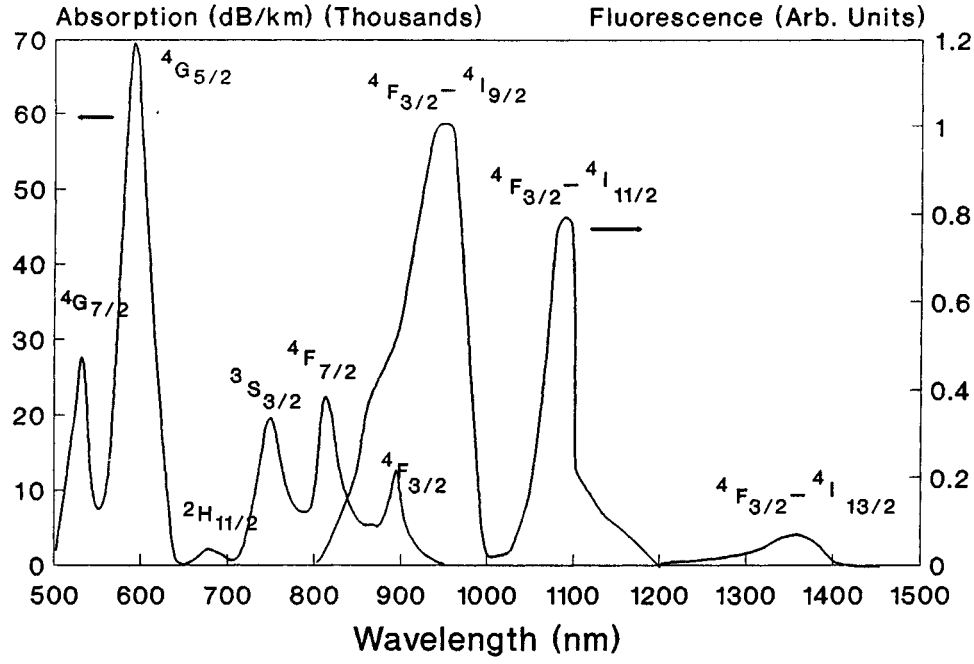


FIGURE 1 Absorption and emission spectra of Nd^{3+} doped germano-silicate fibre (after Townsend [1]).

state absorption in the 500 - 550 nm band. The excited state absorption comprises a near continuum extending from 1100 to 1380 nm. This shifts the oscillating wavelength away from the fluorescent peak towards 1400 nm and therefore eliminates Nd^{3+} doped silica as a host medium for a 1.3 μm amplifier for telecommunications.

C EFFECT OF GLASS COMPOSITION

It is important to consider the effect of glass composition on the properties of Nd^{3+} doped silica. Silica based glass fibre can be fabricated with a range of host compositions large enough to affect fluorescence and absorption peak positions, effective line shapes, line strengths and other spectroscopic properties. The composition is particularly important where a high concentration of Nd^{3+} ions is required, for example in a cladding pumped structure, or where a short cavity is required, for example in a q-switched or single-frequency device. High concentration can lead to devitrification, rare-earth microclustering and concentration quenching, all of which can severely affect the performance of an amplification device.

C1 Alumina and Phosphorus Co-Doping

It is well known from an extensive study of bulk silica by Arai et al [7] that co-doping with alumina and phosphorus has several beneficial effects on the properties of Nd^{3+} doped silica. These co-dopants can significantly increase the solubility of rare-earths in silica, inhibit devitrification and prevent clustering of rare-earth ions.

In a pure silica or germano-silicate host with high Nd^{3+} ion concentration a large proportion of the ions are unavailable for laser action because of microclustering and additionally the transition shows a lower fluorescence intensity than in virtually any other host. However the addition of a small amount of alumina or phosphorus virtually eliminates the fast decay component associated with the microclusters and increases the fluorescence intensity ratio of the $^4F_{3/2}$ to $^4I_{11/2}$ transition from 0.7 to 1.5. An optimised ratio of Al/Nd concentrations of between eight and ten has been determined. In the case of phosphorus doping a ratio of approximately 15:1 is appropriate.

As well as dispersing the microclusters these additional co-dopants also enable realisation of higher average Nd^{3+} concentrations without serious lifetime quenching occurring. This is illustrated in FIGURE 2 for the case of optimised Al co-doping.

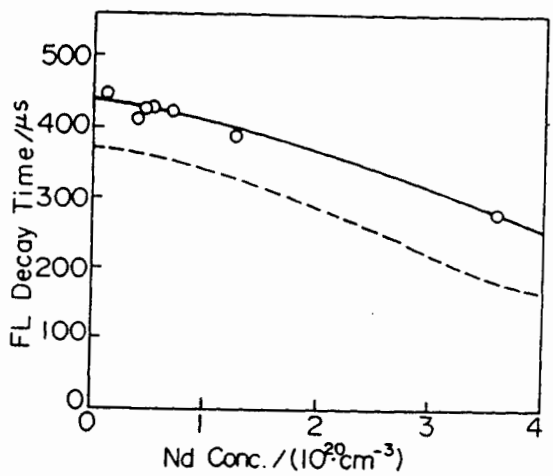


FIGURE 2 The decay time of the $^4F_{3/2}$-$^4I_{11/2}$ fluorescence in an alumino-silicate fibre as a function of Nd^{3+} concentration. The broken line represents that of an ED-2 silicate glass (after Arai et al [7]).

D PRACTICAL DEVICES

D1 $^4F_{3/2}$-$^4I_{11/2}$ Transition

The first demonstration of diode pumped single-mode operation of this transition was in 1985 [4]. The early publications reported lasing at 1088 nm in germano-silicate fibres. The efficiency of these devices was severely limited by microclustering. Currently however an alumino-silicate host is almost universally used for the reasons outlined in the previous section. Highly efficient laser sources pumped by high power diode bars have enabled the output power to be scaled to several tens of watts at 1060 nm [8,9].

D2 $^4F_{3/2}$-$^4I_{9/2}$ Transition

This is potentially a very important transition with applications in remote sensing, non-linear optics (e.g. frequency doubling to the blue) and as a high power pump for Yb or ErYb fibre lasers. The transition is three-level in nature and as such requires that the ground state absorption is bleached before gain can be achieved. Since the first demonstration of this lasing on this transition in 1987 [2], there has been little reported until 1997 when Dragic et al proposed such a source for remote sensing of water vapour. There have so far been no reports of power scaling this transition by cladding pumping. This is because under the weak pumping conditions inherent when double-clad fibre is employed, the strong gain at 1060 nm will lead to ASE self saturation thus suppressing the 940 nm transition irrespective of any wavelength selecting mirrors. However a recently proposed gain limiting structure with annular doping may permit future power scaling of this transition [10].

D3 $^4F_{3/2}$-$^2I_{11/2}$ Transition

As mentioned in Section B lasing on this transition is frustrated by signal excited state absorption. Nevertheless lasing at 1364 nm has been demonstrated in a phospho-silicate Nd^{3+} doped fibre [11]. The slope efficiency was very low however and the gain peak still at too long a wavelength for a practical telecoms amplifier. Further developments concerning this transition have therefore employed compound glasses such as fluorides and phosphates rather than silica based glasses.

E CONCLUSION

Nd^{3+} doped silica provides an excellent host for fibre lasers and amplifiers operating on the four level transition around 1060 nm. Very low threshold can be combined with the capability for power scaling to several tens of watts. The engineering of sources on the three level transition at 940 nm is hindered by competing amplified spontaneous emission at 1060 nm and on the four level transition around 1320 nm by a broadband excited state absorption between 1100 nm and 1380 nm. In most cases an alumino-silicate host is preferred because of improved rare-earth solubility and dispersion of microclusters.

REFERENCES

[1] J.E. Townsend [PhD Thesis, University of Southampton, April 1990]
[2] L. Reekie, I.M. Jauncey, S.B. Poole, D.N. Payne [*Electron. Lett. (UK)* vol.23 (1987) p.884-5]
[3] P.D. Dragic, L.M. Little, G.C. Papen [*Proc. Int. Conf. on Optical Amplifiers and Their Applications* Victoria, BC, Canada, 21-23 July 1997, p.150-2, TuD6.1]
[4] R.J. Mears, L. Reekie, S.B. Poole, D.N. Payne [*Electron. Lett. (UK)* vol.21 (1985) p.738-40]
[5] M. Shimitzu, H. Suda, M. Horiguchi [*Electron. Lett. (UK)* vol.23 (1987) p.768-9]
[6] P.R. Morkel, M.C. Farries, S.B. Poole [*Opt. Commun. (Netherlands)* vol.67 (1988) p.349-52]

[7] K. Arai, H. Namikawa, K. Kumata, T. Honda, Y. Ishii, T. Handa [*J. Appl. Phys. (USA)* vol.59 (1986) p.3430-6]

[8] H. Po et al [*Opt. Lett. (USA)* vol.20 (1995) p.578-80]

[9] H. Zellmer, A. Tunnermann, H. Welling [*Proc. Int. Conf. on Optical Amplifiers and Their Applications* Victoria, BC, Canada, 21-23 July 1997, p.251-2, WC7.1]

[10] J. Nilsson, J.D. Minelly, S. Taccheo, R. Paschotta, D.C. Hanna, A.C. Tropper [*Opt. Lett. (USA)* vol.23 (1998) p.355-7]

[11] F. Hakimi et al [*Opt. Lett. (USA)* vol.14 (1989) p.1060-1]

PART A: SILICA

CHAPTER A4

OPTICAL FIBRE MANUFACTURE

A4.1 Preparation and preform fabrication of silica optical fibres
A4.2 Drawing of silica optical fibres
A4.3 Loss of silica optical fibres
A4.4 Reliability of silica optical fibres

A4.1 Preparation and preform fabrication of silica optical fibres

K. Yoshida

June 1998

A INTRODUCTION

Silica optical fibres are in widespread use for optical telecommunications. These fibres result from volume production using chemical vapour deposition techniques (CVD) such as modified chemical vapour deposition (MCVD), vapour-phase axial deposition (VAD) or outside vapour deposition (OVD). Moreover, the function of optical amplification can be attached to an optical fibre, by doping rare-earth ions into its core glass. The rare-earth doped fibre then becomes an optical amplifier, or fibre laser. Among others, an erbium doped fibre (EDF) serves as a practical, optical amplifier at 1.55 μm. It is usually fabricated using a modification of the CVD technique.

Section B gives a brief explanation of the fabrication of glass and preform for silica optical fibres, and Section C describes rare-earth doped silica optical fibres.

B FABRICATION OF GLASS AND PREFORM FOR SILICA OPTICAL FIBRES

B1 Silica-Based Glass for Silica Optical Fibres

The silica optical fibre consists of a core made from silica-based glass, and a cladding made from pure silica glass or silica-based glass. The silica-based glass for the core includes a dopant for increasing the refractive index; the silica-based glass for the cladding includes a dopant for decreasing the refractive index. By way of illustration, FIGURE 1 presents dopant concentration versus refractive index [1]. Typical dopants used are GeO_2, TiO_2, Al_2O_3 and P_2O_5 for increasing the refractive index, and B_2O_3 and F for decreasing it. These dopants also allow adjustment of the thermal expansion and softening temperatures of glass. In reality, the limits of low-loss fibre fabrication have narrowed the options down to a core of GeO_2 doped silica and a cladding of F doped silica or pure silica-glass.

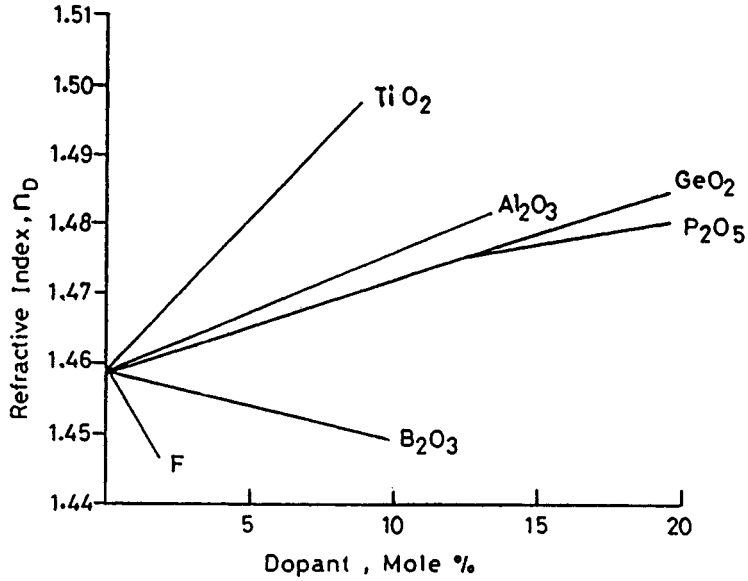


FIGURE 1 Refractive index of common dopants for silica (from [1]).

B2 Fabrication of Preform for Silica Optical Fibres

Fabrication of preforms can be accomplished using several techniques: MCVD [2], VAD [3], OVD [4] and plasma chemical vapour deposition (PCVD) [5], for example. Each method relies on CVD that produces glass from gaseous raw materials. By way of illustration, SiO_2-GeO_2 glass results from a gas mixture of $SiCl_4$-$GeCl_4$ under reaction according to EQNS (1), (2), (3) and (4). The gas constituents are varied to produce various glass compositions.

[oxidation]

$$SiCl_4 + O_2 = SiO_2 + 2Cl_2 \quad (1)$$

$$GeCl_4 + O_2 = GeO_2 + 2Cl_2 \quad (2)$$

[flame hydrolysis]

$$SiCl_4 + 2H_2O = SiO_2 + 4HCl \quad (3)$$

$$GeCl_4 + 2H_2O = GeO_2 + 4HCl \quad (4)$$

MCVD and PCVD are the processes that apply the oxidation reaction in a rotating silica-glass tube, on the inside wall of which fine glass particles of oxide (e.g. SiO_2, GeO_2) deposit in the form of soot. Subsequently, a traversing burner makes the soot layer consolidate into transparent glass. Glass layers, built up in large numbers, are subjected to intense heat so that the silica-glass tube collapses into a solid preform.

VAD and OVD apply the flame hydrolysis reaction and each includes two fabrication stages. The first stage of flame hydrolysis creates a porous body (called 'soot preform') and the second one makes the soot consolidate into a transparent glass preform. In the soot processes, OH^- impurities contained in the soot have to be removed. For this purpose, the soot is heat-treated in a chlorine or thionyl chloride-containing gas [6].

For the CVD, halides such as $SiCl_4$, $GeCl_4$ or $POCl_3$ are used as raw materials. Each halide has high vapour pressure as shown in FIGURE 2 [7]. The magnitude of each vapour pressure exceeds those of transition metal sources, a major cause of loss in an optical fibre. For example, taking $FeCl_3$, a source of Fe impurity ions, the pressure of any of the raw materials is as high as ten million to a billion times ($10^{8\text{-}10}$) that of $FeCl_3$. The significant differential vapour pressures ultimately eliminate transition metal impurities (Fe etc.) in the fabrication of glass by CVD. Thus, CVD is capable of creating high-purity optical fibres, and provides a route for removal of OH^- impurities. Consequently, CVD is judged to be ideally equipped for the fabrication of low-loss fibres.

B3 Novel Fabrication Processes for Silica Optical Fibres

Apart from the CVD-based methods, sol-gel techniques [8] and mechanically shaped preform (MSP) [9] have been proposed for fibre fabrication. However, these have yet to produce low-loss fibres. What have been recently proposed are hybridised processes: colloidal sol-gel processes [10,11], cold isostatic pressing processes (CIP) [12-16] and extrusion forming processes [17]. The hybridised process is one in which a preform is formed by overcladding a CVD-derived core rod with commercially available silica powder. On analysis, the CVD-derived core rod facilitates the production of low-loss fibres, while the commercial silica powder paves the way for less costly fibres.

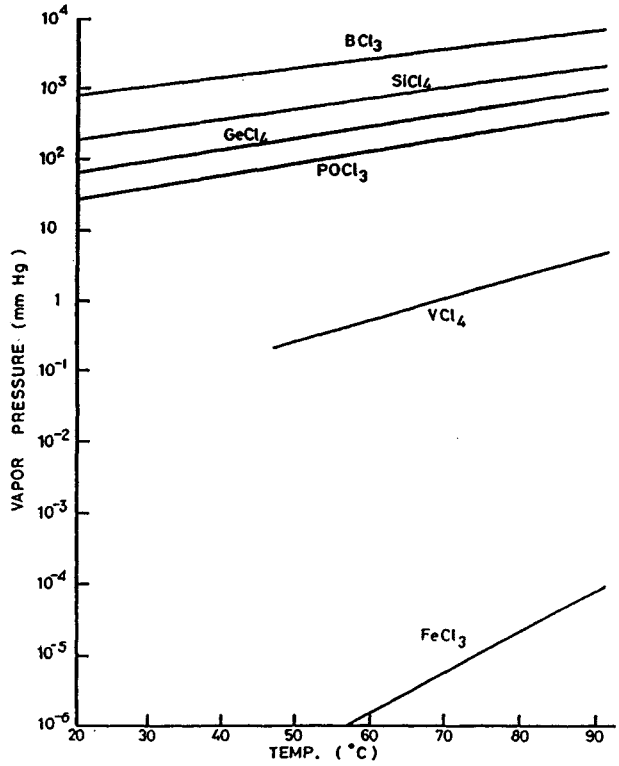


FIGURE 2 Relation of vapour pressures for metal halide additives and potential impurities (from [7]).

C FABRICATION OF GLASS AND PREFORM FOR RARE EARTH-DOPED SILICA OPTICAL FIBRES

C1 Silica-Based Glass for Rare Earth-Doped Silica Fibre

A rare-earth doped silica fibre consists of a core and cladding, with the core also doped with rare-earth ions (e.g. Er^{3+}, Nd^{3+}, Pr^{3+}). It has been found that higher concentrations of rare-earth ions incur clusters of rare-earth ions [18]. These clusters cause the characteristic degradation of optical amplification, called concentration quenching. Nevertheless, where there is some scheme to prevent the growth of clusters of rare-earth ions, high concentrations of rare-earth ions can be applied to provide amplification improvement. Arai et al [19] pointed out a host glass of Al_2O_3-SiO_2, P_2O_5-SiO_2, in which rare-earth ions are soluble enough to appreciably lessen clusters of rare-earth ions, and in turn high concentrations of rare-earth ions become possible. Much research into the host glass has since been carried out, and Miniscalco [20] gave a review of material-dependent properties influencing fibre amplifiers. In fact, it was reported that host glasses GeO_2-Al_2O_3-SiO_2 [21) and Al_2O_3-SiO_2 [22], used for erbium doped fibre (EDF), were proven to be receptive to high concentrations of Er^{3+}-doping and bring out high conversion efficiencies. Likewise it was reported that the Al_2O_3 content of Al_2O_3-SiO_2, which is easy to crystallise, could be made uncrystallisable by adding a small amount of P_2O_5, even with a high Al_2O_3 concentration [23]. Ainslie et al [24] elucidated the fact that Al_2O_3-P_2O_5-SiO_2, even if heavily doped with Er^{3+} or Nd^{3+}, would incur no growth of clusters of rare-earth ions. Thus, while the dopant GeO_2 can be used in silica optical fibres, P_2O_5 or/and Al_2O_3 is also frequently used as a dopant or a co-dopant with GeO_2 for heavy doping of rare-earth ions. Further details regarding the doping of silica fibres can be found in [25-35].

C2 Fabrication of Preform for Rare Earth-Doped Fibres

One of the simplest techniques for fabricating rare-earth doped fibre preforms refers to the rod-in-tube method, which has long been used because of its simplicity [36,37]. This method consists of two steps, to charge a silica-glass tube with core glass and to collapse the charged tube into a solid preform, and is still used as a technique to fabricate heavily Er^{3+}-doped fibres [38].

It would be preferable if rare-earth doped fibres could be fabricated by CVD, as silica optical fibres can be. Some organometallic compounds having a high vapour pressure were prepared [39], and were used for fibre fabrication [40,41], but they are not widely used. Research continues in this area.

Gas-phase doping processes can handle a solid rare-earth source itself. Poole et al [42] announced a modification of MCVD, followed by its alternative means, e.g. porous generator [43] and ampoule [44]. Meanwhile, a modification of the soot process was presented, i.e. sintering core soot subjected to vaporised compounds [45]. In the light of high doping concentrations, the flash-condensation technique was investigated [46].

The solution doping process soaks a porous body in a solution containing rare-earth compounds to dope rare-earth ions. This process was used to investigate the loss resulting from transition metal impurities [47-49], and recently has been the most commonly used method.

FIGURES 3 and 4 illustrate current general methods. FIGURE 3 starts off with a soot preform made in a VAD process. First, the soot is soaked in an alcoholic solution containing rare-earth halide, impregnated with the rare-earth compound, dried and consolidated into a transparent glass core rod. Finally, a cladding of glass is formed on the surface, where a rare-earth doped preform takes shape. FIGURE 4 refers to an MCVD-based method. The soot layer for the core is deposited at low temperature on the inside wall of a silica-glass tube, which is in turn soaked in an alcoholic solution of rare-earth halide, to make the soot layer impregnated with rare-earth material. After being dried, the silica tube is collapsed into a rare-earth doped preform. The CVD method is substantially capable of Al_2O_3 doping. However, the Al_2O_3 source for doping, aluminium chloride, being relatively low in vapour pressure, is often applied in the form of solution doping, in which aluminium nitrate can also be used.

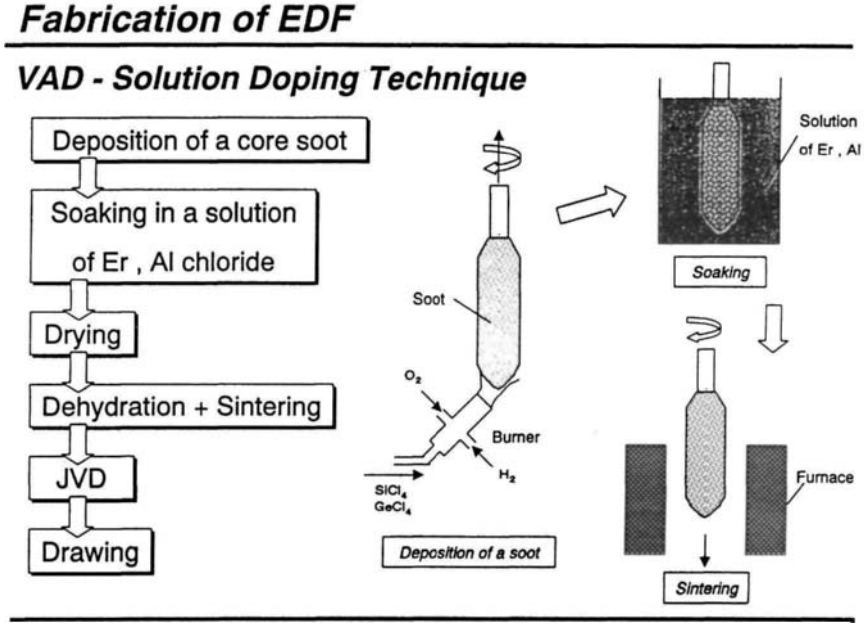


FIGURE 3 VAD-solution doping technique for fabrication of EDF preform.

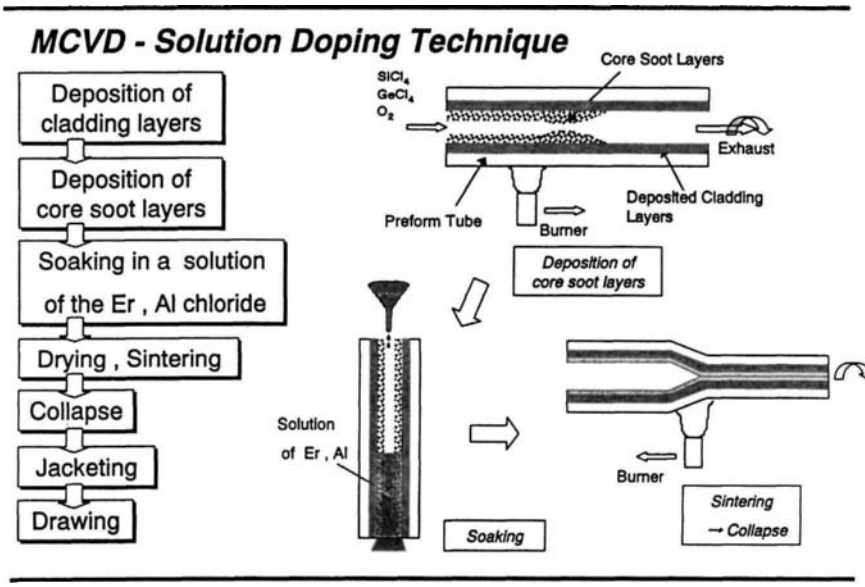


FIGURE 4 MCVD-solution doping technique for fabrication of EDF preform.

Meanwhile, a few more techniques have been proposed for solution doping, for example the aerosol delivery technique [50,51] using an aerosol as a carrier of the doping source to feed into the reaction zone, and the sol-gel technique [52] for forming a rare-earth glass layer on the inside wall of a silica-glass tube by dipcoating.

D CONCLUSION

Current silica optical fibres and rare-earth doped fibres have been reviewed regarding their technical progress, with a focus on the material and production technology.

Silica glass fibres are under volume-production, and their production method seems to have been finalised. However, less costly production means continue to be researched far and wide. For rare-earth doped fibres, the Er^{3+}-doped fibre has come into practical use and is fabricated by solution doping. Even more recently, research has continued the improvement of fibres from the aspects of fibre material and configuration. Also, several technical issues have yet to be resolved, namely practical high doping methods and cost reduction.

REFERENCES

[1] H. Murata [*Handbook of Optical Fibers and Cables* (Marcel Dekker, 1996) p.18]
[2] J.B. MacChesney, P.B. O'Connor, F.V. DiMarcello, J.R. Simpson, P.D. Lazay [*Proc. 10th Int. Congress on Glass* Kyoto, Japan, vol.6 (Ceramics Soc., Japan, 1974) p.40-5]
[3] T. Izawa, N. Inagaki [*Proc. IEEE (USA)* vol.68 (1980) p.2047-54]
[4] A.J. Morrow, A. Sarker, P.C. Schultz [*Optical Fibre Communications, vol.1, Fiber Fabrication* Ed. T. Li (Academic Press, New York, 1985) p.65-95]
[5] P. Geittner, H. Lydtin [*Philips Tech. Rev. (Netherlands)* vol.44 (1989) p.241-9]
[6] K. Chida, F. Hanawa, M. Nakahara, N. Inagaki [*Electron. Lett. (UK)* vol.15 (1979) p.835]
[7] P.C. Schultz [in *Fiber Optics* Eds. B. Bendow, S.S. Mitra (Plenum Press, New York, 1979) p.3-31]
[8] S. Shibata [*J. Non-Cryst. Solids (Netherlands)* vol.178 (1994) p.272-83]
[9] R. Dorn et al [*J. Lightwave Technol. (USA)* vol.9 (1991) p.709-14]

[10] J.B. MacChesney, D.W. Johnson Jr., D.A. Fleming, F.W. Walz [*Electron. Lett. (UK)* vol.23 (1987) p.1005-7]
[11] J.B. MacChesney et al [*Electron. Lett. (UK)* vol.33 (1997) p.1573-4]
[12] K. Yoshida, T. Satoh, N. Enomoto, H. Hihara, T. Yagi, M. Oku [*Electron. Lett. (UK)* vol.32 (1996) p.242-3]
[13] K. Yoshida, T. Satoh, N. Enomoto, T. Yagi, H. Hihara, M. Oku [*Glastech. Ber. (Germany)* vol.69 (1996) p.412-6]
[14] K. Yoshida, T. Satoh, N. Enomoto, T. Yagi, H. Hihara, M. Oku [*J. Ceram. Soc. Jpn. (Japan)* vol.104 (1996) p.501-5]
[15] K. Yoshida, T. Satoh, H. Hihara, M. Oku [*J. Ceram. Soc. Jpn. (Japan)* vol.104 (1996) p.846-9]
[16] K. Yoshida, T. Satoh, N. Enomoto, T. Yagi, H. Hihara, M. Oku [*Electron. Commun. Jpn. (USA)* vol.80 (1997) p.7-15]
[17] K. Yoshida, T. Yagi [*J. Ceram. Soc. Jpn. (Japan)* vol.104 (1996) p.602-7]
[18] K. Arai, H. Namikawa, K. Kumata, Y. Ishii, H. Tanaka, I. Iida [*Jpn. J. Appl. Phys. (Japan)* vol.22 (1983) p.L397-9]
[19] K. Arai, H. Namikawa, K. Kumata, T. Honda, Y. Ishii, T. Handa [*J. Appl. Phys. (USA)* vol.59 (1986) p.3430-6]
[20] W.J. Miniscalco [*J. Lightwave Technol. (USA)* vol.9 (1991) p.234-50]
[21] S.P. Craig-Ryan, J.F. Maaicott, B.J. Ainslie, R. Wyatt [*Technical Digest of ECOC'90 European Conf. on Optical Communications* Amsterdam, 1990 (1990) p.571-4]
[22] Y. Kimura, M. Nakazawa [*Electron. Lett. (UK)* vol.28 (1992) p.1420-2]
[23] J.R. Simpson, J.B. MacChesney [*Electron. Lett. (UK)* vol.19 (1983) p.261]
[24] B.J. Ainslie, S.P. Craig, S.T. Davey, B. Wakefield [*Mater. Lett. (Netherlands)* vol.6 (1988) p.139-44]
[25] R.I. Laming, D.N. Payne, F. Meli, G. Grasso, E.J. Tarbox [*Proc. Top. Meet. Opt. Amp. & Appl.* Monterey, CA, 6-8 Aug. 1990 (1990) MB2]
[26] R.I. Laming, J.E. Townsend, D.N. Payne, F. Meli, E.J. Tarbox [*IEEE Photonics Technol. Lett. (USA)* vol.3 (1991) p.253-5]
[27] J.L. Wagener, P.F. Wysocki, M.J.F. Digonnet, H.J. Shaw [*Opt. Lett. (USA)* vol.19 (1994) p.347-9]
[28] P.F. Wysocki, J.L. Wagener, M.J.F. Digonnet, H.J. Shaw [*Proc. SPIE (USA)* vol.1789 (1992) p.66-79]
[29] P. Myslinski, D. Nguyen, J. Chrostowski [*J. Lightwave Technol. (USA)* vol.15 (1997) p.112-20]
[30] T. Kashiwada, K. Nakazato, M. Ohnishi, H. Kanamori, M. Nishimura [*Proc. 4th Topical Meeting on Optical Amplifiers and Their Applications* Yokohama, Japan, 4-6 Jul. 1993, MA6]
[31] C.G. Atkins, J.F. Massicott, J.R. Armitage, R. Wyatt, B.J. Ainslie, S.P. Craig-Ryan [*Electron. Lett. (UK)* vol.25 (1989) p.910-1]
[32] J.E. Townsend, W.L. Barnes, K.P. Jedrzejewski, S.G. Grubb [*Electron. Lett. (UK)* vol.27 (1991) p.1958-9]
[33] B.N. Samson, L. Dong, J.P. de Sandro, J.E. Caplen [*Electron. Lett. (UK)* vol.34 (1998) p.111-3]
[34] Y. Kimura, M. Nakazawa [*Appl. Phys. Lett. (USA)* vol.53 (1988) p.1251-3]
[35] J.M. Battiato, T.F. Morse, R.K. Kostuk [*IEEE Photonics Technol. Lett. (USA)* vol.9 (1997) p.913-5]
[36] T. Yamashita, S. Amano, I. Masuda, T. Izumitani, A. Ikushima [*Conf. Lasers and Electro-Optics* Anaheim, CA, 25-29 Apr. 1988 (Optical Society of America, 1988) TH2]
[37] E. Snitzer, R. Tumminelli [*Opt. Lett. (USA)* vol.14 (1989) p.757-9]
[38] M.R.X. de Barros, G. Nykolak, D.J. DiGiovanni, A. Bruce, W.H. Grodkiewicz, P.C. Becker [*IEEE Photonics Technol. Lett. (USA)* vol.8 (1996) p.761-3]
[39] R. Tumminelli, E. Snitzer [US Patent no.4,826,288]
[40] R. Tumminelli, F. Hakimi, J. Haavisto [*Opt. Lett. (USA)* vol.16 (1991) p.1098-100]
[41] P.L. Bocko [*Proc. OFC'89, Technical Digest* Houston, USA, Feb. 1989, TUG2]

[42] S.B. Poole, D.N. Payne, M.E. Fermann [*Electron. Lett. (UK)* vol.21 (1985) p.737-8]
[43] B.J. Ainslie, S.P. Craig, S.T. Davey [*Mater. Lett. (Netherlands)* vol.5 (1987) p.143-6]
[44] J.B. MacChesney, J.R. Simpson [*Proc. OFC'85* (1985) WH5 p.100]
[45] W.H. Dumbaugh, P.C. Schultz [US Patent no.1864113 (1975)]
[46] A.L.G. Carter, S.B. Poole, M.S. Sceats [*Electron. Lett. (UK)* vol.28 (1992) p.2009-11]
[47] P.C. Schultz [*J. Am. Ceram. Soc. (USA)* vol.57 (1974) p.309-13]
[48] J.E. Townsend, S.B. Poole, D.N. Payne [*Electron. Lett. (UK)* vol.23 (1987) p.329-31]
[49] T. Gozen, Y. Kikukawa, M. Yoshida, H. Tanaka, H. Shintani [*Proc. OFC'88* New Orleans, Jan. 1988 (1988) WQ1]
[50] T.F. Morse, A. Kilian, L. Reinhart, W. Risen Jr., J.W. Cipolla Jr. [*J. Non-Cryst. Solids (Netherlands)* vol.129 (1991) p.93-100]
[51] T.F. Morse, L. Reinhart, A. Kilian, W. Risen Jr., J.W. Cipolla Jr. [*Proc. SPIE (USA)* vol.1171 (1989) p.72-9]
[52] D.J. DiGiovanni, J.B. MacChesney [*Proc. OFC'91* San Diego, California, 18-22 Feb. 1991 (1991) WA2 p.62]

A4.2 Drawing of silica optical fibres

P.W. Turner and L. Dong

July 1998

A INTRODUCTION

The drawing of optical fibres from silica preforms has, over a short period of time, progressed from the laboratory to become a manufacturing process capable of producing millions of kilometres of telecommunications fibre a year. The basic components and configuration of the drawing tower have remained unchanged for many years. The preform is held in a chuck which has movement in both the x and y planes, and is mounted on a precision feed assembly that lowers the preform into the drawing furnace at a predetermined speed. The fibre is drawn from the molten zone of the preform down the tower to a capstan and drum which controls the fibre diameter. During the drawing process, immediately below the furnace is a non-contact device that measures the diameter of the fibre, the measured diameter is compared to a set diameter and an output signal is generated that is proportional to the difference. The output signal is then used to control the speed of the capstan, speeding up to reduce the diameter or slowing down to increase the fibre diameter. An in-line coating is applied to maintain the fibre strength. FIGURE 1 shows, in schematic form, a fibre drawing tower [1]. Draw towers are commercially available, ranging in height from 3 m to greater than 20 m, with the tower height increasing as the draw speed increases. The increased height is needed to allow the fibre to cool sufficiently before entering the coating applicator, although forced air cooling of the fibre is commonplace in a manufacturing environment.

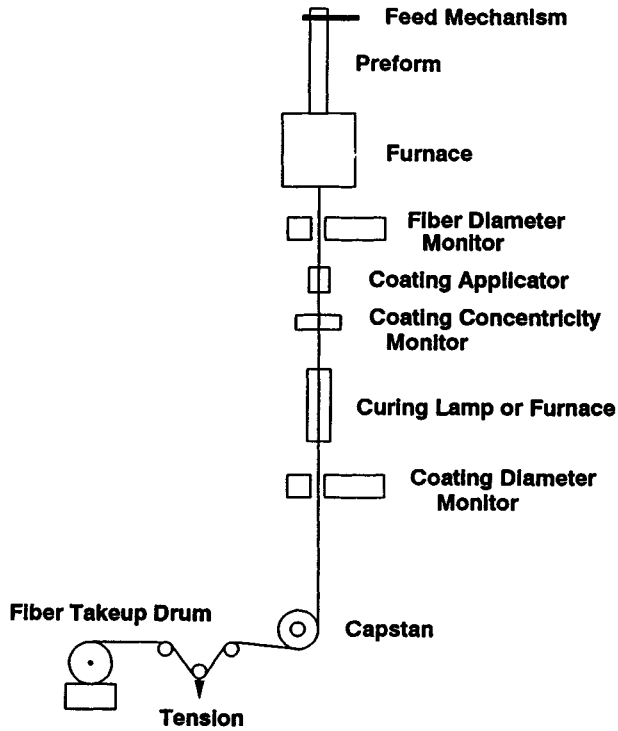


FIGURE 1 Schematic diagram of a typical silica fibre drawing tower.

B HEAT SOURCES

Silica based fibre preforms require heating to temperatures in excess of 2000°C. The preform is suspended in a vertical feed apparatus above the heat source and placed so that the end of the preform protrudes below the hot zone. When the glass reaches a temperature at which it softens to a viscosity of 10^3 to 10^5 Pa s it begins to neck down and elongate. As elongation continues toward the desired diameter, the resulting fibre is drawn down the tower to the coating apparatus and capstan. Any thermal treatment of a glass material is likely to change the glass structure. There is no exception for the fibre drawing process. Stress in the optical fibre from the drawing process can affect the refractive index profile of optical fibre and can be significant in some fibres [2].

B1 Oxyhydrogen Torch

Used in the early stages of fibre drawing development, the oxyhydrogen torch is the simplest heat source but the least desirable as it introduces large variations in fibre diameter due to the turbulence of the flame. Typically four torches would be placed at equal intervals around the preform with water cooling to protect the torches themselves. Heating is obtained by conduction from the flame to the glass.

B2 CO_2 Laser

A CO_2 laser operating around 10.6 microns is a clean and controllable energy source successfully used in laboratory experiments [3]. Energy from the laser is steered via appropriate mirrors to a conical reflector through which the preform passes. The radiation is focused and absorbed by the surface of the preform and its interior is heated by conduction. Fibre diameters can be well controlled but this heat source has found only limited laboratory application as furnaces provide considerably lower cost to energy ratios with comparable diameter control.

B3 Resistance Furnace

A resistance furnace is perhaps the most common and economical heating source used in a fibre drawing tower. A cylindrical furnace with graphite or tungsten elements provides heating to the preform by blackbody radiation. These elements must be surrounded by an inert gas such as nitrogen or argon to prevent oxidation. Gas flow and control is critical to prevent variations in the diameter of the fibre. In addition, the high temperature of the elements may lead to contamination of the preform surface which can weaken the fibre.

B4 Induction Furnace

An induction furnace provides precise clean heating through RF energy which is inductively coupled to a zirconia succeptor ring. This type of furnace is cleaner than the graphite resistance type and is capable of continuous running for several months. It also has the advantage that it does not require a protective inert atmosphere and consequently the preform is drawn in a turbulence-free environment. These advantages result in high strength fibres with good diameter control [4].

C DIAMETER CONTROL

A number of non-contact methods of diameter measurement can be applied to measure fibre diameter [1]. These include shadowgraph methods, laser scanning techniques, lateral interferometry and light scattering techniques. To obtain precise control of the fibre diameter, the deviation signal between the set diameter and measured diameter is fed into the diameter control system. In order to cope with high drawing speeds, sampling rates as high as one thousand times per second are used [5]. The diameter control is strongly affected by the gas flow in the drawing furnace and is less affected by the furnace temperature variation. The furnace gas flow can be used to achieve suppression of fast diameter fluctuations. This is used in combination with drawing speed control to achieve suppression of both fast and slow diameter fluctuations [6]. Current manufacturing processes are capable of producing several hundreds of kilometres of fibre with diameter variations of +/- one micron.

It has also been demonstrated that the fibre diameter can be made to vary in a predetermined fashion for various applications. For example, fibre tapers extending uniformly over several kilometres of fibre have been applied to soliton control [7,8].

D FIBRE COATING

A fibre coating is primarily used to preserve the strength of a newly drawn fibre and therefore must be applied immediately after the fibre leaves the furnace. The fibre coating apparatus is typically located immediately below the diameter measurement gauge to minimise any damage or contamination of the pristine fibre leaving the furnace. A wide variety of coating materials have been applied; however conventional, commercial fibre generally relies on a UV curable polymer acrylate as the primary coating. Coating thickness is typically 50 - 100 microns. Subsequent coatings can then be applied for specific purposes.

A dual coating is often used with an inner primary coating that is soft and an outer, secondary coating which is hard. This ratio of low to high elastic modulus can minimise stress on the fibre and reduce microbending loss. Coating is also one of the limiting factors in the speed of fibre drawing.

Alternative coatings include hermetic coatings of a low melting temperature metal, ceramics or amorphous carbon [9-11]. These can be applied in-line before the polymeric coating. Metallic coatings are applied by passing the fibre through a molten metal while ceramic or amorphous coatings utilise an in-line chemical vapour deposition reactor.

E CONCLUSION

The drawing of silica optical fibre is a mature process which over the years has been developed to provide high reproducibility. Millions of kilometres of fibre now circle the globe and in only a few decades their production has grown from a laboratory procedure to a major worldwide commercial activity. Nonetheless, research activities still exist, with current interest in novel coatings and speciality fibres for newly emerging applications.

REFERENCES

[1] A. Cherin [*An Introduction to Optical Fibres* (McGraw-Hill, 1983) p.173-81]
[2] I. Camlibel, D.A. Pinnow, F.W. Dabby [*Appl. Phys. Lett. (USA)* vol.26 (1975) p.185]
[3] R.F. Jaeger [*Ceram. Bull. (USA)* vol.53 (1976) p.270]
[4] F.V. DiMarcello, A.C. Hart [*Electron. Lett. (UK)* vol.14 (1978) p.578]
[5] M.R. Hadley, D.N. Payne, R.J. Mansfield [*Proc. Sixth European Conf. on Optical Communications* York, UK, 16-19 Sept. 1980 (IEE, London, UK, 1980) p.53-6]
[6] K. Imoto, M. Sumi, G. Toda, T. Suganuma [*J. Lightwave Technol. (USA)* vol.7 (1989) p.115]
[7] V.A. Bogatyrjov, M.M. Bubnov, S.L. Semenov, A.A. Sysoliatin [*Meas. Sci. Technol. (UK)* vol.5 (1994) p.1370]
[8] D.J. Richardson, R.P. Chamberlin, L. Dong, D.N. Payne [*Electron. Lett. (UK)* vol.31 (1995) p.1681]
[9] J. Wysocki [*Appl. Phys. Lett. (USA)* vol.34 (1979) p.17]
[10] K.J. Beales, D.M. Cooper, W.J. Duncan, J.D. Rush [*Proc. OFC'84* (Optical Society of America, USA, 1984) paper W15]
[11] P.J. Lemaire, K.S. Kranz, K.L. Walker, R.G. Huff, F.V. DiMarcello [*Electron. Lett. (UK)* vol.24 (1988) p.1323]

A4.3 Loss of silica optical fibres

A. Bruce

August 1998

A INTRODUCTION

Silica based glasses are transparent from the near-ultraviolet to the mid-infrared range of the electromagnetic spectrum. Loss of silica fibre is now close to the theoretical intrinsic limits in the 1.3 and 1.5 micron telecommunications bands as shown in FIGURE 1 [1]. Such fibres are now routinely obtained [2,3]. Intrinsic limits are dominated by scattering and multiphonon absorption, as discussed earlier in this book [4]. In this Datareview, the extrinsic loss mechanisms which may affect a fibre are examined. Any increased attenuation can have a disproportionately high impact on system performance if it pushes the operation of fibre components such as amplifiers and detectors out of their normal operating range. Optical reliability thus depends on the prevention and management of all loss inducing mechanisms.

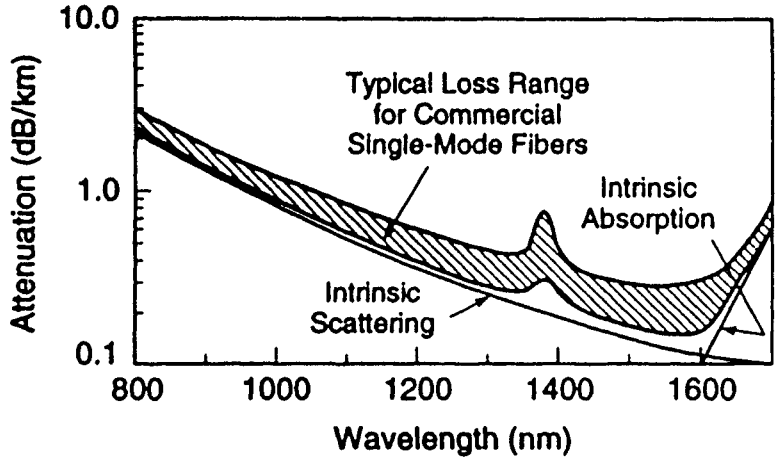


FIGURE 1 NIR attenuation of high-silica, single-mode telecommunication fibres.

B DOPANTS

Pure fused silica consists of oxygen ions with tightly bound electrons resulting in a relatively large energy gap between the valence and conduction bands of about 8.9 eV. To excite these electrons requires ultraviolet photons of wavelength approximately 0.14 microns which defines the UV transmission edge of pure silica fibres. In practice however, a variety of dopants are incorporated into the glasses which alter the UV transparency through the creation of defects or oxygen deficient centres as well as through a change in the intrinsic absorption. FIGURE 2 shows the effect in the UV of several dopants, and FIGURE 3 shows their influence in the NIR and on the intrinsic IR edge [5,6].

For fibres operating near 1.3 and 1.5 microns, GeO_2 is the dopant of choice, producing an acceptable low loss option. However, there is a significant contribution to loss from the GeO defect in the UV [7]. The strength of this absorption depends not only on the germanium doping level and the selection of co-dopants but also on the processing conditions used [8]. In some speciality fibres which contain higher

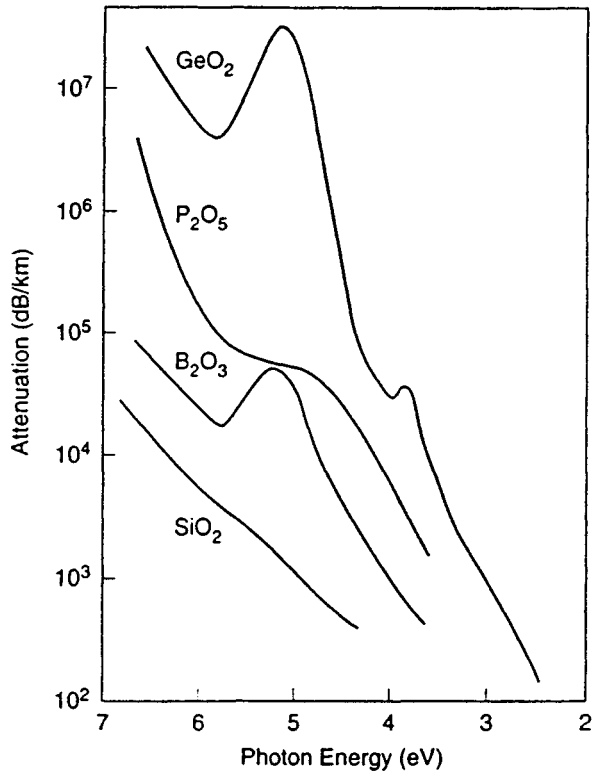


FIGURE 2 UV attenuation of doped SiO_2 glass, including intrinsic and defect absorptions (from [6]).

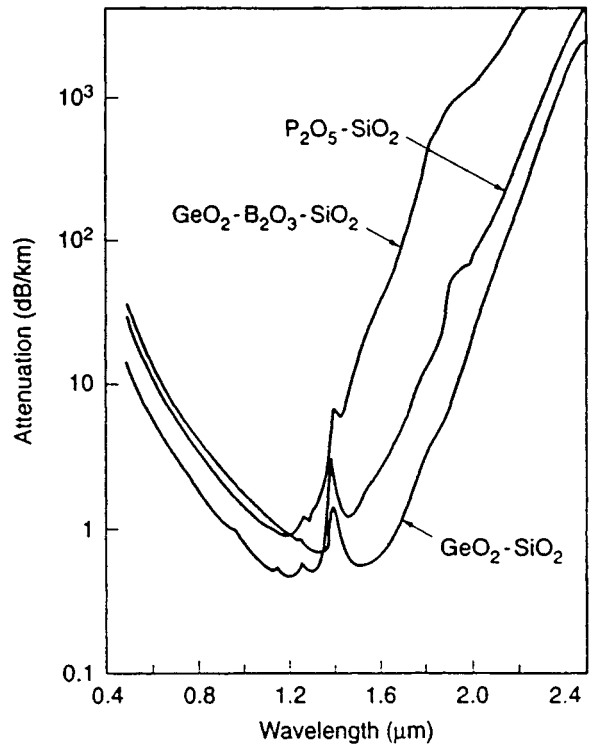


FIGURE 3 NIR attenuation of silica fibres illustrating the effects of different dopants on the intrinsic IR edge (from [5]).

levels of GeO_2, substantial loss at 1550 nm has been observed [9]. This is attributed to the concentration dependence of the defect edge and enhanced scattering due to the higher refractive index differences at the core/clad interface.

C BENDING

As shown in FIGURE 4, macro- and microbending losses manifest themselves as rapid increases in attenuation beyond critical wavelengths [10]. Both are associated with changes in optical mode confinement due to stress-induced changes in refractive index profiles as a result of fibre bending. Dispersion-shifted, single-mode fibre designs are particularly sensitive to these effects. Macrobending is easily envisioned, while microbending is characterised by small amplitude variations of the order of a nanometre with a periodicity of the order of a millimetre. Microbending can result from the expansion mismatches between cable components. Bend loss sensitivity can be reduced by the prudent selection of fibre and cable design.

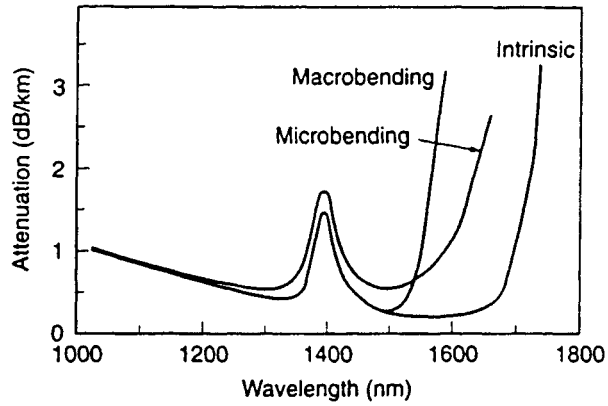


FIGURE 4 Phenomenological illustration of the effects of macro- and microbending on the attenuation of dispersion-shifted single-mode fibres (from [10]).

D MOISTURE

Several factors can result in increased fibre attenuation over a system lifetime and of particular concern is hydrogen and/or moisture penetration into the silica fibre. When a fibre is exposed, moisture can diffuse from the surface to the core of a fibre with an attendant increase in attenuation at the telecommunications wavelengths due to overtone and combination bands associated with the OH^- vibration. This diffusion is relatively slow and can be minimised with the appropriate selection of coatings and packaging. Dopant selection is also a factor, with GeO_2 less susceptible to hydrolysation that P_2O_5. Hydrogen diffusion is more insidious because of its small molecular size and slow reactivity under normal conditions. Diffusion occurs rapidly and is difficult to prevent. FIGURE 5 shows the result of an accelerated test for hydrogen-induced absorption in a standard SiO_2-GeO_2 fibre [11]. The effect is quite substantial and includes

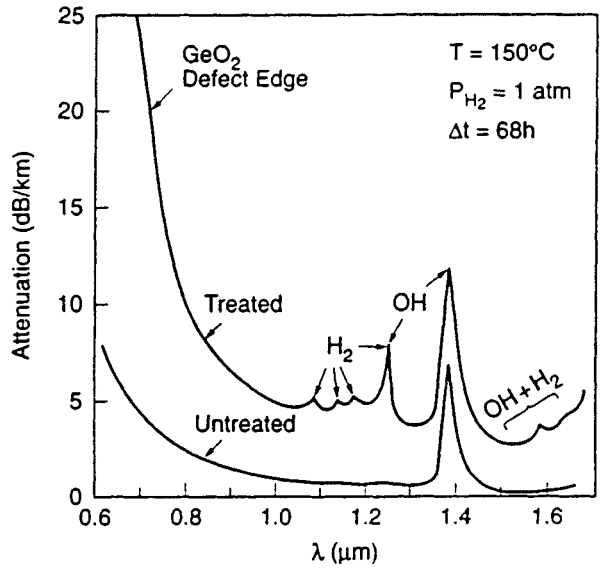


FIGURE 5 Increased fibre attenuation resulting from the exposure of an SiO_2-GeO_2 core fibre to hydrogen at 150°C for 68 hr (from [11]).

absorption due to hydrogen and hydroxyl reaction products. Some hermetic coatings, including amorphous carbon, can limit hydrogen diffusion. These are recommended for use of silica fibre in environments conducive to hydrogen generation. Sources of hydrogen can include polymeric cabling materials and electrolytic reactions involving power supplies and seawater.

E RADIATION

Natural background radiation is sufficient to create defect centres in silica optical fibre which contribute to optical loss. Natural radiation, which is approximately 0.1 to 1 rad/year, can be sufficient to produce significant degradation over system lifetimes. Radiation 'hot spots' on the ocean floor can also be a problem for submarine cables. Standard dopants including P_2O_5 and GeO_2 have been identified as progenitors of such defects; however even pure undoped silica is not immune. Tests done on SiO_2-GeO_2 and SiO_2-GeO_2-P_2O_5 fibres before and after exposure to a ^{60}Co gamma ray source showed the fibre without P_2O_5 to be somewhat more resistant. A dosage of 10^4 rad resulted in a loss increase from 0.8 to 8.0 dB/km at 1.5 microns [12]. At present, there is no complete solution to radiation damage. Radiation hardness is enhanced by avoiding the more-sensitive dopants and shielding some types of radiation by the cable structure.

F CONCLUSION

Silica fibre technology has reached maturity with fibre losses as low as the intrinsic limits. Extrinsic sources of loss include the effect of dopants, bending, moisture and radiation resulting in additional attenuation. However silica fibres currently meet systems needs and their potential is far from exhausted.

REFERENCES

[1] A. Bruce [in *Infrared Fibre Optics* Eds. J.S. Sanghera, I.D. Aggarwal (CRC Press, 1998) ch.2 p.32]

[2] R. Csencsits, P.J. Lemaire, W.A. Reed, D.S. Shenk, K.L. Walker [*Proc. Tech. Digest Conf. Opt. Fiber Comm.* New Orleans, USA, 23-25 Jan. 1984 (Opt. Soc. America, Washington DC, USA, 1984) p.54-5]

[3] H. Yokata et al [*Proc. Tech. Digest Conf. Opt. Fiber Comm.* (Opt. Soc. America, Washington DC, USA, 1986) p.11]

[4] S. Sakaguchi [Datareview in this book: *A1.2 Intrinsic scattering losses of silica glass*]

[5] H. Osanai et al [*Electron. Lett. (UK)* vol.12 (1976) p.549]

[6] N. Shibata [PhD Thesis, Nagoya University, Japan, 1983]

[7] V.B. Neustruev [*J. Phys. Condens. Matter (UK)* vol.6 (1994) p.6901]

[8] L. Dong, J. Pinkstone, P.St.J. Russell, D.N. Payne [*J. Opt. Soc. Am. B (USA)* vol.11 (1994) p.2106]

[9] S.T. Davey, D.L. Williams, D.M. Spirit, B.J. Ainslie [*Proc. SPIE (USA)* vol.1171 (1989) p.181]

[10] D. Marcuse [*Light Transmission Optics* (Van Nostrand Reinhold, New York , 1982)]

[11] A. Tomita, P.J. Lemaire [*Electron. Lett. (UK)* vol.21 (1985) p.71]

[12] H.Itoh, Y. Ohmori, M. Nakahara [*J. Lightwave Technol. (USA)* vol.4 (1986) p.473]

A4.4 Reliability of silica optical fibres

M.J. Matthewson

May 1998

A INTRODUCTION

The total length of silica optical fibre now installed around the world measures in the tens of Gm, the majority of it being for telecommunications applications. While the fibre has proved reliable so far, with most failures being caused by external factors such as 'dig-ups' [1], the huge capital investment involved requires that long term reliability be treated as a serious issue.

FIGURE 1 shows a Weibull probability plot of the strength distribution typical for silica fibre specimens that are several metres in length. The distribution shows a narrow high-strength mode that corresponds to the intrinsic strength of the material. For long enough specimens, a broad low-strength mode is observed which is caused by the presence of extrinsic defects that can be introduced at any stage during manufacture and deployment. Both parts of the distribution can have an impact on reliability.

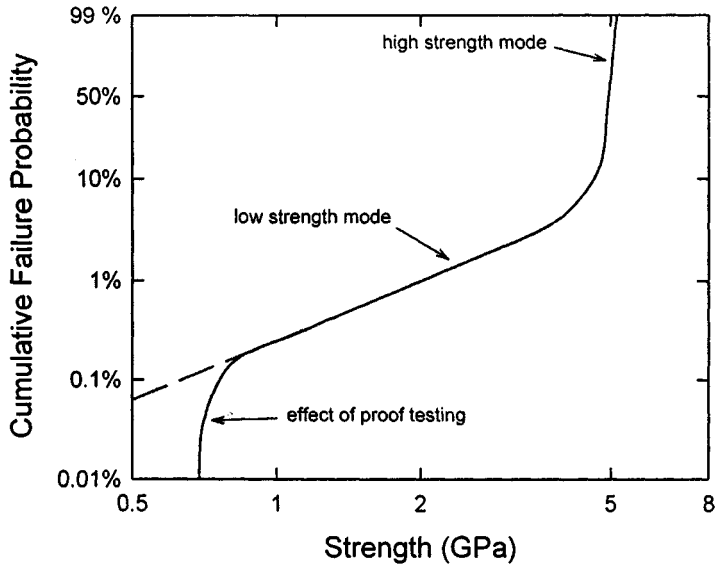


FIGURE 1 Weibull probability plot of the strength distribution typical of specimens several metres in length, showing both the high and low strength modes and the effect of truncation of the low strength mode by proof testing.

B SUBCRITICAL CRACK GROWTH

The weakest flaws in the fibre can lead to delayed failure due to the phenomenon of subcritical crack growth, also known as fatigue. While such flaws do not fail instantaneously under load, they can slowly extend under the combined influence of applied stress and environmental moisture until they reach a critical size, causing failure. For a specimen of initial strength σ_i, the time to failure, t_f, under a static applied load, σ_a, is given by [2]:

$$t_f = B\frac{\sigma_i^{n-2}}{\sigma_a^n} \quad (1)$$

where B and n are fatigue parameters that are determined by accelerated laboratory testing. EQN (1) is then reinterpreted to make reliability predictions with t_f now representing the service life, σ_a the maximum service stress and σ_i the starting strength of the weakest expected flaw. The value of σ_i is controlled by proof testing which removes the weakest defects thus truncating the low strength mode of the strength distribution (see FIGURE 1). However, continued crack growth during unloading from the proof stress means that flaws weaker than the proof stress can survive though such flaws will be rare. Griffioen [3] examines several published models for reliability and proposes a unified model of which the earlier works are particular cases.

The accepted value for n is around 20 for the high strength material but there is considerable variability in the published values, especially for the low-strength material for which values of between 10 and 40 have been reported [4]. Reported values for B show even more variability with accepted values lying between about 10^{-8} and 10^{-5} GPa^2 s.

EQN (1) is derived assuming sharp, stress-free cracks that extend with a power law dependence on stress. These assumptions are hard to justify. In particular, weak defects can have residual thermal or mechanical stresses. 'Real' weak defects are hard to study because of their low frequency and random positions. They have generally been modelled by inducing artificial defects by, for example, abrading the fibre (e.g. [5]) or deliberately applying particulate contaminants to the surface of the fibre preform (e.g. [6]). In general it is found that EQN (1) is conservative in that the weak defects often increase their strength with time [7,5], perhaps due to blunting of the crack tip. However, in a study of flaws induced by indentation, in a narrow region of behaviour the residual stress discontinuously reduced the strength due to delayed nucleation of cracks [8].

Another difficulty with EQN (1) is its assumption of power law crack growth kinetics. A power law is used for mathematical convenience but more physically reasonable models that have an exponential dependence of growth rate on stress predict substantially shorter lifetimes [9,10]; the power law may therefore be unrealistically optimistic.

In summary, considerable progress on modelling weak defects has been made in the last decade. However, the details of the nature of natural defects and their influence on reliability are still poorly understood. The complex mathematical theories applied to fibre reliability describe very simple, ideal defects and are in advance of our understanding of the nature of the natural defects themselves. Further, the paucity of published field data quantifying failure rates, service stresses and environments does not permit adequate comparison of the modelling with field experience.

C ZERO STRESS AGING

The subcritical crack growth model that results in EQN (1) predicts no change in strength if no stress is applied. However, the strength of silica fibre does indeed change in time even in the absence of an applied stress. Weak defects, described in Section B, are reduced in severity by zero stress aging [7,5] with few exceptions [8]. However, high strength fibre (the high strength mode in FIGURE 1) can exhibit severe degradation upon zero stress aging.

High-strength silica fibre is 'pristine' and essentially flaw-free [11]. In moist environments this fibre does exhibit subcritical crack growth, though in this case the 'cracks' at least start at atomic dimensions. However, except for applications in which only short lengths of fibre are used, this behaviour does not

represent a reliability concern because the occasional weak defects will be strength controlling. For those applications that do only use short lengths (a few metres), the subcritical crack growth model (EQN (1)) can be used but with values for the fatigue parameters, B and n, that are appropriate for the high strength material.

The zero stress strength degradation is more of a concern because the strength can degrade to levels where the fibre becomes too fragile to handle for making connections or repairs (less than about 2 to 3 GPa). While such strengths are substantially higher than the occasional weak defects (with strengths near the proof stress) the strength loss is widespread, not localised, and would require replacement of the fibre rather than a repair.

Zero stress aging is now understood to be caused by roughening of the fibre surface produced by corrosion by moisture [12]. This roughness behaves like pits which locally concentrate the stress. While originally thought to be due to dissolution of silica, a perhaps more accurate description is reactive diffusion of water into silica forming a rough diffusion front behind which a gel layer forms [12]. Zero stress aging has been observed to occur in bare as well as polymer coated fibre [13]; it occurs both in humid environments (e.g. 85°C, 85% humidity [14]) and on the time scale of a few years in room temperature water [15]. The degradation can be slowed or delayed by incorporating colloidal silica powder in the polymer coating which presumably acts sacrificially [16]. Some polymer coatings can delay the onset of the aging degradation and it has been proposed that this effect is caused by 'passivation' of the glass surface. However, fibres with such aging resistant coatings still exhibit subcritical crack growth and so are still reacting with moisture. The exact mechanism by which the coating influences aging is not properly understood.

D MEASUREMENT TECHNIQUES

The strength of silica fibre must be measured in order to characterise the strength, stress distribution and stress corrosion (fatigue) behaviour. Gripping the fibre is an important issue since preferential failure can occur at the grips. Several techniques have been developed. The conceptually simplest technique is uniaxial tension in which the fibre ends are gripped by wrapping several times around capstans. This technique is suitable for testing specimens up to several metres in length. Two-point flexure, in which the fibre is bent into a 'U' shape between two platens, enables testing of many fibres simultaneously but has a very short effective test length. It is therefore not useful for looking at long-length strength distributions but is helpful when studying environmental and coating effects, for example. These and other techniques are reviewed in detail elsewhere [17]. A technique worthy of particular mention is a long length continuous tester [18] which involves sequentially stressing 20 metre lengths of fibre. However, the fibre is only loaded up to a given relatively low stress and most of the lengths do not fail; only the occasional weak defect causes failure, thus requiring restarting of the equipment. The results of this test provide statistics on the flaws that just pass the proof test, information which is an important input parameter for lifetime models. Also, this test provides information on the distribution of flaws on a preform and so can help in optimisation of the preform preparation process.

E HERMETIC COATINGS

The reliability concerns described above are all dependent on ambient moisture having access to the fibre surface. Application of a hermetic coating will therefore remove any time dependence of strength. Hermetic coatings generally fall into two categories: metals, usually applied by freezing from the melt, and inorganic compounds (such as carbon and nitrides) typically deposited from the vapour phase. Such coatings are more expensive than the polymers and can add significant microbending loss, especially for the freeze-coated metals. For these reasons, hermetic coatings are usually only used in relatively short

lengths for critical applications where the fibre experiences a harsh environment and where optical loss is not a crucial parameter.

F CONCLUSION

Recent advances have given new insight into the processes that lead to fatigue and aging in silica fibres. Detailed mathematical models for making reliability predictions have been developed. However, the fundamental behaviour of the 'real', non-ideal defects is still poorly understood. Therefore, the predictions of lifetime models need to be treated with circumspection and may not represent worst-case estimates of reliability.

REFERENCES

[1] S.V. Lisle, T.C. Tweedie [*Lightwave (USA)* (November 1993) p.37-50]

[2] A.G. Evans, S.M. Wiederhorn [*Int. J. Fract. (Netherlands)* vol.10 (1974) p.379-92]

[3] W. Griffioen [*Opt. Eng. (USA)* vol.33 (1994) p.488-97]

[4] C.R. Kurkjian, J.T. Krause, M.J. Matthewson [*J. Lightwave Technol. (USA)* vol.7 (1989) p.1360-70]

[5] G.S. Glaesemann [*Proc. 41st Int. Wire & Cable Symp.*, 16-19 Nov. 1992 (IWCS Inc., Eatontown, NJ, 1992) p.698-704]

[6] T. Breuls, T. Svensson [*Proc. SPIE - Int. Soc. Opt. Eng. (USA)* vol.2074 (1994) p.78-82]

[7] H.H. Yuce, P.L. Key, H.C. Chandan [*Proc. SPIE - Int. Soc. Opt. Eng. (USA)* vol.1366 (1991) p.120-8]

[8] M.J. Matthewson, B. Lin, A.P. Stanzeski [*OFC'94 Tech. Digest*, San Jose, CA, 20-25 Feb. 1994 (Opt. Soc. Amer., Washington, DC, 1994) vol.5 p.245-6]

[9] G.M. Bubel, M.J. Matthewson [*Opt. Eng. (USA)* vol.30 (1991) p.737-45]

[10] M.J. Matthewson [*Proc. SPIE - Int. Soc. Opt. Eng. (USA)* vol.CR50 (1994) p.3-31]

[11] C.R. Kurkjian, J.T. Krause, U.C. Paek [*J. Phys. (France)* vol.43 (1982) p.C9-585-6]

[12] V.V. Rondinella, M.J. Matthewson [*Proc. SPIE - Int. Soc. Opt. Eng. (USA)* vol.2074 (1994) p.52-8]

[13] J.T. Krause [*Proc. 5th Eur. Conf. Opt. Commun.*, Amsterdam, Netherlands, 17-19 Sept. 1979 (Philips Res. Labs., Eindhoven, Netherlands, 1979) p.19.1/1-4]

[14] M.J. Matthewson, H.H. Yuce [*Proc. SPIE - Int. Soc. Opt. Eng. (USA)* vol.2290 (1994) p.204-10]

[15] C.R. Kurkjian, M.J. Matthewson [*Electron. Lett. (UK)* vol.32 (1996) p.761-2]

[16] V.V. Rondinella, M.J. Matthewson, C.R. Kurkjian [*J. Am. Ceram. Soc. (USA)* vol.77 (1994) p.73-80]

[17] M.J. Matthewson [*Proc. SPIE - Int. Soc. Opt. Eng. (USA)* vol.CR50 (1994) p.32-59]

[18] G.S. Glaesemann, D.J. Walter [*Opt. Eng. (USA)* vol.30 (1991) p.746-8]

PART A: SILICA

CHAPTER A5

APPLICATIONS

A5.1 Fibre amplifiers based on rare earth-doped silica
A5.2 Fibre gratings in silica optical fibre

A5.1 Fibre amplifiers based on rare earth-doped silica

M.N. Zervas and R.I. Laming

July 1998

A INTRODUCTION

The erbium-doped fibre amplifier (EDFA) [1] has seen rapid development and is now established as a key component in future optical networks. Several excellent texts have been written on this important optical component [2,3]. To date, EDFA development has been driven by specific requirements, primarily in single-channel, point-to-point fibre links. There are, however, many more applications which may require, for example, either broadband or narrowband amplifiers and signal-processing functions. In addition, non-telecommunication applications of silica fibre operating around 1.5 microns can benefit enormously by the use of EDFAs.

Current research on the EDFA is investigating new amplifier designs. The aim of this work is to appropriately modify and optimise the amplifier characteristics for a given application. In this Datareview several modifications to the EDFA are described. In Section B, we discuss the performance of a composite EDFA with an integral isolator. It is shown that this configuration exhibits high gains and quantum-limited noise figure (NF) at relatively low pump powers [4-6]. In Section C, a novel configuration of an optical limiting amplifier is presented which exhibits an input-signal dynamic range in excess of 30 dB [7,8]. Finally, in Section D, an optical equalising amplifier is demonstrated which is based on an erbium-doped twin-core fibre. This fibre geometry shows wavelength-dependent spatial (longitudinal) hole burning, thus increasing the effective inhomogeneous broadening in the amplifier, and provides enhanced output-signal equalisation in a multichannel system.

B COMPOSITE EDFA

A composite-EDFA configuration which incorporates an optical isolator has been investigated theoretically and experimentally. The isolator prevents the build-up of backward-ASE and results in an amplifier with high gain and near-quantum-limited noise figure (NF). The optimum position of the isolator has been calculated as a function of the pump power so that minimum NF and maximum gain are achieved simultaneously. It is shown that under practical pump power at 980 nm, the optimised composite EDFA exhibits a gain improvement of about 5 dB and an NF reduction in excess of 1.5 dB when compared with an optimised conventional EDFA. It is also shown that with further optimisation the composite EDFA can be employed in a practical fibre link as a pre-amplifier without the use of an input isolator. Finally, a high-gain composite EDFA has been experimentally demonstrated which exhibits a gain of 51 dB and NF of 3.1 dB for only 45 mW of pump power at 980 nm.

The amplifier configuration is shown in FIGURE 1. A commercially-available fibre isolator is incorporated into the erbium-doped segment of the EDFA. The active length now comprises two erbium-doped fibre lengths (EDF#1 and EDF#2) with the isolator spliced in between. A wavelength-division-multiplexing (WDM) coupler is used to launch both the pump and signal into the input section (EDF#1), whereupon it is transmitted via the isolator to EDF#2. The amplifier is pumped in the forward direction, i.e. the pump and signal co-propagate. The isolator is designed to transmit the signal, forward-ASE and pump wavelengths with low loss (typical values: pump loss <0.5 dB, signal loss <2.0 dB). Two low-loss WDM fibre couplers (typical loss <0.1 dB) are utilised to extract the residual pump power at point A and re-launch it into the erbium-doped fibre at point B.

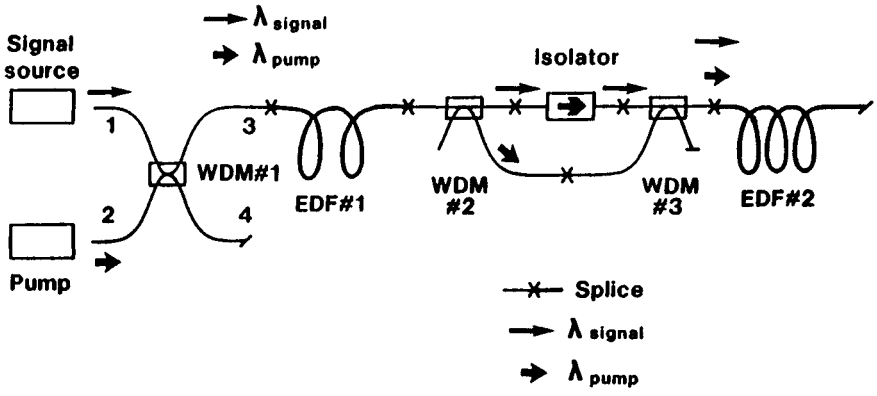


FIGURE 1 Composite-EDFA configuration.

An erbium-doped germano-silicate fibre was used having an NA of 0.24, cutoff wavelength of ~920 nm and erbium absorption of 0.95 dB/m at 1.536 μm. The composite EDFA comprised two fibre lengths of 25 m and 60 m, respectively, which were separated by a polarisation-independent isolator to suppress the backward-travelling ASE. The isolator insertion loss at the signal wavelength was 1 dB. Since the isolator has a very high loss at the pump wavelength of 980 nm, two WDM couplers with insertion losses at the pump/signal wavelengths of 0.11 dB/0.31 dB and 0.16 dB/0.31 dB were incorporated to provide a low-loss by-pass for the pump. The total forward insertion losses between the two sections of amplifier fibre were ~0.6 dB and ~2.1 dB at the pump and signal wavelengths, respectively. The isolation in the reverse direction was greater than 30 dB over a 50 nm bandwidth centred at 1540 nm.

FIGURE 2 shows gain and NF measurements for the composite EDFA. It is shown that gains as high as 54 dB with a corresponding NF of 3.1 dB can be easily obtained. Comparing with the conventional EDFA, we found that for 45 mW of pump power a 75 m length conventional EDFA gives a high gain of 46.6 dB and NF of 4.85 dB, whilst to reduce the NF to about 3.36 dB requires a sub-optimal length of 30 m resulting in a moderate gain of 25.2 dB and corresponding gain-efficiency reduction. On the other hand, for the same pump power the composite EDFA achieves a combination of 51 dB gain and 3.1 dB NF, which represents a very significant improvement. The solid lines in FIGURE 2 correspond to the calculated gain and NF of the composite EDFA. Using this composite amplifier as a pre-amplifier in an optical receiver configuration resulted in a record sensitivity of 102 photons/bit at a transmission rate of 10 Gbit/s [11].

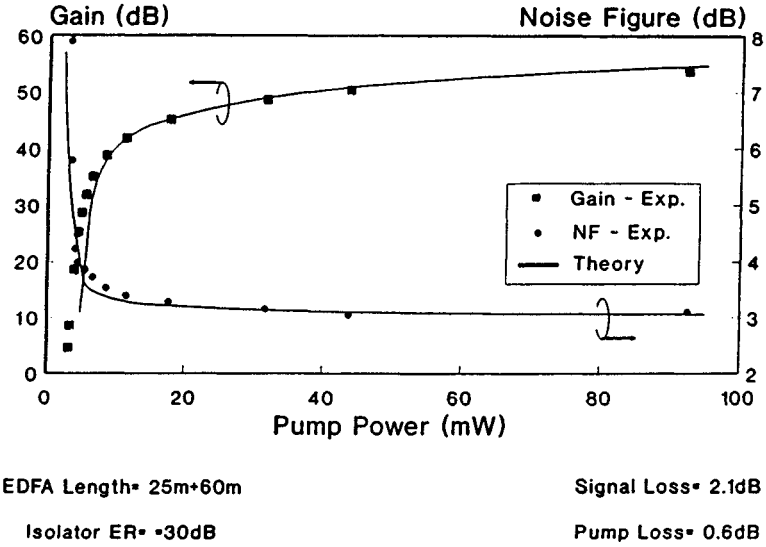


FIGURE 2 Gain and NF measurements for the composite EDFA.

C OPTICAL LIMITING AMPLIFIER

A novel configuration of an erbium-doped-fibre optical limiting amplifier (OLA) is realised by simply introducing a differential lump-loss between the signal and the pump power at a particular point along the fibre. The differential loss between the signal and the pump power can for example be introduced by simply bending tightly the erbium-doped fibre at a particular point along its length. The optical isolator with the two pump-bypassing WDMs used in the composite EDFA (Section B) can be also utilised to provide the differential loss. The OLA exhibits an input-power dynamic range in excess of 35 dB and the capacity to control optically the level of the constant-output signal.

The underlying principle of operation of the proposed OLA is explained with reference to FIGURE 3 where the pump and signal evolution along the normalised fibre length are shown for the two extreme input signal powers of -25 dBm and 0 dBm. The pumping is uni-directional with a pump power of 20 mW. The loss for the signal forward and backward ASE is 2 dB while for the pump it is 0.5 dB. The limiting action is achieved by the balance between the pump and amplified-signal power in stages I and II, before and after the lump-loss position, respectively. In stage I, both signals are amplified, with the low-input-power (-25 dBm) signal attaining lower levels than the high-input-power (0 dBm) one, as expected. However, the pump power is depleted at a slow rate by the low-input-power signal and there is sufficient remnant pump power available in stage II to amplify the attenuated low-input signal to the same level as the high-input signal. On the other hand, although the high-input-power signal attains a higher level throughout stage I, it heavily depletes the pump power which drops below threshold towards the end of stage II and, as a consequence, the signal is slightly attenuated to level-off with the low-input-power one. The signals of intermediate input power evolve in an analogous manner and converge to the same output level.

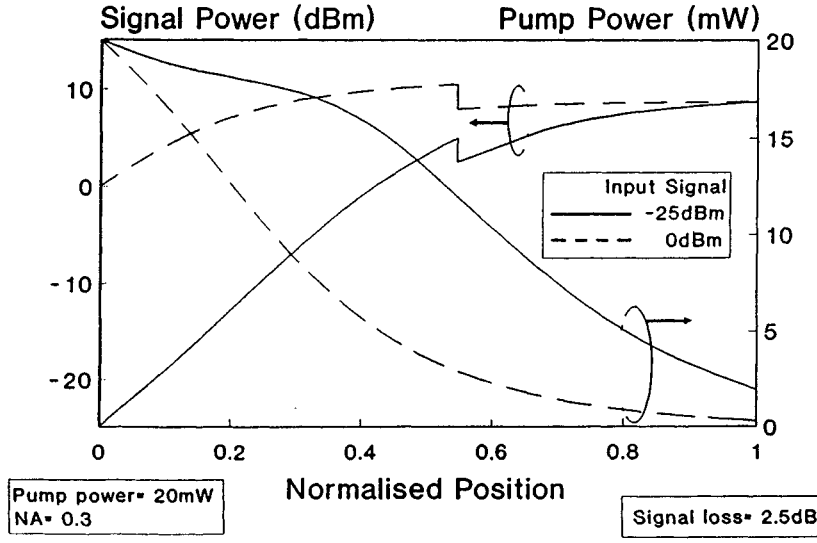


FIGURE 3 Pump- and signal-power evolution along the OLA for input-signal powers of -25 dBm (solid lines) and 0 dBm (dashed lines).

An important feature of the proposed OLA is the possibility of controlling the output signal power optically by varying the input pump power. By increasing the input pump power from 20 mW to 60 mW, the signal output of the OLA increases from ~8 dBm to ~14 dBm and is accompanied by an ~20% increase in the dynamic range of the OLA.

D EQUALISING OPTICAL AMPLIFIER

A novel EDFA configuration is proposed which provides automatic spectral gain equalisation. The device relies on the effective increase in the inhomogeneous broadening in an EDFA by spatial hole burning. The gain medium is a twin core fibre in which both cores are Er^{3+}-doped. The amplifier is configured such that the signal and pump light couple periodically between the two cores along the fibre length (with period approximately proportional to λ^{-3}). One signal exhibits a certain periodic spatial intensity distribution and thus accesses a subset of ions, whilst a different signal wavelength will access a different subset of ions. The gain at the two signal wavelengths is spatially (longitudinally) decoupled and thus for the case when one signal is larger than the others, spatial hole-burning will preferentially decrease its gain resulting in spectral gain equalisation.

An equalising optical amplifier was built and tested. The amplifier consisted of two sections of EDF. The first was a 14 m length of germano-alumino-silica doped fibre with NA of 0.2, cutoff of ~930 nm and absorption at the signal wavelength of ~3 dB/m and was used to boost input signal levels. The output was spliced to one core of a 10 m length of doped twin core fibre. The twin core was fabricated such that both cores were nominally identical with an index difference n of 0.0258 and core radius and separation of 1.43 μm and 4.5 μm respectively. The resulting coupling length is wavelength dependent and estimated to be 1.26 mm (1.2575 mm) at a wavelength of 1.55 μm (1.551 μm). The absorption at the signal wavelength was ~1 dB/m. The output from two signal lasers was employed to probe the amplifier gain simultaneously at two closely-spaced wavelengths in order to investigate spectral gain equalisation. Small sinusoidal modulations at 49 and 51 kHz were superimposed on the CW output of the lasers allowing lock in techniques to discriminate their amplified outputs.

FIGURE 4 shows the gain difference of two channels 1 nm apart as a function of the channel input-power difference, for different fibre lengths. It is shown that the equalisation efficiency increases with the fibre length, due to saturation increase. The ideal case of 1 dB/dB is also shown. Experimental data, obtained with 10 m of fibre, are in excellent agreement with theory. Using this device, gain equalisation rates up to 0.11 dB per dB difference between input signal levels have been demonstrated and should increase the useful bandwidth of cascaded amplifiers. Optimisation of the fibre structure can result in equalisation rates of 0.35 dB/dB [6]. This is shown to be adequate in providing self-regulating spectral characteristics in a four-channel WDM optical link [12].

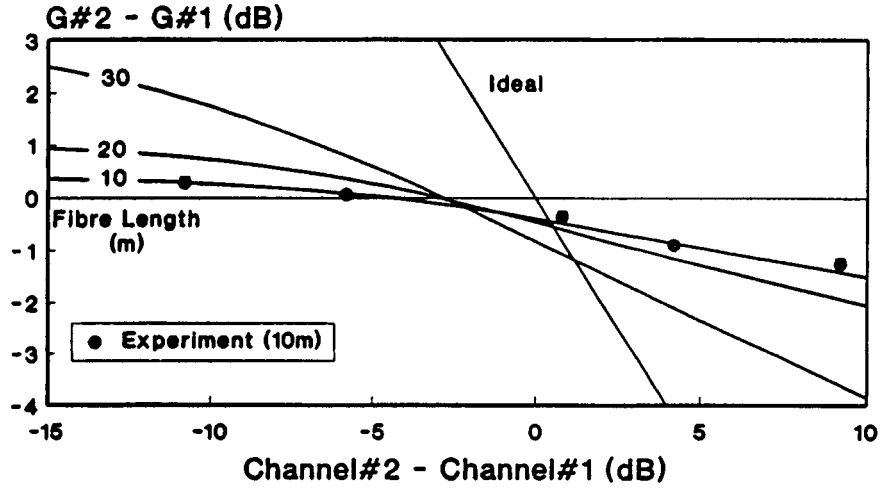


FIGURE 4 Comparison of two-channel gain saturation characteristics for twin-core EDFA and conventional EDFA.

E CONCLUSION

Second-generation EDFAs have been developed by incorporating additional optical components into an ordinary EDFA so that the amplifier response is altered to achieve special functions. Addition of an optical isolator within the erbium-doped fibre prevents the building-up of the backward ASE and results in a composite EDFA which exhibits high gains (>50 dB) accompanied by near-quantum-limited NF (~3.1 dB) at relatively low pump powers (~50 mW). Such a device can be used as a pre-amplifier and enhance the sensitivity of optical receivers.

Incorporation of a lump differential loss between signal and pump results in an efficient optical limiting amplifier with input-signal dynamic range in excess of 30 dB. The constant output of the limiter can be easily adjusted by varying the input pump power. Such a device is useful in cascaded-amplifier links. It can stabilise the signal power against slow, unwanted variations, thus increasing the dynamic range of subsequent optical and electronic devices.

Finally, using a twin-core erbium-doped fibre, i.e. incorporating an additional core into the standard fibre design, results in an amplifier with passive, automatic gain equalisation. Such a device can increase the useful bandwidth of cascaded amplifiers. Gain equalisation rates of 0.11 dB per dB difference between input-signal levels have been demonstrated.

REFERENCES

[1] R.J. Mears, L. Reekie, I.M. Jauncey, D.N. Payne [*Electron. Lett. (UK)* vol.23 (1987) p.1026-8]

[2] M.J.F. Digonet (Ed.) [*Rare Earth Doped Fibre Lasers and Amplifiers* (Marcel Dekker Inc, New York, 1993)]

[3] E. Desurvire (Ed.) [*Erbium Doped Fibre Amplifiers: Principles and Applications* (Wiley Interscience, New York, 1993)]

[4] M.N. Zervas, R.I. Laming, D.N. Payne [*Proc. Third Topical Meeting on Optical Amplifiers and Their Applications* Santa Fe, June 1992, vol.17, Paper FB2, p.162-5]

[5] R.I. Laming, M.N. Zervas, D.N. Payne [*IEEE Photonics Technol. Lett. (USA)* vol.4 (1992) p.1345-7]

[6] M.N. Zervas, R.I. Laming, D.N. Payne [*IEEE J. Quantum Electron. (USA)* vol.31 (1995) p.472-80]

[7] M.N. Zervas, R.I. Laming [*Proc. 18th European Conference on Optical Communication* Berlin, 27 Sept-1 Oct 1992, vol.1, Paper MoA3.1, p.81-4]

[8] O.C. Graydon, M.N. Zervas, R.I. Laming [*J. Lightwave Technol. (USA)* vol.13 (1995) p.732-9]

[9] R.I. Laming, J.D. Minelly, L. Dong, M.N. Zervas [*Proc. Conference on Optical Fibre Communications (OFC '93)/International Conference on Integrated Optics and Optical Fibre Communication (IOOC '93)* San Jose, 21-26 Feb 1993, vol.4, Paper ThD3, p.175-7]

[10] M.N. Zervas, R.I. Laming [*J. Lightwave Technol. (USA)* vol.13 (1995) p.721-31]

[11] R.I. Laming, A.H. Gnauck, C.R. Giles, M.N. Zervas, D.N. Payne [*Proc. Third Topical Meeting on Optical Amplifiers & Their Applications* Santa Fe, 24-26 Jun 1992, postdeadline paper PD13, p.58-61]

[12] C.V. Poulsen, O.C. Graydon, R.I. Laming, M.N. Zervas, L. Dong [*Electron. Lett. (UK)* vol.32 (1996) p.23-5]

A5.2 Fibre gratings in silica optical fibre

L. Reekie

November 1997

A INTRODUCTION

Photorefractive fibre gratings are devices that are rapidly being taken up by the telecommunications and fibre sensor industries due to their wide range of uses. They can be thought of as one-dimensional holograms written directly into the core of a conventional optical fibre which have the capability of reflecting light of a specific wavelength back along the fibre. Like holograms, they are essentially permanent and are written using specialised lasers. They rely on the fact that the refractive index of the germania-doped silica fibre core can be changed by exposure to intense ultraviolet (UV) light; however the exact nature of the photorefractive change is not yet fully understood. In general, it is possible to produce an absolute refractive index change of 10^{-6} - 10^{-3} in most fibres, though it is necessary to use specially designed fibres in order to achieve the highest index change.

B GRATING MANUFACTURING TECHNIQUES

Fibre gratings were first 'discovered' when it was found that light from an Ar^+-ion laser at $\lambda = 514.5$ nm launched into a germania doped silica optical fibre was, after a period of time, being reflected back from the fibre end with high efficiency [1]. The light was being reflected from a region of the core containing a periodic modulation in the refractive index created by the standing wave interference between the incoming beam and the Fresnel reflection (~4%) from the end of the fibre. This effect was weak and difficult to reproduce in a range of different fibre types, and furthermore produced a fibre grating that only worked at the wavelength with which it was written. It was later realised that the photorefractive effect responsible for the grating was a two-photon process centred on an absorption band around $\lambda = 240$ nm [2], and a much higher index change could be generated by writing directly at this wavelength. This required the adoption of a two-beam interference process external to the fibre [3] which had the additional benefit of allowing a much wider range of fibre gratings at different wavelengths to be fabricated (see FIGURE 1). In general, frequency doubled dye lasers, excimer lasers or frequency doubled Ar^+-ion lasers are used. The angle between the two writing beams is chosen to produce a grating with a pitch, Λ, which satisfies the following condition:

$$\lambda_{Bragg} = 2 \cdot n_{eff} \cdot \Lambda$$

where λ_{Bragg} is the centre wavelength of the grating and n_{eff} is the effective refractive index of the mode. Usually, this gives a pitch of 300 - 600 nm for most gratings required in telecommunication and sensor systems.

More recently, silica phase masks have been used to make fibre gratings [4,5]. A phase masks consists of a polished piece of UV-grade silica which has a diffraction grating etched into the surface, the depth and profile of which is designed to maximise coupling into the first order diffracted beams, while minimising the zero-order throughput. The pitch of the phase mask is twice the required pitch of the grating in the fibre. When a fibre is placed in contact with such a grating and illuminated through the mask with UV light, a photorefractive grating will be formed in the core of the fibre. This technique has the advantage that the uniformity of any fibre grating made this way is not limited by the spatial profile or coherence of the writing laser, which can be scanned over the phase mask. This advantage is gained at

the expense of tunability, the wavelength being fixed at the design stage. Phase masks can routinely be made which have a length of several centimetres, so that it is possible to make long fibre gratings using a relatively simple experimental set-up.

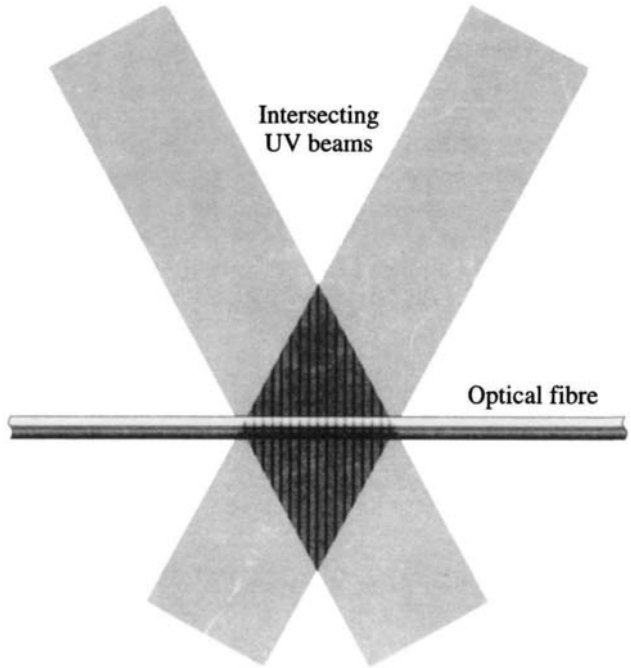


FIGURE 1 Interference fringes created by intersecting UV laser beams create the grating in the core of the fibre.

In addition to making gratings in off-the-shelf fibre, it is also possible to write gratings in fibre as it is being drawn [6]. This has the considerable advantage that the polymer coating which normally protects the fibre does not have to be removed and replaced, improving the physical strength of the grating. The main use however is in fabricating long arrays of gratings for use in multiplexed fibre sensor systems. By using a writing interferometer that can be tuned in wavelength as the fibre is being drawn, the wavelength of each grating in the array can also be selected [7]. A short pulse device such as an excimer laser must be used to write the gratings, and only low reflectivity gratings may be obtained due to the single-shot nature of the writing process.

An alternative method which avoids removal of the coating is to use a polymer which is transparent at the writing wavelength. This can be done either by using a proprietary coating which has low loss at near-conventional writing wavelengths [8] or by using a longer wavelength to write the grating through a standard coating [9]. Both techniques offer solutions to the problems of automated grating fabrication and production of robust grating arrays for fibre sensors.

C FIBRE SENSITISATION

It is not usually possible to obtain a high refractive index change in conventional telecommunication grade fibre. This is partly due to the relatively low germania content, but also to the addition of other dopants such as phosphorus, which weakens the photorefractive effect. One possible way to improve the

index change is to increase the UV absorption of the core by the addition of extra germania. Unfortunately, this raises the index to such an extent that the fibre becomes incompatible with conventional fibre, a high splice loss being obtained due to the difference in the modal spot size. It was found that the addition of boron to the core of the fibre not only lowered the refractive index, as was well known, but also greatly improved the photosensitivity [10]. The boron/germania co-doped silica fibre remains one of the most intrinsically photosensitive fibres to date. This led to a flurry of activity in the search for suitable co-dopants, with varying success. Those tried so far include europium [11], cerium [12], tantalum [13], aluminium [14] and tin [15]. By far the most successful is tin, which has similar photosensitivity to boron co-doped germania, but can be taken to much higher temperature before grating degradation becomes a problem.

The highest index changes are achieved by diffusing molecular hydrogen into the fibre core at high pressure (several hundred atmospheres) prior to writing the grating. Using this technique, refractive index changes of $\Delta n > 10^{-2}$ have been obtained [16]. Part of this index change however can be related to defect centres which have a relatively low activation energy and are not stable at typical industrial operating temperatures. In order to improve the reliability of such gratings, it is necessary to anneal them at elevated temperature, typically ~150°C. In addition, the fibre loss in the wavelength region $\lambda < 1$ μm is increased significantly, with possible repercussions in the field of rare-earth doped fibre lasers.

D TYPES OF GRATING

The conventional photorefractive effect as discussed above consists of an increase in the refractive index of the fibre core with increasing UV fluence - this mechanism is known as Type 1 and is the most commonly observed. Typically, such gratings are stable up to temperatures in the range 200°C - 300°C. Two other grating formation mechanisms are possible, usually referred to as Types 2 and 2A. Type 2A gratings are also photorefractive in nature, the primary difference being that the observed change in the refractive index is negative, not positive. In addition, such gratings are considerably more stable than those of Type 1. This type of grating may be obtained by 'over-exposing' a Type 1 grating; however the process can be very slow if carried out using a laser operating near 240 nm. By writing the grating using an ArF excimer laser operating at $\lambda = 193$ nm, Type 2A gratings may be written in a few minutes, greatly reducing the exposure time.

Type 2 gratings are not photorefractive in nature - rather they are formed when an intense UV laser pulse interacts with a highly absorbing fibre core, creating damage regions along the core/cladding interface [17]. Such gratings have been observed in germania and tin doped fibres. Very high index changes ($\Delta n > 10^{-3}$) can be obtained using this technique using only a single 25 ns pulse from an excimer laser. In addition, due to the nature of the damage mechanism, such gratings are very robust, surviving at temperatures in excess of 800°C. There is however usually a small loss penalty associated with such gratings, rendering them unsuitable for use in multiple grating arrays.

E SPECIALISED GRATINGS AND APPLICATIONS

Fibre gratings are normally designed to reflect light of a specific wavelength propagating in the fundamental mode back along the core of the fibre. By increasing the pitch of the grating to several hundred microns however, the propagation constants of the core and cladding can be matched at various specific wavelengths [18]. This causes light to be coupled into the cladding and ultimately the polymer coating where it is lost. In this manner, efficient bandstop filters can be fabricated which do not couple light into the backward propagating mode, potentially causing problems in optically amplified telecommunication systems. Such gratings are fabricated either using point-by-point exposure of each

individual element, or through a dedicated amplitude mask. The resulting gratings find use as gain equalisers in erbium doped fibre amplifiers for high bit-rate communication links [19].

Using the phase mask production technique, it is possible to fabricate long fibre gratings with properties which vary along the length of the grating. The index profile of the grating may be tapered, or apodised, in order to reduce the sidelobe reflections in the wings of the spectrum. Also, the pitch of the grating may be varied along the length, creating a wavelength chirp in the reflection profile. By combining both of these techniques, it is possible to fabricate a grating which can compensate for the dispersion of a 1.55 μm telecommunications signal transmitted over standard 1.3 μm zero-dispersion fibre [20]. Narrowband gratings can also be used as filters and add/drop multiplexers in multichannel wavelength division multiplexed (WDM) fibre links. Other telecommunication uses include using gratings as stable wavelength selective feedback elements for semiconductor diode and rare-earth doped fibre lasers [21].

Perhaps the most widespread use of fibre gratings to date has been in the area of fibre sensors, where they may be used for sensing strain, temperature, pressure and any other measurand to which the grating can be sensitised [22]. Most commonly they may be configured as strain sensors by using the simple principle that the grating pitch will increase when the fibre is placed under tension, moving the operating point to longer wavelength. Distributed arrays of such gratings in a single length of fibre may be embedded in a composite material for use in 'smart structures' such as an aeroplane fuselage.

F CONCLUSION

Photorefractive gratings in silica optical fibre are finding many uses as stable, robust optical elements in long haul fibre telecommunication and sensor systems. There is still some debate over the exact nature of the photorefractive mechanism in silica; however the physical characteristics of most types of fibre grating are well enough understood for the vast majority of applications.

REFERENCES

[1] K.O. Hill, Y. Fujii, D.C. Johnson, B.S. Kawasaki [*Appl. Phys. Lett. (USA)* vol.32 (1978) p.823]

[2] D.K.W. Lam, B.K. Garside [*Appl. Opt. (USA)* vol.20 (1981) p.440]

[3] G. Meltz, W.W. Morey, W.H. Glenn [*Opt. Lett. (USA)* vol.14 (1989) p.823]

[4] K.O. Hill, B. Malo, F. Bilodeau, D.C. Johnson, J. Albert [*Appl. Phys. Lett. (USA)* vol.62 (1993) p.1035]

[5] D.Z. Anderson, V. Mizrahi, T. Erdogan, A.E. White [*Electron. Lett. (UK)* vol.29 (1993) p.566]

[6] L. Dong, J.L. Archambault, L. Reekie, P.St.J. Russell, D.N. Payne [*Electron. Lett. (UK)* vol.29 (1993) p.1577]

[7] C.G. Askins, M.A. Putnam, G.M. Williams, E.J. Friebele [*Opt. Lett. (USA)* vol.19 (1994) p.147]

[8] R.P. Espindola et al [*Proc. Bragg Gratings, Photosensitivity and Poling in Glass Fibres and Waveguides: Applications and Fundamentals Topical Meeting* Williamsburg, VA, USA, 26-28 Oct. 1997 (Optical Society of America, Washington DC, 1997) p.PD2-1]

[9] D.S. Starodubov et al [*Proc. Bragg Gratings, Photosensitivity and Poling in Glass Fibres and Waveguides: Applications and Fundamentals Topical Meeting* Williamsburg, VA, USA, 26-28 Oct. 1997 (Optical Society of America, Washington DC, 1997) p.PD1-1]

[10] D.L. Williams, B.J. Ainslie, J.R. Armitage, R. Kashyap, R. Campbell [*Electron. Lett. (UK)* vol.29 (1993) p.45]

[11] K.O. Hill et al [*Proc. OFC '91* San Diego, Ca., USA, 18-22 Feb. 1991 (Optical Society of America, Washington DC, 1991) p.PD14]

[12] M.M. Broer, R.L. Cone, J.R. Simpson [*Opt. Lett. (USA)* vol.16 (1991) p.1391]

[13] L. Dong, J.-L. Archambault, E. Taylor, M.P. Roe, L. Reekie, P.St.J. Russell [*J. Opt. Soc. Am. B (USA)* vol.12 (1995) p.1747]

[14] J.T. Kringlebotn, J.-L. Archambault, L. Reekie, D.N. Payne [*Opt. Lett. (USA)* vol.19 (1994) p.2101]

[15] L. Dong, J.L. Cruz, J.A. Tucknott, L. Reekie, D.N. Payne [*Opt. Lett. (USA)* vol.20 (1995) p.1982]

[16] P.J. Lemaire, R.M. Atkins, V. Mizrahi, W.A. Reed [*Electron. Lett. (UK)* vol.29 (1993) p.1191]

[17] L. Dong, J.-L. Archambault, L. Reekie, P.St.J. Russell, D.N. Payne [*Electron. Lett. (UK)* vol.29 (1993) p.1577]

[18] A.M. Vengsarkar, P.J. Lemaire, J.B. Judkins, V. Bhatia, T. Erdogan, J.E. Sipe [*J. Lightwave Technol. (USA)* vol.14 (1996) p.58]

[19] A.M. Vengsarkar, A.M. Pedrazzani, J.B. Judkins, P.J. Lemaire, N.S. Bergano, C.R. Davidson [*Opt. Lett. (USA)* vol.21 (1996) p.336]

[20] F. Ouellette [*Opt. Lett. (USA)* vol.16 (1991) p.303]

[21] I.M. Jauncey, L. Reekie, J.E. Townsend, D.N. Payne, C.J. Rowe [*Electron. Lett. (UK)* vol.24 (1988) p.24]

[22] W.W. Morey, G. Meltz, W.H. Glenn [in *Springer Proceedings in Physics - Optical Fibre Sensors* (Springer-Verlag, 1989) p.526-31]

PART B: OXIDE GLASS

CHAPTER B1

OPTICAL PROPERTIES

B1.1 Transmission of oxide glass
B1.2 Intrinsic scattering losses of oxide glass
B1.3 Refractive index and dispersion of oxide glass
B1.4 Non-linear refractive index of oxide glass

B1.1 Transmission of oxide glass

N. Neuroth

June 1998

A INTRODUCTION

Glasses are materials which do not crystallise when the melt is cooled down. The viscosity increases so fast that the atoms cannot reach their prescribed distances. Their atomic network has deviations from the exact crystal position order [1-5]. The deviations are mainly dependent on the chemical composition of the glass and (to a small degree) on the melting and cooling process. A special group of oxides - called glassformers - is responsible for this behaviour. Examples of network formers are SiO_2, B_2O_3, P_2O_5, GeO_2, As_2O_3 and Sb_2O_3.

Other types of oxides such as alkali oxides and alkaline earth oxides cause interruptions of the network and thus variations of the physical and chemical properties like density, refractive index, thermal expansion and temperature dependence of the viscosity. For fibres with high numerical aperture, glasses with higher refractive index are needed.

Due to the many possible variations of the chemical composition there are many chances to adjust several properties, for instance the refractive index. Also the light transmission is defined by the chemical composition (and to a lower degree by the melting and cooling process).

B INTRINSIC OPTICAL LOSSSES

B1 Electronic Transitions

Transitions of electrons of the atomic shells cause absorption in the ultraviolet spectral region [6,7]. The distribution and intensity of the absorption is influenced by the chemical composition of the glass. In the case of fused silica the electronic transitions cause strong and broad absorptions bands in the ultraviolet with maxima at 109 and 121 nm [8]. By addition of network modifiers these bands are broadened and shifted to longer wavelengths. In FIGURE 1 it is shown how the ultraviolet transmission edge of fused silica is shifted to longer wavelengths by adding small amounts of Na_2O [9]. This modification is caused by non-bridging oxygen. In FIGURE 2 the spectral absorption of binary alkali silicate glasses is shown [10]. We see the influence of the different alkali types. The heavier the alkali type the greater is the shift of the ultraviolet absorption edge to longer wavelengths.

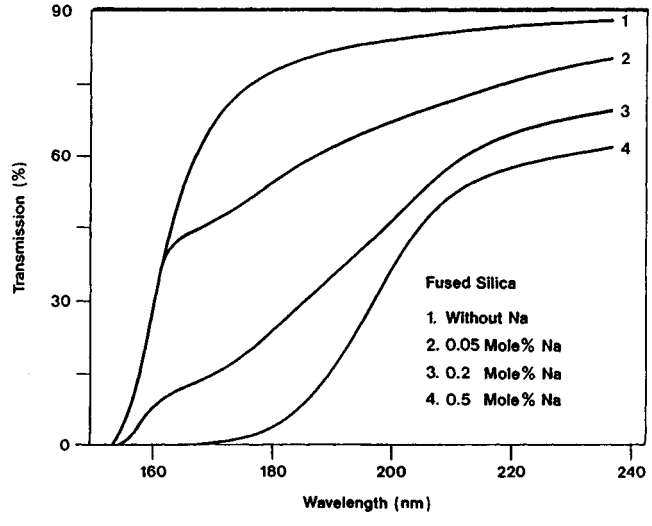


FIGURE 1 Ultraviolet transmission of fused silica with small amounts of Na_2O; sample thickness 1 mm [9].

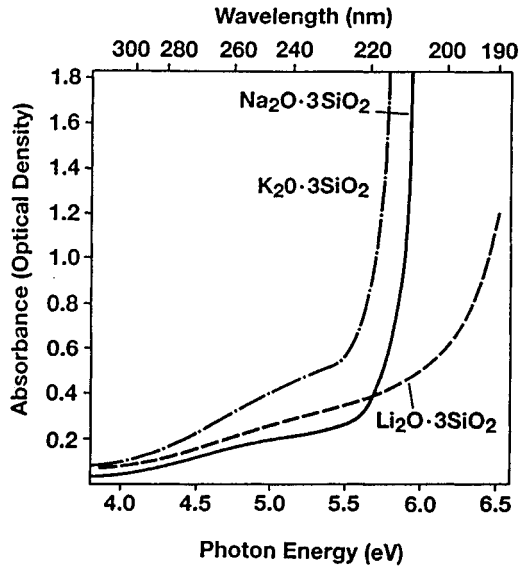


FIGURE 2 Ultraviolet absorption of alkali silicate glasses with different alkali types; sample thickness 2 mm [10].

B2 Molecular Vibrations

Molecular vibrations (for instance Si-O, B-O or P-O) cause strong absorption in the middle infrared region [11,12]. In FIGURE 3 the infrared absorption edge of oxide glasses with different network forming cations is given [13]. The heavier the network forming cation the more the infrared absorption edge is shifted to longer wavelengths.

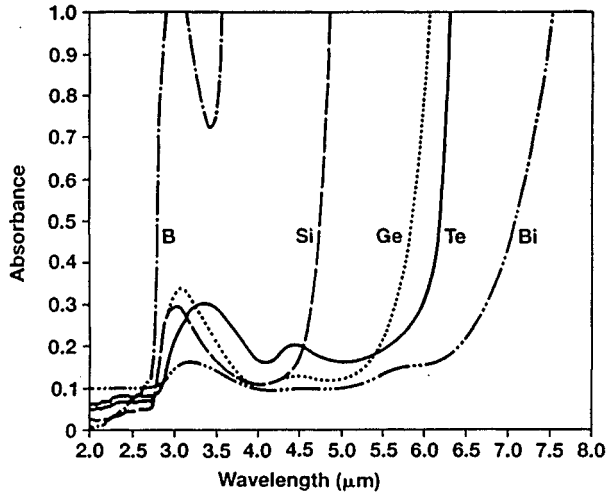


FIGURE 3 Infrared absorption edge of oxide glasses with different network forming cations; sample thickness 1.85 mm, except Bi: 2.00 mm [13].

Mostly the glasses contain OH groups which cause absorption bands in the region 2.5 to 6.5 microns. If glasses with good infrared transmission are wanted one has to reduce or to eliminate the OH-content.

B3 Scattering

Another source of intrinsic loss is light scattering. The Brownian movement of the molecules in the melt causes density fluctuations in the glass melt, which are frozen-in when the melt is cooled down. The density fluctuations cause fluctuations of the refractive index. The consequence is light scattering.

The intensity of the scattering increases with the refractive index of the glass (see Datareview B1.2 and [14]). Another source of scattering can be phase separation of the glass. A third source of scattering may be undissolved particles (contaminants, metals, crystals) or bubbles. This scattering loss is caused by the melting technique. It is not an intrinsic loss.

C EXAMPLES OF THE TRANSMISSION SPECTRA OF OPTICAL GLASSES AND FIBRES

In FIGURE 4 the spectral transmission of three optical glasses is shown: a fluor borosilicate glass and two lead silicate glasses. The sample thickness is 5 mm. In this case the whole visible region is transmitted. In FIGURE 5 the transmission spectra of one and several metre long fibre bundles with a core of lead silicate glass are shown. The blue and green parts of the spectra are diminished. This effect becomes stronger with greater length of the bundle. The absorption peaks at 980, 1280 and 1420 nm are caused by the OH-content.

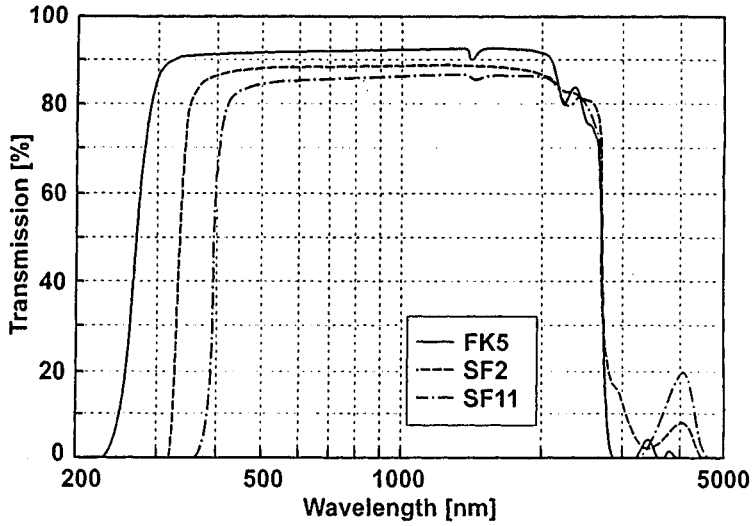


FIGURE 4 Transmission spectra of optical glasses; sample thickness 5 mm [15].

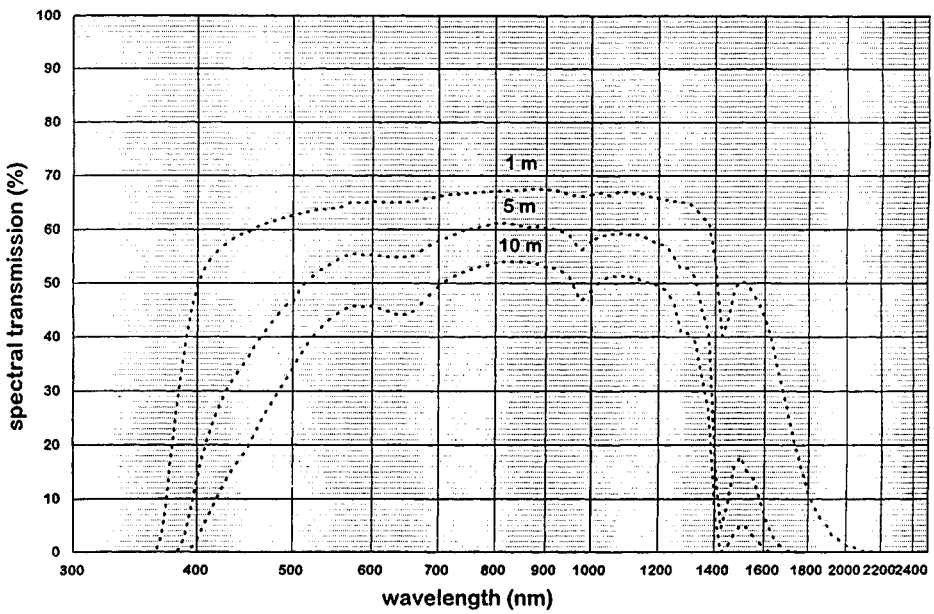


FIGURE 5 Transmission spectra of fibre bundles with a core of lead silicate glass.

D EXAMPLES OF THE ABSORPTION SPECTRA OF FIBRES FROM SPECIAL DEVELOPMENTS

Ten years ago there was intensive development of fibres with very low loss. In TABLE 1 some examples of used glass types are given and in FIGURE 6 the loss spectra of optical fibres made of four of these glass types are demonstrated [16-23]. The lowest loss is in the region 800 to 1100 nm. The bands at 980 and 1300 nm are due to OH-overtone vibrations.

TABLE 1 Composition of different oxide glasses and optical loss of fibres produced thereof.

No.	Glass components	Loss (dB/km)	Wavelength (nm)	Ref
1	SiO_2 - Na_2O - CaO	4.5	850	[16]
2	SiO_2 - K_2O - PbO	27.0	860	[17]
3	SiO_2 - GeO_2 - Na_2O - CaO	8.8	1100	[18]
4	SiO_2 - GeO_2 - B_2O_3 - Na_2O	7.0	890	[19]
5	SiO_2 - ZrO_2 - ZnO et al	8.0 - 15.0	850	[20]
6	SiO_2 - B_2O_3 - R_2O	8.0	850	[21]
7	SiO_2 - B_2O_3 - GeO_2	8.0	850	[22]
8	P_2O_5 - GeO_2 - Ga_2O_3	11.0	840	[23]

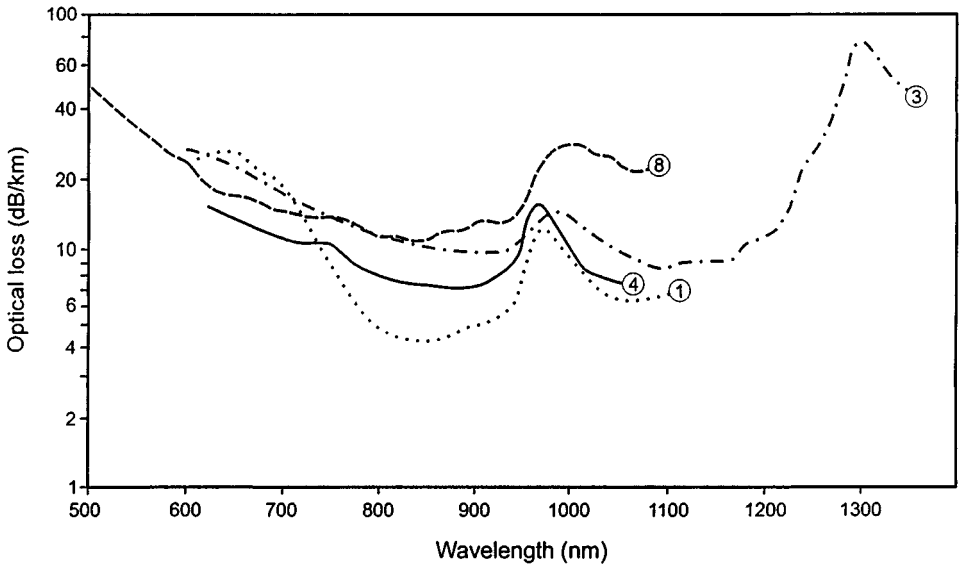


FIGURE 6 Optical loss spectra of fibres from special developments (for glass composition see TABLE 1).

REFERENCES

[1] H. Scholze [*Glass* (Springer, Berlin, 1990)]

[2] W. Vogel [*Glaschemie* 3rd edition (Springer Verlag, Berlin, 1992)]

[3] H. Rawson [*Properties and Applications of Glass* (Elsevier Scientific Publishing Co., Amsterdam, 1980)]

[4] D.R. Uhlmann, N.J. Kreidl [*Glass: Science and Technologie* vol.1 (Academic Press Inc., New York, 1983)]

[5] T.S. Izumitani [*Optical Glass* (Kyoritsu Shuppan Company Ltd., 1984; Lawrence Livermore National Laboratory, American Institute of Physics, Translation Series, 1986)]

[6] G.H. Sigel Jr. [*Treatise on Material Science and Technology* vol.12 (Academic Press, New York, 1997) p.5-89]

[7] G.H. Sigel [*J. Non-Cryst. Solids (Netherlands)* vol.13 (1973/74) p.372-98]
[8] S. Hirota, T. Izumitani, R. Onaka [*J. Non-Cryst. Solids (Netherlands)* vol.72 (1985) p.39-50]
[9] G.H. Sigel Jr. [*J. Phys. Chem. Solids (UK)* vol.32 (1971) p.2373-83]
[10] J.R. Hensler, E. Lell [in *Frontiers in Glass Science and Technology* (Proc. Ann. Meeting International Commission on Glass, Toronto, 1969) p.51-7]
[11] J. Wong, C.A. Angell [*Glass Structure by Spectroscopy* (Marcel Dekker Inc., New York, 1976)]
[12] Gan Fuxi [*Optical and Spectroscopic Properties of Glass* (Springer Verlag, Berlin, 1992)]
[13] W.H. Dumbaugh [*Proc. SPIE (USA)* vol.618 (1986) p.160-4]
[14] J. Schroeder [in *Treatise on Material Science and Technology* vol.12 (Academic Press, New York, 1977) p.158-222]
[15] H. Bach, N. Neuroth [*The Properties of Optical Glass* (Springer Verlag, Berlin, Heidelberg, 1995) p.91]
[16] S. Takahashi, S. Shibata, M. Yasu [*Electron. Lett. (UK)* vol.14 (1978) p.151-2]
[17] N. Neuroth [*Silikat J. (Germany)* vol.17 (1978) p.130-8]
[18] H.H. Brongersma, C.M.G. Jochem, T.P.M. Meeuwsen, P.J.W. Severin, B.A.C.M. Spierings [*Acta Electron. (France)* vol.22 (1979) p.245-54]
[19] K.J. Beales, C.R. Day, A.G. Dunn, P.L. Dunn, G.R. Newns, S. Partington [*Am. Ceram. Soc. Bull. (USA)* vol.59 (1980) p.1119-21]
[20] C.A.C.M. Spierings, C.M.G. Jochem, T.P.M. Meeuwsen, G.E. Thomas [*J. Am. Ceram. Soc. (USA)* vol.67 (1984) p.657-63]
[21] G.R. Newns, K.J. Beales, C.R. Day [*Int. Conf. on Integrated Optics and Optical Fibre Communication* Tokyo, 1977 (Optical Society of America, 1977) p.609-12]
[22] K.J. Beales, C. Day, A.D. Dunn, P.L. Dunn, G.R. Newns, S. Partington [*Am. Ceram. Soc. Bull. (USA)* vol.61 (1982) p.2129-21]
[23] K. Inoue, J. Goto, Y. Kawabata [*Deutsche Patent-Offenlegungsschrift* no.27 46 418 (1978)]

B1.2 Intrinsic scattering losses of oxide glass

S. Todoroki and S. Sakaguchi

June 1997

A INTRODUCTION

Oxides with low scattering compositions are being investigated extensively because of the recent interest in realising low loss oxide fibres. The intrinsic scattering of light is classified as either elastic (Rayleigh scattering) or inelastic (Brillouin and Raman scattering). Of these, Rayleigh scattering normally has the highest intensity. This Datareview provides an overview of these three kinds of scattering in oxide glasses and supplies related references.

B RAYLEIGH SCATTERING

Light scattering by particles smaller than the wavelength of light is called Rayleigh scattering. The 'particles' in glass media consist of frozen-in fluctuations of density and concentration. Since concentration fluctuation is related to diffusion, the temperature at which it is frozen in the glass (~ softening temperature) is higher than that of density fluctuation (~ T_F, fictive temperature) [1]. The theoretical expressions are reviewed elsewhere [1,2].

B1 Density Scattering

The magnitude of the scattering due to density fluctuation is described, by using classical electromagnetic theory and thermodynamics, as follows [2,3]:

$$A_{dens} = \frac{8\pi^3}{3\lambda^4}\left(\rho\frac{\partial\varepsilon}{\partial p}\right)^2 kT_F K_T(T_F) = \frac{8\pi^3}{3\lambda^4} n^8 p^2 kT_F K_T(T_F) \qquad (1)$$

where ρ is the density, ε the permittivity, k Boltzmann's constant, $K_T(T_F)$ the isothermal compressibility at T_F, n the refractive index and p Pockel's photoelastic constant. This equation shows that the scattering decreases as T_F decreases. It is difficult to discuss the compositional dependence of A_{dens} qualitatively for multicomponent oxide glasses because these parameters are not independent of each other and p and K_T are only available in a limited number of compositions.

Lines defined parameter Λ [2,4], which is a measure of the density dependence of bond polarisability (χ), to obtain $n^8p^2 = (n^2 - 1)^2(1 - \Lambda)^2$, and discussed the conditions under which this term is expected to approach zero. Na_2O-Al_2O_3-SiO_2 and CaO-Al_2O_3 glasses are thought to show low density scattering since their glass network frame is 'stuffed' with network modifier ions without accompanying any non-bridging oxygens (see M_2 in FIGURE 1) [4].

B2 Concentration Scattering

Concentration scattering appears when the glass consists of more than one component. Its magnitude is related to the mixing enthalpy of the components, or the activities of each component in the glass, which are both very hard to determine. Thus, concentration scattering is often evaluated from the difference between the experimentally determined scattering coefficient and the theoretically calculated density scattering, i.e. $A'_{conc} = A_{Rayl} - A_{dens}$. Spierings compared A'_{conc} and A_{conc} for K_2O-MgO-PbO-SiO_2 glass [5]. The latter is theoretically derived under the assumption that the glass is an ideal

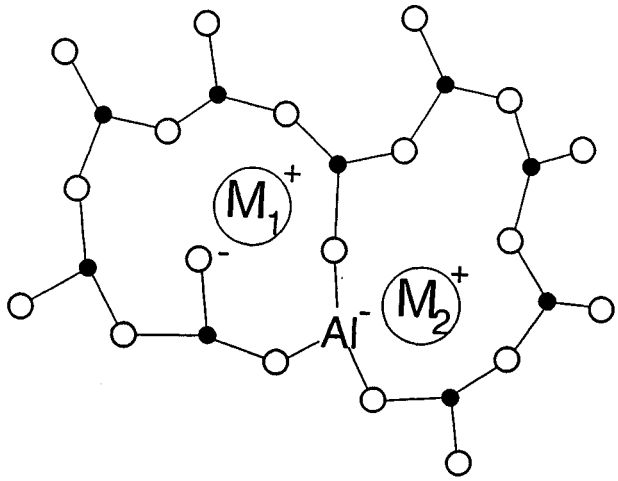


FIGURE 1 A schematic model of the glass network structure. M_1, M_2: network modifier ions accompanied by and without non-bridging oxygen, respectively; large open circle: O; filled circle: tetrahedral network former ions - their fourth bonds project upward or downward from the plane of the drawing.

mixture. Some gaps still remain between them. Lines calculated the compositional dependence of these two scattering coefficients for ternary silicate glasses (SiO_2-$Na_2O.3SiO_2$-$NaAlO_2.3SiO_2$ system which is treated as a regular mixture) [6].

The scattering intensities of commercial optical glasses are known to be larger than that of silica glass [7,8]. Since they usually comprise many components, their concentration scattering becomes large.

B3 Mie Scattering

Anisotropic light scattering by particles not smaller than a wavelength is called Mie scattering. This mostly arises from extrinsic origins, such as crystal precipitation and phase separation [9,10]. Some transparent optical glasses show this type of scattering [8]. This is probably the result of the early stage of phase separation.

C BRILLOUIN AND RAMAN SCATTERING

Light scattering by acoustic and optical phonons is called Brillouin and Raman scattering, respectively. Since the density fluctuation due to acoustic motion is not frozen below T_F, the Brillouin scattering coefficient is described by EQN (1) where T_F is replaced by T [2]. The Brillouin scattering of various oxide glasses was measured to obtain Pockel's coefficients [11-13], which are used in EQN (1).

Since the theoretical representation of Raman scattering intensity is quite complex, some rough approximations must be introduced [2]. Although Raman spectroscopy is widely used for investigating glass structure [14], there have been few reports comparing the absolute intensities of samples [15,16,13].

D CONCLUSION

Scattering properties of glasses are closely related to the thermodynamics in an amorphous state. However, it is difficult to separate density scattering from concentration scattering qualitatively as they include fictive temperature and mixing enthalpy. To achieve this requires the systematic measurement of Pockel's coefficient and isothermal compressibility data for various glasses.

REFERENCES

[1] J. Schroeder [in *Treatise on Materials Science and Technology* vol.12 (Academic Press, New York, 1977) p.157-22]

[2] M.E. Lines [*J. Appl. Phys. (USA)* vol.55 (1984) p.4058-63 and p.4052-7]

[3] D.A. Pinnow, T.C. Rich, J.F.W. Ostermayer, J.M. DiDomenico [*Appl. Phys. Lett. (USA)* vol.22 (1973) p.527-9]

[4] M.E. Lines [*J. Non-Cryst. Solids (Netherlands)* vol.103 (1988) p.279-88]

[5] G.A.C.M. Spierings, T.P.M. Meeuwsen [*J. Non-Cryst. Solids (Netherlands)* vol.66 (1984) p.494-9]

[6] M.E. Lines [*J. Non-Cryst. Solids (Netherlands)* vol.195 (1996) p.249-60]

[7] J. Schroder [*J. Non-Cryst. Solids (Netherlands)* vol.13 (1973) p.313-20]

[8] S. Todoroki, S. Sakaguchi, K. Sugii [*Jpn. J. Appl. Phys. (Japan)* vol.34 (1995) p.3128-33]

[9] M. Tomozawa [in *Treatise on Materials Science and Technology* vol.17 (Academic Press, New York, 1979) p.71-113]

[10] O.V. Mazurin, G.P. Roskova, E.A. Porai-Koshits [in *Phase Separation in Glass* Eds. O.V. Mazurin, E.A. Porai-Koshits (North-Holland, Amsterdam, 1984) ch.4 p.103-42]

[11] J. Schroeder [*J. Non-Cryst. Solids (Netherlands)* vol.40 (1980) p.549-66]

[12] P. Benassi, V. Mazzacurati, G. Ruocco, G. Signorelli [*Phys. Rev. B (USA)* vol.48 (1993) p.5987-96]

[13] P. Benassi, V. Mazzacurati [*Phys. Rev. B (USA)* vol.52 (1995) p.976-81]

[14] H. Scholze [*Glass - Nature, Structure and Properties* (Springer Verlag, 1991)]

[15] F.L. Galeener, J.J.C. Mikkelsen, R.H. Geils, W.J. Mosby [*Appl. Phys. Lett. (USA)* vol.32 (1978) p.34-6]

[16] M.E. Lines, J.B. MacChesney, K.B. Lyons, A.J. Bruce, A.E. Miller, K. Nassau [*J. Non-Cryst. Solids (Netherlands)* vol.107 (1989) p.251-60]

B1.3 Refractive index and dispersion of oxide glass

H. Takebe

July 1997

A INTRODUCTION

Multi-component oxide glasses, which typically consist of glass formers such as SiO_2 and B_2O_3 and modifiers such as Na_2O and CaO, have been studied as alternative materials for low-loss optical fibres for telecommunications. Laser emission of rare-earth ions, especially Nd^{3+} and Er^{3+} ions, has been demonstrated in silicate, phosphate and tellurite glass fibres. Tellurite glass fibre is currently considered as an Er^{3+}-doped fibre amplifier with a broad bandwidth for wavelength-division-multiplexing (WDM) systems.

Refractive index and its dispersion gives us useful information for designing core/clad structure for optical fibres; it also determines the material dispersion, the wavelength dependence of the light wave velocity in transmission. As for laser materials, refractive index dispersion is related to the radiative transition probabilities of active ions and third-order optical non-linearity. This Datareview provides information on refractive index and its dispersion characteristics in multi-component oxide glasses for optical fibres. A good selection of refractive index data for glass in general can be found in [1].

B REFRACTIVE INDEX DATA

The refractive index of oxide glass depends significantly on chemical composition and it is usually characterised at visible wavelengths such as the Na D line (589.3 nm) and the He d line (587.6 nm). TABLE 1 lists refractive indexes of silicate [2,3], aluminosilicate [4] and borosilicate [5] glasses for low-loss optical fibres and phosphate [6] and tellurite [7] glass for fibre lasers and amplifiers. Optical fibres have been successfully fabricated in these glass systems. Multi-component silicate and phosphate glasses have higher refractive indexes in comparison with pure silica glass (n_d = 1.458) due to the incorporation of modifiers such as alkali and alkaline-earth oxides. Tellurite glass containing TeO_2 as a network former possesses a high refractive index of over two, and this characteristic is related to the highly polarisable ion of Te^{4+} [8]. Compositional dependence of refractive index in Na_2O-Al_2O_3-SiO_2 [4], CaO-Al_2O_3-SiO_2 [9] and BaO-Ga_2O_3-GeO_2 [10] glass systems was also studied for the candidates for low-loss optical fibres.

TABLE 1 Refractive indexes of multi-component oxide glasses whose fibres have been successfully fabricated.

Glass composition (mol %)	Refractive index	Ref
19.9 Na_2O - 9.1 CaO - 71 SiO_2	1.518 (n_D)	[2]
30 Na_2O - 10 MgO - 60 SiO_2	1.5138 (n_d)	[3]
16 Na_2O - 6 Al_2O_3 - 78 SiO_2	1.499 (n_D)	[4]
16.9 Na_2O - 32 B_2O_3 - 50.6 SiO_2	1.525 (n_D)	[5]
44 Na_2O - 22.6 Al_2O_3 - 31 P_2O_5 - 2 PbO - 0.4 Er_2O_3	1.5037 (n_D)	[6]
5 Na_2O - 20 ZnO - 75 TeO_2	2.031 (633 nm)	[7]

C FITTING OF REFRACTIVE INDEX DATA

In order to predict refractive indexes at desired wavelengths, refractive index data at specific wavelengths are fitted using a conventional dispersion [3] and a three term Sellmeier [5] equation.

Todoroki et al [3] fitted the refractive index data of Na_2O-MgO-SiO_2 glasses in the region from 0.4 to 3.5 μm using the following equation, where A, B, C, D and E are constants and λ is the wavelength. The errors between measured and calculated values were less than 2×10^{-4}.

$$n = A + \frac{B}{\lambda^2} + \frac{C}{\lambda^4} - D\lambda^2 - E\lambda^4 \quad (1)$$

Mito et al [8] also used the same dispersion equation to fit the data of oxide glasses with basic compositions of new optical fibres in the region from 0.4 to 5.3 μm. The deviation in the fitted index values was approximately 4×10^{-4}. FIGURE 1 shows the refractive index dispersion curves of 30 Na_2O - 10 MgO - 60 SiO_2 (NMS) [3], 65 CaO - 35 Al_2O_3 (CA) [8], 20 Tl_2O - 80 TeO_2 (TT) [8] and 80 PbO - 20 Ga_2O_3 (PG) [8] glasses with the data of silica glass [11] for comparison.

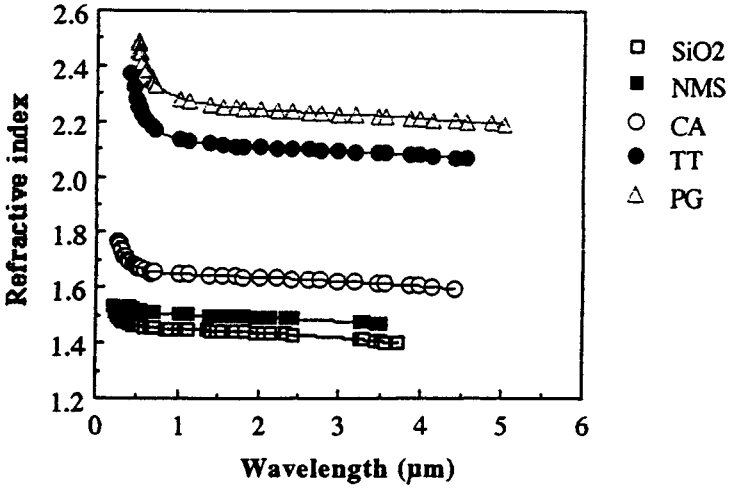


FIGURE 1 Typical refractive index curves for various oxide glasses.

Fleming [5] used a three term Sellmeier dispersion equation, shown as EQN (2), to fit the refractive index data of sodium borosilicate and high silica glasses in the region from 0.4 to 1.5 μm, where λ is the wavelength, A_i are constants related to material oscillator strengths and l_i are oscillator strengths. The average deviation in the fitted index values was better than $\pm 2 \times 10^{-5}$. TABLE 2 shows the fitted Sellmeier coefficients for 16.9 Na_2O - 32.5 B_2O_3 - 50.6 SiO_2 glass [5].

$$n^2 - 1 = \sum_{i=1}^{3} \frac{A_i \lambda^2}{\lambda^2 - l_i^2} \quad (2)$$

TABLE 2 Fitted Sellmeier coefficients for 6.9 Na_2O - 32.5 B_2O_3 - 50.6 SiO_2 glass [5].

A_1	l_1	A_2	l_2	A_3	l_3
0.796468	0.094359	0.497614	0.093386	0.358924	5.999652

D ZERO MATERIAL DISPERSION WAVELENGTH

A component of delay distortion in optical fibres is produced by refractive index dispersion. Material dispersion expressed by EQN (3) is an important property of glass materials for optical fibres to determine the wavelength and width of telecommunication bands [12].

$$M = \frac{\lambda}{c}\frac{d^2n}{d\lambda^2} \tag{3}$$

If one fits the refractive index data of glass by using EQN (1), the material dispersion is determined experimentally by the following equation [3]:

$$M(\lambda) = -\frac{2}{c}\left(\frac{10C}{\lambda^5} + \frac{3B}{\lambda^3} - D\lambda - 6E\lambda^3\right) \tag{4}$$

TABLE 3 shows the zero material dispersion wavelength (ZMDW) with M = 0, λ_0, for some oxide glasses. ZMDW is affected mainly by the absorption due to the electronic transition in the ultraviolet region [8] and the incorporation of modifiers such as Na_2O and MgO promotes the formation of non-bridging oxygen ions with longer resonance wavelengths in comparison with bridging oxygen ions. Therefore, ZMDWs of 16.9 Na_2O - 32.5 B_2O_3 - 50.6 SiO_2 (λ_0 = 1.283), 30 Na_2O - 10 MgO - 60 SiO_2 (λ_0 = 1.502) and 65 CaO - 35 Al_2O_3 (λ_0 = 1.65) glasses are longer than that of silica glass (λ_0 = 1.271). The much longer ZMDWs ($\lambda_0 \geq 2.5$) in the tellurite and heavy-metal gallate glasses are related to the relatively-longer resonance wavelengths of the cations with non-noble gas structure: Te^{4+}, Pb^{2+}, Bi^{3+} and Tl^{+} [8].

TABLE 3 Measured zero material dispersion wavelength λ_0 of multi-component oxide glasses.

Glass composition (mol %)	λ_0 (μm)	Ref
SiO_2	1.271	[3]
16.9 Na_2O - 32.5 B_2O_3 - 50.6 SiO_2	1.283	[5]
30 Na_2O - 10 MgO - 60 SiO_2	1.502	[3]
65 CaO - 35 Al_2O_3	1.65	[8]
20 Tl_2O - 80 TeO_2	2.49	[8]
80 PbO - 20 Ga_2O_3	2.86	[8]
57.1 PbO - 25 Bi_2O_3 - 17.9 Ga_2O_3	2.9	[13]

Materials parameters to predict the ZMDW of new multi-component oxide glasses were reported based on two Sellmeier dispersion [12,14] and Lorentz-Lorenz equations [15].

E CONCLUSION

Refractive index data, the fitting results and zero material dispersion wavelength are presented for multi-component oxide glasses in Sections B - D. The compositional diversity of multi-component oxide glasses leads to the fabrication of high NA (numerical aperture) optical fibres with lower strains. Further investigations are needed to characterise refractive index dispersion as well as the fabrication of low-loss optical fibres for new multi-component oxide glasses.

REFERENCES

[1] N.P. Bansal, R.H. Doremus [*Handbook of Glass Properties* (Academic Press, 1986)]
[2] C.E.E. Stewart, P.W. Black [*Electron. Lett. (UK)* vol.10 (1974) p.53-4]
[3] S. Todoroki, S. Sakaguchi, M. Peeters [*J. Am. Ceram. Soc. (USA)* vol.80 (1997) p.313-6]
[4] D.A. Pinnow, L.G.V. Uitert, T.C. Rich, F.W. Ostermayer, W.H. Grodkiewicz [*Mater. Res. Bull. (USA)* vol.10 (1975) p.133-46]
[5] J.W. Fleming [*Electron. Lett. (UK)* vol.14 (1978) p.326-8]

[6] T. Nishi, K. Nakagawa, Y. Ohishi, S. Takahashi [*Jpn. J. Appl. Phys. (Japan)* vol.31 (1992) p.L177-9]
[7] J.S. Wang, E.M. Vogel, E. Snitzer, J.L. Jackel, U.L. da Silva, Y. Silberberg [*J. Non-Cryst. Solids (Netherlands)* vol.178 (1994) p.109-13]
[8] T. Mito, S. Fujino, H. Takebe, K. Morinaga, S. Todoroki, S. Sakaguchi [*J. Non-Cryst. Solids (Netherlands)* vol.210 (1997) p.155-62]
[9] P.L. Higby, R.J. Ginther, J.D. Aggarwal, E.J. Friebele [*J. Non-Cryst. Solids (Netherlands)* vol.126 (1990) p.209-15]
[10] P.L. Higby, I.D. Aggarwal [*J. Non-Cryst. Solids (Netherlands)* vol.163 (1993) p.303-8]
[11] I.H. Malitson [*J. Opt. Soc. Am. (USA)* vol.55 (1965) p.1205-9]
[12] S.H. Wemple [*Appl. Opt. (USA)* vol.18 (1979) p.31-5]
[13] R.N. Brown [*J. Non-Cryst. Solids (Netherlands)* vol.92 (1987) p.89-94]
[14] K. Nassau [*Bell Syst. Tech. J. (USA)* vol.60 (1981) p.327-37]
[15] S. Fujino [PhD Thesis, Kyushu University, Japan, 1997]

B1.4 Non-linear refractive index of oxide glass

I. Kang and F. Wise

September 1997

A INTRODUCTION

In recent years a considerable effort has been aimed at developing and characterising glasses with large and fast optical non-linearities, motivated largely by the potential application of these materials in all-optical switching devices. Several papers [1-3] offer thorough reviews of progress in this area up until the early 1990s and are highly recommended.

The physical origin of the refractive optical non-linearities of glasses is not understood rigorously. Semi-empirical models of the non-linear response were developed by Miller [4] and by Boling, Glass and Owyoung [5]. To this day the Boling-Glass-Owyoung (BGO) formula for estimating the non-linear index based on the linear optical properties is probably the analysis most commonly employed, and has been a useful guide in the search for highly-non-linear glasses in the absence of a more rigorous theory. Lines developed a bond-orbital theory of the optical non-linearities of alkali-halide crystals [6], and this has been applied to some glasses with some success. It is clear that to obtain a large non-linear refractive index, a large linear refractive index and a small energy gap are desired. In chemical terms, materials with a large number of loosely-bound valence electrons are desired.

B OXIDE GLASSES

The optical non-linearity of 'ordinary' oxide glasses (i.e. glasses not containing heavy elements) is naturally dominated by the oxygen in the structure. Non-bridging oxygen atoms produced by doped cations are more polarisable than bonding oxygens. This is because the non-bonding valence levels are energetically higher than bonding valence levels, and can couple more strongly to conduction levels. Thus, non-bonding oxygens along with the polarisable cations enhance the non-linearity of oxide glasses. Fused silica does not have non-bonding oxygens and thus has the smallest non-linear refractive index among oxide glasses.

The non-linear refractive indices of numerous materials including oxide glasses, the Pb silicate glass SF6 and two tellurite glasses were measured using 3-wave mixing by Adair et al [7]. Nasu and co-workers showed experimentally that non-bonding oxygens are more polarisable than bonding oxygens [8].

C GLASSES DOPED WITH TRANSITION METALS

A number of oxide glasses doped with transition metals have been synthesised and studied. The transition metals with shallow d-electron levels (such as Ti^{4+}, Nb^{5+} and W^{6+}) offer a large number of polarisable valence electrons. According to the bond-orbital theory developed by Lines, the cationic d-band falls below the sp-hybrid conduction band in energy and reduces the bandgap. This gap reduction increases the virtual coupling between the valence band and the d-band, thereby enhancing the (hyper)polarisability.

Sarger and co-workers presented measurements of the linear and non-linear refractive indices of titanium-oxide glasses and tellurite glasses [9]. These measurements were made with a novel femtosecond interferometry technique. Reference [9] also includes an ab initio calculation that

confirms the validity of the phenomenological bond-orbital theory. Nasu et al used third-harmonic generation to determine the non-linear indices of a series of LiTiTe-oxide glasses [10]. Glasses with varying compositions were measured, and non-linear indices as large as forty times that of fused silica were found. Following their own report of relatively high third-order non-linearity in TiNbBNa oxide glass, Vogel and co-workers synthesised two series of glasses in the TiNbNa oxide system [11]. The series were chosen to isolate the contributions of non-bridging oxygens and polarisable cations to the optical properties. Degenerate 4-wave mixing measurements showed that the non-linear indices are proportional to the linear indices of the glasses as predicted by the BGO formula, but the relationship is cation-dependent. In addition, Ti was found to be much more effective than Nb in enhancing the non-linearity.

D GLASSES DOPED WITH POST-TRANSITION HEAVY METALS

Post-transition heavy-metal ions such as Tl^{1+}, Pb^{2+} and Bi^{3+} have the ($6s^2$) electronic configuration, with large ionic radii. As a result, these ions have large polarisabilities. In this system it is well-established that the non-linear index increases with metal-ion concentration. Gallates are preferred over silicates for enhancing the non-linearity owing to their increased densities, which lead to increased linear refractive indices.

Thomazeau et al measured the optical Kerr effect in a variety of doped silicate glasses with 100-fs pulses [12]. These were mostly Pb silicate glasses (Schott SF series), but one Ti-doped glass (Hoya FD60) was also measured. A non-linear index ~45 times that of SiO_2 was measured for SF59 glass. It is worth mentioning that these measurements were made with 620 nm light; the vast majority of previous measurements of non-linear indices were made with 1.06 μm light from an Nd:YAG laser. Even so, good agreement with the BGO formula was found. Hall and co-workers also measured a series of Pb silicate glasses, along with PbBi germanate and PbBi gallate glasses [13]. The non-linear index was found to scale with heavy-metal content, and the PbBi gallate glass RN was found to have a non-linear index approximately six times that of SF59 glass. Later it was found that the non-linearity of similar glasses could be enhanced by a factor of two by replacing lead or bismuth with thallium [14]. The substitution of thallium also shifts the absorption edge of the glass to longer wavelengths, so the figure of merit of the glass (proportional to n_2/α) may actually decrease. Pan et al measured the non-linear indices of a series of Pb borate glasses [15]. These workers found that the non-linear index and the Raman-scattering cross section both increase with lead-oxide content. Borrelli et al reported four-wave mixing measurements of the non-linear indices of a variety of glasses doped with lead, bismuth and thallium [3]. These results agree with measurements made by Kang at a wavelength of ~1 mm on similar glasses [16] and include non-linear indices two orders of magnitude larger than that of fused silica.

E TELLURITE GLASSES

Tellurite glasses utilise the large polarisability of the lone electron pairs of the Te^{4+} ion. Transition-metal oxides or post-transition metal oxides are usually added to enhance the optical non-linearity. References [7], [9] and [10] include the results of measurements of the non-linear indices of tellurite glasses.

F DISPERSION OF THE OPTICAL NON-LINEARITIES

Virtually all reported measurements of the third-order optical non-linearities of glasses (non-linear refraction and two-photon absorption) were made at one or two wavelengths. Kang et al measured the non-linear refractive indices and 2-photon absorption coefficients of a variety of heavy-metal oxide glasses (PbBi borosilicate, PbBi gallate, Pb tellurite and TlBi gallate) at 600, 800, 990 and 1250 nm

[16]. Qualitatively similar variation was found for all samples; the results are exemplified by the data for a TlBi gallate glass shown in FIGURE 1. The steep increase of the non-linearities below 900 nm is probably due to resonant enhancement, given the proximity of the linear absorption edge. The third-order susceptibilities at 600 nm are among the largest values ever reported for glasses, with Re $\chi^{(3)} > 10^{-11}$ esu. The weaker increase between 1250 and 900 nm can be understood from general principles: analysis of the general quantum-mechanical expression for the second hyperpolarisability shows that it should deviate from the static value as a quadratic function of frequency far off resonance [17]. The expression for the off-resonant third-order susceptibility is qualitatively consistent with Kang's results.

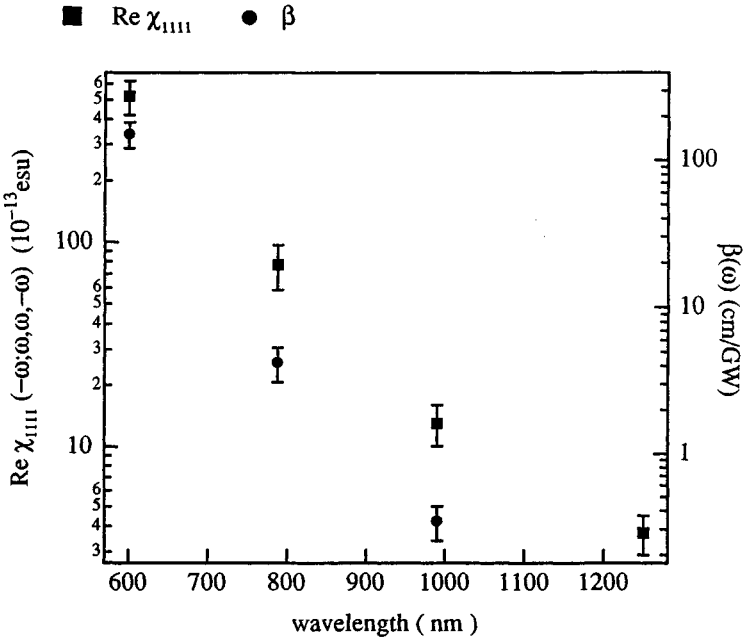


FIGURE 1 Real part of the third-order susceptibility Re $\chi^{(3)}$ (-ω;ω,ω,-ω) and the two-photon absorption coefficient β of a TlBi gallate glass plotted versus wavelength.

G NUCLEAR CONTRIBUTIONS TO THE THIRD-ORDER NON-LINEARITIES

The magnitude of any nuclear contribution to the third-order optical non-linearities was an unresolved issue for many years. Hellwarth and co-workers originally estimated the relative contributions of electronic and nuclear mechanisms to the third-order polarisation of glasses by analysing Raman-scattering spectra along with intensity-induced polarisation changes [18]. Pan et al used the same reasoning to determine the electronic and nuclear contributions to the non-linearities of lead borate glasses [15]. In each case the nuclear contribution was estimated to be 5 - 20% of the total polarisation. Despite the substantial nuclear polarisabilities of most glasses, there was no direct measurement of the nuclear response until Kang et al reported [19] the observation of the coherent nuclear response of glasses. Typical data are shown in FIGURE 2. The clear isolation of electronic and nuclear responses possible in the time domain allows for direct estimation of their relative strengths. The fractional nuclear contribution is 13% in this case, quite similar to the values estimated previously [15,18] for different materials and elements of the response tensor. These experiments also constitute the first observation of coherent phonons in a glass.

H ADVANCES IN MEASUREMENT TECHNIQUES

Prior to 1990, almost all measurements of third-order susceptibilities of glasses were made using 3-wave mixing, 4-wave mixing or third-harmonic generation. In 1989 the z-scan was introduced [20]. This is a simple, single-beam technique that provides the magnitude and sign of the real and imaginary

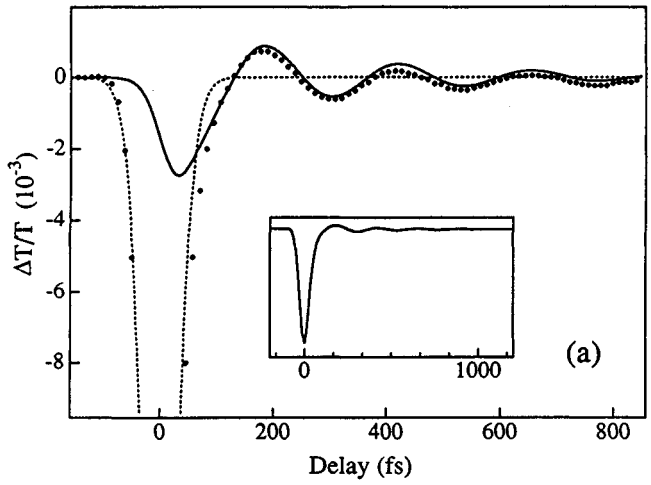


FIGURE 2 Time-resolved z-scan signal from the PbBi oxide glass. Symbols: experimental data; solid line: nuclear contribution calculated from the polarised and depolarised Raman spectra; dotted line: electronic contribution. The total experimental signal is shown in the inset.

parts of $\chi^{(3)}$. The data reported in [15] and [16] were obtained from z-scan measurements. The z-scan is not particularly sensitive; it is difficult to measure non-linear phase shifts ($\Delta\Phi$) less than 0.05 rad using it. The sensitivity is improved to $\Delta\Phi \sim 10^{-3}$ rad in the time-resolved z-scan (used in [19]) because the sample is not moved, so scatter is reduced. Much greater sensitivity is possible using the optical-heterodyne-detected Kerr effect [21] or time-resolved interferometry [22]. Both of these techniques can resolve non-linear phase shifts as small as 10^{-6} rad, but at a cost of significant complexity in the construction and operation of the experiment. Kang et al recently demonstrated that equal and perhaps better sensitivity can be obtained in a very simple experiment based on spectrally resolving a two-beam coupling signal [23]. This technique also gives the magnitude and sign of the real and imaginary parts of $\chi^{(3)}$ in a single experiment. Typical data from a 1 mm piece of fused silica are shown in FIGURE 3; the noise level implies a sensitivity $\Delta\Phi = 3 \times 10^{-6}$ rad.

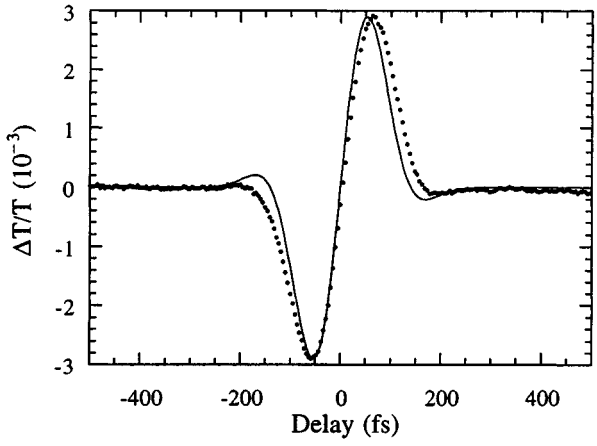


FIGURE 3 Two-beam coupling signal from fused silica (symbols) along with the theoretical fit to the data (solid curve). The peak of the signal corresponds to a non-linear phase shift $\Delta\Phi = 4 \times 10^{-4}$ rad. The trace was obtained using nanojoule-energy pulses from a modelocked laser and noise was reduced by simply averaging 1000 traces (obtained in ~2 minutes).

REFERENCES

[1] M.E. Lines [*J. Appl. Phys. (USA)* vol.69 (1991) p.6876]

[2] E.M. Vogel, M.J. Weber, D.M. Krol [*Phys. Chem. Glasses (UK)* vol.32 (1991) p.231]
[3] N.F. Borrelli, B.G. Aitken, M.A. Newhouse [*J. Non-Cryst. Solids (Netherlands)* vol.185 (1995) p.109]
[4] R.C. Miller [*Appl. Phys. Lett. (USA)* vol.5 (1964) p.17]
[5] N.L. Boling, A.J. Glass, A. Owyoung [*IEEE J. Quantum Electron. (USA)* vol.QE-14 (1978) p.601]
[6] M.E. Lines [*Phys. Rev. B (USA)* vol.41 (1990) p.3383; *Phys. Rev. B (USA)* vol.43 (1991) p.11978]
[7] R. Adair, L.L. Chase, S.A. Payne [*J. Opt. Soc. Am. B (USA)* vol.4 (1987) p.875]
[8] H. Nasu, O. Sugimoto, J. Matsuoka, K. Kamiya [*J. Non-Cryst. Solids (Netherlands)* vol.182 (1995) p.321]
[9] E. Fargin et al [*J. Non-Cryst. Solids (Netherlands)* vol.203 (1996) p.96]
[10] H. Nasu, O. Matsushita, K. Kamiya, H. Kobayashi, K. Kubodera [*J. Non-Cryst. Solids (Netherlands)* vol.124 (1990) p.275]
[11] E.M. Vogel et al [*J. Non-Cryst. Solids (Netherlands)* vol.107 (1989) p.244]
[12] I. Thomazeau, J. Etchepare, G. Grillon, A. Migus [*Opt. Lett. (USA)* vol.10 (1985) p.223]
[13] D.W. Hall, M.A. Newhouse, N.F. Borrelli, W.H. Dumbaugh, D.L. Weidman [*Appl. Phys. Lett. (USA)* vol.54 (1989) p.1293]
[14] J. Yumoto, S.G. Lee, B. Kippelen, N. Peyghambarian, B.G. Aitken, N.F. Borrelli [*Appl. Phys. Lett. (USA)* vol.63 (1993) p.2630]
[15] Z. Pan, S.H. Morgan, B.H. Long [*J. Non-Cryst. Solids (Netherlands)* vol.185 (1995) p.127]
[16] I. Kang, T.D. Krauss, F.W. Wise, N.F. Borrelli, B.G. Aitken [*J. Opt. Soc. Am. B (USA)* vol.12 (1995) p.2053]
[17] D.M. Bishop [*Phys. Rev. Lett. (USA)* vol.61 (1988) p.322]
[18] R. Hellwarth, J. Cherlow, T.-T. Yang [*Phys. Rev. B (USA)* vol.11 (1975) p.964]
[19] I. Kang, S. Smolorz, T. Krauss, F. Wise, N.F. Borrelli, B.G. Aitken [*Phys. Rev. B (USA)* vol.54 (1996) p.R12641]
[20] M. Shiek-Bahae, A.A. Said, E.W. Van Stryland [*Opt. Lett. (USA)* vol.14 (1989) p.955]
[21] D. McMorrow, W.T. Lotshaw, G.A. Kenney-Wallace [*IEEE J. Quantum Electron. (USA)* vol.QE-24 (1988) p.443]
[22] L. Sarger et al [*J. Opt. Soc. Am. B (USA)* vol.11 (1994) p.995]
[23] I. Kang, T. Krauss, F. Wise [*Opt. Lett. (USA)* vol.22 (1997) p.1077]

PART B: OXIDE GLASS

CHAPTER B2

THERMAL AND MECHANICAL PROPERTIES

B2.1 Mechanical properties of oxide glass
B2.2 Viscosity of oxide glass
B2.3 Stability of oxide glass

B2.1 Mechanical properties of oxide glass

D.W. Hewak

August 1998

A INTRODUCTION

The mechanical response of a glass to an applied force is described by various moduli including Young's modulus, Poisson's ratio and the bulk modulus. For common oxide glasses, these parameters have been well characterised [1]. The hardness of a glass is an indication of its vulnerability to surface damage and the ease with which it can be polished. It is usually indicated from the indentation of Knoop or Vickers penetrators. In this Datareview, the measurement and typical values for these mechanical properties of oxide based glasses are presented.

B MODULI

Glass shows an almost perfect brittle-elastic behaviour at temperatures lower than the transformation point, i.e. the deformation is proportional to the stress (Hooke's law). If the ends of a rod are exposed to a stress σ, its relative elongation is given by

$$\Delta l/l = \sigma/E \quad (1)$$

where E is the modulus of elasticity or Young's modulus. As a result of the elongation of the rod its cross-section is decreased. The relation between the relative decrease in the thickness t and the relative elongation is called Poisson's ratio, defined as

$$\Delta t/t \,/\, \Delta l/l = \mu \quad (2)$$

The torsion of a rod is characterised by the modulus of torsion (or shear modulus) G. The properties E, G and μ are characteristic constants of an individual glass type. The relationship between these moduli is given by

$$E = 2(1 + \mu)G \quad (3)$$

Under unilateral stress, Poisson's ratio is the ratio of lateral to longitudinal strain. Reference [1] tabulates the Young's modulus of over two hundred common optical glasses. Recent measurements along with experimental and theoretical research on phosphate and tellurite can be found in [2-8].

The bulk modulus B, also defined as the inverse of the isothermal compressibility, is related to the above moduli by

$$B = E/3(1 - \mu) \quad (4)$$

Measurement of Young's modulus and the torsional rigidity modulus is typically carried out on well annealed glass rods. An electromechanical system is used to induce natural vibrations in the rods between 1 and 10 kHz. Young's modulus is calculated from the transverse vibrations and the torsional rigidity modulus from the torsional vibrations of the rods. Results from a series of glasses are presented in TABLE 1. In FIGURE 1, Young's modulus as a function of temperature is plotted for several oxide glasses.

TABLE 1 Mechanical properties at 589 nm for representative optical glasses.

Glass type	Knoop hardness (N/mm^2)	Young's modulus (10^3 N/mm^2)	Poisson's ratio
Fused silica (SiO_2)	450	70	0.170
Fluorophosphate (FK54)	320	76	0.286
Fluorosilicate (FK5)	450	62	0.205
Fluorozirconate (ZBLAN)	250	54	0.31
Borosilicate (BK7)	520	81	0.208
Barium silicate (SK14)	490	86	0.261
Alkali lead silicate (F2)	370	58	0.225
Lanthanum borate (LaFN2)	450	87	0.294
Lead silicate (SF2)	350	55	0.231
Arsenic trisulphide (As_2S_3)	180	16	0.240

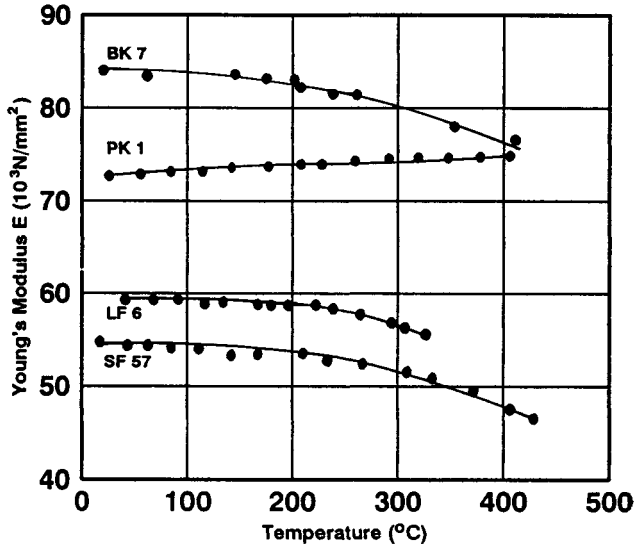


FIGURE 1 Young's modulus as a function of temperature for a number of optical glasses [13].

C MICROHARDNESS

The resistance of a material to indentation is characterised by the indentation hardness. Several testing methods can be used including scratching, abrasion and penetration; however the results are not comparable. Two penetration methods, which yield the Vickers and Knoop hardness, have emerged as standards in the optical glass industry. In both these, indentation from a diamond tool is determined. This serves to characterise the behaviour of a glass with permanent changes in the surface which are due to the penetration of a body. There is some correlation of this deformation with the Young's modulus [1].

Vickers hardness is determined by using a diamond in the form of a square pyramid with an included angle of 136° between the opposite faces. The procedure for measuring Knoop hardness differs by the use of a rhombus-shaped diamond so that the intersections between adjacent facets have included angles of 172.5° and 130.0°, respectively. During pressing of the diamond into a glass plate an elastic and a plastic deformation occurs and after the experiment a permanent indentation is left. With the aid of a microscope, the largest diagonal d of the indentation is measured. The hardness is then defined by

$$HV = 0.1855\ F/d^2, \quad \text{Vickers hardness} \tag{5}$$

$$HV = 1.4233\ F/d^2, \quad \text{Knoop hardness} \tag{6}$$

Representative values of the Knoop hardness are also given in TABLE 1. The indentation hardness depends on the chemical composition of the glass. FIGURE 2 shows the dependence of Knoop hardness on lead content for a series of lead-alkali-silicate glasses.

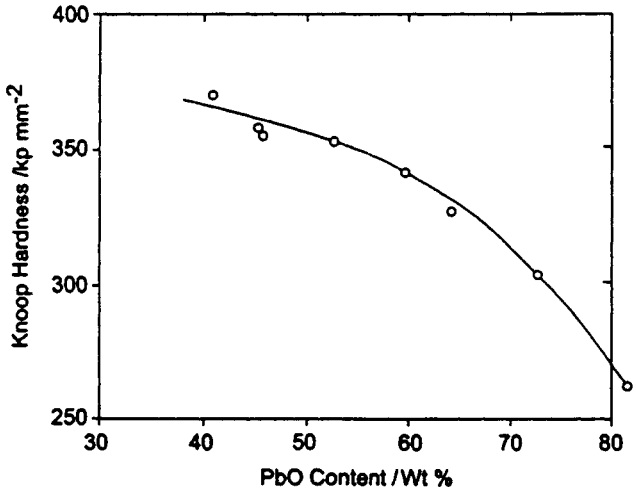


FIGURE 2 The dependence of Knoop hardness on lead content for a series of lead-alkali-silicate glasses [1].

In addition to the mechanical moduli and hardness, other related physical properties are often important. Among these glass strength, and more specifically, brittle fracture, crack growth, fracture probability and fatigue are often characterised [9-12]. Typically of concern for bulk optical components, there are often analogies with glass in fibre form.

REFERENCES

[1] K. Natterman, N. Neuroth, R.J. Scheller [in *The Properties of Glass* Eds. H. Bach, N. Neuroth (Springer, Berlin, 1998) ch.4 p.179-200]
[2] R.E. Mallawany [*J. Mater. Res. (USA)* vol.5 (1990) p.2218]
[3] R.E. Mallawany [*J. Mater. Sci. Lett. (UK)* vol.7 (1988) p.870]
[4] E.F. Lambson, G.A. Saunders, S. Hart [*J. Mater. Sci. Lett. (UK)* vol.4 (1985) p.669]
[5] E.F. Lambson, G.A. Saunders, B. Bridge, R.E. Mallawany [*J. Non-Cryst. Solids (Netherlands)* vol.69 (1984) p.117]
[6] B. Bridge, A.A. Higazy [*Phys. Chem. Glasses (UK)* vol.27 (1986) p.1]
[7] B. Bridge, N.D. Patel, D.N. Waters [*Phys. Status Solidi A (Germany)* vol.77 (1983) p.655]
[8] B. Bridge [*Phys. Chem. Glasses (UK)* vol.29 (1988) p.1]
[9] R.H. Doremus [*Treatise on Materials Science and Technology, vol.22* (Academic Press, New York, 1982) p.170-225]
[10] H. Tada, P.C. Paris, G.R. Lewis [*The Stress Analysis of Cracks Handbook, 2nd Edn.* (Paris Productions, France, 1985)]
[11] W.C. LaCourse ['The Strength of Glass' in *Introduction to Glass Science* Eds. D. Pye, H.J. Stevens, W.C. LaCourse (Plenum, New York, 1972)]
[12] G.W. McLellan, E.B. Shand ['Strength and Strength Testing' in *Glass Engineering Handbook* (McGraw-Hill, New York, 1984)]
[13] [*Schott Optical Glass Catalogue: Types of Optical Glass* (Schott, Mainz)]

B2.2 Viscosity of oxide glass

D.W. Hewak

July 1998

A INTRODUCTION

The viscosity of a glass is one of its most important technological properties. It determines the melting conditions, fining behaviour (removal of bubbles from the melt), annealing temperature, the temperatures of drawing and working, upper temperature of use and devitrification rate. The viscosities of different glasses vary enormously with composition and are strong functions of temperature.

Between their melting points and normal room temperature, glasses pass through a viscosity range of 15 - 20 orders of magnitude and three different thermodynamic states: the melt, the undercooled melt and the frozen melt. These states and the temperatures which define them are indicated schematically in FIGURE 1. The general course of viscosity as a function of temperature is shown in FIGURE 2. A steady and smooth change in viscosity in all temperature regions is a fundamental characteristic of glass [1].

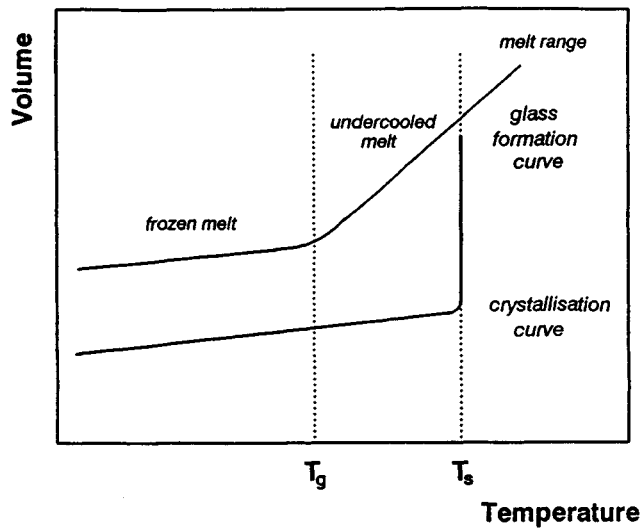


FIGURE 1 Schematic volume-temperature curves for crystallisation and for glass formation.

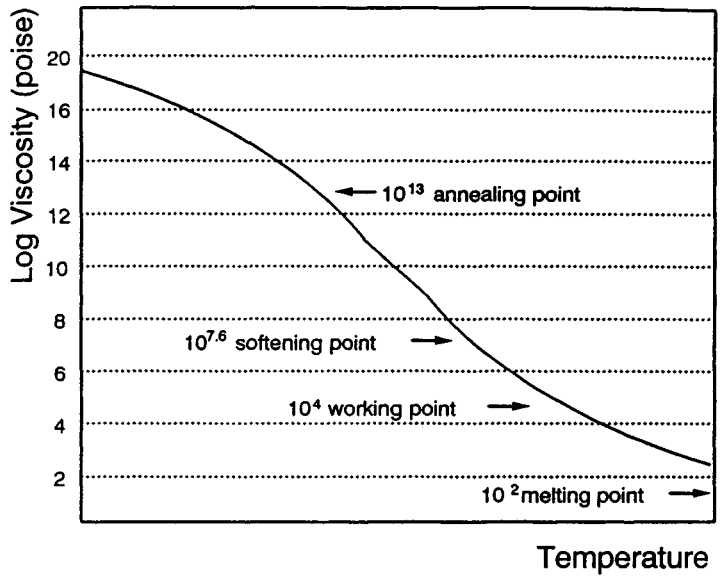


FIGURE 2 Typical viscosity temperature curve showing key temperatures.

In this Datareview, the principle methods of viscosity evaluation of oxide based glasses are reviewed, along with data of compositions of current interest.

B MEASUREMENT METHODS

Unlike silica, whose characteristic temperatures are high [2], or the fluoride [3] and chalcogenide glasses [4], which are prone to devitrification, the measurement of the viscosity of most oxide glasses is relatively straightforward. It is not possible to measure the entire viscosity-temperature curve with one universal apparatus and a series of procedures are used.

When two layers of a fluid move parallel in the same direction but at different velocities, a mutual force is exerted between them [5]. Those fluids for which this force is proportional to the velocity gradient perpendicular to the direction of the fluid flow are called Newtonian fluids. The constant of proportionality is called the (shear) velocity η

$$\tau = \eta\,(T)\,.\,\gamma \qquad (1)$$

where τ is the shear stress and γ is the shear rate. Application of large or rapid shear deformations can lead to non-Newtonian behaviour of the glass melt. The material may exhibit brittle elastic behaviour [6] or the large deformations can lead to a reduction in the viscosity (shear thinning) in these zones [7-10].

B1 Working Point

In the temperature range of the working point ($\eta = 10^3$ poise) the friction of a rotating cylinder in a crucible with molten glass can be used to determine its viscosity [1]. If the gap between the crucible wall and the cylinder surface is small, the viscosity follows from

$$\eta = MD/(4\pi^2R^3\,H\,\omega) \qquad (2)$$

where M is the angular momentum, D the gap thickness, R the cylinder radius, H the height and ω the angular frequency. This technique, which is the principle of the Margules viscometer, offers high precision and accuracy over a viscosity range of 10 to 10^7 poise. Constant rotation works well to 10^4 poise, above which torques can get excessive. At this point, the time required for the rotation to stop between two selected angles is used to calculate the viscosity.

B2 Softening Point

The most widely used primary control viscosity test is the softening point. This test measures viscosity deviations very precisely for a given composition but it does not indicate a viscosity level that is constant for all glasses. The method of test determines the temperature at which a uniform fibre of glass 0.55 to 0.75 mm in diameter and 23.5 cm long elongates under its own weight at a rate of 1 mm per minute when the upper 10 cm of its length is heated in a specified furnace at a rate of approximately 5°C per minute. The elongation is measured with a suitable optical extensometer [1].

A measurement procedure which determines the softening point and permits direct viscosity measurements in this intermediate range is the parallel plate viscometer. This method has long been a standard measurement apparatus and has been well described by Fontana [11].

B3 Annealing Point

For glasses which can be cut and ground, beam bending provides a simple test with several advantages; the sample is in a uniform temperature zone, expansion corrections are negligible and measurements on very hard glass are possible.

The basic apparatus is as follows. A beam of uniform cross section is supported on an alumina muffle, a load is applied at mid-span with a flame-bent sapphire hook, and the mid-point deflection is measured. Viscosity is calculated from the equation:

$$\eta = gS^3/2.4\, I_c\, v\, [M + \rho\, AS/1.6] \qquad (3)$$

where: S = support span, cm
I_c = cross-section moment of inertia of test beam, cm^4
v = midpoint deflection rate, cm/min
A = cross-sectional area of beam, cm^2
ρ = density of glass, g/cm^3
M = applied load, g.

C FITTING OF VISCOSITY DATA

A first guide for measuring the temperature dependence of the viscosity is the Arrhenius law for thermally activated processes

$$\eta = \eta_o \exp (H/RT) \qquad (4)$$

where H is the activation enthalpy necessary for breaking all oxygen bridges (as long as the shear force is small compared with the interatomic forces) and R is the gas constant. This relationship holds well around the annealing temperature. For higher temperatures, the activation enthalpy takes lower values. This effect is connected with the increasing free volume in the glass [12].

A good representation for all temperatures can be obtained with the Vogel-Fulcher-Tammann equation [13]:

$$\eta = \eta_o \exp [Q/R(T - T_o)] \qquad (5)$$

The physical nature of the Vogel-Fulcher-Tammann equation has been discussed a lot, especially with respect to the introduction of a characteristic temperature T_o at which the viscosity becomes infinite. The parallel between the temperature dependence of the natural logarithm of η, $\ln \eta \propto 1/(T - T_o)$, and the paramagnetic susceptibility of ferromagnetic materials above the Curie temperature, indicates that there is a second-order phase transition at T_o.

It has to be emphasised that the Vogel-Fulcher-Tammann equation that gives the equilibrium viscosity is not applicable for a non-equilibrium glass. Usually, the glass transition occurs at temperatures far above T_o, so the second-order phase transition problem is circumvented. Below the glass transition, in the non-equilibrium region, the following modification of Hodge's equation holds [14]:

$$\eta = \eta_o \exp [(Q/R)/T(1 - T_o/T_g)] \qquad (6)$$

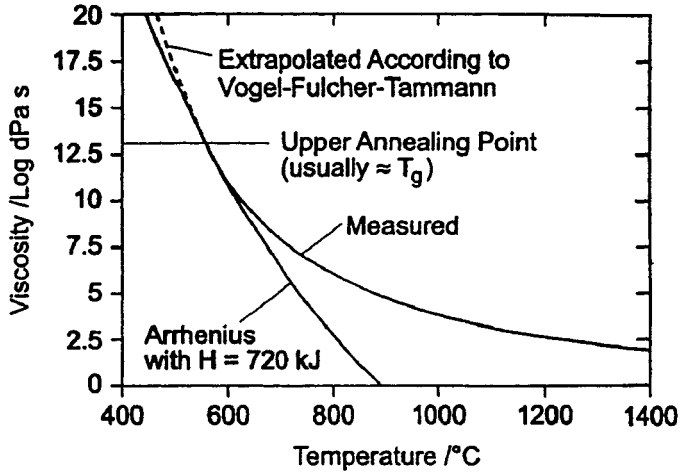


FIGURE 3 Viscosity temperature curve of borosilicate glass from [12].

D CONCLUSION

The rheological behaviour of glass has been discussed in a basic manner applicable to oxide and most traditional glasses. The reference points have been defined and experimental apparatus generally used for measuring viscosity in these ranges reviewed.

REFERENCES

[1] H.E. Hagy [in *Introduction to Glass Science* Eds. L.D. Pye, H.J. Stevens, W.C. Lacourse (Plenum Press, New York, 1972) p.343]
[2] K. Tajima [Datareview in this book: *A2.1 Viscosity of silica glass*]
[3] M. Braglia [Datareview in this book: *C2.2 Viscosity of halide glass*]
[4] D. Hewak, D. Brady [Datareview in this book: *D2.1 Characteristic temperatures of chalcogenide glass*]
[5] A. Dengel [*Rheol. Acta (Germany)* vol.94 (1994) p.133]
[6] M. Coenen [*Glastech. Ber. (Germany)* vol.51 (1978) p.17-20]
[7] J.H. Li, D.R. Uhlmann [*J. Non-Cryst. Solids (Netherlands)* vol.3 (1970) p.127-47 and p.205-24]
[8] J.H. Simmons, R.K. Mohr, C.J. Montrose [*J. Appl. Phys. (USA)* vol.53 (1982) p.4075-80]
[9] P. Manns, R. Bruckner [*Glastech. Ber. (Germany)* vol.61 (1988) p.46-56]
[10] J.H. Simmons, R.K. Mohr, C.J. Montrose [*J. Non-Cryst. Solids (Netherlands)* vol.105 (1988) p.313-22]
[11] E.H. Fontana [*Am. Ceram. Soc. Bull. (USA)* vol.49 (June 1970) p.594-7]
[12] U. Fotheringham [in *The Properties of Optical Glass* Eds. H. Bach, N. Neuroth (Springer, Berlin, 1989) ch.5 p.201-28]
[13] R.H. Doremus [*J. Am. Ceram. Soc. (USA)* vol.49 (1966) p.461]
[14] G.W. Scherer [*Relaxation in Glass and Composites* (Wiley, New York, 1986) p.157]

B2.3 Stability of oxide glass

D.W. Hewak

August 1998

A INTRODUCTION

Glasses have primarily been developed to obtain certain optical characteristics. The extensive group of oxide glasses covers an extremely wide range from chemically inert glass to very easily attacked glasses. The different chemical reactions which may occur between a glass or glass fibre surface and its surrounding environment have been described and explained in the literature [1-5]. In this Datareview, a general survey is made of the ways in which glass can be attacked. Several types of corrosion mechanism have been identified and testing methods proposed for an evaluation of the susceptibility of a glass to attack. In most cases, the main effects are on the glass surface. The behaviour of the outermost layers is of greatest interest since even slight corrosion of the surface can make a glass body useless. In fibre applications, where the ratio of surface to volume is high, slight attack of the surface can destroy the fibre.

B ATTACK BY WATER

Water may be present in excess as a liquid or in deficiency as humidity or droplets. When aqueous solutions react with a glass surface of low resistance, two mechanisms take place: one in dissolving the glass network (dissolution of the glass) and the second an interdiffusion reaction (ion exchange with elements in the surface layer). In either case, OH^- ions destroy the bonds between the ions that give the glass its structure. There is usually an overlap between the two processes. The final result of the overall corrosion process is complex and a function of the environment and the reaction thermodynamics.

Network dissolution may be congruent, when all constituents are extracted into solution at the same time, or selective in the component which is attacked. In the former case, the resulting surfaces can then be blank, without visible changes. Selective removal of only mobile glass constituents results in a layer rich in the immobile network formers. These reactions are characterised by the dissolution velocity and in some cases the glass surface is quickly removed.

When ion exchange is present, selected glass constituents are extracted from the glass when it is exposed to water. If the diffusion velocity is dominant, water molecules diffuse into the surface and can react with cations. In oxide glasses there can be numerous constituents and many of them can form insoluble or poorly soluble new components such as hydroxides or, in the presence of air, carbonates [6,7]. It is generally accepted that this involves an ion exchange between hydrogen and cations such as Na^+ and Ca^{2+}, which results in the development of a surface layer which is compositionally and structurally different from the unreacted glass.

Attack by water can take place extremely slowly and is highly dependent on the amount of water present. With neutral water, the pH value remains practically unchanged when water is present in abundance. If only a little water is present, carbon dioxide from the air can lead to an acidic reaction. An alkaline reaction can result when small quantities of aqueous solution are enriched by alkali ions that migrate from the glass.

C CHEMICAL REACTIONS

Chemical reactions are of concern during processing of glass. Alkaline attack commences at a very significant rate when the pH of a solution has risen to 9. For most oxide glasses, a pH of 8 represents the safe limit that should not be exceeded. Processing such as lapping, grinding and polishing in which a liquid phase is present is of particular concern. During polishing the slurry is progressively enriched by the fine abrasive particles which can be easily leached by water. Alkali ions from the glass can increase the pH value of a neutral slurry: thus pH should be checked and kept within limits to ensure optimum processing conditions. In practice, optical glasses are rarely exposed to acid attacks during processing. During use and handling however, attack by humidity from breath precipitation, fingerprints, etc. can result in weak acidic attack.

D TESTING METHODS

Individual testing methods have been developed by different glass manufacturers and laboratories. The variety of optical glasses and the great number of parameters influencing the chemical attack means a single test cannot cover the whole range of cases. Depending on the pH of the attacking medium, these tests can be roughly divided into three categories: acid resistance tests, alkali resistance tests (including detergent tests), and hydrolytic resistance tests (concerning climate, weather and water). In most of these procedures, solid glass plates are used and compared to each other. In some tests however, glass grains of approximately 500 micron size are used. Typical testing methods are described in TABLES 1 - 3 and further details can be found in [1].

TABLE 1 Testing of acid resistance with two different acids.

Attacking medium	(a) nitric acid, c = 0.5 mol/l, pH = 0.3 (for high resistance glass types) (b) sodium acetate buffer, pH = 4.6 (for glasses with lower resistance)
Temperature	25°C +/- 0.2°C
Duration of test	0.2 - 100 hr
Samples	glass plates polished on all sides 30 mm × 30 mm × 2 mm, edges bevelled
Further conditions	vessel of borosilicate glass stirring to 100 rpm samples fastened with platinum wire are hanging in the solution
Measuring process	weight of the sample before and after treatment visible surface changes
Classification	according to the time which is necessary to etch a surface layer of 0.1 μm (derived from the weight loss per cm^2 and the density)

TABLE 2 Raw optical glass testing of the resistance to attack by aqueous alkaline solution.

Attacking medium	aqueous solution of penta-sodium-triphosphate ($Na5P_3O_{10}$) C = 0.01 mol/l, pH = 10, in excess
Temperature	50°C +/- 0.2°C
Duration of test	0.25 - 16 hr
Samples	glass plates polished on all sides 30 mm × 30 mm × 2 mm, edges bevelled
Further conditions	vessel of silver or stainless steel stirring 100 rpm samples fastened with platinum wire are hanging in the solution
Measuring process	weight of the sample before and after treatment visible surface changes
Classification	according to the time which is necessary to etch a surface layer of 0.1 μm (derived from the weight loss per cm^2 and the density)

TABLE 3 Hydrolytic resistance for water in excess and in deficiency.

Water in excess	
Attacking medium	boiling water, pH neutral, in excess
Temperature	100°C
Duration of test	60 minutes
Samples	freshly prepared glass grains 420 - 590 μm
Further conditions	samples placed in a platinum basket are hanging in the solution
Measuring process	weight of the sample before and after treatment
Classification	water resistance classified by percent weight loss
Water in deficiency	
Attacking medium	saturated water vapour
Temperature	alternating between 40°C and 50°C in cycles of 60 minutes
Duration of test	varying 30 - 180 hr
Samples	glass plates polished on all sides 30 mm × 30 mm × 2 mm, edges bevelled
Further conditions	climate chamber producing alternate condensation on surface followed by evaporation in a one hour cycle
Measuring process	weight of the sample before and after treatment visible surface changes
Classification	measuring percentage of light scatter

E CONCLUSION

These brief explanations are enough to make it clear that no single test method can suffice as a means of describing the chemical behaviour of all optical glasses. The user of a glass must therefore gather all the information he can concerning the chemical behaviour in order to be able to exclude the possibility of disadvantageous changes during processing. Depending on the application in question, the user should base a decision on the results obtained with a number of test methods.

REFERENCES

[1] W. Heimerl, A. Peters [in *The Properties of Optical Glass* Eds. H. Bach, N. Neuroth (Springer, Berlin, 1989) ch.6 p.229-44]

[2] T.S. Izumitani [*Optical Glass* (American Institute of Physics, Translation Series, New York, 1986) p.42]

[3] R.H. Doremus [*Mater. Res. Soc. Symp. Proc. (USA)* vol.125 (1988) p.177-88]

[4] L.L. Hench [*Mater. Res. Soc. Symp. Proc. (USA)* vol.125 (1988) p.189-200]

[5] L.M. Cook [*J. Non-Cryst. Solids (Netherlands)* vol.120 (1990) p.152-71]

[6] H. Bach, F.G.K. Baucke [*Phys. Chem. Glasses (UK)* vol.15 (1974) p.123-9]

[7] H.H. Dunken [in *Treatise on Materials Science and Technology, vol.22, Glass III* Eds. R.H. Doremus, M. Tomozawa (Academic Press, New York, 1982) p.1-74]

PART B: OXIDE GLASS

CHAPTER B3

RARE-EARTH SPECTROSCOPY

B3.1 Spectroscopy of neodymium-doped oxide glass
B3.2 Spectroscopy of erbium-doped oxide glass

B3.1 Spectroscopy of neodymium-doped oxide glass

H. Yanagita, E. Ishikawa and H. Aoki

September 1997

A INTRODUCTION

Since the first laser action was demonstrated in a neodymium-doped glass by Snitzer [1], many types of neodymium-doped laser glasses have been researched and developed. Especially, spectroscopic and physical properties of neodymium-doped oxide glasses were investigated in detail by Lawrence Livermore National Laboratory [2].

This Datareview describes the spectroscopic properties, including absorption, fluorescence and lifetimes, of neodymium-doped oxide glass.

B ABSORPTION

The neodymium ion has a large number of closely spaced and intense absorption bands between the UV and near IR regions. FIGURE 1 illustrates an absorption spectrum of Nd^{3+} doped glass [3]. The $^3F_4$ level is the only metastable state for common oxide glasses because of fast non-radiative decay rates in higher excited levels, and no emission from any other levels can be substantially observed at room temperature. Efficient flash lamp pumped glass laser oscillators and amplifiers around 1.06 μm have been demonstrated based on these characteristics of Nd^{3+}. Some of the absorption bands coincide with the wavelength of laser pumping sources such as the Ar ion laser (514.5 nm) and laser diodes. There have been reports on the absorption spectra of Nd^{3+} in a range of glass systems. Absorption spectra of a wide variety of glass compositions were summarised in [2-4]. They also calculate the integrated absorption cross-section from 400 to 950 nm. A Judd-Ofelt analysis [5-10] has been performed for neodymium in several hosts. As a general tendency, the higher the refractive index, the larger the integrated absorption. This results in the same trend for the stimulated emission cross-sections of the $^3F_4$ level.

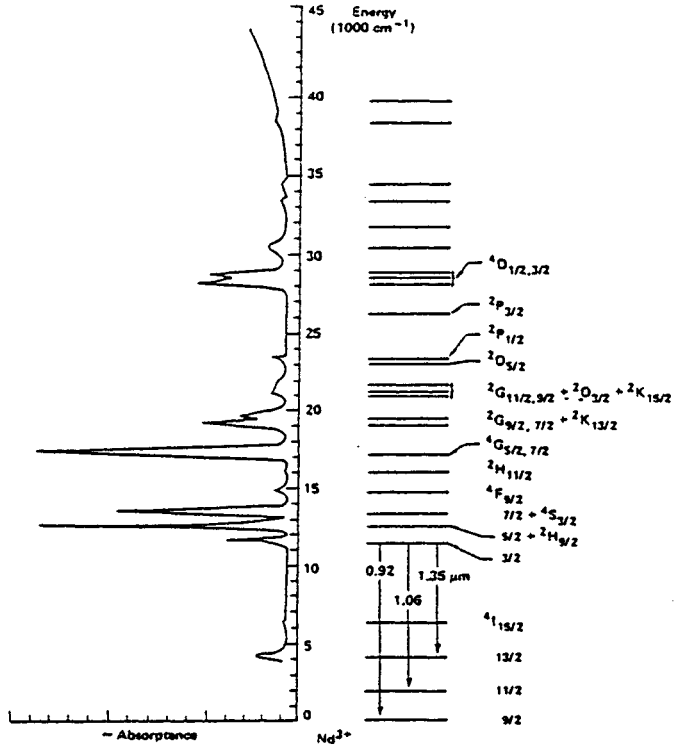


FIGURE 1 Absorption spectrum and energy levels of neodymium ion in glass.

The 810 nm absorption is important for pumping with reliable and low cost AlGaAs laser diodes. This transition is extremely effective for exciting the $^4F_{3/2}$ metastable state, leading to very efficient Nd^{3+}

lasers. Because of the closely spaced excited states, there are some excited state absorptions (ESA) from the $^4F_{3/2}$ state. However the $^4F_{3/2} \rightarrow {}^2D_{5/2}$ ESA transition at around 800 nm is weak and it does not significantly degrade the 810 nm pumping efficiency. For all glasses, Judd-Ofelt analysis reveals that the oscillator strength of this ESA is less than 1% of the ground state absorption (GSA) transition. Thus, high lasing efficiency can be achieved with 810 nm pumping for all compositions.

Peak absorption cross-sections are 1×10^{-20} to 4×10^{-20} cm^2 for this absorption [3]. In contrast with the 580 nm band, the intensity parameters Ω_4 and Ω_6 play a main role for the transition. The variation of Ω_t parameters in silicate and phosphate glasses is shown in FIGURE 2 ([12], data from [7]). Except for alkali-silicate glasses, Ω_4 and Ω_6 increased on increasing the ionic radius of the NWM. In alkali-silicate glasses NWMs with small ionic radius increase Ω_4 and Ω_6, as the lithium ion was very effective [11].

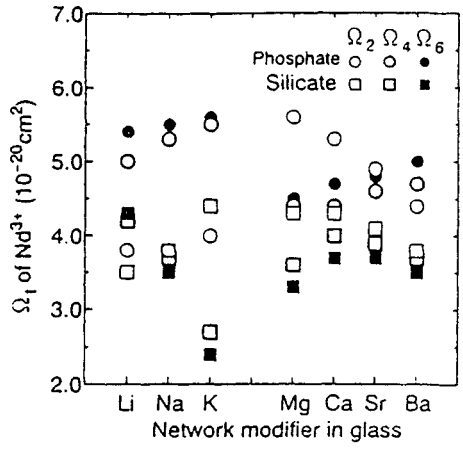


FIGURE 2 Variation of Ω_t parameters of Nd^{3+} in silicate and phosphate glasses.

C FLUORESCENCE

The energy levels and relevant transitions for the pump and fluorescence bands of Nd^{3+} are shown in FIGURE 3. The wavy lines indicate rapid non-radiative transitions. Nd^{3+}-doped glasses have been extensively studied for high peak power amplifier systems to drive nuclear fusion reactions, as well as applications in optical sensors and communications. The broad fluorescence bandwidth of Nd^{3+} in glass allows the construction of tunable sources and broadband amplifiers [13]. The strong $^4I_{9/2}$-$^2H_{9/2}$-$^4F_{5/2}$ absorption transition at about 0.8 μm is effective for exciting the $^4F_{3/2}$ metastable state. Nd^{3+}-doped glass lasers have been operated at 0.92, 1.05 and 1.32 μm on the transitions $^3F_{3/2}$-$^3I_{9/2}$, $^3I_{11/2}$, $^3I_{13/2}$, respectively. The $^4F_{3/2}$-$^3I_{11/2}$ emission of Nd^{3+}-doped glass has been utilised for high peak power and high energy laser applications. The $^4F_{3/2}$-$^3I_{13/2}$ emission (1.32 μm) is used for 1.3 μm band amplifiers in optical fibre communication systems.

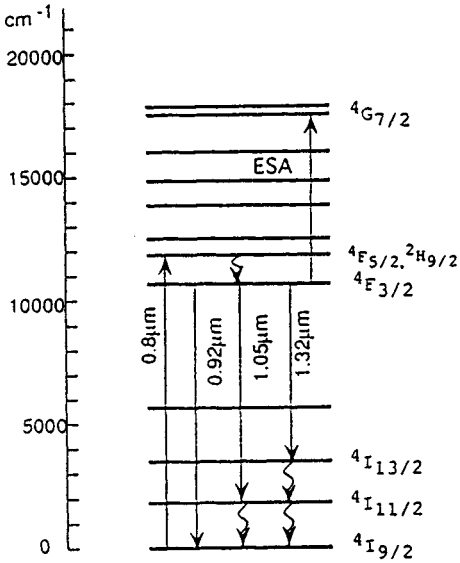


FIGURE 3 Energy level diagram of Nd^{3+}-doped phosphate glass showing the pump band at 0.8 μm and fluorescence bands near 0.92, 1.05 and 1.32 μm.

FIGURE 4 illustrates the $^4F_{3/2}$-$^3I_{11/2}$ fluorescence spectra of Nd^{3+}-doped silicate and phosphate glasses [14], and TABLE 1 lists the fluorescence peak wavelength λ_p, the effective bandwidth $\Delta\lambda_{eff}$ and the stimulated cross-section σ_p of different Nd^{3+}-doped glasses [2]. The fluorescence bands of these glasses are inhomogeneously broadened, i.e. broadened by the site to site variations in the ligand field of rare earth ions in amorphous materials. As shown in TABLE 1 the peak wavelengths become shorter for fluorophosphate and phosphate glasses. This was explained by the nephelauxetic effect which determined the covalent bond character

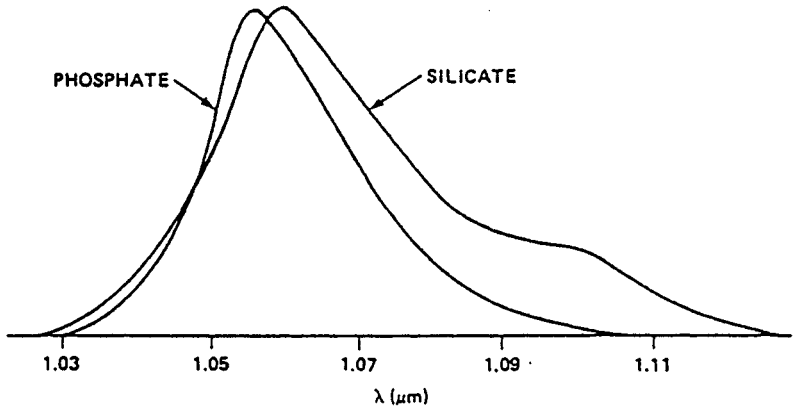


FIGURE 4 The $^4F_{3/2}$-$^4I_{11/2}$ fluorescence spectra of Nd^{3+} for phosphate and silica glass illustrating the effect of network former on the peak wavelength and bandwidth.

[15]. σ_p decreases in the order of phosphate → borate → germanate → silicate. However, large variations in σ_p for a given network former can also be obtained by varying the network modifier ions [7,14].

TABLE 1 The $^4F_{3/2}$-$^4I_{11/2}$ radiative properties of Nd^{3+} for network former variations.

Host glass	Peak wavelength λ_p (nm)	Bandwidth $\Delta\lambda_{eff}$ (nm)	Cross-section σ_p (10^{-20} cm^2)
Silicate	1057 - 1065	34 - 43	0.9 - 3.6
Phosphate	1052 - 1057	22 - 35	2.0 - 4.8
Fluorophosphate	1049 - 1056	27 - 34	2.2 - 4.3
Borate	1054 - 1063	34 - 38	2.1 - 3.2
Germanate	1060 - 1063	36 - 40	1.7 - 2.4
Tellurite	1056 - 1063	26 - 31	3.0 - 5.1

The $^3F_{3/2}$-$^3I_{13/2}$ transitions of Nd^{3+}-ion doped glasses have been investigated for 1.3 μm optical amplifiers. Many glasses exhibit the fluorescence band peaks in the wavelength range utilised in 1.3 μm optical fibre communications [16]. The peak wavelength of $^4F_{3/2}$-$^4I_{13/2}$ transitions varies significantly with glass composition as observed in the 1.06 μm fluorescence. Unfortunately, there is an excited state absorption (ESA) transition ($^4F_{3/2}$-$^4G_{7/2}$) in the 1.3 μm spectral region (see FIGURE 3), which severely reduces the efficiency of the $^3F_{3/2}$-$^4I_{13/2}$ stimulated emission. According to Andrews [17] and Zemon et al [18], the ESA spectrum alters in both wavelength and strength depending on the glass composition. In phosphate, fluorophosphate and fluoride glasses positive gains are observed in the 1.3 μm spectral region. TABLE 2 lists the fluorescence peak wavelength λ_p, the effective bandwidth $\Delta\lambda_{eff}$ and the stimulated cross-section σ_p for some Nd^{3+}-doped oxide glasses. The best composition reported to date was a high fluorine content fluorophosphate glass with peak wavelength as short as 1.295 μm [18]. This glass exhibits gain in the 1.300 - 1.310 μm signal wavelength region. However, the gain is low, and Pr^{3+}-doped fluoride or chalcogenide glass fibres have become more promising for the 1.3 μm fibre amplifier recently [19,20].

TABLE 2 The $^4F_{3/2}$-$^4I_{13/2}$ radiative properties of Nd^{3+} for network former variations.

Host glass	Peak wavelength λ_p (nm)	Bandwidth $\Delta\lambda_{eff}$ (nm)	Cross-section σ_p (10^{-21} cm^2)
Silicate	1325 - 1366	52 - 66	3.1 - 6.7
Phosphate	1323 - 1324	45 - 55	8.9 - 11
Fluorophosphate	1320 - 1324	59 - 60	6.8 - 7.0

D RADIATIVE LIFETIMES

The radiative lifetime is an important parameter as it influences the quantum efficiency. TABLE 3 shows the ranges of radiative lifetimes of the $^4F_{3/2}$ metastable state for various Nd^{3+}-doped oxide glass hosts [2].

TABLE 3 Range of radiative lifetimes for the $^4F_{3/2} \rightarrow {}^4I_{11/2}$ transition of Nd^{3+} in different glasses (from [2]).

Glass	Radiative lifetime
Silicate	170 to 1090 μs
Phosphate	280 to 530 μs
Borate	270 to 450 μs
Germanate	300 to 460 μs
Tellurite	140 to 240 μs

Jacobs and Weber systematically studied the $^4F_{3/2}$ radiative properties of Nd^{3+} in eight different host glasses [14] including four simple oxide glasses, three additional oxide glasses and a fluorophosphate glass. The four simple oxide glasses are phosphate, borate, germanate and silicate glass with the same glass network modifier, when the radiative lifetime increases in the order of phosphate, borate, germanate and silicate glass. The three additional oxide glasses are tellurite, aluminate and titanate glass. The shortest radiative lifetime was observed for the tellurite glass which has a refractive index of >2. It is obvious that the radiative lifetime increases with increasing refractive index. The optimisation of the composition must be individually done for different glass networks to obtain the appropriate radiative parameter values. The large variations of the radiative lifetime are obtained for a given network former by varying the network modifier.

The dependence of the radiative lifetime of neodymium-doped oxide glasses on the glass network modifier has also been reported by Jacobs and Weber [14], and by Toratani et al [21]. The trends for silicate glass are in agreement for both results. The radiative lifetime increases with increasing ionic radius of the alkali modifier in binary and ternary silicate glasses. The changes in the radiative lifetimes with varying alkaline-earth are small. On the other hand, in phosphate glasses, the radiative lifetime is nearly constant with varying alkali ions but decreases in order of Mg-Ca-Sr-Ba.

Extensive research has been undertaken to improve the radiative properties for various glass compositions. Recently, efforts have been made to improve the thermomechanical properties in addition to having better radiative properties. Byun et al reported a neodymium-doped quaternary glass which has improved spectral and thermomechanical properties [22]. Ishii et al reported that clustering Nd^{3+} ions were homogeneously dissolved into the host SiO_2 glass by co-doping of a small amount of Al_2O_3 by using plasma torch CVD [23].

E NON-RADIATIVE DECAY

When an Nd^{3+} ion is excited by absorbing photons or by energy transfer from other ions, it relaxes to the lower energy states via three distinct processes: radiative, with the emission of photons, non-radiative, with the simultaneous emission of several phonons, or energy transfer to another ion. The multiphonon relaxation rate of the metastable state determines the emission efficiency of the transition. Energy transfer is responsible for the concentration quenching in Nd^{3+}-doped glasses. In this section, multiphonon decay and deleterious energy transfer (concentration quenching and OH^- quenching) of Nd^{3+}-doped oxide glasses are reviewed.

If the energy gap between an excited state of a rare earth ion and the next lower state is much larger than the phonon energy of the host glass, the non-radiative decay rate, or multiphonon decay rate (w_{MP}) is inversely proportional to the exponent of the energy gap [24,25]:

$$w_{MP} = C\,[n(T) + 1]^p \exp(-\alpha\,\Delta E) \quad (1)$$

In EQN (1), C and α are host-dependent parameters. ΔE and p indicate the energy gap and the number of phonons required to bridge the gap, respectively. n(T) is the Bose-Einstein occupation number for the effective phonon mode

$$n(T) = [\exp(h\omega/kT) - 1]^{-1} \quad (2)$$

where ω is the phonon angular frequency. The parameters C, α and $h\omega$ are listed in [25,4]. A non-radiative decay rate of an excited state of a rare earth ion can be roughly estimated based on this relationship.

Energy gaps between the excited states of Nd^{3+} are smaller than 2000 cm^{-1} except for that of the $^4F_{3/2}$ state. The w_{MP} for these states are estimated to be larger than 10^6 s^{-1}, and no emission is observed in practice at room temperature. The $^4F_{3/2}$ state of Nd^{3+}, the metastable state for most important transitions, has the energy gap of approximately 5350 cm^{-1} and has the quantum efficiency of higher than 95% in all oxide glasses except borate. Generally, multiphonon decay of the $^4F_{3/2}$ state is not a significant issue in oxide glasses. However, borate glass has a high phonon energy of 1400 cm^{-1}, and it suffers a large non-radiative decay rate of ~3000 s^{-1}. Reported radiative lifetimes of the $^4F_{3/2}$ state in borate glasses range from 270 μs to 450 μs based on a Judd-Ofelt analysis [2]. Therefore, the expected quantum efficiency is only 40 - 55% in this glass system.

Among the transitions from the $^4F_{3/2}$ state, the most important one is the $^4F_{3/2} \rightarrow {}^4I_{11/2}$ transition at 1.06 μm. The lifetime of the terminal state $^4I_{11/2}$ with an energy gap ~2000 cm^{-1} is an important fundamental parameter in determining the design and performance of a high power laser system. Bibeau et al [26] made direct measurements of the terminal state lifetimes of some Nd^{3+}-doped crystals and glasses. The results of 250 - 450 ps and 535 - 740 ps were reported for a phosphate (LG-750) and a silicate (LG-660) laser glass, respectively.

Concentration quenching reduces the emission quantum efficiency on increasing the concentration. In the case of Nd^{3+}, a non-radiative energy transfer between the pair states ($^4F_{3/2}$, $^4I_{9/2}$) and ($^4I_{15/2}$, $^4I_{15/2}$) is possible. This cross-relaxation process is believed to be the primary mechanism for Nd^{3+} concentration quenching [3]. The concentration quenching depends on the glass type. TABLE 4 shows the range of Nd^{3+} ion concentration that reduces the lifetime of the $^4F_{3/2}$ state by a factor of two for some glass systems ([4], data from [25]). The empirical formula relating the observed lifetime τ_{obs} to the ion concentration ρ is

$$\tau_{obs} = \tau_0/[1 + (\rho/Q)^p] \quad (3)$$

where τ_0 is the lifetime in the limit of zero concentration and Q is the quenching concentration listed in TABLE 4. For the cross-relaxation mechanism involving two ions as in this case, p is approximately two [4]. This analysis assumes uniform dispersion of the rare earth ions without clustering. This is the case for multicomponent glasses where the concentration is kept to no more than a few percent.

TABLE 4 Nd^{3+} concentration resulting in a factor of two reduction of the $^4F_{3/2}$ lifetime.

Host glass	Quenching concentration (10^{20} cm^{-3})
Silicate	3.9 - 6.0
Phosphate	3.9 - 8.6
Fluorophosphate	3.0 - 4.0
Fluorozirconate	4.2
Fluoroberyllate	3.8 - 5.3

Another route of non-radiative decay is the energy transfer to the OH^- complex. Generally, oxide glasses prepared by melting contain a large amount of OH^- unless some dehydration processes were employed. The OH^- has a large phonon energy of ~3000 cm^{-1}. It serves as a trap and is extremely effective in quenching the excited Nd^{3+} ions [21,27]. The $^4F_{3/2}$ lifetime decreases with increasing OH^- content. For example, the observed lifetime (τ_{obs}) in a phosphate glass was empirically related to the OH^- concentration, as measured by the absorption coefficient at 2.85 μm (α, cm^{-1}) [3]:

$$\tau_{obs}^{-1}\ (s^{-1}) = 3.3 \times 10^3 + 2.2 \times 10^2\ \alpha \qquad (4)$$

F CONCLUSION

The spectroscopic properties of Nd^{3+}-doped oxide glasses have been reviewed. Characteristics have been reported for a wide variety of glass compositions. References were provided to direct the reader toward further experimental data and theoretical insights.

REFERENCES

[1] E. Snitzer [*Phys. Rev. Lett. (USA)* vol.7 (1961) p.444]

[2] S.E. Stokowski, R.A. Saroyan, M.J. Weber [*Nd-Doped Laser Glass Spectroscopic and Physical Properties* (Lawrence Livermore National Laboratory, M-095, Rev.2, November 1981)]

[3] S.E. Stokowski [in *Handbook of Laser Science and Technology* Ed. M.J. Weber (CRC Press, 1987) vol.1 ch.2.3 p.218]

[4] W.J. Miniscalco [in *Rare Earth Doped Fiber Lasers and Amplifiers* Ed. M.J.F. Digonnet (Marcel Dekker, 1993) ch.2.2 p.50]

[5] W.F. Krupke [*IEEE J. Quantum Electron. (USA)* vol.QE-10 (1974) p.450]

[6] R. Reisfeld, C.L. Jorgensen [in *Handbook on the Physics and Chemistry of Rare Earths* Eds. K.A. Gschneider, L. Eyring (Elsevier Science Publisher, 1987) vol.9 p.1]

[7] T. Izumitani, H. Toratani, H. Kuroda [*J. Non-Cryst. Solids (Netherlands)* vol.47 (1982) p.87]

[8] C.K. Jorgensen, R. Reisfeld [*J. Less-Common Met. (Switzerland)* vol.93 (1983) p.107]

[9] E.W.J.L. Oomen, A.M.A. van Dongen [*J. Non-Cryst. Solids (Netherlands)* vol.111 (1989) p.205]

[10] S. Tanabe, T. Ohyagi, N. Soga, T. Hanada [*Phys. Rev. B, Condens. Matter (USA)* vol.46 (1992) p.3305]

[11] Y. Nageno, H. Takebe, K. Morinaga, T. Izumitani [*J. Non-Cryst. Solids (Netherlands)* vol.169 (1994) p.288-94]

[12] S. Tanabe, T. Hanada, T. Ohyagi, N. Soga [*Phys. Rev. B, Condens. Matter (USA)* vol.48 (1993) p.10591]

[13] R.J. Mears, L. Reekie, S.B. Poole, D.N. Payne [*Electron. Lett. (UK)* vol.21 (1985) p.738-40]

[14] R.R. Jacobs, M.J. Weber [*IEEE J. Quantum Electron. (USA)* vol.QE-12 (1976) p.102-11]

[15] C. Brecher, L.A. Riseberg, M.J. Weber [*Phys. Rev. B (USA)* vol.18 (1978) p.5799-811]

[16] M.J.F. Digonnet [*Rare Earth Doped Fiber Lasers and Amplifiers* (Dekker, New York, 1993) p.63]

[17] L.J. Andrews [*Dig. Conf. on Tunable Solid State Laser* (Optical Society of America, 1987) WB1]

[18] S. Zemon et al [*IEEE Photonics Technol. Lett. (USA)* vol.4 (1992) p.244-7]

[19] Y. Ohisihi et al [*IEICE Trans. Commun. (Japan)* vol.E-77-B (1994) p.421-40]

[20] H. Tawarayama et al [*Proc. Optical Amplifiers and Their Applications* Victoria BC, Canada, 21-23 July 1997 (Optical Society of America, 1997) PD1]

[21] H. Toratani, T. Izumitani [*J. Non-Cryst. Solids (Netherlands)* vol.52 (1982) p.303]

[22] J.-O. Byun et al [*Jpn. J. Appl. Phys. (Japan)* vol.33 (1994) p.4907]

[23] Y. Ishii, H. Namikawa, K. Arai, A. Noda, A. Negishi, T. Hanada [*Yogyo-Kyokai-Shi (Japan)* vol.93 (1985) p.498]
[24] C.B. Layne, M.J. Weber [*Phys. Rev. B (USA)* vol.16 (1977) p.10]
[25] R. Reisfeld, C.K. Jorgensen [*Excited State Phenomena in Vitreous Materials* (Elsevier, 1987) p.1-90]
[26] C. Bibeau, S.A. Payne, H.T. Powell [*J. Opt. Soc. Am. B (USA)* vol.12 (1995) p.1981]
[27] H. Ebendorff-Heidepriem, W. Seeber, D. Ehrt [*J. Non-Cryst. Solids (Netherlands)* vol.183 (1995) p.192]

B3.2 Spectroscopy of erbium-doped oxide glass

S. Tanabe

November 1997

A ABSORPTION OF ERBIUM-DOPED OXIDE GLASS

The assignments and probabilities of optical absorptions due to 4f electronic transitions of Er^{3+} are well understood, since most bands are well separated and their transitions are electric-dipole in nature. Er^{3+} can be said to be one of the best rare earth elements, the transition probabilities of which can be interpreted correctly in Judd-Ofelt theory [1,2] with the smallest errors. The absorption cross sections of electric-dipole transitions in 0.3 - 1.6 μm, where most of the f-f transitions of Er^{3+} are located, can be expressed by sets of reduced matrix elements of unit tensor operators [3], which are characteristic to the ground and excited states and almost independent of the hosts. Since the sets of three values, $\langle\|U^{(t)}\|\rangle^2$ (t = 2, 4, 6), are different for each band, the relative intensities are varied. The dependence of the absorption cross sections on the hosts are explained by the three Judd-Ofelt parameters, Ω_t, which also explain the difference of relative intensities of bands with different hosts.

FIGURE 1 shows typical absorption spectra of Er^{3+}-doped borate glasses with various Na_2O content. The cross sections of the $^2H_{11/2}$ and $^4G_{11/2}$ bands (hypersensitive transition [4]) increase with alkali oxide content, while those of other bands decrease. These features can be explained by the compositional dependence of the Ω_t parameters in FIGURE 2, where Ω_2 increases showing a maximum around x = 25 mol % and the $\Omega_{4,6}$ decrease monotonically with x [5]. The Ω_2 value is considered to increase when the rare earth elements are located at a site with lower symmetry. According to phonon sideband spectroscopy in the local environment of Eu^{3+} ions in borate glass [6], the fractions of the structural units, such as the boroxol rings and tetraborate and diborate groups, change with Na_2O content. Also it is known that the compositional dependences of many physical properties of alkali borate glasses show anomalous behaviour, which is related to the structural changes of borate glasses with alkali content. The maximum of Ω_2 at x = 25 can be due to the distorted local symmetry of Er^{3+} ions in the glass with inhomogeneous structural units.

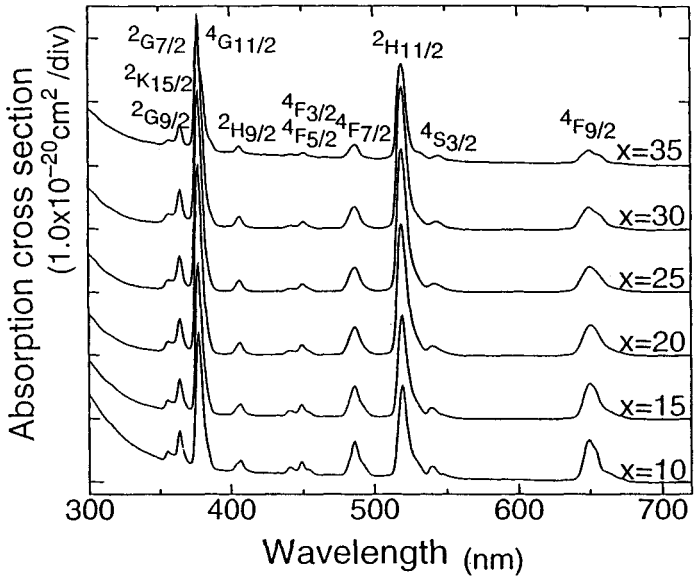


FIGURE 1 Absorption spectra of $(100\text{-}x)B_2O_3$ - xNa_2O - $0.3Er_2O_3$ glasses [5].

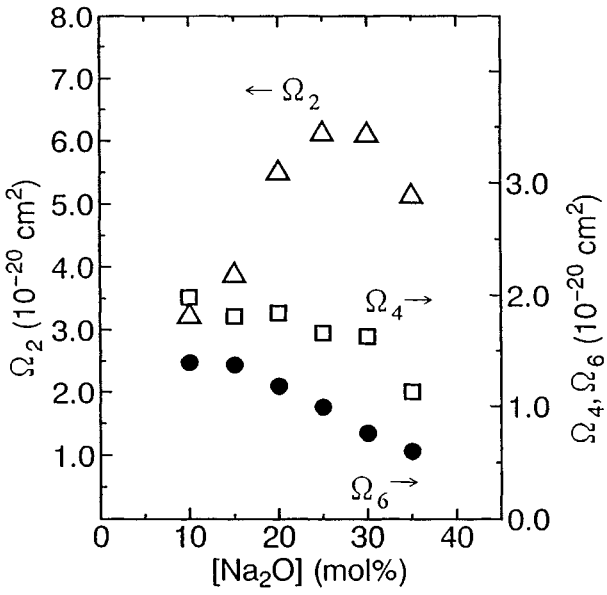


FIGURE 2 Compositional dependence of Ω_t parameters of Er^{3+} ions in borate glasses [5].

Although the Ω_6 values determine the cross-sections of important transitions with practical applications, such as Er^{3+}:$^4I_{13/2}$ - $^4I_{15/2}$ at 1.55 μm and $^4S_{3/2}$ - $^4I_{15/2}$ at 0.55 μm, the controlling factors of the other two parameters have not been well understood. It has been clarified that due to the selection rules of 6j symbols, Ω_6 is most largely dependent on the overlap integrals of 4f and upper-energy orbitals, especially 5d orbitals [7]. By comparing the isomer shift of ^{151}Eu Mössbauer spectroscopy in the same composition, a clear correlation between the IS and the Ω_6 value of Er^{3+} has been shown (FIGURE 3). This fact suggests that the Ω_6 value can be increased by changing the bond covalency of the rare earth-ligand, i.e. the electron density of rare earth orbitals. Among oxide glasses, some phosphate [8] and tellurite glasses show the largest value of Ω_6 as hosts of Er^{3+} and also of Nd^{3+}.

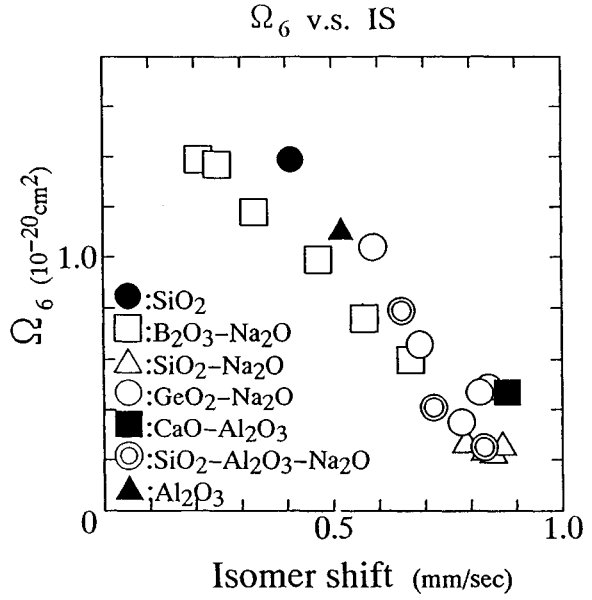


FIGURE 3 Relation between the Ω_6 parameter of Er^{3+} ions and the ^{151}Eu isomer shift in oxide glasses [7].

B FLUORESCENCE OF ERBIUM-DOPED OXIDE GLASS

B1 Visible Fluorescence

Erbium doped oxide glasses are not usually efficient phosphors in the visible region compared with other rare earth phosphors pumped with UV-light. There exist three bands at 410 nm, 550 nm and 660 nm, due to the transitions to the ground state from the $^2H_{9/2}$, $^4S_{3/2}$ and $^4F_{9/2}$ levels, respectively. All these levels have an energy gap less than 3500 cm^{-1}, which makes the quantum efficiency of these levels lower than those of other blue, green and red phosphor elements in oxide glasses with phonon energy higher than 800 cm^{-1}.

At temperatures above 150 K, an emission band can be seen at 530 nm due to the $^2H_{11/2}$ - $^4I_{15/2}$ transition. This emission is due to electronic thermal excitation from the $^4S_{3/2}$ to the $^2H_{11/2}$ level, which obeys a Boltzmann distribution. Although the population of the $^2H_{11/2}$ level even at room temperature is three orders lower than that of the $^4S_{3/2}$ level, the 530 nm emission can be observed. This fact is due to a two orders larger transition probability of $^2H_{11/2}$ - $^4I_{15/2}$ (hypersensitive) than that of $^4S_{3/2}$ - $^4I_{15/2}$, which can be seen in the sets of reduced matrix elements. This emission of the 530 nm band decreases the apparent lifetime of the $^4S_{3/2}$ level, which might result in lower estimation of the radiative quantum efficiency.

Efficient green upconversion emissions are observed by 800 nm pumping in heavy metal oxide glasses such as tellurite, gallate and bismuthate [9].

B2 1.55 μm Fluorescence

Among several fluorescence transitions of Er^{3+}, the $^4I_{13/2}$ - $^4I_{15/2}$ at 1.55 μm is now the most interesting for its practical application in the optical fibre amplifier [10,11]. Since $\Delta J = 1$ (J is the total quantum number) for this transition, it includes the contribution of the magnetic dipole transition, the line strength of which, S^{md}, is independent of ligand field. Usually the fraction of the magnetic dipole transition in the total cross-section is around 30%, and thus the emission cross section of the 1.5 μm fluorescence still depends on the ligand field. According to the sets of reduced matrix elements, the line strength of the electric-dipole is expressed by

$$S^{ed}[^4I_{13/2}: {}^4I_{15/2}] = 0.019\Omega_2 + 0.118\Omega_4 + 1.462\Omega_6 \quad (1)$$

Due to this dependence on Ω_t parameters, the 1.5 μm spectra depend mainly on the value of Ω_6. The emission spectra of Er^{3+}:$^4I_{13/2}$ - $^4I_{15/2}$ in several oxide glasses are shown in FIGURE 4. Among them, the tellurite glass shows the broadest emission band as a host of Er^{3+}:1.5 μm [12]. Thus by utilising their flat and wide gain characteristics the tellurite glasses are now good candidates for EDFAs (erbium doped fibre amplifiers) for WDM (wavelength-division for multiplexing) applications [13], which enables high capacity data rate, multiplexed transfer, branching and insertion resulting in a flexible network architecture.

C RADIATIVE LIFETIMES OF ERBIUM-DOPED OXIDE GLASS

The radiative lifetime is defined as the inverse of the spontaneous emission probability, A, by

$$\tau_R^{-1} = A = A^{ed} + A^{md} \quad (2)$$

where

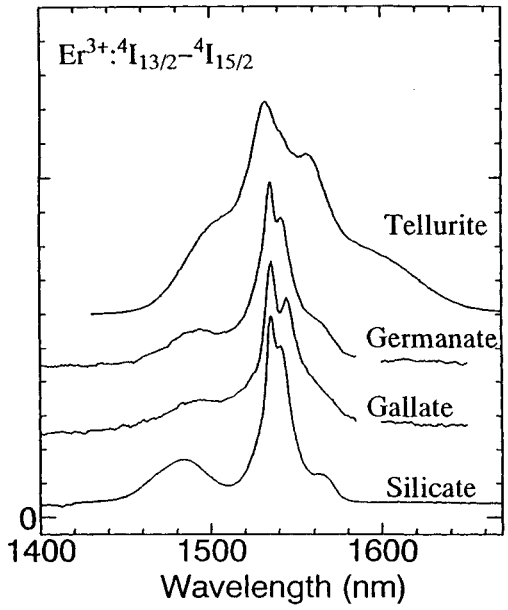


FIGURE 4 Fluorescence spectra of Er^{3+}:$^4I_{13/2} \rightarrow {}^4I_{15/2}$ in several oxide glasses.

$$A_{JJ'}^{ed} = \frac{64\pi^4 e^2}{3h(2J+1)\lambda^3}\left[\frac{n(n^2+2)^2}{9}\right]S_{JJ'}^{ed} \qquad (3)$$

Since the green ($^4S_{3/2}$ - $^4I_{15/2}$) and red ($^4F_{9/2}$ - $^4I_{15/2}$) emissions of Er^{3+} are not hypersensitive transitions (i.e. their $<\|U^{(2)}\|>^2$ are zero), their radiative lifetimes are not very sensitive to the ligand field parameters and almost dependent on the refractive indexes of the host glasses. TABLE 1 shows the refractive index and radiative lifetimes of the $^4S_{3/2}$ and $^4F_{9/2}$ levels in silicate, germanate and aluminate glasses.

TABLE 1 Refractive index and radiative lifetimes of Er^{3+} ions in several oxide glasses.

Sample	n_D	τ_R ($^4S_{3/2}$) (μs)	τ_R ($^4F_{9/2}$) (μs)
60 SiO_2 - 40 Na_2O - 0.3 Er_2O_3	1.520	3145	1992
70 GeO_2 - 30 Na_2O - 0.3 Er_2O_3	1.630	1357	1472
33 Al_2O_3 - 67 CaO - 0.3 Er_2O_3	1.685	1190	635

D NON-RADIATIVE PROPERTIES OF ERBIUM-DOPED OXIDE GLASS

The non-radiative decay of the $^4S_{3/2}$ and $^4F_{9/2}$ levels in oxide glasses are sensitive to the phonon energy ($\hbar\omega$) of the host, because their energy gaps to the next lower levels (ΔE) are small. The non-radiative decay rate due to multiphonon relaxation is expressed by

$$Wp = W_0 \exp(-\alpha\Delta E/\hbar\omega) \qquad (4)$$

where α is a function of electron-phonon coupling of rare earth ions with a host [14] and is almost independent of composition among oxides. Usually the phonon energies of oxide glasses vary with the kind of network forming oxide. They are around 1400 cm^{-1} in borate, 1200 cm^{-1} in phosphate, 1000 cm^{-1} in silicate, 800 cm^{-1} in germanate and aluminate, 700 cm^{-1} in tellurite and 650 cm^{-1} in gallate glasses. Thus only a few phonons are required to bridge the energy gaps of those levels in conventional oxide glasses, leading to lower quantum efficiencies than those of the Tb^{3+}:$^5D_4$ and Eu^{3+}:$^5D_0$ levels,

which are initial levels of efficient green and red emission, respectively. FIGURE 5 shows the multiphonon decay rate of Er^{3+}:$^4S_{3/2}$ and $^4F_{9/2}$ levels as a function of the phonon energy in oxide glasses. Due to their lower phonon energy, the lifetimes of excited levels are longer in heavy metal oxides. Efficient green upconversion emissions are observed in tellurite [9], gallate [9] and aluminate [15] glasses by infrared pumping.

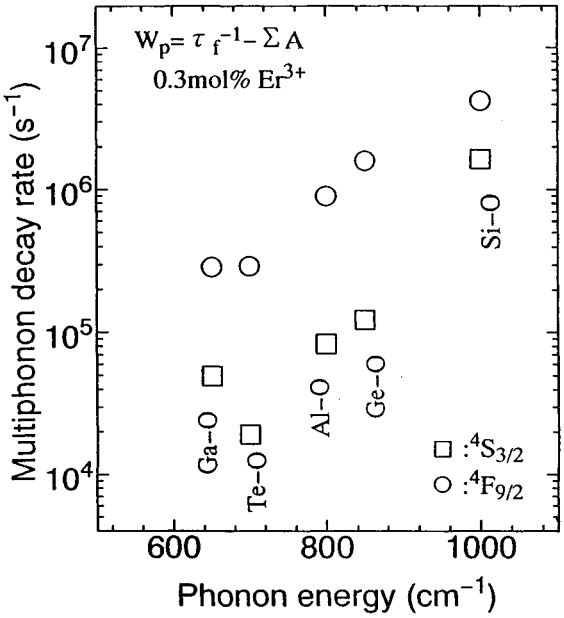


FIGURE 5 Multiphonon decay rate of Er^{3+}:$^4S_{3/2}$ and $^4F_{9/2}$ levels in oxide glasses as a function of their phonon energy.

On the other hand, the $^4I_{13/2}$ level has an energy gap of 6500 cm^{-1} so that the multiphonon decay rate becomes negligible in most oxide glasses. The quantum efficiency of 1.55 μm emission is over 90% even in silicate glasses, which enables silicate hosts to be good materials for EDFA.

REFERENCES

[1] B.R. Judd [*Phys. Rev. (USA)* vol.127 (1962) p.750-61]
[2] G.S. Ofelt [*J. Chem. Phys. (USA)* vol.37 (1962) p.511-20]
[3] M.J. Weber [*Phys. Rev. (USA)* vol.157 (1967) p.262-72]
[4] C.K. Jørgensen, B.R. Judd [*Mol. Phys. (UK)* vol.8 (1964) p.281-90]
[5] S. Tanabe, T. Ohyagi, N. Soga, T. Hanada [*Phys. Rev. B (USA)* vol.46 (1992) p.3305-10]
[6] S. Tanabe, S. Todoroki, K. Hirao, N. Soga [*J. Non-Cryst. Solids (Netherlands)* vol.122 (1990) p.59-65]
[7] S. Tanabe, T. Ohyagi, S. Todoroki, T. Hanada, N. Soga [*J. Appl. Phys. (USA)* vol.73 no.12 (1993) p.8451-4]
[8] S. Tanabe, T. Hanada, T. Ohyagi, N. Soga [*Phys. Rev. B (USA)* vol.48 (1993) p.10591-4]
[9] S. Tanabe, K. Hirao, N. Soga [*J. Non-Cryst. Solids (Netherlands)* vol.122 (1990) p.79-82]
[10] E. Snitzer, R. Woodcock [*Appl. Phys. (USA)* vol.6 (1965) p.45]
[11] R.J. Mears, L. Reekie, I.M. Jauncey, D.N. Payne [*Electron. Lett. (UK)* vol.23 (1987) p.1026]
[12] J.S. Wang, E. Vogel, E. Snitzer [*Opt. Mater. (Netherlands)* vol.3 (1994) p.187-203]
[13] A. Mori et al [*Proc. OFC'97* PD1 (1997) p.1-4]
[14] T. Miyakawa, D.L. Dexter [*Phys. Rev. B (USA)* vol.1 (1970) p.2961-70]
[15] S. Tanabe, T. Ohyagi, T. Hanada, N. Soga [*J. Ceram. Soc. Jpn. (Japan)* vol.101 (1993) p.78-83]

PART B: OXIDE GLASS

CHAPTER B4

OPTICAL FIBRE MANUFACTURE

B4.1 Preparation and melting of oxide glass
B4.2 Drawing of oxide glass optical fibres
B4.3 Loss of oxide glass optical fibres

B4.1 Preparation and melting of oxide glass

W.T. Seeber

March 1998

A INTRODUCTION

The employment of oxide glasses for photonic applications has a long tradition. Their use as materials for lenses and optical windows is well known. More recently, their utilisation as active materials in lasers, amplifiers or switching devices also became important. For transmitting optics, a high degree of purity and homogeneity is required to achieve distortionless transmission. For high-intensity light, e.g. guided in fibres, small amounts of impurities and inclusions can lead to damage. From the earliest use of glasses in technology, it was obvious that for specific purposes a better glass has to be tailored and optimised. The pioneering work of W.V. Harcourt (1789-1871) and O. Schott (1851-1935) in particular provided the basis for today's understanding of the 'chemistry of glass' [1]. In 1936 G.W. Morey used rare elements (e.g. La, Th, Zr, Nb, Ta, W, Mo) to extend the field of oxide glass compositions [2]. Today, almost all elements of the periodic system in numerous combinations have been employed to prepare glasses. Nevertheless, besides the halide glasses [3], only a limited number of oxide glass systems (mainly silicate, phosphate, most recently heavy metal oxide and fluoride phosphate glasses) have proven themselves potential candidates for host matrices for rare earth ions in fibre lasers or amplifiers [4]. Therefore, we will focus on these systems in discussing the basic aspects of preparation and melting.

B TYPICAL OXIDE GLASS SYSTEMS

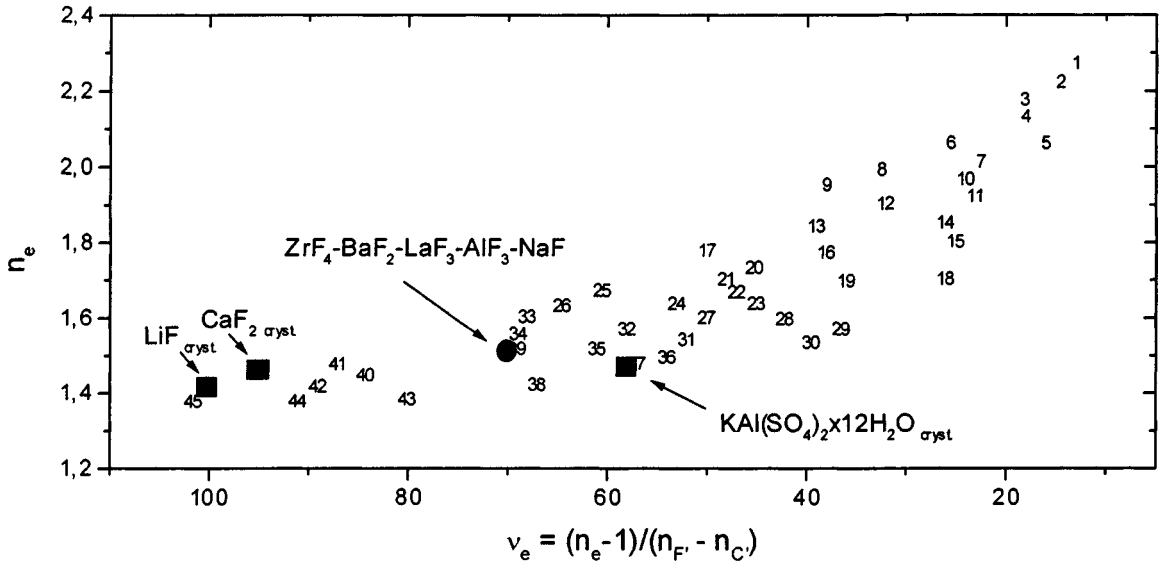
FIGURE 1 makes use of the n_e-ν_e-diagram to give an overview of the main components of important, pure oxide glasses in comparison with pure halide glasses, e.g. ZrF_4-BaF_2-LaF_3-AlF_3-NaF, or mixed-anionic systems, such as fluoride phosphate glasses. The properties of glasses can be tailored by changing the glass composition in a wide range (see e.g. [5-8]); on the other hand, the chemical nature even of pure oxide glasses may be very different [8]. This has an impact on the details of the classic melting process, discussed here. Glasses produced by the chemical vapour deposition technique (CVD) are the subject of other parts of this book - see Datareview A4.1.

C MANUFACTURING OF OPTICAL OXIDE GLASSES

The production of an optical glass is still today a complex challenge; detailed compositions and technological procedures are proprietary and/or kept secret. For a general overview it is useful to divide the manufacturing process into the following stages: selection/preparation of starting materials; melting/fining/homogenisation; casting/forming/annealing; quality assessment. More information can be found, for instance, in [6,8-12].

C1 Selection/Preparation of Starting Materials

It is very useful to select as starting materials inorganic compounds with appropriate decomposition or melting temperatures. This means, for instance, choosing $Al(OH)_3$ or $NaCO_3$ instead of Al_2O_3 or Na_2O, respectively. Pulverised limestone and feldspar have been used formerly as complex materials to introduce CaO, Al_2O_3, SiO_2 or K_2O into the glass. Today, most of the required high-quality starting materials (e.g. H_3BO_3, alkaline and alkaline earth metaphosphates, $Al(PO_3)_3$, GeO_2) are commercially available. Another point is the careful grinding and homogenisation of the batch compounds. It is well



1 TeO_2-$PbBr_2$
2 TeO_2-PbO-$PbOCl_2$
3 TeO_2-La_2O_3
4 TeO_2-Al_2O_3-MgO-SrO-BaO-ZnO
5 PbO-CdO-ZnO-B_2O_3
6 TeO_2-$Ba(PO_3)_2$-$Pb(PO_3)_2$
7 La_2O_3-TiO_2-Ta_2O_5-B_2O_3
8 La_2O_3-ThO_2-Ta_2O_5-B_2O_3
9 ThO_2-Gd_2O_3-Ta_2O_5-Nb_2O_5-B_2O_3
10 La_2O_3-TiO_2-ZrO_2-WO_3-B_2O_3
11 PbO-SiO_2
12 La_3O_3-TiO_2-B_2O_3
13 La_2O_3-Nb_2O_5
14 Sb_2O_3-Al_2O_3-SiO_2
15 PbO-SiO_2
16 ZnO-MoO_3-WO_3-CdO-B_2O_3
17 La_2O_3-ThO_2-CdF_2-B_2O_3
18 NaF-TiO_2-GeO_2
19 Na_2O-BaO-PbO-B_2O_3-SiO_2
20 Li_2O-ZrO_2-La_2O_3-Ta_2O_5-B_2O_3-(MeO)
21 BaO-B_2O_3-SiO_2-La_2O_3-ThO_2
22 La_2O_3-ThO_2-BaO-CaO-MgO-B_2O_3
23 Na_2O-BaO-PbO-B_2O_3-SiO_2
24 BaO-B_2O_3-SiO_2
25 CaF_2-La_2O_3-B_2O_3
26 CaF_2-BaO-B_2O_3
27 Na_2O-BaO-ZnO-PbO-SiO_2
28 Na_2O-PbO-SiO_2
29 $NaPO_3$-$Sr(PO_3)_2$-K_2TiF_6
30 KF-PbF_2-AlF_3-$NaPO_3$-$Mg(PO_3)_2$-$Al(PO_3)_3$
31 Na_2O-K_2O-CaO-SiO_2
32 Na_2O-B_2O_3-SiO_2
33 Na_2O-BaO-B_2O_3-SiO_2
34 BaO-B_2O_3-P_2O_5-Al_2O_3
35 Na_2O-K_2O-CaO-SiO_2
36 KF-AlF_3-K_2TiF_6-Sb_2O_3-PbO-B_2O_3-SiO_2
37 NaF-KF-PbF_2-BeF_2-$Pb(PO_3)_2$
38 Na_2O-B_2O_3-SiO_2-Al_2O_5-F
39 BaO-B_2O_3-P_2O_5-Al_2O_3
40 $Me^{I}F$-ZnF_2-$Me^{II}F_2$-PbF_2-AlF_3-LaF_3-ThF_4-$Al(PO_3)_3$
41 $Me^{II}F_2$-AlF_3-$Me^{II}(PO_3)_2$-$Me^{III}(PO_3)_3$
42 NaF-LaF_3-CeF_3-BeF_2-$Be(PO_3)_2$-$CePO_4$-$La(PO_3)_3$
43 NaF-BaF_2-BeF_2-$NaAlF_6$-$Al_2(SiF_6)_3$-$NaPO_3$
44 NaF-BaF_2-BeF_2-$NaPO_3$
45 KF-AlF_3-BeF_2-$Me^{II}F_2$-CdF_2-LaF_3-CeF_3-ThF_4

FIGURE 1 Overview of main components in optical glasses. n_e and ν_e are the refractive index and Abbe-number, respectively, at λ = 546,06 nm.

known that the reaction pathway during the melting process strongly depends upon the initial particle size of the batch material [13]. Peeler et al [14] investigated the effects of different particle size distributions on the reaction kinetics of melts. They found significant effects, because different intermediate phases will form as the overall particle size distribution varies. Starting materials for soda-lime-silica glass with particles of medium mesh sizes (-270, +325) showed a better melting behaviour than the finer grade material.

Sometimes it is advantageous to press the mixture of inorganic powders into pellets because they can be better handled, and it reduces the sources of impurities. The requirements for purity of used raw materials are usually high and depend on the glass application. Minute impurities consisting of colouring compounds of 3d elements cause losses in light transmission, and can act as unwanted

quenchers of rare earth luminescence in laser devices. Typically the impurity content should be as low as possible, frequently less than 3×10^{-8} % [1,15]. However, special applications require the incorporation of selected ions (e.g. cerium or chromium to act as energy donors for laser ions) [16].

C2 Melting/Fining/Homogenisation

The production of an optical glass is very often a discontinuous process. The melting regime and especially the melting temperature depend on the glass composition (typical range: 1000 - 1600 K). The initial melting stage can be defined as the conversion of all crystalline raw material into the liquid state [14]. With increasing temperatures, the following main reactions take place: dehydration, thermal decomposition of carbonates, phase transformations. At higher temperatures solid state reactions can occur between the intermediate formed oxide phases, and the formation of the first liquid phase can be observed. This liquid phase should coat the remaining refractory compounds of the batch and dissolve these grains to form the batch-free liquid glass melt. Once a melt is obtained, the fining operation can proceed. Fining is the process where bubbles in the melt are caused to dissipate. One has to consider the solubility of gases in melts and glasses because remaining bubbles can create severe problems. Usually, fining agents have to be used to introduce gas bubbles which cause existing bubbles to grow larger in the melt, thereby increasing their destruction rate [12]. These agents can give off oxygen gas (agents such as nitrates, ceric oxide, Sb_2O_3) or SO_2 gas (sulphates), or evaporate from the melt (e.g. NaCl, NH_4Cl). Unfortunately, sodium sulphate as a refining agent, for instance, works at temperatures > 1720 K; Nakajima et al [17] successfully used a sub-atmospheric pressure melting technique to enhance the refining of soda-lime glass at lower temperatures. Besides N_2, O_2 and CO_2, the inert gases are also often found in bubbles. Gausman et al [18] summarise the recent knowledge about solubility of inert gases in a wide variety of glasses. The CO_2 solubility in melts has been discussed, for instance, by Parker et al [19].

The container and stirrer materials of choice in the optical glass melting industry are platinum (Pt) or platinum alloys (Pt/Rh) because they are largely chemically inert to a wide range of compositions and can be heated inductively by microwaves. Nevertheless, some level of Pt-contamination in the form of microscopic particles or of dissolved platinum still remains in the glasses. The Pt-inclusions in particular must be eliminated because they produce fracture sites when irradiated with high-intensity radiation. Campbell et al [20,21] examined the effects of different gas atmospheres, temperature, processing time and container material on the formation of Pt inclusions and the platinum solubility in commercial phosphate laser glasses (Schott's APG-1, LG-750, LG-760 and Hoya's LHG-8). They found that phosphate glasses for high power lasers should contain a minimised Al_2O_3 content.

FIGURE 2 shows schematically a covered inductively-heated Pt crucible for the production of easily-evaporating and crystallising glasses of extreme optical parameters. The disc (a) and the cover (b) are tightly connected with the Pt-stirrer (d) which runs in a 'glass pocket' (c) [22]. The pocket contains a liquid glass of similar composition to that of the glass being produced.

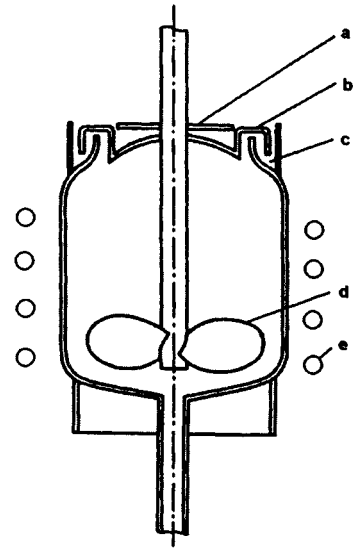


FIGURE 2 Inductively-heated (e) Pt-crucible for melting of easily evaporating glasses. Disc (a) and cover (b) tightly connected with stirrer which runs in so-called 'glass pocket' (after Heidenreich [22]).

Meanwhile, it is convenient to choose amorphous carbon crucibles for the container, together with a graphite furnace under a flowing inert atmosphere (e.g. [15,23]) to avoid Pt-inclusions for instance in fluoride phosphate glasses. For the melting of heavy

metal oxide glasses, for instance, sealed silica glass ampoules or Pt-crucibles [24] may be employed too.

The homogenisation takes place by gas evolution during the melting and through convection-currents resulting from differences in temperature within the crucible. Additionally, the homogenisation has to be supported by stirring or by shaking of the container. For shapes and dimensions of stirring rods and for the liquid flow caused by stirrers, see for instance [11].

C3 Casting/Forming/Annealing

Preforms suitable for the drawing of optical fibres with core-clad structure can be obtained by the rod and tube technique or by using a double-crucible assembly. This consists of an inner crucible filled with the molten core glass and an outer concentric crucible with the cladding glass. The casting procedure requires excellent control of the system. Obviously, the rod and tube method (core and clad glass are melted separately) has some advantages. Usually, the glass liquid is poured into a preheated mould (about 10 K above the transition temperature T_g) and cooled down to room temperature. An essential condition for 'glass formation' from the melt is that the cooling be sufficiently fast to avoid crystal nucleation and growth [25]. On the other hand, too rapid cooling may induce strains in the glass because the molecular arrangements did not have enough time to reach relaxed conditions throughout the sample. Reheating to near the T_g, holding and slow cooling ('annealing') can eliminate these strains (and birefringence) [1]. Practical cooling rates range between 10 and 50 K/hr depending on the glass system and the glass volume. The annealing of a glass presupposes a detailed knowledge of its behaviour at and near the transformation region. Rötger [26] described and explained the phenomena occurring during heating and cooling of glass. To remove strain, the glass sample should be brought to the upper annealing temperature [27], where the strain is removed rapidly. Then the temperature has to be decreased very slowly (often <10 K/hr).

C4 Quality Assessment

The optical glasses for high performance applications have to fulfil stringent requirements - see Datareviews B1.1 and B1.2. The determination of unwanted optical inhomogeneities by light scattering, interferometric techniques (e.g. [28]) or the shadow projection procedure (e.g. [11]) are efficient ways of evaluating the glass sample. The kinds of inhomogeneities can give insight into their source. Hard striae as localised chemical compositional fluctuations with spatial extent essentially in two dimensions result often from the melting and casting process. Soft striae generally result from the forming process [27]. The experimental absorption spectrum in the UV/visible region together with the deconvolution of bands and the employing of molar absorption coefficients of transitional metal ions in specific valence states, can be used to estimate the impurity content in the glass in a simple way [29].

D CONCLUSION

Multi-component oxide glasses such as silicate, phosphate, germanate or fluoride phosphate glasses are being reconsidered for their potential as low loss optical fibres, fibre lasers and amplifiers because of their better glass forming ability compared to halide glasses. The long tradition in development of these glasses, together with the technological know-how in preparation, will be the basis for further improvements.

REFERENCES

[1] W. Vogel [in *Optical Properties of Glass* Eds. D.R. Uhlmann, N.J. Kreidl (The American Ceramic Society, Westerville, 1991) p.1-36 and references cited therein]

[2] G.W. Morey [US patent no.2206081 (1936)]

[3] M. Poulain [Datareview in this book: *C4.1 Preparation and melting of halide glass*]
[4] M. Digonnet [Datareview in this book: *B5.1 Fibre lasers based on rare-earth doped oxide glass*]; T. Mito, S. Fujino, H. Takebe, K. Morinaga, S. Todoroki, S. Sakaguchi [*J. Non-Cryst. Solids (Netherlands)* vol.210 (1997) p.155-62 and references cited therein]
[5] S.E. Stokowski et al [*Laser Program* Annual Report, LLNL, UCRL-50021-78, 1979]
[6] A. Paul [*Chemistry of Glasses* (Chapman and Hall, 1990)]
[7] M.J. Weber [*Wiss. Z. Friedrich-Schiller-Univ. Jena Math.-Nat.wiss Reihe (Germany)* vol.32 (1983) p.239-48]
[8] W. Vogel [*Glass Chemistry* (Springer, 1992)]
[9] J. Lucas, J. Adam [in *Optical Properties of Glass* Eds. D.R. Uhlmann, N.J. Kreidl (The American Ceramic Society, Westerville, 1991) p.60-1]
[10] A.R. Kortan, N. Kopylov, E. Özdas, R. Pafchek [*J. Non-Cryst. Solids (Netherlands)* vol.213-214 (1997) p.90-4]
[11] T.S. Izumitani [*Optical Glass* (American Institute of Physics, 1986)]
[12] R.C. Ropp [*Inorganic Polymeric Glasses* (Elsevier, 1992) p.21-45]
[13] C. Sheckler, D. Dinger [*J. Am. Ceram. Soc. (USA)* vol.74 (1990) p.24-30]; P. Hrma [in *Chemistry of Glasses* Ed. A. Paul (Chapman and Hall, 1990) ch.5 p.157-78]
[14] D.K. Peeler, T.D. Taylor, D.R. Dinger, O.B. Cavin [in *Ceramic Transactions, vol.29, Advances in Fusion and Processing of Glass* Eds. A.K. Varsheneya, D.F. Bickford, P.P. Bihuniak (The American Ceramic Society, Westerville, 1993) p.151-64]
[15] L. Cook, D. Mader [*J. Am. Ceram. Soc. (USA)* vol.65 (1982) p.597]
[16] W. Seeber, D. Ehrt, H. Ebendorff [*J. Non-Cryst. Solids (Netherlands)* vol.171 (1994) p.94-104]
[17] S. Nakajima, S. Takeshita, C. Tanaka, H. Amemiya, K. Kondoh [in *Ceramic Transactions, vol. 29, Advances in Fusion and Processing of Glass* Eds. A.K. Varsheneya, D.F. Bickford, P.P. Bihuniak (The American Ceramic Society, Westerville, 1993) p.396-403]
[18] G.G. Gausman, L.M. Donohoe, J.T. Kohli, J.M. Jewell, J.E. Shelby [in *Ceramic Transactions, vol. 29, Advances in Fusion and Processing of Glass* Eds. A.K. Varsheneya, D.F. Bickford, P.P. Bihuniak (The American Ceramic Society, Westerville, 1993) p.379-90]
[19] C.A. Parker, G.G. Gausman, J.E. Shelby [in *Ceramic Transactions, vol. 29, Advances in Fusion and Processing of Glass* Eds. A.K. Varsheneya, D.F. Bickford, P.P. Bihuniak (The American Ceramic Society, Westerville, 1993) p.391-6]
[20] J.H. Campbell et al [*Elimination of Platinum Inclusions in Phosphate Laser Glasses* (LLNL report UCRL 53932, 1989)]
[21] Y.T. Hayden, J.H. Campbell, S.A. Paine, G.D. Wilke [in *Ceramic Transactions, vol. 28, Solid-State Optical Materials* Eds. A.J. Bruce, B.V. Hiremath (The American Ceramic Society, Westerville, 1992) p.283-96]
[22] E. Heidenreich [*Wiss. Z. Friedrich-Schiller-Univ. Jena Math.-Nat.wiss Reihe (Germany)* vol.32 (1983) p.527]
[23] D. Ehrt, M. Carl, T. Kittel, M. Müller, W. Seeber [*J. Non-Cryst. Solids (Netherlands)* vol.155 (1994) p.405-19]
[24] S. Sakaguchi, S. Todoroki, N. Rigout [*J. Non-Cryst. Solids (Netherlands)* vol.196 (1996) p.58-62]
[25] S.R. Elliott [*Physics of Amorphous Materials* (Longman Scientific & Technical, 1990) p.16-20]
[26] H. Rötger [*Silikattechn.* vol.20 (1969) p.404-7]
[27] G. Günther, R. Meister [*Glastech. Ber. (Germany)* vol.24 (1951) p.1]
[28] A.J. Marker III, W. Pannhorst [in *Ceramic Transactions, vol. 29, Advances in Fusion and Processing of Glass* Eds. A.K. Varsheneya, D.F. Bickford, P.P. Bihuniak (The American Ceramic Society, Westerville, 1993) p.47-54]
[29] W. Seeber, D. Ehrt [*Glastech. Ber. (Germany)* vol.70 no.10 (1997) p.312-5]; W. Seeber [Thesis B, Universität Jena, Germany (1995)]

B4.2 Drawing of oxide glass optical fibres

S. Todoroki and S. Sakaguchi

June 1997

A INTRODUCTION

Oxide glass fibres offer greater freedom than silica-based fibres in the design of functional fibre devices. Some recent examples include Er^{3+}-doped tellurite fibre amplifiers [1], dispersive optical fibres [2], optical current transducers [3] and highly efficient Nd^{3+}-doped fibre lasers [4]. The key to realising such fibre devices is the ability to draw low loss fibres. Oxide glass fibres are generally drawn either by the double-crucible technique or by preform methods [5-7]. This Datareview supplies an overview of these two methods and provides related references.

B REQUIRED PROPERTIES OF RAW GLASSES

Before drawing fibres, we have to prepare two types of raw glass, core and cladding, which satisfy the following requirements.

(1) The refractive index difference (Δn) between them is an appropriate value to form a waveguide structure. The refractive index can be adjusted by changing the glass composition [5], i.e. the metal oxide content (alkali, alkaline earth and heavy metal oxides), the anion content [8], or the whole composition.

(2) Both glasses should be thermally stable, i.e. heat-induced phase separation and/or crystallisation should not occur easily.

(3) Their thermal properties, viscosity and thermal expansion coefficient, should be similar in order to obtain a wide range of possible drawing temperatures and to suppress the losses induced by residual stress [9].

(4) Factors causing extrinsic losses such as bubbles, dust and contamination (Pt colloids from the crucible, ceramic particles, etc.) should be carefully excluded from the glass-making facilities.

Although it is easy to alter the multi-component oxide glass properties discussed in (1) to (3) by changing the glass composition, it is very difficult to find core and cladding compositions which simultaneously satisfy all the requirements. Furthermore, the attenuation of the fibre depends on the heat treatment during the whole process. Thus, their compositions need to be optimised after many drawing trials.

C DEVITRIFICATION OF MELT/GLASS

It is important to manage the temperature of the whole process, particularly that of the drawing tower furnace, in order to suppress the excess loss caused by crystal precipitation. This makes it necessary to understand the mechanism of the crystallisation process, which proceeds via two steps, nucleation and crystal growth [10]. These phenomena are related to the temperature dependence of atom mobility or viscosity (see FIGURE 1).

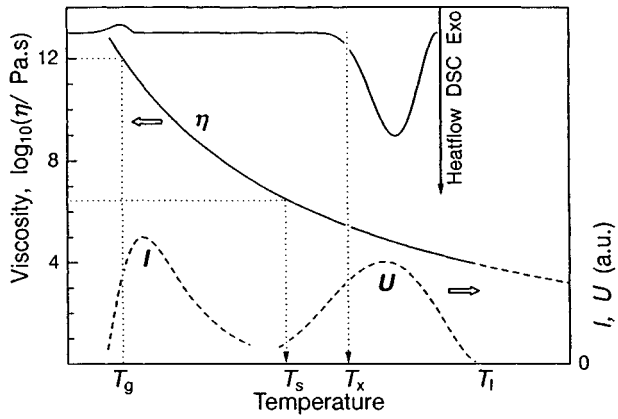


FIGURE 1 A set of model functions showing the temperature dependence of viscosity (η), nucleation frequency (I), crystal growth rate (U) and heatflow (DSC curve). The broken lines indicate that the data are impossible or very hard to determine. T_g: glass transition temperature ($\eta \sim 10^{12}$ Pa s); T_s: softening temperature ($\eta \sim 10^{6.5}$ Pa s); T_x: crystallisation onset temperature; T_l: liquidus temperature.

As the glass is heated, nucleation occurs first, and for silicate glasses, it occurs at ~T_g [10]. It is easy to form nuclei at an interface between the two phases, i.e. the air/glass or crucible/glass interface (heterogeneous nucleation). Then, crystals grow on the nuclei at higher temperature. This is detected by thermal analysis. The onset temperature of the crystallisation peak is usually referred to as T_x. Above the liquidus temperature, T_l, the nuclei disappear and crystallisation does not occur. These two phenomena are quantified by nucleation frequency (I) and crystal growth rate (U). These values are determined by two-stage heat treatment and direct observation of the precipitates [11].

D DRAWING

There are two ways to feed raw glasses into drawing facilities: one involves inserting a solid preform and the other involves two kinds of melt. Which method is used depends on the properties of the glasses/melts being employed, i.e. which is the better way to obtain low loss fibres.

D1 Preform Method

The most basic method for making a step-index preform is the rod-in-tube method. With this technique, a core rod is inserted into a cladding tube. Their surfaces should be carefully polished to suppress the precipitation which occurs during the subsequent heat treatment. Some bubbles are likely to be trapped at the interface between the core and the cladding.

Several methods have been developed for fluoride fibres by which a preform can be made immediately, i.e. built-in casting [12], rotational casting [13], the suction method [14] and the extrusion method [15]. They are also applicable to oxides if the mold can tolerate the high working temperature of the oxide melt. For GeO_2 preforms, the vapour phase deposition process is applicable [16-18]. Since these methods require no polishing process, the precipitation at the interface between the core and the cladding is expected to be smaller than with the rod-in-tube method.

The heat treatment during the process is shown in FIGURES 2(a) - 2(d). During the preparation of raw glasses, the quenched melt is usually kept at near T_g to remove residual stress. This means some nuclei can be formed during the quenching period. Fibres can be drawn above the temperature T_s where macroscopic plastic deformation occurs, i.e. the viscosity becomes less than about $10^{6.5}$ Pa s. T_s can be

determined by viscosity measurements using parallel-plate rheometry [19]. Thus, the fibre drawing temperature is between T_s and T_x (see FIGURE 2(b)).

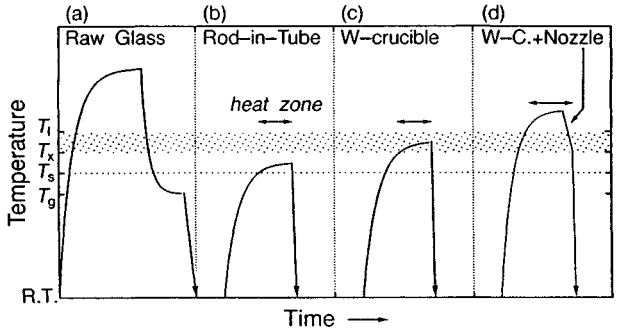


FIGURE 2 Examples of the temperature of the glass/melt/fibre as a function of time during (a) glass preparation and (b - d) the drawing process. U >> 0 in the dotted area.

D2 Melting in Double Crucible

In contrast to the preform method, the raw glasses are heated to a liquid state in a double crucible as shown in FIGURE 3(a). Thus, the melt experiences a temperature higher than T_x. When U is high enough compared with the time in the furnace to precipitate crystals, the crucible should not be heated between T_x and T_l as shown in FIGURE 2(c). Thus, the double crucible is designed so that the melt is heated at above T_l (see FIGURE 2(d)). Once the melt is above T_l, the nuclei disappear and the melt becomes hard to crystallise during the subsequent cooling period. Care must be taken to avoid contamination from the crucible if the working temperature is high.

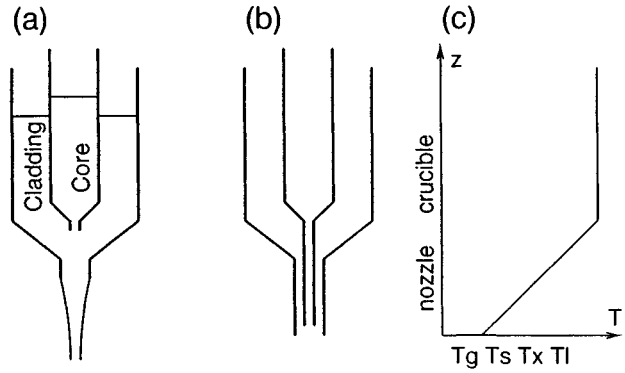


FIGURE 3 Examples of (a) a double crucible, (b) a double crucible with a nozzle, and (c) the temperature profile of (b).

Since the speed at which the melt flows from the crucible should be consistent with the appropriate drawing speed, the crucible is sometimes equipped with a long nozzle as in FIGURE 3(b) in order to provide some resistance to the flow of a low viscosity melt [20]. It is also possible to employ a temperature gradient where the nozzle is cooler than the crucible (see FIGURE 3(c)). The melt moves quickly through the region between T_l and T_x (U >> 0) in the nozzle.

Bubbles form if a metal crucible is used. This is because of a battery effect due to the difference between the alkali ion concentrations of the core and cladding glasses [21]. To avoid this effect, the crucible should be made of an insulator.

E CONCLUSION

The methods described here are vulnerable to contamination and precipitation. Moreover, only a limited amount of fibre can be fabricated at one time. This is because the fibres are drawn from a liquid state, which is hard to control. A new technique without a container is needed by which to fabricate a large preform, such as the methods (VAD, OVD, MCVD etc.) employed for the current silica-based fibres.

REFERENCES

[1] A. Mori et al [*Proc. Conf. Opt. Fiber Commun.* (1997) paper PD-1]; A. Mori, Y. Ohishi, S. Sudo [*Electron. Lett. (UK)* vol.33 (1997) p.863-4]

[2] J. Nishimura, K. Morishita [*J. Lightwave Technol. (USA)* vol.15 (1997) p.294-8]

[3] K. Kurosawa [*Opt. Rev. (Japan)* vol.4 (1997) p.38-44]

[4] J. Wang, L. Reekie, W.S. Brocklesby, Y.T. Chow, D.N. Payne [*J. Non-Cryst. Solids (Netherlands)* vol.180 (1995) p.207-16]

[5] K.J. Beales, C.R. Day [*Phys. Chem. Glasses (UK)* vol.21 (1980) p.5-21]

[6] J.E. Midwinter [*Optical Fibers for Transmission* (Wiley, 1979)]

[7] T. Akamatsu [*J. Lightwave Technol. (USA)* vol.1 (1983) p.580-4]

[8] S. Todoroki, S. Sakaguchi [*Jpn. J. Appl. Phys. (Japan)* vol.35 (1996) p.5374-8]

[9] M. Ohashi, M. Tateda, K. Shiraki, K. Tajima [*IEEE Photonics Technol. Lett. (USA)* vol.5 (1993) p.812-4]

[10] H. Scholze [*Glass - Nature, Structure and Properties* (Springer-Verlag, 1991)]

[11] K. Matsushita, M. Tashiro [*J. Non-Cryst. Solids (Netherlands)* vol.11 (1973) p.471-84]

[12] M. Ohashi, T. Miyashita, T. Manabe [*Phys. Chem. Glasses (UK)* vol.23 (1982) p.196-201]

[13] D.C. Tran, C.F. Fisher, G.H. Sigel [*Electron. Lett. (UK)* vol.18 (1982) p.657-8]

[14] S. Takahashi [*J. Non-Cryst. Solids (Netherlands)* vol.140 (1992) p.172-8]

[15] K. Itoh, K. Miura, I. Masuda, M. Iwakura, T. Yamashita [*J. Non-Cryst. Solids (Netherlands)* vol.167 (1994) p.112-6]

[16] H. Takahashi, I. Sugimoto [*J. Lightwave Technol. (USA)* vol.5 (1984) p.613-6]

[17] T. Hosaka, S. Sudo, K. Okamoto [*Electron. Lett. (UK)* vol.23 (1986) p.24-6]

[18] S. Sakaguchi, S. Todoroki [*Appl. Opt. (USA)* vol.36 no.27 (1997) p.6809-14]

[19] E.H. Fontana [*Am. Ceram. Soc. Bull. (USA)* vol.49 (1970) p.594-7]

[20] S. Sakaguchi, S. Todoroki [*IEICE Trans. Commun. (Japan)* vol.E80-B (1997) p.508-15]

[21] T. Izawa, S. Sudo [*Optical Fibres: Materials and Fabrication* (KTK Scientific Publishers, Tokyo, 1987)]

B4.3 Loss of oxide glass optical fibres

S. Todoroki and S. Sakaguchi

June 1997

A INTRODUCTION

The factors which contribute to optical fibre loss are classified into four types, as listed in TABLE 1. Examples of loss spectra are shown in FIGURE 1. Intrinsic loss determines the ideal minimum loss value of the material and the magnitude of extrinsic loss is dependent on the fabrication process. We provide an overview of these loss factors in oxide glasses and supply related references.

TABLE 1 Loss factors of optical fibre.

	Intrinsic loss	Extrinsic loss
Scattering loss	Rayleigh scattering Raman scattering Brillouin scattering	Crystal precipitation Structural imperfection
Absorption loss	Lattice vibration Electronic oscillation	Impurity

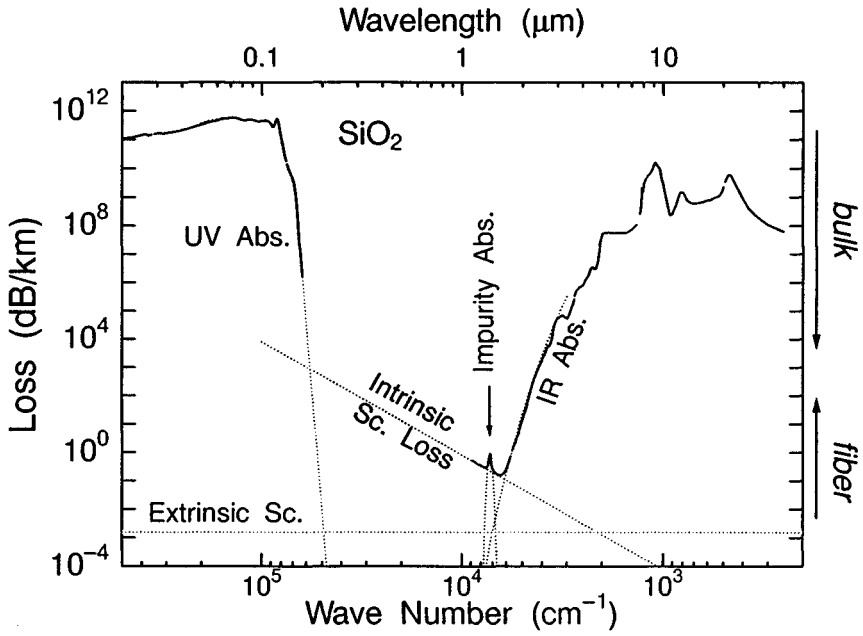


FIGURE 1 Loss spectra of silica glass [1] and fibre [2].

B INTRINSIC LOSS

B1 Scattering Loss

The intrinsic scattering loss of oxide glass fibres is considered to be the same as that of the corresponding bulk glass, which is described in a previous Datareview [3], except that its magnitude may change a little after fibre drawing because of an increase in T_F and heat-induced concentration fluctuation. The loss spectrum exhibits λ^{-4}-dependence.

B2 Absorption Loss

Intrinsic absorption losses in the ultraviolet (UV) and infrared (IR) ranges are due to electron oscillations (mostly in oxygen ions) and lattice vibrations, respectively. The UV absorption peaks shift to a longer wavelength as the electron density on the oxygen ions increases. This can be estimated approximately by using the theoretical optical basicity concept [4]. The slopes of the fundamental IR absorption peaks extend to the near-IR range as a result of their overlapping overtones and combination modes and are empirically expressed as $\alpha = B \exp(-b/\lambda)$. B and b are constants which are determined by fitting the IR absorption spectra.

B3 Estimated Loss

The estimated loss minimum is determined at the crossing point of two of these loss factors, usually scattering and IR absorption. Thus, the theoretical expression is written as

$$\alpha = A/\lambda^4 + B \exp(-b/\lambda) \quad (1)$$

Various glasses with low scattering and/or low IR absorption have been proposed, as shown in TABLE 2, in order to develop optical fibres with a much lower loss than silica glass fibres.

TABLE 2 Predicted loss of oxide glasses for optical fibres.
Ca-Al-O: 5 $KO_{0.5}$ - 2 $NaO_{0.5}$ - 36 CaO - 47 $AlO_{1.5}$ - 10 SiO_2;
Ba-Ga-Ge-O: 27.5 BaO - 12.5 Ga_2O_3 - 60 GeO_2; Ca-P-Ge-O-F: 20 CaO - 40 P_2O_5 - 40 GeO_2;
Na-Al-Si-O: 35.8 Na_2O - 7.2 Al_2O_3 - 57 SiO_2; Na-Mg-Si-O: 30 Na_2O - 10 MgO - 60 SiO_2;
P-Si-O-F: P_2O_5 (8.5 wt%) - F (0.3 wt%) - SiO_2.

System	A	B	B	Loss minimum		Ref
	(μm^4 dB/km)	(dB/km)	(μm)	(dB/km)	@(μm)	
Ca-Al-O	0.17	6×10^{10}	59	0.015	1.9	[5]
GeO_2	2.3	4×10^{10}	58	0.15	2	[6]
Ba-Ga-Ge-O	0.17	1×10^{11}	60	0.03	2	[7]
Ca-P-Ge-O-F	0.7	-	-	0.08	1.77	[8]
Na-Al-Si-O	0.29	6.9×10^{11}	50.6	0.055	1.56	[9]
Na-Mg-Si-O	0.32	6.9×10^{11}	50.6	0.06	1.6	[10]
P-Si-O-F	0.64	6.5×10^{11}	49	0.14	1.56	[11]
Tellurite	0.29	5.75×10^{15}	126.67	0.0035	3.02	[12]
SiO_2 fibre	0.76	6.5×10^{11} [11]	49 [11]	0.154	1.55	[2]

C EXTRINSIC LOSS

C1 Scattering Loss

Extrinsic scattering loss appears as a result of the difference between the actual and ideal structures of the fibre. This is caused by such factors as the precipitation of microcrystals, the inclusion of dust and bubbles, microbending of the waveguide structure due to these particles and microscopic phase separation. The magnitude of this kind of loss is λ-independent. To suppress the precipitation, the heat treatment must be precisely controlled throughout the whole fabrication process (see [13] in this volume).

C2 Absorption Loss

Metal and water contamination cause characteristic absorption peaks in the visible and IR ranges. This contamination originates in the raw materials, fabrication facilities and atmosphere. Fundamental OH absorption peaks appear at 2.8 (free OH groups), 3.5 and 4.25 μm [14]. Tsujikawa applied the

deuteration technique (OH-OD substitution [15]) to the glass melting process and OH absorption was suppressed [16].

C3 Measured Loss

It was in the late 1970s when the loss of multi-component oxide glasses reached several dB/km at ~0.8 μm [17]. TABLE 3 lists work undertaken on oxide glass fibres since the early 1980s. Akamatsu fabricated alkali and alkaline earth free phosphate fibres, by the double-crucible technique, whose scattering coefficient is ~3.3 μm^4 dB/km [18]. Recently, ternary silicate glass fibres have been fabricated in the expectation of a low intrinsic scattering loss [19,16,20]. Their loss values are still high because of the extrinsic scattering loss.

TABLE 3 The minimum measured loss of oxide glass fibres. VAD: vertical axis deposition method; WC: double-crucible method; P: preform method.

Core	Cladding	Process	Loss minimum		Ref
			(dB/km)	@(μm)	
Na-Al-Si-O	Na-Al-Si-O	WC	<100	1.27	[16]
Na-Mg-Si-O	F-doped Na-Mg-Si-O	WC	69*	1.2	[20]
Ga-Ge-P-O	Ga-Si-P-O	WC	2.5	1.1	[18]
P-Si-O	Si-O-F	VAD	0.20	1.55	[21]
Sn_2O_3-doped GeO_2	GeO_2	VAD	4	2	[22]
Nd-Bi-Na-Zn-Te-O	Na-Zn-Te-O	P	900	1.35	[12]

*unpublished result

D CONCLUSION

The ultimate loss value of oxide glass fibres is still not attainable because of a large extrinsic loss. It is therefore necessary to develop a new fabrication process to suppress precipitation and contamination. For this purpose, a knowledge of the thermodynamics of the supercooled melt is essential in order to optimise the fabrication conditions [13].

REFERENCES

[1] H.R. Philipp [*Handbook of Optical Constants* Ed. E.D. Palik (Academic Press, Orlando, 1985) p.749-63]

[2] H. Kanamori et al [*J. Lightwave Technol. (USA)* vol.LT-4 (1986) p.1144-9]

[3] S. Todoroki, S. Sakaguchi [Datareview in this book: *B1.2 Intrinsic scattering losses of oxide glass*]

[4] J.A. Duffy, M.D. Ingram [*J. Non-Cryst. Solids (Netherlands)* vol.144 (1992) p.76-80]

[5] M.E. Lines, J.B. MacChesney, K.B. Lyons, A.J. Bruce, A.E. Miller, K. Nassau [*J. Non-Cryst. Solids (Netherlands)* vol.107 (1989) p.251-60]

[6] S. Sakaguchi, S. Todoroki [*Appl. Opt. (USA)* vol.36 no.27 (1997) p.6809-14]

[7] P.L. Higby, C.I. Merzbacher, I.D. Aggarwal, E.J. Friebele [*Mater. Res. Soc. Symp. Proc. (USA)* vol.244 (1992) p.115-20]

[8] S. Sakaguchi, S. Todoroki, N. Rigout [*Jpn. J. Appl. Phys. (Japan)* vol.34 (1995) p.5615-20]

[9] K. Shiraki, M. Ohashi [*J. Non-Cryst. Solids (Netherlands)* vol.149 (1992) p.243-8]

[10] S. Todoroki, S. Sakaguchi, M. Peeters [*J. Am. Ceram. Soc. (USA)* vol.80 (1997) p.313-6]

[11] K. Tajima, M. Ohashi, K. Shiraki, M. Tateda, S. Shibata [*J. Lightwave Technol. (USA)* vol.10 (1992) p.1532-5]

[12] J.S. Wang, E.M. Vogel, E. Snitzer [*Opt. Mater. (Netherlands)* vol.3 (1994) p.187-203]

[13] S. Todoroki, S. Sakaguchi [Datareview in this book: *B4.2 Drawing of oxide glass optical fibres*]
[14] H. Scholze [*Glass - Nature, Structure and Properties* (Springer Verlag, 1991)]
[15] H. Hosono, T. Kamae, Y. Abe [*J. Am. Ceram. Soc. (USA)* vol.72 (1989) p.294-7]
[16] K. Tsujikawa, M. Ohashi [*OFC'97 Technical Digest* TuB2 (1997) p.2]
[17] K.J. Beales, C.R. Day [*Phys. Chem. Glasses (UK)* vol.21 (1980) p.5-21]
[18] T. Akamatsu [*J. Lightwave Technol. (USA)* vol.1 (1983) p.580-4]
[19] T. Ryan, M. Watanabe, K. Muta, H. Matsuura [*Showa Electr. Wire Cable Rev. (Japan)* vol.43 (1993) p.138-46]
[20] S. Sakaguchi, S. Todoroki [*IEICE Trans. Commun. (Japan)* vol.E80-B (1997) p.508-15]
[21] K. Tajima, Y. Miyajima [*OFC'97 Technical Digest* TuB5 (1997) p.4]
[22] H. Takahashi, I. Sugimoto [*J. Lightwave Technol. (USA)* vol.5 (1984) p.613-6]

PART B: OXIDE GLASS

CHAPTER B5

SELECTED APPLICATIONS

B5.1 Fibre lasers based on rare earth-doped oxide glass
B5.2 Optical fibre amplifier based on rare earth-doped oxide glass

B5.1 Fibre lasers based on rare earth-doped oxide glass

M.J.F. Digonnet

September 1997

A INTRODUCTION

Rare earth doped oxide glass fibre lasers were first demonstrated in the 1960s [1] and investigated again in the 1970s [2], but the field did not blossom until 1985 [3] when long, low-loss doped fibres first became available and optical communications and fibre sensors began to require novel fibre sources and amplifiers. A key feature of fibre lasers that sets them apart from conventional bulk lasers is their waveguiding structure. The fibre's low loss and strong optical confinement result in a low threshold and highly efficient utilisation of the pump power [4], making diode laser pumping possible. Fibre lasers can thus be more compact, easier to manufacture and far less costly than bulk lasers. The overwhelming majority of the work on oxide glass fibre lasers has been done on silica, although some work has covered phosphate glass fibres. This host far exceeds any other glass with regards to thermal and mechanical stability, low loss in a fibre form, and resistance to optical damage. Because of these outstanding properties, and the numerous laser transitions available from triply ionised rare earths, a very large number of silica fibre lasers have been demonstrated, covering a wide range of wavelengths, cavity configurations, and frequency and temporal characteristics. They now compete directly with semiconductor lasers, offering higher brightness, higher fibre-coupled power, different ranges of wavelength and coherence properties, and a greater frequency thermal stability. This technology is mature enough that several sources are now commercialised.

B CW FIBRE LASERS

The most common fibre laser utilises a Fabry-Perot resonator. It is typically formed by placing miniature planar dielectric reflectors in contact with the cleaved or polished ends of the doped fibre (FIGURE 1(a)). The reflectors can also be directly coated onto the fibre ends [5]. When the gain is large enough, the weak Fresnel reflections at the fibre ends can serve as feedback for lasing [6,7]. Fibre lasers are optically end-pumped. The pump beam is coupled with a lens through the high-reflecting mirror, which must be dichroic to transmit the pump but reflect the laser signal. Dielectric resonators can also be replaced by Sagnac fibre loops (FIGURE 1(b)) [8] or fibre gratings (FIGURE 1(c)) [9]. Another important resonator is the all-fibre ring (FIGURE 1(d)) fabricated with a rare-earth doped fibre closed upon itself with a fibre coupler [3,10,11]. For the configurations of FIGURES 1(b) - 1(d), a laser diode pump can be pigtailed directly to the fibre end.

In a typical fibre laser, the output power grows linearly with absorbed pump power above a sharp threshold [3-5]. The pump power required to reach threshold depends on (1) the gain per unit pump power of the laser transition, (2) the round-trip cavity losses δ, and (3) the effective pump mode area [4]. Thus, lower thresholds are produced by reducing the fibre core size and increasing the fibre NA [12]. The slope efficiency (the slope of the output curve) s is the ratio of the output power P_{out} to the absorbed pump power in excess of threshold, $P_{abs} - P_{th}$. For a laser transition with unity quantum efficiency, it is given by $s = (T/\delta)(\lambda_p/\lambda_s)$, where λ_p is the pump wavelength, λ_s the laser wavelength and T the output reflector transmission [4]. If the fibre loss is negligible, as is usual, $\delta = T$ and s approaches λ_p/λ_s. This is the quantum limit: one laser photon is emitted for every absorbed pump photon. Unlike in flashlamp-pumped lasers, such ideal conversions are possible in fibre lasers because the pump wavelength is matched to the dopant absorption transition.

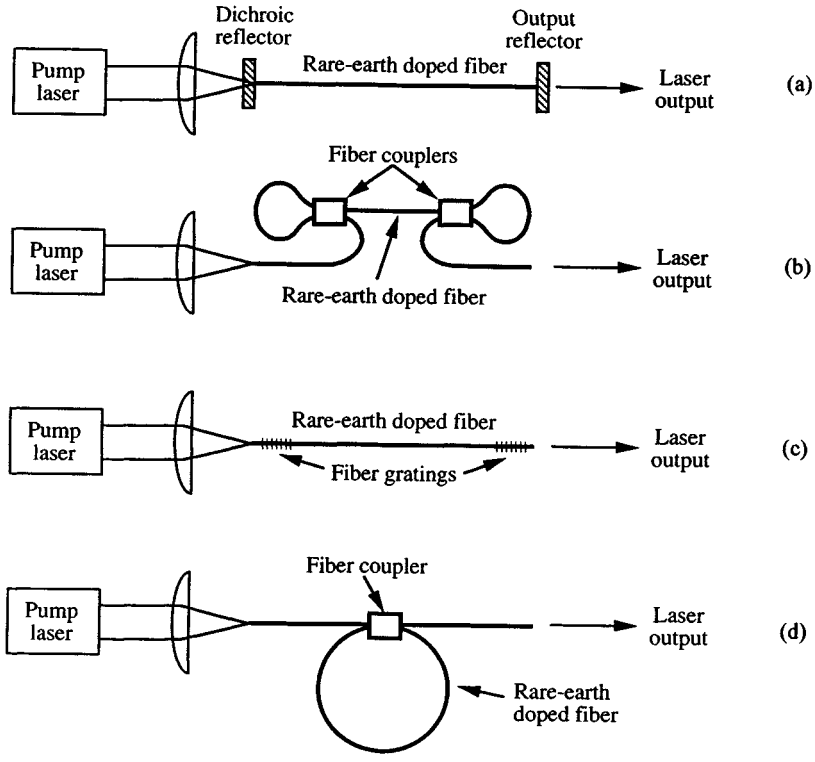


FIGURE 1 Common fibre laser configurations.

TABLE 1 compiles the main wavelength regions demonstrated in CW rare-earth doped silica fibre lasers. They range from the red to mid-IR. Because of the relatively high photon energy of silicates, low energy transitions are strongly non-radiative and laser operation above ~2.1 μm is difficult with all rare-earths. The gain bandwidth of most of the transitions of rare earth ions in glass is broad (~10 - 100 nm). Many fibre lasers are thus widely tunable (see TABLE 1). Tuning has been accomplished with an intracavity bulk-optic grating [13], a wavelength-dependent coupler [14], an acousto-optic tunable filter in a waveguide [15] or fibre [16] form, or a birefringent filter [17]. A good example is the Tm-doped fibre laser, which has been tuned over the widest range (1.65 to 2.05 μm) [17,18]. In lasers based on a three-level transition, the wavelength can be broadly adjusted by proper fibre length selection, as demonstrated with Er^{3+} from ~1.55 to ~1.6 μm [19].

TABLE 1 Wavelength and tuning ranges demonstrated with CW rare-earth doped oxide glass fibre lasers.

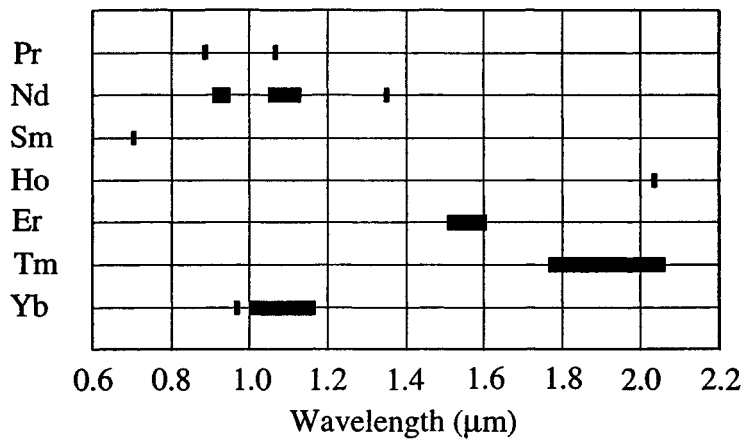


TABLE 2 lists the characteristics of representative CW silica fibre lasers [7,18,20-29]. In many cases the threshold is a few mW and the slope efficiency in the tens of percent range. This is true for important sources such as Er^{3+} (1.55 μm), Nd^{3+} (1.06 μm) and Tm^{3+} (1.9 μm) doped fibre lasers, which are typically laser diode pumped. In a high confinement Nd-doped fibre, a record threshold of only 75 μW was observed, for a slope efficiency of 29% [30]. Other ions (Pr^{3+}, Sm^{3+} and Ho^{3+}) are pumped at short wavelengths not yet available with sufficient power from laser diodes. Frequency up-conversion has been observed in rare-earth doped silica fibres [31] but it is too inefficient to produce lasers.

TABLE 2 Characteristics of representative CW oxide glass fibre lasers; silica for all but [27] (phosphate). With respect to (a) absorbed pump power (l) launched pump power.

Ion	Pump	Laser	Threshold	Slope	Ref
Sm^{3+}	488 nm	0.65 μm	24 $mW^{(a)}$	12.7%$^{(a)}$	[20]
Nd^{3+}	823 nm (LD)	0.938 μm	1.9 $mW^{(a)}$	36%$^{(a)}$	[21]
Yb^{3+}	890 nm	0.98 μm	16 $mW^{(l)}$	40%$^{(l)}$	[22]
Nd^{3+}	822 nm (LD)	1.06 μm	1.3 $mW^{(a)}$	59%$^{(a)}$	[23]
Pr^{3+}	590 nm	1.08 μm	5 $mW^{(a)}$	5%$^{(a)}$	[24]
Yb^{3+}	840 nm	~1.1 μm	8 $mW^{(a)}$	15%$^{(a)}$	[25]
Nd^{3+}	752 nm	1.363 μm	65 $mW^{(a)}$	1%$^{(a)}$	[26]
Nd^{3+}	815 nm	1.363 μm	5 $mW^{(a)}$	10.8%$^{(a)}$	[27]
Er^{3+}	1480 nm (LD)	1.56 μm	4.7 $mW^{(a)}$	90.4%$^{(a)}$	[7]
Er^{3+}	980 nm	1.56 μm	3.2 $mW^{(l)}$	42%$^{(l)}$	[28]
Tm^{3+}	786 nm (LD)	1.9 μm	4.4 $mW^{(l)}$	17%$^{(l)}$	[18]
Ho^{3+}	458 nm	2.08 μm	46 $mW^{(a)}$	1.7%$^{(a)}$	[29]

Er-doped fibre lasers near 1.55 μm, important for optical communications, are extremely efficient. When pumped at 1.48 μm, their efficiency can be within a few percent of the theoretical limit $\lambda_p/\lambda_s \approx 95\%$ [7] (see TABLE 2). Pumping at 980 nm produces a lower, though still quite substantial, efficiency due to the lower λ_p/λ_s ratio (~63%) [28]. Pumping around 800 nm is unfortunately inefficient because of pump excited state absorption (ESA), even when the fibre is co-doped with Yb^{3+} [32].

In all silica-based fibre lasers, the rare earth concentration must be low enough to avoid ion clusters, which can reduce the laser output power significantly [7]. A typical silica fibre laser is thus fairly long, a few tens of cm to a few metres. Phosphate fibres can be doped much more heavily and thus produce much shorter lasers, in the sub-mm range [33].

In 1.36 μm Nd-doped silica fibre lasers, the performance is poor (see TABLE 2) because of signal ESA. Co-doping with P_2O_5 reduces ESA but the laser efficiency is still low [26]. This problem is greatly reduced in phosphate fibres, which have yielded far better performance (see TABLE 2) [27], although with both hosts lasing is forced to occur at longer wavelengths, outside the second communication window.

In diode-pumped fibre lasers, the output power is limited by the maximum pump power that can be coupled into the small fibre core. This problem has been circumvented by using a double-clad fibre, in which the doped core is surrounded by a first (undoped) cladding, itself surrounded by a second (undoped) cladding [34]. The laser diode is coupled into the first cladding. Since the latter is a highly multimoded waveguide, a large fraction of the pump is coupled into it, even if the laser diode is an array of low spatial coherence. A longer fibre must be used to make up for the weaker pump absorption per unit length, which is inconsequential for a four-level laser. This design has produced record CW output powers, for example over 40 W in a 1.1 μm Yb-doped fibre laser [35].

In a laser utilising a low birefringence fibre, the output polarisation is generally not linear and unstable. Several schemes have been developed to produce fibre lasers with a stable, linearly polarised output.

They include using a single-polarisation doped fibre [36], an intracavity fibre polariser [37], or fibre grating reflectors with a slightly polarisation dependent reflectivity [38]. For example, the first method yielded a linearly polarised Nd-doped fibre laser with a 35 dB extinction ratio. Another scheme utilises the anisotropic cross-sections of the ions to produce a single-polarisation laser by pumping a polarisation-maintaining doped fibre with a linearly polarised pump aligned to a fibre axis [39].

C NARROW-LINEWIDTH FIBRE LASERS

A wide range of narrow-linewidth fibre lasers, important for coherent communications, have been developed, mostly with Er^{3+} [10,11,40-47], and occasionally with Nd^{3+} [48] or Yb^{3+} [49]. A first general approach for linewidth narrowing is to introduce a narrowband filter in a linear cavity, in particular a Fabry-Perot etalon made of two fibre gratings [40,48]. A second etalon with a carefully adjusted bandpass suppresses mode hopping [41].

A second general approach involves a fibre ring configuration and an intracavity optical isolator. The latter forces unidirectional oscillation, which eliminates spatial hole burning and facilitates single longitudinal mode operation [10]. Adding a narrow bandpass filter in the ring has reduced the linewidth to 1.4 kHz [40]. With two fibre Fabry-Perot etalons, one to select a single longitudinal mode, the other for frequency tuning, a linewidth under 5.5 kHz and tunability from 1530 to 1575 nm were demonstrated [11]. Narrow-linewidth, frequency-stabilised operation was also reported using an intracavity overlay filter (<68 kHz) [42] or a length of fibre as a birefringent element (240 kHz) [43]. A more complex configuration using a length of unpumped Er-doped fibre as a saturable absorber outside the ring has produced a stable linewidth under 950 Hz [44].

A third general approach is to make the cavity very short (≤1 mm), which is possible with a phosphate fibre [33], or somewhat longer (~5 cm) but with a fibre grating for mode suppression [48]. The weak absorption of the short fibre can be increased by co-doping it with Yb^{3+} (in the case of Er^{3+}) [45]. The master oscillator power amplifier (MOPA) is based on the same principle, but the short fibre laser is followed by a longer doped fibre to amplify the weak laser signal [33,46]. These lasers generally suffer from low tunability (≤5 nm with Er^{3+}). Active noise reduction [46] and means of reducing the dithering associated with it [47] have also been investigated.

D PULSED FIBRE LASERS

Fibre lasers generating short, high peak power pulses are of great interest for many applications, including high-speed communication, non-linear optics, time-domain reflectometry, medicine and sensing. As a result, a large effort has been devoted to develop Q-switched, mode-locked and Q-switched mode-locked fibre lasers, mostly with Er^{3+}, but also with Nd^{3+}, Tm^{3+} and Sm^{3+}.

TABLE 3 summarises the pulse characteristics of representative Q-switched fibre lasers [20,50-53]. Intracavity loss modulation is most often accomplished with a bulk-optic acousto-optic amplitude modulator (AOM) [20,50,52,53]. Other methods include using a dye as a saturable absorber [54], an integrated optic amplitude modulator [55], or a piezoelectric to stretch a fibre grating and modulate its reflectivity [56]. Gain switching has also been reported [57]. Nd- and Er-doped lasers now produce pulse widths of 10 - 30 ns and peak powers of hundreds of watts. The repetition rate at which these characteristics prevail is limited by the upper level lifetime of the ions to 1 - 10 kHz, depending on the ion.

Rare-earth doped silica fibre lasers are particularly well suited to produce very short mode-locked pulses because of their large gain bandwidth. Linear and ring fibre lasers have been mode locked, both passively and actively [58,73]. Common passive techniques utilise a non-linear optical loop mirror

TABLE 3 Characteristics of representative Q-switched silica fibre lasers. AOM: acousto-optic modulator (bulk-optic); FM: fibre modulator; NA: data not available.

Laser ion	Laser wavelength	Pump wavelength	Pump power	Pulse width	Peak power	Rep. rate	Modulator	Ref
Sm^{3+}	0.65 μm	488 nm	NA	370 ns	10 W	NA	AOM	[20]
Nd^{3+}	0.94 μm	825 nm (LD)	~35 mW	80 ns	5.2 W	~1 kHz	AOM	[50]
Nd^{3+}	1.08 μm	825 nm (LD)	17 mW	15.5 ns	110 W	800 Hz	AOM	[50]
Er^{3+}	1.55 μm	980 nm	100 mW	13.5 ns	400 W	100 Hz	FM	[51]
Er^{3+}	1.56 μm	980 nm (LD)	30 mW	20 ns	290 W	500 Hz	AOM	[52]
Tm^{3+}	1.92 μm	792 nm	NA	130 ns	4 W	4 kHz	AOM	[53]

[74], a non-linear amplifying loop mirror [16,61,75], a saturable absorber [59,65], an all-fibre filter [66], additive-pulse mode-locking [60] or the fibre Kerr effect to induce non-linear polarisation modulation [67]. Active mode-locking is usually accomplished by inserting an amplitude modulator (e.g. $LiNbO_3$) in the cavity [63,64]. TABLE 4 lists the pulse characteristics of representative mode-locked fibre lasers. Passively mode-locked lasers easily produce sub-ps pulses. However, they are often, though not always [58], prone to erratic pulse behaviour (pulse drop-out, multiple pulsing and jitter). Active mode-locking is largely immune to these problems, but it produces significantly longer pulses (see TABLE 4). This problem can be alleviated by adding fibre to the laser cavity to induce soliton pulse shortening [63,68]. The shortest uncompressed pulses reported are 77 fs with Er^{3+} [60] and around 42 fs with Nd^{3+} [58]. Pulse energies are typically in the tens of pJ range, and occasionally in the nJ range (see TABLE 4). Repetition rates are typically around 50 MHz with passive mode locking, and as high as 10 GHz with active mode locking. Several other important properties of mode-locked fibre lasers, not listed in TABLE 4, such as pulse drop-out, noise and jittering, have been studied. In particular, several schemes have also been developed to stabilise the pulse train [64,69-71]. Synchronisation of two lasers [72] and of two wavelengths in the same laser [73] have also been accomplished.

TABLE 4 Characteristics of representative mode-locked silica fibre lasers. APM: additive-pulse mode-locking; NALM: non-linear amplifying loop mirror; NPM: non-linear polarisation modulation; NA: data not available.

Laser ion	Laser wavelength	Pump wavelength	Pulse width	Rep. rate	Energy per pulse	Method	Ref
Nd^{3+}	1.06 μm	750 - 800 nm	42 fs	70 MHz	1 nJ	NPM	[58]
Nd^{3+}	1.06 μm	750 - 800 nm	6 ps	52 MHz	1.25 nJ	Sat. abs.	[59]
Er^{3+}	1.55 μm	980 nm	77 fs	45 MHz	90 pJ	APM	[60]
Er^{3+}	1.57 μm	1.48 (LD)	98 fs	210 MHz	10 pJ	NALM	[61]
Er^{3+}	1.55 μm	973 nm (LD)	600 fs	130 MHz	20 pJ	NPM	[62]
Er^{3+}	1.55 μm	980 nm (LD)	800 fs	NA	560 pJ	NALM	[16]
Er^{3+}	1.55 μm	NA	1.3 ps	10 GHz	4.1 pJ	EO modul.	[63]
Er^{3+}	1.55 μm	1480 nm (LD)	6.5 ps	10 GHz	0.18 pJ	EO modul.	[64]
Tm^{3+}	1.9 μm	786 nm (LD)	190 fs	50 MHz	20 pJ	Sat. abs.	[65]

REFERENCES

[1] C.J. Koester, E. Snitzer [*Appl. Opt. (USA)* vol.3 no.10 (1964) p.1182-6]

[2] J. Stone, C.A. Burrus [*Appl. Opt. (USA)* vol.13 no.6 (1974) p.1256-8]

[3] R.J. Mears, L. Reekie, S.B. Poole, D.N. Payne [*Electron. Lett. (UK)* vol.21 no.17 (1985) p.738-40]

[4] M.J.F. Digonnet, C.J. Gaeta [*Appl. Opt. (USA)* vol.24 no.3 (1985) p.333-42]

[5] M. Shimizu, H. Suda, M. Horiguchi [*Electron. Lett. (UK)* vol.23 no.15 (1987) p.768-9]

[6] Y. Kimura, K. Susuki, M. Nakazawa [*Opt. Lett. (USA)* vol.14 no.18 (1989) p.999-1001]

[7] J.L. Wagener, P.F. Wysocki, M.J.F. Digonnet, H.J. Shaw, D.J. Digiovanni [*Opt. Lett. (USA)* vol.18 no.23 (1993) p.2014-6]
[8] I.D. Miller [*Appl. Opt. (USA)* vol.26 no.11 (1987) p.2197-201]
[9] G.A. Ball, W.W. Morey, W.H. Glenn [*IEEE Photonics Technol. Lett. (USA)* vol.3 no.7 (1991) p.613-5]
[10] P.R. Morkel, G.J. Cowle, D.N. Payne [*Electron. Lett. (UK)* vol.26 no.10 (1990) p.632-4]
[11] J.L. Zyskind et al [*Electron. Lett. (UK)* vol.27 no.23 (1991) p.2148-9]
[12] M. Digonnet, K. Liu, H.J. Shaw [*IEEE J. Quantum Electron. (USA)* vol.26 no.6 (1990) p.1105-10]
[13] R. Wyatt [*Electron. Lett. (UK)* vol.25 no.22 (1989) p.1498-9]
[14] C. Yue, J. Peng, B. Zhou [*Electron. Lett. (UK)* vol.25 no.2 (1989) p.101-2]
[15] D.A. Smith, M.W. Maeda, J.J. Johnson, J.S. Patel, M.A. Saifi, A. Von Lehman [*Opt. Lett. (USA)* vol.16 no.6 (1991) p.387-9]
[16] M.-Y. Jeon et al [*IEEE Photonics Technol. Lett. (USA)* vol.8 no.12 (1996) p.1618-20]
[17] D.C. Hanna, R.M. Percival, R.G. Smart, A.C. Tropper [*Opt. Commun. (Netherlands)* vol.75 no.3-4 (1990) p.283-6]
[18] W.L. Barnes, J.E. Townsend [*Electron. Lett. (UK)* vol.26 no.11 (1990) p.746-7]
[19] L. Reekie, I.M. Jauncey, S.B. Poole, D.N. Payne [*Electron. Lett. (UK)* vol.23 no.20 (1987) p.1076-8]
[20] M.C. Farries, P.R. Morkel, J.E. Townsend [*IEE Proc. J (UK)* vol.137 no.5 (1990) p.318-22]
[21] L. Reekie, I.M. Jauncey, S.B. Poole, D.N. Payne [*Electron. Lett. (UK)* vol.23 no.17 (1987) p.884-5]
[22] J.R. Armitage, R. Wyatt, B.J. Ainslie, S.P. Craig-Ryan [*Electron. Lett. (UK)* vol.25 no.5 (1989) p.298-9]
[23] K. Liu, M. Digonnet, K. Fesler, B.Y. Kim, H.J. Shaw [*Electron. Lett. (UK)* vol.24 no.14 (1988) p.838-40]
[24] R.M. Percival, M.W. Phillips, D.C. Hanna, A.C. Tropper [*IEEE J. Quantum Electron. (USA)* vol.25 no.10 (1989) p.2119-23]
[25] D.C. Hanna et al [*Electron. Lett. (UK)* vol.24 no.17 (1988) p.1111-3]
[26] F. Hakimi et al [*Opt. Lett. (USA)* vol.14 no.9 (1989) p.1060-1]
[27] S.G. Grubb, W.L. Barnes, E.R. Taylor, D.N. Payne [*Electron. Lett. (UK)* vol.26 no.2 (1990) p.121-2]
[28] W.L. Barnes, P.R. Morkel, L. Reekie, D.N. Payne [*Opt. Lett. (USA)* vol.14 no.18 (1989) p.1002-4]
[29] D.C. Hanna, R.M. Percival, R.G. Smart, J.E. Townsend, A.C. Tropper [*Electron. Lett. (UK)* vol.25 no.9 (1989) p.593-4]
[30] H. Po, F. Hakimi, R.J. Mansfield, B.C. McCollum, R.P. Tumminelli, E. Snitzer [*Proc. of OSA Meeting* Paper FD-4, October 1986]
[31] D.C. Hanna, R.M. Percival, I.R. Perry, R.G. Smart, J.E. Townsend, A.C. Tropper [*Opt. Commun. (Netherlands)* vol.78 no.2 (1990) p.187-94]
[32] W.L. Barnes, S.B. Poole, J.E. Townsend, L. Reekie, D.J. Taylor, D.N. Payne [*J. Lightwave Technol. (USA)* vol.7 no.10 (1989) p.1461-5]
[33] K. Hsu, C.M. Miller, J.T. Kringlebotn, E.M. Taylor, J. Townsend, D.N. Payne [*Opt. Lett. (USA)* vol.19 no.12 (1994) p.886-8]
[34] H. Po et al [*Proc. of Optical Fiber Communication* OFC'89, Postdeadline paper PD7 (1989)]
[35] S. Grubb et al [*Diode Laser Technology Review* (Albuquerque, NM, 1997)]
[36] J.T. Lin, W.A. Gambling [*Proc. SPIE (USA)* vol.1373 (1990) p.42-53]
[37] J.T. Lin, L. Reekie, L. Li [*Proc. of Conference on Lasers and Electro-Optics* CLEO'87, Paper FP3 (1987) p.358-60]
[38] D. Pureur, M. Douay, P. Bernage, P. Niay, J.F. Bayon [*J. Lightwave Technol. (USA)* vol.13 no.3 (1995) p.350-5]
[39] D. Falquier, D. Lande, J.L. Wagener, M.J.F. Digonnet, H.J. Shaw [*Proc. SPIE (USA)* vol.2289 (1994) p.24-40]
[40] K. Iwatsuki, H. Okamura, M. Saruwatari [*Electron. Lett. (UK)* vol.26 no.24 (1990) p.2033-5]

[41] R.J. Forster, A. Gloag, N. Langford, K. McCallion [*Proc. of Conference on Lasers and Electro-Optics* CLEO'96 vol.9 (1996) p.394-5]
[42] A. Gloag, N. Langford, K. McCallion, W. Johnstone [*J. Opt. Soc. Am. B (USA)* vol.13 no.5 (1996) p.921-5]
[43] R.J. Forster, N. Langford [*Opt. Lett. (USA)* vol.21 no.20 (1996) p.1679-81]
[44] Y. Cheng, J.T. Kringlebotn, W.H. Loh, R.I. Laming, D.N. Payne [*Opt. Lett. (USA)* vol.20 no.8 (1995) p.875-7]
[45] J.T. Kringlebotn, P.R. Morkel, L. Reekie, J.-L. Archambault, D.N. Payne [*IEEE Photonics Technol. Lett. (USA)* vol.5 no.10 (1993) p.1162-4]
[46] G.A. Ball, C.E. Holton, G. Hull-Allen, W.W. Morey [*IEEE Photonics Technol. Lett. (USA)* vol.6 no.2 (1994) p.192-4]
[47] J. Zhang, J.W.Y. Lit, G.W. Schinn, C.Y. Yue [*Proc. of Optical Fibre Communication* OFC'95 vol.8 (1995) p.175-6]
[48] I.M. Jauncey, L. Reekie, J.E. Townsend, D.N. Payne, C.J. Rowe [*Electron. Lett. (UK)* vol.24 no.1 (1988) p.24-6]
[49] R. Paschotta, J. Nilsson, L. Reekie, A.C. Tropper, D.C. Hanna [*Opt. Lett. (USA)* vol.22 no.1 (1997) p.40-2]
[50] B. Barnes, P. Morkel, M. Farries, L. Reekie, D. Payne [*Proc. SPIE (USA)* vol.1171 (1990) p.298-308]
[51] A. Chandonnet, G. Larose [*Opt. Eng. (USA)* vol.32 no.9 (1993) p.2031-5]
[52] F. Séguin, T. Oleskevich [*Opt. Eng. (USA)* vol.32 no.9 (1993) p.2036-41]
[53] P. Myslinski, X. Pan, C. Barnard, J. Chrostowski, B.T. Sullivan, J.-F. Bayon [*Opt. Eng. (USA)* vol.32 no.9 (1993) p.2025-30]
[54] L.A. Zenteno, H. Po, N.M. Cho [*Opt. Lett. (USA)* vol.19 no.2 (1990) p.115-7]
[55] G. Geister, R. Ulrich [*Appl. Phys. Lett. (USA)* vol.56 no.6 (1990) p.509-11]
[56] T. Imai, T. Komukai, T. Yamamoto, M. Nakazawa [*Jpn. J. Appl. Phys. 2 (Japan)* vol.35 no.10A (1996) p.L1275-7]
[57] L.A. Zenteno, E. Snitzer, H. Po, R. Tumminelli, F. Hakimi [*Opt. Lett. (USA)* vol.14 no.13 (1989) p.671-3]
[58] M.H. Ober, M. Hofer, M.E. Fermann [*Opt. Lett. (USA)* vol.18 no.5 (1993) p.367-9]
[59] M. Hofer et al [*Opt. Lett. (USA)* vol.20 no.16 (1995) p.1701-3]
[60] K. Tamura, E.P. Ippen, H.A. Haus, L.E. Nelson [*Opt. Lett. (USA)* vol.18 no.13 (1993) p.1080-2]
[61] M. Nakazawa, E. Yoshida, Y. Kimura [*Electron. Lett. (UK)* vol.29 no.1 (1993) p.63-5]
[62] M.E. Fermann, J.D. Minelly [*Opt. Lett. (USA)* vol.21 no.13 (1996) p.970-2]
[63] T.F. Carruthers, I.N. Duling III [*Opt. Lett. (USA)* vol.21 no.23 (1996) p.1927-9]
[64] K. Tamura, M. Nakazawa [*Opt. Lett. (USA)* vol.21 no.24 (1996) p.1984-6]
[65] R.C. Sharp, D.E. Spock, N. Pan, J. Elliot [*Opt. Lett. (USA)* vol.21 no.12 (1996) p.881-3]
[66] A. Gloag, K. McCallion, W. Johnstone, N. Langford [*Proc. of the Conference on Lasers and Electro-Optics* CLEO'95, Baltimore, MA, USA (1995) p.236-7]
[67] M. Hofer, M.E. Fermann, F. Haberl, M.H. Ober, A.J. Schmidt [*Opt. Lett. (USA)* vol.16 no.7 (1991) p.502-4]
[68] J.D. Kafka, T. Baer, D.W. Hall [*Opt. Lett. (USA)* vol.14 no.22 (1989) p.1269-71]
[69] X. Shan, D.M. Spirit [*Electron. Lett. (UK)* vol.29 no.11 (1993) p.979-81]
[70] G.T. Harvey, L.F. Mollenauer [*Opt. Lett. (USA)* vol.18 no.2 (1993) p.107-9]
[71] M. Nakazawa, E. Yoshida, Y. Kimura [*Electron. Lett. (UK)* vol.30 no.19 (1994) p.1603-5]
[72] G. Sucha, M. Hofer, M.E. Fermann, F. Haberl, D. Harter [*Opt. Lett. (USA)* vol.21 no.19 (1996) p.1570-2]
[73] M. Margalit, M. Orenstein, G. Eisenstein [*Opt. Lett. (USA)* vol.21 no.19 (1996) p.1585-7]
[74] N.J. Doran, D. Wood [*Opt. Lett. (USA)* vol.13 no.1 (1988) p.56-8]
[75] M.E. Fermann, F. Haberl, M. Hofer, H. Hochreiter [*Opt. Lett. (USA)* vol.15 no.13 (1990) p.752-4]

B5.2 Optical fibre amplifier based on rare earth-doped oxide glass

D.W. Hewak

July 1998

A INTRODUCTION

In recent years, telecommunication systems world wide have expanded their capacity requirements to beyond that carried by a single wavelength signal. Wavelength division multiplexing is now providing ultra-high transmission capacity using several channels at wavelengths spaced across the 1.5 micron transmission band. To fully exploit the broad bandwidth fibre networks, amplifiers which operate efficiently and with low noise over the entire WDM wavelength range are required. A typical erbium-doped silica fibre amplifier, though providing extremely practical amplification, cannot boost signals beyond 1625 nm. In this Datareview, progress in developing an erbium-doped tellurite (TeO_2) optical fibre amplifier is reviewed and its performance compared with that of silica and fluoride fibre amplifiers. Activity in this area is currently dominated by research groups in Japan [1-3].

B GLASS AND FIBRE DEVELOPMENT

Tellurite glasses are stable with a wide range of compositions, and active fibre devices have long been considered from these materials [4-7]. Typically these glasses are prepared by melt quenching. Powders are weighed, mixed and transferred to a suitable crucible, for example gold, and heated in a furnace. Melts are cast in preheated brass moulds, either rectangular for bulk glass measurements, or cylindrical for fibre drawing. Wang [8] presents details on a range of TeO_2 compositions, their preparation and their characterisation.

Few details are given on the composition or fabrication procedure for current fibre work used in the erbium doped amplifier. A typical fibre is doped with several hundred ppm of erbium and is a few metres long. Background loss of the fibre is relatively high, as tellurite fibres have undergone far less development than more conventional optical fibre materials. Fibres produced by KDD Research and Development Labs [3] were doped with 880 ppm Er^{3+} by weight and were 5 m in length. The NA and core/cladding diameters are 0.32 and 3.0/125, respectively. The background loss is about 0.28 dB/m at 1300 nm including the loss of cladding modes. FIGURE 1 shows the loss spectrum of fibre prepared by KDD; however this loss was measured on multimode fibre.

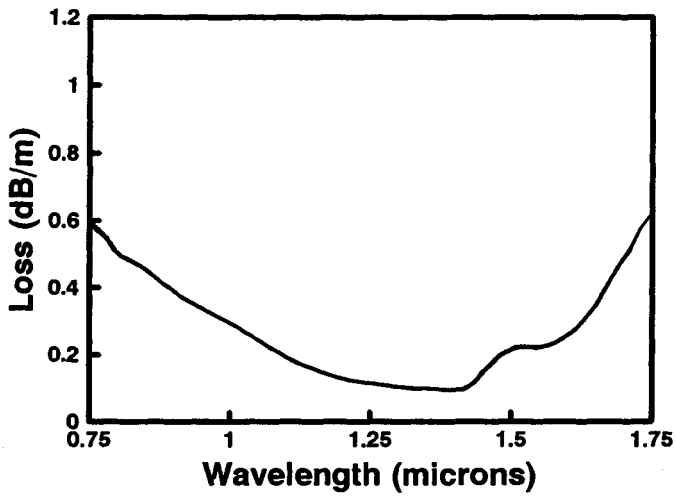


FIGURE 1 Loss spectrum of multimode tellurite fibre [3].

Cladding mode suppression is a problem in these fibres. Since the refractive index of the glass is higher than any coating or index matching oil which could be used to strip these cladding modes, measurements of loss, mode field diameter and cut-off wavelength are difficult.

To prepare this fibre for measurement, the facets are angle polished then PC connected to silica fibres with high NA. The insertion loss at 1300 nm is about 2.0 dB/point, probably due to the mismatching of MFDs between the tellurite and silica.

Preliminary work on fibre strength and stability has been performed. The mean value of the breaking stress is 2.1% which corresponds to a breaking radius of 3.7 mm. To examine the resistance of the fibre to attack by moisture, glass samples were kept at 80°C and 80% humidity for 400 hours. There was no evidence of degradation of the glass surface or crystallisation and no decrease in the transmittance.

C AMPLIFIER PERFORMANCE

As optical fibre quality improves, amplifier performance has been enhanced. As this is currently an extremely active field, gain is steadily on the rise. In 1997, NTT (Japan) published work which showed the pump power dependence of net small signal gain for an 85 cm Er^{3+}-doped tellurite fibre. The fibre was pumped at 978 nm and the signal wavelength was 1560 nm. A gain coefficient of 0.12 dB/mW was obtained as shown in FIGURE 2 with peak gains of about 15 dB. Long wavelength operation was confirmed by lasing a 2.4 m long section of fibre using a Bragg grating at one end of the fibre. The laser operation peak was 1624.5 nm, as measured on an optical spectrum analyser. A gain spectrum is shown in FIGURE 3. This clearly shows the advantages of a tellurite amplifier in providing increased gain at longer wavelengths.

Recent results by KDD [2] in longer fibre lengths improved the gain to 34 dB at 1533 nm from 200 mW of pump at 980 nm. A similar level of gain was obtained by pumping at 1480 nm with less pump power, but at the expense of a higher noise figure. Even so, these fibres still provide room for improvement.

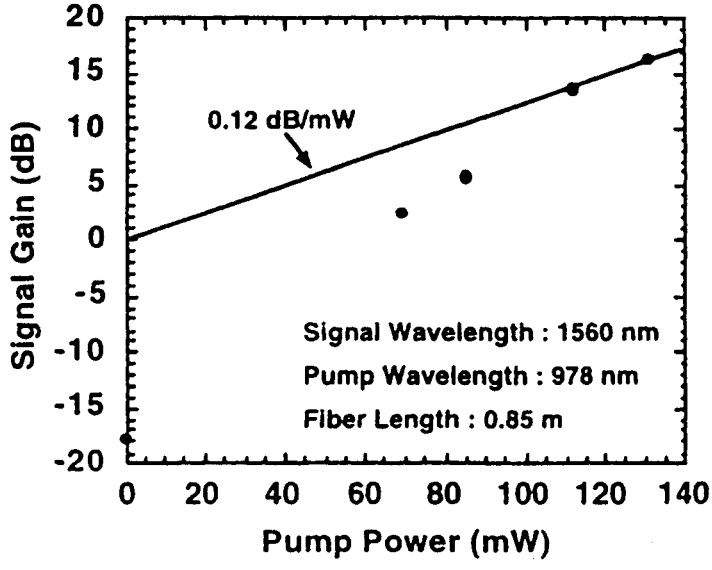


FIGURE 2 Pump power dependence of net small signal gain for an 85 cm Er^{3+} -doped tellurite fibre (from [2]).

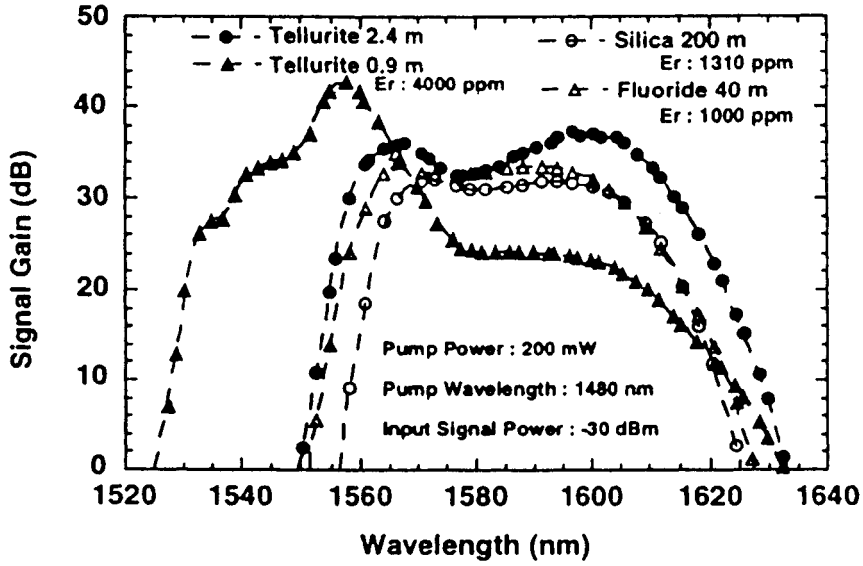


FIGURE 3 Small signal gain spectra of tellurite-based EDFAs with 0.9 and 2.4 m long fibres, a fluoride-based EDFA with a 40 m long fibre and a silica-based EDFA with a 200 m long fibre [2].

D CONCLUSION

Tellurite fibres doped with erbium are now demonstrating gain exceeding 30 dB over a wavelength range which exceeds that of an equivalent silica fibre in the 1.5 micron transmission band. Pumping is feasible with 980 nm laser diodes and there exists further scope for improvement in fibre structure and transmission loss.

REFERENCES

[1] A. Mori, Y. Ohishi, M. Yamada, H. Ono, S. Sudo [*Proc. Eur. Conf. Optical Comm.* Madrid, Spain, 20-24 Sept. 1998]

[2] A. Mori, Y. Ohishi, S. Sudo [*Electron. Lett. (UK)* vol.33 (1997) p.863]

[3] T. Nakai, Y. Noda, T. Tani, Y. Mimura, T. Sudo, S. Ohno [*Proc. OAA* Victoria, BC, Canada (1998) paper PD5-1]

[4] N. Spector, R. Reisfeld, L. Boehm [*Chem. Phys. Lett. (Netherlands)* vol.49 (1977) p.251]

[5] J.S. Wang, E.M. Vogel, E. Snitzer, J.G.H. Sigel [*Proc. Am. Ceram. Soc. Annual Meeting* Cinncinati, OH, 1993]

[6] J.S. Wang, E.M. Vogel, J.G.H. Sigel [*Mater. Res. Soc. Symp. Proc. (USA)* (1991)]

[7] S.E. Stokowski, R.A. Saroyan, M.J. Weber (Eds.) [*Laser Glass Nd-Doped Glass Spectroscopic and Physical Properties, M-95* (Lawrence Livermore National Laboratory, Livermore, 1981)]

[8] J.S. Wang, E.M. Vogel, E. Snitzer [*Opt. Mater. (Netherlands)* vol.3 (1994) p.187-203]

PART C: HALIDE GLASS

CHAPTER C1

OPTICAL PROPERTIES

C1.1 Transmission of halide glass
C1.2 Intrinsic scattering losses of halide glass
C1.3 Refractive index and dispersion of halide glass
C1.4 Non-linear refractive index of halide glass

C1.1 Transmission of halide glass

J.L. Adam

July 1997

A INTRODUCTION

Optical transmission is probably the main physical characteristic of halide glasses in the sense that, except for beryllium fluoride glass, this property easily differentiates halide glasses from traditional oxide glasses. It is because of their broad transmission in the mid-infrared that heavy-metal fluoride glasses, such as those based on zirconium fluoride, were first investigated. Several laboratories went on to extensive research on these materials, for optical applications in wavelength domains where silica glasses cannot operate.

This Datareview is divided into two parts: first, the fluoride glasses section, which deals with glasses comprised of fluorides exclusively, and secondly, the heavy-halide glasses section which includes glasses based on chlorides, bromides and/or iodides and possible mixtures with fluorides. While abundant literature is available on infrared transmission of halide glasses, only scarce and often imprecise information is reported on their UV edge.

In the IR, the position of the edge will be given for 50% transmission (T) or for an absorption coefficient (α) of 1 cm^{-1}, depending on data availability.

B FLUORIDE GLASSES

Fluoride glasses constitute a full class of materials whose compositions are based on tetravalent, trivalent and even divalent fluorides. There are no known compositions with monovalent fluorides as major glass components. Fluoride glasses usually start transmitting around 250 nm in the UV, which corresponds to an energy gap of ≈5 eV. For comparison, pure silica shows a better UV transparency with an energy gap of ≈8 eV ($\lambda \approx 160$ nm). In the infrared, fluoride glasses (except BeF_2) are transparent at wavelengths greater than or equal to 5 μm, depending on the nature of the main cation in the glass. Glasses with large, heavy and lightly-charged elements will possess lower phonon energies and a consequent extended infrared transparency. The IR multiphonon edge may attain 10 μm for ZnF_2-based glasses.

With a refractive index of ≈1.5 at the sodium D-line, fluoride glasses show a nearly constant transmission of ≈92% throughout the visible and near infrared. The loss is due primarily to 4% reflection at each surface of the glass sample.

B1 MF_4-Based Fluoride Glasses

Glasses considered in this section contain ZrF_4, HfF_4 or ThF_4 as a major component. The IR transmission spectrum for ZBLAN (54 ZrF_4 - 23 BaF_2 - 4 LaF_3 - 3 AlF_3 - 16 NaF) fluorozirconate glass is shown in FIGURE 1. The IR edge is in the 5 - 8 μm range with a 50% transmission located at ≈7.1 μm (1400 cm^{-1}) for a 2 mm-thick sample. This is to be compared with silica glass whose transparency starts decreasing at ≈3 μm. The IR edge is due to multiphonon absorption processes related to the fundamental vibration frequencies of the host. For ZBLAN, Zr-F vibrations around 580 cm^{-1} account for the multiphonon absorption, while for silica, the position of the IR edge is due to Si-O vibrations at 1100 cm^{-1}.

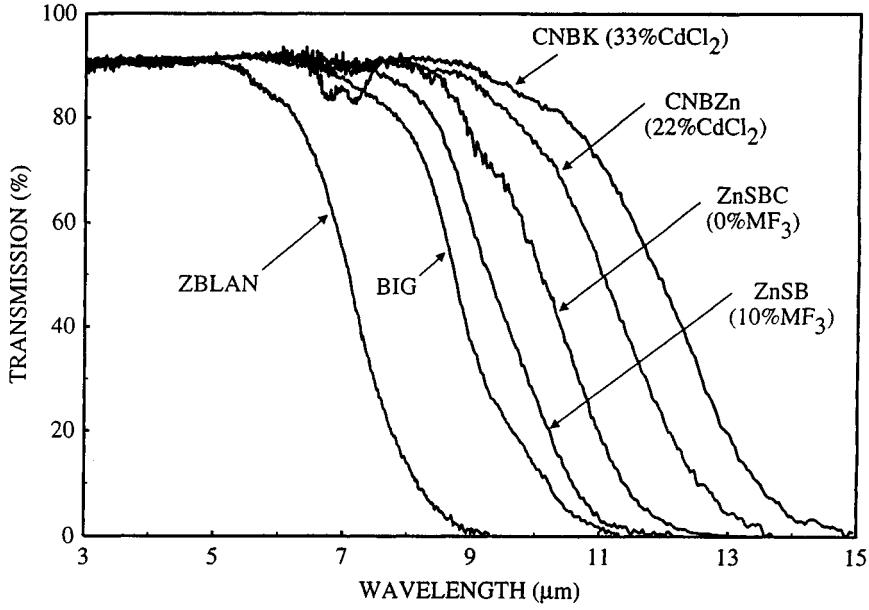


FIGURE 1 Infrared transmission spectra of various fluoride and chloro-fluoride glasses (thickness = 2 mm). Acronyms are detailed in the text and in TABLES 1-4.

When substituting hafnium for zirconium, the larger atomic weight of the former results in fundamental vibrations with lower frequencies and, consequently, with an IR edge shifted towards longer wavelengths. This is well illustrated in FIGURE 2, where the absorption coefficient is found to be lower for HBL glass (HfF_4 - BaF_2 - LaF_3) than for ZBL (ZrF_4 - BaF_2 - LaF_3) at a given wavenumber [1].

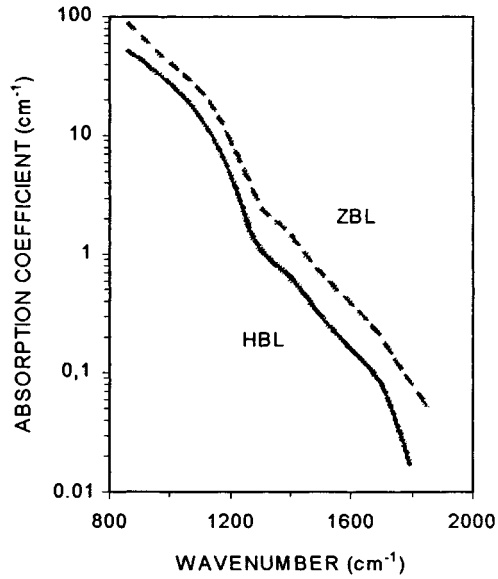


FIGURE 2 Infrared absorption coefficient of HBL and ZBL fluoride glasses [1]. Acronyms are detailed in the text and in TABLE 1.

The IR edges for several ZrF_4, HfF_4 or ThF_4-based fluoride glasses can be found in [2-8], [2,4,9] and [10-12], respectively. Some of them are summarised in TABLE 1. The broader IR transparency of Hf-based glasses is confirmed. In addition, the transmission of ThF_4-based glasses is significantly shifted towards the infrared, with an absorption coefficient of 1 cm^{-1} at a wavenumber of ≈1130 cm^{-1} for TBZnYb. For all compositions, the presence of AlF_3 has a detrimental effect on transmission. This is due to the high fundamental frequency of Al-F bonds, typically 650 cm^{-1}.

TABLE 1 Infrared edge for various fluoride glasses based on tetravalent elements. The edge is given for an absorption coefficient (α) of 1 cm^{-1}. $T_{max} \approx 90\%$ for all samples.

Acronym	Glass composition (mol %)	IR edge at $\alpha = 1\ cm^{-1}$ ($1\ cm^{-1}$)/(μm)	Ref
ZBT	57.5 ZrF_4 - 33.75 BaF_2 - 8.75 ThF_4	1480/6.8	[2]
HBT	57.5 HfF_4 - 33.75 BaF_2 - 8.75 ThF_4	1300/7.7	[2]
ZBL	62 ZrF_4 - 33 BaF_2 - 5 LaF_3	1400/7.1	[3]
ZBLA	62 ZrF_4 - 31 BaF_2 - 5 LaF_3 - 2 AlF_3	1480/6.8	[4]
HBLA	57 HfF_4 - 36 BaF_2 - 3 LaF_3 - 4 AlF_3	1280/7.8	[5]
TBZnYb	30 ThF_4 - 17.5 BaF_2 - 26.5 ZnF_2 - 26 YbF_3	1130/8.8	[10]
TYbZnBA	27 ThF_4 - 27 YbF_3 - 27 ZnF_2 - 15 BaF_2 - 4 AlF_3	1300/7.7	[10]

Bendow and Drexhage have measured the IR absorption for selected temperatures between 85 and 500 K, for ZrF_4 and ThF_4-based fluoride glasses [13,14]. The IR edge is shifted significantly towards higher wavenumbers with increasing temperature.

In the ultra-violet domain, the transmission of ZrF_4 and HfF_4-based fluoride glasses was found dependent on glass processing conditions: atmosphere and crucible material [3,15].

B2 MF_3-Based Fluoride Glasses

Fluoride glasses based on trivalent metals belong essentially to two families with distinct optical properties: InF_3/GaF_3-based glasses and AlF_3-based glasses.

IR transmission for a typical InF_3/GaF_3 glass, referred to as BIG in TABLE 2, is given in FIGURE 1. A shift by more than 1.5 μm in the IR is observed as compared to standard ZBLAN glass. This is due to the lower frequency of In-F bonds ($\approx 510\ cm^{-1}$) with respect to Zr-F. A broad IR transparency is observed for all the indium based glasses listed in TABLE 2 [16-20].

The detrimental effect of aluminium on the IR transparency is obvious for AlF_3-based glasses [21,27]. For ABCYS glass (40 mol % AlF_3), the IR edge is located at 6.4 μm ($\alpha = 1\ cm^{-1}$), as listed in TABLE 2, while for ZBLA and BIG that same edge is at 6.8 μm and 7.8 μm, respectively.

One should note the unique scandium-based glass whose infrared optical transmission is halfway between those of zirconium and hafnium-based glasses [28].

The UV edge has been recorded for AYPMB [24] and for a 50 AlF_3/50 PbF_2 glass [29]. A 50% transmission at ≈ 300 nm is reported for both materials.

B3 MF_2-Based Fluoride Glasses

Except for BeF_2, glasses based on divalent fluorides should show a broader IR transparency than glasses based on indium or zirconium/hafnium. However, if the MF_3 or MF_4 content is too high, glasses behave like indium or zirconium-based glasses. This is well illustrated in TABLE 3 [30-33] where PFeZY and PMG glasses show IR edges comparable to those listed in TABLES 1 and 2. The apparent broad transparency of PZnG glass (T = 50% at 11.9 μm) is due to the small thickness of the sample.

ZnSB and ZnSBC glasses are true divalent glasses and they indeed show, in FIGURE 1, a broad IR transparency up to 9.3 μm for the former and 10.1 μm for the latter, a pure MF_2 fluoride glass.

TABLE 2 Infrared edge for various fluoride glasses based on trivalent elements. The edge is given for 50% transmission (T) or for an absorption coefficient (α) of 1 cm^{-1}. $T_{max} \approx 90\%$ for all samples.

Acronym	Glass composition (mol %)	Thickness (mm)	IR edge at T = 50% (cm^{-1})/(μm)	IR edge at α = cm^{-1} (cm^{-1})/(μm)	Ref
BIG	30 BaF_2 - 18 InF_3 - 12 GaF_3 - 20 ZnF_2 - 10 YbF_3 - 6 ThF_4 - 4 ZrF_4	3	1190/8.4	1290/7.8	[16,17]
BIZYbT	30 BaF_2 - 30 InF_3 - 20 ZnF_2 - 10 YbF_3 - 10 ThF_4	2.43	1100/9.1	1200/8.3	[18,19]
IZBSC	40 InF_3 - 20 ZnF_2 - 15 BaF_2 - 20 SrF_2 - 5 CaF_2	5	1180/8.5	1220/8.2	[20]
ABCYS	40 AlF_3 - 12 BaF_2 - 22 CaF_2 - 16 YF_3 - 10 SrF_2	4	1450/6.9	1560/6.4	[21,22]
AYbPZB	25 AlF_3 - 30 YbF_3 - 15 PbF_2 - 15 ZnF_2 - 15 BaF_2	4.6	1450/6.9	-	[23]
AYPMB	30 AlF_3 - 20 YF_3 - 25 PbF_2 - 10 MgF_2 - 15 BaF_2	4.4	1450/6.9	-	[24]
RAY	35 AlF_3 - 15 YF_3 - 12.5 MgF_2 - 12.5 CaF_2 - 12.5 SrF_2 - 12.5 BaF_2	4	1500/6.7	-	[25]
BATY	28.75AlF_3 - 28.75 YF_3 - 20 BaF_2 - 22.5 ThF_4	3.8	1310/7.6	-	[26]
CLAP	38 AlF_3 - 28.5 PbF_2 - 28.5 CdF_2 - 5 LiF	0.5	1220/8.2	-	[27]
SYB	40 ScF_3 - 20 YF_3 - 40 BaF_2	2.23	1220/8.2	1350/7.4	[28]

TABLE 3 Infrared edge for various fluoride glasses based on divalent elements. The edge is given for 50% transmission (T) or for an absorption coefficient (α) of 1 cm^{-1}. $T_{max} \approx 90\%$ for all samples except for PFeZY ($T_{max} \approx 70\%$).

Acronym	Glass composition (mol %)	Thickness (mm)	IR edge at T = 50% (cm^{-1})/(μm)	IR edge at α = 1 cm^{-1} (cm^{-1})/(μm)	Ref
PFeZY	52 PbF_2 - 23 FeF_3 - 19 ZrF_4 - 6 YF_3	2	1210/8.3	-	[30]
PMG	38 PbF_2 - 20 MnF_2 - 30 GaF_3 - 7 AlF_3 - 5 ZnF_2	-	-	1420/7.0	[31]
PZnG	50 PbF_2 - 25 ZnF_2 - 25 GaF_3	1	840/11.9	-	[32]
ZnSB	47 ZnF_2 - 24 SrF_2 - 10 BaF_2 - 5 CdF_2 - 6 InF_3 - 4 GaF_3 - 2 LaF_3 - 2 NaF	2	1080/9.3	-	[33]
ZnSBC	60 ZnF_2 - 20 SrF_2 - 10 BaF_2 - 10 CdF_2	2	990/10.1	-	[33]

The temperature dependence, from 89 to 473 K, of intrinsic multiphonon absorption has been reported for PMG glass [31]. At a given wavenumber, the absorption coefficient is found to increase significantly with increasing temperature.

BeF_2 glass shows a special behaviour, as far as optical transmission is concerned. Although it is a pure divalent glass, the light and small beryllium cation induces a narrow IR transmission with a cut-off wavelength in the 4 - 5 μm range, comparable to most silica glasses [34,35]. Ohno et al [36] have studied the influence of BeF_2 content on AlF_3-based glasses. The IR edge shifts dramatically from ≈7 μm (50% T) with 0% BeF_2 down to ≈5 μm with only 25 mol % BeF_2.

C HEAVY-HALIDE GLASSES

A very efficient way to improve the IR transparency of fluoride glasses is to substitute a heavy halide for fluorine.

C1 Choro-Fluoride Glasses

A good thermal stability and an increased sensitivity to moisture, compared to pure fluorides, usually characterise glasses containing $CdCl_2$. The IR transmission is directly related to the chlorine content as shown in FIGURE 1 for CNBZn and CNBK glasses whose edges are located at 11 μm and 11.9 μm, respectively [37]. Data for several chloro-fluoride glass compositions are listed in TABLE 4 [37-40]. Mouric et al have calculated the absorption coefficient of CB glass as a function of wavenumber [38]. The resulting IR edge for $\alpha = 1$ cm^{-1} is found to be at ≈11 μm. This compares favourably with 7.8 μm for BIG fluoride and 6.8 μm for ZBLA.

Of course, the presence of zirconium fluoride in the glass composition alters the influence of chlorine ions. Thus, the position of the IR edge for ZBTRb glass at 7.9 μm is the result of dominant Zr-F vibrations. The UV edge for this ZBTRb chloro-fluoride glass is dramatically shifted towards the visible with a 50% transmission at 420 nm. For the pure ZBTRb-F fluoride composition, the UV edge is located at 248 nm [40].

Adam et al [37] and Jha et al [41] have shown the detrimental influence of small Li^+ cations on the IR transparency of cadmium mixed-halide glasses.

C2 Other Heavy-Halide Glasses

Highly hygroscopic and thermodynamically unstable heavy-halide glasses usually exhibit non-standard transmission spectra. This is essentially due to poor optical quality of the glass surfaces (no polishing), unknown thickness and unidentified extrinsic absorption. Thus, the IR transmission of heavy-halide glasses will be characterised by the cut-off wavelength defined as the wavelength at which transmission departs from its maximum.

For pure chloride glasses, the position of the IR cut-off follows the sequence $MCl_4 < MCl_3 < MCl_2 <$ MCl where M represents the dominant cations. This is illustrated in TABLE 5 [42,49] for TNK, BiK, PCK and CuKB glasses and is consistent with the results reported for fluorides in FIGURE 1. The detrimental effect of lithium is also clearly demonstrated for LKBCa chloride glasses whose IR cut-off is at 11 μm only.

For $ZnCl_2$ glass, the IR edge ($\alpha = 1$ cm^{-1}) is at ≈17 μm (590 cm^{-1}) [50] and the UV transmission starts at ≈5 eV (≈44400 cm^{-1}/225 nm) [51].

TABLE 4 Infrared edge for various chloro-fluoride glasses. The edge is given for 50% transmission (T). $T_{maz} \approx 90\%$ for all samples.

Acronym	Glass composition (mol %)	Thickness (mm)	IR edge at T = 50% $(cm^{-1})/(\mu m)$	Ref
CNBZn	22 $CdCl_2$ - 18 CdF_2 - 30 NaF - 20 BaF_2 - 10 ZnF_2	2	910/11	[37]
CNBK	33 $CdCl_2$ - 17 CdF_2 - 34 NaF - 13 BaF_2 - 3 KF	2	840/11.9	[37]
CBN	53 CdF_2 - 11 $BaCl_2$ - 36 NaCl	2	950/10.5	[38]
CB	65 CdF_2 - 33 $BaCl_2$ - 2 $CdCl_2$	1.1	800/12.5	[38]
CNKPb	40 CdF_2 - 10.5 $CdCl_2$ - 23 NaCl - 13 KCl - 6 $PbCl_2$ - 5.5 $BaCl_2$ - 2 CsCl	2	880/11.4	[39]
ZBTRb	50 ZrF_4 - 30 BaF_2 - 5 ThF_4 - 3 LaF_3 - 12 RbCl	3	1270/7.9	[40]

TABLE 5 Infrared cut-off wavelength for various heavy-halide glasses.

Acronym	Glass composition (mol %)	Thickness (mm)	IR cut-off $(cm^{-1})/(\mu m)$	Ref
LKBCa	55 LiCl - 35 KCl - 7.5 $BaCl_2$ - 2.5 $CaCl_2$	-	910/11	[42]
PCK	55 $PbCl_2$ - 35 $CdCl_2$ - 10 KCl	-	550/18	[43,44]
BiK	60 $BiCl_3$ - 40 KCl	1.2	700/14	[45,46]
TNK	40 $ThCl_4$ - 30 NaCl - 30 KCl	0.7	770/13	[47]
TNP	35 $ThCl_4$ - 35 NaCl - 30 $PbCl_2$	-	830/12	[48]
CuKB	50 CuCl - 40 KCl - 10 $BaCl_2$	-	500/20	[49]
PCuAgCs	50 $PbBr_2$ - 22 CuCl - 18 AgBr - 10 CsBr	0.35	500/20	[52]
KZnP	48 KBr - 48 $ZnCl_2$ -4 $PbBr_2$	-	830/12	[53]
-	$ZnBr_2$	0.5	530/19	[54]
AgA	45 AgI - 45 AgF - 10 AlF_3	-	1110/9	[56]
KCP1	40 KI - 30 $CdCl_2$ - 30 $PbCl_2$	-	600/17	[57]
KCP2	40 KI - 30 $CdCl_2$ - 30 $PbBr_2$	-	500/20	[57]
AgCsP1	59 AgX - 39 CsX - 2 PbX_2 (X = 0.38I-0.62Br)	1	670/15	[58]
AgCsP2	50 AgI - 45 CsI - 5 PbI_2	-	≥30 μm	[59]
ZnK	55 ZnI_2 - 45 KI	0.3	430/23	[60]

Br-containing glasses are based on $PbBr_2$, KBr or $ZnBr_2$ [52,54]. Except for KZnP, which contains an appreciable amount of chlorine, the IR cut-off for the other two compositions is located in the 19 - 20 μm range. Nogami et al [55] claimed a 20 μm cut-off wavelength for a multicomponent bromide glass ($ZnBr_2$-$PbBr_2$-TlBr). In the UV domain, the transmission edge for $ZnBr_2$ is slightly shifted towards longer wavelengths (≈5.2 eV, 42000 cm^{-1}, 238 nm) as compared to $ZnCl_2$ glass [51].

Because of the presence of fluorides, the IR cut-off for AgA iodo-fluoride glass remains located around 9 μm as shown in TABLE 5 [56-60]. For iodo-chloride and iodo-bromide glasses, the cut-off wavelength rises to 15 - 20 μm. For pure iodide glasses, ZnK and AgCsP2, IR transparencies of 23 μm and more than 30 μm are reported. Hulme et al [61] and Angell et al [62] have recorded comparative spectra of some iodide and iodo-chloride glasses.

D CONCLUSION

In summary, the numerous data on optical transmission of halide glasses show that they present a broader IR transparency than silica. In addition, on first approximation, the IR transmission increases according to the following sequences:

- $MX_4 < MX_3 < MX_2 < MX$, where M is the dominant cation(s) within the glass and X is a given halide.
- $F < Cl < Br < I$.

When light and small elements such as Li, Be and Al are present the first sequence is usually not valid any more.

REFERENCES

[1] T. Miyashita, T. Manabe [*IEEE J. Quantum Electron. (USA)* vol.18 (1982) p.1432-50]
[2] M.G. Drexhage, C.T. Moynihan, M. Saleh [*Mater. Res. Bull. (USA)* vol.15 (1980) p.213-9]
[3] M. Robinson, R.C. Pastor, R.R. Turk, D.P. Devor, M. Braunstein, R. Braunstein [*Mater. Res. Bull. (USA)* vol.15 (1980) p.735-42]
[4] H. Poignant [*Electron. Lett. (UK)* vol.18 (1982) p.199-200]
[5] C.T. Moynihan et al [*Mater. Res. Bull. (USA)* vol.16 (1981) p.25-30]
[6] M. Matecki, M. Poulain, M. Poulain, J. Lucas [*Mater. Res. Bull. (USA)* vol.13 (1978) p.1039-46]
[7] J. Qiu, K. Maeda, R. Terai [*Phys. Chem. Glasses (UK)* vol.36 (1995) p.70-2]
[8] S. Mitachi [*Phys. Chem. Glasses (UK)* vol.23 (1982) p.190-5]
[9] D.C Tran, G.H. Sigel, B. Bendow [*J. Lightwwave Technol. (USA)* vol.2 (1984) p.566-86]
[10] B. Bendow et al [*J. Am. Ceram. Soc. (USA)* vol.66 (1983) p.C64-6]
[11] Y. Le Page, G. Fonteneau, J. Lucas [*Rev. Chim. Miner. (France)* vol.21 (1984) p.589-600]
[12] M.G. Drexhage et al [*J. Non-Cryst. Solids (Netherlands)* vol.56 (1983) p.51-6]
[13] B. Bendow, M.G. Drexhage, H.G. Lipson [*J. Appl. Phys. (USA)* vol.52 (1981) p.1460-1]
[14] M.G. Drexhage et al [*Appl. Opt. (USA)* vol.21 (1982) p.971-2]
[15] M.G. Drexhage [in *Treatise on Materials Science and Technology* vol.26 (Academic Press, Orlando, 1985) p.151-243]
[16] N. Rigout, J.L. Adam, J. Lucas [*J. Non-Cryst. Solids (Netherlands)* vol.161 (1993) p.161-4]
[17] I. Chiaruttini, G. Fonteneau, J. Lucas, P.S. Christensen, S. Mitachi [*Mater. Sci. Forum (Switzerland)* vol.67-68 (1991) p.245-50]
[18] G. Fonteneau, A. Bouaggad, J. Lucas [*Mater. Sci. Forum (Switzerland)* vol.19-20 (1987) p.41-6]
[19] A. Bouaggad, G. Fonteneau, J. Lucas [*Mater. Res. Bull. (USA)* vol.22 (1987) p.685-9]

[20] Y. Messaddeq, A. Delben, M.A. Aegerter [*J. Mater. Res. (USA)* vol.8 (1993) p.885-9]
[21] T. Iqbal, M.R. Shahriari, G. Merberg, G.H. Sigel [*J. Mater. Res. (USA)* vol.6 (1991) p.401-6]
[22] M.R. Shahriari, T. Iqbal, G.H. Sigel, G. Merberg [*Mater. Sci. Forum (Switzerland)* vol.32-33 (1988) p.99-106]
[23] Y. Wang [*J. Non-Cryst. Solids (Netherlands)* vol.142 (1992) p.185-8]
[24] Y. Wang, N. Sawanobori, S. Nagahama [*J. Non-Cryst. Solids (Netherlands)* vol.128 (1991) p.322-5]
[25] H. Hu, F. Lin, D. Gu, M. Li [*Mater. Sci. Forum (Switzerland)* vol.5 (1985) p.145-54]
[26] M. Poulain, M. Poulain, M. Matecki [*Mater. Res. Bull. (USA)* vol.16 (1981) p.555-64]
[27] J.M. Jewell, E.J. Friebele, I. Aggarwal [*J. Non-Cryst. Solids (Netherlands)* vol.188 (1995) p.285-8]
[28] M. Poulain, M. Poulain, M. Matecki [*Mater. Res. Bull. (USA)* vol.17 (1982) p.661-9]
[29] S. Shibata, T. Kanamori, S. Mitachi, T. Manabe [*Mater. Res. Bull. (USA)* vol.15 (1980) p.129-37]
[30] J. Hang, J.J. Cheng [*J. Non-Cryst. Solids (Netherlands)* vol.109 (1989) p.64-8]
[31] B. Bendow, H.P. Lipson, R.N. Brown, C. Jacoboni, R. de Pape [*Mater. Sci. Forum (Switzerland)* vol.6 (1985) p.483-8]
[32] J.P. Miranday, C. Jacoboni, R. de Pape [*J. Non-Cryst. Solids (Netherlands)* vol.43 (1981) p.393-401]
[33] C. Henriel-Ricordel, J.L. Adam, B. Boulard, C. Sourisseau [*Eur. J. Solid State Inorg. Chem. (France)* vol.34 (1997) p.125-37]
[34] J. Lucas, J.L. Adam [*Glastech. Ber. (Germany)* vol.62 (1989) p.422-40]
[35] C.M. Baldwin, R.M. Almeida, J.D. Mackenzie [*J. Non-Cryst. Solids (Netherlands)* vol.43 (1981) p.309-44]
[36] H. Ohno, N. Igawa, Y. Ishii, N. Umesaki, M. Tokita [*J. Nucl. Mater. (Netherlands)* vol.191-194 (1992) p.525-9]
[37] J.L. Adam, C. Ricordel, J. Lucas [*J. Non-Cryst. Solids (Netherlands)* vol.213-214 (1997) p.30-5]
[38] J.L. Mouric, M. Matecki, M. Poulain, M. Poulain [*Mater. Sci. Forum (Switzerland)* vol.5 (1985) p.135-44]
[39] M. Matecki, M. Poulain [*Mater. Sci. Forum (Switzerland)* vol.32-33 (1988) p.167-72]
[40] A. Elyamani, M. Poulain, S.J. Saggese, G.H. Sigel [*J. Non-Cryst. Solids (Netherlands)* vol.119 (1990) p.187-94]
[41] A. Jha, J.M. Parker [*Phys. Chem. Glasses (UK)* vol.32 (1991) p.1-12]
[42] K. Kadono, K. Mitani, K. Kinigawa, H. Tanaka [*J. Non-Cryst. Solids (Netherlands)* vol.122 (1990) p.214-5]
[43] H. Jiang, H. Sun, F. Gan [*Eur. J. Solid State Inorg. Chem. (France)* vol.28 (1991) p.1277-93]
[44] H. Jiang, H. Sun, F. Gan, B. Yuan [*J. Mater. Sci. Lett. (UK)* vol. 9 (1990) p.1195-6]
[45] C.A. Angell, D.C. Ziegler [*Mater. Res. Bull. (USA)* vol.16 (1981) p.279-83]
[46] E.I. Cooper, C.A. Angell [*J. Non-Cryst. Solids (Netherlands)* vol.56 (1983) p.75-8]
[47] H. Hu, J.D. Mackenzie [*J. Non-Cryst. Solids (Netherlands)* vol.51 (1982) p.269-72]
[48] F. Gan, Y. Dai, H. Hu [*Mater. Sci. Forum (Switzerland)* vol.5 (1985) p.113-20]
[49] K. Kadono, K. Mitani, K. Kinigawa, H. Tanaka [*J. Mater. Sci. Lett. (UK)* vol.9 (1990) p.21-2]
[50] L.G. Van Uitert, S.H. Wemple [*Appl. Phys. Lett. (USA)* vol.33 (1978) p.57-9]
[51] J.A. Duffy, M.D. Ingram [*J. Non-Cryst. Solids (Netherlands)* vol.58 (1983) p.143-4]
[52] F. Ma [*Mater. Sci. Forum (Switzerland)* vol.5 (1985) p.127-34]
[53] M. Yamane, H. Kawazoe, S. Inoue, K. Maeda [*Mater. Res. Bull. (USA)* vol.20 (1985) p.905-11]
[54] H. Hu, F. Ma, J.D. Mackenzie [*J. Non-Cryst. Solids (Netherlands)* vol.55 (1983) p.169-72]
[55] M. Nogami, N. Sawanobori, M. Makihara, J. Hayakawa [*J. Mater. Sci. Lett. (UK)* vol.4 (1985) p.271-2]
[56] T. Komatsu, H. Ur, R.H. Doremus [*J. Non-Cryst. Solids (Netherlands)* vol.69 (1985) p.309-15]
[57] B. Petrova, M. Frumar, E. Stránská, I. Hlozánek [*J. Mater. Sci. (UK)* vol.24 (1989) p.4555-6]

[58] J. Nishii, Y. Kaite, T. Yamagishi [*J. Non-Cryst. Solids (Netherlands)* vol.74 (1985) p.411-5]
[59] K. Kadono, A. Yasuyoshi, K. Nakano, K. Kinugawa, H. Tanaka [*J. Ceram. Soc. Jpn. (Japan)* vol.100 (1992) p.233-5]
[60] H. Nasu, D.P. Yamato, J. Heo, J.D. Mackenzie [*Mater. Sci. Forum (Switzerland)* vol.5 (1985) p.121-6]
[61] J. Hulme, A. Jha, J.M. Parker, A.W. Whitehouse [*Phys. Chem. Glasses (UK)* vol.30 (1989) p.254-9]
[62] C.A. Angell, C. Liu, H.G.K. Sundar [*Mater. Sci. Forum (Switzerland)* vol.5 (1985) p.189-92]

C1.2 Intrinsic scattering losses of halide glass

J.L. Adam

July 1997

A INTRODUCTION

The knowledge of intrinsic scattering losses is of prime importance for determining the theoretical minimum loss of halide glass fibres. In addition to multiphonon absorption [1], and, to a lesser extent, to UV absorption, intrinsic scattering contributes to the total intrinsic attenuation of optical fibres [2]. Of course, extrinsic losses due to light-absorbing impurities, Mie scattering due to defects whose size is similar to the wavelength, and wavelength independent scattering due to larger scattering centres add to the intrinsic contribution. These are detailed elsewhere [3].

In this Datareview, light scattering processes that obey the λ^{-4} dependence demanded by the Rayleigh scattering law are reviewed. The Rayleigh scattering loss (α_{RS}) is simply given by:

$$\alpha_{RS} = A/\lambda^4 \qquad (1)$$

where A is the Rayleigh scattering coefficient expressed in (dB km^{-1} μm^4), with λ in μm units.

Rayleigh scattering includes true intrinsic light scattering from microscopic density and composition fluctuations, and scattering due to sub-micron particles, whose intensity varies with the nature of the glass and the conditions of its preparation. Both processes obey a λ^{-4} dependence, and constitute globally most of the published results on intrinsic scattering. Raman and Brillouin scattering mechanisms, which are typically one or two orders of magnitude smaller than Rayleigh scattering [4], are not considered here.

B HEAVY-METAL FLUORIDE GLASSES

The Rayleigh scattering coefficient was estimated theoretically for some fluoride glasses by means of the following equation:

$$A = 8/3\ \pi^3\ n^8\ p^2\ \beta\ k_B\ T_g \qquad (2)$$

where n is the refractive index of the glass, p is the average photoelastic constant, β is the isothermal compressibility, T_g is the glass transition temperature and k_B is Boltzmann's constant. Rayleigh coefficients as low as $\approx$0.11 and 0.4 dB km^{-1} μm^4 were calculated for two distinct ZrF_4-based glasses, and a value of 0.11 dB km^{-1} μm^4 was estimated for a CaF_2-BaF_2-YF_3-AlF_3 glass [5,6]. This compares favourably with the coefficient of 0.65 dB km^{-1} μm^4 reported for SiO_2 glass.

Attaining the theoretical level of intrinsic Rayleigh scattering necessitates, at first, stringent glass preparation conditions. Especially, the melting conditions play an important role. In order to avoid the particle contamination associated with the use of crucibles for glass melting, Lopez and Baniel have developed a containerless gas film levitation technique [7-9]. They have obtained a Rayleigh coefficient of 0.66 dB km^{-1} μm^4 for a ZBLAN bulk glass, as shown in TABLE 1. This is the lowest value reported to date for that glass.

TABLE 1 Rayleigh scattering coefficient (A) for various heavy-metal fluoride glasses.

Acronym	Glass composition (mol %)	A ($dB\ km^{-1}\ \mu m^4$)	Ref
ZBLAN (levitation)	53 ZrF_4 - 19 BaF_2 - 4 LaF_3 - 4 AlF_3 - 20 NaF	0.66[1]	[9]
ZBLAN	ZrF_4 – BaF_2 - LaF_3 – AlF_3 - NaF	0.70	[10]
ZBLALi	51.5 ZrF_4 - 20.5 BaF_2 - 5.3 LaF_3 - 3.2 AlF_3 - 19.5 LiF	0.69[2]	[11]
ZBLA	57 ZrF_4 - 36 BaF_2 - 3 LaF_3 - 4 AlF_3	0.14[3]	[12,13]
ZBL	62 ArF_4 - 33 BaF_2 - 5 LaF_3	0.78[3]	[14]
HBLA	57 HfF_4 - 36 BaF_2 - 3 LaF_3 - 4 AlF_3	0.62[3]	[13]
HBL	62 HfF_4 - 33 BaF_2 - 5 LaF_3	3.3[3]	[14,15]
TLZnB	27 ThF_4 - 27 LaF_3 - 27 ZnF_2 - 19 BaF_2	5.0[3]	[13]
MnTYbBA	42.5 MnF_2 - 34 ThF_4 - 10 YbF_3 - 8.5 BaF_2 - 5 AlF_3	0.70[3]	[13]

[1]Measured from 0.488 μm to 1.064 μm.
[2]Measured from 0.458 μm to 0.633 μm.
[3]Measured at 0.488 μm.

Moreover, the Rayleigh scattering loss is comparable to that of silica, as shown in FIGURE 1. It is, however, still a factor of six higher than the theoretical limit determined by Shibata et al for zirconium-based fluoride glasses [5].

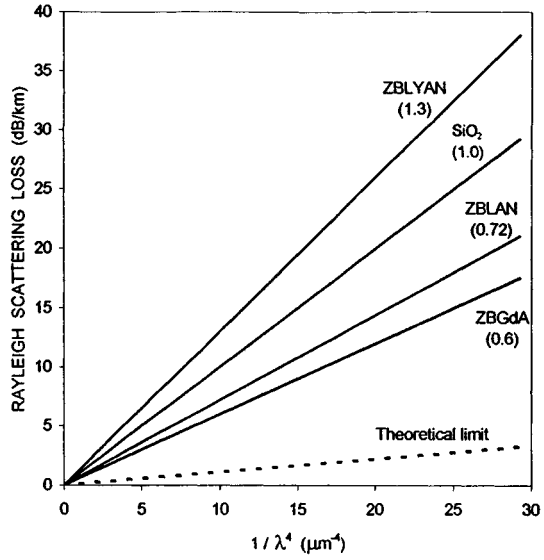


FIGURE 1 Experimental Rayleigh scattering losses of ZBLAN and ZBLA fluoride glasses. The loss for silica glass (not shown) is nearly identical to that of ZBLAN.

The lowest Rayleigh scattering coefficients for fluoride glasses prepared through traditional melting, in platinum or vitreous carbon crucibles, are listed in TABLE 1 [10-15]. A coefficient of 0.70 is obtained for ZBLAN, indicating that Rayleigh losses can also attain a low level in this case, provided that glasses are prepared in a controlled atmosphere and are allowed to solidify in situ.

Schroeder and collaborators have carried out systematic measurements of scattering losses in various fluoride glasses [12-16]. They reported a Rayleigh coefficient as low as 0.14 $km^{-1}\ \mu m^4$ for ZBLA glass prepared under CCl_4/Ar atmosphere. This is considerably lower than that for Suprasil and is extremely close to the theoretical limit, as shown in FIGURE 1.

The fact that addition of NaF in the glass causes an increase in scattering losses is reproducible and has been observed by several authors [14,17,18]. On the basis of a theoretical analysis of scattered light

distribution and SEM observations, Hattori et al suggested that phase separation occurs in alkali-containing fluoride glasses, resulting in increased light scattering [17].

Glasses with poor glass forming ability, such as ZBL or HBL, show significantly higher Rayleigh scattering than their thermally stable counterparts, ZBLA and HBLA [14,15].

All the results presented above were obtained at wavelengths in the visible. However, since the minimum loss of heavy-metal fluoride glasses is at about 2.5 μm, it is desirable to know the experimental values of Rayleigh scattering in the infrared. Thus, Tran et al have measured the scattering losses for a ZBLALi glass at six wavelengths ranging from 2.4 to 3.2 μm [19]. Their results are displayed in FIGURE 2 together with the data for fused silica, extrapolated from results in the visible. The measured light scattering losses obey a typical Rayleigh λ^{-4} behaviour and are lower, by nearly 30%, than that of silica at 2.5 μm.

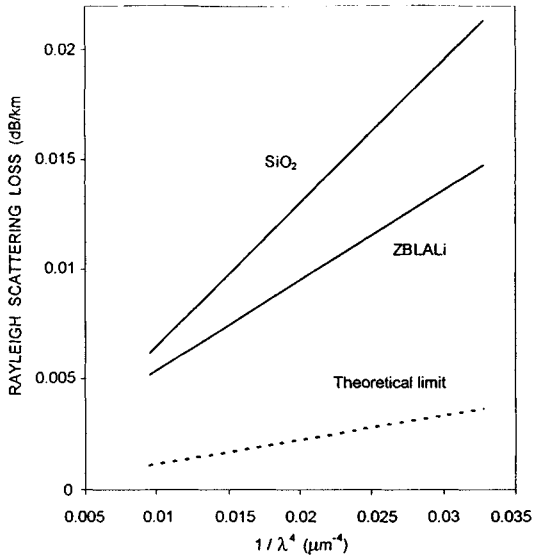


FIGURE 2 Rayleigh scattering losses of ZBLALi fluoride glasses and silica glass in the infrared optical domain (2.4 - 3.2 μm). The silica curve is extrapolated from results in the visible. The theoretical limit is given for Zr-based glasses.

Besides usual measurements of intrinsic light scattering as a function of wavelength, several authors have studied the influence of other parameters. Thus, Tran et al have investigated the angular dependence of light scattering in a ZBLALi glass [11]. Schroeder et al have studied intrinsic light scattering of fluorozirconate glasses as a function of temperature from room temperature to beyond T_g, the glass transition temperature [20,21]. They have concluded that density fluctuations caused by structural relaxations of nanoscale inhomogeneities account for the increase of Rayleigh scattering about T_g. Finally, the relationship between intrinsic light scattering and the various parameters of EQN (2) has been established by Izumitani et al [22]. They have found an almost linear dependence of scattering intensity with p^2, the photoelastic constant.

C HEAVY-METAL FLUORIDE GLASS OPTICAL FIBRES

Scattering measurements have been performed for fluorozirconate optical fibres. The most interesting results are summarised in FIGURE 3 for ZBLYAN fibres (YF_3 containing ZBLAN glass) [17,18], ZBGdA fibres [17,23,24] and ZBLAN fibres [25,26]. The characteristic losses of silica fibres, [17], are shown for comparison.

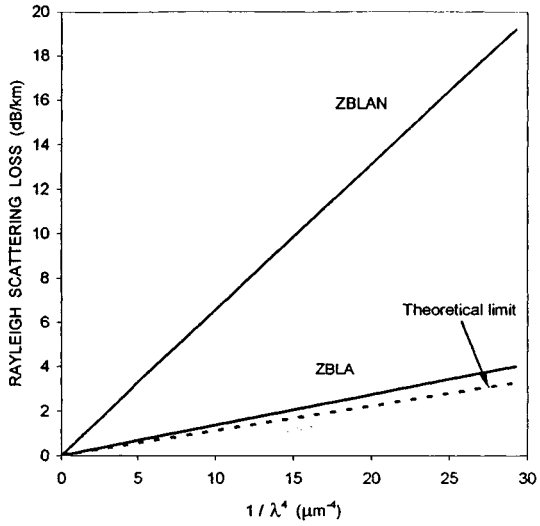


FIGURE 3 Experimental Rayleigh scattering losses for various fluorozirconate optical fibres and silica fibres. The theoretical limit is given for Zr-based glasses. Numbers in brackets are the Rayleigh coefficient (A) expressed in (dB km^{-1} μm^4) units.

A typical λ^{-4} dependence is observed indicating that scattering losses are Rayleigh scattering in nature. Considering the thermal history of fibre glass, which experiences critical heating between T_g and the crystallisation temperature during drawing, a pure Rayleigh behaviour must be considered as a great achievement. This result shows that fibres with particles no greater than the sub-micron scale can be obtained.

With Rayleigh coefficients similar to those measured with bulk glasses, ZBGdA and ZBLAN fibres exhibit significantly lower scattering losses than silica. ZBLYALi fibres were also measured and showed scattering losses comparable to ZBLAN fibres [17].

Day and Tran have found that the addition of lead fluoride to ZBLAN fibres causes a marked increase of the Rayleigh coefficient (A = 1.12 dB km^{-1} μm^4) [25,26]. This is probably due to an increase in the concentration of submicron particles related to the lower stability of ZBLANP glass, as compared to ZBLAN. Similarly, important scattering losses were measured in a ZBLALiP fibre [27].

Measurements performed in the infrared, from 2.4 to 3.2 μm, have revealed a high scattering loss of $(0.61 + 16/\lambda^4)$ for a ZBLAN fibre [28]. This indicates that, in addition to Rayleigh scattering, wavelength independent scattering occurs in this particular fibre.

Comparative minimum loss projections for oxide and halide fibres have been calculated by Van Uitert et al [29].

D OTHER HALIDE GLASSES

Theoretical and measured values of Rayleigh scattering coefficients for BeF_2-based glasses and $ZnCl_2$ glass are listed in TABLE 2. The low theoretical limit, 0.06 dB km^{-1} μm^4, of pure BeF_2 glass was approached experimentally. Thus, for vapour deposited BeF_2, scattering losses as low as 2.4 dB km^{-1} were measured at 0.488 μm (A = 0.14 dB km^{-1} μm^4) [30,31]. Addition of other components such as thorium fluoride [14] or potassium fluoride [29] tend to significantly increase light scattering, except for the four-component BeKCaA glass (A = 0.16 dB km^{-1} μm^4) [29].

TABLE 2 Rayleigh scattering coefficient (A) for BeF_2-based and $ZnCl_2$ glasses.

Acronym	Glass composition (mol %)	Theoretical limit (dB km^{-1} μm^4)	A (dB km^{-1} μm^4)	Ref
BeF_2	100 BeF_2	0.06	0.59[(1)]	[14,30]
BeF_2 (vapour dep.)	100 BeF_2	0.06	0.14[(1)]	[30,31]
BeT	95 BeF_2 - 5 ThF_4	-	4.0[(1)]	[14]
BeKA	75 BeF_2 - 20 KF - 5 AlF_3	-	0.64[(2)]	[29]
BeKCaA	45 BeF_2 - 30 KF - 15 CaF_2 - 10 AlF_3	-	0.16[(2)]	[29]
$ZnCl_2$	100 $ZnCl_2$	1.1	-	[30]

[(1)]Measured at 0.488 μm.
[(2)]Measured at 0.633 μm.

Lines has established that the theoretical limit of the Rayleigh coefficient in vitreous $ZnCl_2$ was 1.1 dB km^{-1} μm^4 [30]. Van Uitert et al have measured light scattering losses of 100 dB km^{-1} at 0.633 μm in $ZnCl_2$ [29]. This is too high a value to be accounted for by Rayleigh scattering only. Mie and/or wavelength independent scattering processes are likely to be present.

Comparative curves of Rayleigh scattering loss for BeF_2, $ZnCl_2$ and some oxide and sulphide glasses have been established by Nassau et al [4].

E CONCLUSION

The theoretical limit for intrinsic scattering losses in zirconium-based fluoride glasses is as low as 0.11 dB km^{-1} μm^4. By using stringent conditions for glass preparation, the typical λ^{-4} dependence demanded by the Rayleigh scattering law is obeyed. The theoretical limit is almost attained for bulk ZBLA fluoride glass with an experimental Rayleigh coefficient of 0.14 dB km^{-1} μm^4.

Rayleigh coefficients of fluoride glasses are significantly lower than that of silica glass, in bulk or fibre configurations.

REFERENCES

[1] J.L. Adam [Datareview in this book: *C1.1 Transmission of halide glasses*]
[2] J. Lucas, J.L. Adam [in *Optical Properties of Glasses* Eds. D.R. Uhlmann, N.J. Kreidl (Am. Ceram. Soc., Westerville, OH, 1991) p.37-85]
[3] [Datareview in this book: *C4.3 Loss of halide glass optical fibre*]
[4] K. Nassau, M.E. Lines [*Proc. SPIE (USA)* vol.484 (1984) p.7-13]
[5] S. Shibata, M. Horiguchi, K. Jinguji, S. Mitachi, T. Kanamori, T. Manabe [*Electron. Lett. (UK)* vol.17 (1981) p.775-7]
[6] H. Poignant [*Electron. Lett. (UK)* vol.17 (1981) p.973-4]
[7] A. Lopez, P. Baniel, P. Gall, J. Granier [*Proc. SPIE (USA)* vol.1590 (1991) p.191-202]
[8] P. Baniel, C. Belouet [*J. Non-Cryst. Solids (Netherlands)* vol.161 (1993) p.1-6]
[9] A. Lopez, P. Baniel, P. Gall, J. Granier [*J. Non-Cryst. Solids (Netherlands)* vol.203 (1996) p.143-52]
[10] P.W. France, M.C. Brierley, S.F. Carter, M.W. Moore, J.R. Williams, C.R. Day [*Mater. Sci. Forum (Switzerland)* vol.32-33 (1988) p.343-8]
[11] D.C. Tran, G.H. Sigel, K.H. Levin, R.J. Ginther [*Electron. Lett. (UK)* vol.21 (1982) p.1046-8]
[12] J. Schroeder et al [*Electron. Lett. (UK)* vol.20 (1984) p.860-2]

[13] J. Schroeder, M. Fox-Bilmont, B.G. Pazol, V. Tsoukala, M.G. Drexhage, O.H. El-Bayoumi [*Proc. SPIE (USA)* vol.484 (1984) p.61-71]
[14] V. Tsoukala, J. Schroeder, G.A. Floudas, D.A. Thompson [*Mater. Sci. Forum (Switzerland)* vol.19-20 (1987) p.637-46]
[15] J. Schroeder et al [*Mater. Sci. Forum (Switzerland)* vol.6 (1985) p.561-70]
[16] M.G. Drexhage [*Mater. Sci. Forum (Switzerland)* vol.5 (1985) p.1-18]
[17] H. Hattori, T. Kanamori, S. Sakaguchi, Y. Ohishi [*Appl. Opt. (USA)* vol.26 (1987) p.650-3]
[18] H. Hattori, S. Sakaguchi, T. Kanamori, Y. Terunuma [*Appl. Opt. (USA)* vol.26 (1987) p.2683-7]
[19] D.C. Tran et al [*Mater. Sci. Forum (Switzerland)* vol.5 (1985) p.339-52]
[20] J. Schroeder, L.G. Hwa, X.S. Zhao, L. Busse, I. Aggarwal [*Mater. Sci. Forum (Switzerland)* vol.67-68 (1991) p.471-6]
[21] J. Schroeder, M.A. Whitmore, M.R. Silvestri, S.K. Saha, C.T. Moynihan [*J. Non-Cryst. Solids (Netherlands)* vol.161 (1993) p.157-60]
[22] T. Izumitani, K. Matsukawa, Y. Wang [*Mater. Sci. Forum (Switzerland)* vol.67-68 (1991) p.453-8]
[23] S. Takahashi [*J. Non-Cryst. Solids (Netherlands)* vol.95-96 (1987) p.95-106]
[24] H. Hattori, Y. Ohishi, T. Kanamori, S. Takahashi [*Appl. Opt. (USA)* vol.25 (1986) p.3549-51]
[25] C.R. Day, P.W. France, S.F. Carter, M.W. Moore, J.R. Williams [*Proc. SPIE (USA)* vol.799 (1987) p.94-100]
[26] P.W. France, S.F. Carter. M.W. Moore, J.R. Williams [*Mater. Sci. Forum (Switzerland)* vol.19-20 (1987) p.381-6]
[27] D.C. Tran, K.H. Levin, C.F. Fisher, M.J. Burk, G.H. Sigel [*Electron. Lett. (UK)* vol.19 (1983) p.165-6]
[28] G. Lu, K.H. Levin, M.J. Burk, D.C. Tran [*Electron. Lett. (UK)* vol.22 (1986) p.602]
[29] L.G. Van Uitert, A.J. Bruce, W.H. Grodkiewicz, D.L. Wood [*Mater. Sci. Forum (Switzerland)* vol.6 (1985) p.591-606]
[30] M.E. Lines [*Am. Rev. Mater. Sci. (USA)* vol.16 (1986) p.113-35]
[31] A. Sarhangi, D.A. Thompson [*Mater. Sci. Forum (Switzerland)* vol.19-20 (1987) p.259-68]

C1.3 Refractive index and dispersion of halide glass

M. Poulain

May 1998

A INTRODUCTION

Refractive index is closely related to composition. It depends on the overall polarisability of the material which is ruled by two parameters: the polarisability of each individual component and the number of elements per unit volume. In ionic solids, anions are the largest ions and their outer electronic shell is more polarisable than that of cations. Fluoride anions are the least polarisable, because fluorine is the most electronegative element. As a consequence, the lowest refractive indices are found in fluorides: only 1.29 for vitreous BeF_2. Larger values are observed for chlorides, and still larger for bromides and iodides. Similarly, the refractive index increases when large and heavy cations enter the material composition.

This simple analysis provides sufficient guidelines for adjusting the refractive index in most halide glasses. The practical difficulty concerns rather the stability of the modified glasses toward devitrification, which directly influences optical quality and fibre drawing ability.

In fluoride glasses, the value of the refractive index may be predicted using the relation introduced by Sun [1]:

$$n - 1 = \sum_i x_i u_i$$

where n is the refractive index, x_i is the mole fraction of the ith component in the glass and u_i is the characteristic refractivity of the ith component.

To some extent, it is surprising that this simple relation could be satisfactory as it does not encompass the variation of the number of elements per unit volume. In fact, the partial molar volume of each glass component is nearly constant in most fluoride glasses and this volume-related factor has only a minor effect.

The values reported by Sun were calculated mainly from fluorberylate glasses. As these glasses are no longer developed, revised results using the measurements implemented during recent years would be useful and lead to more accurate values.

B REFRACTIVE INDEX OF FLUORIDE GLASSES

It is difficult to synthesise fluoride glass samples with a very homogeneous refractive index because the glass melt is very reactive and prone to hydrolysis and vaporisation. In addition, fast cooling rates are required to prevent devitrification. This explains why the accuracy of the values found in the literature is limited. TABLE 1 reports some of them corresponding to standard glasses. The average value is 1.5 for heavy metal fluoride glasses (HMFG). It reflects the small polarisability of the fluorine anions and the larger value for the heavy cations. Smaller refractive index is observed in fluoroaluminate glasses and higher yet in fluorozirconates. Glasses based on hafnium fluoride have a smaller refractive index than fluorozirconates. Although the Hf^{4+} cation is much heavier than Zr^{4+}, it is smaller and less polarisable.

TABLE 1 Composition and refractive index of typical halide glasses.

Glass	Composition (mol %)	n_D
ZBLA	57 ZrF_4, 34 BaF_2, 5 LaF_3, 4 AlF_3	1.519
HBLA	57 HfF_4, 34 BaF_2, 5 LaF_3, 4 AlF_3	1.504
ZBLAN	53 ZrF_4, 20 BaF_2, 5 LaF_3, 4 AlF_3 , 20 NaF	1.498
ZBSFCl	60 ZrF_4, 20 BaFCl, 20 SrFCl	1.542
YABC	20 YF_3, 40 AlF_3, 20 BaF_2, 20 CaF_2	1.440
IZBS	40 InF_3, 20 ZnF_2, 20 SrF_2, 15 BaF_2, 5 CaF_2	1.495
PGICZ	30 PbF_2, 22 GaF_3, 13 InF_3, 18 CdF_2, 13 ZnF_2, 2 GdF_3, 2 NaF	1.595

Various composition changes have been investigated in order to adjust the value of the refractive index in the range needed for the fabrication of optical fibres. Additives have been incorporated in standard fluoride glasses, and their influence quantified [2-5]. Refractive index n generally varies linearly with the concentration of the additive. Lithium, sodium and alkali cations decrease refractive index in fluorozirconates, while lead, cadmium and rare earths have the reverse effect. Substituting zirconium with hafnium also decreases n.

ZBLAN makes the basis of most fluoride glass fibres. The modification of the respective amounts of NaF, AlF_3 and LaF_3 in core and cladding glasses is usually sufficient to obtain a numerical aperture of 0.15 to 0.2. When larger numerical apertures are required, the core refractive index must be increased. Doping with lead fluoride is a common way to do this. However it may induce some problems, e.g. scattering centres at the core/cladding interface. The incorporation of heavy halides such as chlorides is another possibility. The refractive index may also be decreased in the cladding glass. Beryllium fluoride has been used for this purpose, but it has serious disadvantages with respect to chemical durability and phonon energy. In addition, its toxicity raises practical problems.

Adjustments in indium-based fluoride glasses are implemented in the same way. GaF_3/InF_3 substitution decreases n, and the relative amounts of lead and yttrium fluorides may be largely modified leading to large changes in refractive index.

C DISPERSION AND TEMPERATURE DEPENDENCE

The relation between refractive index and wavelength is commonly expressed by the Sellmeier equation:

$$n(\lambda) = A\lambda^{-4} + B\lambda^{-2} + C + D\lambda^2 + E\lambda^4$$

An alternative relation may be used [6]:

$$n_\lambda^2 = f_1\lambda^2 / \left(\lambda^2 - \lambda_1^2\right) + f_2\lambda^2 / \left(\lambda^2 - \lambda_2^2\right)$$

Numerical coefficients are deduced from the experimental measurements. As pointed out above, few data are available and their significance may be limited by the optical quality of the available samples. The pioneering work of Mitachi on the ZrF_4-BaF_2-GdF_3-AlF_3 glasses [7] was confirmed by other studies on fluorozirconate glasses. Experimental measurements have been collected by Gan Fuxi [6]. From these, the values of the parameters f_i and λ_i could be deduced and the corresponding parameters for the various fluorides entering glass composition could be calculated. In this way, dispersion and not only refractive index can be estimated from the chemical composition [6,8]. For most fluoride glasses, dispersion in the visible spectrum corresponds to an Abbe number ranging from 70 to 80. Note that dispersion may be different for core and cladding glasses in an optical fibre. Consequently the numerical aperture estimated from the respective values of n_D may be different at longer wavelength, especially beyond 3 μm.

Until now, the use of HMFG as optical glasses has not been seriously considered, despite the fact that reported values of the partial dispersion makes them attractive materials. This can be understood when considering the problems in obtaining high optical quality samples, and the resulting cost. Solving these problems requires further development.

Material dispersion, which is $d^2n/d\lambda^2$, is also an important parameter for the design of single mode optical fibres. Ideally it should be zero for optimum signal transmission. In fluoride glasses the zero dispersion wavelength λ_0 ranges between 1.5 and 2.0 μm [9,6]. Material dispersion is negative at longer wavelength. However its magnitude remains small and could be compensated by the waveguide design. With fluoroindate glasses this is possible up to 3 μm, and possibly beyond this value [10]. For heavy halide glasses, λ_0 is larger than 2 μm.

Refractive index also changes with temperature. There are two opposite factors: first, atomic polarisability increases with temperature, but so does the average molar volume. The result is that there is a smaller number of more polarisable elements per unit volume. Silica, which has a very low thermal expansion coefficient, exhibits a positive dn/dT, but this temperature coefficient is negative for fluoride glasses [11]: -1×10^{-5} K^{-1} for ZBLA glass.

The non-linear refractive index is low in HMFG, around 1 to 2×10^{-13} esu [12].

Few data are available for heavy halide glasses. As a general rule, optical properties are related to the nature of the anions: refractive index, dispersion and zero dispersion wavelength increase according to the sequence F < Cl < Br < I.

D CONCLUSION

The refractive index lies between 1.45 and 1.55 for most HMFG, and dispersion remains small, with an Abbe number ranging from 70 to 85. Material dispersion is a minimum around 1.7 μm and is slightly negative at longer wavelengths. Most optical properties may be estimated from the chemical composition using semi-empirical models. Refractive index [13] and dispersion are larger when fluorine is replaced by chlorine or heavier halides. However, the practical use of plolyhalide glasses is limited by their poor resistance to moisture and their devitrification tendency.

REFERENCES

[1] N.P. Goldstein, K.H. Sun [*Am. Ceram. Soc. Bull. (USA)* vol.58 (1979) p.1182-4]
[2] S. Mitachi [*Phys. Chem. Glasses (UK)* vol.23 (1982) p.190-5]
[3] R. Lebullenger, S. Benjaballah, C. Le Deit, M. Poulain [*J. Non-Cryst. Solids (Netherlands)* vol.161 (1993) p.217-21]
[4] T. Kogo, M. Onishi, H. Kanamori, H. Yokota [*J. Non-Cryst. Solids (Netherlands)* vol.161 (1993) p.169-72]
[5] J.S. Javorniczky, P.J. Newman, D.R. MacFarlane [*J. Non-Cryst. Solids (Netherlands)* vol.184 (1995) p.336-40]
[6] F. Gan [*J. Non-Cryst. Solids (Netherlands)* vol.184 (1995) p.9-20]
[7] S. Mitachi, T. Miyashita [*Appl. Opt. (USA)* vol.22 (1983) p.2419-25]
[8] P. MacNamara [*Mater. Sci. Forum (Switzerland)* vol.67-68 (1991) p.79-84]
[9] B. Bendow, R.N. Brown, M.G. Drexhage, T. Loretz, R. Kirk [*Appl. Opt. (USA)* vol.20 (1981) p.3688-90]
[10] A. Soufiane, G. Fuxi, H. L'Helgoualch, M. Poulain [*J. Non-Cryst. Solids (Netherlands)* vol.184 (1995) p.36-9]

[11] P. Greason, J. Detrio, B. Bendow, D.J. Martin [*Mater. Sci. Forum (Switzerland)* vol.6 (1985) p.607-10]

[12] J. Lucas, M. Chanthanasinh, M. Poulain, P. Brun, M.J. Weber [*J. Non-Cryst. Solids (Netherlands)* vol.27 (1978) p.273-83]

[13] M. Poulain, A. Elyamani [*Mater. Sci. Forum (Switzerland)* vol.19-20 (1987) p.73-86]

C1.4 Non-linear refractive index of halide glass

T. Catunda and M.L. Baesso

July 1997

A INTRODUCTION

The propagation of intense optical beams through dielectric media induces changes in the refractive index Δn which cause self-focusing, beam breakup and damage in high power laser systems [1,2]. For a laser beam of intensity I, the refractive index is given by $n = n_o + n_2 \langle E^2 \rangle$ with $\Delta n = n_2 \langle E^2 \rangle$ or, alternatively, $\Delta n = \gamma I$, where $\langle E^2 \rangle$ denotes the time average squared amplitude of the optical electric field and I its intensity. In the 1970s, it was realised that refractive-index non-linearities are among the most serious limitations to high-power laser performance and many groups started to measure γ in laser materials. Later it was observed that maximum power transmitted through optical fibres, for telecommunication purposes, is also limited by γ due to self-phase modulation and cross-talk effects.

Besides the effect of γ, which here denotes the contribution of the host glass to the non-linearity, very important refractive index changes appear due to pumping of the upper laser level (which is usually metastable) [3]. The excited state pumping generates heat which causes Δn_{th} due to thermal variation of n_o, thermally induced stress and thermal expansion. Since the laser intensity profile usually has radial symmetry the temperature profile is also radial. Consequently, the thermal effects create a radial refractive index profile acting like a lens, the so called thermal lens effect (TL) [4,5]. Besides TL, excited state pumping causes refractive index changes Δn_{pop} associated with the difference in polarisabilities of the active ions in the metastable excited state versus the ground state, the population lens effect (PL) [6,7]. PL is related to hole burning which is very important in laser systems [8].

In principle, all these effects (γ, TL and PL) are very important [3]. However, the relative magnitude of each one depends on the kind of device, such as a passive optical element (like a window), a laser or an amplifier, pulsed or CW regime of operation, bulk or fibre, the kind of glass and doped ion, etc. In this work we will review the work on γ measurements, PL and TL in halide glasses, where mainly fluoride glasses have been studied.

B GLASS HOST NON-LINEARITY

Optical glasses are classified by their linear refractive index n_o (usually n_d at λ = 587.5 nm) and wavelength dispersion which is quantified by the Abbe number ν_d. TABLE 1 shows experimental results of the non-linear refractive index coefficient, γ, at λ = 1.06 μm, obtained by interferometric [1] and by three-wave mixing techniques [2]. An empirical expression was found to calculate γ_{cal} from n_d and ν_d, that agrees well with γ_{meas} and indicates that γ increases with increasing n_d and dispersion (decreasing ν_d). Fluorozirconate glasses have γ similar to that of silica but glasses with beryllium fluoride as the network former have the lowest n_d and the smallest γ of any solid reported to date. This behaviour is attributed to the lower polarisability of fluorine and fluoride compounds when compared to that of oxygen.

TABLE 1 Calculated (γ_{cal}) and measured (γ_{meas}) non-linear refractive index coefficients.

	n_d	ν_d	$10^{16}\,\gamma_{meas}$ ($cm^2\,W^{-1}$)	$10^{16}\,\gamma_{cal}$ ($cm^2\,W^{-1}$)	Ref
BeF_2	1.275	106	0.75	0.72	[1]
B102	1.340	103	1.0	1.0	[1]
Fluorophosphate	1.492	81	2.0	2.1	[1]
Fluorozirconate	1.52	75.5	3.3	2.5	[2]
Fused silica	1.459	74.5	2.6	3.7	[2]
ED-2 silicate	1.572	57.4	3.8	4.3	[1]
ED-2 silicate	1.572	57.4	4.0	4.3	[2]
SF-6 silicate	1.805	25.4	19	23	[2]

C THERMAL LENS

The propagation of a TEM_{00} gaussian laser beam, either the excitation laser beam itself or a probe beam, is affected by the refractive index profile, or more generally, a profile of the optical path length s. This results in beam spreading (when $ds/dT < 0$) with a reduction in its on-axis intensity, or beam focusing (when $ds/dT > 0$) with an increase in on-axis intensity. By measuring the beam on-axis intensity in the far field, the thermo-optical and/or non-linear properties of the sample can be obtained. This is the main principle of thermal lens [4,5] and Z-scan techniques [6].

The thermal lens (TL) effect is caused by deposition of heat, via a non-radiative decay process after laser energy has been absorbed by the sample. The TL effect can be treated through the calculation of the temporal evolution of the sample temperature profile $\Delta T(r,t)$, caused by a gaussian beam. Several kinds of experimental configurations have been used in TL experiments. The TL transient signal amplitude is proportional to its phase shift given by [4]:

$$\Delta\phi_{th} = \frac{PAL}{K\lambda_p}\varphi\frac{ds}{dT} \tag{1}$$

where P is the excitation laser power, A the absorption coefficient, K the thermal conductivity, λ_p the probe beam wavelength, L the sample length and φ the fraction of absorbed energy converted into heat per photon. If the sample fluorescence quantum efficiency is η, λ_{ex} is the excitation beam wavelength and λ_{em} is the average emission wavelength, then $\varphi = (1 - \eta\lambda_{em}/\lambda_{ex})$. The optical path change with temperature is given by:

$$ds/dT = (n-1)(1 + \nu)l + dn/dT \tag{2}$$

where l is the linear thermal expansion coefficient and ν the Poisson's ratio. Since the first term in EQN (2) is always positive, glasses with negative dn/dT are required to minimise ds/dT. So far all glasses with negative ds/dT are fluoride glasses or contain fluorine.

The characteristic TL signal response time is given by

$$t_c = \frac{w^2}{4D} \tag{3}$$

where $D = K/\rho C$ ($cm^2\,s^{-1}$) is the thermal diffusivity, ρ ($g\,cm^{-3}$) the density, C ($J\,g^{-1}\,K^{-1}$) the specific heat and w (cm) the excitation beam radius.

The thermo-optical properties of fluoride glasses were measured by interferometric [9,10] and thermal lens techniques [5]. We should remark that $dn/dT \propto (\phi - 31)$, where ϕ is the temperature coefficient of the electronic polarisability. Fluoride glasses are known to present very large l, for instance $l \sim 17 \times 10^{-6}$ K^{-1} for ZBLAN, about thirty times larger than the vitreous silica l value [11]. In addition to that, fluorine ions have small ϕ, so consequently fluoride glasses always present negative dn/dT and ds/dT, as shown in TABLE 2.

TABLE 2 Thermo-optical properties of some fluoride glasses.

	10^6 dn/dT (K^{-1})	10^6 ds/dT (K^{-1})	10^3 K (W cm^{-1} K^{-1})	10^3 D (cm^2 s)	Ref
Fluorozirconate	-14.75	-6.06	~4*	~1.5	[9,10]
AlF_3- BeF_2	-8.23	-2.02	-	-	[9]
AlF_3-ZrF_4	-9.42	-2.62	-	-	[9]
Nd:fluorindate	-	-1.7	8.2	3.3	[5]

*estimated value [11]

Time-resolved TL experiments were performed in Er^{+3} and Nd^{+3} doped fluorindade glasses [5], using the two-beams mode mismatched TL configuration. The parameters $\Delta\phi_{th}$ and t_c can be determined by proper fitting of the transient TL signal as shown in FIGURE 1. Using EQN (3) D can be obtained from t_c. However, in order to determine K from D, the product ρC must be known. Bruce [11] analysed data from twelve kinds of fluoride glasses concluding that, at 300 K, the molar specific heat is almost constant ~21.3 J K^{-1} mol^{-1} (86% of the Dulong Petit value). Using this value it was estimated that ρC = 2.5 J K^{-1} cm^{-3} for 1%Nd^{+3} doped fluorindate glass [5], which is close to the ZBLA value 2.58 J K^{-1} cm^{-3} [11].

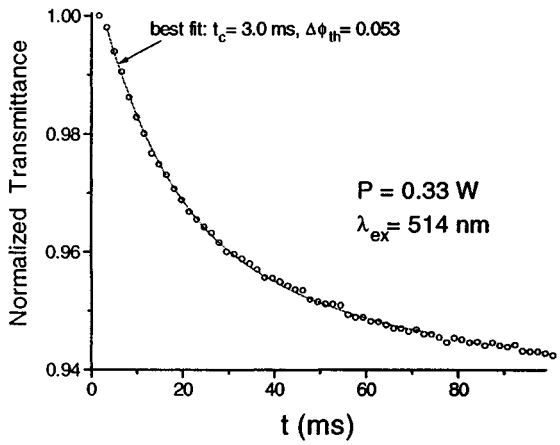


FIGURE 1 Typical time-resolved thermal lens signal (fluorindate glass, 1% Nd fluorindate, L = 2.7 mm). The theoretical fit was calculated as in [4,5].

From the TL experiment $D = 3.3 \times 10^{-3}$ cm^2 s^{-1} was obtained, so $K = \rho CD = 8.2 \times 10^{-3}$ W cm^{-1} K^{-1}. For Nd^{+3} doped glasses, with λ_{exc} = 515 nm and $\lambda_{em} \sim$ 1100 nm, and estimating $\varphi \sim 0.5$, from the $\Delta\phi_{th}$ obtained from the fit of FIGURE 1, from EQN (1) we calculated $ds/dT = -1.7 \times 10^{-6} K^{-1}$.

It is interesting to remark that in EQN (1) $\Delta\phi_{th} \propto P/K$, so $\Delta\phi_{th}$ is proportional to laser power but does not depend on laser intensity (which is determined by beam radius w). This is valid only in the CW regime, in the stationary case $t >> t_c$, where from EQN (3) t_c depends strongly on beam focusing. On the other hand, in the pulsed regime (with pulse width $t_p << t_c$) we can admit that there is no heat diffusion. Supposing also that $t_p << \tau_o$, the excited state population and the refractive index change are proportional to the pulse energy, which is proportional to the average intensity I. Therefore, in the pulsed regime we can write $\Delta n = \gamma_{th} I$, where the thermal coefficient is given by

$$\gamma_{th} = \frac{\varphi \, A t_p}{\rho C} \frac{dn}{dT} \qquad (4)$$

In the case of experiments with nanosecond pulses ds/dT ~ dn/dT because the thermal expansion response time is supposed to be longer than the μs scale.

D POPULATION LENS EFFECT

Several kinds of non-linear optics experiment were made in active ion doped solids, particularly with transition metals and rare earth elements [6-8]. The non-linear effect originates from the dopant ion excited state population, which has a complex susceptibility different from that of the ground state. We call this process population lens (PL) effect, which is responsible for a refractive index change Δn_{pop} proportional to the metastable ion excited state population N_{ex}. In first order (for $I << I_s$) $N_{ex} \sim N_o I/I_s$, where N_o is the total ion concentration and I the laser intensity. The saturation intensity is given by $I_s = \hbar\omega/\sigma\tau_o$ where $\hbar\omega$ is the pump photon energy, τ_o the excited state lifetime and σ the absorption cross section. As N_{ex} is proportional to the laser intensity, we can associate with PL a non-linear refractive index, n_{2pop}, given by $n_{2pop} = \Delta n_{pop}/I$. The laser induced phase shift is given by $\Delta\phi_{pop} = (2\pi/\lambda)\Delta n'_{pop} L$ and can be written as [5]:

$$\Delta\phi_{pop} = (4\pi^2 f_L^2/\lambda n_o)\, \Delta\alpha L N_o I_o/I_s \qquad (5)$$

where $f_L = (n_o + 2)^2/3$ is the Lorenz local field correction factor, $\Delta\alpha$ is the polarisability difference between excited and ground states of the dopant ion, $I_o = 2P/\pi w_o^2$ is the on axis intensity of the gaussian TEM_{00} profile, w_o is the beam radius at focus and P is the laser power.

Another consequence of PL is the fact that the excited state usually has an absorption cross section which is different from the ground state one, and this induces a change in the imaginary part of refractive index $\Delta n''_{pop} = (c/2\omega)N_{ex}\Delta\sigma$, where $\Delta\sigma$ is the absorption cross section difference between excited and ground states.

When saturation effects are taken into account $\Delta n'_{pop} = n'_{2pop} I/(1+I/I_s)$ [6]. Therefore, although n'_{2pop} represents a huge non-linearity, the maximum refractive index change is limited to about $n'_{2pop} I_s$ which is proportional to $\Delta\alpha$. As an example, we will consider the case of Nd^{+3}, which is simpler because it has only one metastable state (the $^4F_{3/2}$ level with $\tau_o \sim 500$ μs). Supposing $\lambda = 800$ nm, $\tau_o = 500$ μs, $\sigma = 10^{-20}$ cm^2, $\Delta\alpha = 10^{-25}$ cm^3 and $N_o = 10^{19}$ cm^{-3}, as typical values for an oxide glass, we obtain $n'_{2pop} \sim 10^{-10}$ cm^2 W^{-1}, $I_s \sim 50$ kW cm^{-2} and $n'_{2pop} I_s \sim 5 \times 10^{-6}$. In Er^{+3} doped fluoride glasses, saturation intensities are even lower due to the longer lifetimes of $^4I_{11/2}$ and $^4I_{13/2}$ levels ($\tau_o \sim 10$ ms).

Using degenerate four-wave mixing, Powell et al measured $\Delta\alpha$ for Nd^{+3} in several different kinds of host material (crystal and glasses) [7]. They observed always $\Delta\alpha > 0$, varying in the range 10^{-26} - 10^{-25} cm^3, with $\Delta\alpha$ increasing in the following order: fluoride crystals, phosphate glasses, silicate glasses and oxide crystals. This behaviour leads to the interpretation that transitions 4f → 5d give the dominant contribution to $\Delta\alpha$ due to their relatively high oscillator strength. The great host dependence is then attributed to the sensitivity of the <4f|r|5d> radial integral to the environment. The low $\Delta\alpha$ observed in fluorides is justified by the high energy of their 5d states and consequent low radial integral.

Most active ion doped solids present simultaneously both PL and TL effects. Therefore it is very important to distinguish these two different contributions. First, we must remark that in both cases the measured signal is proportional to the laser power. However, from EQN (5), $\Delta\phi_p$ is proportional to P/w_o^2 while from EQN (1) $\Delta\phi_{th}$ does not depend on beam focusing and the ratio is given by

$$\frac{\Delta\phi_p}{\Delta\phi_{th}} \propto \frac{K\tau_o\,\Delta\alpha}{w_o^2(ds/dT)}.$$

The signal magnitude depends also on the experiment timescale compared to τ_o and t_c.

Even when $\Delta\phi_p$ and $\Delta\phi_{th}$ have the same order of magnitude these two effects can be distinguished temporally. FIGURE 2 shows single beam time-resolved Z-scan measurements performed at two different chopper frequencies in order to discriminate PL and TL effects in Nd^{+3} doped fluorindate glass [5]. In this experiment the PL effect is faster than the TL, so at high chopper frequency the characteristic Z-scan curve for positive non-linearity was observed and attributed to the PL effect. At lower chopper frequency the curve is inverted because $\Delta s < 0$ and the distance between peak and valley is doubled, as should be expected for a TL Z-scan [13]. From the PL data we calculated $\Delta\alpha \sim 1.3 \times 10^{-26}$ cm^3, which is similar to the values found for fluoride crystals and fluorophosphate glasses [7].

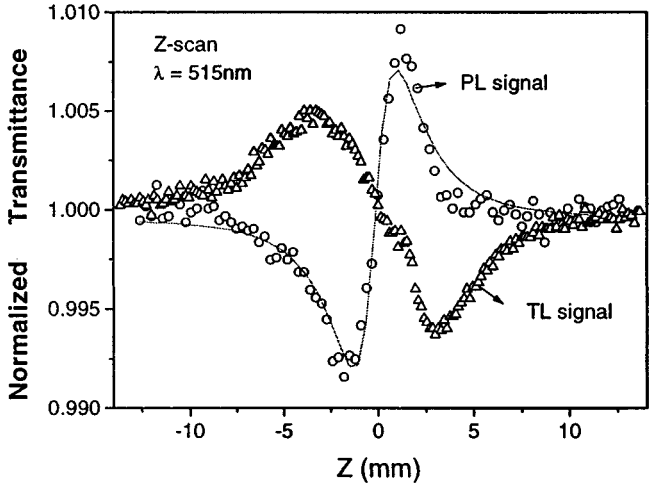


FIGURE 2 Time-resolved Z-scan with chopper frequency f = 90 Hz and P = 0.23 W (triangles) and f = 825 Hz and P = 0.187 W (circles) [12]. Same sample as in FIGURE 1.

E CONCLUSION

In the halide glass family only the non-linear properties of fluoride glasses have been studied. The structural and compositional properties that have been identified as having a significant effect on the linear refractive index also affect γ, PL and TL in a similar way. In Section B, it was shown that γ is directly related to n_d and ν_d, increasing with linear refractive index and dispersion. In Section C, we mentioned that the low polarisability of fluorides implies a low ϕ factor and negative dn/dT. Also for the PL effect, it was observed that in fluorides $\Delta\alpha$ is up to one order of magnitude lower than in oxides.

For a high power pulsed glass laser, it was estimated that γ, TL and PL can give contributions of the same order of magnitude [3]. The general thermo-mechanical properties (particularly the thermal shock parameter) of fluoride glasses are worse than those of silicate and phosphate glasses, so fluorides are not considered good candidates for high power Nd lasers. However, halide glasses have a wide transparency window and low phonon energies, which are particularly interesting properties for special lasers, such as upconversion lasers. Several new kinds of laser have already been demonstrated in fluoride doped glasses (bulk or fibres). Most of theses lasers operate in CW mode with low power. Non-linear effects are particularly important in fibres where high intensities are obtained, even in the CW regime, due to the small core diameter. It is likely that, in the near future, the need for higher power systems will bring more attention to the non-linear properties of halide glasses.

REFERENCES

[1] M.J. Weber, D. Milan, W.L. Smith [*Opt. Eng. (USA)* vol.17 (1978) p.463-9]

[2] R. Adair, L.L. Chase, S. Payne [*J. Opt. Soc. Am. B (USA)* vol.6 (1987) p.875-81]

[3] R.C. Powell, S.A. Payne, L.L. Chase, G.D. Wilke [*Opt. Lett. (USA)* vol.14 (1989) p.1204-6]

[4] M.L. Baesso, J. Shen, R.D. Snook [*J. Appl. Phys. (USA)* vol.75 (1994) p.3732-7]

[5] T. Catunda, M.L. Baesso, Y. Messaddeq, M.A. Aegerter [*J. Non-Cryst. Solids (Netherlands)* vol.213&214 (1997) p.225-30]; S.M. Lima et al [to be published]

[6] V. Pilla, P.R. Impinnisi, T. Catunda [*Appl. Phys. Lett. (USA)* vol.70 (1997) p.817-9]

[7] R.C. Powell, S.A. Payne, L.L. Payne, G.D. Wilke [*Phys. Rev. B (USA)* vol.41 (1991) p.8593-602]

[8] H.J. Eichler, P. Gunter, D.W. Pohl [*Springer Ser. Opt. Sci. (Germany)* vol.50 (1986)]

[9] T. Izumitani, T. Yamashita, M. Tokida, K. Miura, H. Tajima [*Mater. Sci. Forum (Switzerland)* vol.19-20 (1987) p.19-26]

[10] J.M. Jewell, C. Askins, I.D. Aggarwal [*Appl. Opt. (USA)* vol.30 (1991) p.3656-60]

[11] A.J. Bruce [in *NATO on Halide Glasses for Infrared Optics Fiberoptics* Portugal, Ed. R.M. Almeida (Martinus Nijhoff, Dordrecht, 1987) p.149-62]

[12] A.A. Andrade, T. Catunda, R. Lebullenger, A.C. Hernandes, M.L. Baesso [*Electron. Lett. (UK)* vol.34 (1998) p.117-9]

[13] S.J. Sheldon, L.V. Knight, J.M. Thorne [*Appl. Opt. (USA)* vol.21 no.9 (1 May 1982) p.1663-9]

PART C: HALIDE GLASS

CHAPTER C2

THERMAL AND MECHANICAL PROPERTIES

C2.1 Characteristic temperatures of halide glass
C2.2 Viscosity of halide glass
C2.3 Elastic moduli of halide glass
C2.4 Stability of halide glass

C2.1 Characteristic temperatures of halide glass

A. Jha

September 1997

A INTRODUCTION

Halide glasses are predominantly composed of halide anions (X = F^-, Cl^-, Br^- and I^-). The halide glasses, like their silicate counterparts, which have $(SiO_4)^{4-}$ tetrahedra as structural building blocks, are made up of polyanionic complexes, e.g. $(ZrF_6)^{4-}$ and $(CdX_4)^{2-}$ ionic complex units in fluorozirconate and cadmium mixed halide glasses, respectively [1,2]. These structural polyanionic units have weaker bond strengths compared to silicates which can be inferred by comparing the phonon energies of the halide glasses with those of silicates. The phonon energies of silicates are in the range of 1100 cm^{-1} [3] and are significantly higher than those of fluorozirconate and fluorohafnate glasses (580 cm^{-1}) [4] and cadmium mixed halide glasses [5]. Because of the apparent difference in the phonon energies, the characteristic temperatures of halide glasses also differ greatly from those observed in silicate glasses and also between the various families of halide glasses.

B METHODS

The characteristic temperatures of halide glasses are the glass transition (T_g), the onset (T_x) and the peak crystallisation (T_p) temperatures, and the onset of melting (T_m) and the end of melting (T_l) temperatures. These temperatures are determined either by differential scanning calorimetry (DSC) or by differential thermal analysis (DTA) techniques. The value of T_g can also be determined by the dilatometric technique. At T_g, the molar volume and the specific heat change discontinuously. Above T_g, the material behaves as if it were a high viscosity liquid which begins to flow. As the temperature of the material is increased above T_g, the viscosity decreases (i.e. the rate of atomic or ionic transport increases) and the glass crystallisation begins. The onset of crystallisation is manifested by the release of heat due to the formation of thermodynamically more stable bonds in the crystalline phase than are present in the metastable glassy phase. It is possible that the first crystalline phase formed during the devitrification process may not be the equilibrium phase, but it may be more stable than the metastable liquid above T_g. The crystallisation process during the isochronal ramp in DSC or DTA is therefore manifested by the release of energy.

The early phase of crystallisation is dominated by the nucleation of either metastable or stable crystals followed by their growth. The shape of the exothermic peak in a DSC or DTA trace determines the rate of metastable liquid-to-crystal phase transformation. The crystallisation thermal event is usually followed by the melting of metastable or stable crystals. The onset of melting (T_m) in a multicomponent glass-forming system is the temperature at which the first liquid phase forms and the end of melting (T_l) defines the temperature at which the melting of the last remaining crystals in the liquid is complete.

C MEASURED DATA

The characteristic temperatures, measured by DSC and/or DTA techniques, of various types of fluoride and halide glasses are tabulated below and the presented results are classified on the basis of valency of the main component of the glass under consideration. In this data compilation, the heating rate employed is 10 K min^{-1} unless indicated.

TABLE 1 Fluorozirconate and fluorohafnate glasses and their characteristic temperatures [1,2,4].

Composition (mol %)	T_g (K)	T_x (K)	T_p (K)	T_m (K)
52 ZrF_4, 20 BaF_2, 4 LaF_3, 4 AlF_3, 20 NaF (ZBLAN)	548	638	658	715
50 ZrF_4, 40 NaF, 10 BaF_2	488	525	532	-
50 ZrF_4 50 BaF_2	573	604	610	-
75ZrF_4, 15 BaF_2, 10 NaF	534	585	588	-
75 ZrF_4, 25 BaF_2	568	620	623	-
60 ZrF_4, 35 BaF_2, 5 LaF_3	572	618	-	-
60ZrF_4, 35 BaF_2, 5 AlF_3	584	629	-	-
55 ZrF_4, 20BaF_2, 20 NaF, 5 AlF_3	533	598	-	-
50 ZrF_4, 20 BaF_2, 20 LiF, 5 LaF_3, 5 AlF_3 (ZBLALi)	523	630	-	-

Several dozen compositions are well known in the literature but only a few fluorozirconate and fluorohafnate glass compositions are of any practical use. In the fluorozirconate family of glasses, two of the most stable compositions are ZBLAN and ZBLALi and they have been modified to design the core-clad glass preform compositions for fluoride glass fibre fabrication. The most popular commercial core and cladding glasses are based on ZBLANP and ZHBLALi compositions, where the letters P, H and Li in the acronyms designate lead, hafnium and lithium fluorides respectively.

Additions of PbF_2 and HfF_4 as refractive-index modifiers as well as for manipulating the coefficient of thermal expansion are frequently made, so that the overall fibre and glass preform stress is of compressive nature. As a result, the strength of fibres in service is enhanced after providing a suitable coating. For this reason, the T_g of cladding (low refractive index) glass is always maintained slightly higher than the matched core glass.

Selected matched core-clad glass compositions used for commercial fibre fabrications are [4,5]: core 1 (51.5 ZrF_4, 19.5 BaF_2, 5.3 LaF_3, 3.2 AlF_3, 18 NaF, 2.5 PbF_2), clad 1 (53 ZrF_4, 20 BaF_2, 4.0 LaF_3, 3 AlF_3, 20 NaF) and core 2 (53 ZrF_4, 20 BaF_2, 4 LaF_3, 3 AlF_3, 20 NaF), clad 2 (39.7 ZrF_4, 13.3 HfF_4, 18 BaF_2, 4 LaF_3, 3 AlF_3, 22 NaF).

Fluorozirconate glasses can also be prepared without the addition of aluminium fluoride (AlF_3) and by substituting NaF by other alkali halides for designing more efficient Pr-ion glass hosts than the ZBLAN hosts for designing 1.3 μm Pr^{3+}-doped fluoride fibre amplifiers [7]. The glasses can be prepared with additions of LaF_3, InF_3 and YF_3. The characteristic temperatures of stable compositions are listed in TABLE 2.

TABLE 2 Characteristic temperatures of AlF_3-free fluorozirconate glasses. β is the heating rate which was 20 K min^{-1} [7].

Compositions (mol %)	T_g (K)	T_x (K)	T_p (K)	T_m (K)
61 ZrF_4, 11 BaF_2, 4 LaF_3, 2 YF_3, 2 InF_3, 20 NaF	540	624	637	725
61 ZrF_4, 11 BaF_2, 4 LaF_3, 2 YF_3, 2 InF_3, 10 NaF,	551	643	663	725
10 CsF	533	610	623	713
52 ZrF_4, 15 BaF_2, 5 $BaCl_2$, 4 LaF_3, 2 YF_3, 2 InF_3, 15 NaF, 5 NaCl	535	638	658	710
52 ZrF_4, 15 BaF_2, 5 $BaCl_2$, 4 LaF_3, 2 YF_3, 2 InF_3, 5 NaF, 5 NaCl, 10 CsF				

The matched cladding compositions have HfF_4, AlF_3 and LiF and their T_g and T_x vary in the same range as the core glass so as to achieve good fibre drawing conditions and strength.

The trivalent fluoride glass family is classified mainly into three categories and they are fluoroaluminate, fluoroaluminate-phosphate and indium/gallium fluoride glass compositions. The fluoroaluminate family of glasses are primarily based on AlF_3-MF_2-$M'F_3$ compositions where M and M' represent alkaline-earth and prelanthanide or lanthanide metal fluorides respectively. The major constituent is AlF_3 followed by MF_2-type fluorides and LaF_3/YF_3 [8-13]. The addition of monovalent fluorides in fluoroaluminate glasses is known to stabilise the glass compositions [12]. This is also found to be true when sodium fluoride is replaced by the addition of sodium phosphate, resulting in a major change in the characteristic temperatures as a result of the related structural changes.

The indium/gallium fluoride compositions [12-17] are based on AlF_3 glasses except that the indium/gallium fluoride glasses are stabilised by group IIB fluorides (ZnF_2, CdF_2, PbF_2) and infrequently in some compositions GdF_3 and LaF_3 are added [14]. Monovalent fluorides and chlorides are also incorporated for glass stabilisation of $(In,Ga)F_3$-based glasses. The majority of compositions and characteristic temperatures in InF_3 and GaF_3 glass-forming systems were determined by Soufiane and co-workers [14-16]. However indium/gallium fluoride glasses with NaCl were reported by Akella et al [17]. Kanamori and co-workers [18,19], based on the compositions disclosed by Soufiane et al [14-16], designed modified compositions and demonstrated single-mode fibre fabrication in indium/gallium fluoride glass fibres. It has also been reported [20] that the characteristic temperatures of InF_3/GaF_3 glasses are dependent on the processing conditions.

Binary and ternary gallium fluoride based glasses [14] are unstable as indicated by the T_x-T_g difference which ranges from 50 to 75 K.

More recently in order to design Pr-doped fluoride glasses with lower phonon energy than fluorozirconate and indium/gallium fluoride glasses, divalent cadmium mixed halide glasses were investigated by research groups in the UK, France and the US [21-24]. Although a large number of compositions were known before 1990, for example in [25] and references therein, much of the effort to understand the glass formation took place in the wake of designing improved quantum efficiency Pr-doped fluoride fibre amplifiers. TABLE 5 summarises the results for the most stable glass compositions that have been tried for making core/clad glass preforms and for the fabrication of fibres.

TABLE 3 Characteristic temperatures of selected fluoroaluminate and fluoroaluminate phosphate glass compositions [8-13].

Composition (mol %)	T_g (K)	T_x (K)	T_m (K)	Ref
Core glass 30.2 AlF_3, (10.6BaF_2, 3.5MgF_2, 20.2CaF_2, 13.2SrF_2), 10.2 ZrF_4, 8.3 YF_3, 3.8 NaF	663	787	933	[8,9]
37 AlF_3, (12BaF_2, 12MgF_2, 15CaF_2, 9SrF_2), 15 YF_3	699	825	T_l = 1040	[10,11]
37 AlF_3, (8BaF_2, 12MgF_2, 15CaF_2, 9SrF_2), 15 YF_3, 4 $NaPO_3$	713	864	965	[13]
Cladding glass ALS-9	652	813	898	[12]
40 AlF_3, (10BaF_2, 10MgF_2, 27CaF_2, 10SrF_2), 3 $NaPO_3$	694	841	941	[13]

TABLE 4 Characteristic temperatures of InF_3 and GaF_3 based glasses.

Composition (mol %)	T_g (K)	T_x (K)	T_m (K)	Ref
40 InF_3, 20 ZnF_3, 20 SrF_2, 15 BaF_2, 5 CdF_2	564	656	673	[13]
40 InF_3, 20 ZnF_3, 20 SrF_2, 17 BaF_2, 2 GdF_3, 1 LaF_3	567	663	683	[13]
20 GaF_3, 15 InF_3, 30 PbF_2, 15 ZnF_2, 20 CdF_2	528 - 535	617 - 627	624 - 640	[18]

TABLE 5 Characteristic temperatures of cadmium mixed halide glasses.

Composition (mol %)	T_g (K)	T_x (K)	T_p (K)	T_m (K)	Ref
Core glass 45 CdF_2, 10 $BaCl_2$, 30 NaCl, 5 KBr	398	506	511	565	[21]
Cladding glass 50 CdF_2, 10 $BaCl_2$, 30 NaCl, 10 $NaPO_3$	425	555	578	623	[21]
17 CdF_2, 33 $CdCl_2$, 13 BaF_2, 37 NaF	409	519	529	587	[22]
30 CdF_2, 18.5 $CdCl_2$, 8 NaF, 25 NaCl, 12.5 BaF_2, 2 KF, 4 LiF	403	519	549	568	[24]

Much of the work in this area has now ceased owing to the toxicity of cadmium salts. Similarly due to health and safety reasons, the research and development work on ThF_4 containing fluoride fibres has been terminated. The compositions based on BaF_2InF_3-GaF_3-ThF_4 quaternary materials were developed by Charron and co-workers [26] and the characteristic temperatures vary in the range: T_g (605 - 624 K), T_x (733 - 753 K) and T_m (849 - 869 K). These values also change with the addition of AlF_3 and KF. The glasses were drawn into fibres with a 5 dB/m loss between 4 and 4.5 μm wavelength compared to a 0.01 dB/km loss in fluorozirconate fibres.

Finally, monovalent halide glasses based on AgI-CsI were also reported [27,28]. The reason we observe glass formation in such an ionically mobile system is due to the presence of ionic complex formation between CsI and AgI, leading to $[AgX_n]^{n-1}$ ionic structural units. These glasses have a T_g between 303 K and 333 K. The addition of lead bromide stabilises the binary AgI-CsI glass-forming compositions. The glass transmits up to 35 μm and is photo-sensitive.

REFERENCES

[1] R.M. Almeida, J.D. Mackenzie [*J. Chem. Phys. (USA)* vol.76 (1981) p.5954]

[2] A. Uhlherr, D.R. MacFarlane [*J. Non-Cryst. Solids (Netherlands)* vol.161 (1993) p.98]

[3] J.M. Parker, P.W. France [in *Glasses and Glass Ceramics* Ed. M.H. Lewis (Chapman Hall, 1989) p.167]

[4] P.W. France, S.F. Carter, M.W. Moore, C.R. Day [*Br. Telecom Technol. J. (UK)* vol.5 (1987) p.28]

[5] R.S. Deol et al [*J. Non-Cryst. Solids (Netherlands)* vol.161 (1993) p.257]

[6] D.C. Tran [in *Proceedings Optical Fibre Communications (OFC)* Atlanta, GA, 1986, TuA1]

[7] W.G. Jordan, A. Jha, M. Lunt, S.T. Davey, R. Wyatt, W. Rothwell [*J. Non-Cryst. Solids (Netherlands)* vol.184 (1995) p.5]

[8] M.R. Shariari, T. Iqbal, P. Hajcak, G.H. Siegel Jr. [*J. Non-Cryst. Solids (Netherlands)* vol.161 (1993) p.77]

[9] M.R. Shariari, T. Iqbal, P. Hajcak, G.H. Siegel Jr. [*Mater. Res. Forum (Switzerland)* vol.67&68 (1991) p.225]

[10] A.B. Seddon, A.V. Cardoso [*Mater. Res. Forum (Switzerland)* vol.67&68 (1991) p.73]

[11] A.V. Cardoso, P. Korgul, A.B. Seddon [*J. Non-Cryst. Solids (Netherlands)* vol.161 (1993) p.56]
[12] T. Iqbal, M.R. Shariari, G. Weitz, G.H. Siegel Jr. [*J. Non-Cryst. Solids (Netherlands)* vol.184 (1995) p.190]
[13] M. Naftaly, A. Jha [*Technical Report, Advanced Communications Technology & Services* (University of Leeds, April 1996)]
[14] A. Soufiane, M. Poulain [*J. Non-Cryst. Solids (Netherlands)* vol.161 (1993) p.206]
[15] Y. Messaddeq, A. Delben, M. Boscolo, M.A. Aegerter, A. Soufiane, M. Poulain [*J. Non-Cryst. Solids (Netherlands)* vol.161 (1993) p.210]
[16] A. Soufiane, G. Fuxi, H.L. Helgoulch, M. Poulain [*J. Non-Cryst. Solids (Netherlands)* vol.184 (1995) p.36]
[17] A. Akella, E.A. Downing, L. Hesselink [*J. Non-Cryst. Solids (Netherlands)* vol.213&214 (1997) p.1]
[18] T. Kanamori et al [*J. Non-Cryst. Solids (Netherlands)* vol.213&214 (1997) p.121]
[19] T. Kanamori, K. Oikawa, Y. Terunuma, K. Kobayashi, S. Takahashi [*Jpn. J. Appl. Phys. (Japan)* vol.28 (1989) p.L1979]
[20] A. Jha, B.E. Kinsman, E.R. Taylor, G. Kakarantzas [*J. Non-Cryst. Solids (Netherlands)* vol.213&214 (1997) p.101]
[21] S. Jordery, M. Naftaly, A. Jha [*J. Non-Cryst. Solids (Netherlands)* vol.196 (1996) p.199]
[22] G. Zhang, M. Poulain, A. Jha [*J. Non-Cryst. Solids (Netherlands)* vol.184 (1995) p.72]
[23] J. Jiang, G. Zhang, M. Poulain [*J. Non-Cryst. Solids (Netherlands)* vol.184 (1995) p.346]
[24] R.F. Bartholomew, B.G. Aitken, M.A. Newhouse [*J. Non-Cryst. Solids (Netherlands)* vol.184 (1995) p.229]
[25] A. Jha, J.M. Parker [*Phys. Chem. Glasses (UK)* vol.32 (1991) p.1-11 and references therein]
[26] C. Charron, G. Fontenau, J. Lucas [*J. Non-Cryst. Solids (Netherlands)* vol.161 (1993) p.213-6]
[27] J.D. Mackenzie [in *Halide Glasses for Infrared Fibre Optics* Ed. R.M. Almeida (Martinus Nijhoff, Dordrecht, 1987)]
[28] J. Hulme, A. Jha, J.M. Parker, A. Whitehouse [*Phys. Chem. Glasses (UK)* vol.30 no.6 (1989) p.254-9]

C2.2 Viscosity of halide glass

M. Braglia

July 1997

A INTRODUCTION

The viscosity versus temperature and the rheological properties of halide glass are among the most important aspects in the manufacture of optical fibres.

If fibres are to be drawn from a preform, particular attention should be paid to the viscosity in the temperature working range between the T_g glass transition temperature ($10^{12.1}$ Pa s) and the T_x crystallisation onset temperature. On the other hand, if the double crucible method is used to produce fibre, the viscosity dependence on the temperature close to the melting point should be known in order to control the process.

This Datareview discusses the most important work undertaken on the viscosity of halide glass in terms of measurement methods, models, their dependence on temperature, glass composition and rheological properties.

B MEASURING METHODS AND MODELS

Viscosity measurements are very difficult to carry out on halide glass because above the glass transition temperature the nucleation and growth of the crystals increases quickly affecting the viscosity of the glass. Moreover, just below the liquidus temperature the glass can react with the moisture of the air and the growth rate of crystals becomes relevant. These may be the reasons why, in our opinion, little work has been done on the viscosity of halide glass.

TABLE 1 summarises the most important methods which have been used in the viscosity measurements on halide glass. To our knowledge other methods such as falling sphere viscometer, capillary viscometer and rod elongation, not reported in the table, have not been used on halide glass.

TABLE 1 Selection of viscosity measuring methods used for halide glass.

Method	Viscosity range (Pa s)	Ref
Parallel plate	10^4 - 10^8	[1,2]
Penetration	10^6 - 10^{10}	[3,4]
Beam bending	10^7 - 10^{13}	[5]
Rotating cylinder	10^2 - 10^{13}	[6,7]

The viscosity (η) versus temperature measurements of halide glass have been fitted using many equations. The simplest way to describe the temperature dependence of viscosity is by using the Arrhenius equation which is valid only in limited temperature ranges:

$$\eta = \eta_0 \exp\left(\frac{\Delta E}{RT}\right) \qquad (1)$$

where ΔE is the activation energy for the viscous flow, R is the gas constant and η_0 is a constant.

An extension to the Arrhenius equation, proposed by Doolittle [8], takes into consideration the change in the free volume of the glass with the temperature:

$$\eta = \eta_0 \exp\left(\frac{B}{fv_T}\right) \tag{2}$$

where η_0 and B are constants and fv_T is the free volume.

Following the Eyring model [9], based on hole theory, the free volume can be written as:

$$fv_T = C \exp\left(\frac{-\Delta H}{RT}\right) \tag{3}$$

where ΔH is the activation enthalpy for shear viscosity and C is a constant.

Cohen and Grest proposed [10] another form of fv_T:

$$fv_T = (T - T_0) + \left((T - T_0)^2 + 4\,C\,T\right)^{1/2} \tag{4}$$

where T_0 and C are adjustable parameters. Crichton et al [11] showed that the viscosity of fluoride melts could be well fitted by EQNS (2) and (4) where T_0 was close to the liquidus temperature, but with these equations the exactness of the fit is a consequence of the higher number of parameters considered [12].

For glass with high melt viscosity at the liquidus temperature, the Vogel-Fulcher-Tamman [13-15] method has been used to fit the viscosity-temperature data:

$$\eta = A \exp\left(\frac{B}{(T - T_0)}\right) \tag{5}$$

where A, B and T_0 are constants and $T - T_0$ is proportional to the free volume. The value of T_0 is taken to be an ideal glass transition temperature below T_g where the free volume goes to zero. EQN (5) was used to fit the viscosity measurements of many oxide glasses within a wide viscosity range, whereas for fluoride glass systems it can only be used for a limited viscosity range (10^6 - 10^{12} Pa s) [16].

Another equation obtained by Macedo and Litovitz [17], to describe viscosity versus temperature in a wide temperature range, is a combination of EQN (1) with the free volume model used to derive EQN (5):

$$\log \eta = A + \frac{B}{T} + \frac{C}{(T - T_0)} \tag{6}$$

where A and C are constants, and B is the activation energy for the flow unit to jump from one site to the adjacent one. This equation was used by Matusita et al [18] to fit the data for ZBGA glass, but the B values become negative, which is physically meaningless. Therefore they suggested modifying the term B in EQN (6) taking into account the temperature dependence of the flow unit, substituting the second

term of the equation with B/T^n where n is a constant. The quantity $n \cdot B/T^{n-1}$ is assumed to correspond to the activation energy for the flow unit to jump from one site to an adjacent one.

The reader is referred to an interesting review of different viscosity models used to study fluorozirconate and fluoroaluminate glass reported by Jha and Parker [19].

C VISCOSITY MEASUREMENTS IN THE WORKING RANGE

Viscosity measurements in the working range are very important for the drawing process of optical fibres and in particular for the choice of core and cladding glass compositions because the two glasses should have a similar viscosity in order to be drawn from a preform. In this section we consider viscosity reports in the temperature range from above glass transition to below crystallisation onset.

Tran et al [20] measured the viscosity of ZrF_4 - BaF_2 - LaF_3 - AlF_3 glass (ZBLA) in the range from 270°C to 350°C and found that LiF, BiF_3, TlI and PbF_2 reduced the viscosity of the glass. In particular the combination of PbF_2 and LiF was found to be helpful because it decreases the dependence of the viscosity on temperature compared with ZBLA glass. The data obtained were well fitted by the Arrhenius equation.

Similar results were found by Shelby et al [21], who in particular studied the glass system 0.56 ZrF_4 - (0.34-x) BaF_2 - 0.06 LaF_3 - 0.04 AlF_3 - x RF where x = CsF, KF, NaF, LiF. They observed that the effect of alkali fluorides on the viscosity decreases following the sequence Cs>K>Na>Li, which is comparable to the case for silicate systems.

Baniel et al [22] measured and compared the activation energy for viscous flow of different fluorozirconate glass compositions in the temperature range from 288°C to 320°C. They found the following sequence in the activation energy: ZBLANIn<ZBLALi<ZBLAN<ZBLA, where the effect of InF_3 was pointed out for the first time.

Hasz et al [23] showed that the total replacement of ZrF_4 by HfF_4 in a ZBLAN glass has the effect of increasing the viscosity near the glass transition by a factor of about 10^3, but the shapes of the viscosity versus temperature curves are unaffected.

Matusita et al [24] measured the viscosity of the (90-x) ZrF_4 - x BaF_2 - 4 GdF_3 - 6 AlF_3 system (ZBGA) by the penetration method in the range 10^6 - 10^{10} Pa s. The viscosity increases with a higher BaF_2 content.

For similar glass composition ZBGA, the role of NaF was investigated [18]. The replacement of BaF_2 with NaF decreases the viscosity and the numerical values were very well fitted by an equation derived from the Macedo-Litovitz equation [17].

Lin et al [25] used three different methods to measure the viscosity of fluoroaluminate glass (40 AlF_3 - 10 MgF_2 - 30 CaF_2 - 10 BaF_2 - x YF_3 where x = 0, 5, 10, 15, 20) in the range from 1 to 10^{13} Pa s. Measurements were performed by rotating viscometer, for viscosity values $<10^4$ Pa s, by the parallel plate method in the range 10^4 to 10^8 Pa s, and by the beam bending method in the range 10^8 to 10^{13} Pa s. The relationship between the activation energy for the viscous flow and the reciprocal temperature was expressed by two straight lines.

Low viscosity values and small activation energy above the crossover temperature of these two lines suggested that the structure of fluoroaluminate melts is quite similar to that of molten salts rather than that of conventional glass forming liquids.

Shelby et al [26] and Christensen et al [27] used a beam bending viscometer to measure the viscosity in the temperature working range for the following glasses: BZYT (x RF - (19-x) BaF_2 - 27 ZnF_2 - 27 YbF_3 - 27 ThF_4 mol % where RF was LiF or NaF) and BIZYbT (30 BaF_2 - 30 InF_3 - 20 ZnF_2 - 10 YbF_3 - 10 ThF_4 mol %). The viscosity decreased as alkali was substituted for barium.

With regard to cadmium mixed halide glasses, viscosity measurements have recently been carried out by Bartholomew et al [28] and by Naftaly et al [12].

D VISCOSITY MEASUREMENTS OF MELTING GLASS

The viscosity of BeF_2 and BeF_2 LiF glass in the temperature range 575 - 985°C was determined by Mackenzie [29], Moynihan and Cantor [30] and Petrovskij [31]. The behaviour of these glass systems is slightly non-Arrhenian. The BeF_2 viscosity curve is reported in FIGURE 1 where curves of other halide glass systems and silica glass are also shown. As can be seen, the behaviour of the BeF_2 glass is similar to that of SiO_2 in the drawing viscosity range (10^2 - 10^4 Pa s) because the dependence on the temperature is much lower than that of other glass systems. The viscosity of BeF_2 and BeF_2-LiF glass close to the liquidus temperature is more than 10^5 Pa s and this value is quite similar to that of the SiO_2 glass. Considering heavy metal fluoride (HMF) glass, the viscosity around the liquidus temperature is much lower and is included in the range from 10^{-2} to 10^{-1} Pa s.

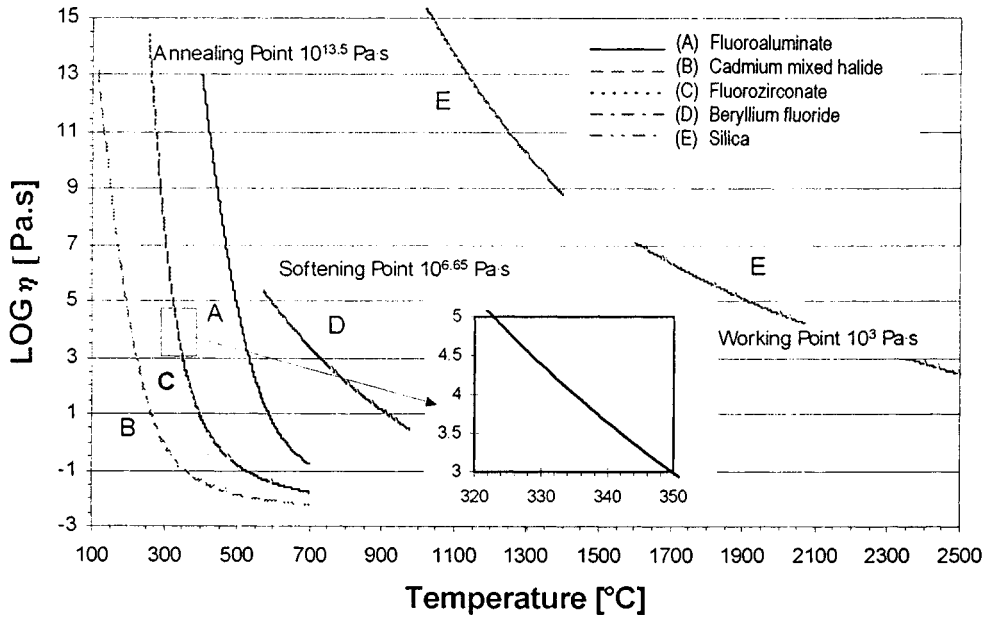


FIGURE 1 Viscosity versus temperature of some halide glass systems compared with silica glass. The viscosity curves have been obtained using the following references: cadmium mixed halide glass [34], fluoroaluminate [19], fluorozirconate [19], beryllium fluoride [37], silica glass [38].

In TABLE 2 the equations used for the curve reported in FIGURE 1 are summarised.

TABLE 2 Viscosity (poise)-temperature equations for different glass systems (1 Pa s = 10 poise).

Glass composition	Equation	Ref
BeF_2	$\eta = 7.603\times10^{-9}\exp\left[\left(52590/RT\right)+\left(1.471\times10^{6}/T^{2}\right)\right]$ (574-979 °C)	[37]
SiO_2	$\log\eta = -6.24+\left(2.69\times10^{4}\right)/T$ (1600-2500 °C) $\log\eta = -12.5+\left(3.73\times10^{4}\right)/T$ (1000-1400 °C)	[38]
$56.5ZrF_4$-$15BaF_2$-$5LaF_3$ $3.5AlF_3$-$20NaF$ (mol %)	$\log\eta = -1.74+388.7\times2/\left[(T-588.3)+\left((T-588.3)^2+4\times3.6\times T\right)^{1/2}\right]$	[19]
$40AlF_3$-$10BaF_2$-$30CaF_2$ $10SrF_2$-$10MgF_2$-$15YF_3$ (mol %)	$\log\eta = -1.54+318.3\times2/\left[(T-818.0)+\left((T-818.0)^2+4\times4.9\times T\right)^{1/2}\right]$	[19]
50 Cd-34 Na-13 Ba-3 K (cat.%) F/(F+Cl) = 59.5%	$\log\eta = -2.679+218.6\times2/\left[(T-527.4)+\left((T-527.4)^2+4\times5555\times T\right)^{1/2}\right]$	[35]

The viscosity of fluorozirconate glass was studied by Hu and Mackenzie [32] in the temperature range from 550 to 950°C. In particular the effect of the composition on glass made of 60 mol % ZrF_4 - 30% BaF_2 - 10% MF_n where MF_n = LiF - NaF - CaF_2 - BaF_2 - ZnF_2 - PbF_2 - AlF_3 - YF_3, LaF_3 or ThF_4 was evaluated.

Generally the divalent fluoride additions decrease the viscosity, while trivalent and tetravalent fluorides have the opposite effect. In any case, the additions change the viscosity values no more than one order of magnitude.

E RHEOLOGICAL PROPERTIES

Rheology was defined by Bingham (1929) as the study of deformation and flow of matter. "Real substances exhibit a wide range of different rheological behaviours, which can be accommodated between the two extremes settled by the linear models of Newton and Hooke" [33].

Glass is a viscoelastic material and if it were completely elastic it would follow Hooke's law where there is proportionality between stress and deformation, while if it were ideally viscous it would follow Newton's law where there is proportionality between the shear stress and shear rate. Components of the two ideals can be represented with a spring (elasticity) and with a damper (viscosity).

Models more or less complicated can be constructed using these components to describe the behaviour of the material. Therefore it becomes important to know if the viscosity depends only on the temperature or on the shear rate as well.

In 1990 Tick and Bocko [34] wrote that HMFGs are Newtonian fluids; before Tick, only Yano et al [35], making measurements on ZBLAN and ZBLALi, observed that above 600°C viscosity curves perfectly overlapped, while in the range below 600°C the profiles were dependent on the shear rate. In order to explain this behaviour, they made two hypotheses, the first one being that some fine crystallites could be present in the melt and the second one considering the effect of some polymer-like or clustered species based on the ZrF_n polyhedron. Up to now nobody has confirmed the same behaviour for the same glass system at this temperature, but another rheological study on fluorozirconate glass with a high

content of PbF_2 (>8 mol %) was performed in the viscosity range $10^{4.5}$ - 10^{10} Pa s, using an oscillating parallel plate and a penetration method [36]. FIGURE 2 shows viscosity versus oscillating frequency measured at three different temperatures in the working range for a glass having the following composition: 52.2 mol % ZrF_4 - 20.4 BaF_2 - 4.1 LaF_3 - 3.1 AlF_3 - 2.0 YF_3 - 10 LiF - 8.2 PbF_2 - 500 ppmw PrF_3 (ZBLAYLiPb). It can be seen that in the working range the non-Newtonian behaviour is more pronounced at higher temperatures.

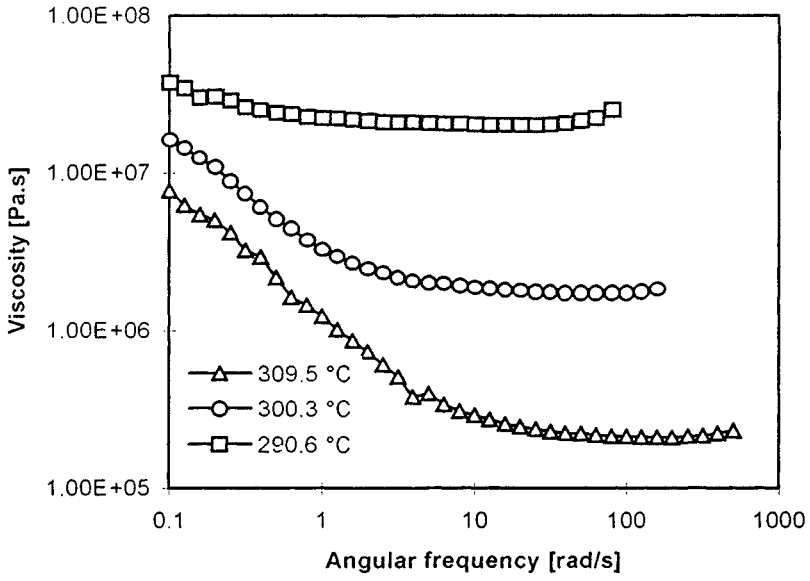


FIGURE 2 Frequency sweep test of fluoride glass (ZBLAYLiPb) at three different temperatures [37].

Another case of non-Newtonian behaviour in halide glass was observed by Naftaly et al [12] in a cadmium mixed halide melt. FIGURE 3 shows the viscosity values measured using the rotating cylinder method at different rotating speeds. Fluoroaluminate glass melt examined in the same work shows instead a near-Newtonian behaviour.

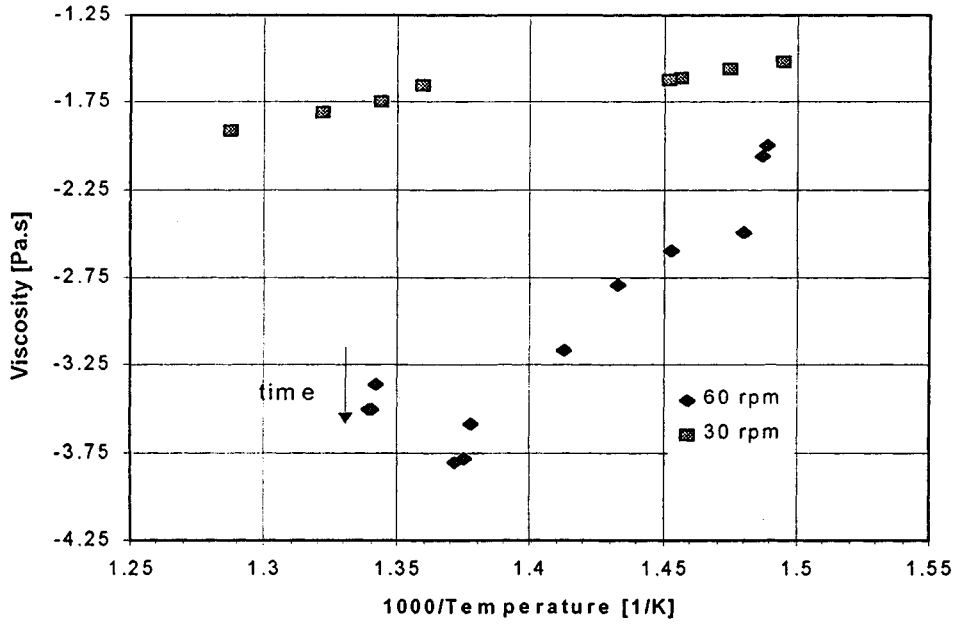


FIGURE 3 Viscosity values of cadmium mixed halide at different rotating speed [12].

The non-Newtonian behaviour, where the viscosity decreases with increasing shear rate at a fixed temperature, can be helpful for drawing fibres. As the drawing speed is raised, the viscosity decreases, and therefore the process temperature and the time spent by the glass in the hot zone of the drawing tower can be reduced. In this way it is possible to reduce the crystallisation, obtaining higher quality optical fibres.

Nevertheless it should be remembered that the fibre drawing process deals with an elongational flow situation rather than an oscillating shear stress, even if the two types of viscosity are usually strictly correlated. Extensional rheometer measurements could be more useful for the drawing process, but up to now as far as we know no publication has been reported on this topic.

REFERENCES

[1] E.H. Fontana [*Am. Ceram. Soc. Bull. (USA)* vol.49 no.6 (1970) p.594]

[2] A.K. Varshneya, N.H. Burlingame, W. Schulze [*Glastech. Ber. (Germany)* vol.63K (1990) p.447-59]

[3] S.V. Nemilov, G.T. Petrowskii [*J. Appl. Chem. (USSR)* vol.36 no.1 (1963) p.208-10]

[4] R. Brueckner, D. Demharter [*Glastech. Ber. (Germany)* vol.48 (1975) p.12]

[5] H. Hagy [*J. Am. Ceram. Soc.(USA)* vol.46 (1963) p.93]

[6] A. Dietzel, R. Brueckner [*Glastech. Ber. (Germany)* vol.28 (1955) p.455]

[7] H. Rawson [in *Properties and Applications of Glass* (Elsevier, Amsterdam, 1980) p.44]

[8] D.K. Doolittle [*J. Appl. Phys. (USA)* vol.22 (1951) p.471]

[9] S. Glasstone, K.J. Laidler, H. Eyring [in *The Theory of Rate Processes* (McGraw Hill, 1941) p.486]

[10] M.H Cohen, G.S. Grest [*Phys. Rev. B (USA)* vol.20 no.3 (1979) p.1077]

[11] S.N. Crichton, R. Mossadegh, C.T. Moynihan [*Mater. Sci. Forum (Switzerland)* vol.19-20 (1987) p.435]

[12] M. Naftaly, A. Jha, E.R. Taylor, K.C. Mills [*J. Non-Cryst. Solids (Netherlands)* vol.213&214 (1997) p.106-12]

[13] H. Vogel [*Phys. Z. (Germany)* vol.22 (1921) p.645]

[14] G.S. Fulcher [*J. Am. Ceram. Soc. (USA)* vol.6 (1925) p.339]

[15] G. Tamman, W. Hesse [*Z. Anorg. Allg. Chem. (Germany)* vol.156 (1926) p.245-7]

[16] M. Koide, K. Matusita, T. Kamatsu [*J. Non-Cryst. Solids (Netherlands)* vol.125 (1990) p.93]

[17] P.B. Macedo, T.A. Litovitz *[J. Chem. Phys. (USA)* vol.42 (1965) p.245]

[18] K. Matusita, M. Koide, T. Komatsu [*J. Non-Cryst. Solids (Netherlands)* vol.140 (1992) p.119-22]

[19] A. Jha, J.M. Parker [*Phys. Chem. Glasses (UK)* vol.30 no.6 (1989) p.220]

[20] D.C Tran, R.J. Ginther, G.H. Sigel [*Mater. Res. Bull. (USA)* vol.17 (1982) p.1177-84]

[21] J.E. Shelby, C.G. Pantano, A.A. Tesar [*J. Am. Ceram. Soc. (USA)* vol.67 (Aug. 1984) p.164-5]

[22] P. Baniel, C. Jacoboni, U. Unrau [*Mater. Sci. Forum (Switzerland)* vol.32-33 (1988) p.601-6]

[23] W.C. Hasz, J.H. Whang, C.T. Moynihan [*J. Non-Cryst. Solids (Netherlands)* vol.161 (1993) p.127-32]

[24] K. Matusita, H. Yamamoto, T. Sudo, T. Komatsu [*Mater. Sci. Forum (Switzerland)* vol.32-33 (1988) p.185-90]

[25] F. Lin, H. Zhang, H. Hu, F. Gan [*Mater. Sci. Forum (Switzerland)* vol.32-33 (1988) p.595-600]

[26] E. Shelby, J.C. Lapp, M.J. Suscavage [*J. Appl. Phys. (USA)* vol.59 no.10 (1986) p.3412-6]

[27] S. Christensen, J. Lucas, S.N. Crichton, C.T. Moynihan [*Mater. Sci. Forum (Switzerland)* vol.32-33 (1988) p.607-10]

[28] F. Bartholomew, A.L. Sadd, P.A. Tick [*J. Non-Cryst. Solids (Netherlands)* vol.203 (1996) p.364-8]
[29] J.D. Mackenzie [*J. Chem. Phys. (USA)* vol.32 no.5 (1960) p.1150-2]
[30] C.T. Moynihan, S. Cantor [*J. Chem. Phys. (USA)* vol.48 (1968) p.114]
[31] G.T. Petrovskij [*Zh. Neorg. Khim.(USSR)* vol.12 (1967) p.485]
[32] H. Hu, J.D. Mackenzie [*J. Non-Cryst. Solids (Netherlands)* vol.54 (1983) p.183]
[33] R. Lapasin, S. Pricl [*Rheology of Industrial Polysaccharides. Theory and Applications* (Blackie Academic & Professional, 1995)]
[34] A. Tick, P.L. Bocko [in *Optical Materials* vol.1 Ed. S. Musikant (Marcel Dekker, Inc., 1990) p.235]
[35] T. Yano, S. Inoue, H. Kawazoe, M. Yamane [*Mater. Sci. Forum (Switzerland)* vol.32-33 (1988) p.583-8]
[36] M. Braglia et al [*J. Non-Cryst. Solids (Netherlands)* vol.213&214 (1997) p.325-9]
[37] S. Cantor, W.T. Ward, C.T. Moynihan [*J. Chem. Phys. (USA)* vol.50 no.7 (1969) p.2874-9]
[38] N.P. Bansal, R.H. Doremus [*Handbook of Glass Properties* (Academic Press, Inc., 1986) p.14]

C2.3 Elastic moduli of halide glass

A. Jha

October 1997

A INTRODUCTION

The elastic modulus is one of the most fundamental properties of glassy materials for determining their suitability in a range of engineering applications including fibre optics. It is determined from the linear part of the stress-strain curve, which follows Hooke's law. The SI unit of elastic modulus is giga Pascal (GPa), and like the heat or enthalpy of formation of a compound reflects the bond strength of the material. The elastic modulus is also known as the Young's modulus. The higher the value of elastic modulus, the stronger the interatomic or inter-ionic bond strength is. For example, the elastic modulus of fused silica, which has a much stronger bond than the fluoride glasses, is approximately 70 GPa compared to less than 60 GPa for fluorozirconate glasses. The glass transition temperature (T_g) of a glass is found to rise in proportion to the elastic modulus. Since the bond strength determines the interatomic or ionic spacing and the phonon vibrations, the fundamental lattice vibration frequency also increases in proportion to the elastic modulus. Other properties such as the acoustic wave velocity and thermal properties are similarly affected. Bulk (K) and shear moduli (G) are dependent on the Young's modulus (E) via EQNS (1) and (2):

$$K = \frac{E}{3(1-2\nu)} \tag{1}$$

$$G = \frac{E}{2(1+\nu)} \tag{2}$$

where ν is the Poisson ratio.

B METHODS

The value of Young's modulus of glassy material can be determined from one of the mechanical testing techniques: the tensile, three-point and four-point bend tests. Besides these conventional destructive methods for determining the Young's modulus, other methods are indentation and acoustic velocity measurement techniques. The latter is a non-destructive method whereas in the indentation method, from the load used for making an indentation and from its geometry, the elastic modulus is calculated [1]. The elastic modulus can also be determined from the rheometric measurement technique together with the viscosity data and shear modulus at a given temperature [2].

The modulus of elasticity of a glassy material can also be estimated using Makashima and Mackenzie's model based on the Madelung constant and dissociation energy [3]. Recently Matecki and Lucas [4] also adopted the Makashima-Mackenzie model and verified its validity for selected fluoride glasses. Using the Makashima-Mackenzie model, the elastic constant can be calculated from EQN (3):

$$E = 2C_M \frac{U}{r^3} \tag{3}$$

where U is the dissociation energy of the lattice or sub-lattice and C_M is called the Madelung constant which can be found out for each component of a halide glass from references [5] and [6].

C VALUES OF MODULI

A large number of elastic moduli data are available within the fluorozirconate system. Most fluorozirconate glasses based on the compositional variations of the ZrF_4-$BaF_2LaF_3AlF_3$-NaF (ZBLAN) system have 50 - 60 GPa, 15 - 24 GPa and 40 - 50 GPa Young's, shear and bulk moduli respectively. The corresponding Poisson's ratios vary between 0.28 and 0.30.

Delben and co-workers [7] measured the velocity of acoustic waves and derived the values of three moduli for each composition in the system 57 ZrF_4 - (28.1-x) BaF_2 - 3.3 LaF_3 - 5 AlF_3 - (6.6+x) NaF ($0 \leq x \leq 13.4$). The authors also measured the Vickers hardness systematically for compositions with 11.6 mol % NaF. The hardness variation with load was established for glasses treated in three different atmospheric and polishing conditions. For the samples prepared inside a dry glove box, the values were found to vary non-linearly between 140 kg mm^{-2} and 210 kg mm^{-2} for corresponding loads of 26 g and 125 g. The reported error in the measurement was ± 10 kg mm^{-2}. The second condition was the exposure of glass samples in an atmosphere of 50% relative humidity for two days. The hardness was measured and found to be similar to the values obtained for the dry glove box samples. The third condition was the samples from the second condition polished down to 0.25 μm. On an average a 10% drop in hardness at smaller loads after polishing was observed compared to previous measurements.

TABLE 1 Elastic constants E (GPa), G (GPa), K (GPa), ν, average acoustic shear wave velocity (V, km s^{-1}) and microhardness (kg mm^{-2}) of ZBLAN glasses with varying NaF molar concentrations.

NaF (%)	E ± 2	G ± 1	K ± 3	V_m ± 0.06	ν	H_v ± 10
7.6	53.3	20.5	44.2	2.400	0.299	-
8.6	51.2	19.9	40.0	2.361	0.286	213
9.6	53.7	20.7	43.6	2.420	0.290	195
10.6	54.2	21.8	46.5	2.430	0.310	208
11.6	54.3	21.0	43.3	2.443	0.290	180
16.6	55.0	21.7	39.1	2.413	0.270	198
20.0	55.0	21.3	43.8	2.497	0.290	220

Zhao and co-workers [8,9] studied the ZrF_4-BaF_2-AlF_3-RF compositions which were, unlike the compositions used by Delben and co-workers [7], without the addition of LaF_3. The modulus variation as a function of the mixed alkali fluoride (RF: LiF, NaF, KF) compositions was investigated. The effect of alkali substitution was more discernible with KF than when LiF replaced ZrF_4. The tables below summarise the effects of alkali ions and mixed-alkali effects on moduli of fluoride glasses.

Ota and Soga [10] observed than in ZBLAN compositions the elastic modulus decreased with increasing temperature between 180 K and 400 K. The values however rise linearly with increasing pressure up to 200 MPa. The variation with pressure was reported to be consistent with the close-packed structure of fluoride glasses.

Matecki and Lucas [4] computed elastic moduli of three different types of fluoride glasses using the Makashima-Mackenzie model. The computed and measured results are compared in TABLE 5. Based on the model approach, Jordery and co-workers [11] estimated and compared the Young's modulus of a cadmium mixed halide glass. The investigators noted that the measurement could have been affected by sensitivity to moisture which has been known to affect the measurement for ZBLAN glasses [7].

TABLE 2 Elastic moduli of some (60-x) ZrF_4 - 10 AlF_3 - 30 BaF_2 - x RF glasses [8].

RF concentration (mol %)	Shear modulus G (GPa)	Young's modulus E (GPa)	Bulk modulus K (GPa)
Glass compositions with LiF			
10	23.2	60.0	48.2
20	22.9	59.4	48.2
30	22.1	57.2	46.9
Glass compositions with NaF			
10	22.0	57.4	49.3
15	21.1	54.8	45.3
20	20.8	54.0	45.1
30	19.5	50.8	43.1
Glass compositions with KF			
10	20.5	53.1	42.6
15	18.8	49.0	41.8
20	17.7	46.3	40.6

TABLE 3 Densities (d, g cm^{-3}), atomic volumes (V_m, cm^3/g-atom), acoustic velocity (km s^{-1}) and elastic moduli (GPa) of 48 ZrF_4 - 24 BaF_2 - 8 AlF_3 - 20 RF glasses [9]. v_l and v_s are the longitudinal and shear acoustic velocities (m s^{-1}).

RF, mol % LiF:NaF	Structural		Acoustic velocity		Moduli			
	d	V_m	v_l	v_s	ν	G	E	K
20:0	4.285	8.159	4.278	2.309	0.2945	22.9	59.4	48.2
15:5	4.288	8.202	4.295	2.321	0.2937	23.1	59.8	48.3
10:10	4.283	8.260	4.261	2.288	0.2974	22.4	58.2	47.9
5:15	4.276	8.323	4.178	2.306	0.2993	21.4	55.5	46.1
0:20	4.260	8.403	4.133	2.207	0.3005	20.8	54.0	45.1

RF, mol % NaF:KF	Structural		Acoustic velocity		Moduli			
	d	V_m	v_l	v_s	ν	G	E	K
20:0	4.260	8.403	4.133	2.207	0.3005	20.8	54.0	45.1
15:5	4.240	8.492	4.146	2.213	0.3008	20.8	54.0	45.2
10:10	4.210	8.603	4.063	2.140	0.3080	19.4	50.9	44.1
5:15	4.176	8.723	4.055	2.132	0.3090	19.0	49.7	43.4
0:20	4.148	8.832	3.957	2.077	0.3098	17.7	46.3	40.6

RF, mol % LiF:NaF	Structural		Acoustic velocity		Moduli			
	d	V_m	v_l	v_s	ν	G	E	K
30:0	4.190	7.981	4.276	2.294	0.2968	22.1	57.2	46.9
25:5	4.202	8.011	4.268	2.284	0.2994	21.9	57.0	47.3
20:10	4.211	8.046	4.281	2.294	0.2986	22.2	57.6	47.7
15:15	4.213	8.095	4.254	2.269	0.3012	21.7	56.4	47.3
10:20	4.204	8.165	4.205	2.250	0.2994	21.3	55.3	46.0
5:25	4.185	8.261	4.225	2.238	0.3050	21.0	54.8	46.8
0:30	4.180	8.320	4.067	2.160	0.3035	19.5	50.8	43.1

TABLE 4 Temperature and pressure dependence of elastic moduli and sound wave velocities [10]. Glass composition (mol %) was 58.3 ZrF_4, 18.4 BaF_2, 14.6 LaF_3, 5.8 NaF and 2.9 AlF_3. Debye temperature θ_D = 316 K.

Temperature dependence	Pressure dependence
$dv_l/dT = -7.98 \times 10^{-4}$ km s^{-1} K^{-1}	$dv_l/dP = 1.672 \times 10^{-1}$ km s^{-1} GPa^{-1}
$dv_s/dT = -4.22 \times 10^{-4}$ km s^{-1} K^{-1}	$dv_s/dP = 3.777 \times 10^{-2}$ km s^{-1} GPa^{-1}
$dK/dT = -2.00 \times 10^{-2}$ GPa K^{-1}	dK/dP = 6.3
$dG/dT = -9.25 \times 10^{-3}$ GPa K^{-1}	dG/dP = 1.2
$dE/dT = -2.41 \times 10^{-2}$ GPa K^{-1}	dE/dP = 3.7

TABLE 5 Comparison of calculated and experimental values of elastic moduli of selected halide glasses. Values in brackets are experimental data.

Glass composition (mol %)	K (GPa)	G (GPa)	E (GPa)	μ
ZrF_4-BaF_2-LaF_3-AlF_3-NaF	40.7 (47.7)	23.4 (20.5)	58.9 (53.8)	0.259 (0.310)
ZrF_4-ThF_4-LaF_3	43.3	25.3	63.5	0.255
BaF_2-InF_3-GaF_3-ZnF_2-ZrF_4-YF_3-ThF_4	30.0	19.1	47.3	0.237
50 CdF_2, 10 $BaCl_2$, 40 NaCl	-	-	38.0 (31.0)	-

Finally the elastic moduli and the glass transition temperatures for different families of glasses are connected in the same way as the melting points of crystalline solids and their elastic moduli. Crystalline solids with high melting point have a proportionately higher value of elastic modulus. In glasses, for example, the high T_g of silica glass (~1473 K) indirectly reflects the bond strength and therefore the elastic modulus (70 GPa), compared to halide glasses whose transition temperatures are lower than 573 K (E < 55 GPa).

REFERENCES

[1] B.R. Lawn, A.G. Evans, D.B. Marshall [*J. Am. Ceram. Soc. (USA)* vol.63 (1980) p.574]

[2] M. Braglia et al [*J. Non-Cryst. Solids (Netherlands)* vol.213&214 (1997) p.326]

[3] A. Makashima, J.D. Mackenzie [*J. Non-Cryst. Solids (Netherlands)* vol.12 (1973) p.35-45]

[4] M. Matecki, J. Lucas [*Mater. Res. Bull. (USA)* vol.29 no.5 (1994) p.473-7]

[5] O. Knacke, O. Kubaschewski, K. Hesselmann [in *Thermochemical Properties of Inorganic Substances* (Springer Verlag, 1991)]

[6] O. Kubaschewski, C.B. Alcock [in *Metallurgical Thermochemistry* 5th edition (Pergamon Press, 1979) p.270-85]

[7] A. Delben, Y. Messaddeq, M.D. Caridade, M.A. Aegerter, J.A. Eiras [*J. Non-Cryst. Solids (Netherlands)* vol.161 (1993) p.166]

[8] X. Zhao, S. Sakka [*J. Non-Cryst. Solids (Netherlands)* vol.99 (1988) p.54]

[9] X. Zhao, H. Kozuka, S. Sakka [*J. Mater. Sci. (UK)* vol.22 (1987) p.4104]

[10] R. Ota, N. Soga [*J. Non-Cryst. Solids (Netherlands)* vol.56 (1983) p.105-10]

[11] S. Jordery, M. Naftaly, A. Jha [*J. Non-Cryst. Solids (Netherlands)* vol.196 (1996) p.199]

C2.4 Stability of halide glass

A. Jha

October 1997

A INTRODUCTION

The definition of the stability of a halide glass includes mainly three aspects which are defined as the thermal, environmental and mechanical, and radiation stabilities. The radiation stability is also referred to as the radiation hardness of a glass. The thermal stability defines the thermodynamic stability of a glassy phase up to the temperature above which the crystalline phase becomes stable, i.e. the temperature at which devitrification begins. Most glasses have a tendency to devitrify above the glass transition temperature (T_g), and the temperature at which the rate of crystal formation becomes discernible and measurable, say for example by using a differential scanning calorimetric (DSC) technique, is called the onset of crystallisation, T_x. The temperature range between T_g and T_x may therefore be used as a guide to define the thermal stability of a glass. The environmental and mechanical stability is usually defined by the chemical and mechanical durability of a glass in a specified service condition, whereas the radiation resistance or stability is the resistance against the damage of the glass structure by high-energy rays and particles. This Datareview compares the thermal and environmental stability of halide glasses and only introduces the types of defect formed when fluoride glasses are exposed to a source of high-energy radiation or particles.

B DEFINITION OF THERMAL STABILITY AND THE MEASURED DATA FOR HALIDE GLASSES

The thermal stability range (ΔT) is defined as the difference between T_x and T_g, i.e. $T_x - T_g$. The larger the differential ΔT, the more stable the glass is considered to be. The ΔT stability parameter is by far the most widely used for halide and non-oxide glasses [1]. Hruby [2] defined the glass stability by combining two different types of characteristic temperature differential: $T_m - T_x$ and $T_x - T_g$, where T_m is the onset of melting of a glass on heating and usually succeeds crystallisation. The Hruby stability parameter, H_r, is defined as the ratio of the two differentials, i.e. $(T_x - T_g)/(T_m - T_x)$. By examining the characteristic temperatures from the DSC, Saad and Poulain [3] defined the 'S' stability parameter, which is expressed as $[(T_x - T_g)(T_p - T_x)/T_g]$. The unit of S is °C. T_p is the peak crystallisation temperature as defined in Datareview C2.1. In the literature, there are other types of stability parameters defined on the basis of the characteristic temperature, and these are excluded from this Datareview. However, the definition of thermal stability, based on the kinetics of phase transformation, is discussed below.

The thermal stability of a halide glass can be rigorously defined by using the equation for the kinetics of phase transformation [4], in which the volume fraction of crystals formed, X, is dependent on time t (s), and the rate constant k (s^{-1}) via the Johnson-Mehl-Avrami (JMA) equation [4]: $-\ln(1 - X) = (kt)^n$. The rate constant k is a temperature dependent quantity and can be expressed in the Arrhenian form, i.e. $k = A_o \exp(-Q/RT)$, where R (J mol^{-1} K^{-1}) and T (K) are the universal gas constant and temperature respectively, and A_o is the pre-exponential expressed in per second units. The JMA equation combined with the equations for nucleation and simultaneous crystal growth [5] yield a time-temperature-transformation (t-t-t) relationship, which is extremely useful in quantitatively estimating the stability of a halide glass against crystallisation and devitrification. The tangent to the nose of the t-t-t curve determines the critical cooling rate (CCR, q^o, s^{-1}) required for a glass-forming liquid to form a glassy phase with a known volume fraction, X, of a crystalline phase. The t-t-t curves can be determined experimentally and q^o estimated from the tangent. The smaller the value of q^o, the greater is the thermal

stability of a glass against devitrification during reheating and crystallisation while quenching. In TABLE 1, the stability parameters of a range of halide glasses are compared.

TABLE 1 A comparison of glass stability parameters for halide glasses. The error in Q has been estimated on the basis of the comparison of the data in the literature.

Glass type	ΔT, K	H_r	S, °C	q^o, min^{-1}	Q ± 10, kJ mol^{-1}	Ref
ZBL	92	-	-	-	302 - 315	[6]
ZBLAN	91	-	-	10	195	[7,8]
ZBLALi	114	-	-	-	190	[6,8]
ZBLALiPb	100	-	-	-	174	[6]
ZBLYIN	84	0.8	4.1	30	165	[8]
ZBLYINC	92	1.1	6.6	24	160	[8]
ZBLYINC(3.4)	103	1.4	7.9	8	170	[8]
InF_3-1	89	0.4	4.3	-	145	[7]
InF_3-2	119	0.7	2.9	-	250	[7]
Cd1	51	0.3	1.0	-	145	[7]
Cd2	68	0.3	1.2	-	150	[7]
Cd3	63	0.3	1.0	-	155	[7]

ZBL: 62 ZrF_4, 33 BaF_2, 5 LaF_3.
ZBLAN: 52 ZrF_4, 20 BaF_2, 4 LaF_3, 4 AlF_3, 20 NaF.
ZBLALi: 52 ZrF_4, 20 BaF_2, 4 LaF_3, 4 AlF_3, 20 LiF.
ZBLALiPb: 49.83 ZrF_4, 16.96 BaF_2, 5.06 LaF_3, 3.16 AlF_3, 20.09 NaF, 4.09 PbF_2.
Other fluorozirconate compositions have already been described in Datareview C2.1.
Cd1: 50 CdF_2, 15 BaF_2, 10 NaF, 10 $BaCl_2$, 15 NaCl.
Cd2: 40 CdF_2, 15 BaF_2, 10 NaF, 8 $BaCl_2$, 13 $NaCl_2$, 5 P_2O_5.
Cd3: 50 CdF_2, 15 BaF_2, 10 Na, 8 NaCl, 7 P_2O_5.
InF_3-1:36 InF_3, 20 ZnF_2, 15 BaF_2, 20 SrF_2, 5 CaF_2, 2 GaF_3, 2 PbF_2.
InF_3-2: 34 InF_3, 20 ZnF_2, 15 BaF_2, 20 SrF_2, 5 CaF_2, 6 GaF_3.

Most of the fluorozirconate family of glasses have a comparable value of the measured apparent activation energy, except for ZBLA and ZBL. While investigating the thermal stability of a halide glass, the range of temperature over which the glassy phase devitrifies is a highly significant parameter for designing defect-free fibre and planar waveguides. The crystallisation range can be readily determined from the dX/dt versus t relationship from the exothermic peak in the DSC. The compositions ZBLAN, ZBLALi, ZBLALiPb and ZBLYINC(3.4) are more stable than others. Janke and Frischat [9] reported that the stability of ZBLAN compositions is also affected by the incorporation of $PtCl_2$ and AgF. In the case of AgF-incorporated glass with compositions ranging between 0.01 and 0.1 mol %, the value of q^o increases from 550 K min^{-1} to 1700 K min^{-1}. The effect of $PtCl_2$ addition on q^o was less dramatic. For a similar composition range of $PtCl_2$, q^o varied between 600 and 1000 K min^{-1}. It is therefore apparent that the minute additions of AgF and $PtCl_2$ have a pronounced effect in reducing the thermal stability of a ZBLAN glass. Mitachi and Tick [10] measured the effect of oxygen addition on the critical cooling rates of ZBLA, HBLA, CLAP and BCYA glasses. Except in ZBLA, the critical cooling rate first decreased with increasing concentrations of oxygen dissolved in the glass and then increased sharply with further increase in oxygen. The observations made in ZBLA showed that the increase in q^o was proportional to the oxygen dissolved in the melt. Rigout et al [11] designed BaF_2-InF_3-GaF_3 (BIG) glasses with less than 15 mol % of ZrF_4 and ThF_4. The glass stability changed with the substitution of InF_3 by KF and NaF, and BaF_2 by AlF_3. The values of H_r were found to change between 0.79 and 1.08.

Shahriari et al [12] and Iqbal et al [13] reported the effects of ErF_3, NdF_3 and PrF_3 on the stability of a fluoroaluminate glass described in Table 3 in Datareview C2.1. The H_r stability parameter was found to vary in the range 0.85 to 1.7, and the measured apparent activation energy for crystallisation was

found to range between 80 kJ and 190 kJ per mole; the lower value of Q corresponded to increasing concentrations of rare-earth fluorides in the glass.

Devitrification characteristics of indium and gallium fluoride based glasses were investigated by Messaddeq et al [14] and Soufiane et al [15]. They reported that for glasses richer in ZnF_2 (20 - 40 mol %), the values of Q range between 135 kJ per mole and 110 kJ per mole, which can be significantly altered with the addition of CaF_2, MgF_2, GdF_3 and PbF_2. For multicomponent indium fluoride glasses, the values of Q range between 210 and 240 kJ per mole. For most GaF_3-containing glasses, the values of Q are found to be typically 5 - 10% larger than for InF_3-based glasses.

The cadmium mixed halide family of glasses was designed by Matecki and Poulain [16]. By measuring the characteristic temperatures as a function of the impurity content, Jordery et al [17] empirically determined the stability of the cadmium mixed halide glasses. Amongst common impurities, OH^{-1} and $(SO_4)^2$ were found to be the most relevant; the former stabilises the glass whereas the latter promotes devitrification. Jordery [18] demonstrated that the stability of cadmium mixed halide is also dependent on the concentration of Pr^{3+} ions in the glass. T_g, T_x and T_p listed below are dependent on the concentrations of PrF_3 in the mixed halide glass of composition 50 (mol %) CdF_2, 10 $BaCl_2$, 30 NaCl and 10 BaF_2. The values of T_m were not found to change significantly.

TABLE 2 Effect of PrF_3 concentration on the characteristic temperatures and ΔT values of CdF_2-based mixed halide glasses [18].

PrF_3, ppmw	T_g, K	T_x, K	T_p, K	ΔT, K
0	409	502	530	93
500	403	476	480	73
1000	403	475	478	72
2000	403	475	478	72
2500	403	475	477	72

Glass compositions based on AgX (X: Cl, I, Br) are sensitive to light and consequently degrade [19]. These glasses also have T_gs above room temperature (310 - 315 K) as indicated in Datareview C2.1. Amongst all known halide glasses, the monovalent AgI based glasses have the lowest thermal stability. In spite of their poor thermal stability, 1 - 2 mm thick glasses can be produced by quenching the melts from 673 K. These glasses can be further stabilised by the addition of smaller anions, say Cl^- instead of I^- ions, and $PbBr_2$ resulting in a larger ΔT gap than in the binary AgI-CsI compositions. The value of T_x rises by nearly 15°C to 95°C in the 55 mol % AgI-33 mol % CsI-12 mol % CsCl compositions compared to a binary composition of 55 mol % AgI-45 mol % CsI glass. The corresponding value of T_g in the binary glass also rises by up to 15°C on partially substituting CsI by CsCl.

C ENVIRONMENTAL DURABILITY

The environmental durability of a halide glass is traditionally defined by its chemical durability. The test procedure for determining the chemical durability is the leach rate experiment described by Simmons and Simmons [20]. Amongst the fluorozirconate family of glasses, the compositions with AlF_3 exhibit the slowest leaching rates in an aqueous environment [20]. It has also been found by Guery et al [21] that the zirconium fluoride glasses with LiF leach at the fastest rate at low pH (<4) and at the slowest rate at high pH (>8). Mitachi and Tick [22] studied the effect of OH^- ion absorption in the CdF_2-LiF-AlF_3-PbF_2 (CLAP) glasses and the molar extinction coefficient (e, 1 mol^{-1} cm^{-1}) was found to be higher than for a typical ZBLA composition. TABLE 3 compares the leach rate data compiled from various references.

TABLE 3 A comparison of the room temperature (298 K) leaching rates (mg cm^{-2} min^{-1}) for halide glasses.

Glass compositions (mol %)	Leach rate (mg cm^{-2} min^{-1})
54 ZrF_4, 15 BaF_2, 6 LaF_3, 4 AlF_3, 21 NaF [20]	6.9
51.8 ZrF_4, 20 BaF_2, 5.3 LaF_3, 3.3 AlF_3, 19.6 LiF [20]	6.0
54 ZrF_4, 15 BaF_2, 6 LaF_3, 4 AlF_3, 21 NaF [20]	10.4
50 CdF_2, 10 $BaCl_2$, 40 NaCl [25]	4020
65 CdF_2, 30 $BaCl_2$, 5 NaCl [25]	2560

The aim of the investigation carried out by Mitachi and Tick was to design an alternative composition that is environmentally more stable than the mixed halide family of glasses reported by Poulain et al [23] and Matecki et al [24]. The mixed halide glasses exhibit a much faster leaching rate than CLAP glasses because of the presence of Cl^{-1} ions. The measured difference between the leaching rates of fluorozirconate and cadmium mixed halide glasses is three orders of magnitude.

D RADIATION RESISTANCE OF HALIDE GLASSES

Like most crystalline solids, high-energy radiation or particles cause structural damage to the glass. The type of damage in the glassy material is dependent on the incident energy. When the incident energy exceeds the energy for the optical bandgap, a significant proportion of the incident energy is transferred to the valence electrons causing some of them to excite to the conduction band. Most of the excited free-electrons thermalise readily, but some remain trapped by escaping recombination. These carriers could form paramagnetic defect centres provided the electronic spin remains unpaired. The energy of the incident beam can also displace ions from their metastable equilibrium sites in the quenched glass to sites which could be more metastable than the as-quenched sites. Such defects are termed Frenkel defects. A particular type of radiation-induced trapping site is also observed in glasses when ions are displaced by means of a mechanism actuated by the electron-hole recombination process. Such a mechanism is called the radiolytic process. A much more extended article on this subject has been recently written by Griscom and Friebele [26], who have compared the results on fluorozirconate and fluorohafnate glasses published by various authors.

The radiation damage technique can also be employed for designing waveguides but to date no successful commercial device exists. The radiation-hard fluorohafnate glasses have also been proposed for use in a high-energy particle detector [27].

REFERENCES

[1] P.W. France, S.F. Carter, M.W. Moore, C.R. Day [*Br. Telecom Technol. J. (UK)* vol.5 (1987) p.28]
[2] A. Hruby [*Czech. J. Phys. B (Czechoslovakia)* vol.32 (1972) p.1187]
[3] M. Saad, M. Poulain [*Mater. Sci. Forum (Switzerland)* vol.19-20 (1987) p.12]
[4] M. Avrami [*J. Chem. Phys. (USA)* vol.7 (1939) p.1103-12 and vol.8 (1940) p.212-24]
[5] A. Jha [*J. Non-Cryst. Solids (Netherlands)* vol.134 (1991) p.157-68]
[6] N.P. Bansal et al [*J. Non-Cryst. Solids (Netherlands)* vol.70 (1985) p.379-96]
[7] M.D. Baro et al [*Mater. Sci. Eng. A (Switzerland)* vol.179/180 (1994) p.308]
[8] W.G. Jordan, A. Jha [*J. Therm. Anal. (UK)* vol.42 (1994) p.759-70]
[9] A. Janke, G.H. Frischat [*J. Non-Cryst. Solids (Netherlands)* vol.213&214 (1997) p.369-74]
[10] S. Mitachi, P. Tick [*Mater. Sci. Forum (Switzerland)* vol.32-33 (1988) p.197-202]
[11] N. Rigout, J.L. Adam, J. Lucas [*J. Non-Cryst. Solids (Netherlands)* vol.161 (1993) p.161-4]
[12] M.R. Shahriari et al [*J. Non-Cryst. Solids (Netherlands)* vol.161 (1993) p.77]
[13] T. Iqbal et al [*J. Non-Cryst. Solids (Netherlands)* vol.213&214 (1997) p.406]

[14] Y. Messaddeq et al [*Mater. Sci. Forum (Switzerland)* vol.67&68 (1991) p.251-6]
[15] A. Soufiane [PhD Thesis, University of Rennes-I, France, 1992, p.133-43]
[16] M. Matecki, M. Poulain [*Mater. Sci. Forum (Switzerland)* vol.19-20 (1987) p.45-54]
[17] S. Jordery et al [*J. Non-Cryst. Solids (Netherlands)* vol.184 (1995) p.263]
[18] S. Jordery [PhD Thesis, Brunel University, Uxbridge, UK, 1995, p.51]
[19] J. Hulme et al [*Phys. Chem. Glasses (UK)* vol.30 (1989) p.256]
[20] C.J. Simmons, J.H. Simmons [in *Fluoride Glass Fibre Optics* Eds. I.D. Aggarwal, G. Lu (Academic Press, San Diego, 1991) p.283 and 9]
[21] J. Guery et al [*Phys. Chem. Glasses (UK)* vol.29 (1988) p.30-6]
[22] S. Mitachi, P. Tick [*J. Non-Cryst. Solids (Netherlands)* vol.135 (1991) p.189-97]
[23] M. Poulain et al [*Mater. Res. Bull. (USA)* vol.18 (1983) p.631-6]
[24] M. Matecki et al [*J. Non-Cryst. Solids (Netherlands)* vol.56 (1983) p.81-6]
[25] A.B. Seddon, W.A. Shah [*J. Non-Cryst. Solids (Netherlands)* vol.128 (1991) p.183-90]
[26] D.L. Griscom, E.J. Friebele [in *Fluoride Glass Fibre Optics* Eds. I.D. Aggarwal, G. Lu (Academic Press, San Diego, 1991) p.309-10]
[27] P.R. Hobson et al [*J. Non-Cryst. Solids (Netherlands)* vol.213&214 (1997) p.147-51]

PART C: HALIDE GLASS

CHAPTER C3

RARE-EARTH SPECTROSCOPY

C3.1 Spectroscopy of praseodymium-doped fluoride glass
C3.2 Spectroscopy of erbium-doped halide glass
C3.3 Spectroscopy of holmium-doped halide glass
C3.4 Spectroscopy of thulium-doped halide glass
C3.5 Spectroscopy of neodymium-doped halide glass

C3.1 Spectroscopy of praseodymium-doped fluoride glass

D.W. Hewak

July 1998

A INTRODUCTION

Currently there is immense interest in the application of fluoride glasses doped with praseodymium in 1.3 micron optical fibre amplifiers [1]. A wide range of fluoride and chloride glass compositions have been melted and spectroscopically evaluated for this purpose. Promising candidates such as those based on zirconium or indium fluorides have also been drawn into fibre and, in some cases, amplification has been demonstrated [2,3]. In this Datareview, we review the spectroscopic properties of praseodymium doped fluoride glasses, with particular emphasis on the 1.3 micron transitions, although results will include the entire range of applications.

B ABSORPTION

As with all the lanthanides, the 4f electronic absorptions of praseodymium are well understood in a variety of glasses. The absorption spectrum of Pr^{3+} in a typical halide glass host, ZBLAN glass based on zirconium fluoride, is illustrated in FIGURE 1. As in most glasses, compared to a crystalline host, the absorption bands are broadened and it is not possible to distinguish sharp lines of the spectra. As a result, some overlapping bands such as the ($^3H_6$, $^3F_2$) cannot be separately resolved.

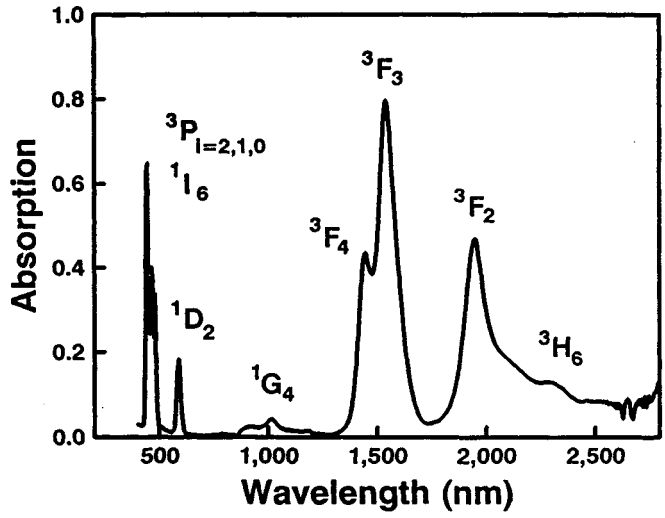


FIGURE 1 Absorption spectra of Pr^{3+} in a typical fluoride glass host.

The spectrum of the absorption bands does not vary significantly from one halide glass host to another, apart from differences in the strength of the absorption which scale with the refractive index. The absorption spectrum is similar to that in oxide-based glasses, but weaker and narrower than that of the chalcogenide glasses. From the absorption spectrum, the absorption cross sections follow through a Judd-Ofelt analysis [4]. This has been performed on many fluoride glasses including the fluorozirconates [5], zinc-cadmium fluorides [6], indium fluorides [7] and mixed-halide [8] glasses. To obtain reliable Judd-Ofelt parameters, the hypersensitive and unresolved transitions of Pr^{3+} are often discarded from the

analysis. Quimby [9] and Hewak [10] have proposed modified Judd-Ofelt techniques which allow all transitions to be considered, thereby improving the accuracy of the procedure when applied to praseodymium.

C FLUORESCENCE

The fluorescence spectra of Pr^{3+} are obtained by pumping with a Ti:sapphire laser tuned to the peak of the $^1G_4$ ground state absorption, a dye laser tuned to the $^1D_2$ level or an argon ion laser pumping into the ^3P manifold, and then analysing the emission on an optical spectrum analyser. FIGURES 2 and 3 provide the fluorescence spectra of Pr^{3+} obtained by pumping at 4976 nm and 1020 nm respectively. Several other typical spectra can be found in [1-8].

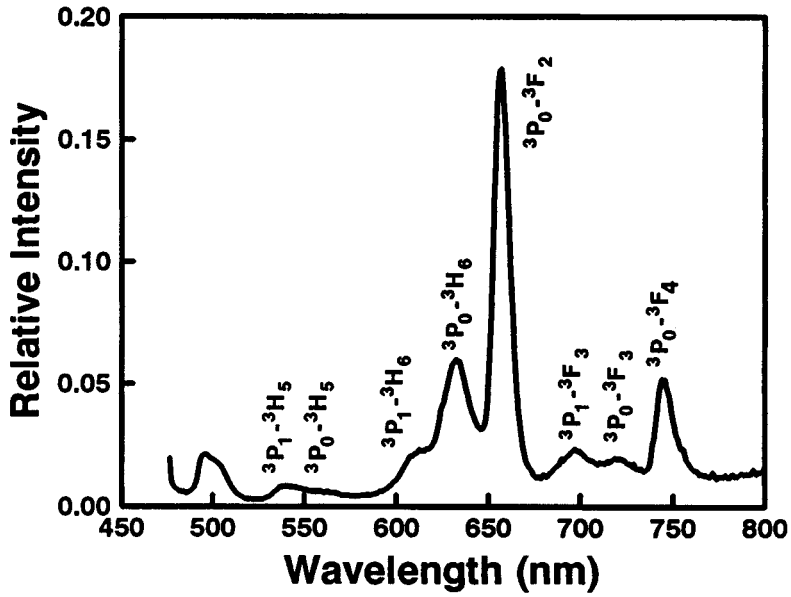


FIGURE 2 Visible emission from Pr^{3+} obtained by excitation at 476.5 nm.

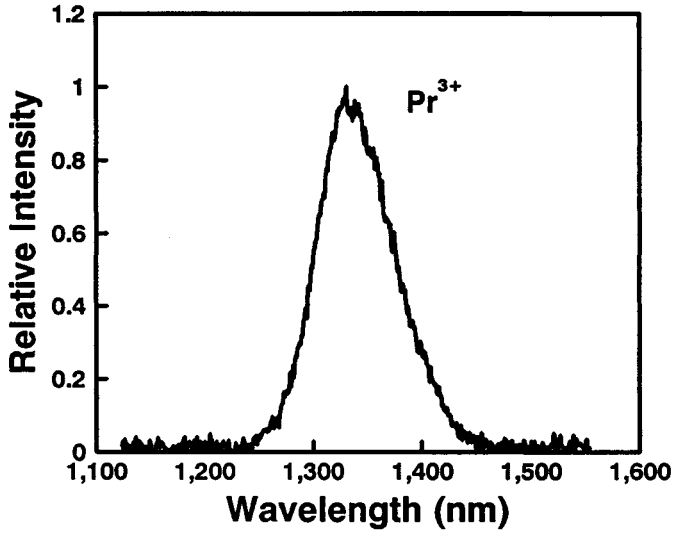


FIGURE 3 1.3 micron emission band obtained by pumping at 1020 nm.

D LIFETIMES

The lifetime of an excited state is a function of the radiative lifetime and all non-radiative decay mechanisms. Non-radiative decay mechanisms include multiphonon decay to a lower energy level and ion-ion interactions, which usually occur above some fixed concentration level. The total lifetime, which is the measured lifetime τ, is given by

$$1/\tau = 1/\tau_{rad} + 1/\tau_{nr} \quad (1)$$

where τ_{rad} and τ_{nr} are the radiative and non-radiative lifetimes respectively. In the absence of any ion-ion interaction, τ_{nr} reduces to the multiphonon lifetime. It is also convenient to state radiative and non-radiative rates, which are the inverse of the lifetimes.

The radiative quantum efficiency of an energy level is the ratio of the measured (total) lifetime to the radiative lifetime; thus for improved amplifier efficiency, long measured lifetimes are sought. Davey [2] has studied a large series of zirconium fluoride based glasses with the aim of optimisation of the $^1G_4$ lifetime for 1.3 micron amplifier applications. Lifetimes varied from 107 μs in ZBLAN glasses to over 240 μs in glasses which incorporated 14 mol % of a chloride. The mixed halide glasses, which contain both fluorides and chlorides of cations, typically including cadmium, initially attracted considerable interest as hosts for Pr^{3+} for this reason. Lifetimes over 320 μs were reported, thus providing predicted quantum efficiencies three times longer than in a pure fluoride glass. However, as the practical difficulties of fibre drawing an unstable, hygroscopic chloride based glass became apparent, interest in these mixed halide glasses evaporated. Today, efforts are concentrated on small improvements to efficiencies using zirconium and indium-based glasses and fibres.

TABLE 1 provides the lifetimes of all energy levels of praseodymium in a fluoride glass host. Lifetimes are measured by exciting the desired level with a chopped pumped beam and detecting the decay of the fluorescence intensity after the pump is switched off.

TABLE 1 Calculated radiative and measured lifetimes for the energy levels of Pr^{3+} in a ZBLAN glass [11].

Energy level	Energy (cm^{-1})	Radiative lifetime (μs)	Total measured lifetime (μs)
$^3P_2$, $^3P_1$, $^3P_0$	20900	37	48
$^1D_2$	17000	241	387
$^1G_4$	9900	2880	129

Lifetimes are concentration dependent and as the Pr^{3+} doping level approaches 500 ppm by weight, ion-ion interactions leading to non-radiative decay are observed.

E NON-RADIATIVE DECAY

In general, the heavy ions and weak ionic bonds of the halide glasses result in a vibrational spectrum consisting of low phonon energies. A consequence of this is that for many transitions completely quenched by non-radiative decay in an oxide host, fluorescence can only be measured when the rare earth is incorporated in a fluoride host. This is certainly the case for the $^1G_4$ level of Pr^{3+}, for which 1.3 micron fluorescence is not observed quenched in a silica host. Even in a fluoride glass, as shown in TABLE 1 above, the total lifetime is dominated by non-radiative decay.

Non-radiative decay rates are estimated from the phonon energy spectrum and the theory of multiphonon decay [12]. For a given host at room temperature, multiphonon decay rates have an exponential dependence

$$W_{mp} = B^* \exp [(-\Delta E + 2hv)\, \alpha] \qquad (2)$$

where α and B^* are experimentally determined parameters which are constant for a given host and independent of the particular rare earth ion.

This method serves only as an approximate guide to non-radiative decay by multiphonon absorption. The maximum phonon energy identified from the Raman spectrum takes into consideration only Raman active vibrational modes and other vibrational modes may not be observed. Further insight into non-radiative properties can be obtained through measurement of the multiphonon edge by transmission or reflection IR spectroscopy or by measurement of the phonon-sidebands [13].

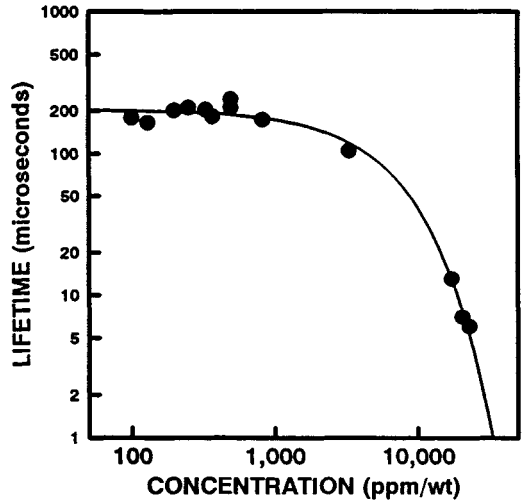


FIGURE 4 Effects of lifetime quenching with increasing Pr^{3+} concentration.

TABLE 2 tabulates the non-radiative decay rates for the $^1G_4$ level in a series of halide glasses. Here the non-radiative lifetime is estimated using EQN (2) and the radiative lifetime from a Judd-Ofelt analysis [4]. The total lifetime is calculated using EQN (1). Measured lifetimes, here the 1/e folding lifetime, are determined from the decay in fluorescence intensity. The measured and calculated quantum efficiencies then follow from the ratios of the measured and calculated total lifetimes to the radiative lifetimes, respectively.

TABLE 2 Multiphonon non-radiative rates for the $^1G_4$ level of Pr^{3+} [1].

Host glass	Maximum phonon energy (cm^{-1})	Non-radiative lifetime (μs)	Radiative lifetime (μs)	Total lifetime (μs)	Measured lifetime (μs)	Quantum efficiency (%)	
						Calculated	Measured
$CdCl_2$	240	3950	2460	1520	80	62	3
$CdCl_2$:CdF_3	370	980	2870	721	322	25	11
CdF_2	270	980	3210	774	184	24	6
InF_3	510	254	5000	255	208	5	4
HfF_4	580	117	2710	106	133	4	5
ZrF_4	580	123	2880	118	129	4	4

It is clear that the non-radiative lifetime increases with decreasing phonon energy, with a corresponding increase in expected quantum efficiency. Measured lifetimes correlate well with total (predicted) lifetimes for the pure fluoride glasses; however as heavier metals (i.e. cadmium) and chlorides are added to the glass compositions, discrepancies result. We attribute the shorter than expected measured lifetimes and thus measured quantum efficiency to additional non-radiative decay mechanisms due to impurities, in particular OH^-. Chlorides are extremely hygroscopic and quenching through OH^- has been quantified [8].

F CONCLUSION

In summary, the spectroscopy of Pr^{3+} in a halide glass host has been reviewed. Key properties including absorption spectra, fluorescence and lifetimes have been described.

REFERENCES

[1] D.W. Hewak et al [*Electron. Lett. (UK)* vol.29 (1993) p.237]

[2] S.T. Davey, D. Szebesta, R. Wyatt, W. Jordan, A. Jha [*Proc. SPIE (USA)* vol.2073 (1993) p.118]

[3] Y. Ohishi, T. Kanamori, T. Nishi, Y. Nishida and S. Takahashi [*Proc. 16th Int. Congress on Glass* Madrid, 1992, vol.2 p.73-8]

[4] M.J. Weber [*J. Chem. Phys. (USA)* vol.48 (1968) p.4774]

[5] J.L. Adam, W.A. Sibley [*J. Non-Cryst. Solids (Netherlands)* vol.76 (1985) p.267]

[6] M.A. Buñel, R. Cases, M.A. Chamarro, R. Alcalá [*Phys. Chem. Glasses (UK)* vol.33 (1992) p.16]

[7] G. Amaranath, S. Buddhudu, F.J. Bryant, L. Xi, B. Yu, S. Huant [*Mater. Res. Bull. (USA)* vol.25 (1990) p.1317]

[8] M.A. Newhouse, R.F. Bartholomew, B.G. Aitken, L.J. Button, N.F. Borrelli [*IEEE Photonics Technol. Lett. (USA)* vol.6 (1994) p.189]

[9] R.S. Quimby, W.J. Miniscalco [*J. Appl. Phys. (USA)* vol.75 (1994) p.613]

[10] J.A. Medeiros, D.W. Hewak, H. Tate [*J. Non-Cryst. Solids (Netherlands)* vol.183 (1995) p.201-7]

[11] D.W. Hewak [*Proc. SPIE (USA)* vol.2073 (1993) p.102]

[12] C.B. Layne, W.H. Lowdermilk, M.J. Weber [*Phys. Rev. B (USA)* vol.16 (1977) p.10-20]

[13] K. Soga, H. Inoue, A. Makishima [*J. Lumin. (Netherlands)* vol.55 (1993) p.17-24]

C3.2 Spectroscopy of erbium-doped halide glass

S. Tanabe

November 1997

A ABSORPTION OF ERBIUM-DOPED HALIDE GLASSES

The absorption spectra due to 4f electronic transitions of Er^{3+} ions are well understood, since most bands are well separated and their transitions are mainly electric-dipole in nature. Er^{3+} is one of the rare earth elements, the transition probabilities of which can be interpreted in the Judd-Ofelt theory [1,2] with the smallest uncertainty. The absorption cross sections of electric-dipole transitions in 0.3 - 1.6 μm, where most of the f-f transitions of Er^{3+} are located, can be expressed by sets of reduced matrix elements of unit tensor operators [3], which are characteristic of the ground and excited states and almost independent of the hosts. Since the sets of three values, $\langle U^{(t)} \rangle^2$ (t = 2, 4, 6), are different for each band, the relative intensities are varied. The dependence of the absorption cross sections on the hosts are explained by the three Judd-Ofelt parameters, Ω_t, which also explain the difference in relative intensities of bands with different hosts.

TABLE 1 shows the compositional variations of refractive index and three Ω_t parameters of doped Er^{3+} ions in various ternary MF_n-BaF_2-YF_3 glasses, where M is Zr, Hf, Al, Ga, Sc, In or Zn [4]. Although compositional variations of Ω_t parameters seem small, there exist some trends. FIGURE 1 shows the relation between the Ω_2 parameters of Er^{3+} and the fluorescence intensity ratio of hypersensitive transitions to a magnetic-dipole transition of Eu^{3+} ions doped in glasses with the same composition. There exists a clear correlation between these values, and Ω_2 takes a larger value in the glasses with higher ionic field strength, Z/r (valence/ionic radius), of the network forming cation, M^{n+}.

TABLE 1 Ω_t parameters of Er^{3+} ions and refractive index of MF_n-BaF_2-YF_3 glasses.

M	Ω_2 (10^{-20} cm^2)	Ω_4 (10^{-20} cm^2)	Ω_6 (10^{-20} cm^2)	n_D
Zr	2.93	1.52	1.02	1.523
Hf	2.84	1.52	1.01	1.508
Al	2.27	1.31	0.98	1.444
Sc	2.17	1.45	1.09	1.500
Ga	2.33	1.51	1.00	1.509
In	2.10	1.59	1.10	1.508
Zn	1.78	1.48	1.12	1.509

Among the three J-O parameters, Ω_6 dominates most the line strength of Er^{3+}:1.55 μm and 0.55 μm transitions according to the sets of reduced matrix elements. Because of the highly ionic character of the Ln-F bond (from the Mössbauer isomer shift [4]) there exists no clear correlation between Ω_6 and bond covalency as in oxide glasses [5,6]. However, the results of EXAFS studies showed a good correlation between the length of the Er-F bond and Ω_6 in the glasses (FIGURE 2). Although the factors affecting the Er-F bond length in glasses are not clear yet, this result suggests some insight into the value of the Ω_6 parameter [6].

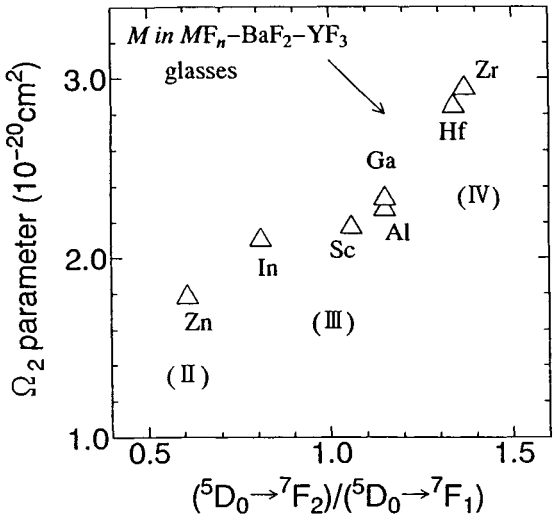


FIGURE 1 Relation between the Ω_2 parameter of Er^{3+} and the ($^5D_0 \rightarrow {}^7F_2$)/($^5D_0 \rightarrow {}^7F_1$) emission ratio of Eu^{3+} in the equivalent glass [4].

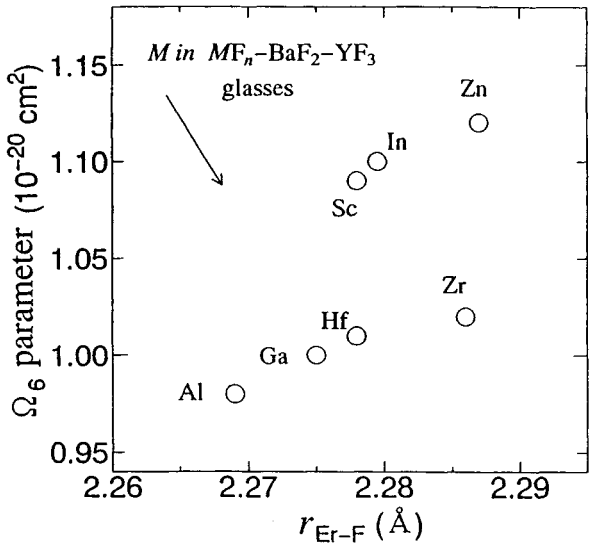


FIGURE 2 Relation between the Ω_6 parameter of Er^{3+} and the Er-F bond length (EXAFS) in fluoride glasses [4].

B FLUORESCENCE OF ERBIUM-DOPED HALIDE GLASS

Compared with oxide glasses, Er-doped halide glasses show much more intense visible emissions under either ultraviolet (Stokes) or infrared (upconversion) excitation. This is due to longer lifetimes of excited levels as a result of low-phonon-energy environments of Er^{3+}.

The comparison of upconversion spectra of erbium doped fluoride glasses by 800 nm pumping ($P = 100$ mW/mm^2) is shown in FIGURE 3 [4]. The main emissions are due to the $^4S_{3/2}$ - $^4I_{15/2}$ transition at 550 nm and to the $^4F_{9/2}$ - $^4I_{15/2}$ transition at 660 nm. The upconversion efficiency varies with fluoride composition owing to different phonon energy and ligand fields. The InF_3-based glass showed the strongest emission among the fluoride glasses [4].

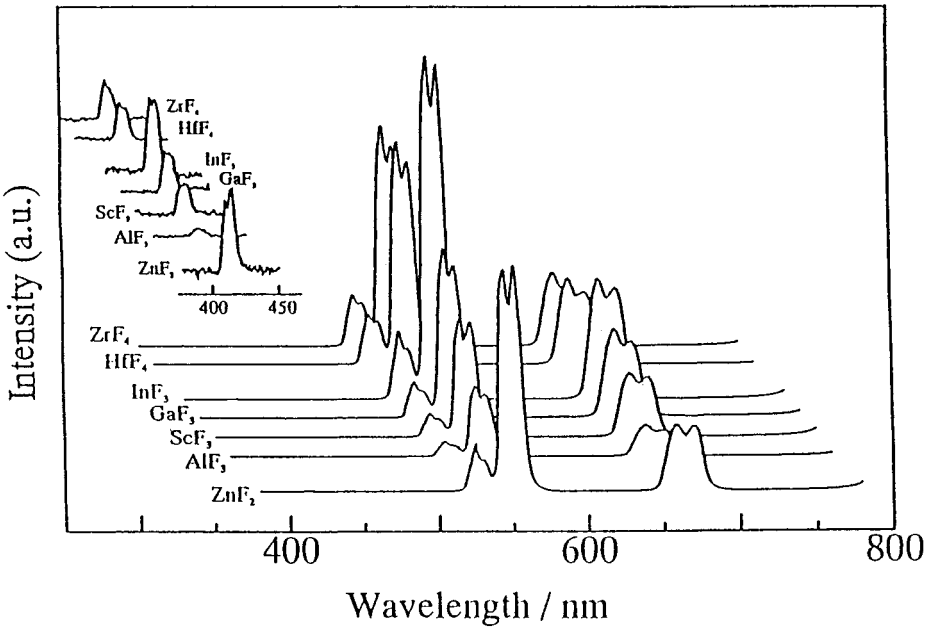


FIGURE 3 Variation of upconversion fluorescence spectra of Er-doped fluoride glasses by 800 nm pumping [4].

Takahashi reported that Er-green upconversion efficiency in a fluorozirconate glass is improved by Cl substitution ($BaF_2 \rightarrow BaCl_2$: FIGURE 4) [7].

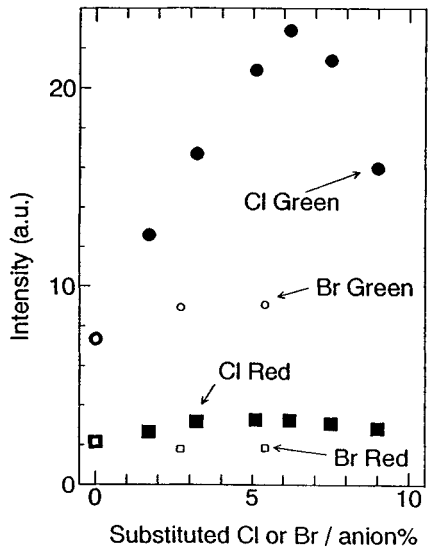


FIGURE 4 Anion substitution dependence of upconversion emission intensities in glasses $58ZrF_4$-(39-x)BaF_2-xBaX_2-$3ErF_3$ (X = Cl or Br) [7].

In addition to the 550 nm and 660 nm upconversion emissions observed in fluorides, Shojiya reported that other chloride and bromide hosts show Er emissions at 560 nm from $^2H_{9/2}$ ($\rightarrow {}^4I_{13/2}$), as well as a strong 410 nm band ($\rightarrow {}^4I_{15/2}$). Also they reported strong Stokes emissions in a CdI_2-based iodide glass at 490 nm from the $^4F_{7/2}$ level, and at 460 nm from the $^4F_{5/2}$ level [8], which has an extremely narrow energy gap. These spectroscopic features are characteristic of heavy metal halide glasses, where the phonon energy is very low and the bandgap is wide enough in visible regions (FIGURE 5).

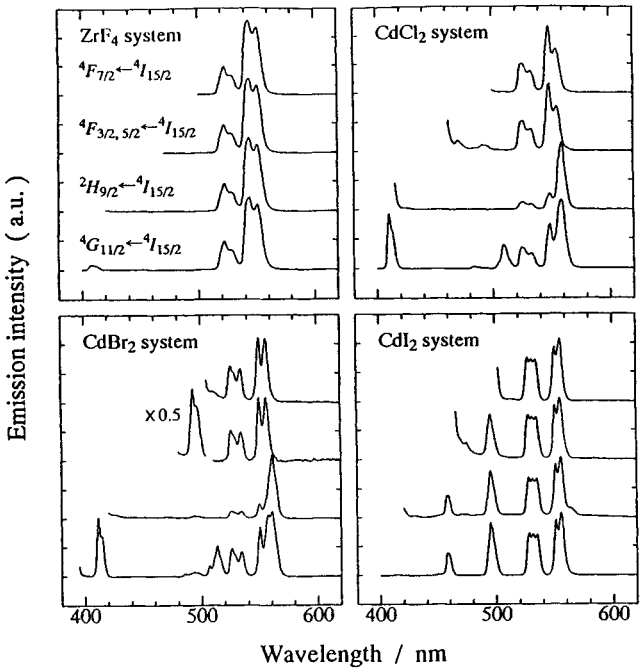


FIGURE 5 Fluorescence spectra of Er^{3+} in the ZrF_4 system and CdX_2 system glasses (X = Cl, Br or I) under $^4G_{11/2}$ (380 nm), $^2H_{9/2}$ (410 nm), $^4F_{3/2,5/2}$ (440 - 460 nm) and $^4F_{7/2}$ (490 nm) excitation [8].

C RADIATIVE LIFETIMES OF ERBIUM-DOPED HALIDE GLASS

Due to small variations of Ω_t parameters and refractive index, the radiative lifetime of Er^{3+} in fluoride glasses shows small compositional variations. TABLE 2 shows the variation of spontaneous emission probabilities from the $^4S_{3/2}$ level in several fluoride glasses [4].

TABLE 2 Emission probability and radiative lifetimes of the Er^{3+}:$^4S_{3/2}$ level in MF_n-BaF_2-YF_3 fluoride glasses.

	Zr	Hf	Al	Sc	Ga	In	Zn
A (s^{-1})							
$^4S_{3/2} \rightarrow {}^4I_{15/2}$	846	813	690	862	759	885	903
$\rightarrow {}^4I_{13/2}$	362	348	295	369	325	379	386
$\rightarrow {}^4I_{11/1}$	30	29	24	31	27	31	32
$\rightarrow {}^4I_{9/2}$	49	47	39	49	44	51	51
$\Sigma A(^4S_{3/2})$	1288	1236	1049	1310	1155	1346	1372
τ_R (μs)	776	809	954	763	866	743	954

D NON-RADIATIVE PROPERTIES OF ERBIUM-DOPED HALIDE GLASS

TABLE 3 shows the variations of fluorescence and non-radiative lifetime and quantum efficiency of the $^4S_{3/2}$ level in the MF_n-BaF_2-YF_3 fluoride glasses. The InF_3-based glass shows the highest quantum efficiency and the AlF_3-based glass shows the largest non-radiative decay rate, largely due to the difference of phonon energy.

TABLE 3 Fluorescence, radiative and non-radiative lifetimes and quantum efficiency of the Er^{3+}:$^4S_{3/2}$ level in fluoride glasses.

	Zr	Hf	Al	Sc	Ga	In	Zn
τ_R (μs)	776	809	954	763	866	743	954
τ_f	491	458	440	464	466	491	453
η_Q (%)	63	57	46	61	54	66	62
τ_{NR}^{-1} (10^2 s^{-1})	7.48	9.47	12.2	8.45	9.91	6.91	8.36

The multiphonon decay rates in halide glasses generally show the following tendency: fluoride > chloride > bromide > iodide. This fact can be seen by careful observation of FIGURE 5 and reasonably understood by the vibrational energy of M-X bonds. Observation of 490 nm and 560 nm emissions is almost impossible in fluoride hosts, which have the highest phonon energy among the four halides. The absence of the 410 nm band from the $^2H_{9/2}$ level in the CdI_2-based glass is due to the smaller bandgap of the iodide host, which quenches the emission from higher levels.

The cross relaxation processes also become dominant in heavily doped halide glasses. FIGURE 6 shows the concentration dependence of the lifetimes of the $^4S_{3/2}$ and $^4F_{9/2}$ levels in a fluorozirconate glass [9]. Due to the difference of possible cross relaxation schemes, their concentration dependence is different. The $^4S_{3/2}$ level is more sensitive to the concentration quenching than the $^4F_{9/2}$ level. This fact affects the concentration dependence of visible upconversion emissions in the fluoride glass (FIGURE 7). Although both 550 nm and 660 nm upconversion emissions are two-step processes by 800 nm

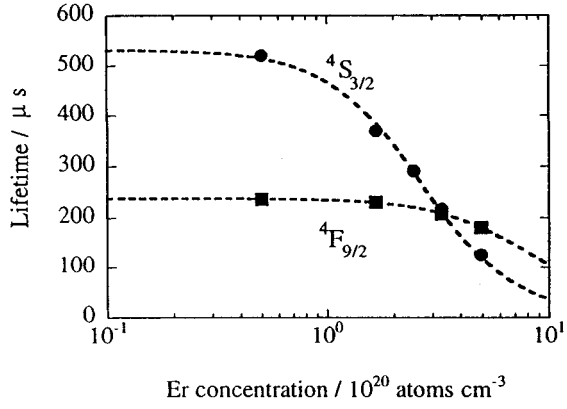


FIGURE 6 Er concentration dependence of fluorescence lifetime of the $^4S_{3/2}$ and $^4F_{9/2}$ levels in $58ZrF_4$-$39BaF_2$-(3-x)LaF_3-xErF_3 glasses [9].

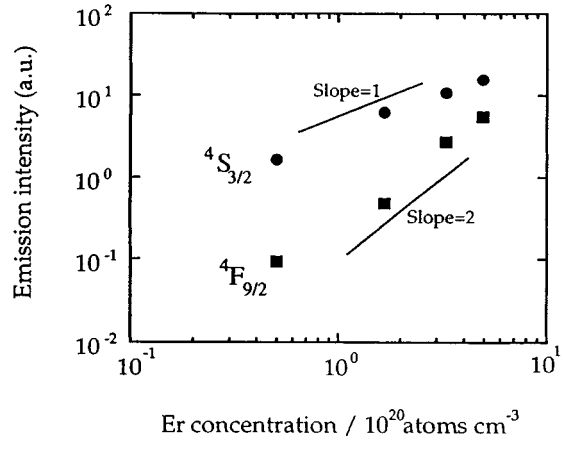


FIGURE 7 Er concentration dependence of the upconversion emission intensity of the $^4S_{3/2} \rightarrow {}^4I_{15/2}$ and $^4F_{9/2} \rightarrow {}^4I_{15/2}$ transitions in $58ZrF_4$-$39BaF_2$-(3-x)LaF_3-xErF_3 glasses.

pumping, the concentration dependence of the 550 nm emission deviates from a quadratic law [9], and the relative ratio of emission intensities changes with the Er concentration.

REFERENCES

[1] B.R. Judd [*Phys. Rev. (USA)* vol.127 (1962) p.750-61]

[2] G.S. Ofelt [*J. Chem. Phys. (USA)* vol.37 (1962) p.511-20]

[3] M.J. Weber [*Phys. Rev. (USA)* vol.157 (1967) p.262-72]

[4] S. Tanabe, K. Takahara, M. Takahashi, Y. Kawamoto [*J. Opt. Soc. Am. B (USA)* vol.12 (1995) p.786-93]

[5] S. Tanabe, T. Ohyagi, S. Todoroki, T. Hanada, N. Soga [*J. Appl. Phys. (USA)* vol.73 (1993) p.8451-54]

[6] S. Tanabe [in *Rare Earths* vol.23 (The Rare Earth Society of Japan, 1993) p.67-93]

[7] M. Takahashi, R. Yokota, Y. Kawamoto, S. Tanabe, K. Hirao [*J. Solid State Chem. (USA)* vol.103 (1993) p.334-40]

[8] M. Shojiya, M. Takahashi, R. Kanno, Y. Kawamoto, K. Kadono [*Appl. Phys. Lett. (USA)* vol.67 (1995) p.2453-5]

[9] M. Takahashi et al [*J. Appl. Phys. (USA)* vol.81 (1997) p.2940-5]

C3.3 Spectroscopy of holmium-doped halide glass

R. Caspary and U.B. Unrau

July 1997

A INTRODUCTION

Spectroscopic research on Ho^{3+} ions in halide glasses has concentrated mainly on the zirconium fluoride class of glasses [1-18]. Another common class is the aluminium fluoride glasses [1,2,20-23] and some work has also been done on barium based glasses [3-5,19,24,25], indate [26] and zinc-cadmium fluoride glasses [27]. It seems, that there has been no work done on non-fluoride holmium doped halide glasses. Besides the halide glasses, there has also been some investigation on holmium doped mixed halide glasses, e.g. fluoroborate [28], fluorophosphate [29] and chlorophosphate [30].

Zirconium in the fluorozirconate glasses can easily be substituted by hafnium without much variation of optical properties and glass stability. Rare earth doping of fluorozirconate (or -hafnate) glasses is usually done by substituting part of the lanthanum ions. BATY and BIZYT glasses contain a large amount of Y^{3+} which can be substituted by Ho^{3+} and Er^{3+} since their ionic radii are close to the Y^{3+} radius [3]. AZF and ZnCd glasses show more critical glass forming ability than the fluorozirconates.

One of the first articles on holmium doped halide glasses was [12]. It is taken as a reference by many authors as it is a rich and comprehensive data source.

B ABSORPTION

The optical absorption spectrum of the rare earth ions from the UV to the mid-infrared originates from transitions between electronic states in the partly filled 4f orbital. These energy levels of the ground configuration are located in an energy range of about 100,000 cm^{-1}, but not all of them can be observed, as the first excited configuration $4f^9 5d$ starts about 50,000 cm^{-1} above the ground level of the ground configuration [31]. FIGURE 1 shows the energy level diagram of Ho^{3+} from the ground level up to 30,000 cm^{-1}.

The electronic states of rare earth ions are normally labelled $^{2S+1}L_J$, where S is the quantum number of the total spin, L = S, P, D, F, G, ... denotes the total orbital angular momentum and J is the total angular momentum. This labelling scheme has to be applied with caution, as J is a good quantum number, but S and L are not. For energy level calculations the electronic states are taken as linear combinations of LS-states in intermediate coupling [31-35].

Absorption spectra are usually obtained from glass samples using a spectrophotometer. This measurement results in an absorption spectrum A(ν) which contains spectral and integral information. The spectral information is used for laser applications as it contains the spectral absorption cross section

$$\sigma_A(\nu) = \frac{-\ln[1 - A(\nu)]}{N l} \qquad (1)$$

where N is the number of rare earth ions per unit volume and l is the thickness of the glass sample. The integral over each absorption band gives the oscillator strength f_{meas} of the appropriate absorption transition.

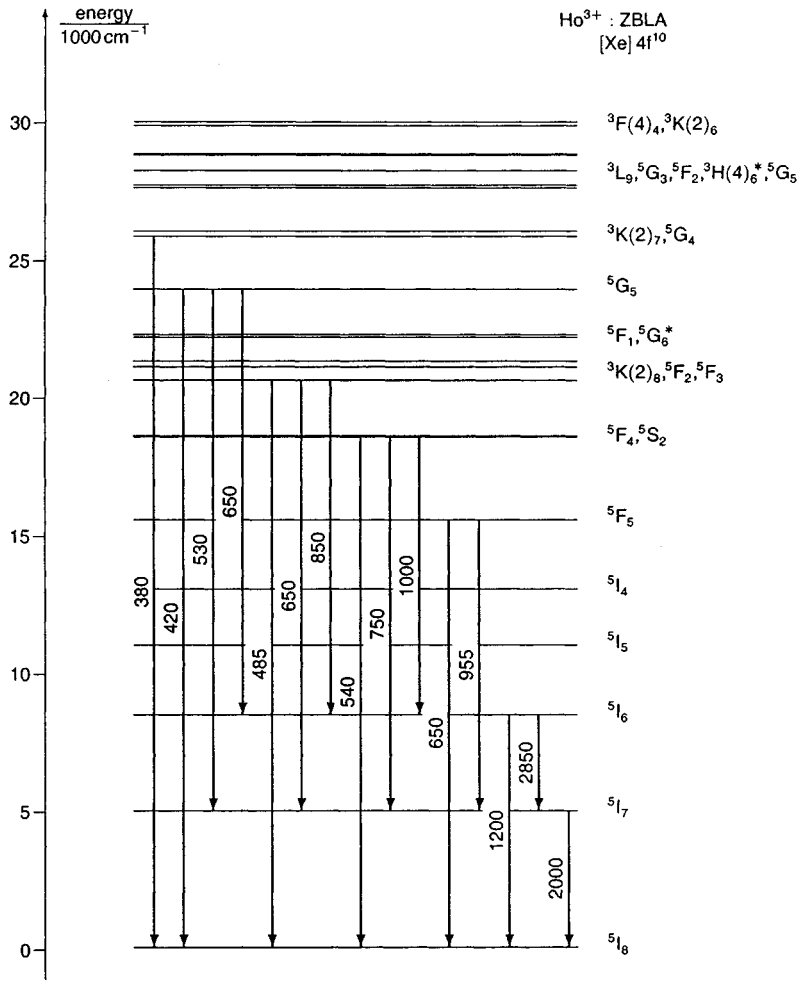


FIGURE 1 Energy levels of Ho^{3+}:ZBLA as calculated for ZBLA(2) in [32]. Levels $^5F_1$ and $^5F_2$ were missing and are taken from Ho^{3+}:ZnBS in the same paper [32]. The stars mark hypersensitive levels, and the arrows show reported fluorescent transitions in fluoride glasses with their wavelengths in nm. Closely spaced levels are labelled from the highest to the lowest level.

In principle, electric dipole transitions between f states are forbidden, as all these states have the same parity. But in practice the electronic states of the rare earth ions contain weak admixings of the 5d configuration and therefore the electric dipole oscillator strengths f_{ed} are typically in the order of 10^{-6} [31]. The magnetic dipole oscillator strengths f_{md} are much smaller for most transitions and in Ho^{3+} only the two transitions shown in TABLE 1 are reported to contain significant magnetic contributions.

TABLE 1 Magnetic dipole oscillator strengths
(n is the index of refraction of the host material).

Glass	$f_{md} \times 10^8$		Ref
	$^5I_8 \rightarrow {}^5I_7$	$^5I_8 \rightarrow {}^3K_8$	
Solution	29.47 n	6.39 n	[36]
Indate	44		[26]
ZnCd	25		[27]
ZBLLi		9.7	[11]
ZBLAN	41.4		[16]

The Judd-Ofelt theory [37,38] in its formulation used today [39] uses three host dependent parameters Ω_2, Ω_4 and Ω_6 per rare earth ion host combination to predict the electric dipole oscillator strengths of all radiative transitions in this combination [39-44].

TABLE 2 gives a survey of the Judd-Ofelt parameters for holmium doped halide glasses and the oscillator strengths the authors used in their calculations. The relative behaviour of the oscillator strengths is more or less host independent with a scaling factor of 2 - 4 for the absolute values. The reported Judd-Ofelt parameters, on the other hand, differ very much from host to host, while there is not much variation in the ZBLA/ZBLAN class. Unfortunately, most authors do not publish their δ_{rms}, which makes comparisons difficult.

C FLUORESCENCE

The arrows in FIGURE 1 show fluorescent transitions reported in the literature. Most authors concentrate on the levels below 30,000 cm^{-1}, and only some publish data of $^3P_1(^3D_3)$ at about 32,900 cm^{-1} [12,40].

The lower energy levels are spaced in distances of 2,000 - 3,500 cm^{-1}. Thus the influence of multiphonon transitions can be expected to be modest for halide glasses (see Section E). For laser applications, the transition $^5I_7 \rightarrow {}^5I_8$ at 2.9 µm is of major interest, but laser action of $^5I_6 \rightarrow {}^5I_7$ at 2.9 µm was also reported [45]. The levels $^5I_5$ and $^5I_4$ are special as most of their reduced matrix elements are particularly small [32,40,41], and therefore the emission and absorption lines of these states are very weak.

From $^5F_5$ onwards, the radiative relaxations of higher lying levels usually terminate at $^5I_8$, $^5I_7$ and $^5I_6$. $^5F_4$ and $^5S_2$ are very closely spaced, which leads to interesting thermalisation effects [12]. The levels $^3K_8$, $^5F_2$ and $^5F_3$ and the levels $^5F_1$ and $^5G_6$ form two closely spaced groups. Fluorescence was only detected from $^5F_3$, whereas $^5G_5$ and $^5G_4$ are separated sufficiently to be seen in emission spectra.

For laser applications, emission cross sections σ_e are of great interest. They are calculated from the fluorescence lines according to [46].

TABLE 3 shows the reported peak wavelengths, effective linewidths and peak emission cross sections of the transitions $^5I_7$, $^5I_6$, $^5F_5$ and $^5S_2$ to the ground level and of $^5S_2$ to $^5I_7$.

D RADIATIVE LIFETIMES

The Judd-Ofelt parameters as the key result of the absorption measurements are used to predict the radiative emission properties of a given rare earth doped material. The spontaneous radiative emission rate from level a to level b is given by [39]

$$A_{ab} = \frac{64\pi^4 \nu^3}{3hc^3(2J+1)} \left(\chi'_{ed} S_{ed} + \chi'_{md} S_{md} \right) \qquad (2)$$

where J is the quantum number of the total angular momentum of the initial state a and S_{ed} and S_{md} are the linestrengths. The electric and magnetic local field correction factors are $\chi'_{ed} = n(n^2 + 1)^2/9$ and $\chi'_{md} = n^3$ where n is the refractive index.

The radiative lifetime τ_a of level a is defined as the inverse of the sum of the radiative emission rates from level a to all lower lying levels b by

TABLE 2 Judd-Ofelt parameters and measured oscillator strengths of ground state absorptions in holmium doped halide glasses.

Glass	f/10^{-8}									$\delta_{rms}/10^{-8}$	Ω_2/pm^2	Ω_4/pm^2	Ω_6/pm^2	Ref
	$^5I_7$	$^5I_6$	$^5I_5$	$^5I_4$	$^5F_5$	$^5S_2/^5F_4$	$^5F_3/^5F_2/^3K_8$	$^5G_6/^5F_1$	$^5G_5$					
AZF											1.86	1.90	1.32	[21]
BATY											2.00	2.00	1.70	[4]
BIZYT		77	14.3		284.8	381.7	242.5	796/-	250	27	1.25	2.38	1.8	[4]
BZYTZ											1.73 ± 0.25	1.89 ± 0.39	1.43 ± 0.26	[25]
Indate	132	70	11		295	394	229	752/-	258		1.07	2.53	1.76	[26]
ZnCd	155	97			317	432	250	698/-	273	27	0.8	2.6	2.0	[27]
HBLAC											3.30	2.22	1.93	[8]
ZBALiN(1)	205	147			308	-/385	176/100/-	2850/-	155		8.13	1.58	2.24	[9]
ZBALiN(2)	170	115			240	-/300	135/80/-	1800/-	125		5.32	1.26	1.84	[9]
ZBALiN(3)	190	125			270	-/340	145/90/-	2250/-	170		6.77	1.31	1.87	[9]
ZBANK(1)	130	80			110	-/135	80/50/-	1050/-	70		3.15	0.74	1.09	[9]
ZBANK(2)	145	105			150	-/200	120/75/-	1380/-	120		4.09	0.97	1.41	[9]
ZBANK(3)	76	56			78	-/95	67/40/-	670/-	63		2.12	0.50	0.73	[9]
ZBLAK											2.20	1.91	1.38	[10]
ZBLLi		36.2			178.4	247.6	132.6	719.8/-	150.1		1.92	1.99	1.36	[11]
ZBLALi											1.99	2.34	1.70	[10]
ZBLA	144.0	72.0	11.6	1.5	276.4	355.4	235.8	1045.6/-	231.9	23	2.28	2.08	1.73	[12]
					316	331	86/-/-	1064	122		2.43	1.67	1.84	[14]
											2.28	2.38	1.79	[15]
											2.43 ± 0.08	1.67 ± 0.15	1.84 ± 0.06	[13]
											2.35	2.25	1.92	[4]
ZBLAN											190	2.09	1.56	[10]
	153.5	82.2	15.6	1.6	284.9	65.9/316.0	109.4/62.3/74.2	1072.3/-	255.3	5.2	2.198	2.444	1.834	[16]

TABLE 3 Peak wavelengths, effective linewidths and peak emission cross-sections of five important transitions in various holmium doped halide glasses.

Glass	$^5I_7 \rightarrow {}^5I_8$			$^5I_6 \rightarrow {}^5I_8$			$^5F_5 \rightarrow {}^5I_8$			$^5S_2 \rightarrow {}^5I_8$			$^5S_2 \rightarrow {}^5I_7$			Ref
	λ_0/nm	$\Delta\lambda_{eff}$/nm	σ_{ep}/pm^2	λ_0/nm	$\Delta\lambda_{eff}$/nm	σ_{ep}/pm^2	λ_0/nm	$\Delta\lambda_{eff}$/nm	σ_{ep}/pm^2	λ_0/nm	$\Delta\lambda_{eff}$/nm	σ_{ep}/pm^2	λ_0/nm	$\Delta\lambda_{eff}$/nm	σ_{ep}/pm^2	
AZF	2035	118	0.53													[21]
BIZYT	2031	146	0.48													[4]
BZYTZ	2010	150 ± 20	0.45	1150	40 ± 5	0.41	648			551						[25]
ZnCd				1155	35	0.5				541	15.8	0.7	753	12.3	0.9	[27]
ZBALiN(1)	1930	80	0.815	1180	50	0.421	640	15	0.986	538	20	0.346				[9]
ZBALiN(2)	1935	78	0.712	1185	48	0.377	641	14	0.898	542	19	0.321				[9]
ZBALiN(3)	1943	75	0.810	1193	47	0.424	644	14	0.958	543	19	0.343				[9]
ZBANK(1)	1949	72	0.602	1197	45	0.317	646	13	0.756	547	18	0.266				[9]
ZBANK(2)	1953	68	0.511	1198	44	0.259	647	12	0.656	550	17	0.229				[9]
ZBANK(3)	1955	65	0.367	1200	42	0.187	650	11	0.499	552	17	0.159				[9]
ZBLLi	2030	800	0.72	1190	500	0.25	640	150	0.82	542	200	0.78	730	200	0.76	[11]
ZBLA							644			540	16		717	47		[14]
	1990	155	0.26										745	10.0	1.93	[47]
							641		0.9	539		1.75	746	8.3	1.0	[13]
	2033	137	0.51													[4]
ZBLAN	2030	145	0.56	1149	48	0.47				545	24	0.39	750	21	0.75	[16]

$$\tau_a = 1/\sum_b A_{ab} \tag{3}$$

and the branching ratio β_{ab} is the probability for an excited level a to relax radiatively to level b:

$$\beta_{ab} = \tau_a A_{ab} \tag{4}$$

TABLE 4 gives an overview of the published calculations of the radiative lifetimes and the branching ratios of the levels $^5I_7$, $^5I_6$, $^5F_5$ and $^5S_2$. It is obvious that the branching ratios do not depend on the glass compositions in contrast to the strong variations of the Judd-Ofelt parameters in TABLE 2. The radiative lifetimes, of course, vary for the different host glasses.

E NON-RADIATIVE PROPERTIES

On changing their electronic state, rare earth ions in solids do not necessarily absorb or emit photons, since they can undergo a variety of non-radiative transitions. The most important ones are multiphonon transitions affecting single ions and energy transfer processes between two ions. Both effects can be investigated separately, as energy transfer is negligible at low dopant concentrations [8,12,25,27,47,48] and multiphonon transitions are vanishing at low temperatures [8,48] and can be neglected for transitions with large energy gaps [5,12].

As all excited states can undergo radiative transitions, multiphonon transitions and energy transfers simultaneously, the lifetime τ consists of three terms according to

$$\tau = \frac{1}{A_{rad} + W_{MP} + W_{ET}} \tag{5}$$

where A_{rad} is the total radiative relaxation rate from EQN (2), and W_{MP} and W_{ET} are the rates of the multiphonon transitions and energy transfers, respectively. The quantum yield η is the radiative portion of the total relaxation rate of a given energy level, which is an important property for laser and amplifier applications:

$$\eta = \tau A_{rad} \tag{6}$$

TABLE 5 contains a collection of published measured lifetimes up to level $^5G_5$. As discussed in Section E2, holmium doped halide glasses show strong concentration quenching and this has to be kept in mind when studying the contents of this table. The lifetime of $^5F_5$ in [16] is larger than the value of other authors, but in this measurement the level $^5F_5$ was excited directly and a sample with low Ho^{3+} concentration was used.

E1 Multiphonon Transitions

The interaction of the f-electrons with vibration modes of the glass matrix allows excited electronic levels to relax by exciting vibrations of the glass network. Unlike the situation in crystals, these vibrations are spatially localised because of the absence of translational invariance in vitreous materials. Nevertheless, the quantised modes are commonly called phonons. The proposed term 'clusterons' [49] would be more accurate but is not in use.

For small energy gaps of the order of kT, the transitions occur very fast in upward and downward directions leading to thermalisation of the involved electronic levels. This happens especially for the

TABLE 4 Calculated radiative lifetimes and branching ratios of four important energy levels of holmium doped halide glasses.

Glass	$^5I_7$	$^5I_6$			$^5F_5$					$^5S_2$						Ref
	τ/μs	τ/μs	β ($^5I_7$)	β ($^5I_8$)	τ/μs	β ($^5I_5$)	β ($^5I_6$)	β ($^5I_7$)	β ($^5I_8$)	τ/μs	β ($^5I_4$)	β ($^5I_5$)	β ($^5I_6$)	β ($^5I_7$)	β ($^5I_8$)	
AZF	17200	8400	0.165	0.835	730	0.003	0.040	0.185	0.772	740	0.015	0.015	0.064	0.364	0.542	[21]
BATY	15100	7500			584					523						[4]
BIZYT	15200	6700	0.085	0.915	494	0.003	0.040	0.181	0.777	467	0.019	0.016	0.066	0.392	0.507	[4]
Indate	13500	6900	0.100	0.900	510	0.003	0.040	0.184	0.773	505	0.018	0.015	0.066	0.384	0.517	[26]
ZnCd					420					400						[32]
ZBALiN(1)	11500	4500	0.095	0.905	460	0.004	0.048	0.194	0.754	350	0.015	0.015	0.060	0.369	0.541	[9]
ZBALiN(2)	14100	5500	0.094	0.906	570	0.004	0.046	0.182	0.722	430	0.015	0.015	0.060	0.369	0.541	[9]
ZBALiN(3)	13800	5400	0.095	0.905	550	0.004	0.048	0.194	0.754	420	0.015	0.015	0.060	0.369	0.541	[9]
ZBANK(1)	18400	7200	0.094	0.906	740	0.004	0.048	0.191	0.757	560	0.015	0.015	0.060	0.369	0.541	[9]
ZBANK(2)	23900	9300	0.094	0.906	960	0.004	0.048	0.191	0.757	730	0.015	0.015	0.060	0.369	0.541	[9]
ZBANK(3)	35500	13400	0.093	0.907	1400	0.004	0.048	0.191	0.757	1100	0.015	0.015	0.060	0.369	0.541	[9]
ZBLLi	17210	8120	0.146	0.854	610	0	0.044	0.186	0.766	220	0.005	0.029	0.072	0.204	0.690	[11]
ZBLA	17300	6500	0.09	0.91	540	0	0.04	0.18	0.77	470	0.02	0.02	0.07	0.37	0.54	[12]
	14900	6000			493					439						[4]
		6500			540					470						[32]
ZBLAN	12650	5840	0.092	0.908	500	0	0.039	0.183	0.775	470	0	0.015	0.064	0.382	0.519	[16]

TABLE 5 Measured lifetimes of the lowest energy levels of holmium doped halide glasses.

Glass	$^5I_7$ τ/μs	$^5I_6$ τ/μs	$^5I_5$ τ/μs	$^5F_5$ τ/μs	$^5S_2$ ($^5F_4$) τ/μs	$^5F_3$ ($^5F_2$, $^3K_8$) τ/μs	$^5G_5$ τ/μs	Concentration	T/K	Ref
AZF	23000[a]	4150 (0.1 mol %)		90	184	2 (0.2 - 8 mol %)[b]	1 (0.5 - 4 mol %)[b]	0.2 mol %		[1][d]
		3200						2.1×10^{20} cm^{-3}		[23]
	26700 (2 cat %)	7000						0.1 cat %		[21,22]
BATY	7700	2350		21	248			0.1%		[3][d]
	11300							0.5 mol %	290	[5][d]
	12700	2350			255			0.18×10^{20} cm^{-3}	295	[4][d]
BIZYT	10700[b]							0.5 - 2 mol %		[24][d]
	8400	3700	47 (0.5%)	31	323			0.1%		[3][d]
	14200[b]							0.1 - 5 mol %	290	[5][d]
	13000	3700			370			0.19×10^{20} cm^{-3}	295	[4][d]
BZYTZ	11500	3800		19.0 - 24.5	294 - 301	1.9	0.5 - 0.8	0.125 mol %		[25]
Indate				29	315			0.1 mol %	300	[26]
ZnCd	15700	2800		30	233			0.2 mol %	300	[27][d]
HBLAC		3200		40	230			0.2 mol %	300[e]	[8]
ZBLA	4200[c]				110			3.20×10^{20} cm^{-3}		[47]
				25	105	1.0	0.2	2 mol %	300	[13]
	4200	2400		27	130			2 mol %	300[e]	[12]
	5200 (5%)	3100	284	27	265			0.5%		[3][d]
	13500[b]							0.1 - 2 mol %	290	[5][d]
	13200	3400			298			0.16×10^{20} cm^{-3}	295	[4][d]
ZBLAN	10700	3100						4 mol %	RT	[17]
	12010	3500		290[a]	300			0.1 mol %		[16]

[a]see text, [b]average lifetime, [c]calculated for 77 K, [d]paper contains lifetimes for various Ho^{3+} concentrations, [e]paper contains lifetimes for various temperatures.

Stark levels of the J-multiplets. Energy gaps larger than the maximum phonon energy $E_{max} = \hbar\omega_{max}$ must be bridged by more than one phonon: hence the name multiphonon transition. These transitions proceed predominantly in the downward direction and lead to high non-radiative relaxation rates for small energy gaps which need only a couple of phonons for the transition.

Multiphonon relaxation rates increase with increasing temperature, and as expressed by EQN (5) this leads to decreasing lifetimes of the electronic levels. This temperature dependence is strong, in particular for levels which are closely spaced to the next lower lying energy level because of their low quantum yield. In the literature, two main theories describing the temperature and energy gap dependence of the multiphonon transitions can be found: the Riseberg-Moos theory [50] and the Huang-Rhys theory [51].

In his approach, Kiel [52] examined the first-order term of the orbit-lattice interaction and carried it to high orders of time dependent perturbation theory to describe the emission of many phonons. Based on this theoretically intractable approach, Riseberg and Moos [50] developed a phenomenological model for crystals, which was applied to glasses by Layne, Lowdermilk and Weber [56].

It is worth noting that rare earth ions have typical Huang-Rhys-Pekar numbers $S_0 << 1$ [53], and it can be shown that in this case the temperature dependence is nearly the same from 0 K to temperatures well above room temperature [12,48].

Both models predict a relaxation rate which decreases strongly with an increasing number of phonons p. Therefore, only the phonons with energy E_{max} are considered, as they lead to the smallest p. These highest energy phonons correspond to stretching vibrations of the network forming components of the glass [8,12,42,43,55,56], and their energy is a key parameter for the non-radiative properties of host materials. Some values for E_{max} in halide glasses are given in TABLE 6.

TABLE 6 Non-radiative properties of halide glasses reported for holmium doped glasses.

Glass	B/s^{-1}	α/cm	E_{max}/cm^{-1}	T/K	Ref
AZF			540		[21,22]
BZYTZ	4.5×10^{10}	5.78×10^{-3}		300	[25]
HBLAC	1.3×10^{9}	5.0×10^{-3}	490	80	[8]
ZBLA	2.8×10^{9}	5.2×10^{-3}	472	80	[8]
ZBLA	1.4×10^{9}	4.5×10^{-3}		300	[27]
ZBLA	1.88×10^{10}	5.77×10^{-3}	460 - 500	80	[12,48]
ZBLA	1.59×10^{10}	5.19×10^{-3}		300	[13,47]
ZBLAN	1.99×10^{5}	2.11×10^{-3}	500	300	[16]
ZnCd	8.4×10^{8}	4.4×10^{-3}		300	[27]
LaF_3	6.6×10^{5}	2.11×10^{-3}	500	300	[16]

For the investigation of multiphonon relaxation rates as a function of the energy gap ΔE, the multiphonon rate is usually simplified [8,12,13,16,21,22,25,27,47,48,50] to

$$W_{MP} = B\, e^{-\alpha \Delta E} \tag{7}$$

However, it should be noted that the parameter B depends on temperature. The reported parameters B and α for holmium-doped halide glasses are listed in TABLE 6. Of course they do not depend on holmium being the dopant. Similar tables, not restricted to halide glasses, can be found in [31,34,42,43,57].

EQN (7) may be used to predict the multiphonon rate for given transitions, but because of the inhomogeneous broadening of the electronic levels, the energy gaps are not known exactly. This leads to

significant errors for small gaps [25], which can be reduced with a numerical fit of the temperature dependence [8,12].

E2 Energy Transfer Between Equal Ions

Ion-ion interactions, for example via dipole-dipole coupling, result in transfer of the excitation energy from one ion to another. The main consequence of the various types of energy transfer, which are discussed extensively in the literature (e.g. [42]), is concentration quenching: the lifetime of energy levels in most cases decreases with increasing dopant concentration [1,3-5,11,16,19,27,47].

In [1], the influence of concentration quenching on upconversion efficiency was studied extensively for a pump wavelength of 647 nm. It was reported that the lifetime of $^5I_7$ increases with increasing holmium concentrations in this case.

E3 Energy Transfer Between Different Species

Co-doping is widely used for tailoring the optical properties of laser glasses. In Ho^{3+}, the 2 µm laser ($^5I_7 \rightarrow {}^5I_8$) is of great interest, but as the absorption bands of Ho^{3+} are not well suited for diode pumping, holmium is co-doped with Tm^{3+} which can be pumped at 790 nm [23,24,58,59]. The energy level diagram in FIGURE 2 shows the three most relevant energy transfer processes. Please note that the labels of the levels $^3H_4$ and $^3F_4$ of Tm^{3+} are sometimes exchanged in the literature. The cross relaxation process (a) is reported to have an efficiency of nearly 100% at Tm^{3+} concentrations of about 8×10^{20} cm^{-3} in AZF [23,58] and 7 mol % in BIZYT [24] which allows the quantum efficiency to reach 2. The energy transfer (b) is very efficient at high Tm^{3+} concentrations in both directions and leads to thermalisation of $^3F_4(Tm^{3+})$ and $^5I_7(Ho^{3+})$ [23,24,58,59]. The process which is believed to be the main loss mechanism of this system is the upconversion process (c) followed by a fast multiphonon decay $^5I_5 \rightarrow {}^5I_6$ [23,58,59].

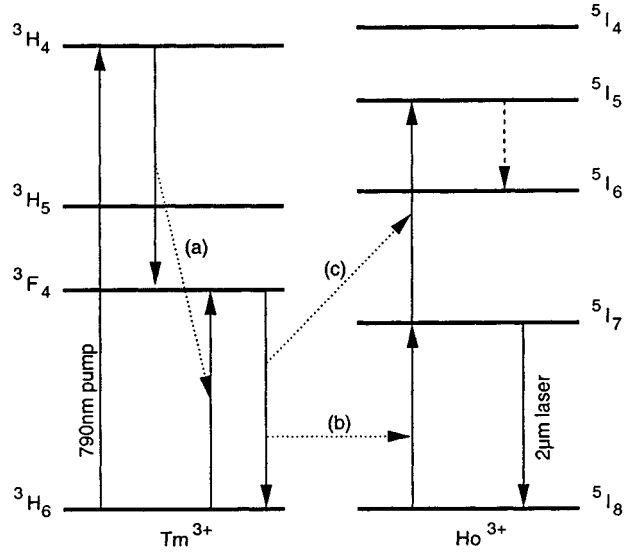


FIGURE 2 Energy transfer paths for Tm^{3+}/Ho^{3+} co-doped halide glasses.

Instead of filling the upper laser level efficiently, co-doping can also be used for depletion of the lower laser level if it is not the ground state. For the laser transition $^5I_6 \rightarrow {}^5I_7$ at 2.9 µm, co-doping with Pr^{3+} and Eu^{3+} was analysed [17].

Recently, there has been increasing interest in upconversion lasers, and for that purpose Ho^{3+} is co-doped with Yb^{3+} pumped at 980 nm [2,6,7,20,22,26]. The two-step upconversion process $^5I_8 \rightarrow {}^5I_6 \rightarrow {}^5S_2$ leads to a green fluorescence at 540 nm ($^5S_2 \rightarrow {}^5I_8$). This fluorescence is reported to be more than 50% stronger in AZF than in ZBLAN [2].

Besides the systems mentioned above, there are papers on some other co-doped systems: e.g. $Er^{3+} \rightarrow Ho^{3+}$ [3,19], $Er^{3+} \rightarrow Tm^{3+} \rightarrow Ho^{3+}$ [5] and $Yb^{3+} \rightarrow Tm^{3+} \rightarrow Ho^{3+}$ [21].

REFERENCES

[1] X. Zou, H. Toratani [*J. Non-Cryst. Solids (Netherlands)* vol.201 (1996) p.37-46]

[2] A. Shikida, H. Yanagita, H. Toratani [*J. Opt. Soc. Am. B (USA)* vol.11 (1994) p.928-32]

[3] B. Moine, A. Brenier, C. Pedrini [*IEEE J. Quantum Electron. (USA)* vol.25 (1989) p.88-96]

[4] C. Guéry [PhD Thesis, Université de Rennes I, 1988]

[5] J.-L. Adam, C. Guéry, J. Lucas, J. Rubin, B. Moine, G. Boulon [*Mater. Sci. Forum (Switzerland)* vol.19-20 (1987) p.573-80]

[6] M.A. Chamarro, R. Cases [*Solid State Commun. (USA)* vol.68 (1988) p.953-7]

[7] M.A. Chamarro, R. Cases [*J. Lumin. (Netherlands)* vol.42 (1988) p.267-74]

[8] R. Cases, M.A. Chamarro [*J. Solid State Chem. (USA)* vol.90 (1991) p.313-9]

[9] S. Buddhudu, F.J. Bryant [*Spectrochim. Acta A (UK)* vol.44 (1988) p.1381-5]

[10] J. McDougall, D.B. Hollis, M.J.P. Payne [*Phys. Chem. Glasses (UK)* vol.35 (1994) p.258-9]

[11] F. Gan, H. Zheng [*J. Non-Cryst. Solids (Netherlands)* vol.95/96 (1987) p.771-6]

[12] K. Tanimura, M.D. Shinn, W.A. Sibley, M.G. Drexhage, R.N. Brown [*Phys. Rev. B (USA)* vol.30 (1984) p.2429-37]

[13] R. Reisfeld, M. Eyal, E. Greenberg, C.K. Jørgensen [*Chem. Phys. Lett. (Netherlands)* vol.118 (1985) p.25-8]

[14] L. Samek, J. Wasylak, K. Marczuch [*J. Non-Cryst. Solids (Netherlands)* vol.140 (1992) p.243-8]

[15] J. Mcdougall, D.B. Hollis, X. Liu, M.J.B. Payne [*Phys. Chem. Glasses (UK)* vol.35 (1994) p.145-6]

[16] L. Wetenkamp [Dr.-Ing.-Dissertation, Fakultät für Maschinenbau und Elektrotechnik der Technischen Universität Braunschweig, 1991]

[17] L. Wetenkamp, G.F. West, H. Többen [*J. Non-Cryst. Solids (Netherlands)* vol.140 (1992) p.25-30]

[18] F. Gan, J. Wang, Y. Chen [*Pure Appl. Opt. (UK)* vol.5 (1996) p.855-62]

[19] B. Moine, C. Pedrini, G. Boulon, A. Brenier, J.L. Adam, J. Lucas [*J. Lumin. (Netherlands)* vol.40&41 (1988) p.692-3]

[20] X. Zou, H. Toratani [*J. Non-Cryst. Solids (Netherlands)* vol.181 (1995) p.87-99]

[21] B. Peng, T. Izumitani [*Opt. Mater. (Netherlands)* vol.4 (1995) p.797-810]

[22] B. Peng, T. Izumitani [*Opt. Mater. (Netherlands)* vol.4 (1995) p.701-11]

[23] X. Zou, H. Toratani [*J. Non-Cryst. Solids (Netherlands)* vol.195 (1996) p.113-24]

[24] A. Brenier, C. Pedrini, B. Moine, J.L. Adam, C. Pledel [*Phys. Rev. B (USA)* vol.41 (1990) p.5364-71]

[25] M. Eyal, R. Reisfeld, C.K. Jørgensen, B. Bendow [*Chem. Phys. Lett. (Netherlands)* vol.139 (1987) p.395-400]

[26] I.R. Martin, V.D. Rodriguez, M. Morales, U.R. Rodriguez-Mendoza, V. Lavin [*J. Appl. Spectrosc. (USA)* vol.62 (1995) p.865-71]

[27] B. Villacampa, V.M. Orera, R.I. Merino, R. Cases, P.J. Alonso, R. Alcala [*Mater. Res. Bull. (USA)* vol.26 (1991) p.741-8]

[28] J.V. Sathyanarayana, T. Balaji, K. Annapurna, S. Buddhudu [*Phys. Chem. Glasses (UK)* vol.37 (1996) p.41-3]

[29] A.V.R. Reddy, K. Annapurna, A.S. Jacob, S. Buddhudu [*Ferroelectr. Lett. (UK)* vol.15 (1993) p.33-44]
[30] K. Subramanyam Naidu, S. Buddhudu [*Mater. Lett. (Netherlands)* vol.14 (1992) p.355-60]
[31] L.A. Riseberg, M.J. Weber [in *Progress in Optics* vol.14 (North-Holland, Amsterdam, 1976) ch.3 p.89-159]
[32] E. Rukmini, C.K. Jayasankar [*Opt. Mater. (Netherlands)* vol.4 (1995) p.529-46]
[33] R.D. Peacock [in *Structure and Bonding* vol.22 (Springer, Berlin, 1975) p.83-122]
[34] W.J. Miniscalco [in *Optical Engineering* vol.37 (Marcel Dekker, New York, 1993) ch.2 p.19-133]
[35] V.J. Pugh, F.S. Richardson, J.B. Gruber, M.D. Seltzer [*J. Phys. Chem. Solids (UK)* vol.58 (1997) p.85-101]
[36] W.T. Carnall, P.R. Fields, K. Rajnak [*J. Chem. Phys. (USA)* vol.49 (1968) p.4412-23]
[37] B.R. Judd [*Phys. Rev. (USA)* vol.127 (1962) p.750-61]
[38] G.S. Ofelt [*J. Chem. Phys. (USA)* vol.37 (1962) p.511-20]
[39] W.T. Carnall [in *Handbook Phys. Chem. Rare Earths* vol.3 (North-Holland, Amsterdam, 1978) ch.24 p.171-208]
[40] M.J. Weber, B.H. Matsinger, V.L. Donlan, G.T. Surratt [*J. Chem. Phys. (USA)* vol.57 (1972) p.562-7]
[41] W.T. Carnall, P.R. Fields, K. Rajnak [*J. Chem. Phys. (USA)* vol.49 (1968) p.4424-42]
[42] R. Reisfeld, C.K. Jørgensen [in *Handbook Phys. Chem. Rare Earths* vol.9 (North-Holland, Amserdam, 1987) ch.58 p.1-90]
[43] R. Reisfeld [in *Spectroscopy of Solid-State Laser-Type Materials* Ed. B. Di Bartolo (Plenum Press, New York, 1987) p.343-96]
[44] W.T. Carnall, P.R. Fields, B.G. Wybourne [*J. Chem. Phys. (USA)* vol.42 (1965) p.3797-806]
[45] L. Wetenkamp [*Electron. Lett. (UK)* vol.26 (1990) p.883-4]
[46] W. Koechner [*Solid-State Laser Engineering* 4th ed. (Springer, Berlin, 1996) p.13-5]
[47] R. Reisfeld, M. Eyal, C.K. Jørgensen [*J. Less-Common Met. (Switzerland)* vol.126 (1986) p.187-94]
[48] M.D. Shinn, W.A. Sibley, M.G. Drexhage, R.N. Brown [*Phys. Rev. B (USA)* vol.27 (1983) p.6635-48]
[49] I. Pócsik [*Physica A (Netherlands)* vol.201 (1993) p.34-7]
[50] L.A. Riseberg, H.W. Moos [*Phys. Rev. (USA)* vol.174 (1968) p.429-38]
[51] K. Huang, A. Rhys [*Proc. R. Soc. Lond. A (UK)* vol.204 (1951) p.406-23]
[52] A. Kiel [in *Quantum Electronics* vol.1 (Columbia University Press, New York, 1964) p.765-72]
[53] W.H. Fonger, C.W. Struck [*J. Lumin. (Netherlands)* vol.17 (1978) p.241-61]
[54] C.W. Struck, W.H. Fonger [*J. Lumin. (Netherlands)* vol.10 (1975) p.1-30]
[55] R.M. Almeida, J.D. Mackenzie [*J. Chem. Phys. (USA)* vol.78 (1983) p.6502-11]
[56] C.B. Layne, W.H. Lowdermilk, M.J. Weber [*Phys. Rev. B (USA)* vol.16 (1977) p.10-20]
[57] R. Reisfeld [in *Radiationless Processes* Ed. B. Di Bartolo (Plenum Press, New York, 1980) p.489-98]
[58] M. Doshida, M. Obara [*Jpn. J. Appl. Phys. (Japan)* vol.34 (1995) p.3562-5]
[59] M. Doshida, K. Teraguchi, M. Obara [*IEEE J. Quantum Electron. (USA)* vol.31 (1995) p.910-5]

C3.4 Spectroscopy of thulium-doped halide glass

T. Sakamoto

July 1997

A INTRODUCTION

Thulium (Tm) ions exhibit various laser transitions in both the visible and infrared wavelength regions. Fluorozirconate glasses and other halide glasses are more efficient hosts for the Tm ions than oxide glasses like silica, germanate and phosphate, because the halide glasses have lower multiphonon emission rates than the oxide glasses. The fluorozirconate glasses are also attractive from the viewpoint that low loss rare earth-doped fibres can be fabricated [1], and indeed some are commercially available. Several laser oscillation and optical amplification events have been reported from Tm-doped fluorozirconate fibres, such as a blue laser at 0.45 or 0.48 μm for application to optical data storage [2-4], lasers and optical amplifiers at 0.8 μm, 1.46 μm and 1.65 μm for optical communications [5-10], and eye-safe lasers at 1.8 - 2.0 μm and 2.3 μm for medical applications and sensors [11-13]. This Datareview provides the optical properties of Tm ions, such as absorption, emission, radiative lifetimes and non-radiative properties. The data are mainly for ZBLALi (ZrF_4-BaF_2-LaF_3-AlF_3-LiF), or ZBLAN (ZrF_4-BaF_2-LaF_3-AlF_3-NaF) glass, which are widely used as fibre materials.

B ABSORPTION OF THULIUM-DOPED HALIDE GLASS

FIGURE 1 shows the energy diagram of Tm ions and the laser transitions observed so far in ZBLAN or ZBLALi glasses/fibres. FIGURE 2 shows the absorption spectra of Tm ions in ZBLALi glass [14,15].

The absorption spectra show wavelengths that may be used as pump lights for laser and optical amplifiers. It is noted that in addition to lasers around the absorption wavelength, lasers around 1.06 μm, such as Nd:YAG lasers, Nd:YLF lasers or Yb-doped fibre lasers are often used as pump sources in conjunction with upconversion, even though the ground state absorption of Tm is very small [3,4,6,7].

Judd-Ofelt analyses [16,17] have been performed by several authors, and TABLE 1 lists the Judd-Ofelt parameters for Tm^{3+} in ZBLALi glass. TABLE 2 shows the predicted spontaneous emission probabilities A_{ij} from the i to the j level [15,18].

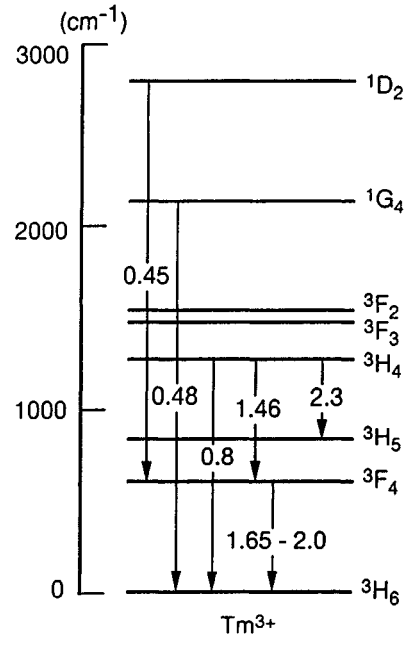


FIGURE 1 Energy diagram of Tm^{3+} ions.

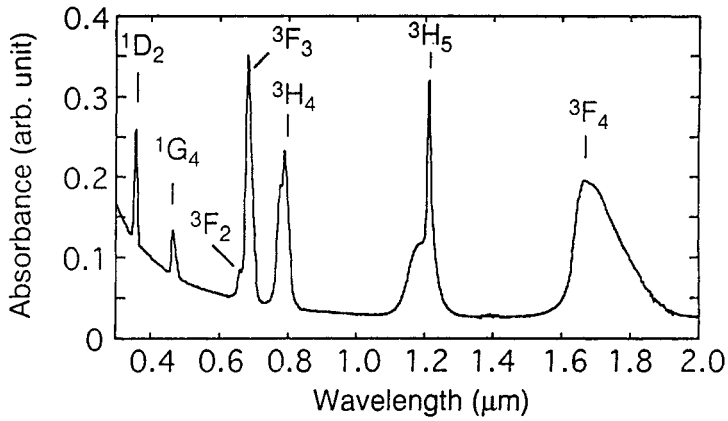


FIGURE 2 Absorption spectra of Tm^{3+} ions.

TABLE 1 Judd-Ofelt parameters of ZBLALi glass.

Ω_2 (10^{-20} cm^2)	Ω_4 (10^{-20} cm^2)	Ω_6 (10^{-20} cm^2)	Ref
2.80	1.91	1.01	[15]
2.31	1.77	1.02	[18]
2.09	1.74	0.91	[19]

TABLE 2 Predicted spontaneous emission probability A_{ij} of Tm^{3+} in ZBLALi glass.

Transition	Average frequency (cm^{-1})	Spontaneous emission probability A_{ij} (s^{-1})	Branching ratio β
$^3F_4 \rightarrow$ $^3H_6$	5546	123.8	1
$^3H_5 \rightarrow$ $^3H_6$	8230	202.5	0.99
$^3F_4$	2684	2.1	0.01
$^3H_4 \rightarrow$ $^3H_6$	12453	615.4	0.86
$^3F_4$	6907	75.1	0.11
$^3H_5$	4223	21.9	0.031
$^3F_3 \rightarrow$ $^3H_6$	14025	1271.9	0.86
$^3F_4$	8479	71.2	0.048
$^3H_5$	5795	130.6	0.089
$^3H_4$	1572	1.64	0.001
$^3F_2 \rightarrow$ $^3H_6$	14684	381.8	0.48
$^3F_4$	9138	278.0	0.35
$^3H_5$	6454	136.5	0.17
$^3H_4$	2231	5.6	0.007
$^3F_3$	659	0.046	5.7×10^{-5}
$^1G_4 \rightarrow$ $^3H_6$	21053	564.7	0.40
$^3F_4$	15506	214.0	0.15
$^3H_5$	12822	449.4	0.32
$^3H_4$	8599	138.3	0.10
$^3F_3$	7027	41.3	0.029
$^3F_2$	6368	11.5	0.008
$^1D_2 \rightarrow$ $^3H_6$	27548	6171.5	0.38
$^3F_4$	22002	7401.1	0.47
$^3H_5$	19318	64.9	0.004
$^3H_4$	15095	821.0	0.052
$^3F_3$	13523	625.2	0.039
$^3F_2$	12864	706.6	0.044
$^1G_4$	6496	92.2	0.005

C FLUORESCENCE OF THULIUM-DOPED HALIDE GLASS

FIGURE 3 shows measured emission cross-sections of various transitions in ZBLALi glass [18]. The cross-sections were calculated from measured fluorescence I(ν) using the following equation [21]:

$$\sigma_e = \frac{\lambda^2 A_{ij}}{8\pi c n^2} \frac{I(\nu)}{\int I(\nu)d\nu}$$

where A_{ij} is the spontaneous emission probability listed in TABLE 2.

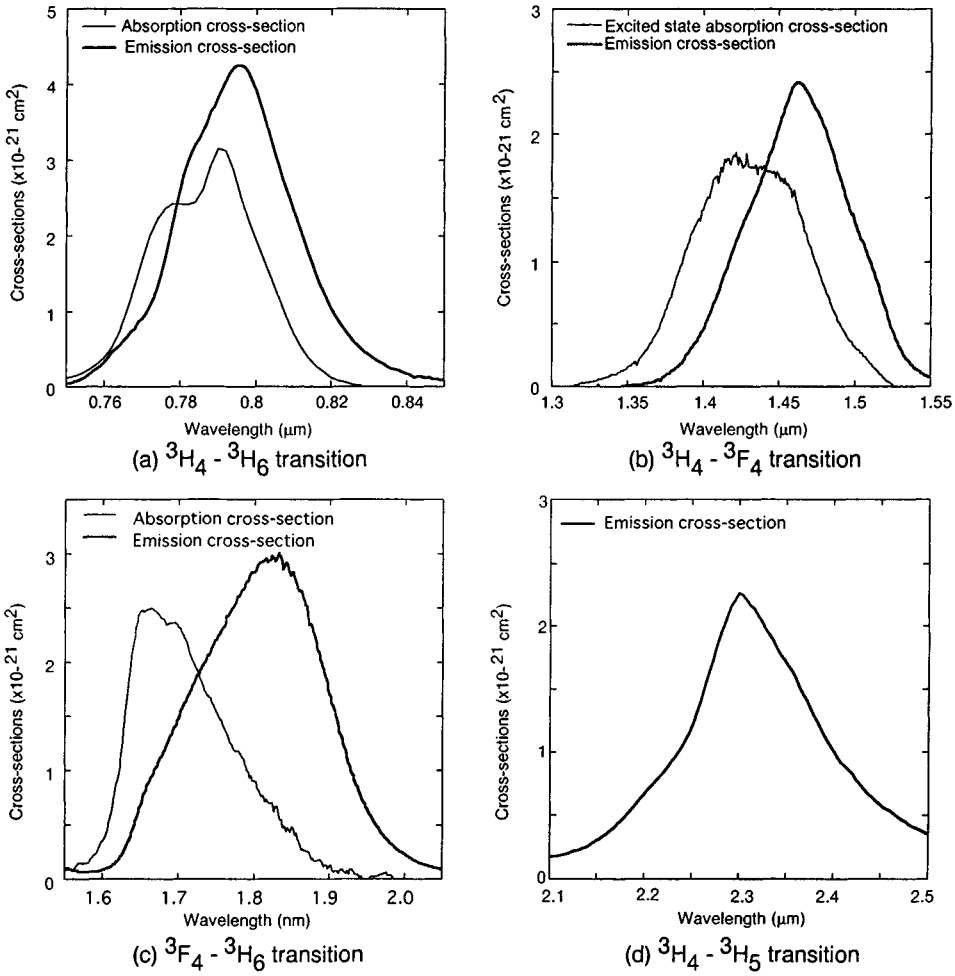


FIGURE 3 Emission cross-sections of Tm^{3+} ions in ZBLALi glass.

In the figure, absorption cross-sections are also indicated for $^3H_4$-$^3H_6$ and $^3F_4$-$^3H_6$. Excited state absorption cross-sections are indicated for the $^3H_4$-$^3F_4$ transition as measured in ZBLALi fibre.

D RADIATIVE LIFETIMES OF THULIUM-DOPED HALIDE GLASS

TABLE 3 lists the predicted and measured radiative lifetimes for $^1D_2$, $^1G_4$, $^3H_4$ and $^3F_4$ levels. Predicted lifetimes τ_{rad} were derived by $1/\Sigma A_{ij}$, where A_{ij} is the spontaneous emission rate from the i to the j level in TABLE 2, and summation is extended to all terminal states j. The lifetimes of $^3F_2$, $^3F_3$ or $^3H_5$ levels are too short to be measured. Every level has a close level on the lower side, and thus non-radiative decay through multiphonon relaxation dominates the lifetimes of the levels.

TABLE 3 Predicted and measured radiative lifetimes of Tm^{3+} ions in ZBLALi glass.

Level	Predicted lifetimes τ_{rad} (ms)	Measured lifetimes τ_{meas} (ms)	Ref
$^1D_2$	0.062	0.055	[15]
$^1G_4$	0.67	0.63	[15]
$^3H_4$	1.40	1.42	[15]
		1.35	[7]
		1.61	[21]
		1.7	[9]
$^3F_4$	8.07	6.8	[8]
		9.0	[7]
		10	[21]
		11	[9]

E NON-RADIATIVE PROPERTIES OF THULIUM-DOPED HALIDE GLASS

Measured lifetimes are given by [15,17]

$$\frac{1}{\tau_{meas}} = \frac{1}{\tau_{rad}} + W_{NR}$$

where W_{NR} is the multiphonon emission rate. From TABLE 3, measured lifetimes agree well with predicted lifetimes for all listed levels. This confirms that the multiphonon emission rate is negligibly small compared to the spontaneous emission rate, and multiphonon emission does not affect the lifetimes of the levels [15].

F CONCLUSION

This review provides optical properties of Tm^{3+} ions in halide glass. Lasers and optical amplifiers can be achieved with Tm-doped ZBLAN fibre in various wavelength regions, such as 0.45 μm, 0.48 μm, the 0.8 μm-band, the 1.4 μm-band, 1.6 - 2.0 μm and 2.3 μm. Their efficiencies are essentially high because of low multiphonon relaxation.

REFERENCES

[1] T. Kanamori, Y. Terunuma, K. Fujiura, Y. Ohishi, S. Sudo [*Proc. 9th Int. Symp. On Non-Oxide Glasses* Hangzou, China, 24-28 May 1994, p.74-9]

[2] M.P. Le Flohic, J.Y. Allain, G.M. Stephan, G. Maze [*Opt. Lett. (USA)* vol.19 (1994) p.1982-4]

[3] S.G. Grubb, K.W. Bennett, R.S. Cannon, W.F. Humer [*Electron. Lett. (UK)* vol.28 (1992) p.1243-4]

[4] I.J. Booth, C.J. Mackechnie, B.F. Ventrudo [*IEEE J. Quantum Electron. (USA)* vol.32 (1996) p.118-23]

[5] R.G. Smart et al [*Electron. Lett. (UK)* vol.28 (1992) p.58-9]

[6] M.L. Denis, J.W. Dixon, I. Aggarwal [*Tech. Dig. Opt. Fiber Commun. Conf. OFC'94* WK10 (1994) p.133-4]

[7] T. Komukai, T. Yamamoto, T. Sugawa, Y. Miyajima [*IEEE J. Quantum Electron. (USA)* vol.31 (1995) p.1880-9]

[8] R.M. Percival, D. Szebesta, S.T. Davey [*Electron. Lett. (UK)* vol.28 (1992) p.671-3]

[9] T. Sakamoto et al [*IEEE Photonics Technol. Lett. (USA)* vol.7 (1995) p.983-5]

[10] T. Sakamoto et al [*IEEE Photonics Technol. Lett. (USA)* vol.8 (1996) p.349-51]
[11] R.G. Smart, J.N. Carter, A.C. Trooper, D.C. Hanna [*Opt. Commun. (Netherlands)* vol.82 (1991) p.563-70]
[12] R.M. Percival, D. Szebesta, C.P. Selzer, S.D. Perrin, S.T. Davey, M. Louka [*IEEE J. Quantum Electron.(USA)* vol.31 (1995) p.489-93]
[13] R.M. Percival, S.F. Carter, D. Szebesta, S.T. Davey, W.A. Stallard [*Electron. Lett. (UK)* vol.27 (1991) p.1912-3]
[14] Y. Ohishi, S. Mitachi, T. Kanamori, T. Manabe [*Phys. Chem. Glasses (UK)* vol.25 (1983) p.135]
[15] J. Sanz, R. Cases, R. Alcala [*J. Non-Cryst. Solids (Netherlands)* vol.93 (1987) p.377-86]
[16] B.R. Judd [*Phys. Rev. (USA)* vol.127 (1962) p.750]; G.S. Ofelt [*J. Chem. Phys. (USA)* vol.37 (1962) p.511]
[17] M.J. Weber [*Phys. Rev. B (USA)* vol.8 (1973) p.54-64]
[18] Measured and estimated by the author.
[19] J. McDouGall, D.B. Hollis [*Phys. Chem. Glasses (UK)* vol.35 (1994) p.258-9]
[20] R. Allen, L. Esterowitz, I. Aggarwal [*IEEE J. Quantum Electron. (USA)* vol.29 (1993) p.303-6]
[21] R. Pafchek, J. Aniano, E. Snitzer, G.H. Sigel Jr. [*Mater. Res. Soc. Symp. Proc. (USA)* vol.172 (1989) p.347-52]

C3.5 Spectroscopy of neodymium-doped halide glass

W.J. Miniscalco

June 1998

A INTRODUCTION

The optical spectroscopy of Nd^{3+}-doped solids has been an active area for several decades. The power and efficiency available from the transition at ≈1050 nm makes Nd^{3+} one of the most important activators for crystalline and bulk glass lasers. The interest in halide glass hosts was originally sparked by the search for improved compositions for use in laser fusion drivers. An invaluable product of this research is the compendium by Stokowski et al of data for more than two hundred Nd^{3+}-doped glasses [1]. Subsequently, interest was renewed when it was found that Nd^{3+}-doped fluoride glasses offered significant advantages over oxide glasses for achieving optical amplification within the 1300 nm optical communications window. This Datareview provides a brief overview of the absorption and emission properties of the most technologically important optical transitions of Nd^{3+}-doped halide glasses, emphasising comparisons to other types of glasses. A more detailed discussion of the optical properties of Nd^{3+}-doped glasses can be found in [2].

B ABSORPTION PROPERTIES

FIGURE 1 presents the energy levels of Nd^{3+}-doped ZBLAN (Zr-Ba-La-Al-Na) fluorozirconate glass based on the positions and linewidths of a measured absorption spectrum. Although glass composition has some influence on the wavelengths of the absorption bands, a more significant effect for Nd^{3+} is the change in strengths of the 580 and 800 nm bands. The 580 nm absorption band ($^4I_{9/2} \rightarrow {}^4G_{7/2} + {}^4G_{5/2} + {}^2G_{7/2}$) dominates in covalent glasses such as silica, while in ionic glasses such as fluorides the 800 nm band ($^4I_{9/2} \rightarrow {}^2H_{9/2} + {}^4F_{5/2}$) has equal or greater strength. The strong 800 nm band is extremely effective for exciting the $^4F_{3/2}$ metastable state, leading to efficient Nd^{3+}-doped lasers and amplifiers pumped by AlGaAs diode lasers. Each level in FIGURE 1 is labelled with the wavelength of the ground state absorption transition terminating on it as well as the wavelength of the excited state absorption (ESA) transition terminating on it that originates from the metastable $^4F_{3/2}$ state. Because of the large number of closely spaced excited states, it is remarkable that Nd^{3+} does not suffer more from ESA. While the $^4F_{3/2} \rightarrow {}^2D_{5/2}$ ESA transition occurs at around 800 nm, it is extremely weak and does not significantly degrade 800 nm pumping. Because the absorption characteristics of Nd^{3+}-doped glasses are good for all glass compositions, the principal consideration for device applications is the performance of the emission transitions and how these depend upon the glass host.

C EXCITED-STATE PROPERTIES

TABLE 1 lists the ranges of $^4F_{3/2}$ radiative lifetimes and branching ratios for some common glass types calculated from a Judd-Ofelt analysis. Silicates exhibit the greatest range in radiative lifetime, more than a factor of six, while fluoroberyllates also have a relatively wide range. As a group, fluoroberyllates have long radiative lifetimes (low relaxation rates). The lower index of refraction for fluoride glasses leads to a longer lifetime for a given stimulated emission cross section, a favourable situation for emission devices operating under steady-state or continuous-wave conditions.

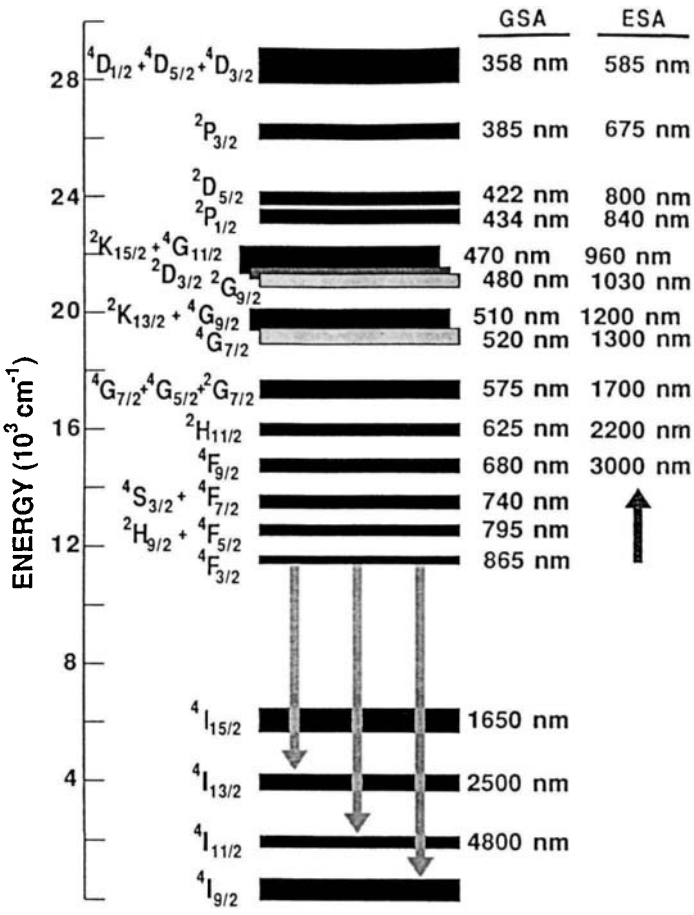


FIGURE 1 Energy levels of Nd^{3+} in a ZBLAN fluorozirconate labelled using Russell-Saunders coupling. The arrows indicate laser transitions demonstrated for glass hosts. The first number to the right of each excited state (GSA) is the wavelength in nanometres of the ground state absorption transition terminating on it. The second number (ESA) is the wavelength of the ESA transition originating on the $^4F_{3/2}$ and terminating on the labelled level.

TABLE 1 Ranges of excited-state properties for Nd^{3+}-doped glasses.

Glass	Radiative lifetime (μs)	Branching ratio $^4F_{3/2} \rightarrow {}^4I_{11/2}$	Branching ratio $^4F_{3/2} \rightarrow {}^4I_{13/2}$
Silica	500	0.450	0.086
Silicate	170 - 1090	0.460 - 0.500	0.080 - 0.097
Borate	270 - 450	0.480 - 0.510	0.091 - 0.100
Phosphate	280 - 570	0.470 - 0.500	0.084 - 0.098
Fluorophosphate	310 - 570	0.490 - 0.520	0.090 - 0.100
Fluorozirconate	430 - 500	0.500 - 0.510	0.093 - 0.095
Fluoroberyllate	480 - 1030	0.490 - 0.520	0.089 - 0.100

Calculated from data of [1].

Non-radiative relaxation depletes excited states through the emission of phonons. This process competes with spontaneous and stimulated radiative emission and can lead to low optical efficiency. Because the ionic bonds of halide glasses are weaker than the covalent bonds of oxide glasses, they have smaller phonon energies. This leads to a lower non-radiative relaxation rate in halide glasses because more phonons must be emitted (making it a higher order process) in order to dissipate the energy of the excited state. Emission has been reported from some of the higher-lying levels for glass hosts [3]. Since non-

radiative relaxation is a serious problem for these states, halide glass hosts are preferred. For the important $^4F_{3/2}$ state, however, relaxation is primarily radiative for the more common glasses with the exception of borates.

D THE $^4F_{3/2} \rightarrow {}^4I_{11/2}$ TRANSITION AT 1050 nm

Because of its importance in high power and high energy laser applications, the $^4F_{3/2} \rightarrow {}^4I_{11/2}$ transition is probably the most thoroughly characterised one for Nd^{3+}-doped glass and crystalline hosts. This band provides four-level operation at room temperature. TABLE 1 indicates some variation in branching ratio within glass type as well as a slight trend among glass types favouring fluoride compositions. Although the $^4F_{3/2} \rightarrow {}^4I_{11/2}$ transition is the principal decay channel for the $^4F_{3/2}$ state, for oxide glasses, and silicates in particular, branching ratios are generally less than 0.5. This is related to the degree of covalent bonding. More ionic glasses like halides favour the $^4F_{3/2} \rightarrow {}^4I_{11/2}$ (1050 nm) and $^4F_{3/2} \rightarrow {}^4I_{13/2}$ (1300 nm) at the expense of the $^4F_{3/2} \rightarrow {}^4I_{9/2}$ (900 nm) transition, and fluorophosphates and fluorides provide better efficiency for emission or optical gain at these wavelengths. TABLE 2 shows a significant trend in the dependence of the peak emission wavelength on glass composition with the ionic halide glasses emitting at shorter wavelengths than oxide glasses due to the nephelauxetic effect. The width of the emission band for this transition also shows a trend with covalency, being narrower for halides than for oxides. There is no significant trend in the peak value of the stimulated emission cross section with glass type because of offsetting trends in linewidth and oscillator strength.

TABLE 2 Properties of the $^4F_{3/2} \rightarrow {}^4I_{11/2}$ transition at 1050 nm.

Glass	Peak cross section (10^{-20} cm^2)	Peak position (nm)	Effective linewidth (nm)
Silica	1.4	1088	54.8
Silicate	0.9 - 3.6	1057 - 1065	33.2 - 43.0
Borate	2.1 - 3.2	1054 - 1062	34.1 - 37.5
Phosphate	2.0 - 4.8	1052 - 1057	22.4 - 34.6
Fluorophosphate	2.2 - 4.3	1049 - 1056	25.8 - 33.3
Fluorozirconate	2.7 - 3.0	1048 - 1049	25.8 - 27.1
Fluoroberyllate	1.6 - 4.4	1046 - 1050	18.9 - 29.0

From [1].

E THE $^4F_{3/2} \rightarrow {}^4I_{13/2}$ TRANSITION AT 1300 nm

For many glasses this emission band peaks within the 1300 nm optical communications window, and this stimulated interest in developing Nd^{3+}-doped fibre lasers and amplifiers. FIGURE 2 illustrates emission spectra for some representative hosts. The position of the peak of the $^4F_{3/2} \rightarrow {}^4I_{13/2}$ transition varies significantly with composition, following the usual trend of the more covalent glasses emitting at longer wavelengths. Other glass compositions fall between those illustrated. As with the 1050 nm transition, the silicates exhibit the broadest emission bands while phosphates and fluorides have the narrowest. Fluorides, fluorophosphates, and borates have the highest branching ratios while those for some silicate compositions are extremely low (TABLE 1). Even the best compositions have values only slightly over 0.1, resulting in significant loss of excitation to the $^4F_{3/2} \rightarrow {}^4I_{11/2}$ channel for devices governed by spontaneous emission.

Initial attempts to obtain gain on this transition for a glass fibre found instead pump-induced loss due to ESA from the competing $^4F_{3/2} \rightarrow {}^4G_{7/2}$ transition, which overwhelms the gain transition for silica [4]. The relative magnitudes of the ESA and stimulated emission cross sections are a property of the host. Theoretical analysis using Judd-Ofelt analysis was used to determine that fluorozirconate glasses should

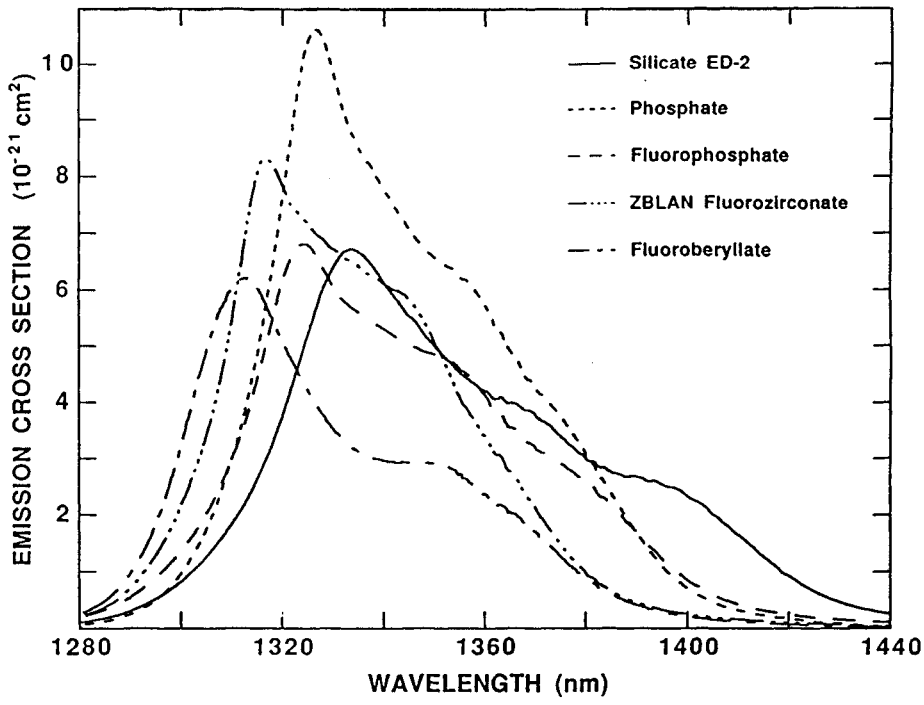


FIGURE 2 $^4F_{3/2} \rightarrow {}^4I_{13/2}$ emission cross section spectra for different glass types. Note that the more covalent silicate is broader and shifted to longer wavelength compared to the more ionic glasses such as the fluorozirconate. Excited at 800 nm. From [2].

be significantly better than silica, and this was confirmed through the demonstration of a ZBLAN fibre laser [5]. FIGURE 3 compares the stimulated emission and ESA cross sections for a ZBLAN glass [6]. The offset between the two bands is present for this composition as well as silica, and gain can only be achieved for wavelengths greater than approximately 1310 nm [7]. To a first approximation, all the

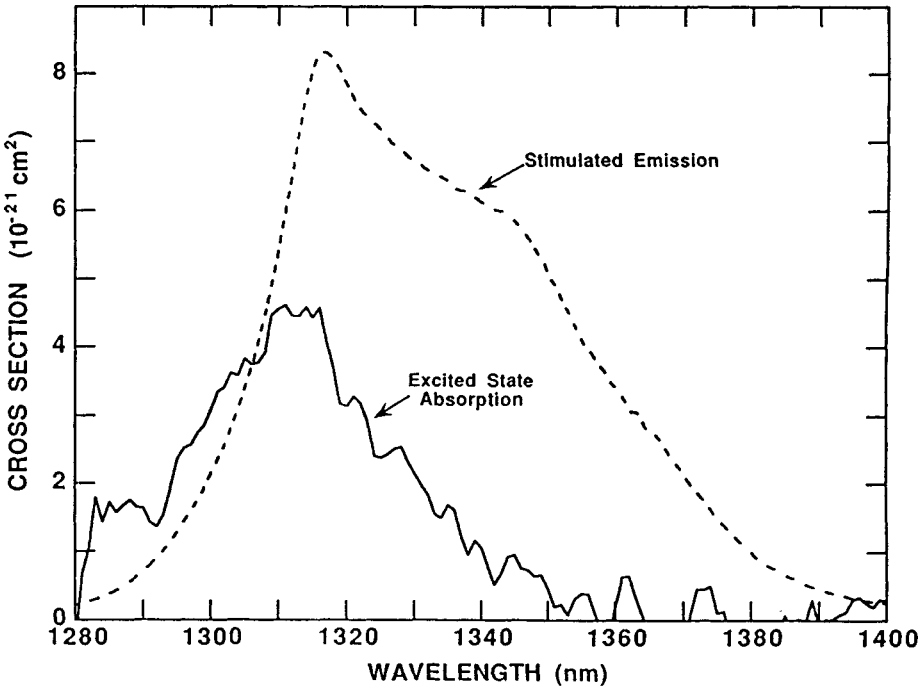


FIGURE 3 Stimulated emission and ESA cross section spectra at 1300 nm for a ZBLAN fluorozirconate glass. Based on the measurements of Zemon et al [6].

energy levels shift together with changes in glass composition, and no significant change in offset between emission and ESA is expected. Some deviations from this rule have been observed [6], but no glass has been found for which the ESA band does not overlap a major portion of the emission band.

REFERENCES

[1] S.E. Stokowski, R.A. Saroyan, M.J. Weber [*Nd-Doped Laser Glass Spectroscopic and Physical Properties* (Lawrence Livermore National Laboratory Report M-095, Rev.2, 1981)]

[2] W.J. Miniscalco [in *Rare Earth Doped Fiber Lasers and Amplifiers* Ed. M.J.F. Digonnet (Marcel Dekker, 1993) ch.2 p.19-133]

[3] T.Y. Fan, R.L. Byer [*J. Opt. Soc. Am. B (USA)* vol.3 (1986) p.1519-25]

[4] I.P. Alcock, A.I. Ferguson, D.C. Hanna, A.C. Tropper [*Opt. Lett. (USA)* vol.11 (1986) p.709-11]

[5] W.J. Miniscalco, L.J. Andrews, B.A. Thompson, R.S. Quimby, L.J.B. Vacha, M.G. Drexhage [*Electron. Lett. (UK)* vol.24 (1988) p.28-9]

[6] S. Zemon et al [*IEEE Photonics Technol. Lett. (USA)* vol.4 (1992) p.244-7]

[7] M.C. Brierley, S. Carter, P.W. France, J.E. Pedersen [*Electron. Lett. (UK)* vol.26 (1990) p.329-30]

PART C: HALIDE GLASS

CHAPTER C4

OPTICAL FIBRE MANUFACTURE

C4.1 Preparation and melting of halide glass
C4.2 Drawing of halide glass optical fibres
C4.3 Loss of halide glass optical fibres
C4.4 Reliability of halide glass optical fibres

C4.1 Preparation and melting of halide glass

M. Poulain

May 1998

A INTRODUCTION

Like most inorganic glasses, halide glasses are prepared simply by cooling a clear melt rapidly enough to prevent crystallisation. Processing includes classical steps: selecting and mixing starting materials, melting, fining, cooling, casting and annealing. However, the specific aspects of halide glasses result in significant differences in the way these glasses must be processed, by comparison with oxide glasses. First, halide melts are very sensitive to hydrolysis and furthermore they are prone to devitrification. In addition, viscosity is very low at liquidus and characteristic temperatures are small: typically, T_g is lower than 300°C and the liquidus temperature lies between 500 and 600°C.

While the generic group of halide glasses encompasses heavy halide glasses as well - chlorides, bromides and iodides - practical development focuses on fluoride systems or fluorochlorides for practical reasons (stability, chemical durability, softening and temperature).

B STARTING MATERIALS

The selection of the starting materials is the first critical step of the preparation. Most commercial halides contain traces of water, and sometimes they are oxyhalides. Contamination may also result from improper storage and handling. Apart from cationic impurities, e.g. transition metals, which induce optical absorption, anionic impurities and organic contaminants may influence the optical quality of the glass. Anionic oxygen usually increases devitrification rate.

Starting materials may be checked by X-ray diffraction and thermal analysis. Visual and microscopic inspection and also classical chemical analysis are helpful. However, the most significant test is glass synthesis itself: it is not always possible to identify the factors which promote devitrification in a given batch. Among other things, starting materials may be contaminated by dust, containers, grinding and mixing devices.

It is wiser to assume that halide powders contain residual water. It may be removed at high temperature and/or low pressure, without hydrolysis. Powder drying depends on the nature of the halides: it may be implemented at room atmosphere above 500°C for earth alkali fluorides, but special processing is required for other fluorides such as ZrF_4. In a general way, two reactions may occur:

$$MX_n, x\,H_2O \rightarrow MX_n + x\,H_2O \quad (1)$$

$$MX_n, x\,H_2O \rightarrow MO_yX_{n-2y} + (x-y)\,H_2O + 2\,y\,HX \quad (2)$$

with M = cation and X = F, Cl, Br or I.

These two reactions are ruled by equilibrium constants K_1 and K_2 which increase strongly with temperature. As long as K_2 is small, dehydration is easily achieved without hydrolysis. Otherwise, a halogenating reagent, e.g. hydracid HX, must be used to prevent oxyhalide formation.

A practical way of removing water traces and preventing hydrolysis consists in adding a small amount of ammonium hydrogenofluoride NH_4HF_2 to the batch. Both HF and NH_4F, which are the byproducts of

NH_4HF_2 pyrolysis, act as fluorinating reagents which inhibit hydrolysis and even convert residual oxides into fluorides. The excess of NH_4F is eliminated in the vapour phase as temperature increases. This process had already been used in the pioneering work of Sun [1], and later for fluorozirconate glass development [2]. It allows oxides to be used as starting materials. However, there are some drawbacks in the ammonium bifluoride processing, as it requires longer time and larger crucibles.

C MELTING AND FINING

The batch is usually melted in a platinum or vitreous carbon crucible. There are interactions and exchanges between melt and crucibles: traces of the previous melt often remain trapped in the walls, even after careful cleaning.

Melting is a simple and fast operation. As it is endothermic, the crucible is overheated to increase heat flow, which means that the furnace temperature is larger than the nominal liquidus temperature. Adsorbed gases and volatile species are evacuated at melting. Some foaming may take place at this stage.

Melting is completed when the liquid is free of solid particles. Then a fining step must be implemented in order to homogenise the material, to oxidise reduced species and reduce the amount of dissolved gas [3]. Because the viscosity of the halide melts is small, no mechanical stirring is required. Temperature is increased to around 200°C above liquidus temperature. An oxidising atmosphere is used to ensure the oxidation of the reduced cations. The origin of the melt reduction is not completely clear. The basic reaction may be written as:

$$M^{n+} + e^- \rightarrow M^{(n-1)+} \qquad (3)$$

A typical example is the pair Zr^{4+}/Zr^{3+}. However, this reaction implies that electrons are formed. Intrinsic reactions are:

$$2\,F^- \rightarrow F_2 + 2\,e^-$$

$$O^{2-} \rightarrow {}^1/_2\,O_2 + 2\,e^-$$

While these reactions may occur at high temperature when equilibrium constants are large enough, it is more probable that reduction is promoted by extrinsic reducing reagents, such as NH_4^+ ions and pyrolitic carbon originating from dust and polymeric impurities in starting materials. In some cases, it is possible to see a carbon layer at the melt surface. In fact, reduced phases are often less soluble in the melt, and consequently lead to the formation of black inclusions in the vitreous matrix.

Depending on melt composition and temperature, some volatile fluorides are likely to escape from the liquid phase. This is the case for ZrF_4, HfF_4 and also $ZrCl_4$ and $AlCl_3$, insofar as chlorides have been introduced in the batch. As a result melt composition may be inhomogeneous. This phenomenon may be limited by using deep crucibles in which the melt surface is small by comparison to the volume. In addition, melt volatilisation is stabilised when the partial vapour pressure of the volatile species has reached the equilibrium value corresponding to the melt temperature.

Some defects may be associated with this phenomenon. As there is a temperature gradient in the atmosphere above the melt, some solid phase, e.g. ZrF_4, may condense from the vapour and fall onto the glass melt. At some stage, this may remain as solid inclusions in the liquid, leading to scattering centres in bulk glass.

Oxidation of the reduced species is implemented during the fining stage, which implies that the atmosphere is oxidising. An alternative choice is to incorporate an oxidising compound, e.g. InF_3:

$$In^{3+} + 2\,e^- \rightarrow In^+$$

$$2\,Zr^{3+} + In^{3+} \rightarrow In^+ + 2\,Zr^{4+}$$

However, this incorporation may increase the crystallisation rate of the melt.

Electrochemical purification has been suggested as an alternative way to remove some cationic impurities and to oxidise the glass melt [4].

D ATMOSPHERE

The control of the atmosphere during processing is critical. First, it must be free of contaminants, especially water. Depending on temperature, water reacts with fluorine anions to form hydroxyl or anionic oxygen, which often enhances devitrification. Dust usually contains water and oxides which react with molten fluorides and promote nucleation.

Special atmospheres may be used to improve glass quality. Intense research has been implemented in this area. CCl_4 was found to be efficient in oxidising the glass melt and in reducing OH concentration [5], but it results in some chlorine incorporation, which may induce platinum corrosion. Other reactive atmospheres include SF_6 and NF_3 [6]. While the potential advantages of reactive atmospheres are not seriously questioned, it appears that dry processing based on dust-free dry air allows the manufacturing of bulk samples with low scattering and high optical quality [7-9].

E CASTING

After fining, the melt is cooled and cast into metallic moulds. Ideally, the melt should be kept above liquidus temperature T_l to prevent nucleus formation. However, viscosity is small at T_l and some volatilisation may occur, which results in cords in bulk glass. Another important point concerns thermal expansion: the volume of solid glass is smaller than that of glass melt. Because the external surface of the sample is frozen first, volume contraction is possible only in the final liquid volume. This leads to the formation of 'vacuum bubbles' along the axis of cylindrical samples. In fact, these bubbles are often filled with low pressure gases evolved from the melt. For this reason, it may be more appropriate to cool the glass melt below T_l in order to limit these problems.

Mould temperature is another parameter. When it is too large, glass adhesion may be significant, and when it is too small, thermal shock results in thermal stresses.

It is also possible to cool the glass melt in conical crucibles. Interactions with the atmosphere are minimised and scattering is often reduced. However, in this approach, it is difficult to avoid bubble formation along the crucible walls.

Containerless melting and cooling have been reported using gas film levitation [10]. Insofar as no contamination arises from the gas film, this results in samples exhibiting low scattering losses.

F ANNEALING

In sample fabrication, very slow cooling rates cannot be used because halide melts crystallise too rapidly. As a consequence, samples have to be annealed to remove the mechanical stresses induced by inhomogeneous cooling. A common way is to hold the sample around T_g for one or two hours and to switch off the annealing furnace. For the fabrication of high quality components, annealing should be studied carefully: as there is a large difference in thermal expansion of solid and liquid, structural relaxation may significantly change the value of some physical parameters such as density and refractive index. Annealing is less critical for optical fibres as the glass is reheated and quenched during fibre drawing.

G CONCLUSION

The synthesis of halide glasses, and among them fluoride glasses, is basically simple. Much care must be taken in the control of the starting materials and hydrolysis at any step of the processing. Temperature and time have to be adjusted for the various steps of the fabrication process. Their values depend on glass composition, batch size and crucible and oven geometry. An empirical approach based on trial and error appears an efficient way to define optimum conditions.

REFERENCES

[1] K.H. Sun [US Patent no.2466507, 1949]
[2] M. Poulain [in *Fluoride Glass Fiber Optics* Eds. I. Aggarwal, G. Lu (Academic Press, Boston, 1992) ch.1 p.1-35]
[3] G.G. Devyatykh, M.F. Churbanov, E.M. Dianov [*Mater. Sci. Forum (Switzerland)* vol.19-20 (1987) p.187-92]
[4] Z. Zhou, P.J. Newman, D.K. Wong, D.R. MacFarlane [*J. Non-Cryst. Solids (Netherlands)* vol.140 (1992) p.297-300]
[5] M. Robinson [*Mater. Sci. Forum (Switzerland)* vol.5 (1985) p.18-34]
[6] T. Nakai, Y. Mimura, H. Tokiwa, O. Shinbori [*IEEE J. Lightwave Technol. (USA)* vol.4 (1986) p.87-9]
[7] G. Mazé, V. Cardin, M. Poulain [*Electron. Lett. (UK)* vol.20 (1984) p.884-5]
[8] Y. Ohishi, S. Sakaguchi, S. Takahashi [*Electron. Lett. (UK)* vol.22 (1986) p.1034-5]
[9] P. France [in *Fluoride Glass Optical Fibres* Ed. P. France (Blackie, 1990) p.100-21]
[10] P. Baniel, C. Belouet [*J. Non-Cryst. Solids (Netherlands)* vol.161 (1993) p.1-5]

C4.2 Drawing of halide glass optical fibres

M. Saad and A. Soufiane

June 1998

A INTRODUCTION

During the last two decades, halide glass optical fibres, especially those drawn from fluoride glass, have experienced extraordinary development due to their unexpected optical properties. Halide glass fibres provide an interesting alternative to silica fibres for both active and passive IR applications. However, drawing halide glass fibres is more complicated than drawing silica glass fibres. Indeed, in spite of the great number of fluoride glass compositions isolated so far, there are only a few among them that could be drawn into fibres. Compared to silica, halide glasses present, in fact, poor chemical durability, poor mechanical properties and high tendency toward crystallisation.

Among all fluoride glass systems investigated so far, zirconium fluoride based glasses are the most stable. Indeed, fibres with optical losses as low as 0.65 dB/km at 2.55 μm [1] have been obtained using ZBLAN and ZBLAN/Pb as cladding and core compositions respectively. However, other fluoride glasses, such as fluoroaluminate and fluoroindate, have been successfully drawn into fibre. For indium fluoride based fibres, losses of lower than 100 dB/km have been reported by Soufiane et al [2] and of 43 dB/km at 3.36 μm by Nishida [3].

B PREFORM PREPARATION

B1 Preforms for Multi-Mode Fibres

Preform preparation is the most important and critical step of the preform drawing technique. Indeed, most imperfections present in the final fibre originate from the preform.

It is well known that processes based on chemical vapour deposition (CVD) are the most suitable techniques to prepare preforms for ultra-low-loss optical fibres. Unfortunately, these processes could not be used to prepare fluoride glass preforms, which contain more than four elements with very different physical and chemical properties. Preform preparation is thus a key step in the development of halide glass optical fibre. Consequently, some techniques have been especially developed and adapted for fluoride glass preform preparation. All these techniques are based on melting and casting processes.

The first core/clad structure was obtained by Mitachi et al [4] by a clad over core method. It consisted of casting a cladding glass melt into a brass mould in which there was a polished core glass rod. The same group has suggested a second method based on jacketing a polished glass rod with appropriate thermoplastic tube such as FEP, which is used as an optical cladding [5]. FIGURE 1 shows these two methods. In both cases optical losses were very high, due to imperfections at the core/cladding interface.

A more appropriate technique, the build-in casting method, has been developed also by Mitachi et al [6]. First, a cladding glass tube is obtained by casting the cladding glass in a preheated mould which is then overturned immediately. The liquid melt in the centre of the mould flows out. The final preform is obtained by casting the core glass into the cladding tube. The great advantage of this method is the good optical quality of the core/clad interface (FIGURE 2). Fibre with losses as low as 1 dB/km has been drawn from preform prepared by this method [7]. However, long length fibres with a regular core

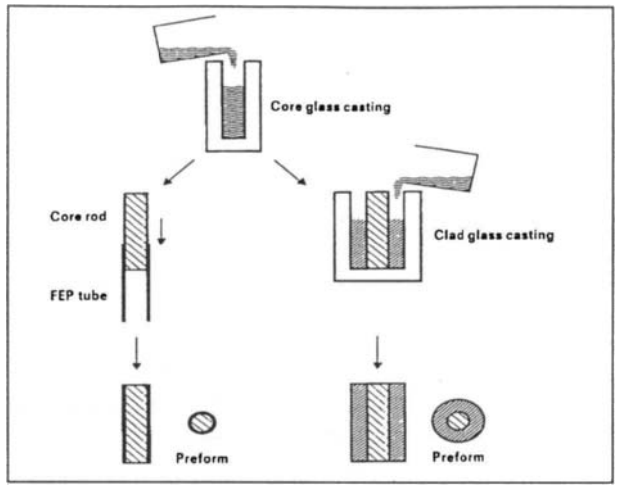


FIGURE 1 FEP jacketing and clad over core techniques (Mitachi et al).

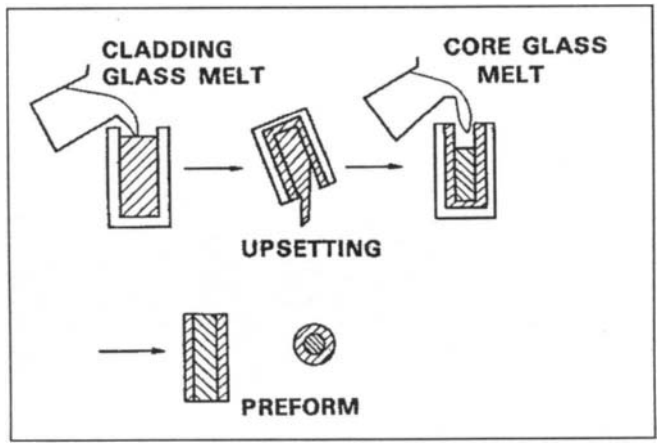


FIGURE 2 Build-in and casting (Mitachi et al).

diameter along the fibre are difficult to obtain. Indeed, preforms show tapered core dimensions along their length.

To overcome this problem, a rotational casting method has been proposed by Tran et al [8]. The cladding tube is prepared by pouring the clad melt into a cylindrical mould, which is rotated at a speed ranging from 3000 to 5000 rpm for a few seconds (FIGURE 3). Using this technique, the inner diameter of the cladding tube could be easily controlled by adjusting the volume of glass melt for a given mould. Fibre drawn from preform prepared by this technique shows transmission losses of about 1 dB/km [9].

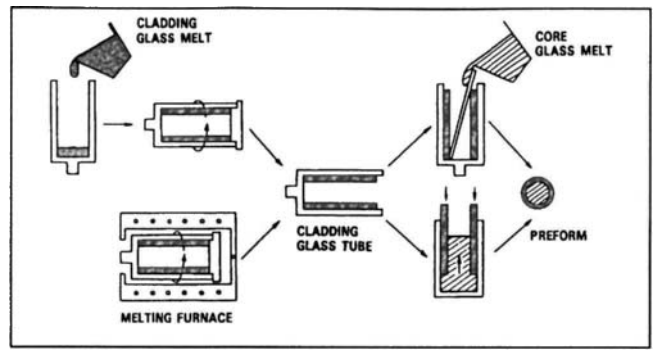


FIGURE 3 Rotational casting (Tran et al).

Using rotational casting under reduced pressure, Carter et al [1] have succeeded in preparing fibre with the lowest loss obtained so far. The fibre loss has been reduced to 0.65 dB/km at 2.59 μm, measured over a 110 m length of fibre. The fibre has a ZBLAN glass cladding and ZBLAN/Pb glass core composition. The core and clad diameters were 70 and 150 μm respectively.

Common problems with all the techniques described above include bubbles and crystal formation at the core/clad interface, which have a drastic influence on both optical and mechanical properties of the fibre. Indeed, the inner surface of the cladding tube is exposed to the inert gas atmosphere and reheated above glass crystallisation temperature by casting the core glass melt. Furthermore, core to clad diameter ratios lower than 0.5 are very difficult to achieve.

Alternatively, to avoid exposure of the inner surface of the cladding glass tube to the inert gas atmosphere, and thus minimise crystals and bubble formation at the core/clad interface, a modified build-in casting technique has been proposed by Sakaguchi et al [10]. A hole is made in the bottom plate of the mould. The cladding glass melt is first cast into a pre-heated brass mould. Then, the core glass melt is cast onto the cladding glass tube before the central part of the cladding glass solidifies. The mould is then shifted to make the central part of molten glass flowing down through the hole in the bottom plate. The core glass melt takes place at the central part of the cladding glass, to form the core-cladding structure (FIGURE 4). Unlike previous methods, the core/clad interface is never exposed to gas atmosphere, and never re-heated above the glass crystallisation temperature. In fact, the two glasses are at the same temperature. Generally, the core/clad diameter ratio is in the 0.5 to 0.6 range.

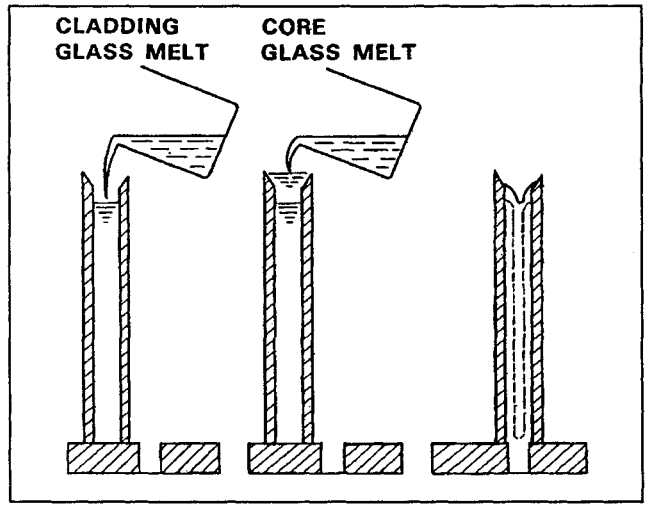


FIGURE 4 Modified build-in and casting (Sakaguchi et al).

In 1992 Clarke et al [11] added some interesting modifications to the technique described above. They used a shutter at the bottom of the mould to let the glass melt flow down, and a taper immediately above the shutter to prevent excess solidification of the glass. The shutter's thickness was fixed to 1mm to limit thermal exchange between the glass and the shutter (FIGURE 5). The time required before opening the shutter was longer than that needed in previous techniques. Thus, a small core diameter, about one-third of the cladding diameter, has been obtained by this technique.

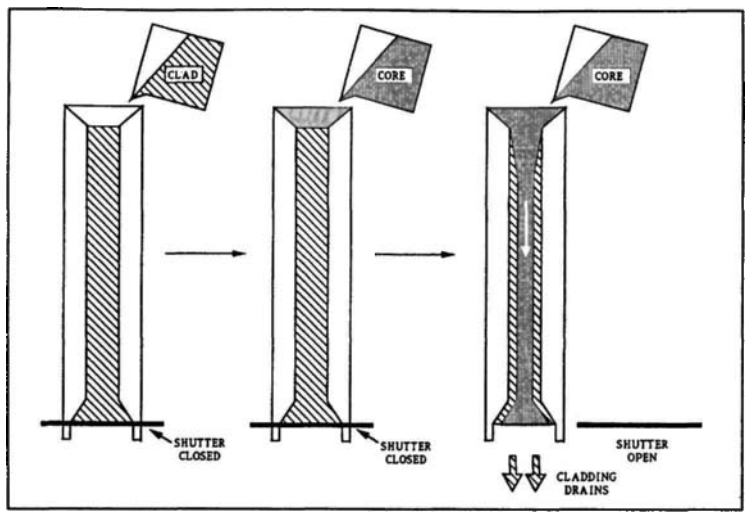


FIGURE 5 Improved modified build-in and casting technique (Clarke et al).

B2 Preforms for Single-Mode Fibres

Preforms for single mode fibre must have a clad/core diameter ratio equal to or greater than 15. So, single-mode fibres could not be directly drawn from preforms prepared by the techniques described above.

Ohishi et al has used a jacketing technique to prepare preforms for fluoride single-mode fibres [12]. This method consists of jacketing a preform with a glass tube (FIGURE 6), which are both prepared by the build-in casting technique. It is very important to obtain a smooth contact between the preform and the tube to achieve low loss single mode optical fibre.

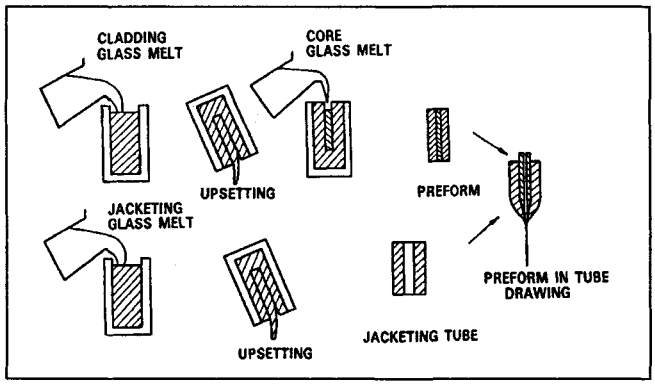


FIGURE 6 Preform preparation for single-mode optical fibre (Ohishi et al).

In order to decrease the core/clad ratio, a suction casting technique was developed by Ohishi et al in 1986 [13]. It is based on a special cylindrical brass mould having a reservoir at the bottom. First, the cladding glass melt is poured into this mould. Then the core glass melt is poured onto the cladding glass before complete solidification of the cladding glass melt. The core glass melt flows into the cladding glass tube by suction phenomena, due to volume constriction during cooling of the cladding glass melt. Core to cladding diameter ratio and preform length could be controlled by controlling the volume of the reservoir. A jacketing process is also necessary to achieve preforms for single mode fibres.

Fibre length is limited to a few hundreds of metres, because of the tapered core along the preform. 200 m single-mode fibres have been obtained with this process. The cladding and core diameters were 130 and 10 μm respectively, with a minimum transmission loss of 8.5 dB/km at 2.2 μm.

Andrews et al used a stretching technique to produce single-mode fluoride optical fibres. It consists of stretching and jacketing a preform, and then drawing the new preform into single-mode fibre [14]. No fibre loss measurement has been reported in this paper.

In order to limit the core diameter fluctuation along the fibre, a modified jacketing method has been proposed by Kanamori et al [15]. A jacketing glass tube and a preform are elongated together to form a preform with a small core diameter. The new preform is then jacketed with a second glass cladding tube and drawn into single-mode fibre. The jacketing tube and preform for elongation were prepared by conventional rotational casting and suction casting techniques respectively. The drawing tube was prepared by rotational casting in a mould with a tapered hole. They have drawn up to 500 m of a single mode fibre, with core and cladding diameters of 2.2 μm and 120 μm respectively. The longitudinal fluctuation of the core diameter over the whole length of the fibre was only 3%.

More recently Refik et al [16] have described a new approach to preparing preforms for single mode fibre by a rapid insertion method. A small core radius glass rod is rapidly inserted into a viscous cladding glass, just before the central glass melt solidifies. They have been able to insert into a viscous cladding glass a core glass rod with a diameter as small as 150 μm. No optical loss value has been reported. The time at which the core rod must be inserted into the glass melt is very critical since the temperature must be high enough to allow easy insertion of the core rod, and low enough to avoid the degradation of the core/clad interface.

Numerous other techniques have been proposed by different researchers, including reactive vapour transport (Tran et al [17]), the tubular crucible technique [18], a core injection technique proposed by Sanghera [19] and an extrusion method proposed by Miura et al [20].

C FIBRE DRAWING

Both double crucible and preform drawing techniques have been used to produce halide glass optical fibres. The first method has been especially developed for oxide glass with low melting temperature; thus only the second technique has proven to be effective in producing low loss fluoride glass optical fibres. Tokiwa et al [21] have prepared up to 500 m of single mode and 700 m of multi-mode fluoride fibres by the double crucible method, but no optical loss results have been reported. Indeed, this technique is effective for drawing long length single and multi-mode fibres, but suffers from poor concentricity of core and cladding, and crystal and bubble formation at the core/clad interface during drawing.

Halide glass fibres with good optical and mechanical properties are very difficult to prepare. This is due to the difficulty in preparing preforms free from crystals or micro bubbles, thermal and mechanical stresses, and the glass viscosity to temperature relationship. To minimise fluctuation of the fibre radius during the drawing process, precise control of drawing temperature is required. Furthermore, moisture must be kept as low as possible in the drawing furnace to avoid fibre surface crystallisation, which would have a drastic influence on mechanical and optical properties of the fibre. Generally, fibres are drawn in a dry inert atmosphere. However, it has been shown that adding NF_3 gas to the furnace atmosphere is effective in suppressing neckdown surface crystallisation, and thus improves the mechanical properties of the fibre [22].

To draw fluoride fibre from preforms, we use a conventional drawing tower similar to that used for silica based fibre. It includes a vertical feed table, a drawing furnace, a diameter controller, an in-line coating system, a tension monitor and a winding drum. FIGURE 7 shows a schematic diagram of a typical fibre drawing tower. While the basic technology used to draw fluoride fibre is similar to that used to draw silica fibre, drawing conditions are completely different. Indeed, drawing temperature, drawing tension and drawing speed are lower for fluoride fibre than those used for silica based fibre. Drawing temperature generally ranges from 290 to 500°C according to the glass system and composition. This temperature increases in the following order for the three fluoride glass systems: fluorozirconate - fluoroindate - fluoroaluminate. Drawing speed varies from 2 to 15 m/min according to drawing temperature, drawing tension and fibre diameter. As for silica based fibres, all these parameters have to be optimised in order to achieve fibres with good optical and mechanical properties. Indeed, it was shown that lower drawing temperature at a fixed speed, and higher speed at a fixed tension, are preferable in order to reduce transmission loss and improve fibre mechanical strength, respectively [23].

Prior to drawing, preforms must be well polished to achieve high strength optical fibres. Both mechanical polishing and chemical etching are used to remove flaws and surface contamination from the surface of fluoride glass preforms. Three solutions have been shown to be effective for improving mechanical properties of fluoride fibres: $ZrOCl_2$, HCl [24]; H_3BO_3, HCl [25]; NH_4NO_3, HNO_3 [26].

D COATING

In order to preserve fibre strength and protect the fibre surface from atmospheric attack, coatings on fibres are necessary. Teflon FEP has been used as an optical coating (n = 1.3); unfortunately it shows poor adhesion to the glass fibre. Furthermore, it has been found that water can easily permeate through FEP and lead to surface attack of the fibre. Currently UV cured polyacrylate coatings are commonly used to protect fluoride fibre. They provide quite good protection and preserve fibre strength. In

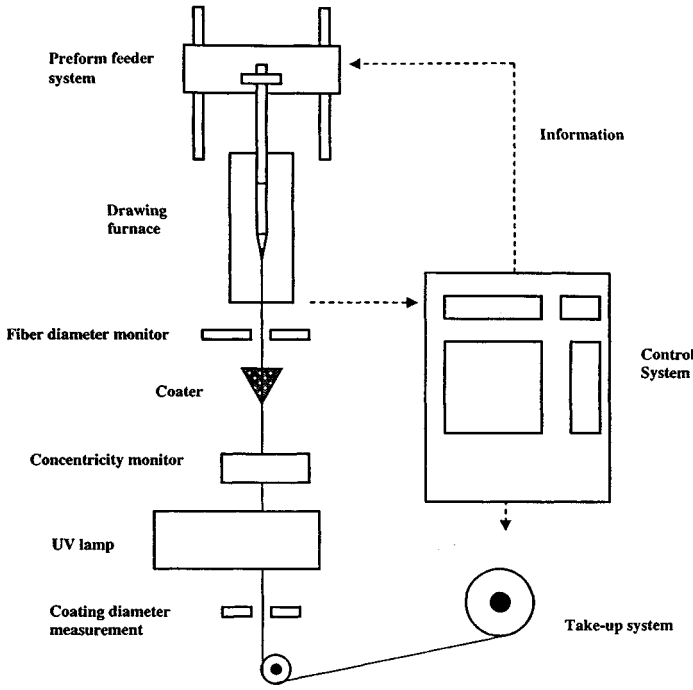


FIGURE 7 Schematic fibre drawing tower.

addition, they present the advantage of being applied on-line during the fibre drawing process. Recently, polyamide has also been successfully used as a coating for heavy metal fluoride glass fibre [27].

E CONCLUSION

Significant and rapid progress has been made in halide glass fibre technology. Indeed, the technology is now very mature, and actual fluoride fibres show good optical and mechanical properties to meet short and medium length application needs. However, further research is required to make optical and mechanical properties of these fibres as close as possible to the theoretical values.

Future development of halide fibres is strongly dependent on preform fabrication improvement. Ultra-low-loss halide glass optical fibres and their use in long length telecommunication links are still a serious but realistic challenge.

REFERENCES

[1] S.F. Carter et al [*Electron. Lett. (UK)* vol.26 no.25 (1990) p.2115-6]
[2] A. Soufiane [PhD Thesis no.829, Rennes 1 University, 1992, p.153]
[3] Y. Nishida, T. Kanamori, T. Sakamoto, Y. Ohishi, S. Sudo [*J. Non-Cryst. Solids (Netherlands)* vol.221 (1997) p.238-44]
[4] S. Mitachi et al [*Electron. Lett. (UK)* vol.17 no.3 (1981) p.128-9]
[5] S. Mitachi, T. Miyashita, T. Manabe [*Phys. Chem. Glasses (UK)* vol.23 no.6 (1982) p.196]
[6] S. Mitachi, T. Miyashita, T. Kanamori [*Electron. Lett. (UK)* vol.17 (1981) p.591-2]
[7] T. Kanamori, S. Sakaguchi [*Jpn. J. Appl. Phys. (Japan)* vol.25 (1986) p.L468-70]
[8] D.C. Tran, C.F. Fisher, G.H. Sigel [*Electron. Lett. (UK)* vol.18 (1982) p.657-8]
[9] G. Lu, I.D. Aggarwal [*Mater. Sci. Forum (Switzerland)* vol.19-20 (1987) p.375-8]
[10] S. Sakaguchi, S. Takahashi [*J. Lightwave Technol. (USA)* vol.LT-5 (1987) p.1219-28]

[11] K. Clarke, Y. Ito [*J. Non-Cryst. Solids (Netherlands)* vol.140 (1992) p.265-8]
[12] Y. Ohishi, S. Mitachi, S. Takahashi [*J. Lightwave Technol. (USA)* vol.LT-2 (1984) p.593-6]
[13] Y. Ohishi, S. Sakaguchi, S. Takahashi [*Electron. Lett. (UK)* vol.22 (1986) p.1034-5]
[14] W. Andrews, D. Coulson, G. Rosman [*J. Non-Cryst. Solids (Netherlands)* vol.140 (1992) p.281-4]
[15] T. Kanamori et al [*J. Non-Cryst. Solids (Netherlands)* vol.213&214 (1997) p.121-5]
[16] A. Refik Kortan, N. Kopylov, E. Özdas, R. Pafchek [*J. Non-Cryst. Solids (Netherlands)* vol.213-214 (1997) p.90-4]
[17] D.C. Tran, M.J. Burke, G.H. Sigel, K.H. Levin [*Proc. OFC'84* TuG2, New Orleans, Louisiana, 1984]
[18] Y. Noda, T. Nakai, N. Norimastu, Y. Mimura, O. Shinbori, H. Tokiwa [*Mater. Sci. Forum (Switzerland)* vol.32-33 (1988) p.1-8]
[19] J.S. Sanghera, B.B. Haribson, I.D. Aggarwal [*J. Non-Cryst. Solids (Netherlands)* vol.140 (1992) p.146-9]
[20] K. Miura, I. Masuda, K. Itoh, T. Yamashita [*Mater. Sci. Forum (Switzerland)* vol.67&68 (1991) p.335-40]
[21] H. Tokiwa, Y. Mimura, T. Nakai, O. Shinbori [*Electron. Lett. (UK)* vol.21 no.24 (1985) p.1131-2]
[22] A. Staudt, A. Schoberth, H.W. Scheider [*Glastech. Ber. (Germany)* vol.62 no.3 (1989) p.88-92]
[23] S. Hiria et al [*Mater. Sci. Forum (Switzerland)* vol.67&68 (1991) p.323-8]
[24] H.W. Scheneider, A. Schoberth, A. Staudt, C. Gerndt [*Electron. Lett. (UK)* vol.22 (1986) p.949-50]
[25] P.H. Klein, P.C. Pureza, W.I. Roberts, I.D. Aggarwal [*Mater. Sci. Forum (Switzerland)* vol.32-33 (1988) p.571-6]
[26] S. Sakaguchi, Y. Hibino, Y. Ohishi, S. Takahashi [*J. Mater. Sci. Lett. (UK)* vol.6 (1987) p.1440-2]
[27] L. Vacha, P.J. Melling [US Patent no.5688553, Nov. 18, 1997]

C4.3 Loss of halide glass optical fibres

D.W. Hewak and M. Saad

August 1998

A INTRODUCTION

The transmission window of halide glasses extends from about 0.2 μm to beyond 8 μm depending on the composition of the glass [1]. However the intrinsic loss of chloride and fluoride glasses has yet to be matched by fibres pulled from these same glasses. FIGURE 1 shows the loss spectrum of a typical low loss fluoride fibre. Major contributors to the losses observed are extrinsic absorptions due to transition metals, rare-earth ions and water. In addition, the relatively low stability of these glasses and propensity to devitrification results in the possibility of crystals and defects which contribute to scattering. This Datareview discusses these mechanisms for loss in a halide fibre.

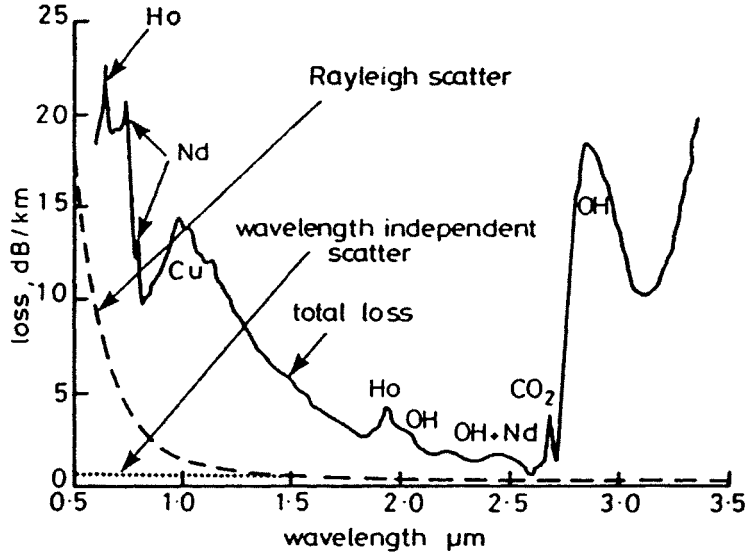


FIGURE 1 Total loss spectrum of a typical ZBLAN fibre, measured over a 110 m length [9].

B ABSORPTION

A complete review of the position of the absorption bands and the absorption coefficients of all major contributors to fluoride fibre loss can be found in [2]. Absorption losses are wavelength dependent and thus different impurities are of concern at different wavelengths of fibre operation. Most research has described losses around 2.55 microns which is the low loss window for ZBLAN fibres. However, impurities such as the transition metals, rare earth ions, oxides, OH^-, molecular ions and dissolved gases contribute to loss across the entire transmission of halide glasses.

B1 Transition Metals

Absorption due to 3d transition metals is one of the main factors in halide fibre loss. Intense absorptions from the visible to the infrared are observed and even levels of 1 ppm of some transition metal ions are sufficient to introduce peak absorption losses of around 1 dB/m. Many of the transition metals exist in

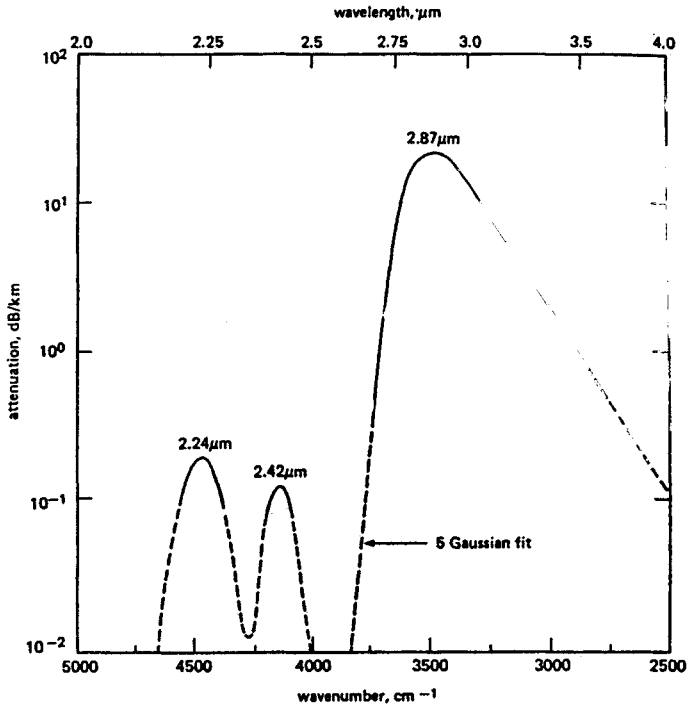


FIGURE 2 Loss spectrum due to OH^- in a ZBLALiPb glass [2].

various oxidation states, depending on whether an oxidising or reducing atmosphere was used during melting. Loss spectra for the transition metals in various oxidation states can be found in [2], while in [3] the calculated effects of various transition metal impurities at levels of 1 ppm are presented. TABLE 1 gives the absorption coefficients for transition metal and rare earth impurities in a fluorozirconate glass.

TABLE 1 Absorption coefficients for transition metal and rare-earth impurities at 2.55 μm in order of absorption strength [4].

Ion	Loss (dB/km per ppm)
Co^{2+}	31.0
Fe^{2+}/Fe^{3+}	28.0
Nd^{3+}	20.0
Ni^{2+}	6.0
Sm^{3+}	2.6
Pr^{3+}	1.8
Eu^{3+}	1.4
Dy^{3+}	0.7
Cu^{2+}	0.14

B2 Rare-Earth Ions

Although there exist a large number of absorption bands associated with the rare-earth elements, their absorption strengths are generally about an order of magnitude less than those of the transition metals. At 2.55 microns, the most deleterious element is Nd, which has an absorptivity of 20 dB/km per ppm. Like the transition metals, the rare earths introduce absorptions from the visible to the infrared. In addition to a reduced absorption coefficient, their absorption bands are also narrower.

B3 Water

Many of the starting halide components contain water-associated impurities because of their high susceptibility to hydrolysis. The presence of OH^- ions has been observed in both bulk halide glass and fibre. The fundamental OH band is centred at about 2.9 μm and has an absorption coefficient of approximately 2 - 5 dB/m per ppm depending on the glass composition [5]. In addition, there are two bands observed at 2.24 and 2.42 μm which are attributed to combination bands with Zr-F and Ba-F, respectively. In addition, an OH^- overtone occurs at 1.44 μm.

Glasses containing alkali elements show less absorption loss, while glasses without alkali seem to vary depending on the ZrF_4 mole fraction and the type and content of additional elements such as LaF_3, GdF_3, YF_3 and AlF_3 which are added to provide thermal stability. The difference in OH^- absorption can probably be attributed to the rigidness of the glass structure [6].

The strong absorption at 2.9 μm can be reduced through processing of the glass under a reactive atmosphere (RAP). The basic principle of RAP is that all non-fluoride components are converted to fluorides, thus eliminating them as sources of extrinsic loss. By bubbling NF_3 through the glass melt at 600°C for 30 minutes, OH^- levels are reduced to only a weak residual absorption due to OH^- on the glass surface [3].

B4 Molecular Ions and Dissolved Gases

Polyatomic molecular ions such as NH_4^+, CO_3^{2-}, NO_3^-, SO_4^{2-} and PO_4^3 have their fundamental absorptions in the infrared region and thus contamination by these ions can limit infrared transmission. A possible source of many of these complex ions is through the NH_4HF_2 which is frequently mixed into a glass melt as a fluorinating agent during glass melting. These contaminants and their absorption bands are summarised in TABLE 2.

TABLE 2 Molecular ion and gas contaminants of fluoride glasses [3].

Ion	Absorption bands (μm)
NH_4^+	3.0, 7.0
CO_3^{2-}	2.9
SO_4^{2-}	4.3, 4.6
PO_4^3	4.8
NO_3^-	none
CO_2	4.252, 2.675, 2.775
CO	4.755

Like OH^-, CO_3^{2-} and NO_3^- can be eliminated by NF_3 processing. SO_4^{2-} can be reduced by melting at high temperature, but PO_4^{3-} is very difficult to eliminate. Dissolved gases can often be removed by prolonged heating or by treatment under vacuum. However, decomposition of these impurities often leads to the formation of oxide impurities which are associated with an increased scattering loss.

C SCATTERING

Crystals, bubbles, oxides and other particles have a different refractive index from the glass and therefore increase scattering loss. The degree of additional scattering loss depends on the size of the particle and the difference in refractive index. This scattering theory has been reviewed in [2]. A significant problem associated with the relatively high loss of halide fibres is the formation of bubbles and crystals. These frequently occur at the core/cladding interface and the centre of the preform.

The magnitude of scattering loss can be measured using an integrating sphere, allowing it to be distinguished from absorption loss. Lu [7] measured the scattering loss in a low-loss (6.8 dB/km at 2.55 μm) fluoride fibre and a scattering level of 1 dB/km. Most of the loss (0.6 dB/km) is due to wavelength independent scattering. The remainder obeys a Rayleigh dependence. Faint pinpoints of light appear to have a negligible effect on scattering and a couple of bright pinpoints has only a small impact. The continuous glow between pinpoints must therefore account for the majority of the scattering loss.

C1 Crystals

A variety of crystals have been observed in bulk glasses and fibres and include AlF_3, LaF_3, β-$BaZrF_6$, α-$BaZr_2F_{10}$, β-$BaZr_2F_{10}$, $NaZrF_5$, $NaBaZr_2F_{11}$, $Na_7Zr_6F_{31}$ and $LaZr_2F_{11}$ [8-12]. The crystallisation tendency of glasses strongly depends on the basic glass composition and dopants that are necessary to give a sufficient refractive index difference between core and cladding glasses. In addition, impurities in the glass such as hydroxyl ions, various complex ions, oxides and metal particles can greatly enhance crystallisation.

Studies have shown that the number of crystals formed on reheating a fluoride glass is independent of the crystallisation nucleation rate. This indicates that homogeneous nucleation is not the predominate mechanism causing crystallisation, but rather it is heterogeneous nucleation [4]. Halide glasses have been prepared that do not exhibit crystallisation on rigorous heating [13]; hence bulk crystallisation is not a limiting problem for ultra low loss fibre.

C2 Bubbles

A major cause of loss in fluoride fibres has been extrinsic scatter from bubbles trapped in preforms during casting. To eliminate bubbles, a reduced pressure casting technique has been developed which significantly lowers fibre loss. Casting and spinning take place in a chamber connected to a vacuum pump resulting in a preform which is visibly free from bubbles [14].

C3 Oxide Impurities

Mitachi [15] has shown that only about 100 ppm of oxide is soluble in a fluorozirconate glass. Thereafter, any excess oxide precipitates out and leads to increased scattering. An increase in the critical cooling rate with increasing oxide content was also observed, indicating that more rapid cooling rates were required to inhibit crystallisation

C4 Other Particles

Non-oxide particles can also contribute to scattering whether or not they act as nucleating sites for crystal growth. The most common particles originate from the crucible material, particularly from the noble metals. Particles of Pt, Au, Rh and Ir have been identified. In addition, some glasses were found to contain submicron sized transition metal phosphides such as Fe-P, Ni-P or Co-P which were probably unmelted raw material impurities [3].

D CONCLUSION

Several extrinsic sources of loss contribute to the loss of halide fibres through the absorption and scattering of light. France [16] has estimated that the minimum loss that could be achieved with a realistic reduction of extrinsic absorption and negligible extrinsic scattering is 0.03 dB/km, about a factor of three higher than the intrinsic loss minimum. This is a factor of seven lower than in a typical silica fibre. This prediction, made over a decade ago, has yet to be realised.

REFERENCES

[1] J.L. Adam [Datareview in this book: *C1.2 Intrinsic scattering losses of halide glass*]

[2] P.W France, M.G. Drexhage, J.M. Parker, M.W. Moore, S.F. Carter [*Fluoride Glass Optical Fibres* (Blackie, London, 1990)]

[3] Y. Mimura, T. Nakai [in *Fluoride Glass Fiber Optics* Eds. I.D. Aggarwal, G. Lu (ISBN 0-12-044505-0, Academic Press, 1991) 'Optical Fibre Loss Mechanisms']

[4] J. Sanghera, L. Busse, I. Aggarwal, C. Rapp [*Fluoride Glass-Based Fibres in Infrared Fiber Optics* Eds. J. Sanghera, I. Aggarwal (CRC Press, New York, 1998) ch.4]

[5] G. Fonteneau [*Mater. Res. Bull. (USA)* vol.19 (1984) p.685]

[6] S. Sakaguchi, S. Takahashi [*J. Lightwave Technol. (USA)* vol.5 (1987) p.1219]

[7] G. Lu, K.H. Levin, M.J. Burk, D.C. Tran [*Electron. Lett. (UK)* vol.22 (1986) p.602-3]

[8] G. Lu, C.F. Fisher, M.J. Burke, D.C. Tran [*Am. Ceram. Soc. Bull. (USA)* vol.63 (1984) p.1416]

[9] N.P. Bansal, R.H. Doremus, C.T. Moynihan, A.J. Bruce [*Mater. Sci. Forum (Switzerland)* vol.5 (1985) p.211]

[10] J.M. Parker, A.G. Clare, A.B. Seddon [*Mater. Sci. Forum (Switzerland)* vol.5 (1985) p.257]

[11] S.F. Carter, P.W. France, M.W. Moore, J.R. Williams [*Mater. Sci. Forum (Switzerland)* vol.19-20 (1987) p.511]

[12] M.W. Moore, P.W. France, S.F. Carter, J.R. Williams [*Proc. 5th Int. Symp. Halide Glasses* Shizuoka, Japan, 1988]

[13] J.S. Sanghera, P. Hart, M.G. Sachon, K.J. Ewing, I.D. Aggarwal [*Mater. Sci. Forum (Switzerland)* vol.7 (1991) p.67-8]

[14] S.F. Carter, M.W. Moore, D. Szebesta, J.R. Williams, D. Ranson, P.W. France [*Electron. Lett. (UK)* vol.36 (1990) p.2115]

[15] S. Mitachi, S. Sakaguchi, H. Shigematsu, S. Takahashi [*Jpn. J. Appl. Phys. (Japan)* vol.24 (1985) p.827]

[16] P.W. France [*Proc. SPIE (USA)* vol.618 (1986) p.51-7]

C4.4 Reliability of halide glass optical fibres

K. Fujiura

August 1997

A INTRODUCTION

Of possible accidents related to the reliability of an optical fibre host, fibre breakage is worse than a loss increase. Such breakages are catastrophic because glass is inherently brittle due to its lack of inelastic flow. The lifetime estimation based on the fracture mechanism [1] has been intensively studied for silica optical fibres [2]. In halide glasses there is ionic bonding between metal ions and halide ions. The nature of this bonding means that the chemical durability and mechanical hardness of these glasses are much lower than those of silicate glasses. In recent years, there has been increasing interest in halide fibre reliability since the emergence of rare-earth doped fluoride optical fibre amplifiers. This Datareview related to the reliability of halide glass optical fibres reports their chemical durability, mechanical strength and estimated lifetime.

B CHEMICAL DURABILITY

Halide glass surfaces can be degraded by a hydrolysis reaction with environmental water. Numerous reports have appeared on the corrosion of heavy metal fluoride glasses in aqueous solution and these provide basic data on the resistance of halide glass to water [3]. The average leach rates of a number of ZrF_4-based compositions were reported to be in the 10^{-3} to 10^{-2} g/cm^2/d range and glasses containing alkalis such as ZrF_4-BaF_2-LaF_3-AlF_3-NaF, ZrF_4-BaF_2-LaF_3-AlF_3-LiF and ZrF_4-BaF_2-LaF_3-AlF_3-LiF-PbF_2 have higher leach rates than those without alkaline ions [4]. FIGURE 1 summarises the leach rates of ZrF_4-based and BaF_2/ThF_4-based fluoride glasses compared with those of silicate glasses [5]. Both fluoride glasses have poor durability compared with Pyrex, but are more durable than SiO_2-Na_2O glass. Fluoroaluminate glasses such as BaF_2-CaF_2-YF_3-AlF_3 have leach rates more than three times lower than those of ZrF_4-based fluoride glasses [6]. Generally, fluoride glasses are more durable than other halide glasses and fluoroaluminate glasses are more durable than fluorozirconate glasses.

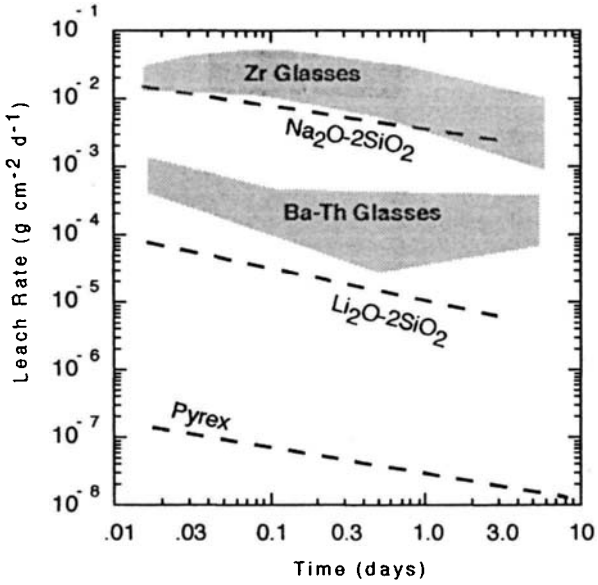


FIGURE 1 Comparison of average leach rates in deionised water of ZrF_4-based and BaF_2/ThF_4-based glasses and silicate glasses at 25°C [5].

The leach rates can be a criterion for the moisture sensitivity of the glass surface. In terms of fibre breakage, the most important problem is surface crystallisation caused by moisture, which might result in the origin of a fracture. Sakaguchi et al [7] have observed EPR peaks of ZrO_2 indicating the importance of water in promoting the formation of flaws and crystallisation. The effects of aging in a humid atmosphere on ZrF_4-based fluoride fibres coated with epoxy-acrylate resin have been investigated. FIGURE 2 [8] shows the results measured at 80°C. The fibre strength is degraded by 50% at 80°C - 90% RH.

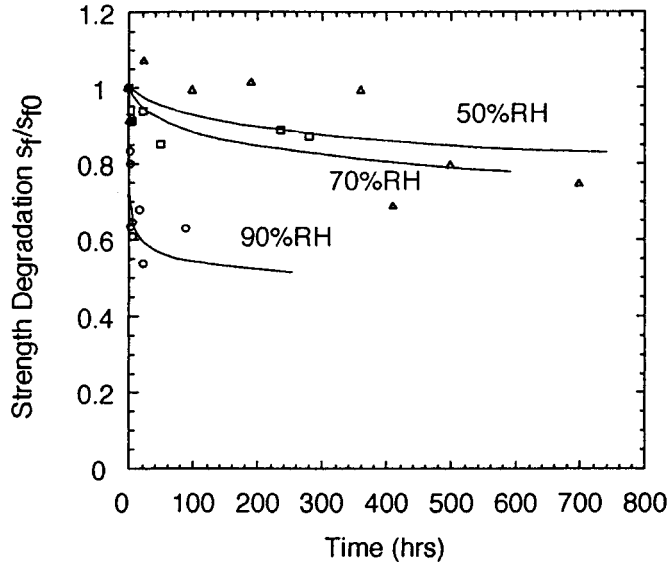


FIGURE 2 Strength degradation resulting from zero-stress aging at 80°C [8].

C MECHANICAL STRENGTH

Microhardness, K_{1c} and elastic constants have been reported for fluoride glasses [9-13]. TABLE 1 shows microhardness, K_{1c} and elastic properties of several kinds of glass [14]. The K_{1c} of fluoride glasses is approximately 40% that of silica glass. This means fluoride glass is softer than silica glass. The mechanical properties listed in TABLE 1 vary considerably according to glass composition and preparation conditions. The values are typical and fall in technologically useful ranges.

TABLE 1 Microhardness, K_{1c} and elastic properties [14].

Glass	Microhardness (GPa)	K_{1c} (MPa $m^{1/2}$)	Young's modulus (GPa)	Shear modulus (GPa)	Poisson's ratio
Fluoride	2.2	0.3	51	20	0.3
Chalcogenide	1.0	0.25	20	7.5	0.26
Silica	7.7	0.75	73.1	31.2	0.17
Silicate	6.2	0.7	71.3	29.2	0.22

The intrinsic strength of fluoride fibre was estimated from both the force needed to separate the atomic layers and K_{1c}. The intrinsic strength is defined as the breaking stress of a flawless sample of a glass material, with no residual stress and in an environment where there is no chemical interaction. The estimated intrinsic strengths are 3.3 GPa and 6.1 GPa from the atomic force and K_{1c}, respectively [14]. The fibre strength has been measured using tensile strength measurement or bend strength measurement. Generally, the bending strength can be larger than the tensile strength because the gauge length for bend measurement is shorter than that for tensile measurement. The tensile strengths of ZrF_4-based fluoride fibres have been reported to be in the 300 to 700 MPa range [15]. These values are less than one quarter of those for commercially available silica fibres.

D LIFETIME ESTIMATION

There has been only one paper regarding the lifetime estimation of halide fibre. This estimation was made for ZrF_4-based fluoride fibres [8]. The lifetime was estimated by using zero-stress aging and dynamic and static fatigue tests. In the estimation, it was assumed that the applied stress was 36 MPa, which corresponded to that applied by a 10 cm-diameter fibre bobbin, and that the allowable failure probability was 10^{-6}. The lifetime was estimated for fibres with strengths of 350 MPa, 400 MPa and 500 MPa. FIGURE 3 shows the humidity dependence of the estimated lifetime at 80°C for ZrF_4-based fluoride fibres with different initial strengths. A sufficient lifetime of over twenty-five years can be guaranteed for fluoride fibres with an initial strength of 500 MPa at 80°C - 80% RH [8]. Results for ZrF_4-based fluoride fibre with a strength of 350 MPa at 80°C and 50% RH have indicated that the predicted lifetime is about sixty-five years at an applied stress of 36 MPa for an allowable failure probability of 0.5 [8]. When the allowable failure probabilities are taken into account, the results from the dynamic and static tests are consistent. The results indicate that fluoride fibres with a strength of 500 MPa have a long-term reliability of over twenty-five years in optical fibre amplifiers in a practical environment such as 80°C - 80% RH [8].

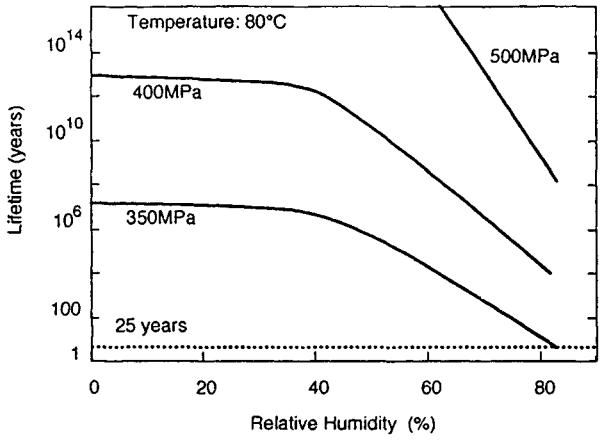


FIGURE 3 Humidity dependence of the estimated lifetime at 80°C for fluoride fibres with different initial strengths [8].

E CONCLUSION

Sections B - D presented data regarding the chemical durability, the mechanical properties and the lifetime estimation of halide glass optical fibres. The data indicate that halide glasses are susceptible to moisture damage which finally causes a fibre breakage and that their mechanical properties are inherently inferior to those of silica glass. The lifetime estimation, however, has demonstrated that long-term reliability can be guaranteed in a practical environment.

REFERENCES

[1] M.A. Saifi [*Proc. SPIE - Int. Soc. Opt. Eng. (USA)* vol.1366 (1990) p.58-70]

[2] H.H. Yuce, F.P. Kapron [*Proc. SPIE - Int. Soc. Opt. Eng. (USA)* vol.1366 (1990) p.144-56]

[3] See for example C.J. Simmons, H. Sutter, J.H. Simmons, D.C. Tran [*Mater. Res. Bull. (USA)* vol.17 (1982) p.1203-10]

[4] C.J. Simmons, J.H. Simmons [*J. Am. Ceram. Soc. (USA)* vol.69 (1986) p.661-9]

[5] C.J. Simmons [*J. Am. Ceram. Soc. (USA)* vol.70 (1987) p.295-300]

[6] T. Iqbal, M.R. Shahriari, G. Merberg, G.H. Sigel Jr. [*J. Mater. Res. (USA)* vol.6 (1991) p.401-6]

[7] S. Sakaguchi, Y. Terunuma, Y. Ohishi, T. Kanamori [*J. Mater. Sci. Lett. (UK)* vol.6 (1987) p.1063-5]

[8] K. Fujiura, K. Hoshino, T. Kanamori, Y. Nishida, Y. Ohishi, S. Sudo [*Tech. Digest of Optical Amplifiers and Their Applications* Davos, Switzerland, 15-17 June 1995 (Optical Society of America, Washington DC, USA, 1995)]

[9] J.J. Mecholsky [*Proc. 2nd Int. Symp. on Halide Glasses* (Renssalaer Polytechnic Institute, USA, 1983) paper 32]

[10] J.J. Mecholsky, A.C. Gonzales, C.G. Patano, B. Bendow, S.W. Freiman [*Proc. 4th Int. Symp. on Halide Glasses* Monterey, USA, 26-29 January 1987 (ISHG, USA, 1987)]
[11] A. Tesar, R.C. Bradt, C.G. Pantano [*Proc. 2nd Int. Symp. on Halide Glasses* Troy, USA, 2-5 August 1983 (ISHG, USA, 1983)]
[12] B.D. Michels, G.H. Frichat [*J. Am. Ceram. Soc. (USA)* vol.64 (1981) p.C-150]
[13] P.J. Weber, J.A. Savage [*J. Non-Cryst. Solids (Netherlands)* vol.20 (1976) p.271-83]
[14] S.F. Carter [in *Fluoride Glass Optical Fibres* Ed. P.W. France (Blackie, 1990) ch.9 p.219-37]
[15] See for example H.W. Schneider, A. Schoberch, A. Staudt, C. Gerndt [*Proc. SPIE - Int. Soc. Opt. Eng. (USA)* vol.799 (1987) p.112-6]

PART C: HALIDE GLASS

CHAPTER C5

SELECTED APPLICATIONS

C5.1 Optical amplifiers based on rare earth-doped halide glass
C5.2 Fibre lasers based on rare earth-doped halide glass

C5.1 Optical amplifiers based on rare earth-doped halide glass

T. Kanamori

September 1998

A INTRODUCTION

We report on current progress in the development of halide glass fibre amplifiers. We describe the fabrication of low-loss Pr^{3+}-doped InF_3-based fibres and their use in constructing efficient Pr^{3+}-doped fibre amplifiers (PDFAs). High gain coefficients of 0.36, 0.30, 0.26 and 0.18 dB/mW are realised for the PDFA using fibres with Δn values of 6.6, 4.6, 3.7 and 2.5%, respectively.

B BACKGROUND

Optical fibre amplifiers are key devices for increasing the transmission distance, speed and capacity of optical communication systems. Recent trends, such as the development of wavelength-division multiplexing (WDM) systems, has meant that fibre amplifiers must meet a variety of requirements. These include high gain, high output power, a low noise figure, a broad and flat gain spectrum, high reliability, low cost, and compactness. Halide glass fibre amplifiers have the potential to meet these requirements.

Since the first demonstration of 1.3 μm amplification using a Pr^{3+}-doped ZrF_4-based fibre, low phonon energy glasses have generated great interest as efficient hosts [1,2]. This is because of the $^1G_4$ to $^3H_5$ transition. There has been a considerable amount of research on new glass hosts for efficient PDFAs. The suggested hosts are the InF_3-based system [3], the InF_3/GaF_3-based system [4], the PbF_2/InF_3-based system [5], mixed-halide glasses [6], chalcogenide glasses such as Ga-La-S [7], Ga-Na-S [8] and As-S [9]. The InF_3-based fluoride glass family is the most promising candidate as the glass host for the next generation of PDFAs in terms of meeting many of the above requirements. The key issue in developing an efficient InF_3-based PDFA for practical use is to reduce the losses of the high-Δn fibres to the level of ZrF_4-based fibre.

C EXPERIMENTAL

C1 Single-Mode Fibre Fabrication

We fabricated single-mode fibres by using a modified jacketing method [10]. The preforms were prepared by the conventional suction-casting method. The jacketing tubes for elongation and fibre drawing were produced by the rotational casting method using moulds with a cylindrical hole and a tapered hole, respectively.

(a) Melting and casting: InF_3 and GaF_3 [3,5] were purified by solvent extraction with acetylacetone in benzene. Fluorides with a high purity of much better than 99.99% were used as the glass materials. Mixtures of the core and cladding materials and NH_4F:HF were melted at 850°C in vitreous carbon crucibles. The melts were cast into metal moulds to produce preforms and jacketing tubes.

(b) Fibre drawing: a preform prepared by suction-casting, which had a tapered core, was elongated together with a straight jacketing tube into a secondary preform. To eliminate the tapered core structure in the secondary preform, a tapered jacketing tube was used for the fibre drawing

process. The secondary preform was inserted into the tapered jacketing tube and drawn into a single-mode optical fibre coated with UV-curable acrylate.

C2 Measurements

The transmission loss spectra were measured using the cutback technique. The signal gain dependence on pump power was measured using the fabricated Pr^{3+}-doped fibre. The fibre was butt-joined to wavelength-division-multiplexing couplers and forward pumped using a Ti:sapphire laser. The pumping wavelength was 1.015 μm, and the signal wavelength and signal level were 1.30 μm and -30 dBm, respectively.

D RESULTS AND DISCUSSION

Single-mode fibres with Δn values of 2.5 and 3.7% were fabricated using the InF_3-based system [3], and 4.6 and 6.6% using the PbF_2/InF_3-based system [5]. A typical transmission loss spectrum is shown in FIGURE 1. The large peaks around wavelengths of 0.6 and 1.0 μm are caused by Pr^{3+}. The small peak at 0.8 μm is due to the cutoff of the first high-order mode. TABLE 1 lists the parameters and transmission losses of the Pr^{3+}-doped fibres we obtained. The transmission losses of the fibres with Δn values of 2.5 and 3.7%, which we fabricated using the InF_3-based system, were effectively reduced to the level of ZrF_4-based single-mode fibre by using purified InF_3 and GaF_3 raw materials. These loss characteristics indicate that the losses of the InF_3-based fibres with Δn values of 2.5% and 3.7% approach the practical level required for fibre amplifiers. By contrast, the fibres with Δn values of 4.6 and 6.6%, fabricated from the PbF_2/InF_3-based system, exhibit a slightly higher loss value. The

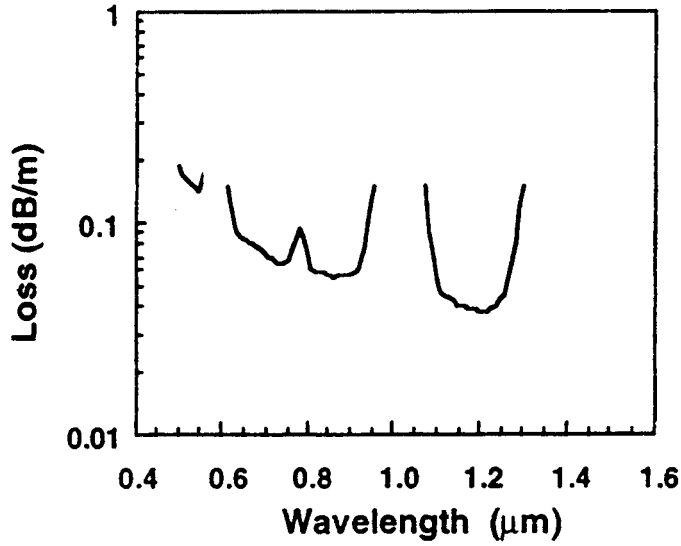


FIGURE 1 A typical transmission loss spectrum.

TABLE 1 Characteristics of Pr^{3+}-doped InF_3-based single-mode fibres (Pr^{3+} content is 500 ppm).

Δn (%)	Glass system	Core diameter (μm)	Cutoff wavelength (μm)	Loss (dB/m @ 1.2 μm)
2.5	InF_3-based glass	2.0	0.9	0.04
3.7	InF_3-based glass	1.8	1.0	0.05
4.6	PbF_2/InF_3-based glass	1.6	1.0	0.18
6.6	PbF_2/InF_3-based glass	1.2	1.0	0.20

difference in the loss levels indicates that the thermal stability of the PbF_2/InF_3-based system must be slightly improved.

FIGURE 2 shows the internal small signal gain dependence on the pump power for 20 m long and 19 m long single-mode fibres with Δn values of 3.7 and 6.6% respectively [11]. The dependence for the most efficient ZrF_4-based fluoride fibre with a Δn of 3.7% is also shown for comparison [12]. An internal small signal gain of 28.2 dB, corresponding to a net gain of 20 dB, for a fibre with a Δn of 6.6% was achieved at a pump power of 100 mW. This net gain is nearly double that of the most efficient ZrF_4-based Er^{3+}-doped fibre. The gain coefficient was increased from 0.18 to 0.36 by increasing the Δn from 2.5 to 6.6% for InF_3-based fibres. It is clear that InF_3-based fibre achieved gain coefficients about 1.3 times higher than ZrF_4-based fibre with the same Δn value.

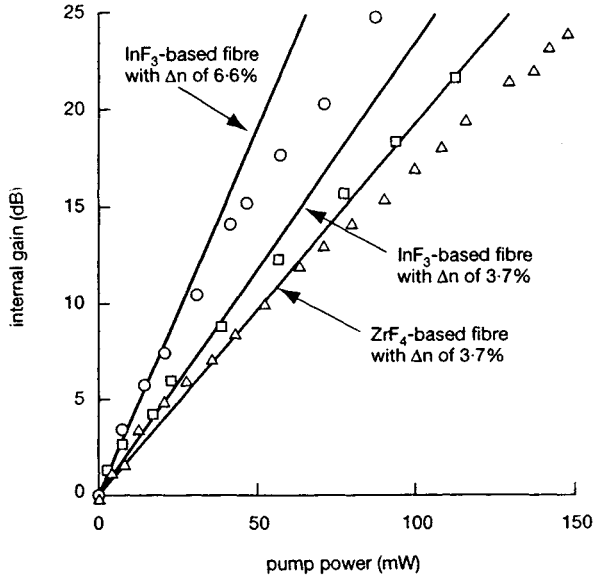


FIGURE 2 Internal small signal gain dependence on the pump power for 20 m long and 19 m long single-mode fibres with Δn values of 3.7 and 6.6% respectively.

E CONCLUSION

We have successfully fabricated low-loss InF_3-based Pr^{3+}-doped single-mode fibres as efficient 1.3 μm band amplification hosts. We achieved high gain coefficients of 0.36, 0.30, 0.26 and 0.18 dB/mW for PDFAs using fibres with Δn values of 6.6, 4.6, 3.7 and 2.5% respectively. We believe that this newly developed PDFA using halide glass fibres will be highly promising for upgrading the current optical transmission systems.

ACKNOWLEDGEMENT

The author acknowledges co-authors Y. Nishida, A. Mori, K. Kobayashi, M. Yamada, T. Shimada, M. Shimizu and Y. Ohishi and thanks K. Nakagawa, K. Hoshino, Y. Terunuma, K. Oikawa, K. Shikano and K. Kato for fibre preparation and H. Kozawaguchi and S. Sudo for their encouragement.

REFERENCES

[1] Y. Ohishi, T. Kanamori, T. Kitagawa, S. Takahashi, E. Snitzer, G.H. Sigel [*Opt. Lett. (USA)* vol.16 (1991) p.1747]

[2] Y. Ohishi, T. Kanamori, T. Nishi, S. Takahashi [*Proc. Int. Cong. Glass* Madrid (1992) p.73]
[3] Y. Nishida, T. Ohishi, T. Kanamori, Y. Teranuma, K. Kobayashi, S. Sudo [*Proc. 19th Euro. Conf. Optical Communication* Montreaux, vol.1 (1993) p.34]
[4] H. Yanagita, K. Itoh, E. Ishikawa, H. Aoki, H. Toratani [*Tech. Dig. OFC'95* San Diego, USA, 26 Feb-3 March 1995 (Opt. Soc. America, Washington DC, USA, 1995) PD2]
[5] Y. Nishida, T. Kanamori, Y. Ohishi, M. Yamada, K. Kobayashi, S. Sudo [*Tech. Dig. OAA'96* Monterey, CA, USA, 11-13 July 1996 (Opt. Soc. America, Washington DC, USA, 1996) PD3]
[6] M.A. Newhouse, B.G. Aitken, R.F. Bartholomew, L.J. Button, N.F. Borrelli [*Tech. Dig. OAA'93* Yokohama, Japan, 4-6 July 1993 (Opt. Soc. America, Washington DC, USA, 1993) p.248]
[7] P.C. Becker, M.M. Broer, V.G. Lambrecht, A.J. Bruce, G. Nykolak [*Tech. Dig. OAA'92* (Opt. Soc. America, Washington DC, USA, 1992) PD5]
[8] H. Tawarayama et al [*Tech. Dig. OAA'97* (Optical Society of America, USA, 1997) PD1]
[9] Y. Ohishi, A. Mori, T. Kanamori, K. Fujiura, S. Sudo [*Appl. Phys. Lett. (USA)* vol.65 (1994) p.13]
[10] T. Kanamori et al [*J. Non-Cryst. Solids (Netherlands)* vol.213&214 (1997) p.121]
[11] T. Shimada et al [*Electron. Lett. (UK)* vol.33 (1997) p.1972]
[12] Y. Ohishi, T. Kanamori, Y. Terunuma, M. Shimizu, M. Yamada, S. Sudo [*IEEE Photonics Technol. Lett. (USA)* vol.6 (1994) p.195]

C5.2 Fibre lasers based on rare earth-doped halide glass

W. Lüthy and H.P. Weber

July 1997

A INTRODUCTION

ZBLAN glass fibres with a core doped with trivalent rare earth ions are extremely well suited as laser materials. The wave-guide properties of the fibre maintain a high intensity of the pump light over long distances and the fluoride glass with its low phonon energies suppresses multi-phonon relaxation and leads to long lifetimes of radiative transitions. As a consequence laser action with low threshold, high efficiency and numerous possibilities of upconversion pumping is possible. Some of the most important laser transitions are given in TABLE 1.

TABLE 1 Laser transitions in RE-doped fluoride glass fibres.

Dopant	Possible co-dopants	Laser wavelengths (nm)	Ref
Praseodymium	Yb^{3+}	491, 520, 615, 635, 695, 715, 885, 910, 1300	[1-5]
Neodymium		381, 412, 1050, 1350	[6]
Holmium	Tm^{3+}	549, 1190, 1850, 2076, 2900	[7,8]
Erbium	Pr^{3+}	550, 850, 1600, 1700, 2710, 3500	[9-12]
Thulium	Yb^{3+}, Tb^{3+}	455, 482, 810, 1470, 1820, 1900, 2300	[13-23]
Ytterbium		1120, 1020	[24,25]

Fibre lasers are developed for numerous applications such as sensors for chemicals [26] or water vapour [27], for ultra-fast components in photonics networks [28] or for medical applications [29].

B LASER CONFIGURATIONS

The set-up of a fibre laser can be extremely simple. With a monomode pump source the pump energy can be injected with the aid of a fibre coupler. With a nearly diffraction limited pump source even a monomode fibre can be excited by directly focusing into the core. With diode arrays as pump source, pumping can be performed by focusing into the cladding of double-clad structures. With double-clad fibres even pumping from the side and multiple pumping from the side is possible [30]. This technique allows scaling of the output power. The mirrors can be directly coated onto the fibre [31] end face, butt coupled or external with optical elements of large numerical aperture and low losses. It is also possible to operate the fibre as a ring laser [32]. In many cases the gain in the fibre is so high that Fresnel reflection from the fibre ends is sufficient to reach threshold.

C TUNABLE LASERS

Tunability in RE^{3+}-doped fibres is possible, if the upper and the lower laser level consist of numerous Stark-sublevels which in a glass are broadened over a large spectral range due to the large number of possible site symmetries of RE^{3+} in the host matrix. If further the lower laser level is identical with the ground-state manifold, then reabsorption of the laser emission occurs and tuning can easily be achieved

by temperature control and fibre length. A higher temperature leads to a higher Boltzmann population of the terminating level and forces the laser to terminate in a higher lying sublevel of the ground state. A longer fibre leads also to reabsorption losses with the same effect. The result for both cases is a shift towards longer wavelengths. Experimentally wavelength tuning has been measured in Tm^{3+} [23,33], in Pr^{3+} [5,34], in Ho^{3+} [7], in Nd [35] and on the green Er^{3+} laser line leading into the $^4I_{15/2}$ ground state [36].

D SHORT PULSES

Q-switch operation has been reported in Er^{3+} [37] and also in Tm^{3+} [14]. Mode locking was realised in Nd^{3+} [4], in Tm^{3+} [38,39] and in Pr^{3+} [40,41], and femto second pulses could be produced [41,42].

E CASCADE LASERS

Probably the most important fluoride fibre laser is the erbium laser operated at 2.71 μm. For this type of laser the use of the fluoride fibre is absolutely necessary since standard silica fibres are nearly opaque for this wavelength. The relevant transitions in erbium are summarised in FIGURE 1. Pumping can be performed with either P_1 at a wavelength of about 970 nm into the $^4I_{11/2}$ level or with P_2 at 791 nm first into the $^4I_{9/2}$ level and then into $^4I_{11/2}$ via a rapid multi-phonon decay. Between the $^4I_{11/2}$ and the $^4I_{13/2}$ lower level a laser transition occurs with the emission wavelength of 2.71 μm.

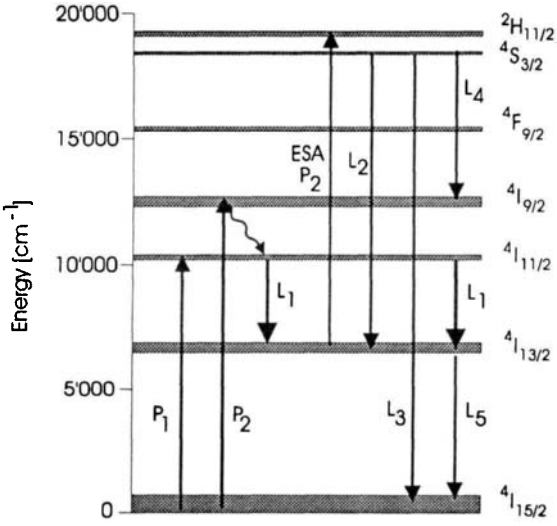


FIGURE 1 Schematic energy level scheme of Er^{3+}:ZBLAN with P_1 the pump line at 970 nm, P_2 the pump line at 791 nm, L_1 the laser transition at 2.71 μm, and L_2 to L_5 the laser lines at 850 nm, 550 nm, 1.7 μm and 1.6 μm respectively.

The output power of the 2.71 μm transition shows a strong saturation limiting the output of a monomode fibre laser to some 10 mW [43]. This saturation is shown [44] not to be based on a bleaching of the ground state but to be due to excited state absorption populating the $^4S_{3/2}$ level (ESA P_2 in FIGURE 1). ESA can not only occur in the way indicated in FIGURE 1, but also from the $^4I_{11/2}$ level. Also in this case after some non-radiative processes $^4S_{3/2}$ is populated.

From this level laser transitions can occur at 550 nm to the ground state, at 850 nm to $^4I_{13/2}$ and at 1.7 μm to $^4I_{9/2}$. The threshold is lowest for the laser line at 850 nm and as soon as this laser oscillates an additional population of $^4I_{13/2}$ occurs thus reducing the inversion for the 2.71 μm laser which then saturates. To avoid this loss mechanism the emission at 850 nm has to be suppressed by minimising the

reflectivity of the laser mirrors for this wavelength. Furthermore it is helpful to use laser mirrors with high reflectance at 1.7 μm. This allows threshold to be reached for the transition L_4 at 1.7 μm which then populates the upper level of the 2.71 μm laser transition and thus increases the inversion and recycles the energy lost by ESA. With these measures the saturation is avoided and unsaturated emission with a slope efficiency of more than 20% can be achieved [10]. Besides this cascade laser [9] also a three cascade erbium laser is possible with the additional transition L_5 from $^4I_{13/2}$ to the ground state [11].

F UPCONVERSION LASERS

The number of available emission wavelengths can be considerably enhanced by upconversion pumping. In this case a population of the upper laser level is reached with the absorption of two or more pump photons. In fibres the concentration of the dopant is generally not high enough to allow upconversion by direct ion-ion interaction. Upconversion is rather based on excited state absorption. In this case a pump photon populates an intermediate level from where a second pump photon can populate the upper laser level [1-3,9,13,15,17-19,34,38,45-56].

G CONCLUSION

In conclusion we have shown that the numerous laser transitions in RE^{3+} doped fluoride fibres can be considerably enhanced by upconversion processes based on excited state absorption and possibly direct ion-ion interaction. Fibre lasers are by no means limited to the mW power level. With suitable double clad geometry, laser operation at the multi-watt level can be achieved.

REFERENCES

[1] H.M. Pask, A.C. Tropper, D.C. Hanna [*Opt. Commun. (Netherlands)* vol.134 no.1-6 (1997) p.139-44]

[2] D.M. Baney, G. Rankin, K.W. Chang [*Opt. Lett. (USA)* vol.21 no.17 (1996) p.1372-4]

[3] D.M. Baney, G. Rankin, K.W. Chang [*Appl. Phys. Lett. (USA)* vol.69 no.12 (1996) p.1662-4]

[4] M. Wegmuller, W. Hodel, H.P. Weber [*Opt. Commun. (Netherlands)* vol.127 no.4-6 (1996) p.266-72]

[5] J.Y. Allain, M. Monerie, H. Poignant [*Electron. Lett. (UK)* vol.27 no.2 (1991) p.189-91]

[6] D.S. Funk, J.W. Carlson, J.G. Eden [*Electron. Lett. (UK)* vol.30 no.22 (1994) p.1859-60]

[7] D.S. Funk, S.B. Stevens, S.S. Wu, J.G. Eden [*IEEE J. Quantum Electron. (USA)* vol.32 no.4 (1996) p.638-45]

[8] L. Wetenkamp [*Electron. Lett. (UK)* vol.26 no.13 (1990) p.883-4]

[9] Ch. Ghisler, M. Pollnau, G. Bunea, M. Bunea, W. Lüthy, H.P. Weber [*Electron. Lett. (UK)* vol.31 no.5 (1995) p.373-4]

[10] M. Pollnau, Ch. Ghisler, G. Bunea, M. Bunea, W. Lüthy, H.P. Weber [*Appl. Phys. Lett. (USA)* vol.66 no.26 (1995) p.3564-6]

[11] M. Pollnau, Ch. Ghisler, W. Lüthy, H.P. Weber, J. Schneider, U.B. Unrau [*Opt. Lett. (USA)* vol.22 no.9 (1997) p.612-4]

[12] H. Tobben [*Electron. Lett. (UK)* vol.29 no.8 (1993) p.667-9]

[13] I.J. Booth, C.J. Mackechnie, B.F. Ventrudo [*IEEE J. Quantum Electron. (USA)* vol.32 no.1 (1996) p.118-23]

[14] A. Saissy, E. Maurice, G. Monnom [*Pure Appl. Opt. (UK)* vol.5 no.1 (1996) p.7-14]

[15] T. Komukai, T. Yamamoto, T. Sugawa, Y. Miyajima [*IEEE J. Quantum Electron. (USA)* vol.31 no.11 (1995) p.1880-9]

[16] R.M. Percival, D. Szebesta, C.P. Seltzer, S.D. Perin, S.T. Davey, M. Louka [*IEEE J. Quantum Electron. (USA)* vol.31 no.3 (1995) p.489-93]
[17] M.P. LeFlohic, J.Y. Allain, G.M. Stephan, G. Mazé [*Opt. Lett. (USA)* vol.19 no.23 (1994) p.1982-4]
[18] R.M. Percival, D. Szebesta, J.R. Williams [*Electron. Lett. (UK)* vol.30 no.13 (1994) p.1057-8]
[19] M.L. Dennis, J.W. Dixon, I. Aggarwal [*Electron. Lett. (UK)* vol.30 no.2 (1994) p.136-7]
[20] R.M. Percival, D. Szebesta, S.T. Davey [*Electron. Lett. (UK)* vol.29 no.12 (1993) p.1054-6]
[21] T. Yamamoto, Y. Miyajima, T. Komukai, T. Sugawa [*Electron. Lett. (UK)* vol.29 no.11 (1993) p.986-7]
[22] R.M. Percival, D. Szebesta, S.T. Davey [*Electron. Lett. (UK)* vol.28 no.20 (1992) p.1866-8]
[23] J.Y. Allain, M. Monerie, H. Poignant [*Electron. Lett. (UK)* vol.25 no.24 (1989) p.1660-2]
[24] C.J. Mackechnie, W.L. Barnes, D.C. Hanna, J.E. Townsend [*Electron. Lett. (UK)* vol.29 no.1 (1993) p.52-3]
[25] J.Y. Allain, M. Monerie, H. Poignant [*Electron. Lett. (UK)* vol.28 no.11 (1992) p.988-9]
[26] F.J. McAleavey, B.D. MacCraith [*Electron. Lett. (UK)* vol.31 no.10 (1995) p.800-2]
[27] B.D. MacCraith, F.J. McAleavey [*Proc. SPIE - Int. Soc. Opt. Eng. (USA)* vol.2360 (1994) p.90-3]
[28] R.P. Davey et al [*Proc. IEE Colloquium on High Speed and Long Distance Optical Transmission* Birmingham, UK, 18 April 1996 (IEE, 1996) p.7/1-7/5]
[29] L. Esterowitz, R. Allen [*Proc. SPIE - Int. Soc. Opt. Eng. (USA)* vol.1048 (1989) p.129-32]
[30] Th. Weber, W. Lüthy, H.P. Weber [*Appl. Phys. B (Germany)* vol.63 (1996) p.131-4]
[31] H. Doring, J. Peupelmann, F. Wenzel [*Electron. Lett. (UK)* vol.31 no.13 (1995) p.1068-9]
[32] Y. Ohishi, T. Kanamori [*Electron. Lett. (UK)* vol.28 no.2 (1992) p.162-4]
[33] R.M. Percival, S.F. Carter, D. Szebesta, S.T. Davey, W.A. Stallard [*Electron. Lett. (UK)* vol.27 no.21 (1991) p.1912-3]
[34] Ping-Xie, T.R. Gosnell [*Opt. Lett. (USA)* vol.20 no.9 (1995) p.1014-6]
[35] T. Komukai, Y. Fukasaku, T. Sugawa, Y. Miyajima [*Electron. Lett. (UK)* vol.29 no.9 (1993) p.755-7]
[36] J.Y. Allain, M. Monerie, H. Poignant [*Electron. Lett. (UK)* vol.28 no.2 (1992) p.111-3]
[37] C. Frerichs, T. Tauermann [*Electron. Lett. (UK)* vol.30 no.9 (1994) p.706-7]
[38] L.M. Yang, D.T. Walton, J. Nees, W.H. Weber [*Electron. Lett. (UK)* vol.32 no.7 (1996) p.658-9]
[39] N. Kishi et al [*Electron. Lett. (UK)* vol.28 no.2 (1992) p.175-7]
[40] T. Sugawa, E. Yoshida, Y. Miyajima, M. Nakazawa [*Electron. Lett. (UK)* vol.29 no.10 (1993) p.902-3]
[41] D.S. Peter, G. Onishchukov, W. Hodel, H.P. Weber [*Electron. Lett. (UK)* vol.30 no.19 (1994) p.1595-6]
[42] M.J. Guy, D.U. Noske, A. Boskovic, J.R. Taylor [*Opt. Lett. (USA)* vol.19 no.11 (1994) p.828-30]
[43] S. Bedö, W. Lüthy, H.P. Weber [*Electron. Lett. (UK)* vol.31 no.3 (1995) p.199-200]
[44] S. Bedö, M. Pollnau, W. Lüthy, H.P. Weber [*Opt. Commun. (Netherlands)* vol.116 (1995) p.81-6]
[45] Y. Zhao, S. Fleming [*Electron. Lett. (UK)* vol.32 no.13 (1996) p.1199-200]
[46] D.M. Baney, L. Yang, J. Ratcliff, Kok Wai Chang [*Electron. Lett. (UK)* vol.31 no.21 (1995) p.1842-3]
[47] S. Sanders, R.G. Waarts, D.G. Mehuys, D.F. Welch [*Appl. Phys. Lett. (USA)* vol.67 no.13 (1995) p.1815-7]
[48] Yuxing-Zhao, S. Fleming, S. Poole [*Opt. Commun. (Netherlands)* vol.114 no.3-4 (1995) p.285-8]
[49] Y. Zhao, S. Poole [*Electron. Lett. (UK)* vol.30 no.12 (1994) p.967-8]
[50] A. Shikida, H. Yanagita, H. Toratani [*J. Opt. Soc. Am. B (USA)* vol.11 no.5 (1994) p.928-32]
[51] D. Piehler, D. Craven, N. Kwong, H. Zarem [*Electron. Lett. (UK)* vol.29 no.21 (1993) p.1857-8]

[52] S.G. Grubb, K.W. Bennett, R.S. Cannon, W.F. Humer [*Electron. Lett. (UK)* vol.28 no.13 (1992) p.1243-4]

[53] T. Komukai, T. Yamamoto, T. Sugawa, Y. Miyajima [*Electron. Lett. (UK)* vol.28 no.9 (1992) p.830-2]

[54] R.G. Smart, D.C. Hanna, A.C. Tropper, S.T. Davey, S.F. Carter, D. Szebesta [*Electron. Lett. (UK)* vol.27 no.14 (1991) p.1307-9]

[55] J.Y. Allain, M. Monerie, H. Poignant [*Electron. Lett. (UK)* vol.27 no.13 (1991) p.1156-7]

[56] C.A. Miller, M.C. Brierley, M.H. Hunt, S.F. Carter [*Electron. Lett. (UK)* vol.26 no.22 (1990) p.1871-3]

PART D: CHALCOGENIDE GLASS

CHAPTER D1

OPTICAL PROPERTIES

D1.1 Transmission of chalcogenide glass
D1.2 Intrinsic scattering in chalcogenide glass
D1.3 Refractive index and dispersion of chalcogenide glass
D1.4 Non-linear refractive index of chalcogenide glass

D1.1 Transmission of chalcogenide glass

D.J. Brady

November 1997

A INTRODUCTION

The use of silica for fibre optics is a well established technology based on its excellent properties, such as thermal and environmental stability, and extremely low optical loss in the near infrared (NIR). Good reasons must be used to select another material over silica for optical fibres or components. One such reason is the requirement for mid infrared (MIR) optical transparency; where the silica transmission window closes at 2 μm for windows, lenses etc., chalcogenide glasses can be used up to 15 μm or greater (TABLE 1 lists the transmission windows for various chalcogenide glasses that have been extensively reported in the literature). This is useful for a wide range of scientific and industrial applications: as fibre for transmission of high power MIR lasers, for example Er:YAG (2.94 μm) [1], CO (~5 μm) [2], and CO_2 (~10.6 μm) [3] used in medical, aerospace and industrial cutting and welding applications; for chemical and remote sensing (many industrially important compounds and gases have very strong fundamental absorptions in the MIR giving the possibility of very sensitive detectors working in this wavelength range); and as 'bulk' glass for MIR windows, lenses and other optical components for spectroscopy and imaging. Some chalcogenide glasses are also suitable hosts for rare-earth doping for MIR laser sources [4]. The advantages of using glasses over crystalline materials are that they are cheap and easy to produce, and may be drawn to fibre, with all the advantages that a fibre geometry brings. This Datareview describes the processes which affect the width and position of the optical transmission window, namely the electronic absorption edge (UV edge), the multiphonon edge (IR edge) and the weak absorption tail.

TABLE 1 Approximate transmission windows of some chalcogenide glasses.

Glass	Typical composition	Transmission window ($\alpha \leq 1$ cm^{-1}) μm	Ref
GaLaS	$70Ga_2S_3{:}30La_2S_3$	0.57 - 9.5	[16]
GaLaSCsSI	$65Ga_2S_3{:}10La_2S_3{:}25CsCl$	0.48 - 8.8	[10]
AsS	As_2S_3	0.6 - 11	[11]
AsGeSe	$As_{38}Ge_5Se_{57}$	0.84 - 16	[11]
GeSeTe	$Ge_{22}Se_{20}Te_{58}$	~1.7* - 17	[16]

* Taken from fibre attenuation.

B ELECTRONIC ABSORPTION EDGE

Chalcogenide glasses may be considered as amorphous semiconductors with an energy gap E_g. Incident photons with energies greater than E_g excite an electron from the valence band to the conduction band, generating an electron-hole pair, and are absorbed in the process. The free carrier mobilities and lifetimes of amorphous materials are generally very low due to defect states in the bandgap, and recombination of the electron-hole pair will occur by a multistep process with the emission of phonons rather than photons. The absorption edge is a function of frequency that follows an empirical rule first proposed by Urbach [5] that predicts the absorption coefficient at the UV edge to be

$$\alpha_{uv} = \alpha_o \exp\left(\frac{\hbar\omega - E_g}{\Delta E}\right) \quad (1)$$

where $\hbar\omega$ is the energy of the incident photons, E_g is the energy gap of the glass and ΔE is the Urbach slope, a material dependent parameter. Dow and Redfield [6] proposed a quantitative mechanism for the Urbach tail based on local field variation, created by optical phonons, impurities, dangling bonds, or other potential fluctuations associated with disorder induced tunnelling of an electron away from a hole, under excitation by photons.

Wood et al [7] used approximations to EQN (1) to give the general shape of the electronic absorption edge shown in FIGURE 1. For the high absorption region (A) (α > 10exp4 cm^{-1}, or ~4exp6 dB m^{-1})

$$\hbar\omega\alpha \sim (\hbar\omega - E_g)^{\gamma} \quad (2)$$

where the constant γ is usually equal to 2 or 3. Below $\alpha \sim$ 10exp4 (regions B and C) the absorption coefficient is larger than given by EQN (2), and Wood et al [7] claim that in the compound glasses they studied (As_2S_3, $Ge_{33}As_{12}Se_{55}$, $Ge_{26}Sb_{12}Se_{60}$) the absorption coefficient obeyed

$$\alpha \sim \exp\left(\frac{\hbar\omega}{E}\right) \quad (3)$$

with $E_B < E_C$. Region B is usually taken as the UV absorption edge as A is difficult to measure (α = 10exp4 cm^{-1} gives 100 absorption lengths for a 10 μm thick film). Region C is described as the 'weak absorption tail' which extends from the electronic absorption edge across the transmission window to the multiphonon edge, and in low loss chalcogenide fibres is the dominant loss mechanism over Rayleigh scattering. Ramachandran et al have measured the absorption coefficient, in the visible and UV, of As_2S_3 glass thin films as a function of photon energy [8].

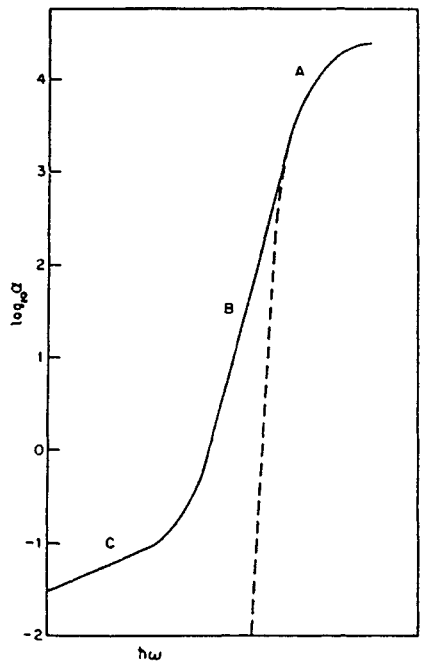


FIGURE 1 UV absorption edge for amorphous materials [7].

Chalcogenide glasses are deliberately composed of heavy ions, that are weakly bonded. This gives the glass a low phonon energy and hence its extended infrared transparency (see Section C). It also gives rise to large numbers of vacancies and dangling bonds on the amorphous lattice, which gives a large density of states in the bandgap (mobility gap) [7]. These states are not available for conduction, but can have electrons excited to them from the valence band, which gives rise to absorption even for photons with small energies. The density and type of defects and hence the strength of the weak absorption tail will obviously be strongly dependent on the exact preparation details of the glass [7,10]. Due to the differences in bonding, oxide glasses do not suffer from a significant weak absorption tail. FIGURE 2 shows a plot of fibre attenuation against λ^{-1} for an AsSSe glass [10], clearly illustrating the position of the weak tail (WAT) and the effect on the attenuation of the fibre. It can be seen that the weak tail is a much more significant source of loss than that from the predicted Rayleigh scatter.

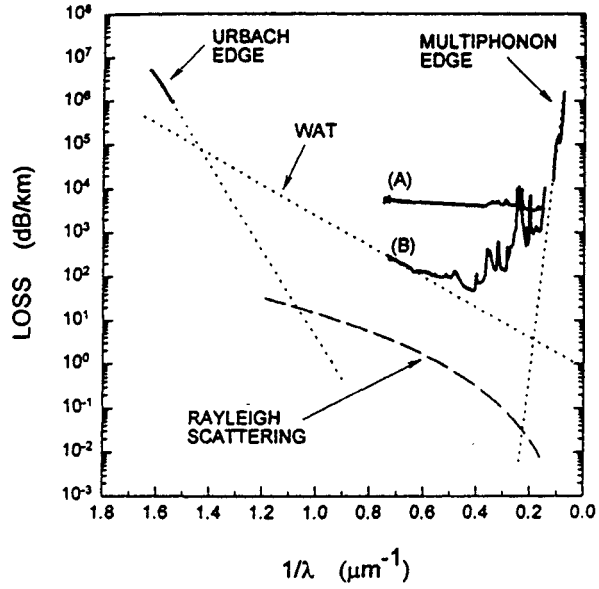


FIGURE 2 Absorption coefficient of AsSeS glass showing the UV, IR and weak absorption edges [9].

The position of the electronic absorption edge is heavily dependent on the composition of the glass. FIGURE 3 shows the electronic absorption edge for GaLaS, GaLaSCsCl, AsS, AsGeSe and GeSeTe glasses. There is wide variation of short wavelength transmission possible; for example in the chalcohalide glass $65Ga_2S_3{:}10La_2S_3{:}25CsCl$ [11] the transmission extends well into the visible, whereas for an $As_{38}Ge_5Se_{57}$ glass [10,12,13] the transmission window closes in the near infrared.

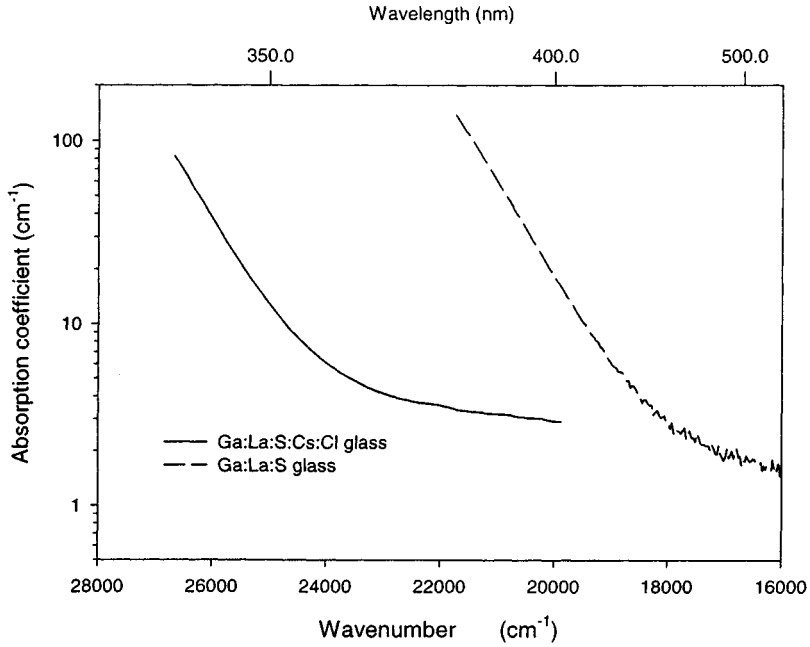


FIGURE 3(a) UV absorption edges of GaLaS and GaLaSCsCl glasses [11].

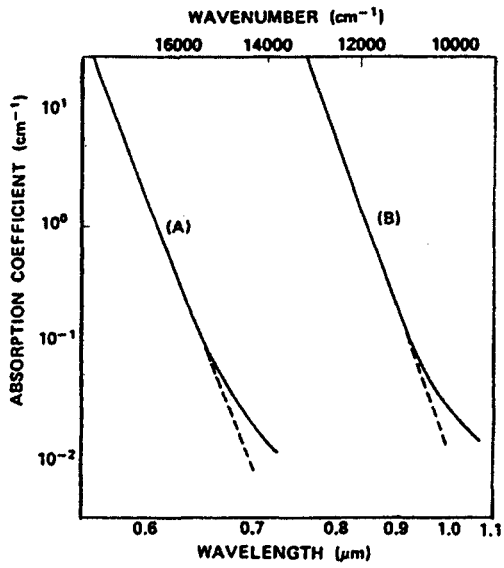


FIGURE 3(b) UV absorption edges of AsS(A), and AsGeSe(B) glasses [13].

C MULTIPHONON PROCESSES

Of the three types of phonon that can interact with photons, optic, Raman and acoustic (via the photostrictive effect), only the optic phonon modes are of concern here. Long wavelength photons can excite optic phonon modes in the glass and are elastically absorbed with the generation of phonons, at wavelengths corresponding to the multiphonon absorption edge of the glass [14]. For the reasons presented simply above, chalcogenide glasses have a low maximum phonon energy (compared to silica ~1100 cm^{-1}, ZBLAN ~590 cm^{-1} and the chalcogenide glass GaLaS ~425 cm^{-1}; other chalcogenides can have lower phonon energies) which results in the multiphonon edge shifting to longer wavelengths in these materials. The shape and position of the multiphonon edge contains information about the structure and bonding in the glass, and many workers use this and reflection spectroscopy to determine vibrational modes of the glass matrix [10,13,15]. In doped glasses, low phonon energy also results in lower non-radiative decay rates from excited levels, giving a high quantum efficiency for transitions between closely spaced dopant energy levels. According to Van Uitert et al [16] the multiphonon edge may be fitted with a simple exponential of the form

$$\alpha_{mp} = A \exp\left(\frac{a}{\lambda}\right) \tag{4}$$

and is usually fitted at high attenuations, so extrapolations to low attenuations should be treated with caution, as uncertainty in the slope at high attenuations can give rise to significant errors in the low loss regime. Using EQN (4) coupled with EQNS (3) and (2) it is possible to give sensible predictions as to the minimum loss in a glass (see FIGURE 2), although theoretical minimum attenuation predictions would involve calculating the scattering attenuation for the glass (see Datareviews D1.2 and D4.4). The multiphonon edges for glasses given in TABLE 1 are shown in FIGURE 4.

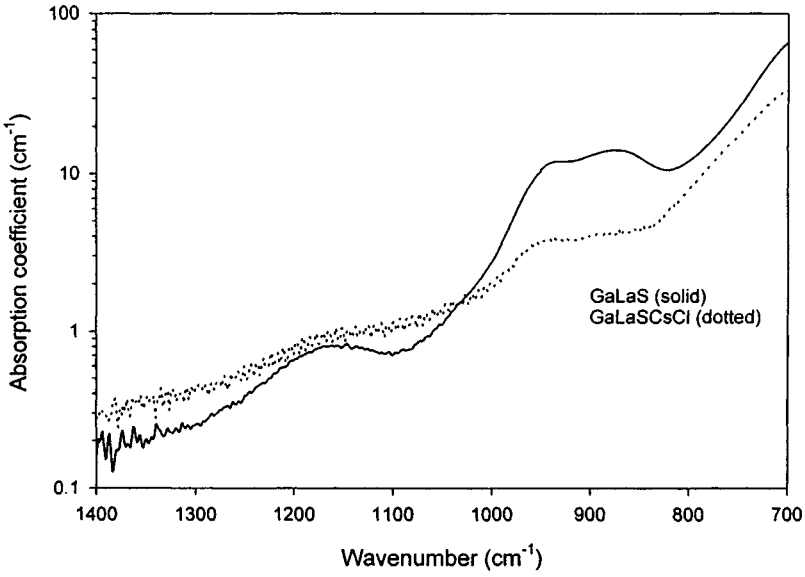


FIGURE 4(a) IR absorption edges of GaLaS and GaLaSCsCl glasses [11].

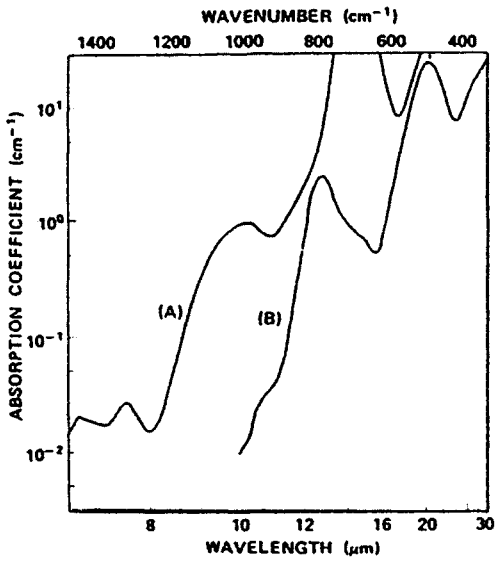


FIGURE 4(b) IR absorption edges of AsS(A) and AsGeSe(B) glasses [13].

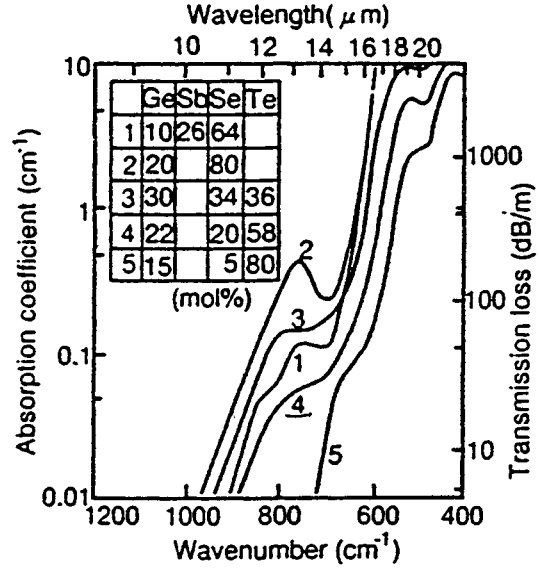


FIGURE 4(c) IR absorption edge of GeSeTe glass [16].

D CONCLUSION

FIGURES 3 and 4 show the edges of the transmission windows for various chalcogenide glasses which have been extensively studied by various authors. Fibres of GaLaS or As_2S_3 are clearly not suitable for transmission of the technologically important 10.6 μm CO_2 laser, but may be used for 2.94 μm Er:YAG and 5 μm CO laser transmission, whereas glasses based on GeAsSeTe can be drawn to fibre with losses ~1 - 2 dB m^{-1} at 10.6 μm and 5 μm, but have much higher losses at 2.94 μm [19]. It can be seen that the glasses composed of lighter chalcogens, such as sulphur based glasses (e.g. GaLaS [17]), generally have a transmission window that covers shorter wavelengths than glasses such as GeAsSeTe, that contain heavy chalcogens. This gives the advantage that these materials may at least in part be characterised by NIR and visible sources (e.g. Ti:Sapphire, HeNe) and detectors (e.g. Si, InGaAs), rather than more complex sources (e.g. Tm:YAG), and less sensitive detectors (e.g. InSb). It also means that the short

wavelength pump required to excite many doped glasses suffers lower attenuation in chalcogenides such as GaLaS.

REFERENCES

[1] A.G. Antipenko et al [*Kvantovaya Elektron. Mosk. (Russia)* vol.22 (1995) p.523-5]

[2] S. Somkuampanit et al [*Opt. Lasers Eng. (UK)* vol.23 (1995) p.221-31]

[3] S. Sato, K. Igarashi, M. Taniwaki, K. Tanimoto, K. Kikuchi [*Appl. Phys. Lett. (USA)* vol.62 (1993) p.669-71]

[4] T. Schweizer, B.N. Samson, R.C. Moore, D.W. Hewak, D.N. Payne [*Electron. Lett. (UK)* vol.33 (1997) p.414-5]

[5] P.W. France [*Fluoride Glass Fibre Optics* (CRC Press, 1990) p.61-2]

[6] J.D. Dow, D. Redfield [*Phys. Rev. B (USA)* vol.5 (1972) p.594-610]

[7] D.L. Wood, J. Tauc [*Phys. Rev. B (USA)* vol.5 (1972) p.3144-51]

[8] S. Ramachandran, J.C. Pepper, D.J. Brady, S.G. Bishop [*J. Lightwave Technol. (USA)* vol.15 (1997) p.1371-7]

[9] J.S. Sanghera, V.Q. Nguyen, P.C. Pureza, R.E. Miklos, F.H. Kung, I.D. Aggarwal [*J. Lightwave Technol. (USA)* vol.14 (1996) p.743-8]

[10] T. Kanamori, Y. Terunuma, T. Miyashita [*Rev. Electr. Commun. Lab. (Japan)* vol.32 (1984) p.469-77]

[11] J. Wang et al [*Appl. Phys. Lett. (USA)* vol.71 (1997) p.1753-5]

[12] G.G. Devyatykh, M.F. Churbanov, I.V. Scripachev, E.M. Dianov, V.G. Plotnichenko [*Int. J. Optoelectron. (UK)* vol.7 (1992) p.237-54]

[13] T. Kanamori, Y. Terunuma, S. Takahashi, T. Miyashita [*J. Non-Cryst. Solids (Netherlands)* vol.69 (1985) p.231-42]

[14] W.J. Tropf, M.E. Thomas, T.J. Harris [*Handbook of Optics* vol.2 (McGraw-Hill, 1995) p.33.12-33.20]

[15] A.M. Efimov [*J. Non-Cryst. Solids (Netherlands)* vol.203 (1996) p.1-11]

[16] L.G. Van Uitert, A.J. Bruce, W.H. Grodkiewicz, D.L. Wood [*Mater. Sci. Forum (Switzerland)* vol.6 (1985) p.591-606]

[17] D.W. Hewak et al [*Electron. Lett. (UK)* vol.32 (1996) p.384-5]

[18] T. Katsuyama, H. Matsumura [*J. Appl. Phys. (USA)* vol.76 no.4 (1994) p.2036-40]

[19] J.S. Sanghera et al [*J. Lightwave Technol. (USA)* vol.12 (1994) p.737-41]

D1.2 Intrinsic scattering in chalcogenide glass

D.J. Brady

November 1997

A INTRODUCTION

The transmission window of chalcogenide glasses is of interest when selecting a glass to satisfy particular requirements, for example as a window material or lens, where scattering effects may usually be safely ignored. In glass fibres, however, we are more interested in the processes that limit the attenuation in the gap between the electronic and multiphonon absorption edges. The weak absorption tail has already been discussed [1] as being analogous with the electronic edge so this Datareview will be constrained to a discussion of scattering effects in chalcogenide glasses, which are of considerable significance for fibre materials. There are three main groups of scattering centres: intrinsic from material considerations, extrinsic from impurities and defects, and phonon scattering. All three arise from local permittivity fluctuations, differing in the mechanism by which the fluctuations are generated. The intrinsic forms of scattering are: Rayleigh directly from permittivity changes, Raman, and Brillouin from phonon scattering. The last two are not of significance for optical loss, but have technological importance so will be discussed briefly.

B RAYLEIGH SCATTERING

The structure of glass is often assumed to be a uniformly amorphous solid. This is not the case. On a microscopic scale there are static density fluctuations that are 'frozen' into the matrix by cooling from the melt. The presence of density fluctuations is a thermodynamically driven process that is described in terms of its fictive temperature. This is the temperature at which an equivalent structure would exist in equilibrium, and is often assumed to be the lowest temperature at which flow can take place which, in an annealed glass, approximates to the glass transition temperature, T_g [2]. Scattering also arises from compositional fluctuations in the glass that can be calculated from thermodynamic considerations. Chalcogenide glasses have particularly strong refractive index (n) variations with composition (c) compared to other glasses [3] (for example $\delta n/\delta c = 0.42$ at 1.7 μm, in GaLaS glass [4]). Rayleigh scattering is proportional to λ^{-4} so is much less important for longer wavelengths, and applies for perturbations that are much smaller than the wavelength of light.

The scattering from density fluctuations is given by Lines [5]:

$$\alpha = \left(\frac{8\pi^3}{3\lambda^4}\right)\left\langle(\Delta\varepsilon)^2\right\rangle \upsilon_e \qquad (1)$$

where $\langle(\Delta\varepsilon)^2\rangle$ is the mean squared fluctuation in permittivity, and υ_e is the volume over which it occurs. Pinnow et al [6] defined the expression to be

$$\alpha_{(density)} = \frac{8\pi^3}{3\lambda^4} n^8 p^2 \beta_c K_B T_g \qquad (2)$$

where n is the refractive index, p is the photoelastic coefficient, β_c is the isothermal compressibility (at T_g), K_B is Boltzmann's constant and the glass transition temperature is T_g, here used as an approximation to the fictive temperature. Following the method of Olshansky [7] EQN (3) may be approximated as

$$\alpha_{(density)} = \frac{8\pi^3}{3\lambda^4}\left(n^2 - 1\right)^2 \beta_c K_B T_g \tag{3}$$

In a multi-component glass, fluctuations in composition also give rise to Rayleigh scattering and must be added to the density scattering effect. Lines [5] followed a thermodynamic approach to finding the fluctuations in the glass composition and converted these into fluctuations in dielectric permittivity ε from which the loss coefficient can be evaluated as

$$\alpha_{(conc)} = \frac{32\pi^3 M}{3\lambda^4 N_o \rho}\sum_{i\neq m}\left(\frac{\partial\varepsilon}{\partial c_i} - \frac{\partial\varepsilon}{\partial c_m}\right)^2\left(\frac{c_i + c_m}{c_i c_m} - \frac{2zW_{ab}}{kT}\right)^{-1} \tag{4}$$

where M is the average molecular weight, N_o is Avogadro's constant, ρ is the density of the system, c_i is the concentration of the ith component, z is the coordination number of particles in the system (assumed to be the same for all species present) and W_{ab} is the heat of formation of the glass from molecular species a and b. This is a well established technique for calculating optical power losses from such thermodynamic fluctuations. The equation can be considerably simplified for the case of a binary system if the mixture is assumed to be ideal, i.e. there is no spinodal decomposition, and no heat released upon glass formation; $W_{ab} = 0$, and EQN (4) becomes

$$\alpha_{(conc)} = \frac{32\pi^3 M}{3\lambda^4 N_o \rho}\left(\frac{\partial\varepsilon}{\partial c}\right)^2 c(1-c) \tag{5}$$

where the amount of one component is (c) and of the other (1 - c). This expression was used to estimate the concentration Rayleigh scattering in GaLaS glass, with EQN (4) used for GaLaSCsCl glass. $\partial\varepsilon/\partial c$ for each type of glass was calculated from refractive index measurements of glass compositions varied about the compositions given in TABLE 1, and by using the fact that $n^2 = \varepsilon$ far from a fundamental absorption. Other workers have neglected the component of the scattering from compositional fluctuations when calculating the minimum loss of their glasses, although it is clear, at least for GaLaS and GaLaSCsCl glasses, that the compositional scattering is significantly stronger than the density scattering effects [8].

TABLE 1 Examples of chalcogenide glasses with Rayleigh and compositional scattering coefficients.

Glass	Typical composition	Rayleigh coefficient k (m^3); ($\alpha_{rs} = k\lambda^{-4}$)	Compositional coefficient c (m^3); ($\alpha_{cs} = c\lambda^{-4}$)
GaLaS	$70Ga_2S_3{:}30La_2S_3$	6.1exp-28	1.2exp-26
GaLaSCsCl	$65Ga_2S_3{:}5La_2S_3{:}25CsCl$	-	1.05exp-24
AsS	As_2S_3	7.2exp-29	-

C RAMAN SCATTERING

At the multiphonon edge of a glass, photons are absorbed by interactions with optic phonons. Raman scattering can be described quantum mechanically as absorption of a photon by a molecule, which then re-emits the photon (in an arbitrary direction, hence scattered) whilst making a vibrational transition [9]. This imparts a frequency shift to the photon determined by the vibrational modes in the glass. This forms

the basis of a very powerful technique for examining phonons in a glass - Raman spectroscopy [10]. Lines also calculated the attenuation for Raman scattering, from which the salient point to note is that its dependence on wavelength is λ^{-4}, which gives it a constant relationship with Rayleigh scattering (it is several orders of magnitude smaller) assuming the temperature remains constant [11].

D BRILLOUIN SCATTERING

Acoustic phonons may also indirectly interact with photons. An acoustic phonon distorts the local structure of the glass, which periodically alters the permittivity via the photostrictive effect. This can generate scattering when the photon satisfies the Bragg angle for the induced grating [12]. The scattering attenuation generated is larger than that from Raman scattering (still much less than Rayleigh), and is also found to be proportional to λ^{-4} [6]. As the acoustic wave is travelling there is also an associated frequency shift, from the Doppler effect, of the scattered photon. This frequency shift from the fundamental, as with Raman scattering, can be used to generate gain at the shifted frequency, and lasers may be constructed using this effect [13]. The intensity of Brillouin scattering is dependent on temperature, and the frequency shift from Brillouin scattering is dependent on both strain and temperature in the material, giving further uses of this effect for distributed fibre sensors [13].

E CHALCOGENIDE GLASSES

Little work has been done on the intrinsic scattering losses of chalcogenide glasses, as most systems are currently dominated by either extrinsic scattering losses or impurity absorption bands and the weak tail [14-16]. However, many workers have used theoretical calculations of the intensity of the Rayleigh scattering (EQN (3)) to predict the minimum possible losses in optical fibres. For example in As_2S_3 fibres the minimum loss is predicted to be 0.05 dB km^{-1} at 5 μm [17] using Rayleigh scattering as the lower limit. However fibre losses to date have only achieved ~20 dB km^{-1} [17] due to the effects of the weak absorption tail, and extrinsic scattering. As_2S_3 is the most widely reported chalcogenide glass, and the system on which most work has been done. FIGURE 1 shows attenuation against wavelength^{-1} for an

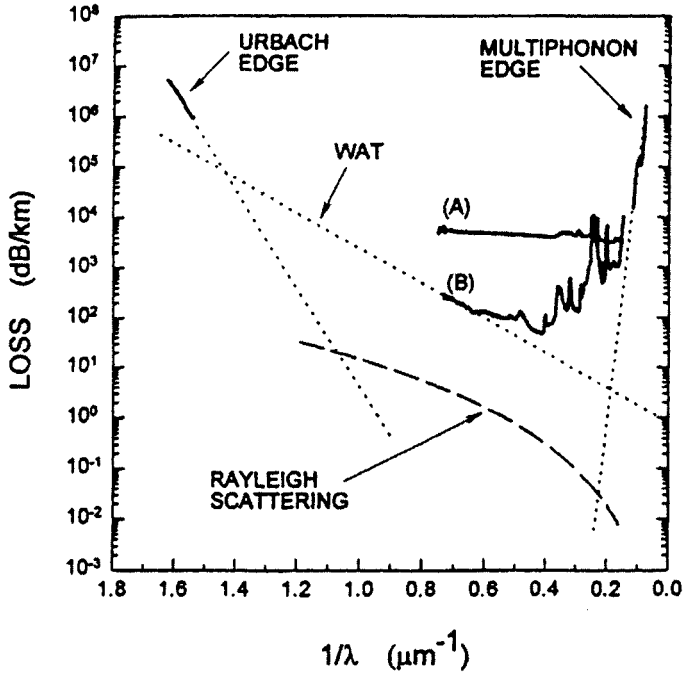


FIGURE 1 Attenuation versus wavelength plot for AsSSe glass fibre fabricated using (A) as received materials, and (B) purified materials. From Sanghera et al [17].

AsSeS glass [17], including two fibre attenuation plots A and B. Fibre A was drawn from unpurified materials, and the loss is dominated by extrinsic scattering. In fibre B the loss in the transmission window is dominated by the weak absorption tail. It can be seen that the Rayleigh scattering losses do not give an accurate picture of the minimum or actual attenuation in the material. For the chalcogenide glass GaLaS the calculated Rayleigh scattering curves are shown in FIGURE 2. Included in the calculated scattering loss is scattering from compositional variations. The plot is shown with the electronic and multiphonon edges included to give a better overview of these glasses. As yet, the weak tail is not resolved in these glasses.

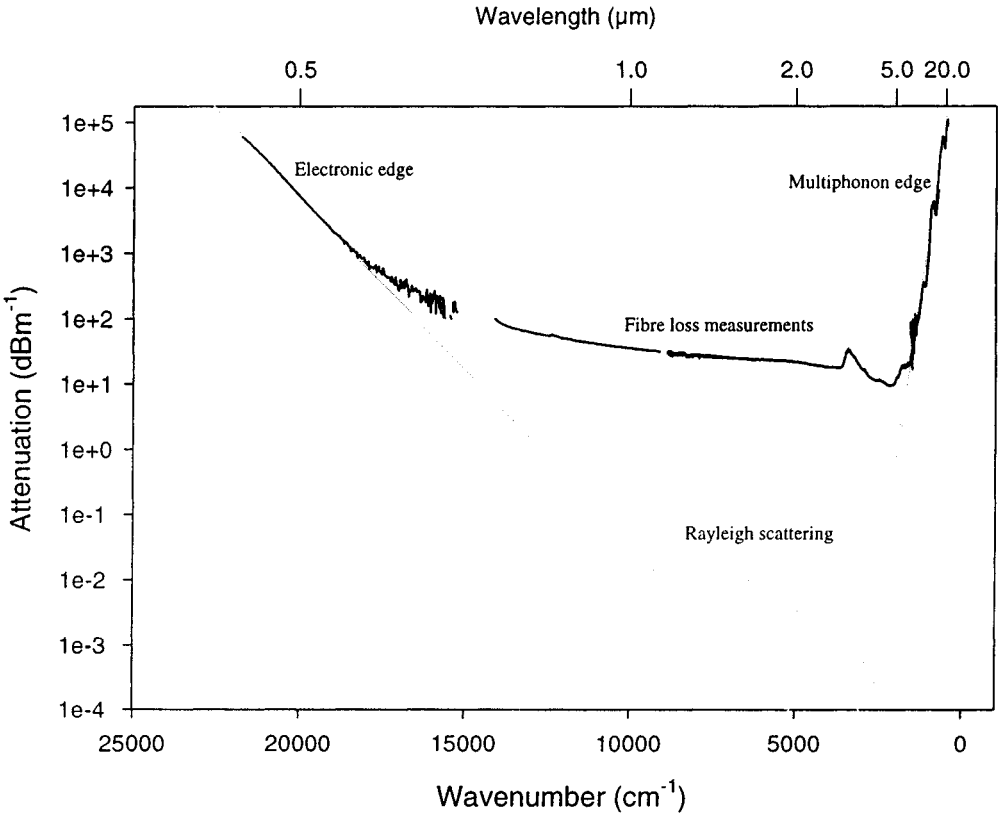


FIGURE 2 Attenuation versus wavelength plot for GaLaS glass.

F CONCLUSION

Intrinsic scattering in chalcogenide glasses is something that most workers have (optimistically) used to predict the minimum loss in their material system. It is, however, at the time of writing a limit that is far from being approached. Current limitations on the optical loss of a material are either extrinsic scattering from crystallites, bubbles or impurities, or absorption from the weak tail and impurities in the chalcogenide glasses.

REFERENCES

[1] D.J. Brady [Datareview in this book: *D1.1 Transmission of chalcogenide glasses*]
[2] J. Zaraycki [in *Glasses and the Vitreous State* (Cambridge University Press, 1991) ch.2]
[3] K. Saito, A.J. Ilkushima, T. Ito, A. Itoh [*J. Appl. Phys. (USA)* vol.81 (1997) p.7129-34]
[4] D.J. Brady, T. Schweizer, J. Wang, D.W. Hewak [to be submitted]

[5] M.E. Lines [*J. Appl. Phys. (USA)* vol.55 (1984) p.4052-7]
[6] D.A. Pinnow, T.C. Rich, F.W.Ostermayer, M. DiDomenico [*Appl. Phys. Lett. (USA)* vol.22 (1973) p.527-9]
[7] R. Olshansky [*Rev. Mod. Phys. (USA)* vol.51 (1979) p.348-51]
[8] [This work and [4]]
[9] G.P. Agrawal [in *Non-Linear Fibre Optics* (Academic Press, 1995) ch.8 p.316-7]
[10] W. Hayes, R. Louden [*Scattering of Light by Crystals* (Wiley Interscience, 1978)]
[11] G.P. Agrawal [in *Non-Linear Fibre Optics* (Academic Press, 1995) ch.9 p.370-1]
[12] C. Lin [*J. Lightwave Technol. (USA)* vol.4 (1986) p.1103-14]
[13] G.J. Cowle, D.Y. Stepanov [*Opt. Lett. (USA)* vol.21 (1996) p.1250-2]
[14] T. Katsuyama, H. Matsumura [*J. Appl. Phys. (USA)* vol.76 (1994) p.2036-40]
[15] J.S. Sanghera, L.E. Busse, I.D. Aggarwal [*J. Appl. Phys. (USA)* vol.75 (1994) p.4885-91]
[16] D. Lezal, K. Konak, S. Polakova, B. Petrovska [*J. Non-Cryst. Solids (Netherlands)* vol.161 (1993) p.301-3]
[17] J.S. Sanghera, V.Q. Nguyen, P.C. Pureza, R.E. Miklos, F.H. Kung, I.D. Aggarwal [*J. Lightwave Technol. (USA)* vol.14 (1996) p.743-8]

D1.3 Refractive index and dispersion of chalcogenide glass

H. Takebe

July 1997

A INTRODUCTION

Chalcogenide glass fibres have been attractive not only as passive transparent media in the infrared region for numerous applications, e.g. infrared imaging, high power delivery of CO_2 (10.6 μm) and Er:YAG (2.94 μm) lasers, and chemical sensors at 3 - 12 μm, but also as active optical devices such as 1.3 μm optical amplifiers, infrared lasers at 2 - 5 μm and photonic switches. The refractive index and dispersion of chalcogenide glasses have been evaluated mainly for designing core/clad structure at desired wavelengths. The refractive index also relates to some important optical properties for active devices such as radiative transition probabilities of rare-earth ions for fibre lasers and third-order non-linearities for photonic switches. This Datareview provides refractive index data at specific wavelengths, zero material dispersion wavelengths and partial dispersion characteristics for chalcogenide glasses.

B REFRACTIVE INDEX DATA

The refractive index of chalcogenide glass has been characterised at the desired wavelengths for its applications and at its transparent wavelengths. Since almost all chalcogenide glasses have high refractive indexes over 2, accurate refractive index data is obtained mainly by the minimum deviation method using prism samples. TABLE 1 shows refractive indexes of sulphide, selenide and mixed selenide telluride glasses [1-7]. Optical fibres have been successfully fabricated in these systems, although they still have relatively high transmission losses of over 1 dB/m. The refractive index of chalcogenide glasses increases in the order of network forming constituents: S < Se < Te due to their polarisabilities [8]. Refractive indexes of Ge-As-Se based glasses in the region from 1 to 11 μm [9], and the compositional dependence of the refractive index in $As_{40}S_{(60-x)}Se_x$ glasses at 5 μm [10] and in Ge-Ga-S glasses at 587.6 nm [11] have also been reported.

TABLE 1 Refractive indexes of chalcogenide glasses whose fibres have been successfully fabricated.

Glass composition (at% or mol%)	Refractive index	Ref
$As_{40}S_{60}$	2.65017 (n_d)	[1]
	2.395 (3 μm)	[2]
$64Ga_2S_3$:$36La_2S_3$	2.58 (500 nm)	[3]
$Ge_{25}S_{75}$	2.113 (n_d)	[4]
$As_{40}Se_{60}$	2.7840 (8 μm)	[5]
$Ge_{30}As_{15}Se_{55}$	2.4972 (8 μm)	[5]
$Ge_{25}Se_{75}$	2.37 (3 μm)	[6]
$Ge_{28}Sb_{12}Se_{60}$ (core)/	2.628 (3 μm)	[6]
$Ge_{32}Sb_8Se_{60}$ (clad)	2.537 (3 μm)	[6]
$Ge_{25}As_{20}Se_{25}Te_{30}$ (core)/	2.940 (8.5 μm)	[7]
$Ge_{20}As_{30}Se_{30}Te_{20}$ (clad)	2.862 (8.5 μm)	[7]
$Ge_{27}Se_{17}Te_{55}Tl_1$ (core)/	3.080 (10.6 μm)	[7]
$Ge_{27}Se_{18}Te_{55}$ (clad)	3.042 (10.6 μm)	[7]

C FITTING OF REFRACTIVE INDEX DATA

There are a few reports on the fitting of refractive index data for chalcogenide glasses. Rodney et al [1] fitted the data of $As_{40}S_{60}$ glass using a five term Sellmeier dispersion equation, where λ is the wavelength, and K_i and λ_i are the fitting coefficients shown in TABLE 2.

$$n^2 - 1 = \sum_{i=1}^{i=5} \frac{K_i \lambda^2}{\lambda^2 - \lambda_i^2} \tag{1}$$

TABLE 2 Fitting coefficients for a five-term Sellmeier dispersion equation for $As_{40}S_{60}$ glass [1].

i	λ_i^2	K
1	0.0225	1.8983678
2	0.0625	1.9222979
3	0.1225	0.8765134
4	0.2025	0.1188704
5	750	0.9569903

The average deviation between computed and measured values was about 7×10^{-5}. Klocek and Colombo [6] presented the fitting result for $Ge_{28}Sb_{12}Se_{60}$ glass by using a five term Herzberger polynomial

$$n = A_1 + \frac{A_2}{(\lambda^2 - 0.028)} + \frac{A_3}{(\lambda^2 - 0.028)^2} + A_4\lambda^2 + A_5\lambda^4 \tag{2}$$

The fitting coefficients A_1 - A_5 are listed in TABLE 3. FIGURE 1 shows the refractive index dispersion curves of $As_{40}S_{60}$ and $Ge_{28}Sb_{12}Se_{60}$ glasses using the fitting EQNS (1) and (2). TABLE 4 lists their zero material dispersion wavelengths (ZMDWs), where the material dispersion $M = (\lambda/c)(d^2n/d\lambda^2) = 0$. Shibata also showed the refractive index dispersion curve of $Ge_{25}S_{75}$ glass in the region from 0.5 to 3.5 μm [12].

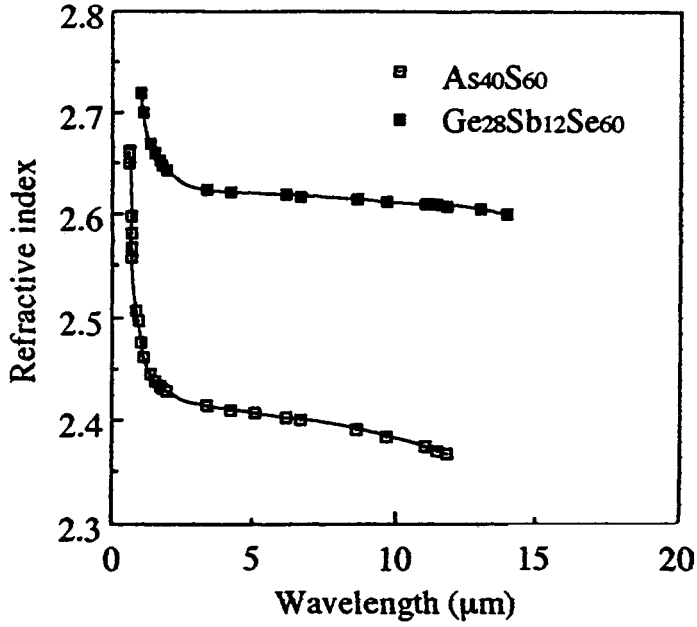


FIGURE 1 Refractive index dispersion curves of $As_{40}S_{60}$ and $Ge_{28}Sb_{12}Se_{60}$ glasses using EQNS (1) and (2).

TABLE 3 Fitting coefficients for a five-term Herzberger polynomial for $Ge_{28}Sb_{12}Se_{60}$ glass [6].

	0.9 - 2.5 μm	2.5 - 6.0 μm	6.0 - 14.0 μm
A_1	2.609048	2.616916	2.612545
A_2	0.1113049	0.1265583	0.3536862
A_3	-0.725286×10^{-3}	-0.129672	-3.561954
A_4	-0.196917×10^{-2}	$-0.1171826 \times 10^{-3}$	-0.8917×10^{-6}
A_5	$-0.1546277 \times 10^{-3}$	$-0.1154375 \times 10^{-6}$	$-0.3215095 \times 10^{-6}$

TABLE 4 Zero material dispersion wavelengths of $As_{40}S_{60}$ and $Ge_{28}Sb_{12}Se_{60}$ glasses.

Glass	λ_o (μm)	Ref
$As_{40}S_{60}$	4.89	[4]
$Ge_{28}Sb_{12}Se_{60}$	6.72	[6]

D PARTIAL DISPERSION IN THE INFRARED REGION

Refractive index dispersion of oxide optical glasses has been evaluated by the Abbe number $\upsilon_d = (n_d - 1)/(n_F - n_C)$, where n_d, n_F and n_C are refractive indexes at 0.5876 μm (He d-line), 0.4861 μm (H_2 F-line) and 0.6563 μm (H_2 C-line), respectively. In contrast, the wavelength dependence of the refractive index of chalcogenide glasses is characterised by partial dispersion within their transparent or desired wavelength ranges. Savage [2] evaluated the refractive index dispersion of chalcogenide glasses in the infrared region, typically As-S, As-Se, Ge-As-Se and Ge-As-Se-Te glasses, by two types of reciprocal dispersion coefficient, $\upsilon_{3\text{-}5}$ and $\upsilon_{8\text{-}12}$. The former coefficient expresses the reciprocal dispersion from 3 to 5 μm, and the latter from 8 to 12 μm. TABLE 5 summarises the results. $\upsilon_{8\text{-}12}$ increases monotonically with increasing As concentrations in Ge-As-Se glasses. $\upsilon_{3\text{-}5}$ decreases and $\upsilon_{8\text{-}12}$ increases monotonically with increasing Te concentrations in Ge-As-Se-Te glasses. There are no systematic dependences of the partial dispersions on Ge concentration in Ge-As-Se and Ge-As-Se-Te glasses. This may concern Ge-O impurities in Ge-containing chalcogenide glasses [2,11].

TABLE 5 Refractive indexes and partial dispersion of chalcogenide glasses in the infrared region [2].

Glass (at%)	$n_{3\ \mu m}$	$n_{4\ \mu m}$	$n_{5\ \mu m}$	$\upsilon_{3\text{-}5}$*	$n_{8\ \mu m}$	$n_{10\ \mu m}$	$n_{12\ \mu m}$	$\upsilon_{8\text{-}12}$**
$As_{40}S_{60}$	2.395	2.390	2.386	154				
$As_{40}Se_{60}$								
$Ge_{10}As_{20}Se_{70}$					2.4649	2.4954	2.4526	119
$Ge_{10}As_{30}Se_{60}$					2.6254	2.6201	2.6135	135
$Ge_{10}As_{40}Se_{50}$					2.6108	2.6067	2.6016	176
$Ga_{20}As_{10}Se_{70}$					2.5628	2.5583	2.5528	156
$Ge_{30}As_{10}Se_{60}$					2.4408	2.4347	2.4271	104
$Ge_{30}As_{15}Se_{55}$					2.4972	2.4914	2.4840	113
$Ge_{30}As_{20}Se_{50}$					2.5690	2.5633	2.5560	120
$Ge_{30}As_{13}Se_{47}Te_{10}$	2.6118	2.6057	2.6024	171	2.5952	2.5897	2.5829	129
$Ge_{30}As_{13}Se_{37}Te_{20}$	2.7412	2.7342	2.7342	162	2.7229	2.7178	2.7117	154
$Ge_{30}As_{13}Se_{27}Te_{30}$	2.8818	2.8732	2.8732	144	2.8610	2.8563	2.8509	185

* $\upsilon_{3\text{-}5} = (n_4 - 1)/(n_3 - n_5)$, ** $\upsilon_{8\text{-}12} = (n_{10} - 1)/(n_8 - n_{12})$.

E CONCLUSION

Refractive index data, their fitting results, zero material dispersion wavelengths and partial dispersion in the infrared region are presented for chalcogenide glasses. This Datareview summarises the data for sulphide, selenide and mixed selenide telluride glasses whose fibres have been successfully fabricated. Further investigations on refractive index dispersion with systematic compositional variation are needed, as well as on the preparation of high-purity chalcogenide glasses for low-loss optical fibres.

REFERENCES

[1] W.S. Rodney, I.H. Malitson, T.A. King [*J. Opt. Soc. Am. (USA)* vol.48 (1958) p.633-6]
[2] J.A. Savage [*J. Non-Cryst. Solids (Netherlands)* vol.47 (1982) p.101-16]
[3] J. Flahaut, M. Guittard, A.M. Loireau-Lozac'h [*Glass Technol. (UK)* vol.24 (1983) p.149-56]
[4] T. Miyashita, T. Manabe [*IEEE J. Quantum Electron. (USA)* vol.QE-18 (1982) p.1432-50]
[5] J.A. Savage, P.J. Webber, A.N. Pitt [*Appl. Opt. (USA)* vol.16 (1977) p.2938-41]
[6] P. Klocek, L. Colombo [*J. Non-Cryst. Solids (Netherlands)* vol.93 (1987) p.1-16]
[7] J. Nishii, T. Yamashita, T. Yamaguchi [*Appl. Opt. (USA)* vol.28 (1989) p.5122-7]
[8] J. Tessman, A.H. Kahn, W. Shockley [*Phys. Rev. (USA)* vol.92 (1953) p.890-5]
[9] L.G. Aio, A.M. Efimov, V.F. Kokorina [*J. Non-Cryst. Solids (Netherlands)* vol.27 (1978) p.299-307]
[10] J. Sanghera, V.Q. Nguyen, I.D. Aggarwal [*J. Am. Ceram. Soc. (USA)* vol.79 (1996) p.1324-8]
[11] K. Abe, H. Takebe, K. Morinaga [*J. Non-Cryst. Solids (Netherlands)* vol.212 (1997) p.143-50]
[12] S. Shibata [PhD Thesis, Hokkaido University, Japan, 1982, p.186-220]

D1.4 Non-linear refractive index of chalcogenide glass

I. Kang and F. Wise

September 1997

A INTRODUCTION

In recent years considerable effort has been aimed at developing and characterising glasses with large and fast optical non-linearities, motivated largely by the potential application of these materials in all-optical switching devices. Several papers [1-3] offer thorough reviews of progress in this area up until the early 1990s and are highly recommended.

The physical origin of the refractive optical non-linearities of glasses is not understood rigorously. Semi-empirical models of the non-linear response were developed by Miller [4] and by Boling, Glass, and Owyoung [5]. To this day the Boling-Glass-Owyoung (BGO) formula for estimating the non-linear index based on the linear optical properties is probably the analysis most commonly employed, and has been a useful guide in the search for highly-non-linear glasses in the absence of a more rigorous theory. Lines developed a bond-orbital theory of the optical non-linearities of alkali-halide crystals [6], and this has been applied to some glasses with some success. It is clear that to obtain a large non-linear refractive index, a large linear refractive index and a small energy gap are desired. In chemical terms, materials with a large number of loosely-bound valence electrons are desired.

B SULPHIDE GLASSES

Adair and co-workers pointed out that the large polarisability and hyperpolarisability of the S^{2-} ion implies large linear (n_o) and non-linear (n_2) refractive indices for sulphide glasses [7]. In addition, the high densities possible with sulphide glasses contribute to achieving large linear indices, which in turn imply large non-linear indices through the BGO formula. A shortcoming of the sulphide glasses is the tendency to have large linear absorption, which is a consequence of relatively long-wavelength absorption edges [8]. With regard to the non-linear-optical properties, much less work has been done on sulphide glasses than on oxide glasses.

C As_2S_3 GLASS FIBRES

Chalcogenide glass fibres show much promise as non-linear media for applications in all-optical switching, and this motivated much of the work in this area. Asobe and co-workers reported a series of studies of As_2S_3-based fibres. These workers used an optical Kerr shutter configuration to measure the non-linear index of As_2S_3 fibre and to demonstrate optical switching at repetition rates as high as 80 GHz [9]. The non-linear index was inferred from cross-phase modulation of a probe pulse, and the value $n_2 = 9.3 \times 10^{-15}$ cm^2/W was obtained at 1.55 μm. The non-linear index of As_2S_3 fibre at 1.3 μm was measured using both self-phase [10] and cross-phase [11] modulations. The results fall between 2×10^{-14} cm^2/W and 4.2×10^{-14} cm^2/W ($\chi^{(3)} = 5 \times 10^{-12}$ - 1.2×10^{-11} esu).

D BULK CHALCOGENIDE GLASSES

Nasu et al have reported using third-harmonic generation to measure the non-linearities of a variety of chalcogenide glasses [12-14]. These include As_2S_3, GeS, GeAsS, GeAsSSe and AsSSe glasses. Nasu and co-workers found that $\chi^{(3)}$ increases with increasing mass density in the chalcogenide glasses. In addition, the addition of Se to the glass dramatically increases $\chi^{(3)}$. Values as high as $\chi^{(3)} = 10^{-11}$ esu were obtained, which is near the largest value reported for a glass and comparable to the non-linearity of organic compounds.

Later measurements of sulphide glasses produced non-linear indices substantially smaller than those obtained with third-harmonic generation. Hall et al used degenerate four-wave mixing to determine the non-linearities of a variety of oxide glasses as well as As_2S_3 glass [15]. These workers report $\chi^{(3)} = 1.7 \times 10^{-12}$ esu for As_2S_3 glass, a value ~7 times smaller than that found using third-harmonic generation. Although the non-linear index is large, As_2S_3 glass suffers from two-photon absorption even at 1.06 μm. Borrelli and co-workers used degenerate four-wave mixing to determine $\chi^{(3)}(-\omega; \omega, \omega, -\omega)$ for LaGa sulphide, Ge sulphide, and some tellurite glasses [3]. Kang et al measured the non-linear indices of LaGa sulphide and GeGa sulphide glasses at several wavelengths between 600 and 1250 nm [16]. Values of $\chi^{(3)}$ as high as 3×10^{-11} esu were found at 600 nm, and good agreement with the values presented in [3] was obtained. The two-photon absorption coefficients of the LaGa sulphide and GeGa sulphide glasses are very small ($\beta < 0.01$ cm/GW) for wavelengths of 1 μm and beyond.

The discrepancies between the results reported by Nasu et al [12-14] and those of Borrelli et al [3] and Kang et al [16] have not been resolved completely. It should be mentioned that a third-harmonic generation experiment determines $\chi^{(3)}(-3\omega; \omega, \omega, \omega)$, which in general is not equal to $\chi^{(3)}(-\omega; \omega, \omega, -\omega)$, the susceptibility that is proportional to n_2 and most pertinent to applications in optical switching. The difference between the susceptibilities with different frequency arguments is likely to be significant when there is a large three-photon-resonant enhancement of the third-harmonic generation, which is likely to be the case in the glasses studied by Nasu et al. The measurements of Borrelli et al and Kang et al are the only direct measurements of $\chi^{(3)}(-\omega; \omega, \omega, -\omega)$ for bulk sulphide glasses. Another possible source of uncertainty arises from the fact that the third-harmonic generation is measured relative to a reference sample. Nasu et al used fused silica as a reference in their measurements. However, they used a value of n_2 for fused silica that is seven times larger than the value used by Adair et al [7]. It seems likely that the discrepancy in the value of the non-linear index of the reference sample accounts for much of the discrepancy in the inferred values of the non-linear indices of the sulphide glasses.

E DISPERSION OF THE OPTICAL NON-LINEARITIES

Virtually all reported measurements of the third-order optical non-linearities of glasses (non-linear refraction and two-photon absorption) were made at one or two wavelengths. Kang et al measured the non-linear refractive indices and two-photon absorption coefficients of three heavy-metal sulphide glasses (LaGa sulphide, GeGa sulphide, and GeGaBa sulphide) at 600, 800, 990 and 1250 nm [16]. Qualitatively similar variation was found for all samples; the results are exemplified by the data for an LaGa sulphide glass shown in FIGURE 1. The steep increase of the non-linearities below 900 nm is probably due to resonant enhancement, given the proximity of the linear absorption edge. The third-order susceptibilities at 600 nm are among the largest values ever reported for glasses, with Re $\chi^{(3)} > 10^{-11}$ esu. The weaker increase between 1250 and 900 nm can be understood from general principles: analysis of the general quantum-mechanical expression for the second hyperpolarisability shows that it should deviate from the static value as a quadratic function of frequency far off resonance [17]. The expression for the off-resonant third-order susceptibility is qualitatively consistent with Kang's results.

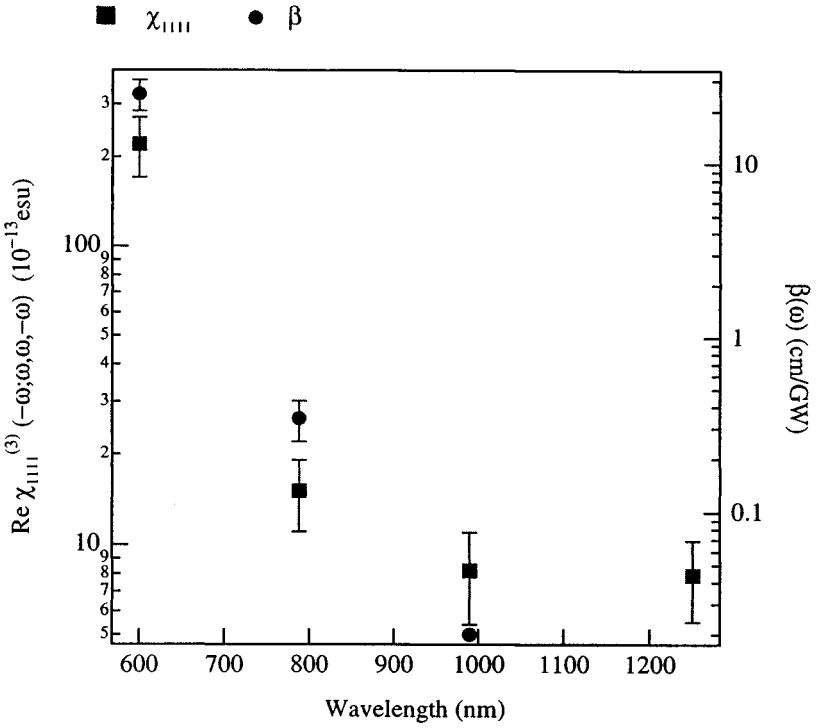


FIGURE 1 Real part of the third-order susceptibility Re $\chi^{(3)}(-\omega; \omega, \omega, -\omega)$ and two-photon absorption coefficient β of an LaGa sulphide glass plotted versus wavelength.

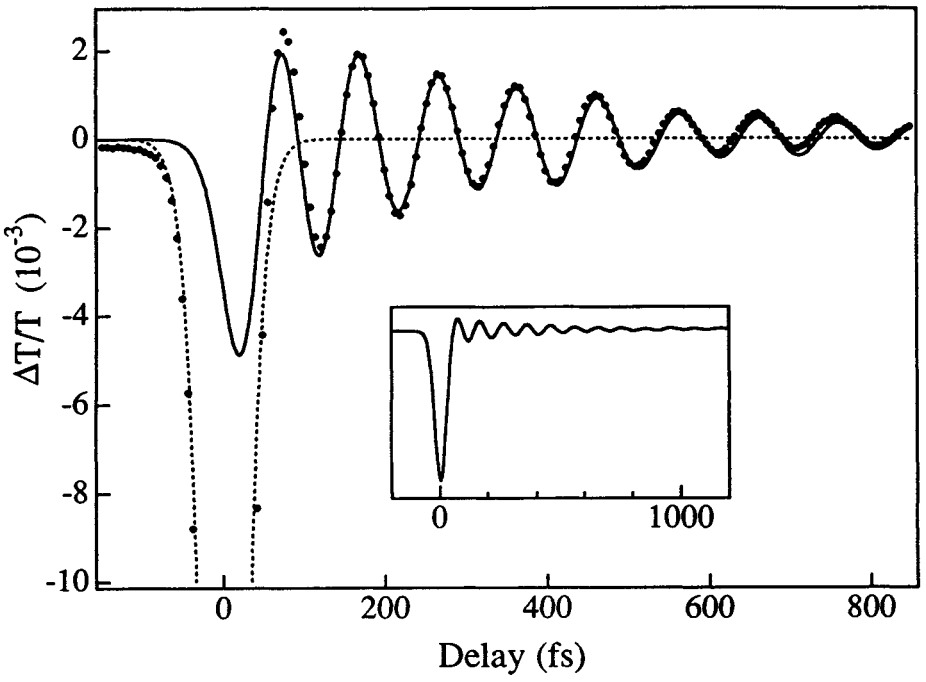


FIGURE 2 Time-resolved z-scan signal from a GeGa sulphide glass. Symbols: experimental data; solid line: nuclear contribution calculated from the polarised and depolarised Raman spectra; dotted line: electronic contribution. The total experimental signal is shown in the inset.

F NUCLEAR CONTRIBUTIONS TO THE THIRD-ORDER NON-LINEARITIES

The magnitude of any nuclear contribution to the third-order optical non-linearities was an unresolved issue for many years. Hellwarth and co-workers originally estimated the relative contributions of electronic and nuclear mechanisms to the third-order polarisation of glasses by analysing Raman-scattering spectra along with intensity-induced polarisation changes [18]. Pan et al used the same reasoning to determine the electronic and nuclear contributions to the non-linearities of lead borate glasses [19]. In each case the nuclear contribution was estimated to be 5 - 20% of the total polarisation. Despite the substantial nuclear polarisabilities of most glasses, there was no direct measurement of the nuclear response until Kang et al reported the observation of the coherent nuclear response of glasses [20]. Typical data are shown in FIGURE 2. The clear isolation of electronic and nuclear responses possible in the time domain allows for direct estimation of their relative strengths. The fractional nuclear contribution is 13% in this case, quite similar to the values estimated previously [18,19] for different materials and elements of the response tensor. These experiments also constitute the first observation of coherent phonons in a glass.

G ADVANCES IN MEASUREMENT TECHNIQUES

Prior to 1990, almost all measurements of third-order susceptibilities of glasses were made using three-wave mixing, four-wave mixing or third-harmonic generation. In 1989 the z-scan was introduced [21]. This is a simple, single-beam technique that provides the magnitude and sign of the real and imaginary parts of $\chi^{(3)}$. The data reported in [16] were obtained from z-scan measurements. The z-scan is not particularly sensitive; it is difficult to measure non-linear phase shifts ($\Delta\Phi$) of less than 0.05 rad using it. The sensitivity is improved to $\Delta\Phi \sim 10^{-3}$ rad in the time-resolved z-scan (used in [20]) because the sample is not moved, so scatter is reduced. Much greater sensitivity is possible using the optical-heterodyne-detected Kerr effect [22] or time-resolved interferometry [23]. Both of these techniques can resolve non-linear phase shifts as small as 10^{-6} rad, but at a cost of significant complexity in the construction and operation of the experiment. Kang et al recently demonstrated that equal and perhaps better sensitivity can be obtained in a very simple experiment based on spectrally resolving a two-beam coupling signal [24]. This technique also gives the magnitude and sign of the real and imaginary parts of $\chi^{(3)}$ in a single experiment. Typical data from a 1 mm piece of fused silica are shown in FIGURE 3; the noise level implies a sensitivity of $\Delta\Phi = 3 \times 10^{-6}$ rad.

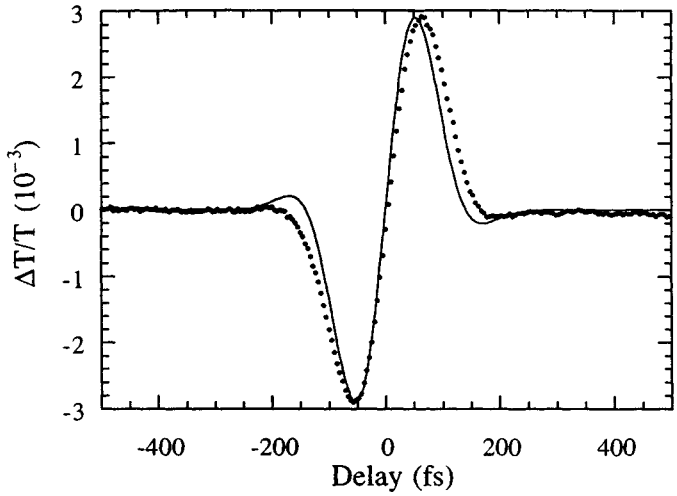


FIGURE 3 Two-beam coupling signal from fused silica (symbols) along with the theoretical fit to the data (solid curve). The peak of the signal corresponds to a non-linear phase shift $\Delta\Phi = 4 \times 10^{-4}$ rad. The trace was obtained using nanojoule-energy pulses from a modelocked laser and noise was reduced by simply averaging 1000 traces (obtained in ~2 minutes).

REFERENCES

[1] M.E. Lines [*J. Appl. Phys. (USA)* vol.69 (1991) p.6876]

[2] E.M. Vogel, M.J. Weber, D.M. Krol [*Phys. Chem. Glasses (UK)* vol.32 (1991) p.231]

[3] N.F. Borrelli, B.G. Aitken, M.A. Newhouse [*J. Non-Cryst. Solids (Netherlands)* vol.185 (1995) p.109]

[4] R.C. Miller [*Appl. Phys. Lett. (USA)* vol.5 (1964) p.17]

[5] N.L. Boling, A.J. Glass, A. Owyoung [*IEEE J. Quantum Electron. (USA)* vol.QE-14 (1978) p.601]

[6] M.E. Lines [*Phys. Rev. B (USA)* vol.41 (1990) p.3383; *Phys. Rev. B (USA)* vol.43 (1991) p.11978]

[7] R. Adair, L.L. Chase, S.A. Payne [*J. Opt. Soc. Am. B (USA)* vol.4 (1987) p.875]

[8] M.E. Lines [*J. Appl. Phys. (USA)* vol.55 (1984) p.4052]

[9] M. Asobe, H. Kobayashi, H. Itoh, T. Kanamori [*Opt. Lett. (USA)* vol.18 (1993) p.1056]

[10] M. Asobe, K. Suzuki, T. Kanamori, K. Kubodera [*Appl. Phys. Lett. (USA)* vol.60 (1992) p.1153]

[11] M. Asobe, T. Kanamori, K. Kubodera [*IEEE Photonics Technol. Lett. (USA)* vol.4 (1992) p.362; *IEEE J. Quantum Electron. (USA)* vol.29 (1993) p.2325]

[12] H. Nasu, Y. Ibara, K. Kubodera [*J. Non-Cryst. Solids (Netherlands)* vol.110 (1989) p.229]

[13] H. Nasu, K. Kubodera, M. Kobayashi, M. Nakamura, K. Kamiya [*J. Am. Ceram. Soc. (USA)* vol.73 (1990) p.1794]

[14] H. Nasu, J. Matsuoka, K. Kamiya [*J. Non-Cryst. Solids (Netherlands)* vol.178 (1994) p.23]

[15] D.W. Hall, M.A. Newhouse, N.F. Borrelli, W.H. Dumbaugh, D.L. Weidman [*Appl. Phys. Lett. (USA)* vol.54 (1989) p.1293]

[16] I. Kang, T.D. Krauss, F.W. Wise, N.F. Borrelli, B.G. Aitken [*J. Opt. Soc. Am. B (USA)* vol.12 (1995) p.2053]

[17] D.M. Bishop [*Phys. Rev. Lett. (USA)* vol.61 (1988) p.322]

[18] R. Hellwarth, J. Cherlow, T.-T. Yang [*Phys. Rev. B (USA)* vol.11 (1975) p.964]

[19] Z. Pan, S.H. Morgan, B.H. Long [*J. Non-Cryst. Solids (Netherlands)* vol.185 (1995) p.127]

[20] I. Kang, S. Smolorz, T. Krauss, F. Wise, N.F. Borrelli, B.G. Aitken [*Phys. Rev. B (USA)* vol.54 (1996) p.R12641]

[21] M. Shiek-Bahae, A.A. Said, E.W. Van Stryland [*Opt. Lett. (USA)* vol.14 (1989) p.955]

[22] D. McMorrow, W.T. Lotshaw, G.A. Kenney-Wallace [*IEEE J. Quantum Electron. (USA)* vol.QE24 (1988) p.443]

[23] L. Sarger et al [*J. Opt. Soc. Am. B (USA)* vol.11 (1994) p.995]

[24] I. Kang, T. Krauss, F. Wise [*Opt. Lett. (USA)* vol.22 (1997) p.1077]

PART D: CHALCOGENIDE GLASS

CHAPTER D2

THERMAL AND MECHANICAL PROPERTIES

D2.1 Characteristic temperatures of chalcogenide glass
D2.2 Viscosity of chalcogenide glass

D2.1 Characteristic temperatures of chalcogenide glass

D.W. Hewak and D.J. Brady

September 1998

A INTRODUCTION

In considering a glass system for fibre optic applications, the characteristic temperatures form an important set of data which will determine if the material can be drawn into fibre, the level of crystallisation which may be induced during drawing and compatible materials for core-clad structures. In this Datareview, the characteristic temperatures, in particular the glass transition, crystallisation and melting temperatures, along with the coefficient of thermal expansion of chalcogenide glass will be reviewed. Also discussed are their measurement and application in fibre drawing for several typical chalcogenide glasses.

B CHARACTERISTIC TEMPERATURES

It is generally true that any crystalline solid can be made amorphous if cooled sufficiently rapidly from above its melting point; for example amorphous metals require cooling of the order of 10^6 K/s for formation. They are however glasses only if they have a glass transition temperature, T_g [1]. Glasses will show a continuous decrease in volume as they are cooled from high temperatures through a super-cooled region until their T_g is reached where the coefficient of thermal expansion changes (usually decreases), but remains continuous. T_g is the intersection between the glass solid and glass liquid phases as shown in FIGURE 1. It is dependent on cooling rate, and increases with increasing cooling rate [2]. Unlike glass, crystalline materials exhibit a discontinuity in the volume of the material upon passing through the melting point.

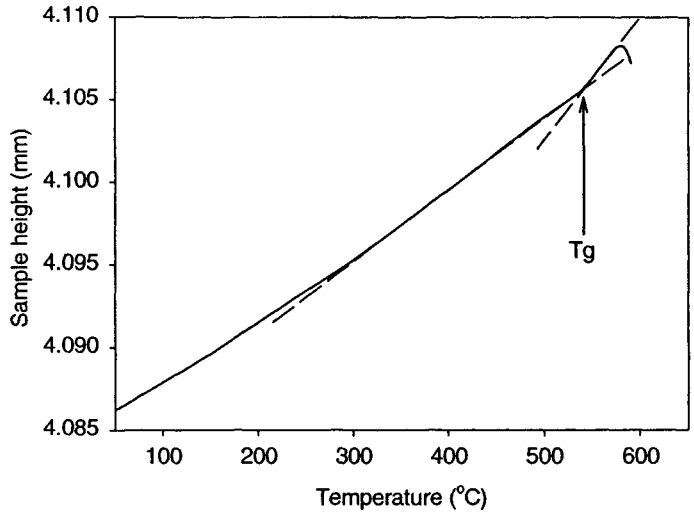


FIGURE 1 Determination of T_g from the expansion coefficient (Ga:La:S glass).

The lack of such a discontinuity in glasses is due to their viscoelastic property where the viscosity of the glass constantly increases upon cooling. The viscosity becomes so great that the mass transport for crystallisation has such a large time constant that crystallisation is effectively prevented. Glasses can, however, devitrify if held above T_g for long enough, the time and temperature for which is determined

by the composition of the glass. The onset of crystallisation is denoted T_x and the peak crystallisation temperature is denoted T_p as shown in the differential thermal analysis (DTA) curve given in FIGURE 2. Both these temperatures are heating rate dependent. As heating continues, any crystals may begin to melt. The onset of melting is denoted T_m and is indicated in FIGURE 2 by the first endothermic event. This is followed by the liquidus, T_l, the temperature at which crystal melting is complete.

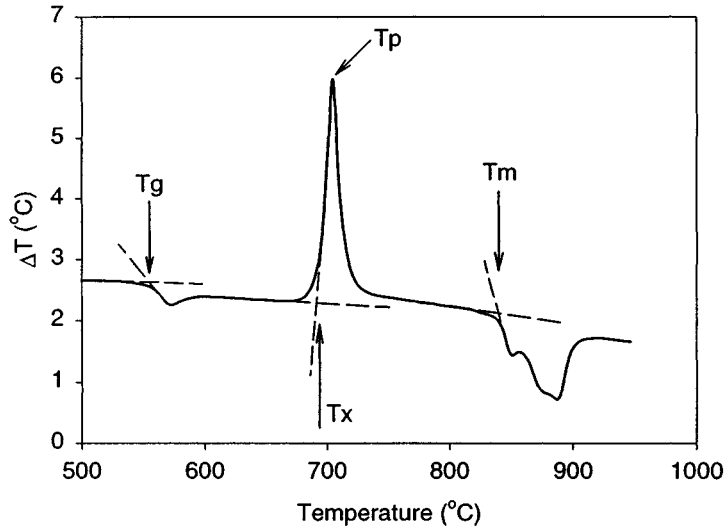


FIGURE 2 Typical DTA trace for Ga:La:S glass.

There are also three defined temperatures in terms of the viscosity of the glass. The strain point is the temperature at which the viscosity of the glass is approximately $10^{14.6}$ poise. At this viscosity the glass will tend to flow rather than fracture, and stresses in the glass will be relieved in hours. The annealing point is the temperature at which the viscosity is approximately $10^{13.4}$ poise, and stresses in a glass at this temperature will be relieved in minutes. The final temperature is the softening point, where the glass has a viscosity of approximately $10^{7.6}$ poise. At or above this temperature the glass can be worked. In FIGURE 1, the drop in sample height at high temperatures is due to plastic deformation of the sample [3,4].

C MEASUREMENT OF THE CHARACTERISTIC TEMPERATURES

There are several techniques for measuring these characteristic temperatures; however differential scanning calorimetry (DSC) and differential thermal analysis (DTA) are now the most common. In our own work, we prefer DTA for the higher temperatures that can be reached. The instrument used for our measurements is the Perkin-Elmer DTA7. The measurement principle is based on the difference in temperature between two alumina cups, both of which are at the centre of a uniform temperature furnace. One cup holds an inert material (alumina powder), and the other holds a small piece of glass (of known mass), contained in alumina powder to provide good thermal contact. As the furnace is ramped up, any changes in the glass that require or release heat are recorded as a function of temperature. In this way, T_g, T_x, T_p and the melting point T_m can all be measured.

A typical DTA trace for gallium based chalcogenide glass is shown in FIGURE 2. The transition temperatures marked on the diagram are calculated as the intercepts of two tangents to the curve, one before and one after the feature. The left hand axis is the difference in temperature between the thermocouples. The slight slope in the curve is due to the thermocouple being at slightly different heights in the furnace.

A commercial thermo-mechanical analyser (Perkin-Elmer TMA7) with a high displacement sensitivity (up to 50 nm) and temperature range up to 1000°C can be used for thermal expansion measurements. The sample is cylindrical in shape, typically of dimensions 5 mm in both thickness and diameter, and held between two Inconel plates. Expansion coefficients are measured with a 10 mN load. The procedure is to measure the expansion coefficient of the Inconel plates before that of the sample and plates composite. In this way the expansion coefficient of the sample alone can be extracted. Heating is from room temperature to the point where the sample begins to deform, and the deflection is measured as a function of temperature. The expansion coefficient is given directly from the slope of the line. It is also possible to find T_g from expansion coefficient data as shown in FIGURE 1, although the DTA is likely to be more accurate.

D CRYSTALLISATION DURING FIBRE DRAWING

Criteria for a glass which allow good fibre drawing are that the separation of T_g and T_x should be large, the width of the crystallisation peak T_p - T_x should also be large, and the separation of T_m and T_p should be small. These can readily be understood in terms of what is happening to the glass. The temperature T_g determines the intersection of the glass solid and glass liquid phases, so any fibre drawing needs to be at temperatures above T_g. If T_x - T_g is small, the material will tend to crystallise at or before drawing, and may not draw at all. It may also be used as a guide to the maximum working temperature of the glass as a glass held above T_g will eventually crystallise.

If the width of the crystallisation peak is large, then some crystallisation may take place, but not as rapidly as in the case where this peak is strong and narrow. The latter indicates one clearly defined crystalline event which completes very quickly once started, potentially making fibre very difficult to draw, particularly if T_x - T_g is also small. A wider peak indicates the possibility of more than one crystal event. In this case, crystallisation may be sluggish, and not complete unless the temperature increases. Here the 'confusion principle' applies with crystallisation being suppressed by competing phases [3].

If T_m - T_p is small, then the viscosity of the glass at the crystallisation temperature will be low (viscosity of the liquid ~10^1 poise); however for fibre drawing we require a higher viscosity (10^4 - 10^6 poise), allowing drawing at temperatures significantly lower than the onset of crystallisation. If viscosity data are known, then the actual separation between the drawing temperature and the onset of crystallisation can be calculated and serves as a useful indicator of fibre drawing potential. It has been shown that careful optimisation of the composition can result in significant gains in thermal stability with correspondingly enhanced fibre drawing properties.

E EXAMPLES

TABLE 1 presents glass transition values for a series of chalcogenide glasses, in order of decreasing T_g. As heavier chalcogenides are incorporated in the glass, T_g and all characteristic temperatures tend to drop. TABLE 2 indicates the wide variation in thermal stability and ease of fibre drawing which can be obtained through compositional modifications of a glass. Starting from a base composition of approximately 70% gallium sulphide, lanthanum sulphide, sodium sulphide, cesium chloride and lanthanum oxide are all added to form a stable glass composition. While all of these compositions have been drawn into multimode fibre, there are clear differences in ease of fibre drawing and propensity to crystallisation which are reflected in their characteristic temperatures. In our experience, pure Ga:La:S based glasses are most difficult to draw and prone to a variety of crystallisation events. Introduction of a chloride or oxide dramatically improves fibre drawing and prospects for a crystal free fibre, though at the expense of other glass properties [5-10]. There is a clear correlation between the width of the crystallisation peak T_p - T_x and the difference between the drawing temperature T_η and the peak crystallisation temperature T_p in this series of glasses.

TABLE 1 Glass transition temperatures of various chalcogenides [11,12].

Composition	T_g (°C)
$Ga_{20}La_{20}S_{60}$	556
$Ge_{25}Ga_5S_{70}$	450
$Ge_{30}As_{20}Se_{50}$	361
$Ge_{28}Sb_{12}Se_{60}$	300
$Ge_{20}As_{30}Se_{30}Te_{20}$	236
$Ge_{27}Se_{18}Te_{15}$	205
$As_{40}S_{60}$	204
$As_{40}Se_{60}$	178
$Ge_{20}S_{80}$	170
$Ge_{20}Se_{80}$	154

TABLE 2 Comparison of thermal properties of a series of gallium sulphide based chalcogenide glasses.

Composition	T_g (°C)	T_x (°C)	T_p (°C)	T_m (°C)	$T_{\eta=10^6}$ (°C)	$T_p - T_x$ (°C)	$T_p - T_g$ (°C)	$T_P - T_\eta$ (°C)	α $\times 10^{-6}$/°C
$66Ga_2S_3{:}34Na_2S$	484	599	616	720	570	17	115	46	14.5
$70Ga_2S_3{:}30La_2S_3$	556	681	705	830	656	24	149	49	8.95
$70Ga_2S_3{:}5La_2S_3{:}25CsCl$	501	682	712	797	615	32	211	97	13.9
$70Ga_2S_3{:}30La_2O_3$	556	738	810	971	676	72	254	134	7.46

T_g is the glass transition, T_x is the onset of crystallisation, T_p is the peak crystallisation, T_m is the onset of melting, $T_{\eta=10^6}$ is the temperature at which the viscosity is 10^6 poise (generally the upper limit for fibre drawing) and α is the coefficient of thermal expansion.

REFERENCES

[1] J.S. Bowder, S.S. Ballard, P. Klocek [in *Handbook of Infrared Optical Materials* Ed. P. Klocek (Marcel Dekker, New York, 1991) p.151]

[2] S.R. Joshi, A. Pratap, N.S. Saxena, M.P. Saksena, A. Kumar [*J. Mater. Sci. Lett. (UK)* vol.13 (1994) p.77-9]

[3] R.H. Doremus [*Glass Science* (Wiley, New York, 1973) ch.2]

[4] D.J. Brady, J. Wang, D.W. Hewak [Datareview in this book: *D2.2 Viscosity of chalcogenide glass*]

[5] J. Wang et al [*Appl. Phys. Lett. (USA)* vol.71 (1997) p.1753-5]

[6] R.S. Brown, W.S. Brocklesby, D.W. Hewak, B.N. Samson [*J. Lumin. (Netherlands)* vol.66-7 (1995) p.278-84]

[7] S.P. Morgan, I.M. Reaney, R. Buckley, D. Furniss, A.B. Seddon [*J. Am. Ceram. Soc. (USA)* in press]

[8] I.M. Reaney, S.P. Morgan, R. Li, A.B. Seddon [*Proc. 11th Int. Symp. on Non-Oxide and New Optical Glass* Sheffield, UK, 6-10 September 1998, paper D4]

[9] S.P. Morgan, D. Furniss, A.B. Seddon, W.M. Moore [*J. Non-Cryst. Solids (Netherlands)* vol.213 (1997) p.72-8]

[10] S.P. Morgan, I.M. Reaney, R. Buckley, D. Furniss, A.B. Seddon [*J. Am. Ceram. Soc. (USA)* vol.81 (1998) p.1913-8]

[11] J.S. Sanghera, I.D. Aggarwal (Eds.) [*Infrared Fibre Optics* (CRC Press, Boca Raton, USA, 1998)]

[12] J. Nishii, Y. Kaite, T. Yamagishi [*Phys. Chem. Glasses (UK)* vol.28 (1987) p.55-8]

D2.2 Viscosity of chalcogenide glass

D.J. Brady, J. Wang and D.W. Hewak

July 1998

A INTRODUCTION

Chalcogenide glasses for drawing into optical fibres have been a topic of interest for over thirty years. Since the late 1960s a wide range of germanium, selenium and tellurium based compositions have been explored for infrared transmission [1]. More recently, gallium based glasses have undergone study for active devices, in particular a 1.3 micron optical fibre amplifier [2,3]. For all these fibre applications knowledge of the viscosity behaviour as a function of the temperature is important. When fibre drawing from a preform, viscosities in the region of 10^4 - 10^6 poise are required. With crucible drawing, fibre drawing takes place near the melt temperature, at viscosities around 10 poise. Despite the importance of this parameter, there are few systematic studies of the viscosity of chalcogenide glasses.

In this Datareview, the principle methods of viscosity evaluation of chalcogenide glasses are reviewed, along with data for compositions of current interest.

B MEASUREMENT METHODS

As with the fluoride glasses [4], viscosity measurements tend to be difficult to carry out with some chalcogenide glass compositions. The viscosity curves of these glasses as a function of temperature are steep, resulting in a relatively small working range. Within this range, the glasses are prone to crystallisation [5] which alters the viscosity. At the liquidus temperature, some compositions are volatile, while others react with moisture or air. None the less, a variety of methods of viscosity measurement are applicable to the chalcogenide glasses, as described in the table below.

TABLE 1 Methods for viscosity measurement suitable for chalcogenide glasses.

Method	Viscosity range	Ref
Parallel plate	10^4 - 10^8	[6,7]
Penetration	10^6 - 10^{10}	[8,9]
Bending beam	10^7 - 10^{13}	[10]
Rod elongation	10^4 - 10^6	[11,12]
Tube viscometers	10^1 - 10^2	[13,14]
Rotational viscometer	10^1 - 10^2	[15]

Conventional viscometry techniques such as parallel plate, penetration and bending beam methods have been applied to a wide variety of solid materials, not only glasses, and the procedures are well documented [14]. Further details on the application of the parallel plate method are presented later in this Datareview.

Rod elongation requires the preparation of a glass rod which is placed in a furnace and heated until it softens and stretches. This can be done with or without additional tension. From measurements of the tension, and the initial and final diameters of the rod, the viscosity at the furnace temperature follows. This method is analogous to the preform drawing technique and the information it yields is directly relevant to fibre fabrication.

Tube viscometers, including the Ostwald, Ubbelohde and Cannon Fenske types, measure the time for fluids to flow through a capillary and fill or empty a reservoir bulb. For these viscometers, gravity is the force applied to cause flow. Both the glass and the entire viscometer must be heated. If the apparatus is silica based, the flow of the molten glass within can be monitored visually. Further details of this method are presented later in this Datareview.

Rotating cylinder methods, applicable to glasses near their liquidus temperature, or low viscosity fluids in general, are common and well documented [14,15].

C FITTING OF VISCOSITY DATA

There are several equations to which viscosity as a function of temperature can be fitted. These have been described in [4], found earlier in this book.

D PRACTICAL EXAMPLES

D1 Viscosity of Ga:La:S Glass by the Parallel Plate Method

The viscosity of Ga:La:S glass in the range 10^5 to 10^{11} poise has been determined using the technique of parallel plate rheometry [7]. A commercial thermo-mechanical analyser (Perkin-Elmer TMA7) with a high displacement sensitivity (up to 50 nm) and temperature range up to 1000°C was used. The sample is cylindrical in shape, typically of dimensions 5 mm in both thickness and diameter, and is held between two parallel plates of Inconel, 0.1 mm thick and 8 mm in diameter. The sample chamber is purged with helium to ensure rapid temperature equilibrium. The sample is held at T_g for ten minutes to give a sample free of stresses, which would interfere with the measurement. The compression as a function of time and temperature is recorded as the temperature is increased at a rate of 2 - 10°C/min under a constant force of between 50 and 2000 mN, depending on the viscosity range of interest. For fibre drawing this is 10^4 to 10^6 poise, for which the ideal set of parameters was a load of 200 mN with a heating rate of 10°C. Recording is stopped once the diameter of the sample approaches that of the plates. The viscosity was calculated using:

$$\eta = \frac{2\pi F h^5(t)}{3V\left[\frac{dh(t)}{dt}\right]\left[2\pi h^3(t) + V\right]} \qquad (1)$$

where η is the viscosity in poise, F is the applied force in dynes (1 dyne = 10^{-2} mN), h(t) is the sample thickness at time t (in cm), dh(t)/dt is the compression rate at time t in cm/s, and V is the sample volume.

The viscosity of Ga:La:S as a function of composition is shown in FIGURE 1. The limit of the viscosity measurements was around 10^6 poise or the viscosity required for fibre drawing, and the slight curve at the end of each measurement was due to the width of the sample approaching that of the plates, with sample compression becoming correspondingly more difficult and EQN (1) no longer applying. As more Ga_2S_3 is introduced to the glass, the viscosity drops. As different compositions must be used to give different refractive indices for core-clad fibres, the core and cladding will have different viscosities. The situation is made slightly more complex by the fibre drawing technique, where a stream of inert gas passes over the outside of the preform, cooling the cladding. This type of system can lead to problems in obtaining a circular core.

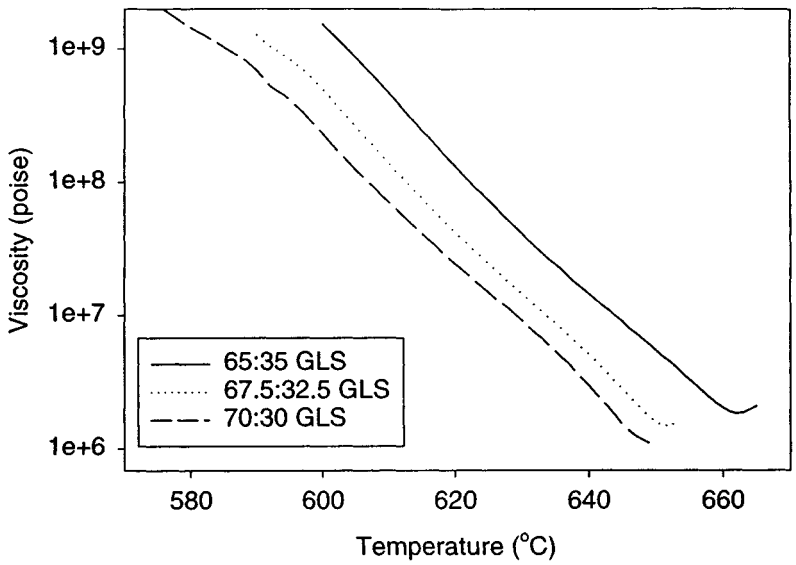


FIGURE 1 Results of parallel plate viscometry measurements applied to a series of Ga:La:S glasses.

D2 High Temperature Viscosity of As:Ga:Ge Glasses

One possible method for the fabrication of As:Ga:Ge fibres is the double crucible method. As these glasses are volatile at the melt temperature, conventional viscometry is problematic; thus Fretz et al [15] employed a modified Ostwald-type viscometer to determine the viscosity of this family of glasses.

A sealed tube viscometer is fabricated from fused silica. It consists of a reservoir connected by a tube to a bulb as illustrated in FIGURE 2. The sealed tube, loaded with the glass to be measured, is placed in a furnace and heated to about 100°C above the measurement temperature. The viscometer is oriented 180° from the position shown in the figure and the higher temperature ensures that all of the glass drains to the bottom of the reservoir and off the surface of the viscometer. After this has occurred, the temperature is adjusted to the measurement temperature and allowed to equilibrate before a measurement is taken.

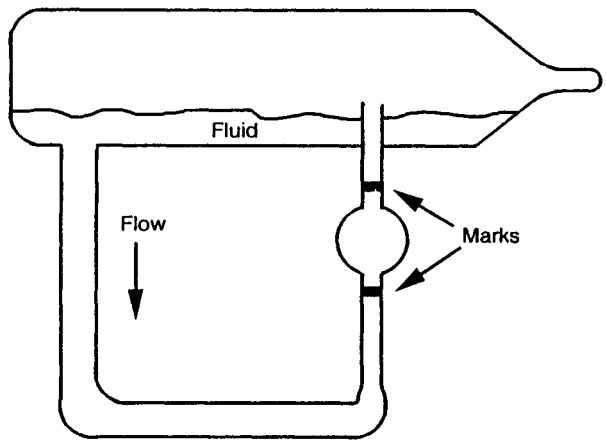


FIGURE 2 Illustration of the modified Ostwald viscometer used for the viscosity measurement of As:Ga:Ge glasses.

For the measurement, the apparatus is rotated back to the orientation shown in FIGURE 2 and the time of flow between the two marks on either side of the bulb is timed to the nearest second. Measurement errors are typically less than 3%. The viscosity was obtained by fitting the data to a modified Poiseuille equation [15]:

$$\eta = \rho A t - (\rho B/t) \qquad (2)$$

where η is the viscosity in poise, ρ is the density at 25°C, t is the time of flow for the fluid between the marks, and A and B are calibration constants obtained by using the apparatus to measure two fluids of known viscosity.

E CONCLUSION

The viscosity of chalcogenide glasses is an important rheological parameter, in particular for fibre optic applications. Many conventional methods of viscosity measurement can be applied to this glass, though care is needed around the crystallisation and liquidus temperatures.

REFERENCES

[1] T. Kanamori, Y. Terunuma, S. Takahashi, T. Miyashita [*J. Lightwave Technol. (USA)* vol.2 (1984) p.607]

[2] J. Kobelke, J. Kirchof, M. Scheffler, A. Schwuchow [*Proc. OAA* Monterey, CA, USA, 11-13 July 1996 (Opt. Soc. America, Washington DC, USA, 1996) p.127-8]

[3] D.W. Hewak et al [*Electron. Lett. (UK)* vol.32 (1996) p.384-5]

[4] M. Braglia [Datareview in this book: *C2.2 Viscosity of halide glass*]

[5] D. Hewak, D. Brady [Datareview in this book: *D2.1 Characteristic temperatures of chalcogenide glass*]

[6] E.H. Fontana [*J. Am. Ceram. Soc. (USA)* vol.49 (1970) p.549]

[7] J. Wang [*Mater. Lett. (Netherlands)* vol.31 (1997) p.99-103]

[8] S.V. Nemilov, G.T. Petrowskii [*J. Appl. Chem. of the USSR (USA)* vol.36 pt.I (1963) p.208-10]

[9] R. Brueckner, D. Demharter [*Glastech. Ber. (Germany)* vol.48 (1975) p.12]

[10] H. Hagy [*J. Am. Ceram. Soc. (USA)* vol.46 (1963) p.93]

[11] U.C. Paek, R.B. Runk [*J. Appl. Phys. (USA)* vol.49 (1978) p.4417]

[12] U.C. Paek, C.M. Schroeder, C.R. Kurkjian [*Glass Technol. (UK)* vol.29 (1988) p.263]

[13] K.-D. Pohl, R. Bruckner [*Phys. Chem. Glasses (UK)* vol.22 (1981) p.150]

[14] G. Barr [*A Monograph of Viscometry* (Oxford University Press, UK, 1931)]

[15] E.R. Fretz, R.F. Bartholomew, B.G. Aitken, M.L. Powley [*Proc. 10th Non-Oxide Glass Symposium* Corning, New York, 19-22 June 1996]

PART D: CHALCOGENIDE GLASS

CHAPTER D3

RARE-EARTH SPECTROSCOPY

D3.1 Spectroscopy of praseodymium-doped chalcogenide glass
D3.2 Spectroscopy of neodymium-doped chalcogenide glass
D3.3 Spectroscopy of thulium/holmium-doped chalcogenide glass
D3.4 Spectroscopy of dysprosium-doped chalcogenide glass

D3.1 Spectroscopy of praseodymium-doped chalcogenide glass

W.S. Brocklesby

April 1998

A INTRODUCTION

The chalcogenide glasses exhibit transmission from the visible or near infrared far into the IR. The IR absorption edge is attributed to absorption of photons by the glass matrix, and the visible cut-off is due to absorption by the bands of the semiconductor. The refractive index of the chalcogenides is typically high (greater than 2.0) which indicates large oscillator strengths for rare-earth dopant transitions [1].

The rare-earth ion solubility in chalcogenides varies greatly, depending on their composition. Many different glasses have been tried, including GeS_2-Ga_2S_3 [2] (GeGaS) and derivatives, Ga_2S_3-La_2S_3 (GLS) [3] and halide modified GLS [4], $GeAsS_2$ [5] and As_2S_3 [6]. In the cases of the GeGaS and GeAsS systems, the rare earth ions are relatively insoluble unless some modifier is added. Many different modification schemes have been used, including Ge-S-I [7] and GeGaS-alkali halides [8]. Ga_2S_3-Na_2S glass has also been successfully made into low-loss fibres [9]. In all cases, glass samples with high concentrations are typically used for absorption measurements, and low concentration samples are used for emission measurements, where concentration quenching can distort results.

Solubility in GLS glass is high. The ionically bonded lanthanum creates negatively charged spaces within the structure that have high coordination numbers. The rare-earth ions will displace lanthanum and enter these charged areas. It is expected that the bonds to the rare-earth ion in GLS glass will be more covalent than the bonds to the rare-earth ion in oxide glasses. This is expected to lead to a strong spectral shift due to the nephelauxetic effect.

B Pr^{3+} ABSORPTION LEVELS

From a chalcogenide glass with a relatively large bandgap, like GLS, emission can be seen from bands up to the $^1D_2$ level, at ~590 nm. FIGURE 1 shows the absorption spectra of Pr^{3+} in GLS glass. The absorption lines correspond to transitions from the ground state $^3H_4$ level to the upper Stark manifolds. The absorption lines for Pr^{3+} in GLS glass are broadened and shifted in wavelength relative to the same Pr^{3+} absorption lines with a silica glass host. The broadening is largely inhomogeneous (see Section D) and the shift in peak position is due to the nephelauxetic effect.

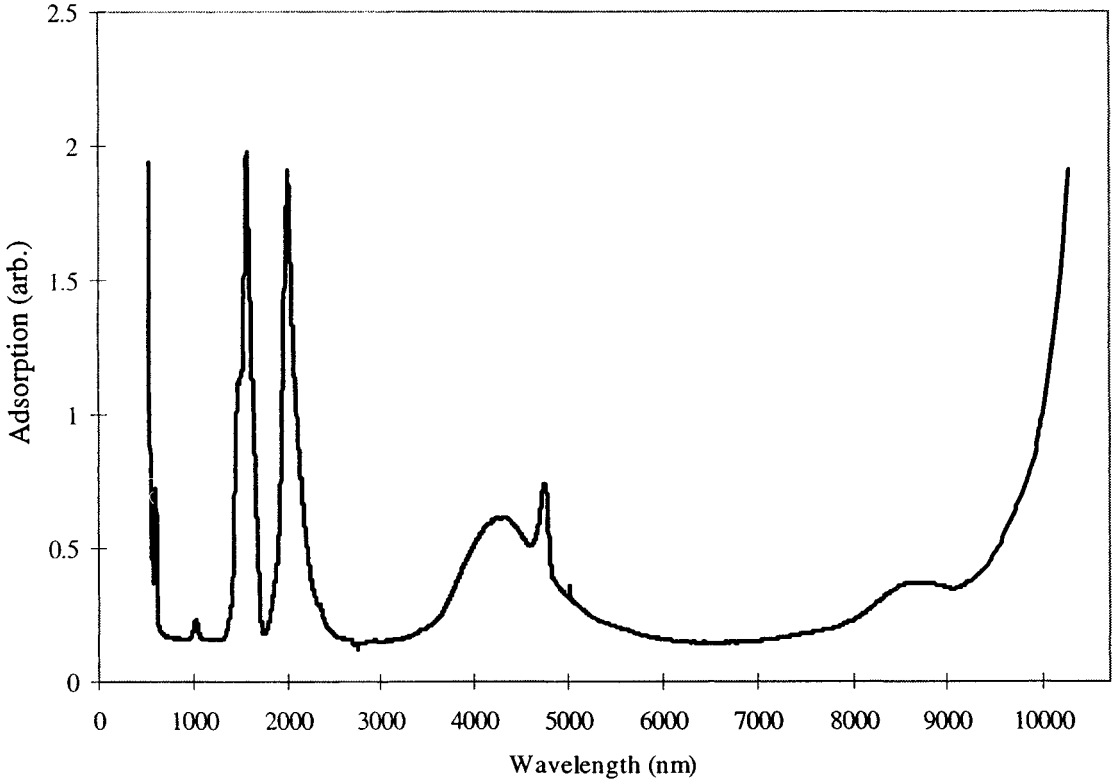


FIGURE 1 Absorption spectrum of Pr-doped GLS glass.

C ABSORPTION STRENGTHS AND RADIATIVE LIFETIMES

Calculation of absorption strengths and radiative lifetimes in chalcogenide glasses is similar to calculation for many other solid hosts [10]. However, the Pr^{3+} ion does have some associated difficulties in all hosts. The commonest way to calculate absorption strengths and thus radiative lifetimes for rare-earth-doped insulators is to use Judd-Ofelt [11] theory. This takes as its input the measured absorption strengths of a few optical transitions, and can predict from these data absorption strengths, radiative lifetimes and branching ratios for other transitions of the system. Unfortunately, Judd-Ofelt calculations for the Pr^{3+} ion are notoriously error-prone. The principal reason for this is that Judd-Ofelt theory relies on the approximation that the 5d levels of the rare earth ion are widely-spaced in energy from the 4f levels. Although true for many rare earth ions, the 5d levels of the Pr ion are significantly closer to the 4f levels than most, resulting in significant errors in J-O calculations. Several schemes have been put forward to amend the J-O calculations to take the 4f-5d spacing into account [12]. If these modified Judd-Ofelt calculation techniques are not used, then the values of the $\Omega_{2,4,6}$ parameters can turn out to have unphysical values. J-O calculations for chalcogenide glasses are made more complicated by the fact that the absorption of the visible $^1D_2$ level and higher energy levels of Pr^{3+} is typically obscured by the band edge and weak absorption tails of the glass. To achieve accurate absorption spectra, the background glass absorption has to be removed from the measured absorption spectra.

The Pr^{3+} ion also exhibits hypersensitive upper levels, which again complicates the Judd-Ofelt calculation. In GLS glass, the Judd-Ofelt calculation for the predicted radiative lifetime for the $^1G_4$ level gives a value of (512 ± 50) μs [13]. The large error illustrates the particular difficulties in the Judd-Ofelt measurement in this glass and dopant system.

Typical J-O parameters for Pr^{3+} in chalcogenide glasses are given in TABLE 1. From these parameters, it is possible to calculate the radiative rates between any two levels.

TABLE 1 Judd-Ofelt parameters for several chalcogenide glasses.

Host glass	Ω_2 ($\times 10^{-20}$ cm^2)	Ω_4 ($\times 10^{-20}$ cm^2)	Ω_6 ($\times 10^{-20}$ cm^2)
GLS [3]	9.8	2.8	5.5
GLS [14]	7.3 ± 0.9	6.2 ± 0.6	3.9 ± 0.2
GeS_x [15]	9.6 ± 3.9	15.4 ± 4.7	4.4 ± 1.9
GNS [9]	10.5	11.6	5.2

D FLUORESCENCE OF Pr-DOPED CHALCOGENIDE GLASS

Chalcogenide glasses act as efficient hosts for the observation of fluorescence from rare earth dopants, because their low phonon energies mean that non-radiative decay is much less prevalent than in oxide glasses (see Section E). The other effect of the reduction in multiphonon decay is that some of the more common laser and amplifier pumping schemes used in silica glasses do not work. This is because the non-radiative decay channels that are part of the pumping cycle for three- or four-level lasers are less probable than photon emission from the pump levels.

Broadening on chalcogenide glasses follows the pattern seen on other glasses, with both homogeneous and inhomogeneous components in approximately equal orders of magnitude at room temperature. One notable difference between broadening in chalcogenide hosts and other glass hosts has been observed in GLS glass. In the GLS system, the inhomogeneous broadening is correlated between different electronic levels [16]. The end result of this is that line narrowing can be seen at room temperature, which may affect the gain bandwidths of lasers or amplifiers based on these materials.

E NON-RADIATIVE PROPERTIES

Chalcogenide glasses typically have much lower vibrational energies than oxide or fluoride glasses because of the different strength and nature of the chemical bonds that form them. A typical Raman spectrum of GLS glass is shown in FIGURE 2 [17]. The highest energy vibrations supported by the glass are at about 400 cm^{-1}, compared to 600 cm^{-1} for fluoride glasses such as ZBLAN, and 1100 cm^{-1} for silica glasses. The effect of this very low maximum vibrational energy in the glass is to reduce rates of non-radiative decay very significantly, and to extend the absorption edge considerably further into the infrared. GLS glass exhibits a maximum phonon energy of ~390 cm^{-1}, and GeGaS glass has a maximum vibrational energy of ~430 cm^{-1} [18].

Chalcogenide glasses have lower multiphonon decay rates than most other common fibre materials, and thus exhibit higher quantum efficiencies for many rare earth transitions. In the case of the important 1.3 μm transition of Pr^{3+}, the quantum efficiency can be measured directly without the use of Judd-Ofelt theory. A method has been described by Quimby et al [19] which makes use of the level structure of Pr^{3+}. This method relies on the measurement of fluorescence from a visible transition with known quantum efficiency, which has a known branching ratio to the top level of the 1.3 μm transition, and produces results which approximately confirm those from modified Judd-Ofelt theory. This technique provided a basis for more detailed exploration of the change in properties of the Pr^{3+} emission with modification of the host [20], which would be impossible by more conventional and less accurate methods.

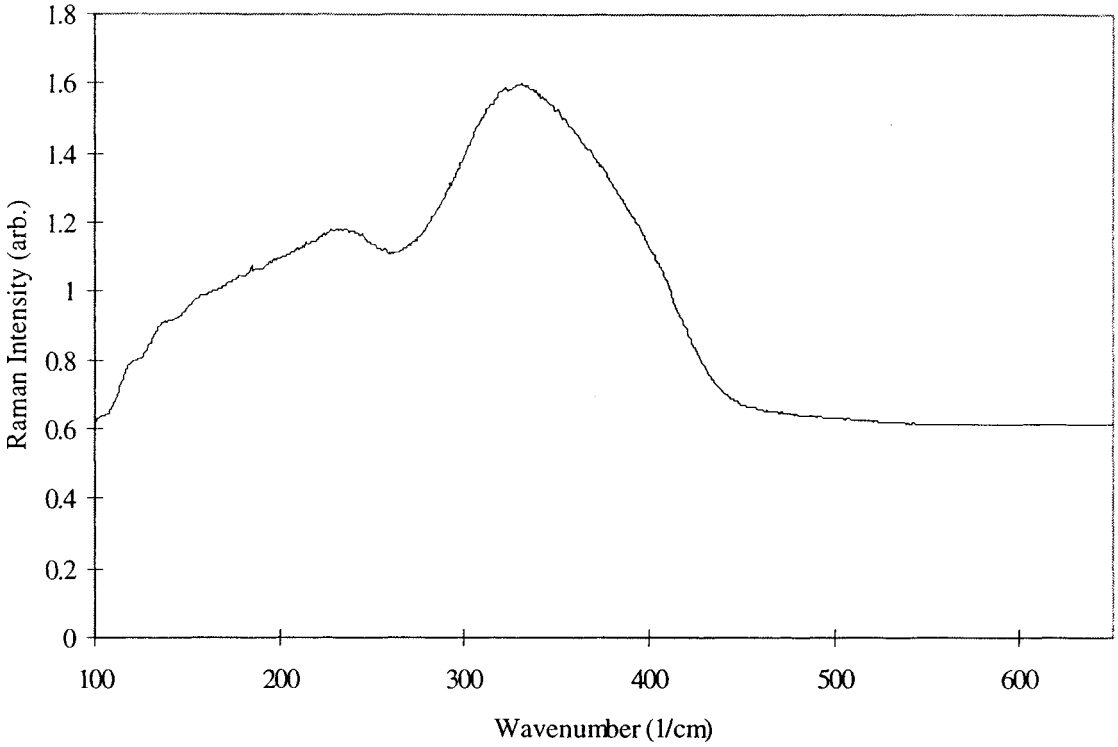


FIGURE 2 Typical Raman spectrum of GLS glass.

REFERENCES

[1] G.F. Imbusch, R. Kopelman [in *Laser Spectroscopy of Solids* Eds. W.M. Yen, P.M. Selzer (Springer, New York, 1981) p.3]

[2] K. Wei, D.P. Machewirth, J. Wenzel, E. Snitzer, G.H. Sigel [*J. Non-Cryst. Solids (Netherlands)* vol.182 (1995) p.257-61]

[3] P.C. Becker, M.M. Broer, V.G. Lambrecht, A.J. Bruce, G. Nykoliak [*Proc. OAA '92* postdeadline paper PD5 (Santa Fe, 1992) p.20]

[4] J. Wang et al [*Appl. Phys. Lett. (USA)* vol.71 no.13 (1997) p.1753]

[5] D.P. Machewirt, K. Wei, V. Krasteva, R. Datta, E. Snitzer, G.H. Sigel [*J. Non-Cryst. Solids (Netherlands)* vol.213 (1997) p.295-303]

[6] J. Kirchhof, J. Kobelke, M. Scheffler, A. Schwuchow [*Electron. Lett. (UK)* vol.32 no.13 (1996) p.1220-1]; Y. Ohishi, A. Mori, T. Kanamori, K. Fujiura, S. Sudo [*Appl. Phys. Lett. (USA)* vol.65 no.1 (1994) p.13]

[7] V.M. Krasteva, G.H. Sigel Jr., S.L. Semjonov, M.M. Bubnov, M.I. Belovolov [*J. Non-Cryst. Solids (Netherlands)* vol.213 (1997) p.304-11]

[8] D. Marchese, G. Kakarantzas, A. Jha [*J. Non-Cryst. Solids (Netherlands)* vol.196 (1996) p.314-9]

[9] E. Ishikawa, H. Tawarayama, K. Itoh, H. Aoki, H. Yanagita, H. Toratani [*Technical Report of IEICE, OPE96-111* (1996) p.7]

[10] See for example [*Laser Spectroscopy of Solids* Eds. W.M. Yen, P.M. Selzer (Springer, New York, 1981)]

[11] B.R. Judd [*Phys. Rev. (USA)* vol.127 (1962) p.750]; G.S. Ofelt [*J. Chem. Phys. (USA)* vol.37 (1962) p.511]

[12] J.A. Medeiros Neto, D.W. Hewak, H.Tate [*J. Non-Cryst. Solids (Netherlands)* vol.183 (1995) p.201-7]

[13] D.W. Hewak et al [*Electron. Lett. (UK)* vol.32 (1996) p.384]
[14] D.W. Hewak et al [*IEEE Photonics Technol. Lett. (USA)* vol.6 no.5 (1994) p.609]
[15] D.R. Simmons, A.J. Faber, H. de Waal [*Opt. Lett. (USA)* vol.20 no.5 (1995) p.468]
[16] W.S. Brocklesby, A. Pearson [*J. Lumin. (Netherlands)* vol.59 (1994) p.333-40]
[17] Although the Raman spectrum and vibrational spectrum of a material are typically not the same thing, in the case of glasses, lowering of the symmetry of the bonds means that almost all vibrational modes are both Raman and IR active. Thus the Raman spectrum illustrates the positions of the highest vibrational levels well.
[18] A. Tverjanovich, Yu. S. Tveryanovich, S. Loheider [*J. Non-Cryst. Solids (Netherlands)* vol.208 (1996) p.49-55]
[19] R.S. Quimby, K.T. Gahagan, B.G. Aitken, M.A. Newhouse [*Opt. Lett. (USA)* vol.20 (1995) p.2021]
[20] J.R. Hector et al [*J. Non-Cryst. Solids (Netherlands)* accepted, 1998]

D3.2 Spectroscopy of neodymium-doped chalcogenide glass

T. Schweizer

November 1997

A INTRODUCTION

The main reason for studying rare-earth doped chalcogenide glasses is their low phonon energy which leads to low non-radiative decay rates of rare-earth energy levels and good infrared transparency. The trivalent neodymium ion (Nd^{3+}) has not been studied widely as a dopant for chalcogenide glasses because the main fluorescent energy level ($^4F_{3/2}$) is separated by a large gap from the next lower lying level and hence does not suffer from competing non-radiative multiphonon decay. Instead the Nd^{3+} ions have been used as convenient test ions to show the influence of the chalcogenide glass host on the rare-earth dopants and to perform initial laser experiments. About a dozen Nd^{3+} doped chalcogenide glasses have been reported in the literature [1-8], most of which are sulphide glasses of which gallium lanthanum sulphide glass (GLS) is the most extensively studied system [9-13] and the only system with reported laser action in bulk and fibre form [14-16]. For these reasons this Datareview will concentrate on the spectroscopy of Nd^{3+} doped GLS glass and give references to other sulphide glass systems.

B ABSORPTION, FLUORESCENCE AND LIFETIME SPECTROSCOPY

FIGURE 1 depicts the ground state absorption spectrum of a 1.5 mol% Nd^{3+} doped GLS glass. The graph is plotted on a reciprocal wavelength scale in order to show the real energy gaps between the levels. The UV edge of the glass appears at 500 nm, and the multiphonon edge starts at 8 μm.

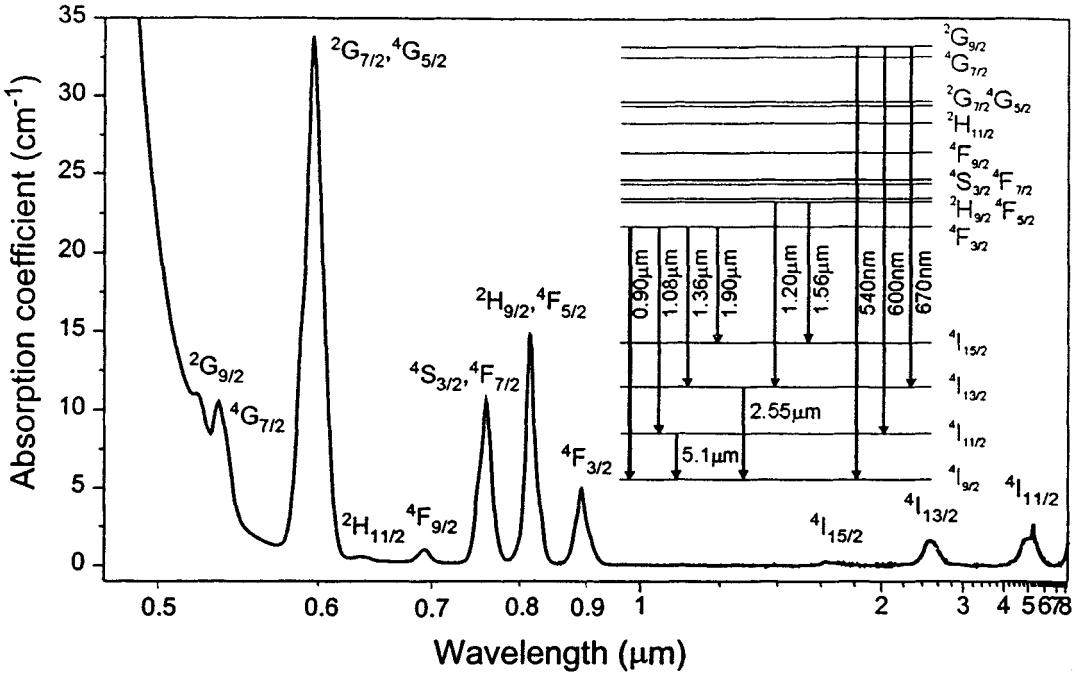


FIGURE 1 Ground state absorption spectrum of $70Ga_2S_3{:}28.5La_2S_3{:}1.5Nd_2S_3$ glass and energy level diagram with fluorescent transitions.

An interesting feature in the absorption spectrum is the strength of the absorption band at 600 nm ($^2G_{7/2}$, $^4G_{5/2}$ levels) compared to the band at 815 nm ($^2H_{9/2}$, $^4F_{5/2}$ levels). In fluorozirconate glasses these two bands are about equal in strength [17,18]. The $^4I_{9/2} \rightarrow {}^4G_{5/2}$ transition is one of the so called hypersensitive pseudoquadrupolar transitions which show strongly increased intensities in host media which are highly polarisable (covalent bonding, high refractive index) and provide an inhomogeneous surrounding for the rare-earth dopants [19,20]. The intensity of these transitions increases with increasing Judd-Ofelt parameter Ω_2 [22,23] which has large values in covalent host materials such as chalcogenide glasses [18]. TABLE 1 contains spectroscopic data for a number of chalcogenide glasses along with a silicate and a fluorozirconate glass.

TABLE 1 Judd-Ofelt parameters of Nd^{3+} doped glasses, peak emission wavelengths and emission cross sections of the $^4F_{3/2} \rightarrow {}^4I_{11/2}$ transition and calculated radiative lifetimes of the $^4F_{3/2}$ level.

Glass	Ω_2 (10^{-20} cm^2)	Ω_4 (10^{-20} cm^2)	Ω_6 (10^{-20} cm^2)	λ_{peak} (nm)	$\sigma_{SE}(\lambda_{peak})$ (10^{-20} cm^2)	τ_{calc} (μs)	Ref
As_2S_3	-	-	-	1090	-	-	[1]
				1080			[2]
Ga:Na:S	8.2	5.3	3.8	1080	8.0	109	[3]
Ga:Ge:As:S	4.42	9.10	6.79	1078	-	90	[4]
$70Ga_2S_3$:$30La_2S_3$	7.70	7.65	4.86	1078	6.96	61	this work
$3Ga_2S_3$:$1La_2S_3$	6.65	4.39	4.67	1077	7.95	73	[10,11]
$3Al_2S_3$:$1La_2S_3$	9.45	4.84	6.54	1077	8.20	102	[10,11]
Ge:As:Ga:Sb:S	-	-	-	1077	-	-	[5]
25Ge:5Ga:70S	10.6	9.29	7.08	-	-	74	[6]
LG-680 silicate	3.4	5.0	5.1	1061	2.9	333	[17]
Fluorozirconate	1.7	3.3	3.9	1049	2.7	497	[17]

The list of the Judd-Ofelt intensity parameters shows an increase in parameter Ω_2 going from ionic fluorozirconate glasses to more covalent silicate glasses and on to even more covalent chalcogenide glasses. The increase in the line strength of the hypersensitive 600 nm absorption band in chalcogenide glasses is therefore attributed to the more covalent bonding compared to the ionic bonding in fluorozirconate glasses.

The $^4F_{3/2}$ level is the level with the largest energy gap between it and the next lower lying level ($^4I_{15/2}$) and the only metastable level in the Nd^{3+} system independent of the host material. The four common emission bands from the $^4F_{3/2}$ level are shown in FIGURE 2 (see also inset in FIGURE 1).

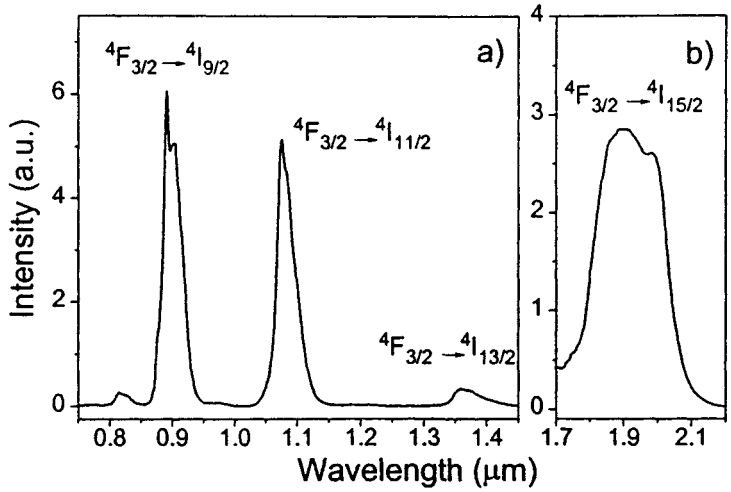


FIGURE 2 Emission bands from the metastable $^4F_{3/2}$ level of (a) 1 mol% Nd_2S_3 doped GLS glass pumped at 875 nm and measured with an ANDO spectrum analyser and (b) 1.5 mol% Nd_2S_3 doped GLS glass pumped at 815 nm with a Ti:sapphire laser and measured with a 300 nm monochromator and a liquid nitrogen cooled InSb detector ((a) and (b) not to scale).

There are two noteworthy points about the fluorescence spectra. Firstly, the peak emission wavelengths are shifted to longer wavelength in chalcogenide glasses compared to silicate and fluorozirconate glasses.

The glasses in TABLE 1 are listed in order of decreasing peak emission wavelength of the $^4F_{3/2} \rightarrow {}^4I_{11/2}$ transition. The shift to longer emission wavelengths in chalcogenide glasses, the so called nephelauxetic effect, has been attributed to the high covalency of the glass bonds [3,18,21]. Secondly, the measured branching ratios of the 900 nm, 1080 nm and 1360 nm bands (50%, 43% and 7%) which correspond well to the calculated branching ratios (49%, 43%, 7% and <1% for the 1.9 μm band) also reflect the covalency of the glass bonds. In more ionic glasses the 1080 nm band has the largest branching ratio with a value of typically >50% [17,18].

The measured lifetime of the $^4F_{3/2}$ level should correspond, within experimental error, to the radiative lifetime obtained from the Judd-Ofelt calculation (TABLE 1) as long as the Nd^{3+} concentration and the excitation power are kept low to avoid ion-ion interactions. FIGURE 3(a) shows the lifetime of the $^4F_{3/2}$ level as a function of the Nd_2S_3 concentration in GLS glass pumped at 890 nm with a Ti:sapphire laser. For low concentrations the measured lifetime is slightly higher than the calculated value (TABLE 1). The lifetime of the $^4F_{3/2}$ level is considerably lower in chalcogenide glasses than in silicate and fluorozirconate glasses, an unfavourable property for laser operation. This is partially counteracted by the larger emission cross sections in chalcogenide glasses (TABLE 1). The στ-product which is inversely proportional to the laser threshold, however, is still smaller in chalcogenide glasses because the spontaneous transition probability (inverse of the lifetime) increases more rapidly with increasing refractive index (high in chalcogenide glasses) than the emission cross section [24].

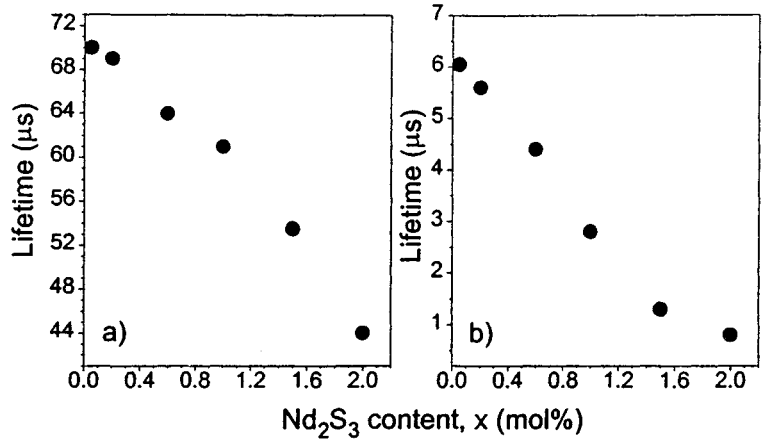


FIGURE 3 Lifetime of $^4F_{3/2}$ (a) and $^2G_{9/2}$, $^4G_{7/2}$ (b) levels versus Nd_2S_3 content, x, in $70Ga_2S_3$:$(30\text{-}x)La_2S_3$:xNd_2S_3 glass under 890 nm (a) and 514 nm (b) excitation.

The situation changes for transitions from levels close to the next lower lying levels. In this case the lifetimes are considerably longer in chalcogenide glasses due to reduced multiphonon decay rates, making chalcogenide glasses the favourable choice as laser materials for this sort of transition.

The lifetime decreases with increasing Nd^{3+} concentration due to the well known cross-relaxation ($^4F_{3/2}$, $^4I_{9/2}$) → ($^4I_{15/2}$, $^4I_{15/2}$). This process was found to be rather pronounced in chalcogenide glasses with their ground state splitting ($^4I_{9/2}$) of around 500 cm^{-1} exceeding the 450 cm^{-1} value which separates the weak from the strong concentration quenching regime [3,25].

At higher excitation powers the probability for the interaction between two excited Nd^{3+} ions increases providing an additional decay channel for the $^4F_{3/2}$ level. One ion decays to the ^4I levels and the other is upconverted to higher energy levels leading to visible upconversion emission from the $^2G_{9/2}$, $^4G_{7/2}$ levels (see inset in FIGURE 1). FIGURE 4 shows the upconversion emission of a 0.05 mol% Nd_2S_3 doped GLS fibre with a 14 μm core and a 230 μm outer diameter pumped at 815 nm by a Ti:sapphire laser. The three emission bands in the green, orange and red show a double peak structure with varying peak ratios which reflect the branching ratios and the relative population of the thermally coupled $^2G_{9/2}$, $^4G_{7/2}$ levels. The yellow upconversion emission is visible for pump powers as low as 1 mW. The lifetime quenching of the $^2G_{9/2}$, $^4G_{7/2}$ levels (FIGURE 3(b)) is significantly stronger than for the $^4F_{3/2}$ level (FIGURE 3(a)), indicating more efficient cross-relaxation processes. For the lifetime measurements the $^2G_{9/2}$, $^4G_{7/2}$ levels were excited directly with the 514 nm line of an Ar^+ ion laser. The decay time of the

$^2G_{9/2}$, $^4G_{7/2}$ levels under 815 nm Ti:sapphire upconversion pumping is 30 μs which is much longer than under direct 514 nm pumping and is about half the value of the $^4F_{3/2}$ level lifetime. This indicates that the upconversion emission is caused by interaction between two excited Nd^{3+} ions in the $^4F_{3/2}$ level and not by excited-state absorption. If the visible upconversion emission were caused by excited-state absorption the lifetime under 815 nm pumping would be similar to the lifetime under 514 nm pumping. The radiative lifetimes of the $^2G_{9/2}$, $^4G_{7/2}$ levels (22 μs and 21 μs) derived from the Judd-Ofelt calculations combine to a radiative lifetime of 11 μs for the thermally coupled levels. This is considerably longer than the measured lifetime for low Nd^{3+} concentration (6 μs) indicating that multiphonon decay is an important decay channel for the $^2G_{9/2}$, $^4G_{7/2}$ levels due to the small energy gap of 1900 cm^{-1} (5.2 μm). The lifetime shortening caused by multiphonon decay would, however, be much more severe in silicate and fluorozirconate glasses with higher phonon energies. The upconversion emission is a loss process for laser transitions starting from the $^4F_{3/2}$ level [14-16].

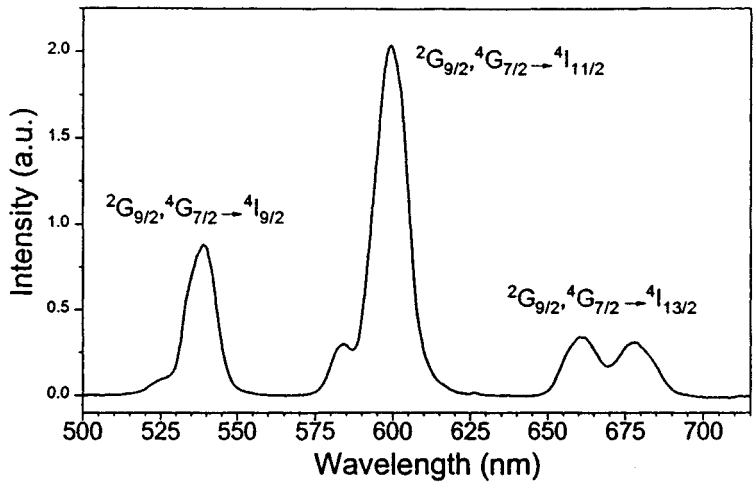


FIGURE 4 Visible upconversion emission of 0.05 mol% Nd_2S_3 doped GLS glass fibre pumped at 815 nm with a Ti:sapphire laser and measured with a liquid nitrogen cooled CCD array spectrometer.

The low phonon energy of chalcogenide glasses also gives rise to new Nd^{3+} emission bands that cannot be observed in other glasses.

FIGURE 5 shows two fluorescence bands from the $^2H_{9/2}$, $^4F_{5/2}$ levels at 1.2 μm and 1.56 μm (see also FIGURE 1) at either side of the 1.36 μm band from the metastable level ($^4F_{3/2}$) under 815 nm Ti:sapphire pumping.

The intensities of the 1.2 μm and 1.56 μm bands are of the same order of magnitude as that of the 1.36 μm band, despite the small energy gap of about 1000 cm^{-1} (10 μm) to the next lower lying level, displaying the low phonon energy of the chalcogenide glass. The radiative transitions from the $^2H_{9/2}$, $^4F_{5/2}$ levels bypass the $^4F_{3/2}$ level (see FIGURE 1) and reduce the pump efficiency for laser transitions starting from the $^4F_{3/2}$ level under 815 nm pumping [14-16].

The low multiphonon decay rates in chalcogenide glasses also lead to measurable fluorescence from the lower Nd^{3+} energy levels in the mid-infrared wavelength region which has not been reported in silicate and fluorozirconate glasses (see FIGURE 1). FIGURE 6 shows the emission bands from the $^4I_{13/2}$ and $^4I_{11/2}$ levels at 2.55 μm (a) and 5.1 μm (b) for 815 nm pumping. The 5.1 μm ($^4I_{11/2} \rightarrow {}^4I_{9/2}$) band that cannot be measured completely due to limitations of the equipment will only have some minor contribution from the $^4I_{13/2} \rightarrow {}^4I_{11/2}$ transition which is expected to overlap with the $^4I_{11/2} \rightarrow {}^4I_{9/2}$ transition.

The $^4I_{13/2} \rightarrow {}^4I_{11/2}$ transition is competing with the stronger $^4I_{13/2} \rightarrow {}^4I_{9/2}$ transition (2.55 μm) and the $^4I_{13/2}$ level is only populated by the 1.36 μm and 1.90 μm transitions whereas the $^4I_{11/2}$ level is populated by the much stronger 1.08 μm transition and has a branching ratio of 100% (see FIGURE 1).

The population of the lower energy levels, which is commonly assumed to be negligible in higher phonon energy laser materials, could lead to gain saturation and reabsorption for laser transitions starting from the $^4F_{3/2}$ level [14-16].

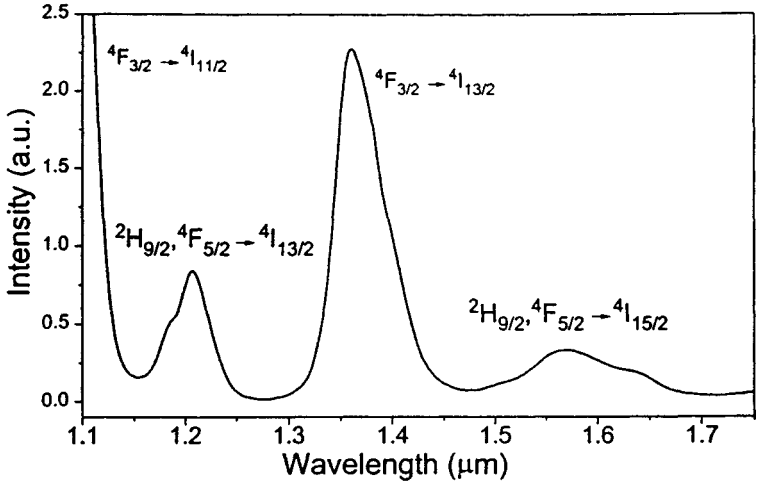


FIGURE 5 Emission from $^2H_{9/2}$, $^4F_{5/2}$ levels in 1.5 mol% Nd_2S_3 doped GLS glass pumped at 815 nm with a Ti:sapphire laser and measured with a 300 mm monochromator and a liquid nitrogen cooled InSb detector.

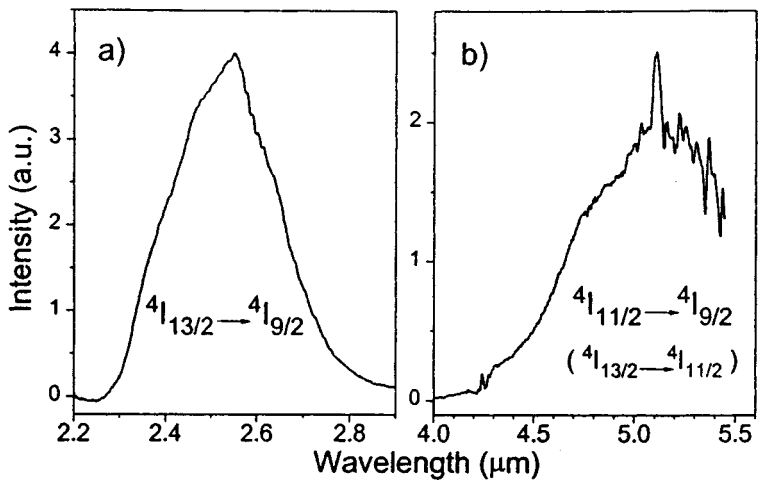


FIGURE 6 Emission from the two lowest Nd^{3+} levels, $^4I_{13/2}$ (a) and $^4I_{11/2}$ (b), in 1.5 mol% Nd_2S_3 doped GLS glass pumped at 815 nm with a Ti:sapphire laser and measured with a 300 mm monochromator and a liquid nitrogen cooled InSb detector.

The mid-infrared emission shows the potential of chalcogenide glasses as promising materials for mid-infrared lasers. The problem of pumping the lower Nd^{3+} levels directly and efficiently could be avoided by using a cascade lasing scheme including the 1.36 μm or 1.08 μm transitions, respectively. Such a pumping scheme has been realised in an Nd^{3+} doped fluoride crystal with simultaneous laser operation at 1.35 μm and 5.15 μm [26].

C CONCLUSION

The spectroscopic differences in the absorption, fluorescence and lifetime measurements of Nd^{3+} doped chalcogenide glasses compared to silicate and fluorozirconate glasses have been outlined using Nd^{3+} doped gallium lanthanum sulphide glass as an example. The measurements reflect the influence of the covalent glass bonds and the low phonon energy on the spectroscopy of the Nd^{3+} ions and show the potential of chalcogenide glasses as materials for new laser transitions, in particular in the mid-infrared wavelength region.

REFERENCES

[1] J. Heo [*J. Mater. Sci. Lett. (UK)* vol.14 (1995) p.1014]

[2] J.-F. Viens et al [in *Conference on Lasers and Electrooptics* vol.11 of 1997 OSA Technical Digest Series (Optical Society of America, Washington DC, 1997) p.249]

[3] B. Viana, M. Palazzi, O. LeFol [*J. Non-Cryst. Solids (Netherlands)* vol.215 (1997) p.96]

[4] A. Belykh et al [*J. Non-Cryst. Solids (Netherlands)* vol.213&214 (1997) p.238]

[5] A. Mori, Y. Ohishi, T. Kanamori, S. Sudo [*Appl. Phys. Lett. (USA)* vol.70 (1997) p.1230]

[6] K. Abe, H. Takebe, K. Morinaga [*J. Non-Cryst. Solids (Netherlands)* vol.212 (1996) p.143]

[7] J.V. Sathyanarayana, K. Annapurna, S. Buddhudu [*J. Alloys Compd. (Switzerland)* vol.224 (1995) p.97]

[8] Y.S. Tver'yanovich, S.V. Degtyarev, S.S. Pivovarov, N.V. Belyakova [*Glass Phys. Chem. (Russia)* vol.23 (1997) p.80]

[9] R. Reisfeld, A. Bornstein [*Chem. Phys. Lett. (Netherlands)* vol.47 (1977) p.194]

[10] R. Reisfeld [*Ann. Chim., Sci. Mater. (France)* vol.7 (1982) p.147]

[11] A. Bornstein, R. Reisfeld [*J. Non-Cryst. Solids (Netherlands)* vol.50 (1982) p.23]

[12] J. Flahaut, M. Guittard, A.M. Loireau-Lozac'h [*Glass Technol. (UK)* vol.24 (1983) p.149]

[13] L. Mattoa Jr., A.G. Clare [*Phys. Chem. Glasses (UK)* vol.34 (1993) p.244]

[14] T. Schweizer, D.W. Hewak, D.N. Payne, T. Jensen, G. Huber [*Electron. Lett. (UK)* vol.32 (1996) p.666]

[15] T. Schweizer, B.N. Samson, R.C. Moore, D.W. Hewak, D.N. Payne [*Electron. Lett. (UK)* vol.33 (1997) p.414]

[16] T. Schweizer [Datareview in this book: *D5.2 Fibre lasers based on rare-earth doped chalcogenide glass*]

[17] S.E. Stokowski, R.A. Saroyan, M.J. Weber [*Laser Glass, Nd-Doped Laser Glass, Spectroscopic and Physical Properties* vol.1&2 (Lawrence Livermore National Laboratory, University of California, Livermore, California, 1981)]

[18] M.J.F. Digonnet (Ed.) [*Rare Earth Doped Fibre Lasers and Amplifiers* (Marcel Dekker Inc., 1993) p.50-72]

[19] C.K. Jørgensen, B.R. Judd [*Mol. Phys. (UK)* vol.8 (1964) p.281]

[20] C.K. Jørgensen, R. Reisfeld [*J. Less-Common Met. (Switzerland)* vol.93 (1983) p.107]

[21] C.K. Jørgensen [*Orbitals in Atoms and Molecules* (Academic Press, New York, 1962)]

[22] B.R. Judd [*Phys. Rev. (USA)* vol.127 (1962) p.750]

[23] G.S. Ofelt [*J. Chem. Phys. (USA)* vol.37 (1962) p.511]

[24] M.J. Weber, J.D. Myers, D.H. Blackburn [*J. Appl. Phys. (USA)* vol.52 (1981) p.2944]

[25] F. Auzel [*Mater. Res. Bull. (USA)* vol.14 (1979) p.223]

[26] A.A. Kaminskii [*Inorg. Mater. (USA)* vol.20 (1984) p.782]

D3.3 Spectroscopy of thulium/holmium-doped chalcogenide glass

J. Heo

July 1997

A INTRODUCTION

Laser actions in the 2.0 μm wavelength region from Ho^{3+}-doped glasses and crystals provide potential for applications in medicine, eye-safe laser radar and chemical sensing. However, efficiencies of the laser actions were low mainly due to lack of suitable absorption bands for the semiconductor laser pumping. Therefore, co-doping of Tm^{3+} as a sensitiser has been used as a viable alternative [1-4] since it has a strong absorption band at 800 nm wavelength. Work on the co-doping of Tm^{3+}/Ho^{3+} into chalcogenide glasses is scarce, while there have been many studies with fluoride glass hosts. Low solubility of rare-earth ions in chalcogenide glasses (<0.3 wt.% in most cases [5]) hampered the systematic investigation of the co-doping before the rediscovery of Ge-Ga-S glasses with solubility in excess of 1.5 wt.% [6,7]. This Datareview presents the absorption and emission properties of Tm^{3+}/Ho^{3+} doped into $Ge_{25}Ga_5S_{70}$ (at.%) glass together with the analysis of the energy transfer [8] between Tm^{3+} and Ho^{3+}.

B ABSORPTION OF THULIUM/HOLMIUM-DOPED CHALCOGENIDE GLASS

The absorption spectrum of chalcogenide glass doped with Tm^{3+}/Ho^{3+} is presented in FIGURE 1. Locations of the energy bands were similar to those recorded from other hosts except for some minor differences originating from the different ligand field. Therefore, each absorption band was assigned with term symbols following Carnall et al [9,10]. Energy levels higher than the $^1G_4$ level of Tm^{3+} were not clearly identified because of the strong intrinsic bandgap absorption in the host glass. The absorption spectrum of Tm^{3+}/Ho^{3+} co-doped glass confirmed that the absorbance of the Tm^{3+}:$^3H_4$ level near 798 nm is high while that of the Ho^{3+}:$^5I_6$ level near 900 nm is low.

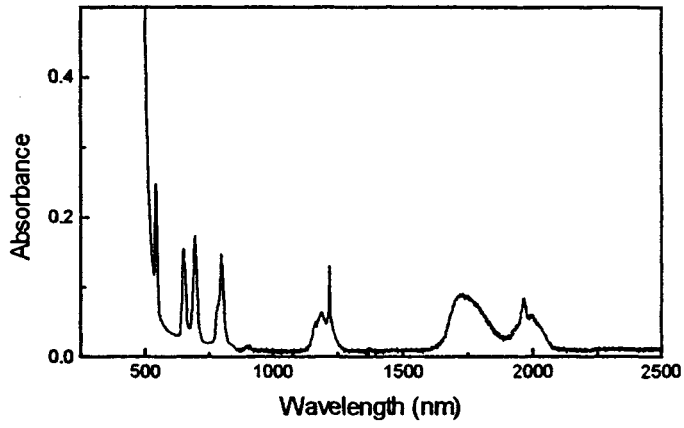


FIGURE 1 Absorption spectrum of Tm^{3+}/Ho^{3+} co-doped $Ge_{25}Ga_5S_{70}$ glass.

C FLUORESCENCE OF THULIUM/HOLMIUM-DOPED CHALCOGENIDE GLASS

Intensities of emissions at 1.80 μm (Tm^{3+}:$^3F_4 \rightarrow {}^3H_6$) and 2.02 μm ($Ho^{3+}$:$^5I_7 \rightarrow {}^5I_8$) from $Ge_{25}Ga_5S_{70}$ glasses increased with increasing Tm^{3+} concentration while Ho^{3+} was fixed at 0.7 wt.% as shown in FIGURE 2. A rapid increase in 2.02 μm emission intensities with the addition of Tm^{3+} provides strong evidence for an efficient energy transfer from Tm^{3+} to Ho^{3+} in chalcogenide glasses. This phenomenon became more evident when the concentration of Tm^{3+} reached 1.0 wt.%, probably because of the enhanced cross-relaxation of $^3H_4$, $^3H_6 \rightarrow {}^3F_4$, $^3F_4$. When the Ho^{3+} concentration increased with a fixed

Tm^{3+} content of 1.0 wt.%, intensities of 1.80 μm fluorescence from Tm^{3+} decreased sharply with a rapid increase in 2.02 μm emission (FIGURE 3).

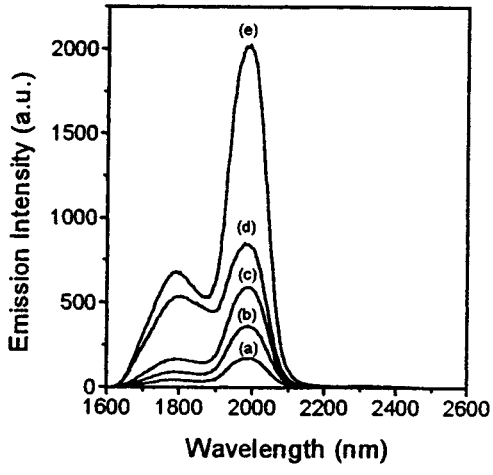


FIGURE 2 Emission intensities of $Ge_{25}Ga_5S_{70}$ glass with Tm^{3+} concentrations of (a) 0.1, (b) 0.3, (c) 0.5, (d) 0.7 and (e) 1.0 wt.% with Ho^{3+} concentration being fixed at 0.7 wt.%. Pump wavelength was 798 nm (Tm^{3+}:$^3H_6 \rightarrow {}^3H_4$).

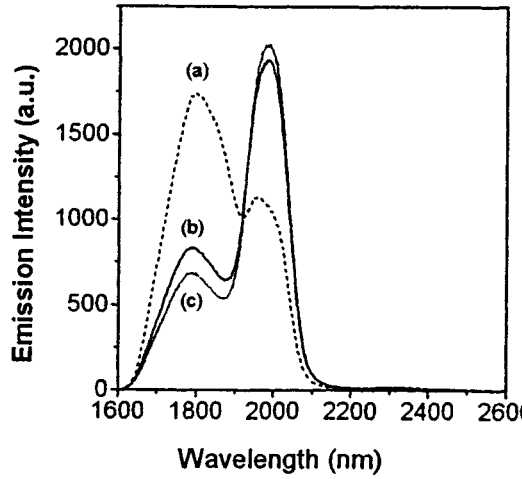


FIGURE 3 Emission of infrared fluorescence as Ho^{3+} concentration increased: (a) 0.1, (b) 0.5 and (c) 0.7 wt.%. Pump wavelength was 798 nm (Tm^{3+}:$^3H_6 \rightarrow {}^3H_4$).

D RADIATIVE LIFETIMES OF THULIUM/HOLMIUM-DOPED CHALCOGENIDE GLASS

Lifetimes of the Ho^{3+}:$^5I_7$ level decreased with the increase in Tm^{3+} and Ho^{3+} concentration (TABLE 1). For instance, when the Ho^{3+} concentration was fixed at 0.1 wt.%, the lifetime of the $^5I_7$ level was approximately 4.81 ms with 0.1 wt.% of Tm^{3+} and decreased to 3.15 ms with increasing Tm^{3+} content to 1.0 wt.%. When the Ho^{3+} concentration was fixed at 0.7 wt.%, values ranged between 3.40 ms and 2.64 ms. Direct comparisons between the various hosts were not possible due to the vastly different levels of co-doping concentration, but lifetimes measured in this study were generally comparable with those for fluoride glasses reported previously [4,11].

TABLE 1 Measured lifetimes (ms) of the Ho^{3+}:$^5I_7$ level in $Ge_{25}Ga_5S_{70}$ glasses.

Ho^{3+} (wt.%)	Tm^{3+} (wt.%)				
	0.1	0.3	0.5	0.7	1.0
0.1	4.81 (± 1.2)	4.15 (± 0.5)	4.17 (± 0.4)	3.60 (± 0.4)	3.15 (± 0.3)
0.7	3.40 (± 1.2)	3.36 (± 1.0)	3.30 (± 0.8)	2.27 (± 0.5)	2.64 (± 0.5)

E NON-RADIATIVE PROPERTIES OF THULIUM/HOLMIUM-DOPED CHALCOGENIDE GLASS

Energy transfer between Tm^{3+} and Ho^{3+} can be expressed using the rate equations based on the analysis of Yeh et al [12] modified for the present Tm^{3+}/Ho^{3+} case. Details and assumptions for the analysis can be found elsewhere [8]. FIGURE 4 illustrates that the transfer rates for both directions increased with addition of Ho^{3+} while the Tm^{3+} content was fixed at 1.0 wt.%. Specifically, the forward ($Tm^{3+} \rightarrow Ho^{3+}$) rate grew much faster than the backward transfer which agrees well with the results obtained from

indium-based fluoride glasses using a similar approach [4]. In addition, transfer rates increased monotonically even when the acceptor concentration reached values close to the donor concentration. In fact, it was verified that 2.02 μm emission intensities from Ho^{3+} increased with Ho^{3+} addition up to 0.7 wt.% with Tm^{3+} fixed at 1.0 wt.% (FIGURE 2).

Radiation from the excited states of rare-earth ions is dissipated through a variety of non-radiative processes. One of the most important processes is the conversion of the photons to thermal energy by multiphonon relaxation via the local vibrations with neighbouring atoms. It is clear that the multiphonon relaxation in chalcogenide glass is several orders of magnitude less than that for other hosts, especially for transitions between two closely-spaced energy levels.

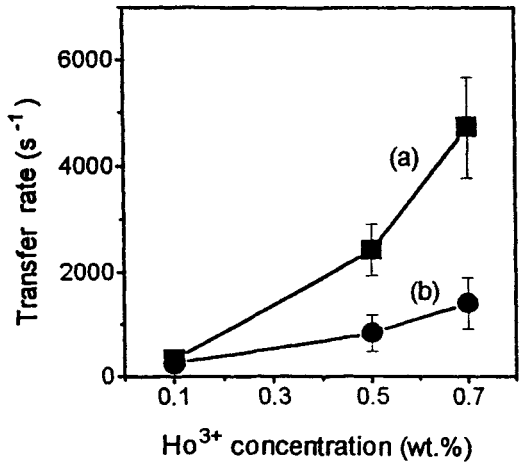


FIGURE 4 Dependence of energy transfer rates between (a) $Tm^{3+} \rightarrow Ho^{3+}$ and (b) $Ho^{3+} \rightarrow Tm^{3+}$ with increasing Ho^{3+} (acceptor) concentrations. Lines are drawn as guides to the eye.

F CONCLUSION

Chalcogenide glasses are potential host materials for rare-earth ions because of their reduced phonon energy which in turn results in low multiphonon relaxation. This characteristic feature becomes important especially when emissions at the mid-infrared wavelength are desired. In this respect, co-doping of Tm^{3+} and Ho^{3+} into chalcogenide glasses for 2.0 μm fluorescence is an adequate approach to take.

REFERENCES

[1] R.M. Percival, D. Szebesta, S.T. Davey, N.A. Swain, T.A. King [*Electron. Lett. (UK)* vol.28 (1992) p.2064-6]

[2] R.M. Percival, D. Szebesta, S.T. Davey, N.A. Swain, T.A. King [*Electron. Lett. (UK)* vol.28 (1992) p.2231-2]

[3] J.Y. Allain, M. Monerie, H. Poignant [*Electron. Lett. (UK)* vol.27 (1991) p.1513-5]

[4] A. Brenier, C. Pedrini, B. Moine, J.L. Adam, C. Pledel [*Phys. Rev. B (USA)* vol.41 (1990) p.5364-71]

[5] Y.B. Shin, J.N. Jang, J. Heo [*Opt. Quantum Electron. (UK)* vol.27 (1995) p.379-86]

[6] K. Wei, D.P. Machewirth, J. Wenzel, E. Snitzer, G.H. Sigel Jr. [*Opt. Lett. (USA)* vol.19 (1994) p.904-6]

[7] K. Wei, D.P. Machewirth, J. Wenzel, E. Snitzer, G.H. Sigel Jr. [*J. Non-Cryst. Solids (Netherlands)* vol.182 (1995) p.257-61]

[8] Y.S. Kim, W.Y. Cho, Y.B. Shin, J. Heo [*J. Non-Cryst. Solids (Netherlands)* vol.203 (1996) p.176-81]

[9] W.T. Carnall, P.R. Fields, B.G. Wybourne [*J. Chem. Phys. (USA)* vol.42 (1965) p.3797-806]

[10] W.T. Carnall, P.R. Fields, K. Rajnak [*J. Chem. Phys. (USA)* vol.49 (1968) p.4412-23]

[11] G. Huber, P. Mitzscherlich, T.Y. Fan, R.L. Byer [*J. Lumin. (Netherlands)* vol.40&41 (1988) p.509-10]

[12] D.C. Yeh, R.R. Petrin, W.A. Sibley, V. Madigou, J.L. Adam, M.J. Suscavage [*Phys. Rev. B (USA)* vol.39 (1989) p.80-90]

[13] R. Reisfeld [*Ann. Chim. (France)* vol.7 (1982) p.147-60]
[14] D.C. Yeh, W.A. Sibley, M. Suscavage, M.G. Drexhage [*J. Appl. Phys. (USA)* vol.63 (1987) p.266-75]

D3.4 Spectroscopy of dysprosium-doped chalcogenide glass

B.N. Samson and T. Schweizer

September 1998

A INTRODUCTION

The dysprosium ion (Dy^{3+}) has been studied to a much smaller extent than the more common rare-earth ions such as neodymium, erbium and thulium. In particular Dy^{3+} doped glasses have hardly been investigated at all. This apparent lack of interest is caused by the nature of the energy level structure which is shown in FIGURE 1.

The energy levels up to an energy of about 13300 cm^{-1} (0.75 μm, $^6F_{1/2}$) are separated by energy gaps smaller than 3300 cm^{-1}, i.e. fluorescence from these energy levels is quenched in conventional oxide glasses and oxide crystals. Emission is usually observed in the visible wavelength range from the $^4F_{9/2}$ level which is the lower level of a second set of closely spaced energy levels at energies of 20800 cm^{-1} (0.48 μm) and higher (not shown in FIGURE 1) [1]. These energy levels are not measurable in most chalcogenide glasses due to the UV absorption edge in the visible wavelength region [2]. However, in chalcogenide glasses emission is observed from the lower set of energy levels offering the potential for new devices which cannot be realised in conventional oxide and fluoride glasses.

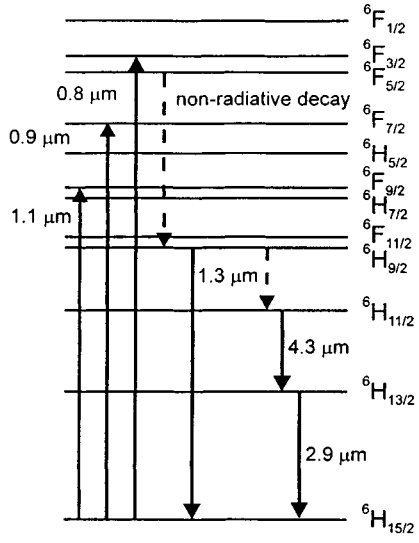


FIGURE 1 Energy level diagram of Dy^{3+} along with pump and fluorescent transitions.

There are two applications for Dy^{3+} doped chalcogenide glasses that have recently been covered in the literature, both of which make use of the low phonon energy inherent in this family of glasses. The first makes use of the ground state transition that occurs at a wavelength around 1.3 μm, a technologically important wavelength corresponding to the second low loss window in silica fibre and the zero dispersion wavelength of the currently installed fibre base. There has been considerable interest in the possibility of making an optical fibre amplifier operating at this wavelength to complement the erbium doped fibre amplifier (EDFA) which operates within the third telecom window around 1.5 μm. The second application is in the area of mid-infrared fibre lasers, in particular devices operating at wavelengths suitable for remote sensing or gas sensing applications.

This Datareview presents the spectroscopy of Dy^{3+} doped gallium lanthanum sulphide glass (GLS) as a representative example of Dy^{3+} doped chalcogenide glasses and gives references to other glass systems.

B ABSORPTION, FLUORESCENCE AND LIFETIME SPECTROSCOPY

B1 Absorption

The energy level diagram and a typical absorption spectrum for a Dy^{3+} doped chalcogenide glass are shown in FIGURES 1 and 2. The UV absorption edge of the GLS glass appears at 0.5 μm, and the multiphonon edge starts at 8 μm (not shown in FIGURE 2). Excitation of the Dy^{3+} ions into the

absorption bands at 0.8, 0.9, 1.1 and 1.3 μm populates the fluorescent ($^6F_{11/2}$, $^6H_{9/2}$), $^6H_{11/2}$ and $^6H_{13/2}$ levels.

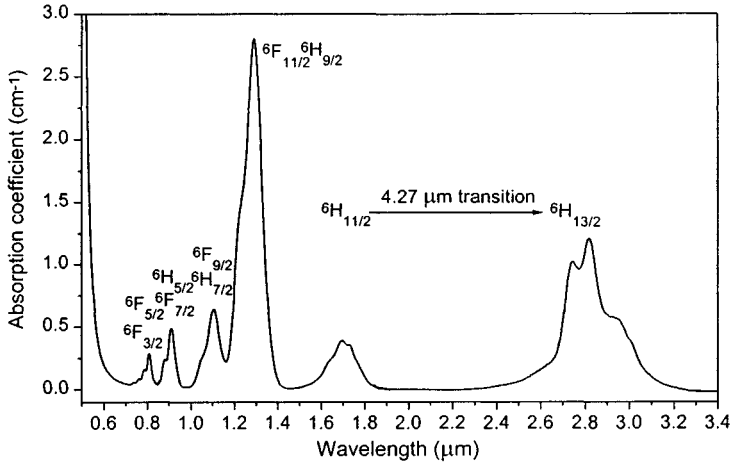


FIGURE 2 Room temperature absorption spectrum of 9900 ppm Dy^{3+} doped GLS glass [16].

B2 1.3 μm Fluorescence from the ($^6F_{11/2}$, $^6H_{9/2}$) Energy Level

The $^6F_{11/2}$ and $^6H_{9/2}$ energy levels are not resolved in the glass absorption spectrum (FIGURE 2) and are normally treated as one energy level for most analysis. The first reported measurements of fluorescence at 1.3 μm in a Dy^{3+} doped chalcogenide glass were simultaneously reported in doped gallium lanthanum sulphide [3] and doped germanium gallium sulphide glasses [5] (see FIGURE 3).

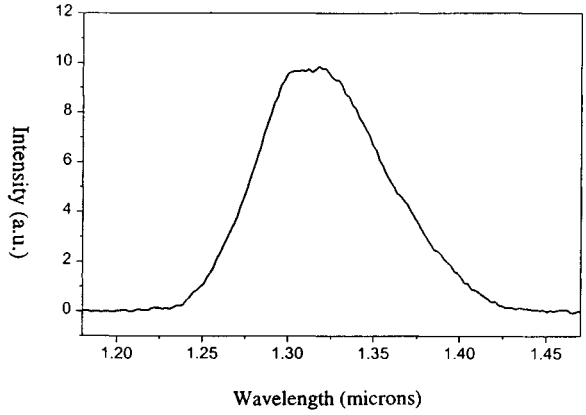


FIGURE 3 Room temperature 1.3 μm fluorescence spectrum of Dy^{3+} doped GLS glass pumped at 0.907 μm [3].

Other reported Dy^{3+} doped chalcogenide glasses include arsenic trisulphide [5], indium modified arsenic trisulphide [6], germanium arsenic sulphide [6,7], germanium indium sulphide [6], barium indium gallium germanium selenide [8], germanium arsenic selenide [9] and modified germanium arsenic selenide [10]. Despite the short measured fluorescence lifetime for the ($^6F_{11/2}$, $^6H_{9/2}$) energy level, typically in the region of 20 - 60 μs for sulphide glasses [6], an estimate of the quantum efficiency based on a Judd-Ofelt analysis of the radiative rates suggests that efficient amplification could be achieved at 1.3 μm in these glasses. Alternative methods of estimating the quantum efficiency have since been published based on a three level McCumber analysis (~19%) [11] and a value derived from the temperature dependence of the 1.3 μm fluorescence lifetime (~13%) [12]. Obviously the quantum efficiency varies with glass composition and is strongly dependent on the glass phonon energy since the energy gap for this transition is only ~1700 cm^{-1} and is strongly quenched in glasses with a high non-radiative decay rate. However, the radiative rate for the ($^6F_{11/2}$, $^6H_{9/2}$) → $^6H_{15/2}$ transition is also strongly dependent on the glass composition, particularly since the $^6F_{11/2}$ → $^6H_{15/2}$ transition is a hypersensitive transition with a large value for the $\langle U^{(2)} \rangle^2$ reduced matrix element [1]. The transition linestrength then becomes hypersensitive to the Judd-Ofelt parameter Ω_2, a parameter commonly used as an indicator of the type of bonding within the glass. Large values for Ω_2 and hence high radiative rates are found in covalent glasses. This explains the high radiative rates, more than a

factor of ten larger than in Dy^{3+} doped fluoride glasses, for the $^6F_{11/2} \rightarrow {}^6H_{15/2}$ transition in chalcogenide glasses [1]. This coupled with low non-radiative decay rates gives rise to the high quantum efficiencies for the 1.3 μm transition in Dy^{3+} doped chalcogenide glasses. Indeed a radiative quantum efficiency of 90% for the ($^6F_{11/2}$, $^6H_{9/2}$) level has recently been reported in modified GeAsSe glasses which have lower phonon energies than sulphide glasses due to the replacement of the sulphur ions with the heavier selenium ions [10].

There are a number of advantages in the use of a Dy^{3+} doped chalcogenide glass over a praseodymium (Pr^{3+}) doped chalcogenide glass [13,14] for application as a 1.3 μm fibre amplifier. An optimised Dy^{3+} doped device is expected to require a considerably shorter fibre length than that found in Pr^{3+} doped amplifiers, thus significantly relaxing the tolerance on fibre background loss [10,15]. Furthermore, the longer pump wavelength (~1.26 μm compared with 1.02 μm) required for a Dy^{3+} doped device will reduce any deleterious effects from pumping close to the glass absorption edge.

B3 Mid-Infrared Fluorescence from the $^6H_{11/2}$ and $^6H_{13/2}$ Energy Levels

Efficient fluorescence at mid-infrared wavelengths in rare-earth doped chalcogenide glasses is again a direct result of the low non-radiative decay rates, coupled with the high radiative rates found in many of these glasses. Using this long wavelength emission to achieve efficient lasing at mid-infrared wavelengths becomes possible because of the extended infrared transmission [2] resulting from the low phonon energies of the chalcogenide glasses. This becomes especially important in the case of fibre lasers where the fibre length may be metres, placing a tight tolerance on the glass and fibre losses. Indeed many chalcogenide glasses are better suited for applications as mid-infrared lasers where the fibre loss is lower than that found in the near infrared [2].

In the case of Dy^{3+} doped chalcogenide glasses fluorescence at 2.9 μm ($^6H_{13/2} \rightarrow {}^6H_{15/2}$ transition) and at 4.3 μm ($^6H_{11/2} \rightarrow {}^6H_{13/2}$) was first reported by Heo [5] in doped As_2S_3 glass, this latter transition corresponding with a fundamental absorption in carbon dioxide making a fibre laser operating at this wavelength a potential source for gas sensing applications (see FIGURE 4). The branching ratio for the ($^6H_{11/2} \rightarrow {}^6H_{13/2}$) transition is estimated to be ~14%, which is easily enough to achieve lasing in a fibre form with a low threshold power suitable for diode laser pumping [16].

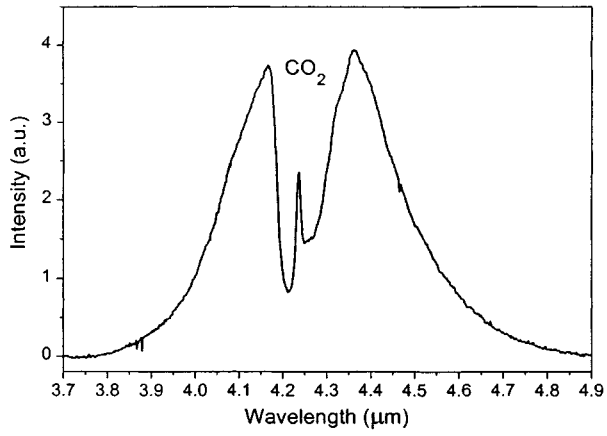


FIGURE 4 Room temperature 4.3 μm Dy^{3+} fluorescence spectrum of Dy^{3+}/Er^{3+} co-doped GLS glass pumped at 0.985 μm with CO_2 absorption.

B4 Lifetimes

The effects of Dy^{3+} concentration on the lifetimes of the $^6H_{13/2}$, $^6H_{11/2}$ and ($^6F_{11/2}$, $^6H_{9/2}$) energy levels in doped chalcogenide glass have been studied in [12]. In GLS glass the lifetimes of the above levels are about 3600 μs, 1300 μs and 55 μs, respectively. The lifetime of the ($^6F_{11/2}$, $^6H_{9/2}$) level can be increased

from 55 μs to 300 μs by changing the host from a sulphide glass to a lower phonon energy selenide glass [8]. The onset of concentration quenching in Dy^{3+} doped GLS glass appears to occur at fairly low levels of rare-earth concentration (~1000 ppm) for all of these levels. The effects of other rare-earth co-dopants such as terbium (Tb^{3+}) [12], thulium (Tm^{3+}) [17] and erbium (Er^{3+}) (FIGURE 4) on these energy levels have also been studied in chalcogenide glasses.

B5 Excitation

Finally, the excitation of dysprosium ions by means of pumping the chalcogenide glass and utilising an energy transfer mechanism between the glass and rare-earth is discussed in [9]. Such a process opens up the possibility of broadband pumping of the Dy^{3+} doped chalcogenide devices discussed above.

C CONCLUSION

This review has introduced the basic spectroscopic data and possible applications of Dy^{3+} doped chalcogenide glasses. Spectroscopic data have been given mainly for Dy^{3+} doped GLS glasses but can easily be extended to other sulphide glasses which are included in the references. Dy^{3+} doped chalcogenide glass fibres could find application as optical amplifiers at 1.3 μm and fibre laser sources for CO_2 gas sensing.

REFERENCES

[1] S. Tanabe, T. Handa, M. Watanabe, T. Hayashi, N. Soga [*J. Am. Ceram. Soc. (USA)* vol.78 (1995) p.2917]

[2] D.J. Brady [Datareview in this book: *D1.1 Transmission of chalcogenide glass*]

[3] D.W. Hewak, B.N. Samson, J.A. Medeiros Neto, R.I. Laming, D.N. Payne [*Electron. Lett. (UK)* vol.30 (1994) p.968]

[4] K. Wei, D.P. Machewirth, J. Wenzel, E. Snitzer, G.H. Segel [*Opt. Lett. (USA)* vol.19 (1994) p.904]

[5] J. Heo [*J. Mater. Sci. Lett. (UK)* vol.14 (1995) p.1014]

[6] D.P. Machewirth, K. Wei, V. Krasteva, R. Datta, E. Snitzer, G.H. Sigel Jr. [*J. Non-Cryst. Solids (Netherlands)* vol.213&214 (1997) p.295]

[7] J. Heo, Y.B. Shin [*J. Non-Cryst. Solids (Netherlands)* vol.196 (1996) p.162]

[8] L.B. Shaw, D.T. Schaafsma, J. Moon, B. Harbison, J.S. Sanghera, I.D. Aggarwal [in *Conference on Lasers and Electrooptics* vol.11 of 1997 OSA Technical Digest Series (Optical Society of America, Washington DC, 1997) p.255]

[9] D.A. Turnbull, S.Q. Gu, S.G. Bishop [*J. Appl. Phys. (USA)* vol.80 (1996) p.2436]

[10] L.B. Shaw, B.J. Cole, J.S. Sanghera, I.D. Aggarwal, D.T. Schaafsma [in *Optical Fiber Communication Conference 1998* vol.2 of 1998 OSA Technical Digest Series (Optical Society of America, Washington DC, 1998) p.141]

[11] B.N. Samson, J.A. Medeiros Neto, R.I. Laming, D.W. Hewak [*Electron. Lett. (UK)* vol.30 (1994) p.1617]

[12] B.N. Samson, T. Schweizer, D.W. Hewak, R.I. Laming [*J. Lumin. (Netherlands)* to be published 1998]

[13] W.S. Brocklesby [Datareview in this book: *D3.1 Spectroscopy of praseodymium-doped chalcogenide glass*]

[14] H. Tawarayama [Datareview in this book: *D5.1 Fibre amplifiers based on rare-earth doped chalcogenide glass*]

[15] B.N. Samson, T. Schweizer, D.W. Hewak, R.I. Laming [*Opt. Lett. (USA)* vol.22 (1997) p.703]

[16] T. Schweizer, D.W. Hewak, B.N. Samson, D.N. Payne [*Opt. Lett. (USA)* vol.21 (1996) p.1594]

[17] J. Heo [*J. Non-Cryst. Solids (Netherlands)* vol.212 (1997) p.151]

PART D: CHALCOGENIDE GLASS

CHAPTER D4

OPTICAL FIBRE MANUFACTURE

D4.1 Preparation and melting of chalcogenide glass
D4.2 Purification of chalcogenide glass
D4.3 Drawing of chalcogenide glass optical fibres
D4.4 Loss of chalcogenide glass optical fibres

D4.1 Preparation and melting of chalcogenide glass

A.J. Faber

September 1997

A INTRODUCTION

The group of chalcogenide glasses includes glassy materials containing one or more of the chalcogen elements S, Se and Te but no O [1]. Chalcohalide glasses are based on the chalcogen elements with additions of a halogen.

The best sulphide glass forming systems are based on the glass formers As_2S_3, GeS_2 and the Ga_2S_3-La_2S_3-system.

Vapour phase techniques have been used to prepare chalcogenide glass films [2], but melting is the common technique used to prepare chalcogenide bulk glasses.

B RAW MATERIALS

Chalcogenide glasses can be prepared both from elemental precursors like S, Te, Se, Ge, As, Ga, etc. and from compound precursors like sulphides and selenides.

For obtaining highly transparent glasses without impurity absorptions, very pure (5N - 10N) raw materials are used. The most important impurities include metal contaminants and hydrogen, oxygen and carbon components [2,3]. Dissolved in the glass, even in low concentrations in the ppm range, these impurities give rise to unwanted infrared optical absorptions and can act as nuclei for heterogeneous crystallisation. Therefore, semiconductor grade elemental raw materials (Ge, Ga, As) with a minimised surface area (e.g. ingots), in view of surface oxide contaminants, are used [4].

As an example, FIGURE 1 shows the infrared transmittance spectra of GeS_2-glasses produced from different Ge and S starting materials, taken from [5].

The chalcogen elements like S and Se can be purified by a distillation process in vacuum, under an inert or under a reactive atmosphere, like S_2Cl_2, $SeCl_2$ or H_2S [2,6,7]. Furthermore, for oxygen removal, gettering agents like aluminium or magnesium, e.g. in the form of metal strips, have been employed [4,8,9].

Thermal pre-treatment of raw materials like Ge and Sb is not adequate to reduce the surface oxide contaminants, since the oxide vapour pressures are lower than the elemental vapour pressures. To reduce surface oxides, these elements are sometimes pre-treated chemically by acid etching, e.g. with nitric or sulphuric acid, although the effect of these pre-treatments is often dubious (see FIGURE 1).

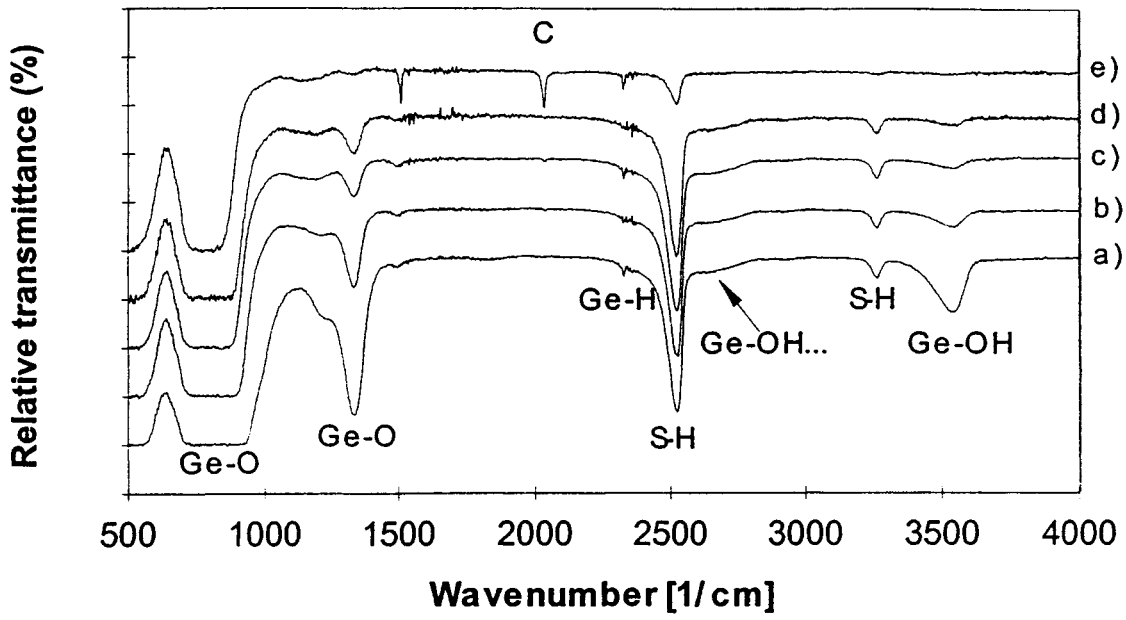


FIGURE 1 IR transmittance spectra of various GeS_2 glasses. The sample thickness is 2 mm. The starting materials for (a) to (e) are: (a) Ge pieces treated with HNO_3 and S powder; (b) Ge pieces and S powder; (c) Ge broken ingots and S powder; (d) Ge broken ingots treated with HNO_3 and S powder; (e) Ge broken ingots treated with HNO_3 and S pieces.

C MELTING

Once the raw materials have been pre-treated, they are weighed and charged into the melting container in an inert atmosphere, usually inside a glove box with an Ar atmosphere at levels of <1 ppm water vapour and oxygen.

Vitreous silica ampoules, vitreous carbon and boron nitride are employed as crucible materials [1,2,11]. In most cases, vitreous silica is an adequate crucible material, but the silica surface can be attacked by some batch components, like La_2S_3 and Si, resulting in contamination of the melt and possibly in sticking of the glass after cooling. To minimise OH-contamination from silica ampoules during the melting process, silica with a low ppm OH level should be used. Prior to batching and melting, the silica ampoules may be etched with hydrofluoric or nitric acid and heat-treated in vacuum, e.g. at 1000°C for eight hours, in order to remove adsorbed water and organic contaminants.

Since many of the raw materials and most of the resulting chalcogenide glass melts have high vapour pressures at the melting temperatures and oxidation or hydrolysis of the melt must be prevented, melting is carried out in sealed systems. Thus, after batching, the silica ampoule is sealed off by an oxy fuel burner, while being evacuated to a vacuum of less than 10^{-4} mbar (0.01 Pa).

For melting, the sealed ampoule is transferred to an electric furnace and heated gradually to the melting temperature in order to prevent explosions due to high vapour pressures of the batch components. Typical melting temperatures of chalcogenide glasses lie in the range 700 - 1000°C, depending on the specific composition. To ensure homogenisation of viscous melts, the melt is agitated by horizontally rotating and/or rocking the silica ampoule (see e.g. [4]). Melting temperatures are maintained for several hours, typically between eight and twenty hours. It is not expected that much longer melting times will

improve glass quality [2,10]. On the contrary, the contamination of the melt by the ampoule wall will increase for longer melting times.

In some studies (e.g. [2,11]) an additional process step for reducing any residual contamination by distillation of the glass during melting is reported. This can be done by using an ampoule with two chambers in a two zone furnace. The temperature in one zone of the furnace is raised while keeping the temperature of the other zone a few hundred °C cooler, so that the melt distils from one chamber to the other. However, during distillation purification of these glasses, dissociative evaporation of the chalcogenides can occur, resulting in deviating compositions of the distilled glass compared to the initial glass [2].

D COOLING

The cooling process must be well controlled to obtain crystal-free and crack-free glasses. In [12] the critical (minimum) cooling rate of GeS_2-based glasses is computed to be higher than 3°C/min, assuming homogeneous nucleation and simultaneous 3D-crystal growth of the nuclei. Mostly the cooling rate in the melting furnace is not high enough for obtaining crystal-free chalcogenide glasses. In these cases the sealed ampoule containing the melt is quenched in ambient air, in water or in other liquids. After quenching, the glass in the ampoule is annealed at a temperature around the glass transformation temperature, typically for one hour, and then slowly cooled down to room temperature (maximum rate of about 1°C/min).

REFERENCES

[1] A.B. Seddon [*J. Non-Cryst. Solids (Netherlands)* vol.184 (1995) p.44-50]

[2] G.G. Devyatykh, E.M. Dianov, V.G. Plotnichenko, I.V. Skiripachev, M.V. Churbanov [*Vysokochistye Veshchestva (Russia)* no.1 (1991) p.7-36]

[3] M.F. Churbanov [*J. Non-Cryst. Solids (Netherlands)* vol.184 (1995) p.25-9]

[4] J.M. Parker, A.B. Seddon [in *High Performance Glasses* Eds. M. Cable, J.M. Parker (Blackie, Chapman and Hall, New York, 1992) p.252-86]

[5] D.R. Simons, A.J. Faber, H. de Waal [*J. Non-Cryst. Solids (Netherlands)* vol.185 (1995) p.283-8]

[6] T. Katsuyama, K. Ishida, S. Satoh, H. Matsumura [*Appl. Phys. Lett. (USA)* vol.45 no.9 (1984) p.925-7]

[7] S. Shibata, T. Manabe, M. Horiguchi [*Jpn. J. Appl. Phys. (Japan)* vol.20 no.1 (1981) p.L13-6]

[8] I. Inagawa, R. Iizuka, T. Yamagishi, R. Yokota [*J. Non-Cryst. Solids (Netherlands)* vol.95&96 (1987) p.801-8]

[9] A.M. Reitter, A.N. Sreeram, A.K. Varshneya, D.R. Swiler [*J. Non-Cryst. Solids (Netherlands)* vol.139 (1992) p.121-8]

[10] S.P. Morgan, D. Furniss, A.B. Seddon, M.W. Moore [*J. Non-Cryst. Solids (Netherlands)* vol.213&214 (1997) p.72-8]

[11] M.T. Tuzzolo, D.J. McEnroe, M.G. Drexhage [*Mater. Res. Soc. Symp. Proc. (USA)* vol.172 (1990) p.185-91]

[12] D. Marchese, G. Kakarantzas, A. Jha [*J. Non-Cryst. Solids (Netherlands)* vol.196 (1996) p.314-9]

D4.2 Purification of chalcogenide glass

M.F. Churbanov

July 1997

A INTRODUCTION

Glasses, formed by chalcogenides of III-V group elements, are an efficient and promising group of optical materials. Their application, especially in fibre optics in the middle IR range [1-5], made it necessary to determine the composition and origin of impurities, to develop methods of production of glasses with low impurity content, and to investigate the effect of impurities on glass properties. The present status of these problems is considered below, with As-S and As-Se glass systems as examples which have been systematically studied since 1980 [2-5].

B IMPURITIES IN CHALCOGENIDE GLASSES

The data on composition and content of impurities in chalcogenide glasses are obtained by analysing bulk samples and optical fibres by IR-spectroscopy, element analysis and laser ultramicroscopy. Hydrogen, oxygen, carbon and silicon, in the form of compounds with each other as well as with the elements constituting the macrocomponents of glass, are the impurities which cause the selective absorption. TABLE 1 gives the positions of impurity absorption bands in the transmission spectra of glasses.

TABLE 1 Absorption bands in transmission spectra of chalcogenide glasses due to impurities.

Compound or functional group leading to absorption	Position of the maximum of absorption band (μm)
OH	2.92
SH	4.01; 3.65; 3.11; 2.05
SeH	7.8; 4.57; 4.12; 3.53; 2.32
AsH	5.02
GeH	4.95
AsO	12.6; 9.51; 8.6; 7.88; 7.45
SeO	10.68
GeO	12.8; 7.9
SiO	9.0 - 9.5
H_2O	6.31; 2.86; 2.79
CO_2	4.33
COS	4.95
CS_2	6.68; 4.65
CSe_2	7.8
Non-identified bands due to carbon presence	4.65; 5.17; 5.56; 6.0

Impurities of substances that are poorly soluble in chalcogenide melts are present in glasses in the form of heterogeneous inclusions of submicron size. Carbon comprises the majority of impurity inclusions in As-S and As-Se systems [6]. Some inclusions in the glasses with germanium and tellurium content consist of silicon dioxide [7]. The starting substances and the container material where the glass-forming compounds are synthesised are the sources of impurities in chalcogenide glasses. The content of impurities of carbon, oxygen and hydrogen in commercial samples of chalcogens and of arsenic is 1 - 10 ppm, and of inclusions with a size of 0.08 - 0.3 μm is 10^6 - 10^7 cm^{-3}.

C PREPARATION OF HIGH-PURITY CHALCOGENIDE GLASSES

The anion component of chalcogenide glasses (sulphur, selenium, tellurium) is less volatile as compared to oxygen in quartz and silicate glasses. On the other hand, the volatility of chalcogens is comparable with that of the chalcogenides of arsenic and germanium which are the glass-forming substances. These distinctions preclude the direct application of the well-developed methods for the production of high-purity quartz glass, and especially the method of chemical vapour deposition, to the production of chalcogenide glasses. Chalcogenide glasses of optical grade are produced by solidification of the glass-forming melt. The initial charge with low impurity content is melted in evacuated sealed ampoules made of quartz glass at the time-temperature modes which provide the production of a microhomogeneous melt. The degree of glass purity is determined by the impurity content in the starting substances, by entry of impurities into the melt from the container, and by contamination of the charge components during their loading into the reactor. Below different variants for the preparation of high-purity charge are given.

C1 Charge from Purified Elements

This variant is applicable to the production of all the glasses. The existing problems are connected with high content of the gas-forming impurities (C, H, N, O) and of the submicron-size particles in the initial substances. Methods of production of chalcogens and of arsenic with gas-forming impurity content lower than 0.5 - 1 ppm and with submicron particle content less than $(2 - 5) \times 10^4$ cm^{-3} have been developed [8-11].

Selenium, tellurium and arsenic can be oxidised by air during contact with the environment even at room temperature. Thus, the starting high-purity substances are loaded into the container for the glass synthesis during evaporation in oil-free vacuum.

C2 Charge from Glass-Forming Compounds of Technical Quality

Commensurability in volatility of the arsenic chalcogenides, chalcogens and arsenic allows preparation of a pure charge for the production of As-S and As-Se glasses by purification of arsenic sulphide and selenide of technical quality. Vacuum distillation in an open and closed system allows a 3 - 10 times decrease of the content of impurities of highly volatile substances and of submicron particles [5]. The purification efficiency is very sensitive to the evaporation rate and to the melt viscosity. To remove the oxygen, chemically bound with glass macrocomponents, a small amount of magnesium (aluminium, rare-earth elements) was added to the melt of the compound being purified which binds oxygen into magnesium oxide. After heating at 700 - 800°C the melt was subjected to vacuum distillation. The distillate was used as a charge which was melted and a glass-forming melt was formed. A special feature of the process is the difference in macrocomposition of the distillate and of the initial chalcogenide melt. As_2S_3 distillate is enriched with arsenic during vacuum distillation.

C3 Charge with Arsenic Monosulphide as the Arsenic-Containing Component

Ultrapurification of arsenic from submicron particles, consisting mainly of carbon, by the method of vacuum sublimation is of low efficiency at the acceptable values of arsenic evaporation rate [11]. The particles accumulate on the surface of the sublimated arsenic which decreases during distillation of the starting load. To produce glasses with As/S ratio equal to 1/1 and less, arsenic monosulphide was used as an arsenic-containing component of the charge [12]. Arsenic monosulphide is not a glass-forming substance with low viscosity and that is why there is no noticeable accumulation of particles on the surface and in the near-surface layer during distillation. A product with particle content equal to 2×10^4 cm^{-3} was obtained during vacuum distillation at sufficiently high evaporation rate ($n \times 10^{-4}$ cm^3/cm^2 s).

Two- and three-component glasses were obtained from the purified arsenic monosulphide by melting it with the required amount of chalcogenide, e.g.

$$As_4S_4 + S_2 \rightarrow 2As_2S_3$$

$$As_4S_4 + Se_2 \rightarrow 2As_2S_2Se$$

C4 Charge Prepared by Decomposition of Volatile Inorganic Hydrides

The synthesis of germanium chalcogenides by melting the elements is accompanied by impurity entry from the container walls due to the high temperature (≥900°C) of the process. In the case of Ge-Se and Ge-As-Se glass systems, a high-purity charge was obtained by decomposition of the hydrides of germanium, arsenic and selenium. Thermal decomposition of the hydride mixtures was carried out in the mode of normal (deflagration) burning. The reaction develops due to the heat liberated at decomposition of thermally unstable monogermane and that is why there is no substantial heating of the reactor walls. The solid product of the reaction is the charge that can be obtained in the form of powder or in the melted form. The charge for the synthesis of the As-Se glass system can be obtained by plasmo-chemical decomposition of the mixture of the hydrides of arsenic and selenium [13].

The synthesis of glass-forming chalcogenides and homogenisation of the melt are carried out in the range 750 - 950°C depending upon the nature of the glass obtained. The duration of the high-temperature stage depends on the loading mass and can change from several hours to several tens of hours. At such high temperature hydrogen, silicon and oxygen enter the melt at a noticeable rate from the walls of quartz containers. For example, from quartz glass, containing 100 atomic ppm of hydrogen, the latter enters the melts of chalcogenide glass at the rate V (g cm^{-2} s^{-1}), depending on temperature according to the expression [4,5]:

$$\ln V = -11.2 - \left(\frac{15300}{T}\right); (873\,K \leq T \leq 1023\,K)$$

This means that the hydrogen impurity content in the chalcogenide glass can reach 10 atomic ppm due only to its entry from the container walls. Special preparation of quartz containers, including annealing in a certain time-temperature mode and application of protective coatings, allows a considerable decrease of the contaminating effect. During synthesis of germanium chalcogenides in quartz glass containers the following reaction between germanium and silicon dioxide takes place:

$$Ge + SiO_2 \rightarrow GeO + SiO$$

As a result the chalcogenide glass is contaminated by silicon and oxygen mainly in the form of heterogeneous particles [7]. In this case it is efficient to use containers made from non-oxide materials. The silicon impurity content in glasses obtained in a boron nitride container is lower than that in glasses obtained in a quartz-glass container [5]. In experiments conducted to prepare pure materials, glass samples are obtained with the following impurity contents: metals - 0.1 - 0.01 ppm-weight; silicon - ≤0.1 - 0.5 ppm-weight; carbon, oxygen - (0.5 - 2) ppm-weight; hydrogen - 0.02 atomic ppm; submicron particles - $\leq 2 \times 10^4$ cm^{-3}.

D EFFECT OF IMPURITIES ON OPTICAL PROPERTIES OF CHALCOGENIDE GLASSES

The effect of impurities is most pronounced in the optical losses and radiation strength of chalcogenide glasses. According to theoretical calculations the minimum optical losses in A_2S_3 and As_2Se_3 glasses are equal to $(6 - 7) \times 10^{-2}$ dB/km between 4 and 6 μm [14]. In view of the experimental values of the extinction coefficient for SH, the SeH-group, CO_2, COS and CS_2, the content of these impurities in glasses with optical losses at the level of the intrinsic values should not exceed 0.05 - 1 ppb. The lowest value of optical losses in chalcogenide glass optical fibres is equal to 23 dB/km at 2.4 μm [15], i.e. it exceeds by approximately 10^3 times the theoretically calculated value. It conforms to a high content of impurities, mainly of hydrogen.

It is found that the volume damage threshold of As_2S_3 glass under the effect of YAG-Er laser radiation is very sensitive to the presence of heterogeneous inclusions of submicron size in the glass.

E CONCLUSION

Up to the present time methods of preparation of glasses with oxygen, carbon, hydrogen and silicon impurity content of 0.1 - 0.02 ppm have been developed. Further research should lead to preparation of glasses with the content of these impurities at the level of several ppb. This will allow determination of the values of the intrinsic optical properties of chalcogenide glasses.

REFERENCES

[1] T. Katsujama, H. Matsumura [*Infrared Optical Fibers* (Adam Hilger, Bristol, 1989)]
[2] A.V. Vasiliev et al [*Dokl. Akad. Nauk SSSR (Russia)* vol.300 (1988) p.859-62]
[3] G.G. Devyatykh et al [*Int. J. Optoelectron. (UK)* vol.7 (1992) p.237-54]
[4] M.F. Churbanov [*J. Non-Cryst. Solids (Netherlands)* vol.140 (1992) p.324-30]
[5] M.F. Churbanov [*J. Non-Cryst. Solids (Netherlands)* vol.184 (1995) p.25-9]
[6] I.V. Scripachev et al [*Vysok. Veshch. (Russia)* no.4 (1993) p.186-90 (in Russian)]
[7] B. Voigt, G. Dresler [*J. Non-Cryst. Solids (Netherlands)* vol.58 (1983) p.41-7]
[8] M.F. Churbanov, I.V. Scripachev [*Vysok. Veshch. (Russia)* no.3 (1988) p.92-107 (in Russian)]
[9] G.G. Devyatykh, M.F. Churbanov [*High-Purity Substances* vol.3 no.6 (1989) p.927-46]
[10] M.F. Churbanov, V.S. Shiryaev [*Vysok. Veshch. (Russia)* no.2 (1996) p.5-13 (in Russian)]
[11] M.F. Churbanov et al [*Vysok. Veshch. (Russia)* no.6 (1995) p.38-43 (in Russian)]
[12] G.G. Devyatykh et al [Patent of RF No.1721997 (April 2, 1995)]
[13] N.I. Voronin et al [*Dokl. Akad. Nauk SSSR (Russia)* vol.281 (1987) p.121-4 (in Russian)]
[14] M.E. Lines [*J. Appl. Phys. (USA)* vol.55 (1984) p.4058-66]
[15] A.V. Vasiliev et al [*Kvantovaya Elektron. Mosk. (Russia)* vol.20 (1993) p.109-12 (in Russian)]

D4.3 Drawing of chalcogenide glass optical fibres

J.S. Sanghera and I.D. Aggarwal

August 1998

A INTRODUCTION

Chalcogenide fibres are technologically important materials since they transmit in the 1 - 12 μm wavelength region and can therefore enable numerous IR applications including laser power delivery, chemical sensing and amplifiers for telecommunications when doped with appropriate rare earth ions [1]. Consequently the manufacture of low loss fibres becomes extremely important. Chalcogenide glass fibres are drawn from preforms or using the double crucible process and the details of these are described below. The fibres can consist of a core-only structure or possess a glass cladding. Typically the fibres will have a protective polymer coating for mechanical/abrasion resistance.

B PREFORM ROUTE TO FIBRES

A preform is a glass rod which consists of a central core rod and an outer cladding tube. Traditional melt casting techniques such as built-in-casting [2] and rotational casting [3] cannot be used since the chalcogenide glass melts possess high vapour pressures which lead to loss of components through volatilisation during traditional casting-type processes. This causes changes in the glass composition leading to refractive index change as well as scattering at the core/clad interface due to bubble formation and glass soot deposition. Therefore, alternative preform fabrication processes have been developed such as the rod-in-tube process [4]. In this process, the core glass rods are obtained by direct melting and quenching in the quartz ampoules and can therefore be made to almost any diameter and length. If needed they can be ground and polished down to the desired diameter. The cladding glass tubes are made by spinning the molten cladding glass in the quartz ampoule while cooling the assembly to the glass transition temperature and then annealing. Alternatively, cladding tubes can be core drilled from larger glass billets, but this is less desirable due to associated scattering losses. The inner diameter of the cladding tube is slightly larger (~50 μm) than the core rod diameter which is subsequently inserted into the tube. The rod-in-tube assembly can be collapsed either prior to fibre drawing or during the fibre draw process. An advantage of collapsing prior to fibre drawing using a low temperature isostatic pressing process [5] is reduced scattering losses due to significantly fewer bubbles and glass soot trapped at the core/cladding interface.

The preforms are subsequently drawn into fibres on a fibre draw tower (FIGURE 1) under an inert atmosphere and in the viscosity range of 10^3 - 10^6 poise. The laser-mike is used for monitoring the fibre diameter fluctuations. The preform feed rate into the furnace, the furnace temperature and the capstan/winding drum speed are used to control the fibre diameter. The preform can be initially coated with a heat shrinkable Teflon tube and drawn into fibre or a UV-curable acrylate or thermoset coating can be applied in-line.

Single-mode fibres are needed for rare earth ion-doped fibre laser and amplifier applications where considerably higher power densities can be obtained in single-mode fibres. While it is not practical to make a single mode preform directly, it is possible to stretch a typical preform obtained from the rod-in-tube process. This elongated preform is then inserted in a cladding glass tube, collapsed, and the whole stretch-and-insert process repeated several times until the appropriate core/clad ratio is attained (FIGURE 2).

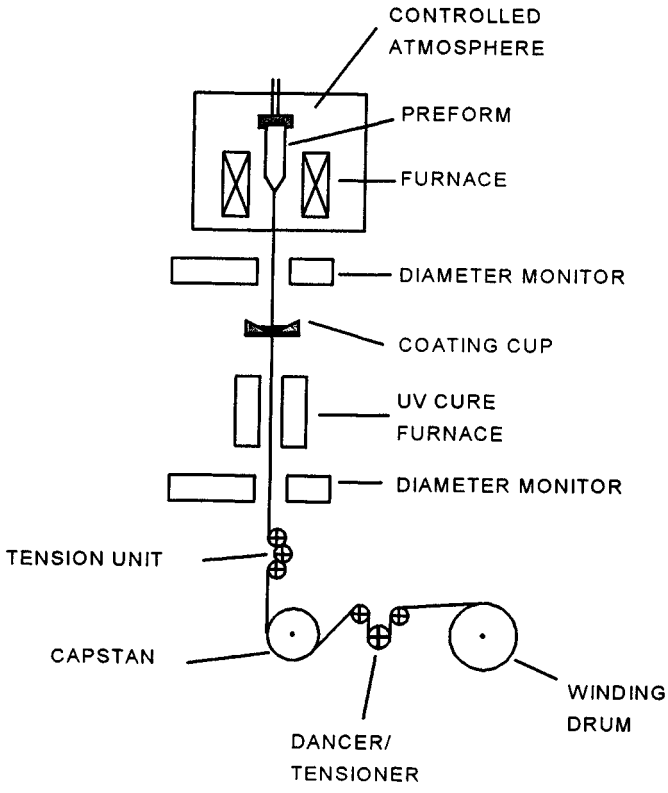


FIGURE 1 Fibre drawing tower.

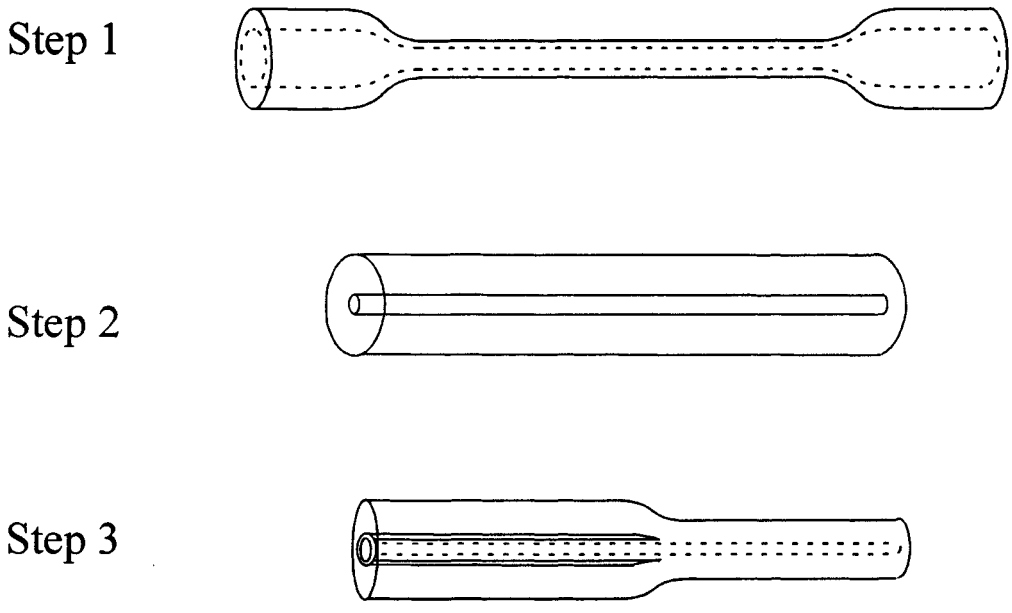


FIGURE 2 The fabrication of a single mode fibre using the stretch-and-insert process: step 1, a multimode preform is initially stretched; step 2, a cladding glass tube is cast; step 3, the stretched preform is inserted into the cladding tube. The structure is then collapsed, and the process repeated several times prior to drawing single mode fibre.

An extrusion process, similar to that used for fluorozirco-aluminate glasses [6], has been used to fabricate preforms from core and cladding glass disks made from the Ga-Na-S glass system with Pr in the core glass [7]. Such a preform has been drawn directly into a single mode fibre. The question arises whether this particular technique can be used to make long lengths of uniform diameter rare-earth doped single mode fibre. This is important from the viewpoint of commercialisation of these doped fibres for 1.3 μm fibre amplifier systems in telecommunications.

C DOUBLE CRUCIBLE PROCESS

In the double crucible process, the core and cladding glasses are remelted in concentric quartz crucibles which have small holes in their bases [8]. FIGURE 3 shows a schematic of a double crucible process setup. Once the core melt has reached a viscosity of 10^3 - 10^6 poise, it flows through the hole and into the cladding glass melt whereupon both core and cladding glasses flow out of the second hole in the bottom of the crucible. Under optimised processing conditions, the ensuing fibre possesses a defect-free and concentric core/clad structure. The processing is performed under an inert atmosphere of argon. The fibre diameter is controlled by independent pressure control above the core and cladding glass melts, respectively, as well as by the furnace temperature and draw speed. An outer polymer coating, such as a UV-curable acrylate or thermoset polymer, is applied in-line. The double crucible process can be used to make multimode and single mode fibres [9] by appropriate control of the parameters.

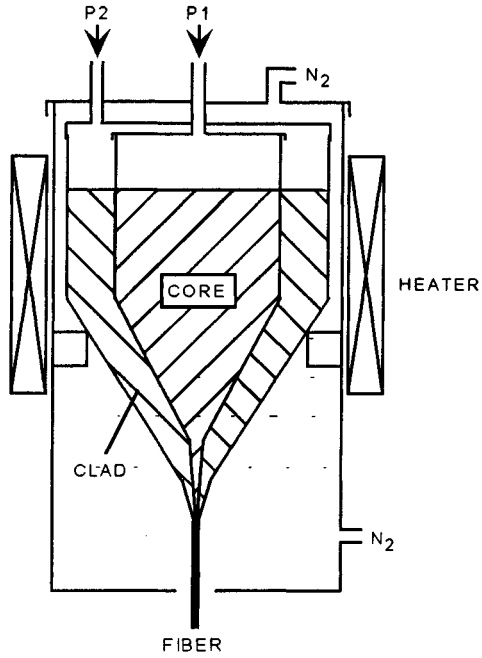


FIGURE 3 Double crucible process for fibre drawing.

REFERENCES

[1] J.S. Sanghera, I.D. Aggarwal (Eds.) [*Infrared Fiber Optics* (CRC Press Inc., Boca Raton, 1998)]

[2] Y. Ohishi, S. Mitachi, S. Takahashi [*J. Lightwave Technol. (USA)* vol.LT-2 no.5 (1984) p.593]

[3] D.C. Tran, C.F. Fisher, G.H. Sigel Jr. [*Electron. Lett. (UK)* vol.18 (1982) p.657]

[4] J. Nishii, T. Yamashita, T. Yamagishi [*Appl. Opt. (USA)* vol.28 (1989) p.5122]

[5] J.S. Sanghera, P.C. Pureza, R.E. Miklos, I.D. Aggarwal [US Patent no.5,735,927 (1998)]
[6] K. Itoh, K. Miura, I. Masuda, M. Iwakura, T. Yamashita [*J. Non-Cryst. Solids (Netherlands)* vol.167 (1994) p.112]
[7] H. Tawarayama et al [*Proc. Optical Fiber Conf.* Victoria, Canada (1997) PD1-1]
[8] J.S. Sanghera et al [*Proc. SPIE - Int. Soc. Opt. Eng. (USA)* vol.2396 (1995) p.71]
[9] R. Mossadegh et al [*J. Lightwave Technol. (USA)* vol.16 no.2 (1998) p.214]

D4.4 Loss of chalcogenide glass optical fibres

J.S. Sanghera and I.D. Aggarwal

August 1998

A INTRODUCTION

The transmission window of chalcogenide glasses is highly dependent upon the chalcogen element. For example, sulphide, selenide and telluride fibres transmit to about 7, 10 and 12 μm, respectively [1]. Therefore, the choice of glass composition is strongly dictated by the application. For instance, telluride based glasses are more appropriate for transmission in the 8 to 12 μm atmospheric window whereas sulphides possess lower loss in the 2 to 5 μm window.

The fibre optical losses are routinely measured with an FTIR method between 1.3 and 12 μm using the cut-back technique [2] or using a broad band IR source and monochromator. The fibre endfaces can be cleaved or polished but care must be taken to prevent scratching of the chalcogenide glass surface, which is inherently softer than oxide and fluoride glasses.

B ESTIMATED MINIMUM OPTICAL LOSSES

The question arises as to what is the predicted theoretical minimum loss of these glasses. For example, it has been postulated that As_2S_3 and As_2Se_3 based glasses possess minimum losses of <0.1 dB/km at about 5 μm based on the intersection of the Rayleigh scattering and multiphonon absorption curves [3]. Unfortunately, these chalcogenide glasses possess small bandgaps and hence there is a contribution from the weak absorption tail (WAT) to the total loss. FIGURE 1 shows the loss versus 1/wavelength plot for a sulphide fibre sample which had a minimum loss of 0.047 dB/km at 2.4 μm [4]. Although the calculated Rayleigh scattering ($\alpha_{RS} = 11.7\lambda^{-4}$) pins the minimum loss below 0.1 dB/km, the contribution from the WAT is significant such that the predicted minimum loss is about 4 dB/km at 5.3 μm. The contribution from the WAT is not well understood for selenide and telluride glasses and so similar estimations have not been performed.

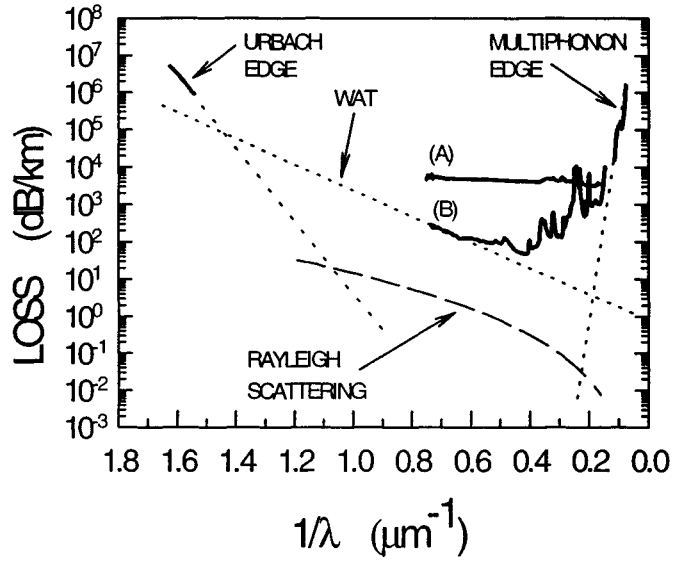


FIGURE 1 The attenuation versus 1/wavelength plot for $As_{40}S_{55}Se_5$ glass fibre fabricated using (A) poor quality chemicals and (B) purified chemicals, respectively.

C MEASURED OPTICAL LOSSES

The actual measured losses in As-S based fibres at around 5 μm are much higher. FIGURES 2 and 3 show the measured losses of sulphide (As-S based) fibres and telluride (Ge-As-Se-Te based) fibres, respectively, which are obtained on a routine basis in the infrared. Also shown for comparison are the champion loss results reported in the literature for the same compositions. The As-S glass system has received significantly more attention than the other glass systems since it contains fewer elements to purify, is very stable towards crystallisation and consequently has demonstrated the lowest losses to date. These fibres transmit in the 1 - 6.5 μm region. Routine losses of about 200 dB/km are readily obtained on long fibre lengths (>20 metres) [5], although champion losses of 23 dB/km have been reported [6].

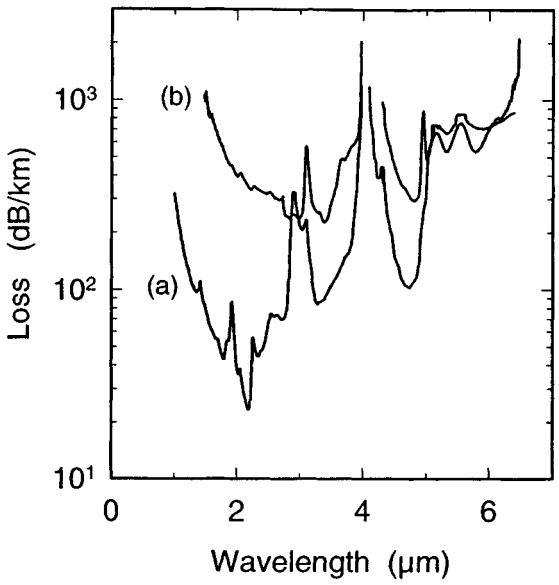


FIGURE 2 The optical loss of sulphide fibres demonstrating (a) record low loss and (b) routine loss.

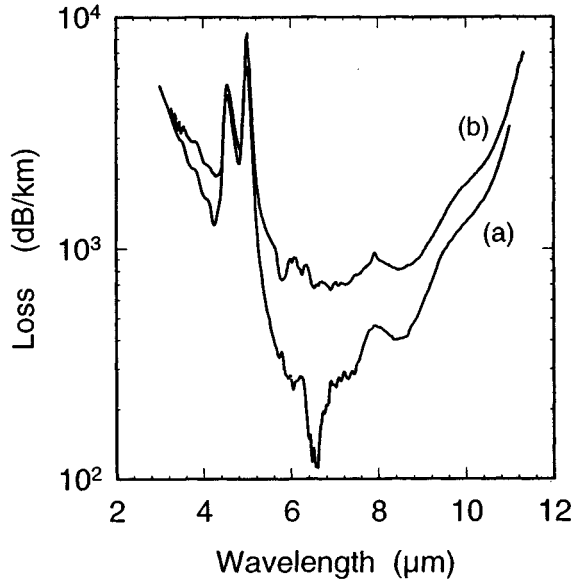


FIGURE 3 The optical loss of telluride fibres demonstrating (a) record low loss and (b) routine loss.

The telluride fibres tend to be less stable, contain more elements which need to be purified and hence exhibit higher losses, more typically 500 to 1000 dB/km on long fibre lengths [7]. However, champion losses of about 200 dB/km have been demonstrated [7]. These fibres transmit in the 3 - 12 μm region.

D EXTRINSIC ABSORPTION AND SCATTERING LOSSES

While extrinsic absorption from impurities leads to discrete absorption bands in the infrared region, extrinsic scattering from defects and impurities can cause wavelength dependent and/or wavelength independent scattering losses in this wavelength region.

TABLE 1 lists the impurity absorption bands along with their estimated concentrations in these fibres. The main impurity bands are related to hydrogen and oxygen containing species whose concentrations are in the part per billion up to several parts per million range.

TABLE 1 Estimated concentration of typical impurities in sulphide and telluride fibres.

Impurity absorption	Wavelength (μm)	Absorption loss (dB/m)	Extinction coefficient (dB/m/ppm)*	Impurity concentration (ppm)
Sulphide fibres				
H-S	4.0	5	2.3 [8]	2.2
O-H	2.9	0.3	5.0 [10]	0.06
Telluride fibres				
H-Se	4.5	3.0	1.1 [8]	2.7
Ge-H	5.0	6.0	-	-
H_2O	6.3	0.07	34.0 [11]	0.002
Ge-O	7.9	0.16	2.6 [9]	0.06

* References in parentheses.

Typical defects which have been identified in these glasses and fibres include bubbles, amorphous carbon, silica and alumina [12]. FIGURE 4 shows how the calculated scattering efficiency factor, Q, varies with defect radius at a wavelength of 5 μm. Q is related to the relative refractive index, particle size and wavelength [13]. The slope is indicative of the type of scattering behaviour, namely Rayleigh (λ^{-4}), Rayleigh-Gans (λ^{-2}) and wavelength independent scattering (λ^{0}). The effects for carbon are complex because there is both a real and an imaginary component to its refractive index. TABLE 2 lists the defect size which gives rise to the appropriate scattering behaviour. For a given particle size, bubbles exhibit the largest scattering since they possess the largest values of Q. This magnitude is related to the large index difference between bubbles (n = 1) and sulphide glass (n = 2.4). The actual scattering contribution from bubbles may be higher since large bubbles may be drawn into long capillaries in fibres. Also shown in FIGURE 4 and listed in TABLE 2 are data for As_2S_3 crystals. These data are for comparative purposes even though these crystals have not been identified in As_2S_3 glass under normal processing conditions. It is possible to estimate the maximum number of defects in order to attain a loss of 4 dB/km in a 1 km length of fibre with a core diameter of 150 μm. Estimates for the maximum number of tolerable particles with 0.5 μm radius include 12,800 bubbles, 16,000 carbon particles, 23,200 SiO_2 particles, 40,000 Al_2O_3 crystals and 156,000 As_2S_3 crystals, indicating the detrimental role of these particles, especially bubbles. Bubbles can be trapped at the core/clad interface or within the core and cladding glasses due to inappropriate processing. Therefore, great care must be taken when fabricating chalcogenide glass fibres.

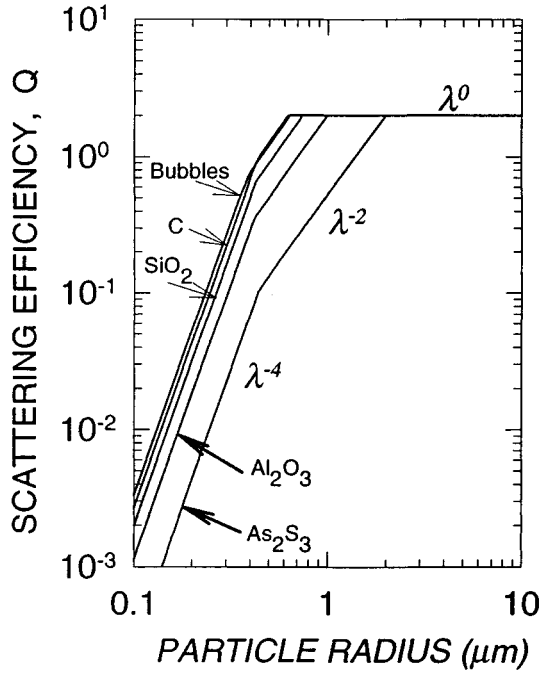


FIGURE 4 Scattering efficiency factor, Q, as a function of defect radius at a wavelength of 5 μm in As_2S_3 glass.

TABLE 2 The defect radius, x (in μm), causing λ^{-4}, λ^{-2} and λ^{0} scattering behaviour at a wavelength of 5 μm in As_2S_3 glass.

Defect	λ^{-4}	λ^{-2}	λ^{0}
Bubble	$x < 0.4$	$0.4 < x < 0.6$	$x > 0.6$
Carbon	$x < 0.4$	$0.4 < x^* < 0.6$	$x > 0.6$
SiO_2	$x < 0.4$	$0.4 < x < 0.7$	$x > 0.7$
Al_2O_3	$x < 0.4$	$0.4 < x < 1.0$	$x > 1.0$
As_2S_3	$x < 0.45$	$0.45 < x < 2.0$	$x > 2.0$

* Carbon exhibits complex behaviour.

REFERENCES

[1] J. Nishii, T. Yamashita [in *Infrared Fiber Optics* Eds. J.S. Sanghera, I.D. Aggarwal (CRC Press Inc., Boca Raton, 1998)]

[2] R.D. Driver, G.M. Leskowitz, L.E. Curtiss, D.E. Moynihan, L.B. Vacha [*Mater. Res. Soc. Symp. Proc. (USA)* vol.172 (1990) p.169]

[3] E.M. Dianov, M.Yu. Petrov, V.G. Plotnichenko, V.K. Sysoev [*Sov. J. Quantum Electron. (USA)* vol.12 (1982) p.498]

[4] J.S. Sanghera, V.Q. Nguyen, R.E. Miklos, P.C. Pureza, F.H. Kung, I.D. Aggarwal [*J. Lightwave Technol. (USA)* vol.14 (1996) p.743]

[5] J.S. Sanghera, I.D. Aggarwal [*Proc. Int. Congress on Glass* San Francisco, CA, USA, 5-10 July 1998]

[6] A.V. Vasilev et al [*Quantum Electron. (USA)* vol.23 (1993) p.89]

[7] J.S. Sanghera, V.Q. Nguyen, P.C. Pureza, F.H. Kung, R. Miklos, I.D. Aggarwal [*J. Lightwave Technol. (USA)* vol.12 (1994) p.737]

[8] G.E. Devyatykh, M.F. Churbanov, I.V. Scripachev, E.M. Dianov, V.G. Plotnichenko [*Int. J. Optoelectron. (UK)* vol.7 (1992) p.237]

[9] J. Nishii, T. Yamashita, T. Yamagishi [*J. Mater. Sci. (UK)* vol.24 (1989) p.4293]

[10] G. Fonteneau [*Mater. Res. Bull. (USA)* vol.19 (1984) p.685]

[11] F.M. Ernsberger [*J. Am. Ceram. Soc. (USA)* vol.60 (1977) p.91]

[12] J.S. Sanghera, L.E. Busse, I.D. Aggarwal [*Appl. Phys. (USA)* vol.75 (1994) p.4885]

[13] G. Mie [*Ann. Phys. (Germany)* vol.25 (1908) p.377]

PART D: CHALCOGENIDE GLASS

CHAPTER D5

SELECTED APPLICATIONS

D5.1 Fibre amplifiers based on rare earth-doped chalcogenide glass
D5.2 Fibre lasers based on rare earth-doped chalcogenide glass
D5.3 Optical switches based on chalcogenide glass

D5.1 Fibre amplifiers based on rare earth-doped chalcogenide glass

H. Tawarayama

March 1998

A INTRODUCTION

The Pr^{3+}-doped fibre amplifier (PDFA) has been attractive as a new amplifier for 1.3 μm optical telecommunication networks. High gain amplification has already been demonstrated using fluoride fibres [1-3]. However, compared with Er^{3+}-doped fibre amplifiers (EDFAs), their gain coefficients are considerably lower because of low radiative quantum efficiencies of the $^1G_4$ - $^3H_5$ transition at 1.3 μm.

Chalcogenide glasses, which have lower phonon energies and higher refractive indices than fluoride glasses, have been expected to be good host materials for high efficiency PDFAs. Excellent emission properties of Pr^{3+} in several chalcogenide glasses, such as large stimulated emission cross-sections and long fluorescence lifetimes, have been reported [4]. Here we describe high efficiency optical amplification in Pr^{3+}-doped Ga-Na-S (GNS) chalcogenide fibre [5].

B HOST GLASS

In order to fabricate a low loss Pr^{3+}-doped single-mode fibre, it is necessary for host glasses to overcome some problems. These are the solubility of rare-earth ions, the thermal stability and the transparency at pump (1.02 μm) and signal (1.31 μm) wavelengths. GNS glasses reported by Palazzi [6] were thermally stable and were able to incorporate large amounts of rare-earth ions. The colour of GNS glasses is pale yellow and the absorption edge is about 400 nm. Therefore, the background losses of Pr^{3+}-doped GNS fibre at the pump and the signal wavelengths become low.

C EMISSION PROPERTIES

TABLE 1 shows the fluorescence lifetime τ_f, the branching ratio β, the quantum efficiency η and the stimulated emission cross-section σ_{se} of the $^1G_4$ - $^3H_5$ transition for a GNS glass calculated by Judd-Ofelt analysis as well as for a ZrF_4-based fluoride glass [1]. The quantum efficiency and the relative gain parameter $\sigma_{se}\tau$ for 500 ppm Pr^{3+} concentration were 56% and 40.0 × 10^{-25} cm^2 s respectively, which were greatly improved from 3.4% and 3.8 × 10^{-25} cm^2 s for the ZrF_4-based fluoride glass. Therefore, a much higher gain coefficient than that of the ZrF_4-based fluoride glass is expected by using the GNS glass.

TABLE 1 The fluorescence lifetime τ_f, the branching ratio β, the quantum efficiency η and the stimulated emission cross-section σ_{se} of the $^1G_4$ - $^3H_5$ transition for a GNS glass.

Glass	τ_f (× 10^{-21} cm^2)	σ_{se} (μs)	β (%)	η (%)
GNS glass	370	10.8	57	56
ZrF_4-based fluoride glass [1]	110	3.48	64	3.4

D AMPLIFICATION CHARACTERISTICS

A Pr^{3+}-doped GNS single-mode fibre with a numerical aperture of 0.31, a core diameter of 2.5 μm and attenuation loss of 1.2 dB/m at 1.31 μm was used in our amplifier trial. Pr^{3+} concentration in the core glass was 750 ppm. For the measurement of the amplification characteristics, a bi-directional pumping configuration shown in FIGURE 1 was employed. The pump source was a Ti:sapphire laser operating at 1.017 μm and the pump power was monitored with a power meter. The arrows with dotted and solid lines show the paths of the pump and the signal lights respectively. The GNS fibre was butt-jointed to a silica fibre with a high numerical aperture. The fibre length used for the measurement was 6.1 m.

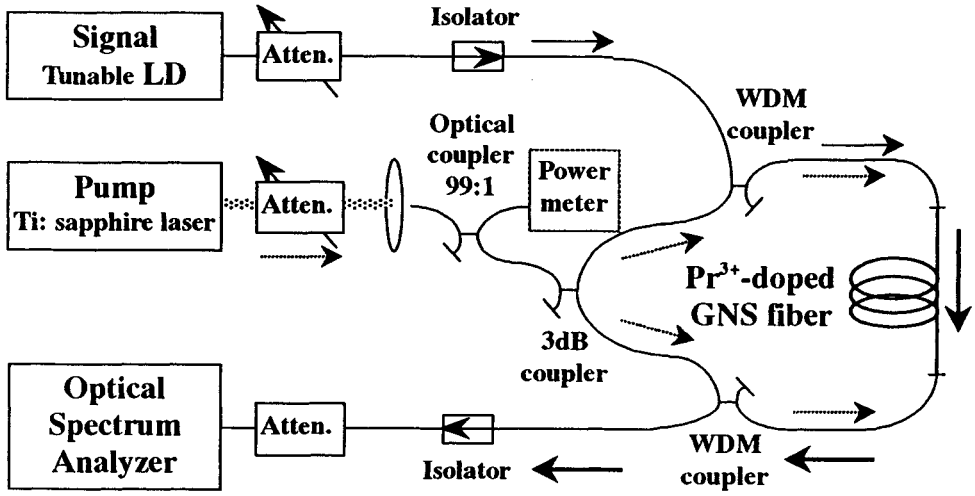


FIGURE 1 Experimental setup for amplification characteristics.

FIGURE 2 shows the gain spectrum in the 1.3 μm region. The input signal level was -8 dBm or -30 dBm and the pump power was 90 mW. The net gain was the highest at 1.34 μm for both signal levels and the maximum net gain of 32 dB was obtained. In the case of ZrF_4-based fluoride fibre, the single pass gain obtained at the same pump power is less than 10 dB [3].

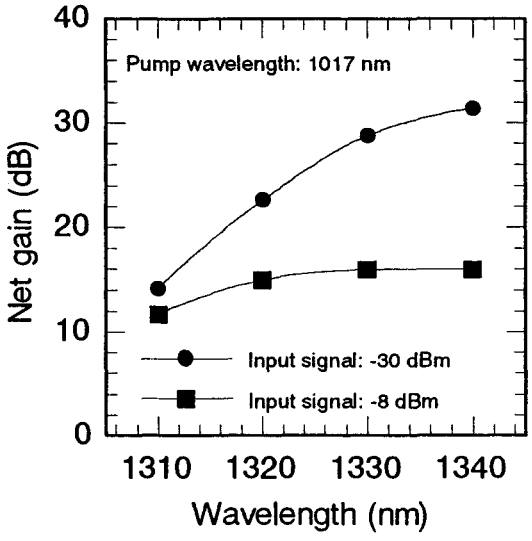


FIGURE 2 The gain spectrum in the 1.3 μm region.

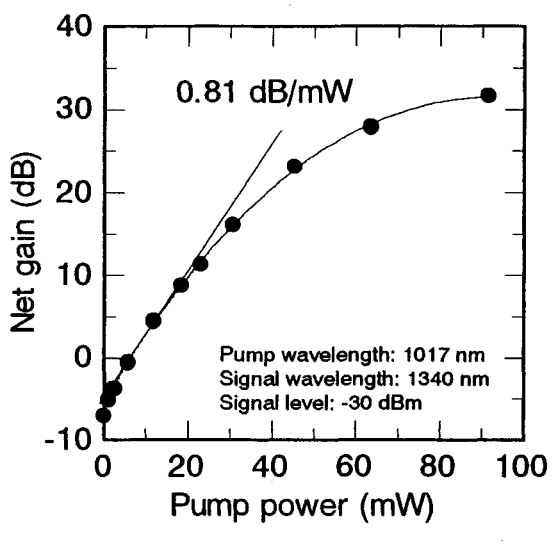


FIGURE 3 The pump power dependence of the net gain at 1.34 μm.

FIGURE 3 shows the pump power dependence of the net gain at 1.34 μm. The input signal level was -30 dBm. A gain coefficient of 0.81 dB/mW was achieved, much higher than 0.24 dB/mW for ZrF_4-based fluoride fibre [1]. To the best of our knowledge, the maximum gain coefficient ever reported for a PbF_2/InF_3-based fluoride fibre was 0.36 dB/mW [3]. Highly efficient optical amplification was confirmed for GNS fibre. The amplifier performance can be improved by lowering the background loss at the pump and the signal wavelengths as well as by optimising the Pr^{3+} concentration and the fibre structure.

E CONCLUSION

High efficiency optical amplification in the 1.3 μm region was demonstrated in Pr^{3+}-doped GNS chalcogenide single-mode fibre. The highest gain coefficient of 0.81 dB/mW and a net gain of 32 dB at a pump power of 90 mW were obtained at 1.34 μm.

REFERENCES

[1] Y. Ohishi et al [*IEICE Trans. Commun. (Japan)* vol.E77-B (1994) p.421-40]

[2] H. Yanagita, K. Itoh, E. Ishikawa, H. Aoki, H. Toratani [*Tech. Digest of Conf. on Optical Fiber Communication* San Diego, California, USA, 26 Feb.-3 March 1995 (Optical Society of America, Washington DC, USA, 1995) paper PDP2]

[3] Y. Nishida, T. Kanamori, Y. Ohishi [*Tech. Digest of Conf. on Optical Fiber Amplifiers and Their Applications* Monterey, California, USA, 11-13 July 1996 (Optical Society of America, Washington DC, USA, 1996) paper PDP3]

[4] See, for example, D.R. Simons, A.J. Faber, H. de Waal [*J. Non-Cryst. Solids (Netherlands)* vol.185 (1995) p.283-8]

[5] H. Tawarayama et al [*Tech. Digest of Conf. on Optical Fiber Amplifiers and Their Applications* Victoria, BC, Canada, 21-23 July 1997 (Optical Society of America, Washington DC, USA, 1997) paper PDP1]

[6] M. Palazzi [*C.R. Acad. Sci. (France)* vol.299 (1984) p.529-32]

D5.2 Fibre lasers based on rare earth-doped chalcogenide glass

T. Schweizer

November 1997

A INTRODUCTION

The first demonstration of laser action in a rare-earth doped glass fibre by Snitzer [1] triggered off world wide activities to realise fibre lasers at a large variety of emission wavelengths ranging from the ultraviolet [2] to the mid-infrared [3]. Specific applications require different laser wavelengths which in turn require different rare-earth dopants and host materials. Chalcogenide glasses offer some advantages over oxide and fluoride glasses. The small phonon energies of the glass matrix lead to extended infrared transparency and low non-radiative decay rates of rare-earth energy levels; the covalent nature of the glass bonds (high refractive index) increases the radiative decay rates and emission and absorption cross sections (see [4-9] for more details). Based on these favourable properties chalcogenide glasses have been proposed as new laser materials, in particular for new laser transitions from energy levels close to the next lower lying level such as the 1.3 μm transitions in praseodymium [6] and dysprosium [9] and new mid-infrared transitions [10-13]. Most of the research is focused on sulphide glasses which offer transparency at convenient pump wavelengths in the visible and near-infrared wavelength regions compared to the opaque selenide and telluride glasses [4,13]. Most of the rare-earth doped sulphide glass laser work in turn concentrates on trivalent neodymium (Nd^{3+}) as the active ion which is used rather as a convenient test dopant than as a dopant with promising new transitions [7,10,14-24]. Out of this group of glasses Nd^{3+} doped gallium lanthanum sulphide (GLS) glasses have been studied in greatest depth and are the only chalcogenide glasses with reported laser action in bulk glass and fibre form [7,14-18,25,26]. After a brief introduction to other proposed neodymium doped chalcogenide laser glasses this Datareview will therefore focus on neodymium lasers in GLS glass.

B LASERS BASED ON NEODYMIUM-DOPED SULPHIDE GLASSES

A number of Nd^{3+} doped sulphide glasses such as As_2S_3 [10,20], Ga:Ge:As:S [21], $3Al_2S_3$:$1La_2S_3$ [15,16], Ge:As:Ga:Sb:S [19], Ge:Ga:S [22] and Ga:Na:S [24] have been proposed as new laser materials and studied mainly in bulk glass form. Viens et al [20] reported 1080 nm fluorescence from As_2S_3 waveguides which were thermally evaporated onto oxidised silicon wafers and doped with Nd^{3+} using ion implantation. Internal gain in an Nd^{3+} doped sulphide fibre was reported for the first time by Mori et al [19]. The fibre with a 1000 ppm Nd^{3+} doped Ge:As:Ga:Sb:S core glass and a Ge:As:S cladding glass was fabricated using the rod-in-tube technique, and had a core diameter of 5 μm and a cladding diameter of 120 μm, a cut-off wavelength of 2.1 μm, and a transmission loss of 10 dB/m at 1.3 μm. A 5 cm long fibre showed a maximum internal gain of 6.8 dB for a pump power of 180 mW. Net signal gain was not obtained.

Nd^{3+} doped gallium lanthanum sulphide (GLS) glass has been studied extensively [14-18], and a summary of the spectroscopic properties can be found in this book [7]. The first laser operation in a rare-earth doped chalcogenide glass was achieved in this system [25]. A 1.42 mm thick glass disk with the composition $70Ga_2S_3$:$28.5La_2S_3$:$1.5Nd_2S_3$ was placed in a hemispherical laser cavity and pumped with a Ti:sapphire laser at either 815 nm or 890 nm. FIGURE 1 shows the output power versus the absorbed pump power of the 1080 nm laser transition ($^4F_{3/2} \rightarrow {}^4I_{11/2}$) for 890 nm pumping.

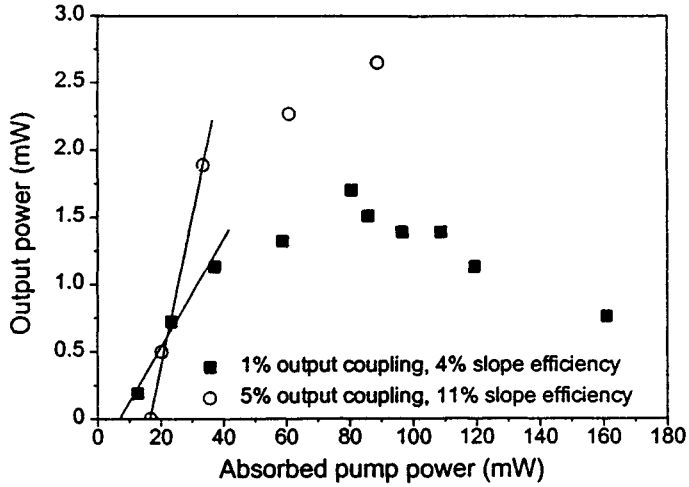


FIGURE 1 Output power against absorbed pump power of 1080 nm Nd^{3+} doped GLS glass laser pumped at 890 nm [23].

The laser operated in the continuous wave regime at room temperature. The threshold power is reasonably low but the rollover of the output power indicates strong thermal problems in the laser material. Similar thermal problems and measurements of the focal length of the thermal lens have been reported by Viana et al in Nd^{3+} doped Ga:Na:S glass [24]. The authors concluded that laser action in their system was prevented by thermal lensing and the high threshold power which is caused by the short lifetime of the $^4F_{3/2}$ level, and proposed several solutions to this problem such as reduction of the chopped pump duty cycle, convex polishing of the glass end faces and the fabrication of guiding structures such as waveguides and fibres.

Advances in chalcogenide glass fibre fabrication [27] enabled the realisation of an Nd^{3+} doped GLS glass fibre laser [26]. The fibre which was fabricated using the rod-in-tube method was doped with 0.05 mol% Nd_2S_3 and had a 14 μm core and a 230 μm diameter. The fibre laser behaviour of a Ti:sapphire pumped (815 nm) 22 mm long fibre with a high reflecting input mirror and three different output mirrors and wavelengths is shown in FIGURE 2. As expected the output power does not roll over at high pump powers showing the advantage of the fibre geometry.

The fibre laser was initially reported to be self-pulsing with pulse width of about 0.2 μs and regular pulse spacing between 2 and 3.5 μs [26]. Further experiments showed that the self-pulsing behaviour is not inherent to the fibre itself but depends on the alignment of the resonator mirrors and the focusing objective. FIGURE 3 shows the two different lasing regimes (continuous wave and self-pulsing) which could be switched on and off by changing the alignment of the output mirror. A graph showing a train of single equidistant pulses can be found in [26]. We can therefore report true CW laser action at room temperature at this point.

To our knowledge, there are no other chalcogenide glass fibre lasers reported in the literature although a number of different glasses with different rare-earth dopants have been proposed as new laser materials, in particular for mid-infrared fibre lasers, a wavelength range which is not accessible by common silica fibre lasers.

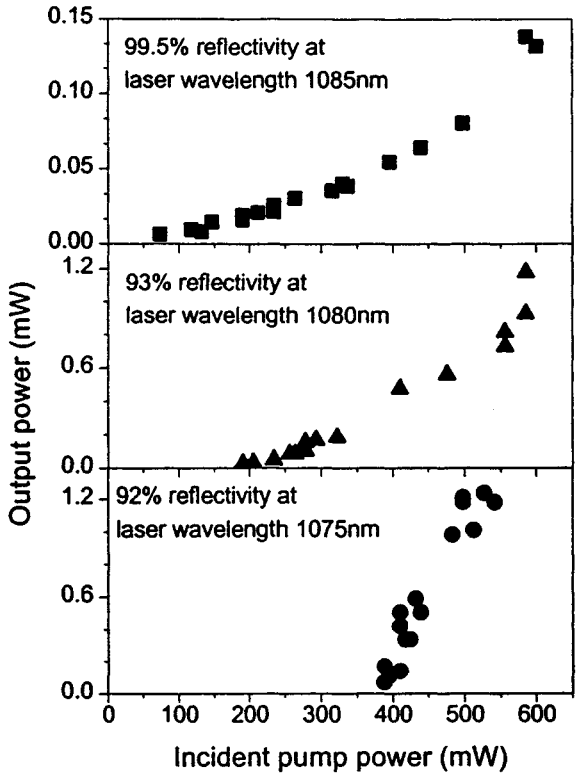


FIGURE 2 Output power against incident pump power of Nd^{3+} doped GLS glass fibre laser for different output mirrors and laser wavelengths pumped at 815 nm [24].

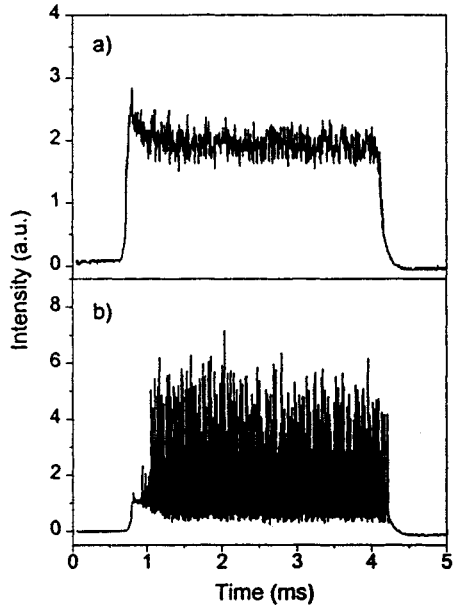


FIGURE 3 Continuous wave (a) and self-pulsing (b) laser behaviour of the Nd^{3+} doped GLS glass fibre laser (chopped pump source for clarity).

C CONCLUSION

Fibre lasers based on chalcogenide glasses are still in their infancy but the proof of principle in the form of the demonstration of an Nd^{3+} doped fibre laser, the numerous reports in the literature on new potential laser transitions, and the advances in fibre fabrication show a promising future for new chalcogenide glass fibre lasers.

REFERENCES

[1] E. Snitzer [*Phys. Rev. Lett. (USA)* vol.7 (1961) p.444]

[2] D.S. Funk, J.W. Carlson, J.G. Eden [*Electron. Lett. (UK)* vol.30 (1994) p.1859]

[3] J. Schneider [*Electron. Lett. (UK)* vol.31 (1995) p.1250]

[4] D.J. Brady [Datareview in this book: *D1.1 Transmission of chalcogenide glass*]

[5] H. Takebe [Datareview in this book: *D1.3 Refractive index and dispersion of chalcogenide glass*]

[6] J.R. Hector [Datareview in this book: *D3.1 Spectroscopy of praseodymium-doped chalcogenide glass*]

[7] T. Schweizer [Datareview in this book: *D3.2 Spectroscopy of neodymium-doped chalcogenide glass*]

[8] J. Heo [Datareview in this book: *D3.3 Spectroscopy of thulium/holmium-doped chalcogenide glass*]

[9] B.N. Samson [Datareview in this book: *D3.4 Spectroscopy of dysprosium-doped chalcogenide glass*]

[10] J. Heo [*J. Mater. Sci. Lett. (UK)* vol.14 (1995) p.1014]

[11] T. Schweizer, D.W. Hewak, B.N. Samson, D.N. Payne [*Opt. Lett. (USA)* vol.21 (1996) p.1594]

[12] T. Schweizer, D.W. Hewak, B.N. Samson, D.N. Payne [*J. Lumin. (Netherlands)* vol.72-74 (1997) p.419]

[13] L.B. Shaw, B.B. Harbison, B. Cole, J.S. Sanghera, I.D. Aggarwal [*Optics Express (USA)* vol.1 (1997) p.87]

[14] R. Reisfeld, A. Bornstein [*Chem. Phys. Lett. (Netherlands)* vol.47 (1977) p.194]

[15] A. Bornstein, R. Reisfeld [*J. Non-Cryst. Solids (Netherlands)* vol.50 (1982) p.23]

[16] R. Reisfeld [*Ann. Chim. (France)* vol.7 (1982) p.147]

[17] J. Flahaut, M. Guittard, A.M. Loireau-Lozac'h [*Glass Technol. (UK)* vol.24 (1983) p.149]

[18] L. Mattos Jr., A.G. Clare [*Phys. Chem. Glasses (UK)* vol.34 (1993) p.244]

[19] A. Mori, Y. Ohishi, T. Kanamori, S. Sudo [*Appl. Phys. Lett. (USA)* vol.70 (1997) p.1230]

[20] J.-F. Viens et al [in *Conference on Lasers and Electrooptics* vol.11 of 1997 OSA Technical Digest Series (Optical Society of America, Washington DC, 1997) p.249]

[21] A. Belykh et al [*J. Non-Cryst. Solids (Netherlands)* vol.213&214 (1997) p.238]

[22] K. Abe, H. Takebe, K. Morinaga [*J. Non-Cryst. Solids (Netherlands)* vol.212 (1996) p.143]

[23] Y.S. Tver'yanovich, S.V. Degtyarev, S.S. Pivovarov, N.V. Belyakova [*Glass Phys. Chem. (Russia)* vol.23 (1997) p.80]

[24] B. Viana, M. Palazzi, O. LeFol [*J. Non-Cryst. Solids (Netherlands)* vol.215 (1997) p.96]

[25] T. Schweizer, D.W. Hewak, D.N. Payne, T. Jensen, G. Huber [*Electron. Lett. (UK)* vol.32 (1996) p.666]

[26] T. Schweizer, B.N. Samson, R.C. Moore, D.W. Hewak, D.N. Payne [*Electron. Lett. (UK)* vol.33 (1997) p.414]

[27] D.W. Hewak [Datareviews in this book: *D4.3 Drawing of chalcogenide glass optical fibres*; *D4.4 Loss of chalcogenide glass optical fibres*]

D5.3 Optical switches based on chalcogenide glass

M. Asobe

August 1997

A INTRODUCTION

Various kinds of materials are being studied as non-linear optical media to achieve strong interaction between individual light signals. Utilising the non-linear refractive index or absorption change induced by very short optical pulses, one can switch one light signal by using another light signal, with ultrafast response time. Such 'all-optical' switching may be useful to break through the operation speed limit of electrical circuits in the field of future high-speed optoelectronics. To accomplish the non-linear interaction efficiently, it is desirable that the employed non-linear optical medium possess high non-linearity, high power density and a sufficiently long interaction length. Recently, it has been revealed that chalcogenide glass shows promise to fulfil these requirements. This Datareview introduces the recent research progress on the application of chalcogenide glass to all-optical switching.

B FEATURES OF CHALCOGENIDE GLASS AS A NON-LINEAR MATERIAL

Materials exhibit several kinds of non-linear optical effect depending on the operating wavelength. With a wavelength near the electronic absorption edge, various resonant non-linear effects in chalcogenide glass have been reported, such as light-induced structural change [1], absorptive non-linearity [2] and a thermal index change [3]. Although these resonant effects possess large non-linearity, it is difficult to utilise these effects, and slow response time limits the operation speed. In contrast, with a wavelength longer than the electronic absorption edge, ultrafast non-linearity due to third-order electronic polarisation is guaranteed. For example, a typical chalcogenide glass such as As_2S_3 possesses good transparency at a wavelength of 0.7 to 10 μm. Thus some types of chalcogenide glass can be used as non-resonant material at communication wavelengths (1.3 ~ 1.55 μm). The drawback of non-resonant operation is that the non-linearity is relatively small, so a waveguide structure is necessary in order to keep a high power density within the long interaction length. Conventional silica fibre has been one of the most commonly used non-resonant non-linear media in all-optical switching [4]. This is because glass is suitable for fabricating a long fibre type waveguide. However, the small non-linearity of silica glass requires that the fibre be extremely long, for example a few kilometres. To overcome this problem of length, the chalcogenide glass is attractive because of its high non-linearity. A study on non-linear optical susceptibility $\chi^{(3)}$ using third harmonic generation (THG) revealed that As_2S_3 glass has a level of non-linearity two orders of magnitude higher than that of silica glass [5]. One of the significant features of chalcogenide glass is that it possesses such high non-linearity at a non-resonant wavelength.

C NON-LINEAR OPTICAL PROPERTIES OF THE CHALCOGENIDE GLASS FIBRE

TABLE 1 summarises the non-linear refractive index n_2, two-photon absorption coefficient α_2, two-photon figure of merit and group velocity dispersion (GVD) of As_2S_3 glass. The non-linear refractive index n_2 of the As_2S_3 glass fibre was measured directly by optical Kerr shutter experiments with wavelengths of 1.3 μm and 1.55 μm [6,7]. In any case, it was confirmed that As_2S_3 glass possesses an n_2 value about two orders of magnitude larger than that of silica glass ($n_2 = 3.2 \times 10^{-20}$ m^2/W). As shown in TABLE 1, the n_2 value at 1.3 μm was measured to be larger than that at 1.55 μm. There is the

possibility that the n_2 value depends on the wavelength because of the two-photon resonance near 1.3 μm [8].

TABLE 1 Non-linear and linear optical parameters of As_2S_3-based glass fibre.

Wavelength λ (μm)	n_2 (m^2/W)	α_2 (m/W)	$\frac{2\alpha_2\lambda}{n_2}$	GVD (ps/km nm)
1.3	4.0×10^{-16}	6.2×10^{-15}	9.3×10^{-3}	660
1.55	2.0×10^{-16}	$<4.0 \times 10^{-12}$	<0.5	410

In highly non-linear materials, not only the non-linear refractive index but also two-photon absorption (TPA) is enhanced. TPA limits the transmittable optical power and thereby the attainable non-linear phase shift in all-optical switching [9]. To avoid limitations in the attainable phase shift due to TPA, the figure of merit (FOM), $2\alpha_2\lambda/n_2$, should be much smaller than 1. The TPA coefficient α_2 can be estimated by measuring the transmittance change of a single beam as a function of the incident power. From a single beam experiment, the FOM of As_2S_3 glass at a wavelength of 1.55 μm was estimated to be small enough, as shown in TABLE 1 [10]. The TPA coefficient at 1.3 μm could not be measured directly by the single beam experiment because of the limited available light source power [6]. From the Kerr shutter experiment at 1.3 μm it was confirmed that the FOM is at most less than 0.5. Non-linear optical properties of chalcogenide glasses other than As_2S_3 are not clear at present. Glass with a higher refractive index, for instance As_2Se_3, may have higher non-linearity. Such materials, however, should have large TPA coefficient depending on the operation wavelength. Therefore materials should be chosen with consideration of enhancement of TPA and wavelength of interest.

As far as the phase-shift limitation is concerned, the TPA does not affect the all-optical applications of As_2S_3-based glass fibres at communication wavelength. There is, however, another problem related to TPA. It is well known that chalcogenide glass undergoes a structural change when exposed to light near the bandgap wavelength [1]. We expect that TPA could cause the same structural change, which would lead to optical damage or a birefringence change. Throughout the experiments at the 1.55 μm wavelength, no optical damage was observed, in contrast to the experiment at 1.3 μm where we expect a higher TPA coefficient. Further study is required to clarify the mechanism of the structural change and the reliability of the chalcogenide fibres.

Insofar as the materials are used with non-resonant wavelength, ultrafast response is guaranteed. In fact, the non-linear response of the As_2S_3-based glass fibres was confirmed to be instantaneous, that is, within a few hundred femtoseconds, with a wavelength of 1.55 μm [10]. Switching speed, however, is primarily determined by GVD if the material response is instantaneous, that is, within the optical pulse width. As shown in TABLE 1, As_2S_3 glass has a large normal dispersion around the communication wavelength. Thus, unlike the conventional silica fibre, it is difficult to control the GVD of the fibre by changing the fibre structure, and the GVD of the fibre is mostly determined by material dispersion. Certain care should be addressed to pulse broadening and walk-off effects due to GVD.

D ALL-OPTICAL SWITCHING USING CHALCOGENIDE FIBRE

To accomplish all-optical switching utilising non-linear refractive index change, one has to convert the phase modulation into intensity modulation by using some kind of interferometric configuration. In most interferometers, signal light is divided into two paths and ideally only one of the resulting signals suffers a non-linear phase shift induced by a gate pulse within a non-linear medium. Finally the two separate signals are combined to give interference and the phase modulation is converted into intensity modulation.

One of the most simply configured interferometers is the optical Kerr shutter [6]. In this configuration the orthogonal polarisation along the fibre acts as the two distinct paths of an interferometer, so that no additional fibre optics are required. FIGURE 1 shows the principle of the optical Kerr shutter. The polarisation of the signal and gate pulses is offset by 45 degrees. A gate pulse induces a phase shift difference between two signal components whose polarisation is parallel and perpendicular to that of the gate. The phase shift difference $\Delta\Phi$ is given as follows:

$$\Delta\Phi = \Delta\Phi_{\parallel} - \Delta\Phi_{\perp} = \Delta\Phi_{\parallel} - \frac{1}{3}\Delta\Phi_{\parallel} = \frac{2}{3}\frac{4\pi n_2}{3\lambda_s A_{eff}} P_g L \qquad (1)$$

where $\Delta\Phi_{\parallel}$, $\Delta\Phi_{\perp}$ are phase shifts in parallel and perpendicular polarisation, λ_s is the signal wavelength, A_{eff} is the effective core area, P_g is the gate power and L is the length of the non-linear medium. When the phase shift difference reaches π, the polarisation of the signal is switched by 90 degrees. Thus the non-linear phase shift is converted to intensity modulation by passing the signal through a polariser. TABLE 2 summarises the all-optical switching performance using As_2S_3 fibre. In the first demonstration of the Kerr shutter using a 50 cm-long As_2S_3 fibre at 1.3 μm, the switching power was 14 W [6]. Afterwards, laser-diode driving became possible with the assistance of an erbium-doped fibre amplifier (EDFA) at 1.55 μm and the switching power has been reduced to 3 W using a 1 m-long small-core fibre [7].

TABLE 2 All-optical switching performance using As_2S_3-based fibres.

Configuration	Wavelength (μm)	Core size (μm)	Loss (dB/m)	Fibre length (m)	Switching power (W)
Kerr	1.3	6	6.0	0.5	14
Kerr	1.55	3	3.0	1.2	3
NOLM	1.55	2.5	0.6	4	0.4

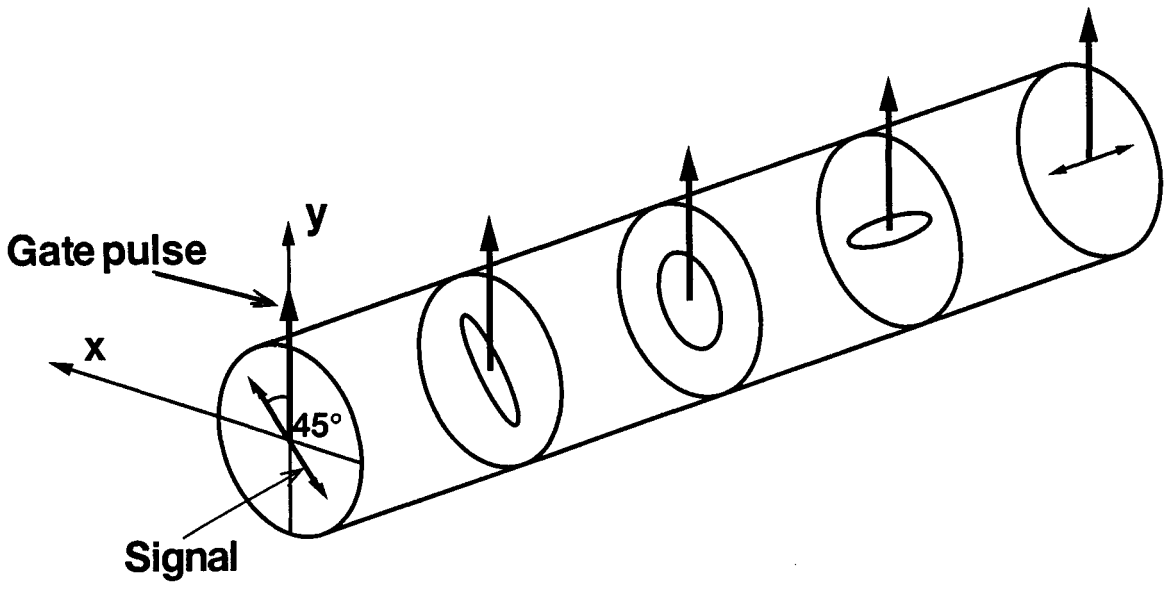


FIGURE 1 Principle of optical Kerr shutter.

Although the optical Kerr shutter offers a simple configuration, it does not necessarily afford the lowest switching power. The phase shift in perpendicular polarisation reduces the effective phase shift difference. By comparison, the non-linear optical loop mirror (NOLM) utilises the difference in phase shift between two signal beams which propagate along the fibre in the same and the opposite directions

as the gate pulse [11]. In the NOLM the phase shift of the counter-propagating beam is negligible, so that the effective phase shift difference is 1.5 times larger than that of EQN (1). Recently, switching with an NOLM using an As_2S_3-based fibre has been demonstrated [12]. FIGURE 2 shows the schematic experimental setup. The NOLM consists of 3 dB fibre couplers, a gate/signal combiner, 4 m of As_2S_3 based fibre and a polarisation controller. The edges of As_2S_3 based fibres are anti-reflection coated and butt-jointed to conventional silica-based fibre optics. Gate and signal pulses are generated by gain switching of DFB laser diodes and amplification with an erbium-doped fibre amplifier. The NOLM acts like a mirror for signals in the absence of the gate pulse. When the gate pulse is launched, and the phase shift difference between co-propagating and counter-propagating signals reaches π, the signal is switched to the output port as illustrated in FIGURE 2. As summarised in TABLE 2, the switching power was reduced to 0.4 W using the NOLM configuration with a low-loss fibre. This switching power is comparable to that of a silica-based NOLM 6 km in length [4]. FIGURE 3 shows the results of the demultiplexing experiment. All-optical demultiplexing of a 40 GHz pulse train into 4 GHz was successfully demonstrated.

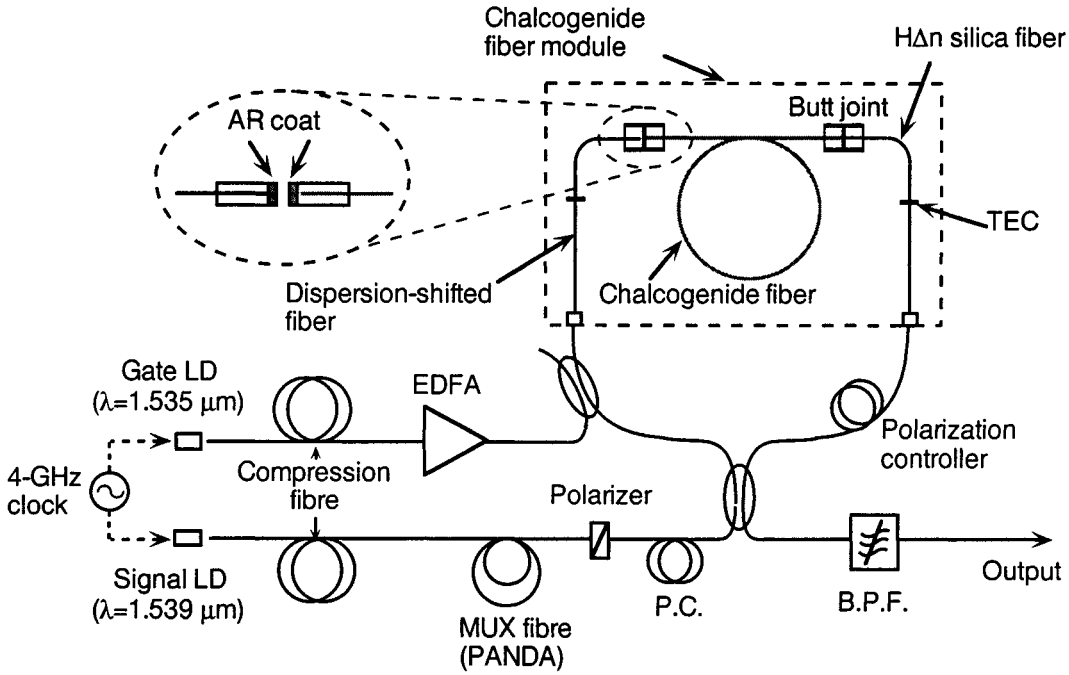


FIGURE 2 Experimental setup of all-optical switching with an NOLM using As_2S_3-based fibre.

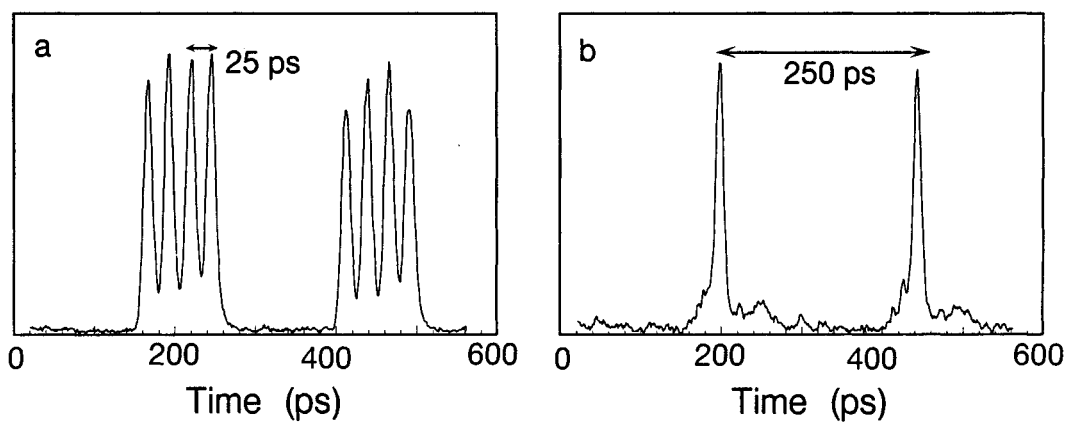


FIGURE 3 Temporal waveforms of (a) input signal and (b) switched signal in all-optical demultiplexing experiment.

To further reduce the switching power, one of the simplest ways is to increase the interaction length by using a longer fibre. If we use a longer fibre, however, the large GVD causes walk-off between the gate and the signal, which limits the effective interaction length [6]. To overcome this limitation, fabrication of As_2S_3-based fibre grating is being studied [13]. By extending the fabrication technique to chirped grating, the GVD limitation could be relaxed.

E CONCLUSION

Recent progress in studies on the application of chalcogenide glass fibre to all-optical switching has been reviewed. The non-linear refractive index of As_2S_3-based fibre was measured to be two orders of magnitude higher than that of silica fibre. All-optical switching using the As_2S_3-based fibre was demonstrated in the Kerr shutter and NOLM configurations. The large GVD of the fibre might restrict its applicable length.

Future challenges are summarised as follows:

(1) Transmission loss of the fibre should be further reduced to reduce the switching power.

(2) The mechanism of photo-induced damage and the reliability of the fibre should be clarified.

(3) The fabrication of chirped grating and its application to all-optical switching should be promoted.

REFERENCES

[1] A.E. Owen, A.P. Firth, P.J.S. Ewen [*Philos. Mag. B (UK)* vol.52 (1985) p.347]
[2] R.L. Fork, C.V. Shank, A.M. Glass, A. Migus, M.A. Bosch, J. Shah [*Phys. Rev. Lett. (USA)* vol.43 (1979) p.394]
[3] R. Ranganathan, M. Gal, P.C. Taylor [*Phys. Rev. (USA)* vol.37 (1988) p.10216]
[4] K. Uchiyama, S. Kawahishi, H. Takara, T. Morioka, M. Saruwatari [*Electron. Lett. (UK)* vol.30 (1994) p.873]
[5] H. Nasu, K. Kubodera, H. Kobayashi, M. Nakamura, K. Kamiya [*J. Am. Ceram. Soc. (USA)* vol.4 (1990) p.1794]
[6] M. Asobe, T. Kanamori, K. Kubodera [*IEEE J. Quantum Electron. (USA)* vol.29 (1993) p.2325]
[7] M. Asobe, H. Itoh, T. Miyazawa, T. Kanamori [*Electron. Lett. (UK)* vol.29 (1993) p.1966]
[8] M. Sheik-Bahae, D.C. Hutchings, D.J. Hagan, E.W.V. Stryland [*IEEE J. Quantum Electron. (USA)* vol.27 (1991) p.1296]
[9] V. Mizarahi, K.W. Delong, G.I. Stegeman, M.A. Saifi, M.J. Andrejco [*Opt. Lett. (USA)* vol.14 (1989) p.1140]
[10] M. Asobe, T. Kanamori, K. Naganuma, H. Itoh, T. Kaino [*J. Appl. Phys. (USA)* vol.77 (1995) p.5518]
[11] K.J. Blow, N.J. Doran, B.K. Nayar, B.P. Nelson [*Opt. Lett. (USA)* vol.15 (1990) p.248]
[12] M. Asobe, T. Ohara, I. Yokohama, T. Kaino [*Electron. Lett. (UK)* vol.32 (1996) p.1396]
[13] M. Asobe, T. Ohara, I. Yokohama, T. Kaino [*Electron. Lett. (UK)* vol.32 (1996) p.1611]

Index

Index terms	Links			
A				
Abbe number				
fluoride glass	177	181		
oxide glass	134			
silica glass	15			
absorption cross-sections				
erbium-doped silica fibre	46			
neodymium-doped halide glass	244			
neodymium-doped oxide glass	120			
thulium-doped halide glass	238			
acid resistance tests	115			
acoustic shear wave velocity				
fluoride glass	203			
alkali resistance tests	115			
annealing point	110	112	197	306
atomic volume				
fluoride glass	204			
B				
Bragg grating devices	3	5	6	
branching ratio				
dysprosium-doped chalcogenide glass	332			
holmium-doped halide glass	229	230		
neodymium-doped chalcogenide glass	322	324		
neodymium-doped halide glass	241	242		
praseodymium-doped chalcogenide glass	355			
thulium-doped halide glass	237			
Brillouin frequency				
pressure dependence	32			
silica glass	32			
Brillouin scattering	8	9	93	291
broadband amplifiers	120			
bubbles	263	350	351	
build-in casting method	253			

This page has been reformatted by Knovel to provide easier navigation.

Index terms	Links		
bulk modulus			
halide glass	202		
oxide glass	107		
pressure dependence	205		
silica glass	29		
temperature dependence	205		
C			
cascade lasers	276	277	324
cascaded-amplifier links	79		
casting			
build-in method	253		
halide glass	251		
oxide glass	136		
rotational	254		
suction	256		
chalcogenide glass			
cooling rate	339		
crystallization onset temperature	306		
dispersion	295		
dysprosium-doped	330		
electronic absorption edge	283		
glass transition temperature	305		
impurities	340		
inclusions	340		
intrinsic scattering	289		
IR absorption edge	285		
IR transmittance spectra	338		
melting	338	339	
melting onset temperature	306	338	
microhardness	266		
neodymium-doped	320		
non-linear refractive index	298		
non-linearity	362		
partial dispersion	296		
peak crystallization temperature	306		
Poisson's ratio	266		
praseodymium-doped	315	355	
preparation	337		
purification	340		
raw materials	337	338	
Rayleigh scattering coefficient	290		

This page has been reformatted by Knovel to provide easier navigation.

Index terms **Links**

chalcogenide glass *(Continued)*
refractive index 294
shear modulus 266
thermal expansion coefficient 305 308
third-order susceptibility 299 300 362
thulium/holmium doped 326
transmission 283
UV absorption edge 283
viscosity 309
Young's modulus 266
zero material dispersion wavelength 295 296
chalcogenide glass fibre
defects 350 351
drawing 307 308 344
dysprosium-doped 332 333
group velocity dispersion 362 363
impurities 349 350
loss 287 291 292 343 348
neodymium-doped 322 323
non-linear refractive index 298 362 363
preforms 344
two-photon absorption coefficient 362 363
two-photon figure of merit 362 363
upconversion emission 322 323
chemical durability
halide glass 208 209
halide glass fibre 265 266
chemical sensing 326
clad over core technique 253 254
coatings for optical fibres 64 71 72 257 258
344 346
cold isostatic pressing 56
colloidal sol-gel processes 56
compressibility
pressure dependence 30 33
silica glass 29 30 33
temperature dependence 29 30
concentration quenching 57 123 222 229 233
315 322
concentration scattering 92 93

This page has been reformatted by Knovel to provide easier navigation.

Index terms	Links				
cooling rate					
chalcogenide glass	339				
critical	206	207			
crack velocity					
oxide glass	109				
silica glass	37				
cristobalite	33				
critical cooling rate	206	207			
crystallization curve	110				
crystallization onset temperature	139	189	206	208	306
CW fibre lasers	149	359	360		

D

Debye temperature					
fluoride glass	205				
defect centres					
silica glass	5				
demultiplexing	365				
density					
fluoride glass	204				
density scattering	92				
dielectric permittivity	289	290			
differential thermal analysis	306	307			
diode pumped lasers	50	151			
dispersion					
chalcogenide glass	295				
chromatic	15				
fluoride glass	177				
group velocity	13				
oxide glass	96	97			
silica glass	12				
dispersive optical fibres	138				
distillation purification					
chalcogenide glass	339	341			
distributed-feedback fibre lasers	43				
double crucible melting	140	257	346		
drawing					
chalcogenide glass	307	308			
chalcogenide glass optical fibres	344				
characteristic temperature criteria	307				
halide glass optical fibres	253	271			

This page has been reformatted by Knovel to provide easier navigation.

Index terms	Links				
drawing *(Continued)*					
oxide glass optical fibres	138				
silica optical fibres	62				
drawing tower	257	258	344	345	
dysprosium-doped chalcogenide glass	330				
absorption spectra	330	331			
excitation	333				
fluorescence	331	332			
lifetime	332	333			
UV absorption edge	330				
E					
elastic modulus: see Young's modulus					
electric dipole oscillator strength					
holmium-doped halide glass	225				
electronic absorption bandgap					
silica glass	13	14			
electronic absorption edge					
chalcogenide glass	283				
electrostriction	18	20	21		
emission cross-sections					
erbium-doped silica fibre	46				
holmium-doped halide glass	226	228			
neodymium-doped chalcogenide glass	321	322			
neodymium-doped halide glass	243	244			
praseodymium-doped chalcogenide glass	355				
thulium-doped halide glass	238				
environmental durability					
halide glass	208	209			
equalising optical amplifier	78				
erbium-doped-fibre amplifiers	43	75	128	130	138
	156				
composite configuration	75	76			
fluoride	158				
gain	75	157	158		
gain equalization	78				
noise figure	75	76			
optical limiting amplifier	77				
oxide glass	128	130	138		
silica	75	158			
tellurite	156				

This page has been reformatted by Knovel to provide easier navigation.

Index terms			Links
erbium-doped halide glass	218		
absorption spectra	218		
fluorescence	219		
Judd-Ofelt parameters	218	219	
non-radiative decay	221		
radiative lifetime	221	222	
Stokes emission	220		
upconversion efficiency	219	220	
erbium-doped oxide glass	126		
absorption spectra	126	127	
fluorescence	128	129	
non-radiative decay	129	130	
radiative lifetime	128	129	
refractive index	129		
erbium-doped silica	43		
absorption	44		
energy-level transitions	43		
erbium-clustering effects	43		
excited-state absorption	44	45	
fluorescence	44	45	
fluorescence lifetime	45	46	
optical pumping	43	44	
extinction coefficient			
chalcogenide glass fibre	350		
extrusion forming	56	257	346

F

fatigue			
oxide glass	109		
silica fibre	69	70	
fibre amplifiers: see also erbium-doped-fibre amplifiers, praseodymium-doped-fibre amplifiers			
dysprosium-doped chalcogenide glass	330	332	
erbium-doped silica	43	57	75
erbium-doped tellurite	156		
neodymium-doped silica	50		
oxide glass	128	130	138
praseodymium-doped chalcogenide glass	355		
praseodymium-doped halide glass	271		
fibre gratings			
chalcogenide glass	366		
chirped	366		

This page has been reformatted by Knovel to provide easier navigation.

Index terms	Links			
fibre gratings *(Continued)*				
doping effects	82			
fibre sensitisation	81	82		
manufacturing techniques	80	81		
silica	80			
Type1	82			
Type 2	82			
Type 2A	82			
fibre lasers				
cascade	276	277	324	
configurations	150	275		
CW fibre lasers	149	359	360	
distributed feedback	43			
dysprosium-doped chalcogenide glass	332			
erbium-doped fluoride glass	276	277		
fluoride glass	184			
mid infrared	283	324	330	332
mode-locked	152	153	276	
narrow linewidth	152			
neodymium-doped halide glass	243	244		
neodymium-doped oxide glass	138			
neodymium-doped silica	50			
neodymium-doped sulphide glass	358			
pulsed	152	153	359	360
Q-switched	152	153	276	
rare earth-doped fluoride glass	275			
rare earth-doped oxide glass	149			
slope efficiency	149	151	277	
tuning	150	152	275	276
upconversion	277			
fictive temperature				
silica fibre	9	38		
figure of merit				
chalcogenide glass fibre	362	363		
fining				
halide glass	250	251		
oxide glass	135			
fluorescence				
dysprosium-doped chalcogenide glass	331	332		
erbium-doped halide glass	219			
erbium-doped oxide glass	128	129		
erbium-doped silica	44	45		

This page has been reformatted by Knovel to provide easier navigation.

Index terms	Links		
fluorescence *(Continued)*			
holmium-doped halide glass	226	228	
neodymium-doped chalcogenide glass	321	323	324
neodymium-doped oxide glass	120	121	
praseodymium-doped chalcogenide glass	317		
praseodymium-doped fluoride glass	214		
thulium-doped halide glass	238		
thulium/holmium-doped chalcogenide glass	326	327	
fluorescence lifetime			
dysprosium-doped chalcogenide glass	331		
erbium-doped fluoride glass	222		
erbium-doped silica	45	46	
praseodymium-doped chalcogenide glass	355		
fluoride glass: see also heavy metal fluoride glass			
Abbe number	177	181	
acoustic shear wave velocity	203		
atomic volume	204		
bulk modulus	203		
crystallization onset temperature	190		
Debye temperature	205		
density	204		
dispersion	177		
erbium-doped	219		
glass transition temperature	190		
IR absorption	161		
longitudinal acoustic velocity	204	205	
melting temperature	190		
microhardness	266		
molar specific heat	182		
non-linear refractive index	180	181	
peak crystallization temperature	190	192	
Poisson's ratio	203	204	266
praseodymium-doped	213		
preparation	249		
Rayleigh scattering coefficient	170		
refractive index	161	176	181
rheology	198	199	
shear modulus	203	266	
thermal conductivity	182		
thermal diffusivity	182		
thermal expansion coefficient	182		
transmission	161		

This page has been reformatted by Knovel to provide easier navigation.

Index terms **Links**

fluoride glass: *(Continued)*
- UV absorption 163
- Vickers hardness 203
- viscosity 196
- Young's modulus 203 266
- zero dispersion wavelength 178

fluoride glass fibre
- core-clad compositions 190
- drawing 253
- lifetime 267
- loss 192 253
- Rayleigh scattering loss 172 173
- tensile strength 266

fracture strength
- oxide glass 109
- silica glass 35

Frenkel defects 209

frozen melt 110

G

gas sensing 330 332

gettering agents 337

glass formation curve 110

glass preparation
- atmosphere control 251
- chalcogenide glass 337
- halide glass 249
- oxide glass 133
- silica 55

glass transition temperature 139 189 205 206 208 249 289 305

group velocity dispersion
- chalcogenide glass fibre 362 363 366

H

halide glass: see also fluoride glass, heavy halide glass
- Abbe number 181
- acoustic shear wave velocity 203
- annealing 252
- atomic volume 204
- bulk modulus 203

This page has been reformatted by Knovel to provide easier navigation.

Index terms	Links		
halide glass: *(Continued)*			
casting	251		
characteristic temperatures	189	205	208
Debye temperature	205		
density	204		
erbium-doped	218		
fining	250	251	
glass transition temperature	205		
holmium-doped	224		
intrinsic scattering loss	170		
IR absorption	161		
longitudinal acoustic velocity	204	205	
melting	250		
neodymium-doped	241		
non-linear refractive index	180		
non-Newtonian behaviour	198		
Poisson's ratio	203	204	
praseodymium-doped	213		
preparation	249		
refractive index	176	181	218
shear modulus	203		
stability	206		
starting materials	249	250	
thulium-doped	236		
transmission	161		
UV absorption	163	165	167
Vickers hardness	203		
viscosity	194		
Young's modulus	203		
halide glass fibre: see also fluoride glass fibre			
chemical durability	265	266	
dispersion	178		
drawing	253		
loss	254	260	
mechanical strength	266		
multi-mode	253	257	
Rayleigh coefficient	173		
Rayleigh scattering loss	173		
reliability	265		
single-mode	256	257	
heavy halide glass			
dispersion	178		

This page has been reformatted by Knovel to provide easier navigation.

Index terms **Links**

heavy halide glass *(Continued)*
refractive index 178
transmission 165
zero dispersion wavelength 178
heavy metal fluoride glass
dispersion 178
intrinsic scattering loss 170
non-linear refractive index 178
refractive index 176 177
viscosity 197
holmium-doped halide glass 224
absorption 224
branching ratio 229 230
co-doped systems 233 234
electric dipole oscillator strength 225
fluorescence 226 228
Judd-Ofelt parameters 226 227
magnetic dipole oscillator strength 225
measured lifetime 229 231
non-radiative properties 229 231
radiative lifetime 226 229 230
homogenization
oxide glass 136
Hruby stability parameter 206 207
hydrolytic resistance tests 115 116
water in deficiency 116
water in excess 116
hypersensitive pseudoquadrupolar transitions 321 331

I

intrinsic scattering loss
chalcogenide glass 289
doping effects 9 10
halide glass 170
oxide glass 88 89 92 93
silica fibre 8
silica glass 8
IR absorption
halide glass 161
oxide glass 88 143
silica glass 3 4 6

This page has been reformatted by Knovel to provide easier navigation.

Index terms	Links			
IR absorption *(Continued)*				
temperature dependence	163			
IR absorption edge				
chalcogenide glass	285			
IR transmittance spectra				
chalcogenide glass	338			
isostatic pressing	344			
isothermal compressibility	290			
J				
jacketing technique	253	254	256	271
Judd-Ofelt parameters				
erbium-doped halide glass	218	219		
erbium-doped oxide glass	126			
holmium-doped halide glass	226	227		
neodymium-doped chalcogenide glass	321			
neodymium-doped oxide glass	120			
praseodymium-doped chalcogenide glass	317			
praseodymium-doped fluoride glass	213	214		
thulium-doped halide glass	236	237		
K				
Kerr shutter	364			
Knoop hardness				
oxide glass	108	109		
Kramers-Kronig analysis	3			
L				
laser radar	326			
lattice absorption frequency				
silica glass	13			
leach rate				
halide glass	208	209	265	
lifetime	215			
see also non-radiative lifetime, radiative lifetime				
holmium-doped halide glass	231			
measured	215	216	231	
praseodymium-doped fluoride glass	215	216		
lifetime quenching	215	216		
liquidus temperature	139	189	249	306

This page has been reformatted by Knovel to provide easier navigation.

Index terms **Links**

longitudinal acoustic velocity
fluoride glass 204 205
loss
bending effects 67
chalcogenide glass fibre 348
dopant effects 9 10 65
extrinsic 142 262 263 349
fluoride glass fibre 192 253
halide glass fibre 260 272
hydrogen effects 67 68
impurity effects 260 349
intrinsic scattering 8 88 89 92 93
142 170 189
moisture effects 67 262
oxide glass 88 89 92 93
oxide glass fibre 90 142
radiation effects 68
silica fibre 8 65
silica glass 8

M

Madelung constant 202
magnetic dipole oscillator strength
holmium-doped halide glass 225
master oscillator power amplifier 152
mechanical strength
fluoride glass fibre 266
silica fibre 266
medical applications 236 275 326
melting
double crucible 140 257 346
chalcogenide glass 338
halide glass 250
oxide glass 135
melting onset temperature 189 206 306 338
microhardness
chalcogenide glass 266
fluoride glass 266
oxide glass 266
silica glass 266
mid infrared lasers 283 324 330 332

This page has been reformatted by Knovel to provide easier navigation.

Index terms	Links				
mid infrared optical transparency	283				
Mie scattering	93	174			
mode-locked fibre lasers	152	153	276		
modified chemical vapour deposition	56	58	59		
molar specific heat					
fluoride glass	182				
multiphonon processes	229	232			
chalcogenide glass	286	287	317	323	328
	348				
N					
narrow-linewidth fibre lasers	152				
neodymium-doped chalcogenide glass	320				
absorption spectra	320	321			
branching ratio	322	324			
emission cross-section	321	322			
fluorescence	321	323	324		
Judd-Qfelt parameters	321				
multiphoton decay	323				
radiative lifetime	321	322			
neodymium-doped chalcogenide glass fibre					
upconversion emission	322	323			
neodymium-doped halide glass	241				
absorption	241	242			
branching ratio	241	242			
emission cross-sections	243	244			
non-radiative decay	242	243			
radiative lifetime	241	242			
neodymium-doped oxide glass	119				
absorption cross-section	120				
absorption spectra	119	120			
fluorescence	120	121			
non-radiative decay	122				
radiative lifetime	122	123			
neodymium-doped silica	48				
absorption	48	49			
co-doping effects	49				
energy-level transitions	50				
fluorescence	48	49			
nephelauxetic effect	120	243	315	322	
network formers	87				

This page has been reformatted by Knovel to provide easier navigation.

Index terms	Links		
non-linear optical loop mirror	364		
non-linear phase shift	301		
non-linear refractive index			
chalcogenide glass	298		
chalcogenide glass fibre	298	362	363
cross-phase modulation	19	20	
doping effects	99	100	
four-wave mixing	20		
halide glass	180		
heavy metal fluoride glass	178		
oxide glass	99		
self-phase modulation	18	19	
silica fibre	17		
silica glass	19		
non-radiative decay			
energy transfer processes	233	234	
erbium-doped halide glass	221		
erbium-doped oxide glass	129	130	
holmium-doped halide glass	229	231	
multiphonon transitions	229	232	
neodymium-doped halide glass	242	243	
neodymium-doped oxide glass	122		
praseodymium-doped chalcogenide glass	317		
praseodymium-doped fluoride glass	215		
thulium-doped halide glass	239		
thulium/holmium-doped chalcogenide glass	327	328	
non-radiative lifetime			
erbium-doped fluoride glass	222		
praseodymium-doped fluoride glass	216		

O

optical absorption			
defect centres	5		
dissolved gaseous species	6		
dysprosium-doped chalcogenide glass	330	331	
erbium-doped halide glass	218	219	
erbium-doped oxide glass	126	127	
halide glass	161		
halide glass fibre	260		
holmium-doped halide glass	224		
impurities	6	260	340
neodymium-doped chalcogenide glass	320	321	

This page has been reformatted by Knovel to provide easier navigation.

Index terms	Links	
optical absorption *(Continued)*		
neodymium-doped halide glass	241	242
neodymium-doped oxide glass	119	120
oxide glass	87	88
oxide glass fibre	90	
praseodymium-doped chalcogenide glass	315	316
praseodymium-doped fluoride glass	213	214
silica fibre	4	
silica glass	3	44
thulium-doped halide glass	236	237
thulium/holmium-doped chalcogenide glass	326	
optical absorption coefficient		
chalcogenide glass	283	
fluoride glass	261	262
silica glass	3	
optical communications	236	
optical current transducers	138	
optical data storage	236	
optical fibre fabrication: see also drawing		
chalcogenide glass	337	
halide glass	249	
oxide glass	133	
rare earth-doped silica	57	
silica	55	
optical limiting amplifier	77	
optical switches	298	362
demultiplexing	365	
loss	364	
non-linear optical loop mirror	364	
optical Kerr shutter	364	
phase shift	364	365
switching power	364	
outside vapour deposition	56	
oxide glass		
Abbe number	134	
annealing	136	
bulk modulus	107	
casting	136	
crack growth	109	
dispersion	96	97
erbium-doped	126	

This page has been reformatted by Knovel to provide easier navigation.

Index terms	Links				
oxide glass *(Continued)*					
fatigue	109				
fining	135				
forming	136				
fracture strength	109				
homogenization	136				
intrinsic scattering loss	88	89	92	93	
IR absorption	88	143			
Knoop hardness	108	109			
loss spectra	142				
melting	135				
microhardness	266				
neodymium-doped	119				
non-linear refractive index	99				
optical absorption	87	88			
Poisson's ratio	107	108	266		
preparation	133				
Rayleigh scattering	92	93			
refractive index	95	96	134		
Sellmeier coefficients	96				
shear modulus	107	266			
shear velocity	111				
stability	114				
third-order susceptibility	101	102			
transmission	87				
UV absorption	88	143			
Vickers hardness	108				
viscosity	110	139			
Young's modulus	107	108	266		
oxide glass fibre					
drawing	138				
loss	142				
optical loss spectra	90				
preforms	139	140			
transmission spectra	89				

P

partial dispersion					
chalcogenide glass	296				
peak crystallization temperature	189	190	192	206	208
	306				
photoelectric constant	172	290			

This page has been reformatted by Knovel to provide easier navigation.

Index terms			Links
photonic switches	294		
photonics networks	275		
photorefractive gratings	80		
plasma chemical vapour deposition	56		
Poisson's ratio			
halide glass	202	266	
oxide glass	107	108	266
silica fibre	31		
silica glass	29	266	
strain effects	31		
temperature dependence	29	30	
polymorphism			
silica glass	31		
population lens effect	180	183	184
praseodymium-doped chalcogenide glass	315	355	
absorption spectra	315	316	
branching ratio	355		
emission cross-section	355		
fluorescence	317	355	
Judd-Ofelt parameters	316	317	
non-radiative properties	317		
quantum efficiency	355		
radiative lifetime	316		
Raman spectrum	317	318	
praseodymium-doped-fibre amplifiers	271	355	
chalcogenide glass	355		
fabrication	271	272	
gain	271	273	355
halide glass	271		
single-mode fibre	271	355	356
transmission loss	272		
praseodymium-doped fluoride glass	213		
absorption spectra	213	214	
fluorescence	214		
Judd-Ofelt analysis	213	214	
lifetime	215	216	
non-radiative decay	215		
quantum efficiency	215		
pre-amplifiers	75	79	
preform fabrication			
chalcogenide glass optical fibres	344		

This page has been reformatted by Knovel to provide easier navigation.

Index terms	Links				
preform fabrication *(Continued)*					
halide glass optical fibres	253				
oxide glass optical fibres	139	140			
rare earth-doped silica optical fibres	58	59			
silica optical fibres	56	58	59		
pulsed fibre lasers	152	153	359	360	
purification					
chalcogenide glass	340				
charge	341	342			
Q					
Q-switched fibre lasers	152	153	276		
quantum efficiency					
dysprosium-doped chalcogenide glass	331	332			
erbium-doped fluoride glass	222				
holmium-doped halide glass	233				
praseodymium-doped chalcogenide glass	317	355			
praseodymium-doped fluoride glass	215				
quantum yield	229				
R					
radiation resistance					
halide glass	209				
radiative lifetime					
dysprosium-doped chalcogenide glass	332	333			
erbium-doped fluoride glass	221	222			
erbium-doped oxide glass	128	129			
holmium-doped halide glass	226	229	230		
neodymium-doped chalcogenide glass	321	322			
neodymium-doped halide glass	241	242			
neodymium-doped oxide glass	122	123			
praseodymium-doped chalcogenide glass	316				
praseodymium-doped fluoride glass	215	216			
thulium-doped halide glass	238	239			
thulium/holmium doped chalcogenide glass	327				
radiolytic process	209				
Raman effect	18				
Raman scattering	8	9	93	290	291
Raman spectrum					
praseodymium-doped chalcogenide glass	317	318			

This page has been reformatted by Knovel to provide easier navigation.

Index terms	Links				
rapid insertion method	256				
Rayleigh ratio	8				
Rayleigh scattering	8	92	93	289	350
	351				
concentration scattering	92	93			
density scattering	92				
Mie scattering	93	174			
Rayleigh scattering coefficient					
chalcogenide glass	290				
fluoride glass	171	173			
halide glass	170	171	173	174	
Rayleigh scattering loss					
chalcogenide glass fibre	348				
fictive temperature dependence	9				
fluoride glass fibre	172	173			
halide glass	170				
oxide glass	92	93			
silica fibre	9	10	173		
silica glass	8	172			
temperature dependence	172				
Rayleigh-Gans scattering	350	351			
reactive vapour transport	257				
refractive index: see also non-linear refractive index					
chalcogenide glass	294				
erbium-doped oxide glass	129				
fluoride glass	161	176	181	218	
oxide glass	95	96	134		
silica fibre	17				
silica glass	12	55			
temperature dependence	178				
reliability					
chemical durability	265	266			
halide glass optical fibres	265				
hermetic coatings	71	72			
lifetime estimation	267				
mechanical strength	266				
silica optical fibres	69				
subcritical crack growth	69	70			
zero stress aging	70	71	267		
remote sensing	50	330			

This page has been reformatted by Knovel to provide easier navigation.

Index terms	Links				
ring laser	275				
rod-in-tube method	58	139	344		
rotational casting	254				
S					
S stability parameter	206	207			
scattering efficiency factor	350				
Sellmeier coefficients					
oxide glass	96				
silica glass	12				
sensors	50	81	83	236	275
	283	326	330	332	
shear modulus					
density dependence	32				
halide glass	202	266			
oxide glass	107	266			
pressure dependence	30	205			
silica glass	29	266			
strain effects	31				
temperature dependence	29	205			
shear thinning	111				
shear velocity					
fictive temperature dependence	31	32			
oxide glass	111				
silica glass	31	32			
silica fibre					
absorption cross-sections	46				
defect centres	5				
doping effects	57				
drawing	62				
emission cross-sections	46				
erbium-doped	43	58	59		
fabrication	55				
fictive temperature	9	38			
impurities	6				
intrinsic scattering loss	8				
loss	65				
neodymium-doped	48				
non-linear refractive index	17				
optical absorption spectra	4				
Poisson's ratio	31				

This page has been reformatted by Knovel to provide easier navigation.

Index terms			Links
silica fibre *(Continued)*			
Rayleigh scattering loss	9	10	173
reliability	69		
static fatigue	35		
silica glass			
Abbe number	15		
Brillouin frequency	32		
bulk modulus	29		
compressibility	29	30	33
crack velocity	37		
defect centres	5		
dispersion	12		
doping effects	55		
electronic absorption bandgap	13	14	
erbium-doped	43		
fracture strength	35		
glass transition temperature	205		
impurities	6		
intrinsic scattering loss	8		
IR absorption	3	4	6
lattice absorption frequency	13		
microhardness	266		
neodymium-doped	48		
non-linear refractive index	19		
optical absorption	3		
Poisson's ratio	29	266	
polymorphism	31		
Rayleigh scattering loss	8	172	
refractive index	12	55	
Sellmeier coefficients	12		
shear modulus	29	266	
shear velocity	31	32	
stability	35		
static fatigue	35	37	38
structure	33		
thermal expansion coefficient	33		
transmission	3		
UV absorption	3	5	6
viscosity	25		
Young's modulus	29	30	266
zero-dispersion wavelength	15		
single-mode fibre fabrication	344		

This page has been reformatted by Knovel to provide easier navigation.

Index terms	Links				
softening point	110	111	139	197	306
solution doping	58	59			
soot	56	58			
spontaneous emission probability					
thulium-doped halide glass	237				
stability					
acid resistance tests	115				
alkali resistance tests	115				
attack by water	114				
chemical durability	208	209			
chemical reactions	115				
halide glass	206				
hydrolytic resistance tests	115	116			
leaching rates	208	209			
oxide glass	114				
radiation resistance	209				
silica glass	35				
thermal	206				
static fatigue					
mechanisms	37	38			
silica fibre	35				
silica glass	35	37	38		
water effects	37	38			
strain point	306				
strain sensors	83				
stress corrosion cracking	37				
stretch-and-insert process	344	345			
structure					
silica glass	33				
submarine cables	68				
suction casting	256				

T

telecommunication systems	83				
tellurite glass	156				
tellurite glass fibre	156	157			
breaking stress	157				
loss spectrum	156				
moisture resistance	157				
tensile strength					
fluoride glass fibre	266				

This page has been reformatted by Knovel to provide easier navigation.

Index terms	Links				
tensile strength *(Continued)*					
silica fibre	266				
thermal conductivity					
fluoride glass	182				
thermal diffusivity					
fluoride glass	182				
thermal expansion coefficient					
chalcogenide glass	308				
fluoride glass	182				
measurement	307				
silica glass	33				
thermal lens effect	180	359			
thermal stability					
halide glass	206				
third-order optical non-linearities	301				
nuclear contribution	301				
third-order polarization	301				
third-order susceptibility	17	101	102	299	362
thulium-doped halide glass	236				
absorption	236	237			
branching ratio	237				
fluorescence	238				
Judd-Ofelt parameters	236	237			
non-radiative properties	239				
radiative lifetime	238	239			
spontaneous emission probability	237				
thulium/holmium-doped chalcogenide glass	326				
absorption spectra	326				
fluorescence	326	327			
non-radiative properties	327	328			
radiative lifetime	327				
transmission					
chalcogenide glass	283				
halide glass	161				
oxide glass	87				
oxide glass fibre	89				
silica glass	3				
transmission window					
chalcogenide glass	283				
tubular crucible technique	257				

This page has been reformatted by Knovel to provide easier navigation.

Index terms	Links				
two-photon absorption coefficient					
chalcogenide glass	299	300			
chalcogenide glass fibre	362	363			
dispersion	299	300			
U					
undercooled melt	110				
upconversion lasers	234	277	322	323	
Urbach tail	284	348			
UV absorption					
chalcogenide glass	283	330			
halide glass	163	165	167		
oxide glass	88	143			
silica glass	3	5	6		
UV lithography	3	5			
V					
vacuum distillation	341				
vapour-phase axial deposition	56	58			
Vickers hardness					
fluoride glass	203				
oxide glass	108				
viscosity					
chalcogenide glass	309				
doping effects	26				
halide glass	194				
measurement methods	309				
oxide glass	110	139			
shear rate dependence	198				
silica glass	25				
temperature dependence	25	110	112	113	139
	194	311			
W					
wavelength independent scattering	350	351			
weak absorption tail					
chalcogenide glass	284	285			
chalcogenide glass fibre	348				
working point	110	111	197		

This page has been reformatted by Knovel to provide easier navigation.

Index terms	Links				
Y					
Young's modulus					
chalcogenide glass	266				
halide glass	202	266			
oxide glass	107	108	266		
pressure dependence	30	203	205		
silica glass	29	30	266		
strain effects	30				
temperature dependence	29	108	203	205	
Z					
z-scan	101	102	184	300	301
zero-dispersion wavelength					
chalcogenide glass	295	296			
fluoride glass	178				
halide glass	178				
oxide glass	97				
silica glass	15	97			
temperature dependence	15				
zero stress aging	70	71	266		

This page has been reformatted by Knovel to provide easier navigation.